Optimal Design
with Advanced Materials

The Frithiof Niordson Volume

Proceedings of the IUTAM Symposium on
Optimal Design with Advanced Materials,
Lyngby, Denmark, 18-20 August, 1992

Edited by

Pauli PEDERSEN

Department of Solid Mechanics
The Technical University of Denmark
Lyngby, Denmark

This book is printed on acid-free paper.

Printed in The Netherlands.

PREFACE

Early 1990 a proposal for a IUTAM Symposium with the title "Optimal Design with Advanced Materials" was submitted, and approved by the Bureau of IUTAM to take place in Lyngby, Denmark during the dates 18th to 20th of August 1992. This time schedule made it possible also to mark the 70th birthday of Professor Frithiof Niordson.

The scientific committee pointed out the importance of joining scientists with a primary background in mechanics, materials and mathematics, respectively. To further improve the cooperation between these groups is of vital importance, and not an easy task. The cooperation with the scientific committee is highly appreciated.

Optimal design with advanced materials is a very active and challenging domain within applied mechanics. Several research groups conduct basic research in the area and there is a need to coordinate these activities and to discuss the mechanical as well as the computational aspects in an international forum. The increasing use of advanced materials, such as anisotropic fiber composites and ceramics, necessitates new development to be made within constitutive modelling and the computational methods of analysis, sensitivity analysis and optimization. A new dimension of optimal design is opened by the direct tayloring and design of new materials. The research area is increasingly active and the results of the research will find rapid application in the high technology industries. The two important research areas, homogenization and smart materials/structures, are within the scope of the Symposium. The symposium brought together 60 scientists from 18 countries working in mechanics and mathematics related to optimal design and materials. The 31 contributions stimulated the exchange of ideas and many went home with ideas for further research.

Financial support for the Symposium was generously provided by the International Union of Theoretical and Applied Mechanics (IUTAM). Further, the Symposium was sponsored by the Danish Center for Applied Mathematics and Mechanics (DCAMM), Technical University of Denmark, Danfoss A/S, Grundfos A/S, Otto Mønsted Foundation and Danish Technical Research Council (STVF Programme on Computer Aided Design). This financial support is greatly appreciated.

The ordering of the published papers agrees with the order of presentation at the Symposium. The division into sections and the headings of the sections should not be too deeply interpreted, because these decisions were taken on an early stage without detailed information.

It is my hope that the proceedings will prove useful for our further research with these interesting problems. No doubt a number of important results are still to be obtained. The clear tendencies towards closer cooperation between scientists with basis background in mechanics, materials, and mathematics will undoubtedly prove fruitful.

Finally I would like to thank the local organizing committee and the technical staff of the Department of Solid Mechanics, primarily Ms. Bente Brask Andersen and Mr. Robert Zetterlund for valuable help.

Lyngby, december 1992

Pauli Pedersen
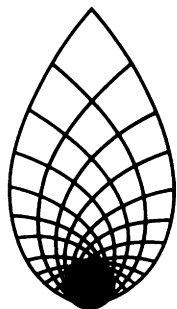
I U T A M Symposium on

OPTIMAL DESIGN
WITH ADVANCED MATERIALS

LYNGBY DENMARK

Tuesday 18th – Thursday 20th August 1992

Organized by Department of Solid Mechanics
The Technical University of Denmark

Scientific Committee:

H. Abé, Tohoku University, Japan
N.V. Banichuk, Inst. for Problems in Mechanics, USSR
H. Eschenauer, Universität Siegen, Germany
John W. Hutchinson, Harvard University, USA
B.L. Karihaloo, The University of Sydney, Australia
G. Sacchi Landriani, Politecnico di Milano, Italy
K.A. Lurie, Worchester Polytechnic Institute, USA
Z. Mroz, Polish Academy of Sciences, Poland
Niels Olhoff, Aalborg Universitetscenter, Denmark
Pauli Pedersen, Technical University of Denmark, Denmark (Chairman)
Franz G. Rammerstorfer, Techn. University of Vienna , Austria
G. Rozvany, Essen University, Germany
M.A. Save, Faculte Polytechnique de Mons, Belgium
Werner Schiehlen, University of Stuttgart, Germany
John E. Taylor, The University of Michigan, USA
A.B. Templeman, The University of Liverpool, UK

Local Organizing Committee:

Jes Christoffersen, Department of Solid Mechanics
Jarl Jensen, Department of Solid Mechanics
Arne Gudmann Nielsen, Department of Solid Mechanics
Pauli Pedersen, Department of Solid Mechanics
Preben Terndrup Pedersen, Department of Ocean Engineering
Viggo Tvergaard, Department of Solid Mechanics

Sponsors:

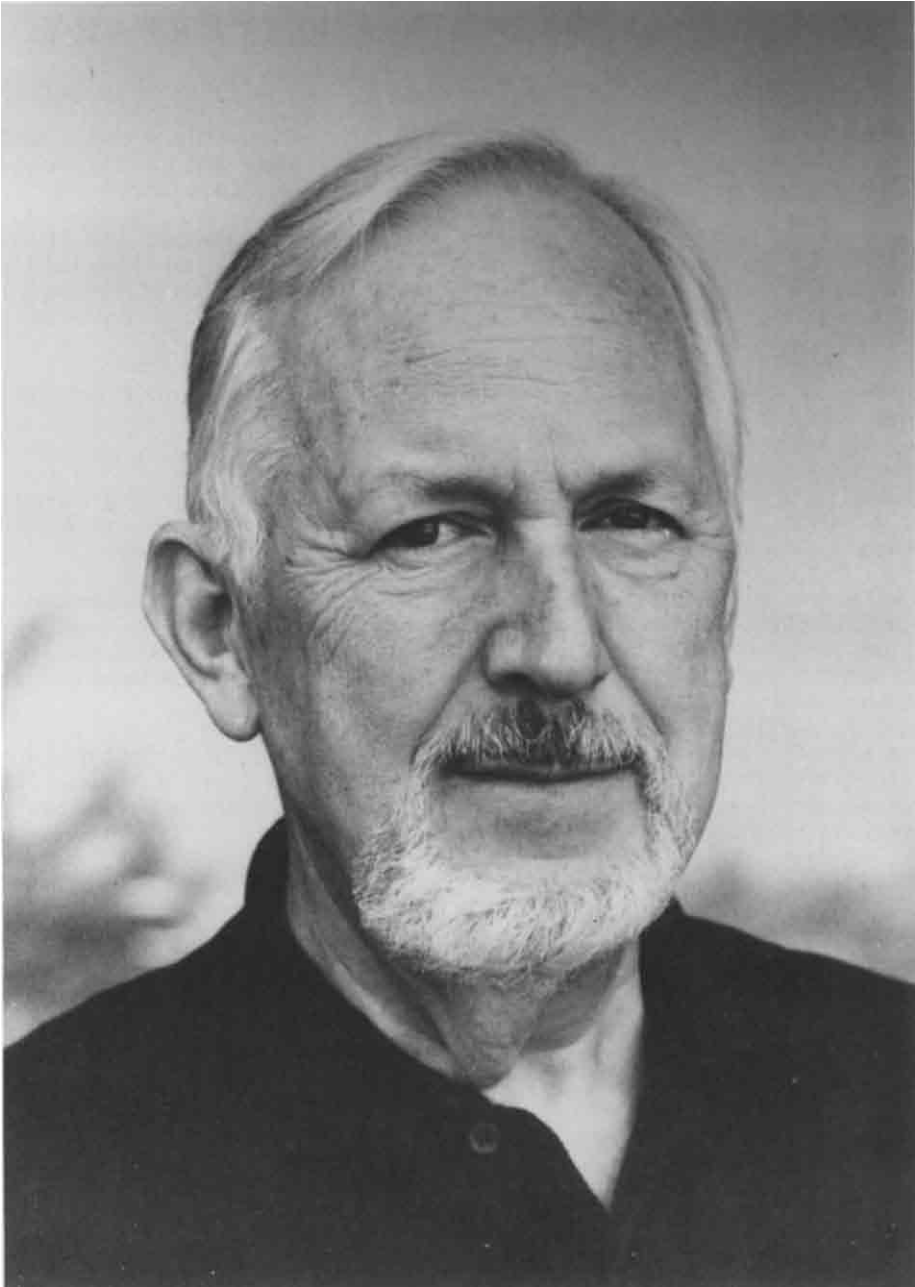|	
IUTAM	International Union of Theoretical and Applied Mechanics
DCAMM/DTH	Danish Center for Applied Mathematics and Mechanics/ Technical University of Denmark
STVF	Danish Technical Research Council (Programme on Computer Aided Design)

Otto Mønsteds Fond

GRUNDFOS

Fabrikant Mads Clausens Fond, DANFOSS

Frithiof Igor Niord Niordson

FRITHIOF NIORDSON ANNIVERSARY

Frithiof Igor Niord Niordson was born on August 1, 1922 in Johannesburg, South Africa, with a Russian mother and a Swedish father. It is likely that this international background of his has contributed to his later genuinely cosmopolitan orientation.

He received his basic engineering education and obtained his Bachelor and Masters Degrees at the Royal Institute of Technology in Stockholm in the years 1946 and 1947 respectively, a student of Folke K.G. Odqvist. As such he was one of the group of Odqvist's students that should later prove extremely successful as Professors of Technology in the Nordic Countries.

Following his Swedish education he continued his studies at Brown University, Providence where he obtained the degree of Ph.D. in Applied Mathematics in 1952 as a student of William Prager.

He began his professional career as an engineer, founding his own consulting bureau in 1952 in Sweden. Emphasis was on what should later become his main subject: analysis of strength and vibration of structures, in this case particularly gas turbines.

In 1958 he was appointed Full Professor at the Technical University of Denmark where a group of older, but foresighted, professors anticipated the need for mechanical engineers proficient in strength of materials and vibration, fields that had hitherto been given a rather low priority in the curriculum. In 1965 he founded the Department of Solid Mechanics.

To us, his early students, it was a shock − and a revelation − to be introduced to, e.g., the theory of shells given in a form modelled over the general theory of relativity. The use of the more theoretical models was emphasized, and "The mathematical toolbox" of the engineer was a central concept in the education.

Another important aspect of his activities was his endeavour to connect the people around him to the surrounding world. His first conspicuous success in this respect was his organization of the IUTAM Symposium on Thin Shells held at the Technical University of Denmark in 1967. Ever since then, extensive contact on the professional − and personal − level with foreign scientists has been created and maintained.

His cosmopolitan orientation is reflected in the many international tasks with which he has been trusted: Danish delegate in IUTAM 1960−1984. Secretary General of the Union 1968−1976, President 1976−1980, Vice President 1980−1984. Elected member of its General Assembly since 1984. Member of Advisory Group for Aeronautical Research and Development, AGARD. Foreign member of The Royal Swedish Academy of Sciences. Member of the Polish Society of Theoretical and Applied Mathematics. Centennial Year Honorary Membership of the ASME.

He also has been most active in Danish groupings concerned with the technical sciences: Member of the Danish Academy of the Technical Sciences since 1962. Originator of the Danish Center of Applied Mathematics and Mechanics and served as its secretary general since its beginning in 1969. DCAMM is a forum for cooperation between eight departments of the Technical University of Denmark and is very helpful in placing Denmark on the scientific world map. Member of the board of directors of the Northern Europe University Computing Center 1970−1984, and deservedly so, since

he was one of the first in Scandinavia to apply automatic computing in the technical sciences. Dean of the Faculty of Mechanical Engineering of the Technical University of Denmark in 1975–1991.

His scientific interest lies primarily within the theory of vibration, the theory of plates and shells, and – to a large degree combining the two – within the newer subject of structural optimization. His reputation as a scientist relies also on his fundamental work on optimization and problems related to this, e.g. inverse eigenvalue problems, and on basic results concerning thick shells and plates. In 1985 he finished the excellent monograph on "Shell Theory", a book of high reputation. He has also worked on complex problems of experimental mechanics relating to high–rate plastic deformations.

The above is a brief description of Frithiof Niordson's scientific career. Impressive as it is, it hinges on only one – be it important – facet of his personality. Few have more facets than he. Few are better company. His strong, but well founded, views on politics, be it international, domestic, or university, are appreciated by anyone who endeavours to take up the discussion. On occasions where the subject has been sailing, horseback riding, or skiing (his favorite sports) one is given the opportunity to participate in a no less heated discussion. Again, it is educational and never dull. Whenever he is cheerful and he is most of the time – he may take pleasure in entertaining himself and present company with some of his childrens toys. He might have chosen a position as a market place entertainer (e.g. the sorcerer). Instead he chose a brilliant scientific career, bringing up The Department of Solid Mechanics to an international standard. For this we, his colleagues, are grateful to him.

Publications by Frithiof Niordson

Scientific Papers

Buckling of Conical Shells Subjected to Uniform External Lateral Pressure
Transactions of the Royal Institute of Technology, Sweden, No. 10 (1947)

Vibrations of a Cylindrical Waterfilled Tube
Proc. of the 8th Int. Congress on Theoretical and Applied Mechanics, Istanbul, 1952

Transmission of Shock Waves in Thinwalled Cylindrical Tubes
Transactions of the Royal Inst. of Techn., Stockholm, No. 57 (1952)

Vibrations of a Cylindrical Tube Containing Flowing Fluid
Acta Polytechnica, Vol. 3, No. 2 (1954)
(Also published as Proceedings of the Royal Institute of Technology, No. 73)

Vibration of Turbine Blades with Loose Hinge Support
Acta Polytechnica Vol. 3, No. 3 (1954)
(Also published as Tekniska Skrifter No. 154)

Vibration of Rotating Twisted Beams
Tekniska Skrifter No. 161 (1957)

Computation of Critical Speeds with an Electronic Computer
(in Swedish)
Ingeniøren, No. 22, Nov. 1959

A Method for Solving Inverse Eigenvalue Problems
In "Recent Progress in Applied Mechanics"
The Folke Odqvist Volume (Eds. Bertram Broberg, Jan Hult, Frithiof Niordson)
Almqvist & Wiksell, Stockholm. John Wiley & Sons, New York 1959.

On the Linear Theory of Stability of Thin Elastic Shells
Bygningsstatiske Meddelelser Vol. 32, No. 1 (1961)

Strength and Design of Pipe Systems
(in Swedish)
Bygningsstatiske Meddelelser Vol. 33, No. 1 (1962)

A Unit of Testing Materials at High Strain Rates
Experimental Mechanics, January 1965.

On the Optimal Design of a Vibrating Beam
Quart. of Applied Mathematics, Vol. 23, No. 1, pp. 47-53 (1965)

The Tallest Column (with Joseph B. Keller)
J. of Math. Mechanics, Vol. 16, No. 5, pp. 443-446 (1966)

On the Inverse Eigenvalue Problem for Vibrating Plates
(in Russian)
In "Problems in Mechanics of Solid Deformable Bodies"
The Novoshilov Anniversary Volume
USSR Academy of Sciences, Leningrad 1970

A Note of the Strain Energy of Elastic Shells
Int. J. Solids Structures, Vol. 7, pp. 1573-1579 (1971)

A Review of Optimal Structural Design (with Pauli Pedersen)
Proc. 13th Int. Congr. Theor. Appl. Mech., Moscow 1972.

Designing Vibrating Membranes (with J.W. Hutchinson)
In "Continuum Mechanics and Related Problems of Analysis"
The N.I. Muskhelishvili Anniversary Volume, pp. 581-590,
USSR Academy of Sciences, Moscow 1972

Optimal Design of Vibrating Cantilevers (with B.L. Karihaloo)
J. of Optimization Theory and Applications, Vol. 11, No. 6 (1973)

Optimal Design of a Circular Shaft in Forward Precession (with B.L. Karihaloo)
In "Optimization in Structural Design", Proc. of the IUTAM Symposium, Warsaw 1973
Springer-Verlag 1975

Improvment of the Stodola Method at Close Eigenvalues (with J.J. Simmonds)
(In Russian)
In "Progress in the Mechanics of Deformable Bodies"
The Galerkin 100 year Anniversary Volume
USSR Academy of Sciences, Moscow 1975

Symbolic and Algebraic Manipulation Languages and their Application in Mechanics
(with Jarl Jensen)
Structural Mechanics Software Series (Ed. W. Pilkey).
University of Virginia 1976

A Consistent Refined Shell Theory
In "Complex Analysis and its Applications"
The Ilya Nestorovich Vekua Anniversary Volume
USSR Academy of Sciences, Moscow 1978

Some Problems Concerning Singularities of Optimal Beams and Columns (with N. Olhoff)
Main Lecture, GAMM-Tagung 1979, ZAMM Vol. 59, pp. 16-26

An Asymptotic Theory for Vibrating Plates
Int. J. Solids Structures Vol. 15, pp. 167-181.

Variational Methods in Optimization of Structures
In "Trends in Solid Mechanics" (Eds. J.F. Besseling and A. van der Heijden).
Proc. Symp. dedicated to the 65 birthday of W.T. Koiter.
Delft University Press, 1980.

Optimal Design of Elastic Plates with a Constaint on the Slope of the Thickness Function
Int. J. Solids Structures Vol. 19, No. 2, pp. 141-151 (1983)

Some New Results Regarding Optimal Design of Elastic Plates
In "Optimization Methods in Structural Design" (Eds. H. Eschenauer and N. Olhoff).
Proc. Euromech Colloquium No. 164, Univ. of Siegen, FR Germany 1982, pp. 380-386.

Free Vibrations of Thin Elastic Spherical Shells
Int. J. Solids Structures Vol. 20, No. 7, pp 667-687 (1984)

The Spectrum of Free Vibrations of a Thin Elastic Spherical Shell
Int. J. Solids Structures Vol. 24, No. 9, pp. 947-961 (1988)

Scientific Books

Introduction to the Theory of Elasticity
(in Swedish)
Polyteknisk Forenigs Forlag 1962.
Also published by Akademisk Forlag, Copenhagen 1963

Recent Progress in Applied Mechanics
The Folke Odqvist Volume
Almqvist & Wiksell, Stockholm 1967
(Editor with B. Broberg and J. Hult)

Theory of Thin Shells
Proceedings of the IUTAM Symposium, Copenhagen 1967
Springer-Verlag 1969
(Editor)

Dynamics of Rotors
Proceedings of the IUTAM Symposium, Lyngby 1974
Springer-Verlag 1975
(Editor)

Theoretical and Applied Mechanics
Proceedings of the XVth Int. Congr. of Theor. Appl. Mech., Lyngby 1984
Elsevier Science Publishers B.V. 1985
(Editor with N. Olhoff)

Shell Theory
North-Holland Series in Applied Mathematics and Mechanics
Elsevier Science Publishers B.V. 1985

Topology design using a material with self-optimizing microstructure

C. S. Jog and R.B. Haber[a]
M.P. Bendsøe[b]

[a]Department of Theoretical and Applied Mechanics
University of Illinois at Urbana-Champaign
Urbana, Illinois
U.S.A

[b]Matematisk Institut
Danmarks Tekniske Højskole
Lyngby
Denmark

1. INTRODUCTION

The earliest literature on topology optimization involves layout problems. For example, Prager, Rozvany and others have studied layout optimization of truss structures, a problem which results in optimal designs with many thin, 'truss-like' members [1], [2]. The first attempts to optimize continua over variable topologies were based on macroscopic partitions of the candidate structure domain into solid and void regions [3]. However, it was found that this formulation of the topology optimization problem is not well-posed [4]. Kohn and Strang obtained a well-posed, relaxed formulation by quasiconvexification and, alternatively, by homogenization of a microstructural model [4]. The relaxed problem can be approximated using a finite element grid on a fixed domain [5]. Bendsoe and Kikuchi explored this approach using a microstructure that approximates the optimal configuration [6].

In this study we are concerned with topology optimization procedures based on the exact optimal microstructure. In the following sections, we develop displacement based formulations of the relaxed topology optimization problem and carry out analytical optimization of the distributed microstructural design parameters. We obtain a reduced problem in the form of a two-field, inf-sup problem that generates a mixed finite element method.

2. STATEMENT OF THE TOPOLOGY OPTIMIZATION PROBLEM

We consider the problem of finding the stiffest structure that can be obtained by distributing a given volume of material $\bar{V}$ within a domain $\Omega \subset R^2$. We assume a homogeneous, linear

elastic, isotropic material, small deformations, plane stress conditions, a single static loading case and that all interior boundaries are traction free.

We present the strong forms of the governing equations and the boundary conditions and the corresponding variational problems. The section closes with the formulation of the topology optimization problem.

2.1. STRONG FORM OF THE BOUNDARY VALUE PROBLEM

Let Ω be an open domain with boundary Γ. The boundary is composed of two open, disjoint regions, $\Gamma = \overline{\Gamma_u \cup \Gamma_t}$. The following governing equations and boundary conditions apply.

$$\nabla \cdot \tau + b = 0 \quad \text{in} \quad \Omega \tag{1}$$

$$\varepsilon(u) = \frac{1}{2}(\nabla u + (\nabla u)^T) \quad \text{in} \quad \Omega \tag{2}$$

$$\tau = C{:}\varepsilon \quad \text{in} \quad \Omega \tag{3}$$

$$t(\tau, n) = \tau \cdot n \quad \text{on} \quad \Gamma \tag{4}$$

$$u = \bar{u} \quad \text{on} \quad \Gamma_u \tag{5}$$

$$t = \bar{t} \quad \text{on} \quad \Gamma_t \tag{6}$$

τ is the stress tensor, u is the displacement vector, ε is the strain tensor, b is the body force vector, t is the traction vector, n is the unit normal vector to the surface Γ, $\bar{u}$ is a vector of prescribed displacements, $\bar{t}$ is a vector of prescribed tractions and C is the material stiffness tensor.

2.2. VARIATIONAL FORM OF THE GOVERNING EQUATIONS

We replace the strong form of the problem using the principle of minimum potential energy.

Find the displacement field u that solves $\min_{v \in V_u} \Pi(v)$ such that equations (2)-(4) are satisfied, where

$$\Pi(v) = \int_\Omega W(\varepsilon(v)) \, d\Omega - \int_{\Gamma_t} (\bar{t} \cdot v) \, d\Gamma - \int_\Omega (b \cdot v) \, d\Omega \tag{7}$$

and $V_u = \{v \in H^1(\Omega) \ : \ v = \bar{u} \ \text{on} \ \Gamma_u\}$.

W is the strain energy density function which, for a linear elastic material, is given by,

$$W(\varepsilon) = \frac{1}{2}\varepsilon^T C \varepsilon \tag{8}$$

If we base the formulation on the principle of minimum complementary energy we obtain,

Find τ which solves $\underset{\sigma \in V_\tau}{min} \Pi_c(\sigma)$ such that equations (3) and (4) are satisfied, where

$$\Pi_c(\sigma) = \int_\Omega W_c(\sigma)\,d\Omega - \int_{\Gamma_u} (t \cdot \bar{u})\,d\Gamma \tag{9}$$

and $V_\tau = \{ \sigma \in L_2(\Omega) : (\nabla \cdot \sigma) + b = 0 \text{ in } \Omega , t(\sigma, n) = \bar{t} \text{ on } \Gamma_t \}$.

W_c is the complementary energy density for a linear elastic material given by,

$$W_c(\tau) = \frac{1}{2}\tau^T D \tau \quad ; \qquad D = C^{-1} \tag{10}$$

2.3. STATEMENT OF THE TOPOLOGY OPTIMIZATION PROBLEM

We are interested in finding a configuration of solid and void regions within the domain Ω that maximizes the stiffness of the resulting structure, such that the total volume of material equals a specified value $\bar{V}$. No restriction is placed on the topology of the configuration of the solid part of Ω. One way to formulate this problem is to introduce the indicator function $X(x)$ given by,

$$X(x) = \begin{cases} 1 & \text{if } x \in \Omega_1 \\ 0 & \text{if } x \in \Omega_2 \end{cases} \tag{11}$$

where Ω_1 and Ω_2 are the solid and void regions in Ω, respectively. The volume of the structure is given by $\int_\Omega X(x)\,d\Omega$ and the elasticity tensor at each point is $C = X(x)\,C_{solid}$ where C_{solid} is the elasticity tensor of the solid material.

The following *compliance functional* measures the flexibility of the structure.

$$J = \int_{\Gamma_t} (\bar{t} \cdot u)\,d\Gamma - \int_{\Gamma_u} (t \cdot \bar{u})\,d\Gamma + \int_\Omega (b \cdot u)\,d\Omega \tag{12}$$

Maximizing the stiffness of a structure corresponds to minimizing the compliance J. For a linear elastic material, Clapeyron's work theorem [7] gives the following relations.

$$\Pi = -\frac{J}{2} \tag{13}$$

$$\Pi_c = \frac{J}{2} \tag{14}$$

Therefore, maximizing the stiffness is equivalent to minimizing the complementary energy or maximizing the potential energy. Alternative forms of the maximum stiffness problem are stated as:

- Displacement formulation:

$$\sup_{X(x) \in V_x} \quad \inf_{u \in V_u} \quad \int_\Omega W(\varepsilon)\,d\Omega - \int_{\Gamma_t} (\bar{t} \cdot u)\,d\Gamma - \int_\Omega (b \cdot u)\,d\Omega \tag{15}$$

subject to equations (2)-(4) and $C = X(x)\, C_{solid}$

- Stress formulation

$$\inf_{X(x) \in V_x} \quad \inf_{\tau \in V_\tau} \quad \int_\Omega W_c(\tau)\,d\Omega - \int_{\Gamma_u} (t \cdot \bar{u})\,d\Gamma \tag{16}$$

subject to equations (3), (4) and $D = X(x)\, D_{solid}$.

The set of admissable designs for the above problems is defined as,

$$V_x = \{ Y : Y(x) = 0 \text{ or } 1 \quad \forall x \in \Omega, \int_\Omega Y(x)\,d\Omega = \bar{V} \}.$$

Several researchers have studied this problem. Early approaches considered only macroscopic patterns of solid and void [3]. However, the macroscopic problem is not well-posed [4]. As a result, attempts to optimize finite element models based on the macroscopic approach fail to converge to a macroscopic pattern of solid and void regions in the limit of mesh refinement. Kohn and Strang showed that a tractable, relaxed form of the problem can be obtained either by quasiconvexification of the macroscopic optimization problem or, equivalently, by introducing microstructure to the design space [4]. The process of relaxation leads to a well-posed problem and tends to eliminate artificial local minima that arise in the macroscopic optimization problem [5]. The introduction of microstructure transforms the optimization task from the determination of the indicator function $X(x)$ to the determination of distributions of microstructural parameters, as explained below.

3. OPTIMUM MATERIAL DISTRIBUTION AND EFFECTIVE MATERIAL PROPERTIES

Studies of the bounds on the effective properties of composite mixtures of two materials show that for plane elasticity, the stiffest composite material for a fixed ratio of the two constituent materials can be obtained by a rank-2 layering, as shown in Fig. 1 ([8], [9], [10]). The rank-2 composite is constructed as follows. First, a rank-1 composite is constructed of alternating layers of the stiffer and the more flexible materials. The averaged densities of the stiff and flexible layers are designated γ and $1 - \gamma$, respectively. The rank-2 composite is then constructed of alternating layers of the stiff material and the rank-1 composite with average densities δ and $1 - \delta$, respectively. The characteristic length scales of the rank-1 and rank-2 layerings must be of different orders of magnitude. Furthermore, the rank-1 layering direction is perpendicular to the rank-2 direction. The bulk density of the stiff material is [11],
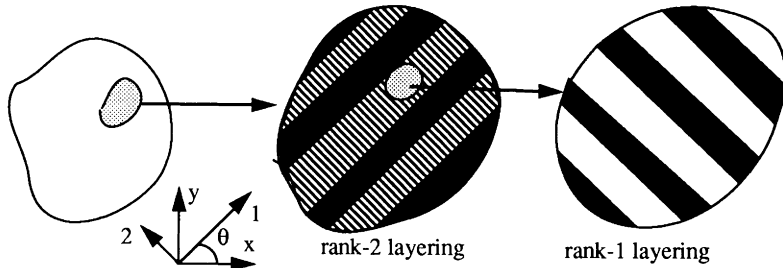
$$\rho = \delta + \gamma - \gamma\delta \tag{17}$$

Fig. 1 Construction of a rank-2 composite

In the context of shape optimization of a homogeneous material with voids, we assign void properties ($X = 0$) to the flexible material in the rank-2 composite. Then ρ in equation (17) gives the bulk density of the rank-2 material and the volume constraint is expressed as,

$$\int_\Omega \rho d\Omega = \bar{V} \tag{18}$$

The effective material properties of the rank-2 composite can be derived using the formulas of homogenization [11]. Assuming that the primary layering of density δ is aligned along the direction 1 (as shown in Fig. 1), the effective properties are:

$$C_{1111} = \frac{\gamma E}{\delta\gamma(1-\nu^2)+(1-\delta)} \qquad C_{2222} = \delta E + \delta^2\nu^2 C_{1111}$$

$$C_{1122} = \frac{\nu\delta\gamma E}{\delta\gamma(1-\nu^2)+(1-\delta)} \qquad C_{1212} = 0 \tag{19}$$

where E is the Young's modulus and ν is the Poisson's ratio of the solid isotropic material. The tensor components in (19) correspond to the effective properties of the homogenized material in a material coordinate system that is inclined at an angle θ to the global reference frame (Fig. 1). The effective properties in the global reference frame can be found using the standard coordinate transformation formulas for the elasticity tensor.

The process of relaxation expands the macroscopic design space and the outer subproblems in (15) and (16) are transformed accordingly. Now we seek the supremum of the potential energy (or the infimum of the complementary potential energy) over $\theta(x)$, $\delta(x)$ and $\gamma(x)$ instead of $X(x)$. The analytical optimization of these functions is discussed in the following section.

4.   ANALYTICAL OPTIMIZATION OF THE MICROSCOPIC DESIGN FUNCTIONS

We now express the volume constraint in the displacement formulation (equation (15)) using a Lagrange multiplier technique.

- Displacement problem DP0:

$$\begin{array}{cc} \underset{\theta, \delta, \gamma}{sup} & \underset{u \in V_u}{inf} & L_u(\theta, \delta, \gamma, u, \lambda) \end{array} \tag{20a}$$

subject to $0 \le \delta \le 1$, $0 \le \gamma \le 1$, $\dfrac{\partial L_u}{\partial \lambda} = 0$ and equations (2)-(4); where

$$L_u(\theta, \delta, \gamma, u, \lambda) = \int_\Omega W(\varepsilon) \, d\Omega - \int_{\Gamma_t} (\bar{t} \cdot u) \, d\Gamma - \int_\Omega (b \cdot u) \, d\Omega - \lambda \left(\int_\Omega \rho \, d\Omega - \bar{V} \right) \tag{20b}$$

In the case of the sup-inf problem given by equation (20a), it is not obvious that the 'sup' and 'inf' operators can be interchanged. However, it has recently been demonstrated that finding the supremum of L_u with respect to θ and the ratio of δ to γ under fixed ρ can be carried out before taking the infimum of L_u over the kinematically admissible displacement fields without changing the results [12]. In the following, we interchange the sup and inf operators to arrive at subproblems that can be solved analytically. Diagrams of the optimization problems that are obtained by successive interchanges of the sup and inf operators in problem DP0, each followed by analytical optimization of one of the microstructure design variables, are shown in Fig. 2. Each analytical solution of a subproblem leads to a reduced optimization problem with fewer unknowns. Apparently, it is not possible to interchange the order of maximization over ρ and minimization over u in the second reduced problem DP2. Therefore, we cannot obtain a third reduced optimization problem in terms of the displacements only. The following sections present the detailed development of the reduced optimization problems for the displacement formulation.

4.1. FIRST REDUCED PROBLEM: ANALYTICAL OPTIMIZATION OF THE DIRECTION OF ORTHOTROPY (θ)

Equation (20a) in problem DP0 is equivalent to [12],

$$\begin{array}{cccc} \underset{\delta, \gamma}{sup} & \underset{u}{inf} & \underset{\theta}{sup} & L_u(\theta, \delta, \gamma, u, \lambda) \end{array} \tag{21}$$

The angle of orthotropy, θ, is the angle between the material axes (1-2) and the coordinate axes of the global reference frame, while the principal angle ψ is the angle between the direction of the first principal strain (ε_I) and the coordinate axes. Pedersen ([13], [14]) has shown that the stiffest microstructure is obtained by aligning the material axes with the principal strain axes (for maximizing the potential energy) or the principal stress axes (for minimizing the complementary potential energy). That is, if we assume that $C_{1111} > C_{2222}$ and choose ε_I and ε_{II} such that $|\varepsilon_I| > |\varepsilon_{II}|$ the stiffest structure is obtained for $\theta = \psi$. This result is valid for composites having low shear stiffness, that is materials which satisfy $C_{1111} + C_{2222} - 2C_{1122} - 4C_{1212} > 0$, which is the case for our rank-2 composite. Also, it is easy to see that the axes of principal stress, the axes of principal strain and the axes of orthot-
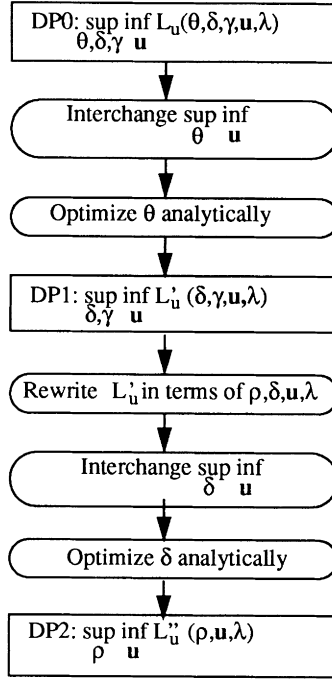
Fig. 2 Generation of reduced optimization problems
in the displacement formulation

ropy are aligned in the stiffest microstructure. Next, we use this result to eliminate θ as a design variable.

Noting the alignment of the principal axes and the optimal axes of orthotropy and combining equations (3) and (8), we find that the strain energy density of a material with an optimal material angle θ is given by,

$$W'(\varepsilon) = \frac{1}{2} (C_{1111}\varepsilon_I^2 + C_{2222}\varepsilon_{II}^2 + 2C_{1122}\varepsilon_I\varepsilon_{II}) \tag{22}$$

where C_{1111}, C_{2222}, and C_{1122} are functions of the layer densities δ and γ (equation (19)). The principal strains, ε_I and ε_{II}, can be expressed in terms of the Cartesian strain components to get the following expressions for the strain energy density.

$$(\varepsilon_{xx} + \varepsilon_{yy}) \geq 0 \; : \; W'(\varepsilon) = \frac{(2\alpha_1 (\varepsilon_{xx}^2 + \varepsilon_{yy}^2) + 8C_{1122}\varepsilon_{xx}\varepsilon_{yy} + \beta_1\gamma_{xy}^2 + 2\alpha_2\kappa (\varepsilon_{xx} + \varepsilon_{yy}))}{8}$$

$$(\varepsilon_{xx} + \varepsilon_{yy}) \leq 0 \; : \; W'(\varepsilon) = \frac{(2\alpha_1 (\varepsilon_{xx}^2 + \varepsilon_{yy}^2) + 8C_{1122}\varepsilon_{xx}\varepsilon_{yy} + \beta_1\gamma_{xy}^2 - 2\alpha_2\kappa (\varepsilon_{xx} + \varepsilon_{yy}))}{8}$$

$$\tag{23}$$

where $\alpha_1 = C_{1111} + C_{2222}$, $\alpha_2 = C_{1111} - C_{2222}$, $\beta_1 = C_{1111} + C_{2222} - 2C_{1122}$ and

$\kappa = \sqrt{(\varepsilon_{xx} - \varepsilon_{yy})^2 + \gamma_{xy}^2}$. Note that $\alpha_2 \geq 0$ due to the convention that $C_{1111} \geq C_{2222}$.

The strain energy density function described by equation (23) is that of a fictitious "adaptive" rank-2 material whose material axes rotate so as to always remain coincident with the instantaneous principal strain axes. Even though our rank-2 composite is constructed from a linear elastic material, the response of the rotating adaptive material is nonlinear elastic, as can be seen in equation (23). An effective tangent material stiffness matrix for the adaptive material can be derived based on the energy density function in equation (23). The tangent stiffness matrices for the two cases, $\varepsilon_{xx} + \varepsilon_{yy} < 0$ and $\varepsilon_{xx} + \varepsilon_{yy} > 0$ are distinct and positive definite. However, the tangent stiffness matrix and the stresses are discontinuous for $\varepsilon_{xx} + \varepsilon_{yy} = 0$ ($\varepsilon_I = -\varepsilon_{II}$) and some of the terms in the tangent stiffness matrix are unbounded for $\kappa = 0$ ($\varepsilon_I = \varepsilon_{II}$). These problems are eliminated if δ and γ are continuously optimized as in section 4.2.

After carrying out the maximization over θ in equation (21), we get the following displacement formulation.

• Displacement problem DP1:

$$\sup_{\delta, \gamma} \quad \inf_{u \in V_u} \quad L_u'(\delta, \gamma, u, \lambda) \tag{24a}$$

subject to $0 \leq \delta \leq 1$, $0 \leq \gamma \leq 1$, $\dfrac{\partial L_u'}{\partial \lambda} = 0$ and equations (2)-(4); where

$$L_u'(\delta, \gamma, u, \lambda) = \int_\Omega W'(\varepsilon)\, d\Omega - \int_{\Gamma_t} (\boldsymbol{i} \cdot \boldsymbol{u})\, d\Gamma - \int_\Omega (\boldsymbol{b} \cdot \boldsymbol{u})\, d\Omega - \lambda \left(\int_\Omega \rho\, d\Omega - \overline{V} \right) \tag{24b}$$

4.2. SECOND REDUCED PROBLEM: ANALYTICAL OPTIMIZATION OF THE LAYER DENSITY δ

We can interchange the order of the maximization over δ and minimization over $\boldsymbol{u}$ in equation (24a) without changing the results [12]. Problem DP1 is restated as,

$$\sup_{\rho} \quad \inf_{u \in V_u} \quad \sup_{\delta} \quad L_u'(\delta, \rho, u, \lambda) \tag{25a}$$

subject to $0 \leq \delta \leq \rho \leq 1$, $\dfrac{\partial L_u'}{\partial \lambda} = 0$ and equations (2)-(4); where

$$L_u'(\delta, \rho, u, \lambda) = \int_\Omega \tilde{W}'(\varepsilon)\, d\Omega - \int_{\Gamma_t} (\boldsymbol{i} \cdot \boldsymbol{u})\, d\Gamma - \int_\Omega (\boldsymbol{b} \cdot \boldsymbol{u})\, d\Omega - \lambda \left(\int_\Omega \rho\, d\Omega - \overline{V} \right) \tag{25b}$$

$\tilde{W}'(\varepsilon)$ is the same as $W'(\varepsilon)$ in equation (22), except that the elastic moduli are expressed as functions of δ and ρ (using equation (17)), rather than δ and γ.

For the displacement formulation, the Kuhn-Tucker optimality condition for the design variable δ leads to,

$$\frac{\partial}{\partial \delta} \tilde{W}'(\varepsilon) = 0 \tag{26}$$

if neither the upper nor the lower-bound constraints on δ are active.

Solving equation (26) gives two roots for the optimal layer density δ. We derived expressions for the two roots using lengthy hand-calculations and confirmed them using a symbolic computation package. The corresponding optimal layer densities γ can be derived from equation (17) as a function of ρ and the principal strains. The expressions for the optimal layer densities according to equation (26) are given by equation (27). In the following, we use the term 'mode' to describe which expression for the optimal value of δ governs. For example, mode-I and mode-II materials are rank-2 composites where δ assumes the values of the alternative roots of equation (26). Mode-III and mode-IV materials represent rank-2 composites where the lower-bound and upper-bound constraints on δ, respectively, are active.

$$\text{mode-I: } \delta = \frac{\varepsilon_I (1 + \nu\rho - \rho) + \varepsilon_{II}}{\nu\varepsilon_I + (2 - \rho - \nu + \nu\rho)\varepsilon_{II}} \qquad \text{mode-II: } \delta = \frac{\varepsilon_I (\nu\rho + \rho - 1) + \varepsilon_{II}}{\nu\varepsilon_I + (2 - \rho + \nu - \rho\nu)\varepsilon_{II}}$$

$$\gamma = \frac{\varepsilon_I + \varepsilon_{II}(1 + \nu\rho - \rho)}{(1 - \nu)(\varepsilon_I - \varepsilon_{II})} \qquad\qquad \gamma = \frac{\varepsilon_I + \varepsilon_{II}(\nu\rho + \rho - 1)}{(1 + \nu)(\varepsilon_I + \varepsilon_{II})} \tag{27}$$

$$\text{mode-III: } \delta = 0 \qquad\qquad\qquad \text{mode-IV: } \delta = 1$$

$$\gamma = \rho \qquad\qquad\qquad\qquad \rho = 1$$

Substitution of the above expressions for the layer densities in equation (19) verifies our starting assumption that $C_{1111} \geq C_{2222}$ for mode-I, mode-II, mode-III and mode-IV materials. In the special cases of $\varepsilon_I = -\varepsilon_{II}$ and $\varepsilon_I = \varepsilon_{II}$, it can be verified that $C_{1111} = C_{2222}$. Thus the problems which arise in the first reduced problem do not occur here.

The ranges of validity for mode-I, mode-II, mode-III and mode-IV materials as functions of ρ and the principal strain ratio, k, are given next. By convention, we choose ε_I and ε_{II} such that $|\varepsilon_I| \geq |\varepsilon_{II}|$ and define the principal strain ratio as, $k = \varepsilon_{II}/\varepsilon_I$. Since $|\varepsilon_I| \geq |\varepsilon_{II}|$, we have $-1 \leq k \leq 1$. The criterion that $0 < \delta < 1$ in the mode-I and mode-II regions in equation (27) gives

$$\text{mode-I: } \frac{1 + k}{1 - \nu} < \rho < 1 \qquad \text{mode-II: } \frac{1 - k}{1 + \nu} < \rho < 1 \tag{28}$$

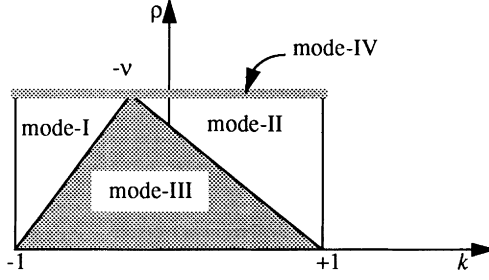We obtain the following ranges for the four modes using equation (28) (see Fig. 3).

Fig. 3. Ranges of validity of the various modes

mode-I: $\dfrac{1+k}{1-v} < \rho < 1$ mode-II: $\dfrac{1-k}{1+v} < \rho < 1$

mode-III: $0 \le \rho \le \dfrac{1+k}{1-v}$ and $0 \le \rho \le \dfrac{1-k}{1+v}$ mode-IV: $\rho = 1$

$$(29)$$

The lower shaded zone in Fig. 3 represents the mode-III region where the constraint $\delta \ge 0$ is active and we have a rank-1 material. Accordingly, the material can only sustain a uniaxial stress state in mode-III.

Combining the expressions for the optimal layer densities (equation (27)), the effective material properties (equation (19)) and the strain energy density (equation (22)), we get the following expressions for the strain energy density of the optimized rank-2 material.

mode-I: $W''(\rho, \boldsymbol{u}) = \dfrac{E\,(\varepsilon_I^2 + 2\varepsilon_I \varepsilon_{II}\,(1 - \rho + v\rho) + \varepsilon_{II}^2)}{2\,(1-v)\,(2 - \rho + v\rho)}$

mode-II: $W''(\rho, \boldsymbol{u}) = \dfrac{E\,(\varepsilon_I^2 - 2\varepsilon_I \varepsilon_{II}\,(1 - \rho - v\rho) + \varepsilon_{II}^2)}{2\,(1+v)\,(2 - \rho - v\rho)}$

mode-III: $W''(\rho, \boldsymbol{u}) = \dfrac{1}{2}\rho E \varepsilon_I^2$ mode-IV: $W''(1, \boldsymbol{u}) = \dfrac{E\,(\varepsilon_I^2 + 2v\varepsilon_I \varepsilon_{II} + \varepsilon_{II}^2)}{2\,(1 - v^2)}$

$$(30)$$

The expression for W'' for a mode-IV material coincides with $W''(1, \boldsymbol{u})$ for the mode-I and mode-II materials. Hence, from here on we treat the mode-IV material as a special case of the mode-I and mode-II materials with $\rho = 1$. The expressions in equation (30) can be written directly in terms of the Cartesian strain components as

mode-I: $W''(\rho, \boldsymbol{u}) = \dfrac{E\,(\varepsilon_{xx}^2 + \varepsilon_{yy}^2 + \gamma_{xy}^2/2 + 2\,(1 - \rho + v\rho)\,(\varepsilon_{xx}\varepsilon_{yy} - \gamma_{xy}^2/4))}{2\,(1-v)\,(2 - \rho + v\rho)}$

mode-II: $W''(\rho, \boldsymbol{u}) = \dfrac{E\,(\varepsilon_{xx}^2 + \varepsilon_{yy}^2 + \gamma_{xy}^2/2 - 2\,(1 - \rho - v\rho)\,(\varepsilon_{xx}\varepsilon_{yy} - \gamma_{xy}^2/4))}{2\,(1+v)\,(2 - \rho - v\rho)}$

$$(31)$$

$W''(\rho, \boldsymbol{u})$ for a mode-III material is given by equation (23) with $\alpha_1 = \alpha_2 = \beta_1 = \rho E$ and $C_{1122} = 0$ (since $\delta = 0$).

Equation (31) corresponds to the strain energy density function of a fictitious hyperelastic material, composed of an adaptive rank-2 composite with fixed bulk density ρ, whose material axes rotate so as to remain aligned with the instantaneous principal strain axes and in which the layer densities are continuously adjusted (according to equation (27)) to remain optimal under the current strain state. Surprisingly, the resulting stress-strain relations ($\tau_{ij} = \dfrac{\partial W''}{\partial \varepsilon_{ij}}$), for both the mode-I and the mode-II materials, are linear.

$$
\text{mode-I: } \tau_{xx} = \frac{E(\varepsilon_{xx} + (1 - \rho + \nu\rho)\varepsilon_{yy})}{(1 - \nu)(2 - \rho + \nu\rho)} \qquad \text{mode-II: } \tau_{xx} = \frac{E(\varepsilon_{xx} - (1 - \rho - \nu\rho)\varepsilon_{yy})}{(1 + \nu)(2 - \rho - \nu\rho)}
$$

$$
\tau_{yy} = \frac{E(\varepsilon_{yy} + (1 - \rho + \nu\rho)\varepsilon_{xx})}{(1 - \nu)(2 - \rho + \nu\rho)} \qquad \tau_{yy} = \frac{E(\varepsilon_{yy} - (1 - \rho - \nu\rho)\varepsilon_{xx})}{(1 + \nu)(2 - \rho - \nu\rho)}
$$

$$
\tau_{xy} = \frac{E\rho(1 - \nu)\gamma_{xy}}{2(1 - \nu)(2 - \rho + \nu\rho)} \qquad \tau_{xy} = \frac{E\gamma_{xy}}{2(1 + \nu)}
$$

$$\tag{32}$$

The layering of the rank-1 material corresponding to mode-III is colinear with the numerically larger (ε_I) principal strain direction. This also generates a constitutive model equivalent to that of an adaptive hyperelastic material. However, in this case the effective stress-strain relation is nonlinear and the tangent stiffness matrix is singular. Nonetheless, one can derive a positive-definite secant material stiffness matrix for the mode-III region which is continuous at the mode-I/mode-III and mode-II/mode-III boundaries (see Fig. 3) and which generates stresses that are consistent with the rank-1 microstructure.

Equation (32) is rearranged to obtain the mode-I and mode-II material stiffness matrices. mode-I material:

$$
\boldsymbol{C} = \boldsymbol{C}''(\rho, E, \nu) = \tilde{E}\begin{bmatrix} 1 & 1 - \rho + \nu\rho & 0 \\ 1 - \rho + \nu\rho & 1 & 0 \\ 0 & 0 & \dfrac{(1 - \nu)\rho}{2} \end{bmatrix} \tag{33}
$$

$$
\tilde{E} = \frac{E}{(1 - \nu)(2 - \rho + \nu\rho)}
$$

mode-II material:

$$C = C''(\rho, E, \nu) = \tilde{E} \begin{bmatrix} 1 & -(1-\rho-\nu\rho) & 0 \\ -(1-\rho-\nu\rho) & 1 & 0 \\ 0 & 0 & \dfrac{(2-\rho-\nu\rho)}{2} \end{bmatrix} \tag{34}$$

$$\tilde{E} = \frac{E}{(1+\nu)(2-\rho-\nu\rho)}$$

For $\rho = 1$, both the mode-I and the mode-II material stiffness matrices coincide with the stiffness matrix of a solid isotropic material without microstructure.

$$C''(1, E, \nu) = C_{solid}(E, \nu) \tag{35}$$

After carrying out the optimization over the layer density δ in equation (25a), the second reduced form of the displacement problem is obtained.

- Displacement problem DP2:

$$\underset{\rho}{sup} \quad \underset{u \in V_u}{inf} \quad L_u''(\rho, u, \lambda) \tag{36a}$$

subject to equation (28), $\dfrac{\partial L_u''}{\partial \lambda} = 0$ and equations (2)-(4); where

$$L_u''(\rho, u, \lambda) = \int_{\Omega} W''(\rho, u)\, d\Omega - \int_{\Gamma_t} (\bar{t} \cdot u)\, d\Gamma - \int_{\Omega} (b \cdot u)\, d\Omega - \lambda \left(\int_{\Omega} \rho\, d\Omega - \bar{V} \right) \tag{36b}$$

In our experience, it is not permissible to interchange the order of the inf and sup operators on u and ρ. Hence, we cannot find a third reduced displacement problem.

5. PROBLEM DP2 AS A MIXED VARIATIONAL STATEMENT

The second reduced displacement problem DP2 is an inf-sup problem, corresponding to a two-field, mixed variational formulation. The stationary condition of $L_u''(\rho, u, \lambda)$ with respect to u yields the usual weak form of the equilibrium equation, and the stationary condition with respect to the bulk density ρ yields a weak form of the optimality criterion,

$$\frac{\partial}{\partial \rho} W''(\rho, u) - \lambda = 0 \tag{37}$$

which is valid provided that the constraint $0 \le \rho \le 1$ is not active. These two equations (supplemented by the constraint equations) determine the two fields, u and ρ. As with any mixed variational problem, care must be taken in choosing the function spaces for u and ρ. Finite element formulations based on the problem DP2 must satisfy the Babuska-Brezzi stability conditions [15]. We discuss this matter in greater detail in sections 6 and 8.

6. FINITE ELEMENT MODEL

Among the three displacement-based problems, DP2 involves the least number of design variables and guarantees an analytically optimal microstructure. We construct a mixed finite element method for DP2 in which the density and the displacement fields are parameterized as,

$$u = N_u \hat{u}$$
$$\rho = N_\rho \hat{\rho} \tag{38}$$

N_u and N_ρ are matrices containing the displacement and density basis functions and $\hat{u}$ and $\hat{\rho}$ are unknown parameter vectors. The choice of the basis functions for the displacement and density fields is critical to achieving a stable solution. When the domain is discretized using quadrilateral elements with an 8-node displacement model and a bilinear density field (possibly discontinuous across element boundaries), the solution is unstable in regions where the upper and lower bound constraints on the density are not active. Similarly, a discretization using a 4-node displacement model and a constant density distribution within each element and a discretization using a 9-node displacement model and a discontinuous bilinear density field generate unstable solutions. However, a mesh using an 8-node displacement model with a piecewise constant density distribution gives a stable solution. We attribute the problems of the unsuccessful models to Babuska-Brezzi type instabilities.

7. SOLUTION METHOD

We employ an iterative procedure to solve the mixed variational problem. We alternately solve the equilibrium problem for the displacement field, subject to a fixed distribution of bulk density, and optimize the bulk density distribution, subject to a fixed displacement field. An analytically optimal microstructure (for the current bulk density and displacement estimates) is maintained at all times. Although the stiffness analysis is nonlinear due to the rank-1 (mode-III) material, we carry out only one equilibrium iteration before updating the design. This serves to spread the cost of the nonlinear equilibrium iterations over a number of design cycles.

The redesign step is an iterative procedure. We seek a density distribution that satisfies equation (37) in a weak sense in the perforated region Ω_p where the bounds on ρ are inactive.

$$\int_{\Omega_p} N_\rho^T \left(\frac{\partial}{\partial \rho} W'' (\rho, u) - \lambda \right) d\Omega = 0 \tag{39}$$

This leads to the following heuristic update formula for the density parameters.

$$\hat{\rho}^{k+1} = min \left\{ \left(\frac{\int_{\Omega_p} \frac{\partial}{\partial \rho} W'' (\rho, u) N_\rho d\Omega}{\lambda \int_{\Omega_p} N_\rho d\Omega} \right) \hat{\rho}^k, 1.0 \right\} \tag{40}$$
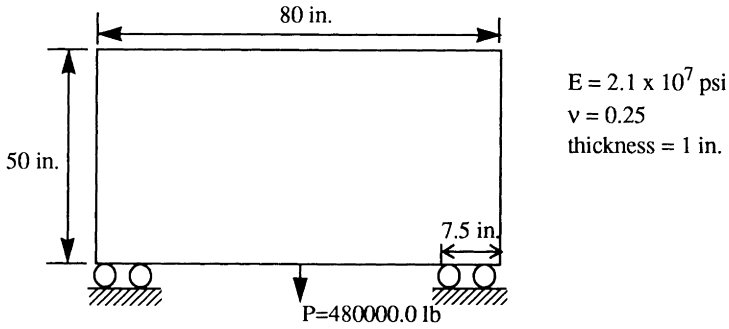
Fig.4 Deep beam loaded along its bottom edge

We next calculate the current volume of the structure ($\int_\Omega \rho d\Omega$). Since our estimate of the

Lagrange multiplier is not likely to be exact, we get a volume residual $R = \bar{V} - \int_\Omega \rho d\Omega$. We

use a Newton-Raphson procedure (using an approximate expression for the sensitivity of the residual R with respect to λ derived using equation (40)) to improve the estimate of λ. This in turn gives new values of the bulk density ρ via equation (40). Iterations on λ and ρ are repeated until the volume constraint is satisfied within a specified tolerance. Then a new equilibrium iteration is begun.

8.   NUMERICAL EXAMPLE

A deep beam rests on two supports and carries a point load at the center of its bottom edge (see Fig. 4). Plane stress conditions are assumed. Two optimization problems with prescribed volume fractions 60% and 20% respectively, are considered. We use a 40×32 mesh of square elements with 8-node displacement functions and constant density to model half the structure. For the 60% volume fraction case, we obtain the stable solution shown in Fig. 5a, yielding $J = 71733$ lb-in. after 40 iterations. For the 20% volume fraction case we obtain the stable solution shown in Fig. 5b with $J = 159580$ lb-in. after 60 iterations.

9.   CONCLUSIONS

Analytical optimization of the microstructural parameters in the homogenized topology design problem leads to a series of reduced problems which form the basis for a family of computational solution procedures. The second reduced displacement problem DP2 appears to be an attractive choice for use with stiffness solution procedures. The interpretation of this formulation as a mixed variational problem has significant consequences with respect to the Babuska-Brezzi stability criterion in the construction of finite element models.

Although we have been able to get near-optimal designs with the current update strategy, terminal convergence is slow, and we would like to find a more effective redesign strategy.
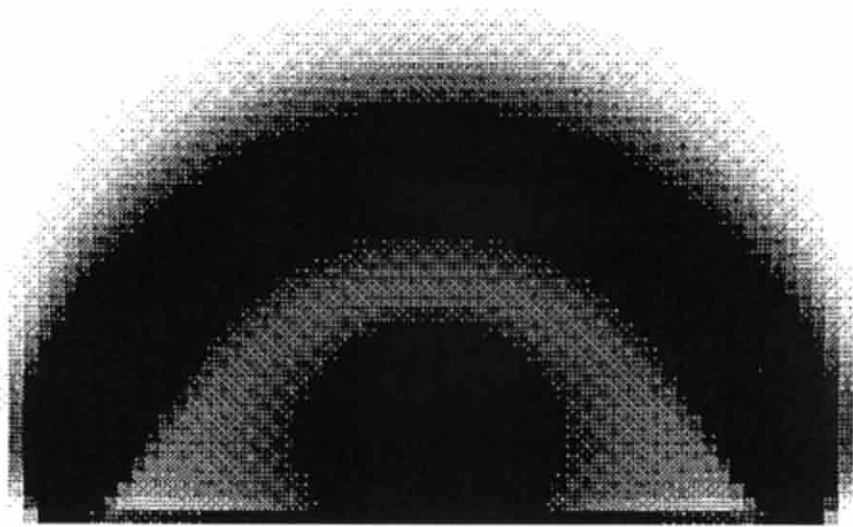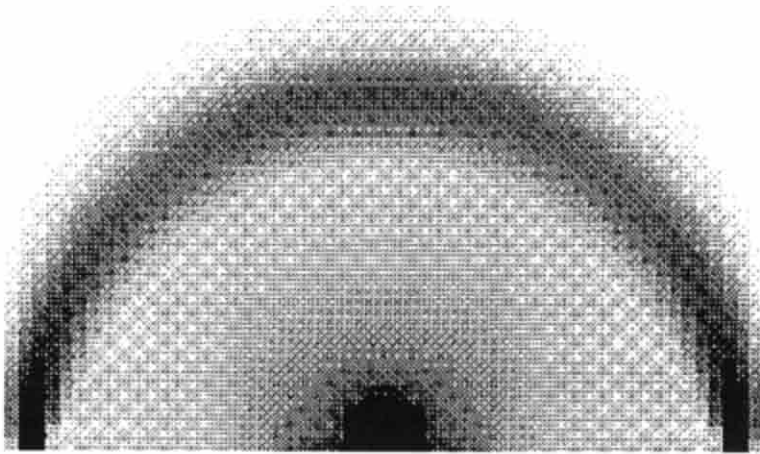
Fig. 5   Stable solutions obtained using 8 node displacement/constant density elements
for specified volume fractions of a) 60% and b) 20%

Another computational problem is associated with the non-uniqueness of the displacement so-
lution for the rank-1 material in mode-III regions. This slows the convergence of the equilibri-

um iterations and introduces nonlinear character to what is otherwise a linear stiffness problem.

Currently, we carry out the optimization using a fixed finite element mesh. We plan to explore adaptive strategies to control error in both the displacement solution and the satisfaction of the optimality criterion for design. Thus, a unified method for adapting the models for u and ρ is needed. This will ensure accurate resolution of the optimal geometry and the corresponding displacement solution.

All of our current effort has been directed towards finding the exact solution to the relaxed form of the topology optimization problem. The relaxed problem can generate optimal designs in which parts of the structure have intermediate densities between zero and one. However, in many practical situations we would like the final design to be comprised solely of macroscopic solid and void regions. Hence, we plan to penalize intermediate densities to force all points to either a solid or void condition. Extensions to three dimensions, multiple load cases, nonlinear materials and alternative objectives are also of interest.

ACKNOWLEDGEMENTS

REFERENCES

[1] Prager, W.; Rozvany G. (1977) Optimization of structural geometry. Dynamical Systems, A. Bednarek and L. Cesari eds., Academic Press, 265-294

[2] Rozvany, W. (1987) Structural design via optimality criteria. Martinus Nijhoff

[3] Cheng, K. T.; Olhoff, N. (1981) An investigation concerning optimal design of solid elastic plates. Int. J. Solids Structures, 17, 305-323

[4] Kohn, R. V.; Strang, G. (1986) Optimal design and relaxation of variational problems. Comm. Pure Appl. Math., 39, 1-25 (Part-I), 139-182 (Part-II) and 353-377 (Part-III)

[5] Kohn, R. (1990) Composite materials and structural optimization. Proc. Workshop on Smart/Intelligent Materials and Systems, Honolulu, March. Technomic Press

[6] Bendsoe, M.; Kikuchi, N. (1988) Generating optimal topologies in structural design using a homogenization method. Comp. Meth. Appl. Mech. Engrg, 71, 197-224

[7] Sokolnikoff, I. S. (1987) Mathematical theory of elasticity. Robert Krieger Publishing Company, Florida

[8] Avellaneda, M. (1987) Optimal bounds and microgeometries for elastic two-phase composites. SIAM J. App. Math., 47, 1216-1228

[9] Avellaneda, M. (1989) Bounds on the effective elastic constants of two-phase composite materials. Proc. Sem. College de France, X, H. Brezis, J.-L. Lions (Eds), Pitman, London

[10] Avellaneda, M.; Milton, G. W. (1989) Bounds on the effective elasticity tensor of composites based on two-point correlations. Proc. of the A.S.M.E Energy Technology Conference and Exposition, Houston, Texas

[11] Bendsoe, M. P. (1989) Optimal shape design as a material distribution problem. Structural Optimization, 1, 193-202

[12] Lipton R. (1992) Private communication

[13] Pedersen, P. (1989) On optimal orientation of orthotropic materials. Structural Optimization, 1, 101-106

[14] Pedersen, P. (1990) Bounds on elastic energy in solids of orthotropic materials. Structural Optimization, 2, 55-63

[15] Brezzi, F.; Fortin, M. (1991) Mixed and Hybrid Finite Element Methods. Springer-Verlag

Simulation of Natural Adaptation of Bone Material and Application in Optimum Composite Design

T.J. Reiter and F.G. Rammerstorfer

Institute of Lightweight Structures and Aerospace Engineering, Vienna Technical University, Austria

Abstract

An algorithm for the simulation of the stress induced remodeling of bone material is presented. The applicability of this method in the field of biomechanics as well as to the design improvement of technical structures is shown in several examples.

1. NOMENCLATURE

U	Strain energy density
U_{eff}	Effective strain energy density
U_n	Homeostatic strain energy density
n_i	Number of load cycles in load case i
ρ_a	Apparent density
ρ_c	(Maximum) density of cortical bone
ΔX	Growth increment perpendicular to the surface
$\Delta \rho$	Change of apparent density
ϵ_{ij}	Strain tensor
σ_{ij}	Stress tensor
β, γ, s, U_{n0}	Model parameters
$C_{X1,2}, C_{\rho1,2}$	Remodeling parameters
E	Young's modulus
G	Shear modulus
ν	Poisson's ratio
K	Bulk modulus
ξ	Particle volume fraction
m, C	Material parameter in Paris-law
$\alpha_1, \alpha_2, k_0, k_1$	Model parameters
$\frac{da}{dN}$	Fracture growth rate per load cycle

2. INTRODUCTION

Unlike normal technical materials such as steel or concrete, bone material as a living tissue has the ability to react to environmental influences by changing its shape and

internal architecture with respect to its functional requirements. Special classes of bone cells are capable of maintaining a steady process of bone resorption and deposition, leading – on a macroscopic observation level – to a quasistatic equilibrium state, which reflects the mechanical loading environment a given bone is exposed to. Changes in the actual stress/strain pattern within the bone will tend to stimulate pronounced cell activity resulting in a resorption of bone material in regions of low loading levels and *vice versa* a deposition of new material in highly stressed zones, giving rise to a new equilibrium state. This functional adaptation can be considered as a 'natural implementation' of some minimum weight optimization procedure, even though the resulting configuration does not necessarily constitute an optimum in a rigorous mathematical sense. However, massive alterations of loading conditions following the implantation of prostheses or implants as used in orthopaedic or dental surgery may lead to detrimental remodeling reactions. While the physical and biomechanical processes which are responsible for transmitting mechanical stimuli into actual bone cell activity are still not fully understood, several attempts have been made to obtain phenomenologically based mathematical formulations, relating local bone growth rates to common mechanical parameters like stress- or strain tensors, v'Mises equivalent stresses etc. *via* simple mathematical equations [Frost 1964; Cowin *et al.* 1985,1987; Carter *et al.* 1987, 1989, 1990; Huiskes *et al.* 1987].

The remodeling algorithm formulated here to simulate stress induced functional adaptation of bone can be introduced to advantage in the improvement of the design of technical structures as will be shown later.

3. REMODELING MODEL

In the present study the difference between an actual effective strain energy density (SED), U_{eff}, and an homeostatic SED, U_n, serves as an appropriate mechanical stimulus to predict bone remodeling processes. Due to the multiple loading conditions and individual loading time histories experienced by a bone in the course of a typical time period, U_{eff} is calculated by an appropiate superposition of the SED-values derived from a number of discrete load cases, weighted according to the corresponding number of load cycles [Carter *et al.* 1987]:

$$U_{eff} = \left(\sum_i \frac{n_i}{\sum_j n_j} U_{(b)_i}^k \right)^{\frac{1}{k}} \tag{1},$$

where $U_{(b)}$ for load case i is given by

$$U = \frac{1}{2} \sigma_{ij} \epsilon_{ij} \tag{2}$$

or by the 'bulk' SED

$$U_b =: \frac{\rho_c}{\rho_a} U \tag{3},$$

which better reflects the strain energy actually stored in the mineralized tissue. In eqn.(1) k acts as a weighting parameter of the degree of influence of load magnitude and the number of loading cycles, respectively.

The homeostatic SED, U_n, which represents the site specific balanced state of no bone remodeling is given by

$$U_n = U_{n0} + \alpha_1 \rho_a \qquad (4),$$

approximating the influence of the apparent density ρ_a. The deviations between U_{eff} and U_n must exceed a certain threshold level to cause any remodeling activity, so that a 'lazy zone' around U_n is assumed.
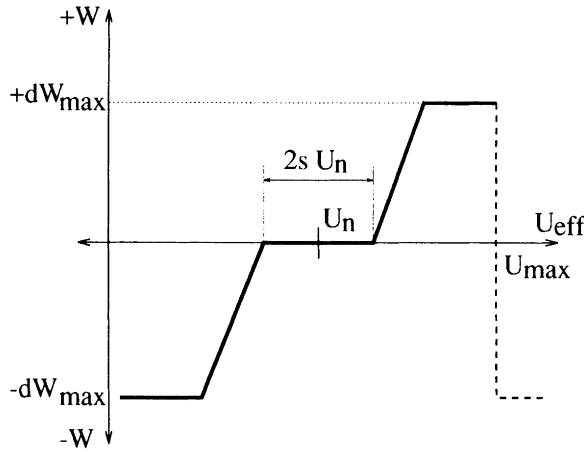
Fig.(1) Qualitative relationship between U_{eff}, and the bone remodeling reaction W.

Fig.(1) shows the principal relationship between U_{eff} and the bone material deposition/resorption. Any SED level exceeding U_{max} causes actual bone cell damage, leading to overstrain necrosis. Due to biological cell activity limits, certain growth rate bounds have to be taken into consideration ($+/-\Delta W_{max}$). Applying this model to the simulation of surface remodeling (i.e. ΔX as surface growth perpendicular to the surface) we derive:

$$\Delta X = \begin{bmatrix} \Delta X_{min} & \Delta X < \Delta X_{min} \\ C_{X1}[U_{eff} - U_n(1-s)] & U_{eff} < U_n(1-s) \\ 0 & U_n(1-s) \leq U_{eff} \leq U_n(1+s) \\ C_{X2}[U_{eff} - U_n(1+s)] & U_{eff} > U_n(1+s) \\ \Delta X_{max} & \Delta X > \Delta X_{max} \end{bmatrix} \qquad (5)$$

Under the assumption of isotropic bone material behaviour the changes due to internal remodeling can be expressed by the change in apparent density $\Delta\rho$, thus giving:

$$\Delta\rho = \begin{bmatrix} \Delta\rho_{min} & \Delta\rho < \Delta\rho_{min} \\ C_{\rho 1}[U_{eff} - U_n(1-s)] & U_{eff} < U_n(1-s) \\ 0 & U_n(1-s) \leq U_{eff} \leq U_n(1+s) \\ C_{\rho 2}[U_{eff} - U_n(1+s)] & U_{eff} > U_n(1+s) \\ \Delta\rho_{max} & \Delta\rho > \Delta\rho_{max} \end{bmatrix} \qquad (6).$$

From experimental investigations [Carter and Hayes 1977], in which cortical bone was treated simply as densified trabecular bone (i.e. the two tissues are assumed to consist of the same material, differing only in porosity), the Young's modulus of bone material (the Poisson ratio ν is assumed to be constant) can be approximated by

$$E = \beta_1 \rho_a^\gamma \qquad (7)$$

It should be noted that theoretical investigations [Gibson and Ashby 1988] for the relation between E and ρ_a taking into account the foam-like microstructure of bone material, predict γ-values between 2 and 3. As shown later materials with different microstructures (e.g. particle reinforced materials) can be handled in an analogous way.

3.1 Biomechanical Example - Bone Remodeling around a Dental Implant

Combining the above formulated remodeling scheme with a linear Finite Flement code, an iterative computer procedure is implemented to allow quantitative predictions of adaptive bone remodeling processes. In each timestep a FE-Analysis has to be performed and the FE-representation of the model has to be adapted according to the current distribution of U_{eff}.

Using this procedure for the simulation of internal bone remodeling, the formation of bone mass around a natural tooth and a tooth-shaped implant (both modeled by 2-D plane-stress finite elements) under normal masticatory loads is predicted, starting from a configuration of constant bone density. The natural tooth is supported in the jaw bone by an encapsulating periodontal membrane of small stiffness, while the implant is assumed to be directly attached to the surrounding bone.
As shown in Fig.(2), the model of the natural tooth with a periodontal membrane gives rise to a concentration of bone mass all around the alveolus, whereas the tooth-shaped implant without a periodontal membrane causes not only a significantly different density distribution lacking this encapsulating cortical pocket, but also results in a funnel-shaped resorption zone due to overstrain necrosis in the upper part of the bone tissue in the immediate vicinity of the implant.
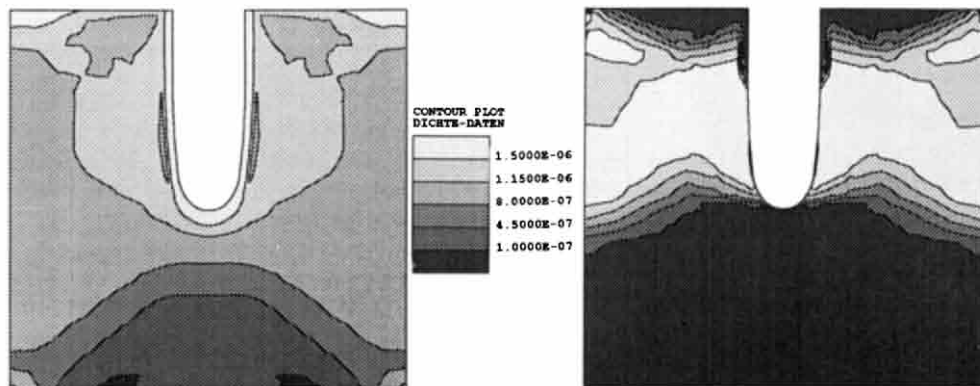
CONTOUR PLOT
DICHTE-DATEN

1.5000E-06
1.1500E-06
8.0000E-07
4.5000E-07
1.0000E-07

Fig.(2) Distribution of apparent bone density around a) A natural tooth sourrounded by a periodontal membrane and b) An implant without a periodontal membrane, resulting in a funnel-shaped resorption zone.

4. TOPOLOGY OPTIMIZATION BY FUNCTIONAL ADAPTATION

During the last decades there have been major advances in the field of structural optimization, taking advantage of new developments based either on Optimality Criterion or Mathematical Programming Methods, particularly as far as shape optimization and sizing problems are concerned. A relatively new branch in this expanding research field is refered to as topology optimization, its aim being the developing of methods for finding an optimal structure for a mechanical configuration which is only defined by its loading environment and its boundary conditions [eg. Bendsøe and Kikuchi 1988, Suzuki and Kikuchi 1990].

The above remodeling algorithm can be considered as a simple and natural (and in some sense nature's) approach to this class of problems, and it is closely related to the approach of Bendsøe and Kikuchi. Starting from a possible design domain which is discretized by finite elements of homogeneous density (and stiffness) an internal remodeling simulation is started (using U instead of U_b as stimulus), which generates a clear structural design within a few iterations (the convergence rate depends on the chosen growth-rate-parameters and on the problem under consideration). As mentioned in the introduction, there is no proof of uniqueness or optimality for these solutions. However, it will be shown that for certain problems this method yields the actual optimum structures. It turns out that the objective function of this approach is the minimum overall compliance which in most cases also leads to optimized structures in respect to stress criteria. In [Pedersen 1991] it is shown that for elastic structures the minimization of the overall compliance is equivalent to the local criterion of constant strain energy density throughout the structure, which exactly corresponds to the assumption of some optimal homeostatic U_n-value in the 'natural' approach presented here.

4.1. Topology-Finding Examples

Starting with a rectangular design domain of homogeneous density which has pinned boundary nodes at the left side the topologies shown in Fig.(3) are obtained, depending on the loading conditions. The derived topology in the case of a single vertical load (Fig.(3b)) shows the well known optimum solution with two 45°-bars, whereas a single horizontal force yields a single horizontal strut. Fig.(3d) gives the result for a single load under 45° which differs essentially from Fig.(3c), illustrating the solution under combination of two loadcases according to case (a) and case (b) using eqn.(1)
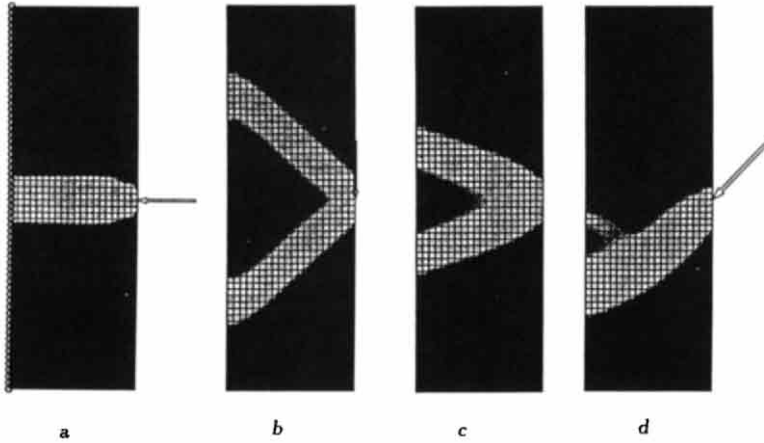

Fig.(3) 'Cantilever Beam': a) Single horizontal load, b) Single vertical load, c) Combination of a) and b), d) Single load under 45°.

The result for the 'aircraft support beam' problem [eg. Bendsøe, Rasmussen and Rodrigues 1991] obtained by functional adaptation is shown in Fig.(4). Again a rectangular design domain is used. The left-hand boundary nodes are pinned and a single vertical force is applied to the lower right-hand corner.

5. FUNCTIONAL ADAPTATION OF PARTICLE REINFORCED COMPOSITES

Since bone material can be considered as a highly sophisticated natural composite (collagen fibers reinforced by hydroxyapatite crystals building the material for the struts (trabiculae) of the complex foam-like structure of spongy bone), the extension of the present functional adaptation algorithm to structural optimization (or rather structural design improvement) in connection with artificial composite materials suggests itself. In the following, linear elastic materials, reinforced by spherical particles (in particular the SiC/Al metal matrix composite system) are considered, where the particle volume fraction ξ replaces the apparent density ρ_a as the variable material parameter. Due to
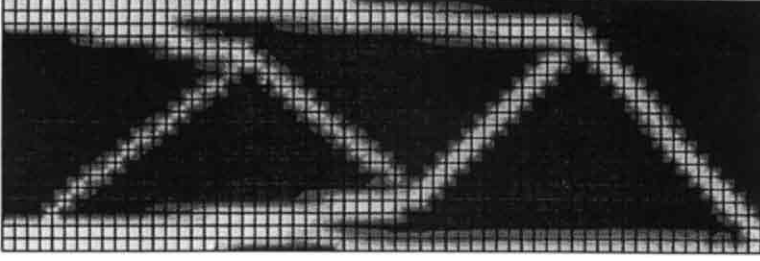
Fig.(4) 'Aircraft support beam' - Problem.

the different material behaviour as compared to bone tissue several changes have to be introduced into the remodeling procedure.

7.1. Material Description

Although eqn.(7) gives a good approximation for foam-like microstructures, it does not hold in any way for particle reinforced materials. Following [Benveniste 1987], a Mori-Tanaka mean-field approach is utilized to obtain analytical formulas for the linear elastic material parameters of the composite depending on the particle volume fraction ξ. Since matrix (Al), reinforcing particles (SiC), and the resulting composite show isotropic material behaviour, the Young's Modulus E and the Poisson's ratio ν can be calculated by:

$$E = \frac{9KG}{3K + G} \tag{8}$$

$$\nu = \frac{3K/2 - G}{3K + G} \tag{9}$$

where the effective bulk and shear moduli of the composite are given by

$$K = K^{(m)} + \frac{\xi(K^{(p)} - K^{(m)})(3K^{(m)} + 4G^{(m)})}{3K^{(m)} + 4G^{(m)} + 3(1 - \xi)(K^{(p)} - K^{(m)})} \tag{10}$$

$$G = G^{(m)} + \frac{\xi(G^{(p)} - G^{(m)})[5G^{(m)}(3K^{(m)} + 4G^{(m)})]}{5G^{(m)}(3K^{(m)} + 4G^{(m)}) + 6(1 - \xi)(K^{(m)} + 2G^{(m)})(G^{(p)} - G^{(m)})} \tag{11}.$$

The index (m) stands for matrix and (p) stands for particles (SiC). As can be seen in Fig.(5), which shows the functions $E = E(\xi)$ and $\nu = \nu(\xi)$ for particle reinforced Aluminum SiC/Al99, the dependency of these parameters on ξ differs essentially from a simple rule of mixture prediction, which gives just straight lines.
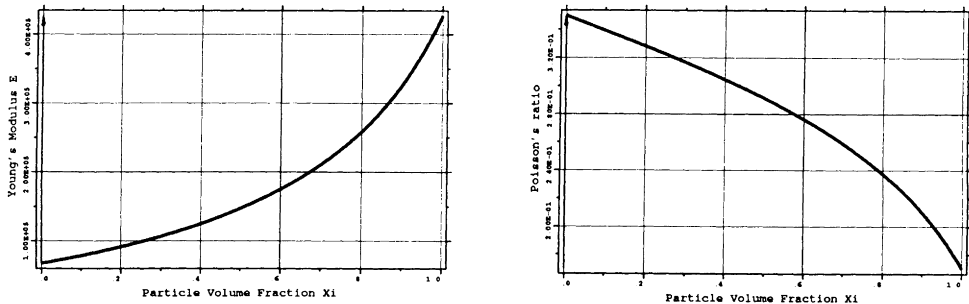

Fig.(5) Young's modulus, $E = E(\xi)$ and Poisson's ratio $\nu = \nu(\xi)$ for particle reinforced aluminum calculated by Mori-Tanaka mean-field approach.

In conjunction with fracture mechanics, the classical formulation of the Palmgreen-Miner fatigue concept for cyclic loading under consideration of different loadcases may written as

$$\Delta \sigma eff = \left(\sum_i \frac{n_i}{\sum_j n_j} \Delta \sigma_i^m \right)^{\frac{1}{m}} \tag{12},$$

with m standing for the exponent in the classical Paris-law

$$\frac{da}{dN} = C \ \Delta K^m \tag{13}.$$

Equation.(1) can be interpreted as an alternative formulation of eqn.(12) setting $k = 2m$. For SiC particle reinforced Aluminum experimental investigations [eg. Davidson 1989; Botstein et al. 1990; Kumai et al. 1992] show a dependency between the particle volume fraction ξ and the parameters of the Paris-law $m(\xi)$ and $C(\xi)$ $(\Delta K_{th}(\xi))$. This is introduced into the remodeling scheme by using polynomial approximations:

$$U_n = U_{n0} + \alpha_1 \xi + \alpha_2 \xi^2 ... \tag{14}$$

$$k = k_0 + k_1 \xi ... \tag{15}.$$

7.2. Example: Design of a Composite Hinge

To show the applicability of the remodeling algorithm for the design improvement of structures using particle reinforcement, a hinge problem as illustrated in Fig.(6a) is investigated. Two different loadcases (a single load, acting at an angle of $10°$ to the horizontal and a single vertical load, both loads being cosine distributed around the corresponding half of the load bearing circle) are considered. To find a proper topology for this problem a rectangular design domain with a circular hole is discretised by finite elements (2/D plane stress) and subjected to the two loadcases. Fig.(7a) shows the FE-mesh and the U_{eff} distribution at the starting configuration of a homogeneous particle volume fraction of $\xi = 0.2$. To enable the system to find a suitable topology it is given the capability of 'removing' material by introducing a foam-like material microstructure following eqn.(7) once the minimum ξ-value of 0.0 has been reached. The topology derived by internal remodeling (see Fig.(8a)) is used as a basis for a new FE-discretization as shown in Fig.(8b). In the next step a combined surface and internal remodeling simulation is performed, allowing the particle volume fraction to vary between 0.0 and 0.6. Fig.(6b) shows the final ξ-distribution at the end of the simulation. Fig.(8a) and Fig.(8b) give the U_{eff}-distribution at the beginning and the end of the remodeling process.
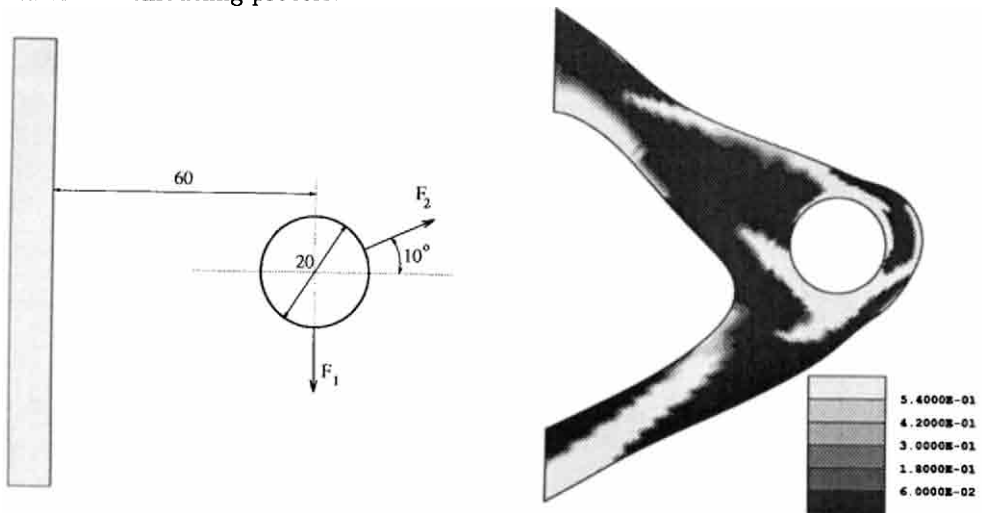
Fig.(6) 'Hinge-Problem', a) Principal problem illustration, ($F_1 = F_2 = 250\ N$ per unit thickness - cosine distributed, $U_n = 8.0e - 4$); b) Final solution of shape and particle volume fraction distribution obtained by remodeling simulation.

6. CONCLUSIONS

A biologically based remodeling algorithm has been presented, which is capable of giving good results in simulating stress induced functional adaptation reactions of bone material in a quantitative way. It also can serve as an efficient tool for finding proper topologies for technical structures as well as for design improvements of structures, especially in cases where continuous changes in the material parameters are fabricable (i.e. functionally gradient materials).
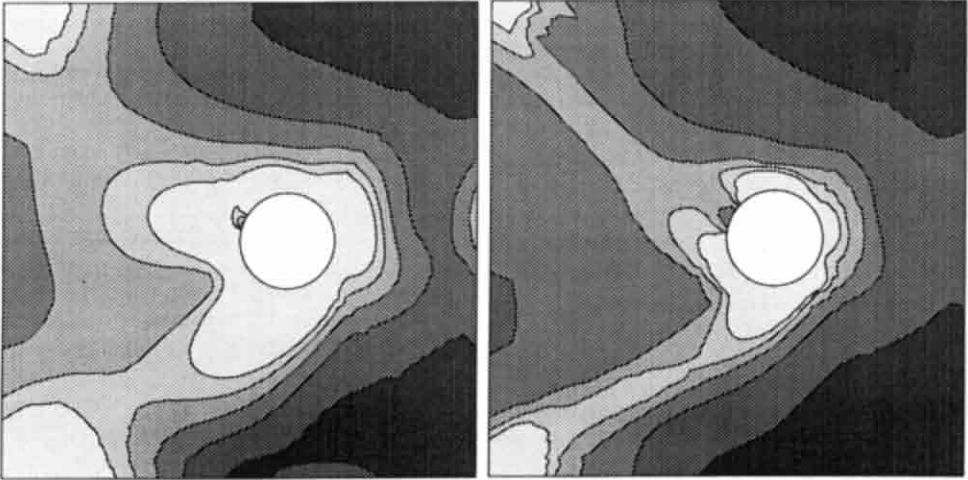
Fig.(7) 'Hinge-Problem', U_{eff} - Distribution at the beginning a) and at the end b) of the internal remodeling simulation in the preliminary topology search (step 1).
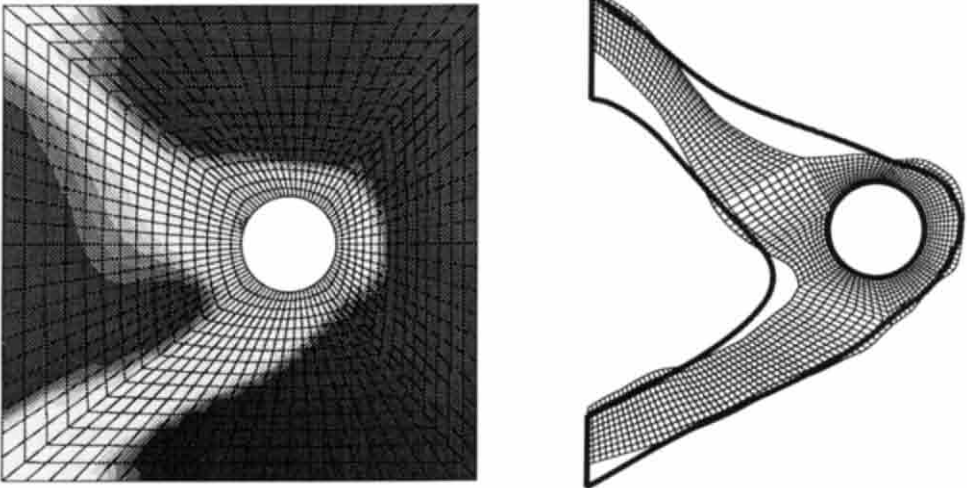
Fig.(8) 'Hinge-Problem', a) Topology (density distribution) obtained by remodeling simulation, b) FE-Mesh for second remodeling step (at the start of step 2) and final shape (outlined).

Fig.(9) 'Hinge-Problem', a) U_{eff} distribution at the start (a) and at the end (b) of the second remodeling step.

7. REFERENCES

Bendsøe, M.P. and Kikuchi, N., 'Generating optimal topologies in structural design using a homogenization method', *Comput. Meths. Appl. Mech. Eng.* **71**, 1988, pp. 197-224.

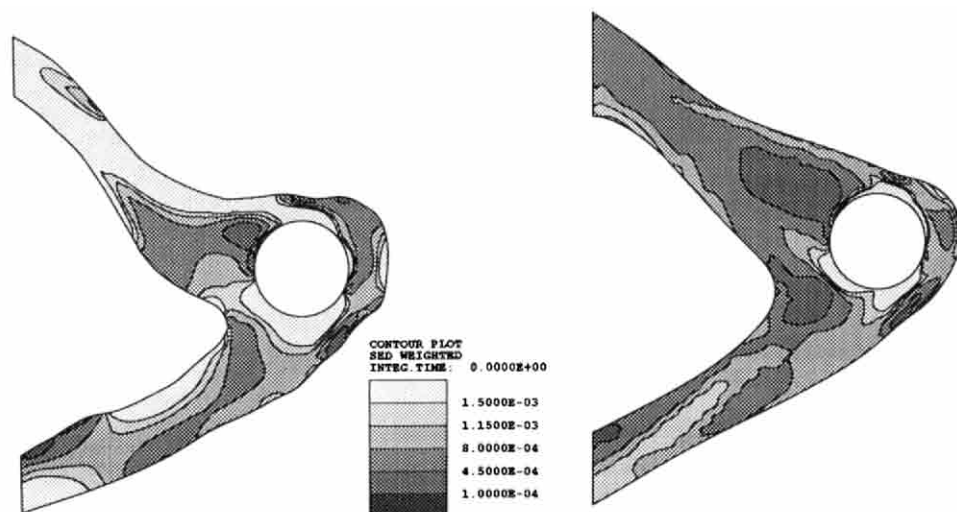Bendsøe, M.P., Rasmussen, J. and Rodrigues, H.C., 'Topology and boundary shape optimization as an integrated tool for computer aided design', in: Engineering optimization in design processes, ed.: Eschenauer, Mattheck and Olhoff, Springer-Verlag, Heidelberg, 1991, pp. 27-34.

Benveniste, Y., 'A new approach to the application of Mori-Tanaka's theory in composite materials', *Mechanics of Materials* **6**, 1987, pp. 147-157.

Botstein, O., Arone, R. and Shpigler, B., 'Fatigue crack growth mechanisms in Al-SiC particulate metal matrix composites', *Mat. Science and Eng.* **A128**, 1990, pp. 15-22.

Carter, D.R. and Hayes, W.C., 'The compressive behaviour of bone as a two-phase porous structure', *J. Bone and Joint Surg.* **59-A**, 1977, pp. 954-962.

Carter, D.R., Fyhrie, D.P. and Whalen, R.T., 'Trabecular bone density and loading history: regulation of connective tissue biology by mechanical energy', *J.Biomech.* **20**, 1987, pp. 785-794.

Carter, D.R., Orr, T.E. and Fyhrie, D.P., 'Relationship between loading history and femoral cancellous bone architecture', *J.Biomech.* **22**, 1989, pp. 231-244.

Carter, D.R., Fyhrie, D.P., 'Femoral head apparent density distribution predicted from bone stresses', *J.Biomech.* **23**, 1990, pp. 1-10.

Cowin, S.C., Hart, R.T., Balser, J.R. and Kohn, D.H., 'Functional adaptation in long bones: Establishing *in vivo* values for surface remodeling rate coefficients', *J.Biomech.* **18**, 1985, pp. 665-684.

Cowin, S.C., 'Bone remodeling of diaphyseal surfaces by torsional loads: theoretical predictions', *J.Biomech.* **20**, 1987, pp. 1111-1120.

Davidson, D.L., 'The growth of fatigue cracks through particulate SiC reinforced aluminum alloys', in: Advances in fracture research, ed.: Salama, Ravi-Chandar, Taplin, Rama Rao, ICF7 Vol. 4, Proceed. of Seventh International Conference on Fracture, Houston, Texas, March 1989, pp. 3021-3028.

Frost, H.M., 'The laws of bone structure', C.C.Thomas, Springfield, IL., 1964

Gibson, L.J. and Ashby M.F., 'Cellular Solids - Structure and Properties', Pergamon Press, Oxford,New York, 1988.

Huiskes, R., Weinans, H., Grootenboer, H.J., Dalstra, M., Fudala, B. and Slooff, T.J., 'Adaptive bone-remodeling theory applied to prosthetic-design analysis', *J.Biomech.* **22**, 1987, pp. 1135-1150.

Kumai, S., Yoshida, K., Higo, Y. and Nunomura, S., 'Effects of the particle distribution on fatigue crack growth in particulate SiC/6061 aluminium alloy composites', *Int. J. Fatigue* **14/2**, 1992, pp 105-112.

Pedersen, P., 'On thickness and orientational design with orthotropic materials', *Struct. Optim.* **3/2**, 1991, pp. 69-78

Suzuki, K. and Kikuchi, N., 'Shape and topology optimization by a homogenization method', in: Sensitivity analysis and optimization with numerical methods, AMD-Vol. 115, ASME, 1990, pp.15-30.

OPTIMAL DESIGN OF ANISOTROPIC STRUCTURAL ELEMENTS

N.V.BANICHUK

Academy of Sciences, Moscow

Abstract

Rational distribution of material in plate - like structures are studied. Emphasis is placed on the fundamental eigenfrequencies maximization for unrestrained plates subjected to planar harmonic vibrations. The problem of finding the optimal orientation of orthotropic properties for an elastic plates is investigated with the help of variational formulation of the problem and necessary optimality conditions. The successive optimization method based on redesign and sensitivity analysis is applied. Computed optimum designs are compared with conventional layouts.

In recent years, a number of new design coucepts have emerged. One of them is concerned with optimal positioning of elastic symmetry planes in an orthotropic body. This concept is very fruitfull for structures made of composite materials, for complex effectively orthotropic structures and especially for large space structures. Because of the high cost of lifting mass to orbit there is a great incentive in making large space structures light and therefore flexible. The natural frequency spectrum of such structures is typically quite dense and the fundamental eigenfrequency is very low. On the other hand, many of these structures, especially antenna structures, have very stringent requirement on their dynamical stiffness and

shape accuracy. Therefore, these structures have to be optimally designed to achive the required performance without increasing in structural mass. In some cases this goal can be succesfully solved with the help of orientational design, which does not require the additional structural mass.

The basic idea of designing of structures with the best orientation of the principal axes of orthotropy was realized in the past decade in a series of the papers. Necessary coditions for the optimal positioning of elastic symmetry planes in an orthotropic body were derived by Banichuk (1979), Seregin and Troitski (1981). The problem of maximization of integral stiffness has been considered by these authors. Some of the obtained analytical and numerical results were described by Banichuk (1983). Restricting ourselves to plane problems for 2-D locally orthotropic structures we shall note recent papers by Landriani and Rovati (1991) Pedersen (1989, 1990), Tomsen (1991). Note also the paper by Pedersen (1991) devoted to combined thickness and orientational design of locally orthotropic structures.

In this paper the internal structure of the plate are seen as two dimensional locally orthotropic solids. This approximation can be assumed acceptable as for some complex built in effectively orhotropic structures as for the structures made of composite materials. The variational problem governing the amplitude displacement function behavior and the optimization problem of finding the best orientation of the principal axes of orthotropy are formulated. Optimality conditions are derived and analysed. These conditions allows for a nonunique orientation of orthotropy axes. As for statical cases dynamical optimality conditions show that the stress and strain principal axes are collinear. Necessary optimality conditions and design sensitivity analysis formulas are implemented in successive

optimization algorithm and optimal designs for square, rectangular and hexagan plates are calculated.

1.BASIC ASSUMPTION AND OPTIMIZATION PROBLEM.

Let us consider the planar harmonic vibrations of unrestrained plate defined by the formulas.

$$\tilde{u} = u(x,y) \ e^{i\omega t}, \quad \tilde{v} = v(x,y) \ e^{i\omega t} \qquad (1.1)$$

where x-y-z- Cartesian coordinate system (z axis is perpendicular to the plate); ω – the smallest eigenfrequency of free vibrations; $\tilde{u}$, $\tilde{v}$ – planar displacement of median surface of the plate in the directions opf the x and y coordinates, respectively; $u = u(x,y)$, $v = v(x,y)$ – amplitude displacements; i imaginary unit, t – time. Fundamental eigenfrequency of planar vibrations can be evaluated with the help of Rayleigh variational principle.

$$\omega^2 = min_{u,v} \ (^V/_T) \qquad (1.2)$$

Amplitude expressions of potential energy V and kinetic energy $\omega^2 T$ are given in the following form.

$$V = \frac{1}{2} \int_\Omega \{A_{11} \ u_x^2 + 2A_{12} \ u_x v_y + A_{22} v_y^2 + 2A_{16} u_x (u_y + v_x) +$$

$$+ 2A_{26} v_y (u_y + v_x) + A_{66} (u_y + v_x) \} \ d\Omega \qquad (1.3)$$

$$\omega^2 T = \frac{1}{2} \ \rho \omega^2 \int_\Omega (u^2 + v^2) \ d\Omega \qquad (1.4)$$

Partial derivatives of u and v with respect to x and are denoted u_x, u_y, v_x, v_y, while Ω $(x,y) \in \Omega$ denotes the domain in x-y plane occupied by the material.

We adopt that the material properties do not change in the direction of the z-axis. Assume also that the plate is locally orthotropic and that the values of the orthotropic constants A_{11}^o, A_{12}^o, A_{22}^o, A_{66}^o are known for the axes of orthotropy ξ and η. The direction of the ξ-η axes of orthotropy, relative to the x-y axes is given by the angle $\alpha(x,y)$, where α-is the angle between the x and ξ axes.(Fig.1).
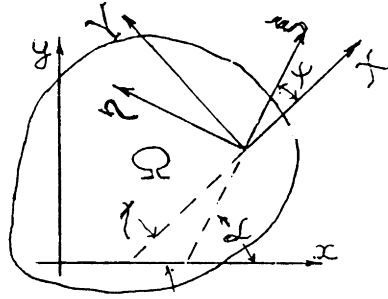
Fig.1 Coordinate systems.

In the fixed x-y coordinate system, the orthotropic elastic moduli $A_{11},\ldots,A_{66}$ are related to the assigned orthotropic constants $A_{11}^{o},\ldots,A_{66}^{o}$ in the $\xi-\eta$ system by means of next equation.

$$A_{11}(a)= C_1 Cos^4 a + C_2 Sin^4 a + C_3 \qquad (1.5)$$

$$A_{22}(a)= C_2 Cos^4 a + C_1 Sin^4 a + C_3$$

$$A_{12}(a)= (C_1 + C_2) Cos^2 a Sin^2 a + A_{12}^{o}$$

$$A_{66}(a)= (C_1 + C_2) Cos^2 a Sin^2 a + A_{66}^{o}$$

$$A_{16}(a)= Cos\, a\, Sin\, a\, (C_1 Cos^2 a - C_2 Sin^2 a)$$

$$A_{26}(a)= Cos\, a\, Sin\, a\, (C_1 Sin^2 a - C_2 Cos^2 a)$$

$$C_1 = A_{11}^{o} - C_3, \quad C_2 = A_{22}^{o} - C_3, \quad C_3 = A_{12}^{o} + 2A_{66}^{o}$$

The spectrum of free planar vibrations of unrestrained plate has three zero eigenfrequencies, corresponding rigid body displacements in x and y directions and rigid body rotation with respect to z-axis. There fore we use the next orthogonality conditions for elastic modes and rigid body modes to determine the non zero eigenfrequencies by means

$$\int_\Omega u\, d\Omega = 0, \quad \int_\Omega v\, d\Omega = 0 \qquad (1.6)$$

$$\int_\Omega (xv + yu)\, d\Omega = 0$$

of Rayleigh quotient V/T minimization. The boundary conditions for free edges of plate are a "natural"

conditions for the Rayleigh quotient, so there is no need to satisfy these conditions a priory. The problem of optimization consists in determining the best orientation of the axes of orthotropy from the condition of maximum behavior of the fundamental eigenfrequency.

$$J_* = max_\alpha \; \omega^2(\alpha) = max_\alpha \; min_{u,v} \; \frac{V(\alpha, u, v)}{T(u, v)}$$

2. OPTIMALITY CRITERIA.

First variation of the optimized functional with respect to design variable α has the form.

$$\delta_\alpha \omega^2 = \frac{1}{T} \delta_\alpha V = \frac{1}{T} \int_\Omega \frac{\partial f}{\partial \alpha} \delta \alpha \; \partial\Omega \qquad (2.1)$$

$$f = \frac{1}{2} A_{11}(\alpha) u_x^2 + A_{12}(\alpha) u_x v_y + \frac{1}{2} A_{22}(\alpha) v_y^2 + A_{16}(\alpha) u_x (u_y + v_x)$$
$$+ A_{26}(\alpha) v_y (u_y + v_y) + \frac{1}{2} A_{66}(\alpha)(u_y + v_x^2) \qquad (2.2)$$

For the sake of ease in obtaining the conditions for stationary behavior of ω^2 as we vary α, and to cut short our exposition, we introduce at each point (x,y) a system of principal X-Y axes of deformation and denote the components of the strain tensor in this coordinate system by $\varepsilon_X, \varepsilon_Y$ and ε_{XY} (with $\varepsilon_{XY} = 0$). Let ψ and χ denote the angle between the x and X axes, respectively, so that $\psi = \alpha - \chi$ (see Fig.1). The quantities ε_x, ε_y, ε_{xy} and ε_X, ε_Y, ε_{XY} are related to each other by the wellknown formulas.

$$\varepsilon_X = \varepsilon_x Cos^2\chi + \varepsilon_y Sin^2\chi + \gamma_{xy} Sin \chi Cos \chi \qquad (2.3)$$

$$\varepsilon_Y = \varepsilon_x Sin^2\chi + \varepsilon_y Cos^2\chi + \gamma_{xy} Sin \chi Cos \chi$$

$$\varepsilon_{XY} = \frac{1}{2} (\varepsilon_y - \varepsilon_x) Sin 2\chi + \frac{1}{2} \gamma_{xy} Cos 2\chi = 0$$

Equation (2.2) for f may now be rewritten as

$$f = \frac{1}{2} A_{11}(\psi)^2 \varepsilon_X + A_{12}(\psi) \varepsilon_X \varepsilon_Y + \frac{1}{2} A_{22}(\psi) \varepsilon_Y^2 = (NCos^2\psi +$$
$$+ QCos^2\psi)(\varepsilon_X - \varepsilon_Y) + R \qquad (2.4)$$

$$N = \frac{1}{2} (C_1 + C_2)(\varepsilon_x - \varepsilon_y)$$

$$Q = (C_1 \varepsilon_Y - C_2 \varepsilon_X)$$

$$R = \frac{1}{2} A_{22}^0 \varepsilon_X^2 + A_{12}^0 \varepsilon_X \varepsilon_Y + \frac{1}{2} A_{11}^0 \varepsilon_Y^2$$

wrere ε_X and ε_Y are given by Eq (2.3). Thus, the functional ω^2 is expressed as a function of the angles ψ and χ, by means of Eqs.(1.5),(2.3),(2.4). These angles satisfy the constraint $\psi + \chi = a$. To derive necessary conditions for an extremum, we require the first variation of the functional ω^2, which depends on the variations δa, δu and δv, to be zero. As we vary ω^2 by varging u, v, and a the quantities a, u, and v are regarded as independent of each other. Therefore, the angle χ may also be regarded as independent of a, where χ enters into Eqs. (2.3) and (2.4). The same assumption can be made concerning χ in the third relation of Eq.(2.3); i.e.., in this formula χ depends only on the components of the strain tensor $\tan 2\chi = \gamma_{xy} / 2(\varepsilon_x - \varepsilon_y)$. Therefore, in finding the first variation we can substitute $\partial f / \partial a = \partial f / \partial \psi$. As we vary a the conditions of stationary behavior of ω^2 becomes

$$\delta_a \omega^2 = \frac{1}{T} \int_\Omega \frac{\partial f}{\partial a} \, \delta a \; d\Omega = \frac{1}{T} \int_\Omega \frac{\partial f}{\partial \psi} \, \delta \psi \; d\Omega = 0 \qquad (2.5)$$

$$\frac{\partial f}{\partial \psi} \equiv (\varepsilon_X - \varepsilon_Y) \sin 2\psi (2N\cos^2\psi + Q) = 0 \qquad (2.6)$$

This condition contains four different ways of orienting the axes.

1) $\psi = 0$ \hfill (2.7)

2) $\psi = \frac{\pi}{2}$

3) $\cos^2\psi = -\frac{Q}{2N}$, $0 \le -\frac{Q}{2N} \le 1$

4) $\varepsilon_x = \varepsilon_y$

If we adopt the third way of orienting the axes of orthotropy, we find that this is possible only if the inequality of (2.7) is satisfied. Let us explain this by representing f by quadratic formula with tharee terms $f = Nt^2 + Qt + R$ where the variable t is $t = \cos^2\psi$. Since t varies on the interval $0 \le t \le 1$, the extremum of f, as a function of t may occur either at the boundary points $t=0$

or $t=1$, which corresponds to 1) and 2), or it can occur at an interior point. The inequality of Eq.(2.7) simply states that t must be chosen in the interval [0,1].

Let us discuss the mechanical interpretation of the necessary optimality conditions (2.7). To this purpose write the stress strain relations in principal strain axes $X-Y$ $(\varepsilon_{XY}= 0)$.

$$\sigma_X= A_{11}(\psi)\varepsilon_X + A_{12}(\psi)\ \varepsilon_Y \qquad (2.8)$$

$$\sigma_Y= A_{12}(\psi)\varepsilon_X + A_{22}(\psi)\varepsilon_Y$$

$$\sigma_{XY}= A_{16}(\psi)\varepsilon_X + A_{26}(\psi)\varepsilon_Y$$

Consider the ways 1) and 2) of orienting the orthotropy axes. Using (1.5) and (2.8) with $\psi = 0$, $\pi/2$ we obtain $A_{16}(\psi) = A_{26}(\psi) = 0$, $\sigma_{XY}= 0$. Consequently the principle strain axes coincide with the principle stress axes for these ways.

If the third way of orienting the axes of anisotropy is considered with

$$Cos\ \psi = -\ \frac{Q}{2N} = \frac{C_2\ \varepsilon_X - C_1\ \varepsilon_Y}{(C_1+C_2)(\varepsilon_X-\varepsilon_Y)}$$

we arrive at the following result using (1.5) and (2.8).

$$\sigma_{XY}= Cos\ \psi\ Sin\ \psi\ \{(C_1 + C_2)(\varepsilon_X - \varepsilon_Y)Cos^2\psi + C_1\varepsilon_Y- C_2\varepsilon_X\} = 0$$

Hence the coincidence of the principle strain axes and the principle stress axes is realized.

Consider the way 4) from (2.7). If $\varepsilon_X = \varepsilon_Y$, then strain tensor is spherical. Consequently arbitrary axes and particularly the principal stress axes can be taken as principal strain axes.

Thus the strain tensor and stress tensor are coaxial for optimal plate.

3.NUMERICAL RESULTS.

The optimization problem (1.7) was solved numerically for square, rectangular and hexagonal plates with the help of successive optimization method described by Banichuk

(1983). The computational algorithm is based on design sensitivity analysis formulas and finite element technique. If the optimized eigenfrequency become multiple, then it takes into account the additional conditions of coincidence of the eigenfrequencies. For all cases we assumed $A_{11}^o = 1.02$, $A_{22}^o = 0.34$, $A_{12}^o = 0.08$, $A_{36}^o = 0.16$.

Optimal distribution of orthotropy axes orientational is shown in Fig.2 for square plate. This distribution
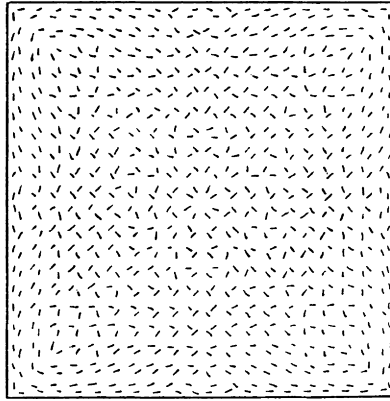
Fig.2 Optimal design of square plate for planar vibrations. corresponds to the smallest eigenfrequency $J_* = \omega_1 = 2.001$. The multiplicity of the eigenfrequency ω_1 is equal to 4. To compare the optimal distribution of orthotropy axes with conventional layouts we computed the frequency spectrums for the plates of unit area shown in Figs.3-5, and
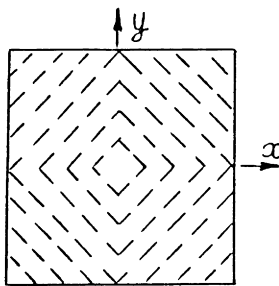
Fig.3 Conventional design for square plate.
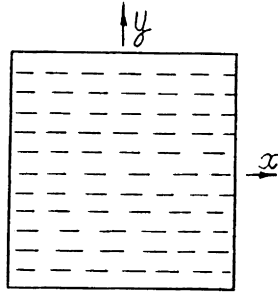
Fig.4 Conventional design for square plate.
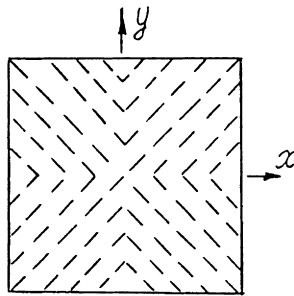
Fig.5 Conventional design for square plate.

displayed them in Table 1. First column of the Table 1 corresponds to the optimal plate shown in Fig.2.

Table 1. Eigenfrequencies of planar vibrations for square plates with optimal and conventional designs.

	Fig.2	Fig.3	Fig.4	Fig.5
ω_1	2.001	1.796	1.522	1.639
	(4)	(1)	(1)	(2)
ω_2	2.516	1.812	1.575	1.787
	(1)	(1)	(1)	(1)
ω_3	2.692	1.813	1.782	1.989
	(1)	(2)	(1)	(1)
ω_4	3.075	2.078	2.097	2.021

	(2)	(1)	(1)	(1)
ω_5	3.957	2.204	2.359	2.350
	(1)	(1)	(1)	(1)
ω_6	3.982	2.679	2.611	2.838
	(2)	(2)	(1)	(2)

Second, third and fourth columns correspond tot he plates presented respectively in Figs.3-5. The numbers in round brackets indicate the multiplicity of the eigenfrequencies. The result of the solving of optimization problem for the rectangular plate $(-0.25 \leq x \leq 0.25, -1 \leq y \leq 1)$ of unit area is illustrated in Fig.6. The optimized functional $J_* = \omega_1 = 1.426$ is simple for the optimal distribution of orthotropy axes orientation. The first eigenfrequency and the highest eigenfrequencies of the optimal plate planar
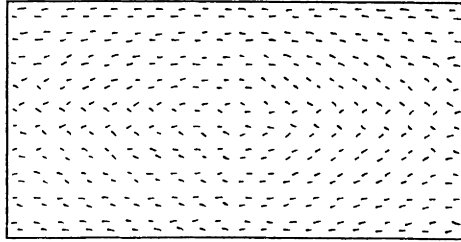
Fig.6 Optimal design of rectangular plate for planar vibrations.
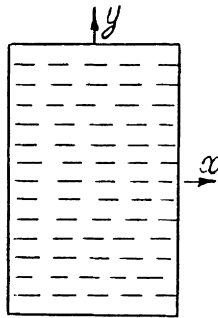
Fig.7 Conventional design of rectangular plate.
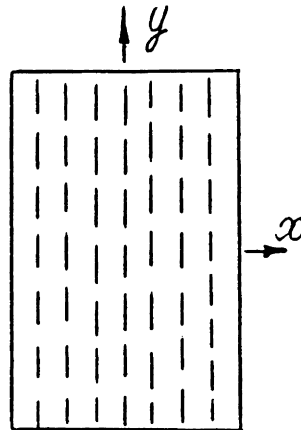
Fig.8 Conventional design of rectangular plate.

vibrations are displayed in the first column of the Table 2
For comparison the frequency spectrums were computed also
for the plates with nonoptimal orthotropy axes orientations
show in Fig.7,8. The computed values are represented
respectively in the second and third columns of the Table2.

Table.2 Eigenfrequencies of planar vibrations for
rectangular plates with optimal and conventional designs.

	Fig.6	Fig.7	Fig.8
ω_1	1.426	0.857	1.259
	(1)	(1)	(1)
ω_2	1.772	1.264	1.690
	(1)	(1)	(1)
ω_3	1.896	1.515	2.159
	(1)	(1)	(1)
ω_4	2.540	2.239	2.406
	(1)	(1)	(1)
ω_5	2.581	2.243	2.481
	(1)	(1)	(1)
ω_6	2.656	2.528	2.520
	(1)	(1)	(1)

ω_7	2.809	3.139	2.599
	(1)	(1)	(1)
ω_8	2.827	3.191	2.728
	(1)	(1)	(1)

The optimal solution of the first nonzoro eigenfrequency maximization problem for the hexagan plate with unit area is illustrated in Fig.9.
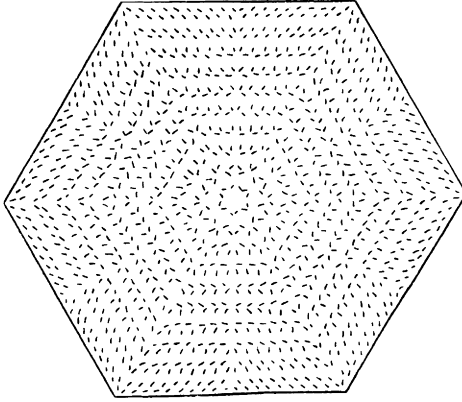
Fig.9 Optimal design of hexagan plate for planar vibrations.
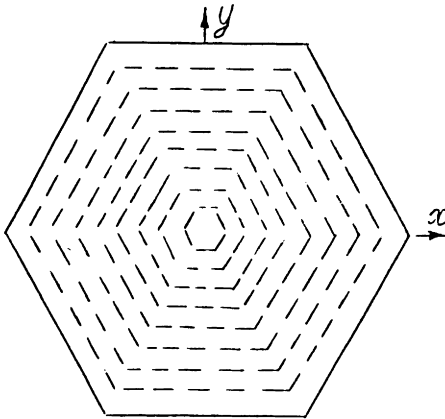
Fig.10 Conventional design of hexagan plate.
The multiplicity of the maximized functional $J_* = 1.988$ is

equals to *4*. The frequency spectrum of the plate with optimal distribution of orthotropy axes orientation is displayed in the first column of the Table.3. Next columns correspond to the plates with nonoptimal layouts shown respectively in Figs.10,11.
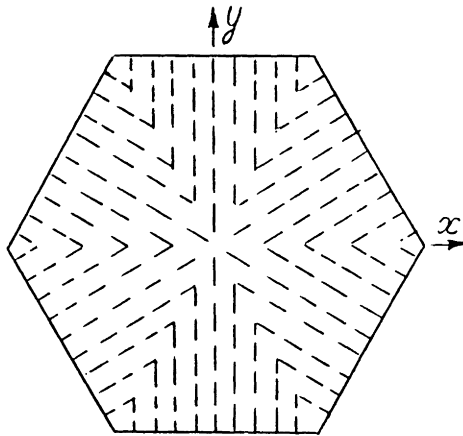
Fig.11 Conventional design of hexagan plate.

Note that in practical applications, questions concerning optimization of anisotropic properties arise not only in this pure form. We usually consider problems of finding the best shape of structural parts, usig materials with given anisotropic properties, so we need optimize simultaneously the shape and orientation of the axes of anisotropy for the elastic structures (Banichuk (1983)).

Note also that for layed composite plates and structures the combined optimization of thickness and anisotropic properties distributions is very perspectivi as was shawn by Pedersen (1991).

Table 3. Eigenfrequencies of planar vibrations for hexagan plates with optimal and conventional designs.

	Fig.9	Fig.10	Fig.11
ω_1	1.988	1.788	1.734
	(4)	(2)	(2)

ω_2	2.632	2.417	1.859
	(1)	(2)	(2)
ω_3	2.929	2.541	2.342
	(2)	(1)	(1)
ω_4	2.982	2.743	2.528
	(1)	(1)	(1)
ω_5	3.049	3.021	2.629
	(1)	(1)	(1)
ω_6	3.696	3.436	3.181
	(1)	(2)	(1)
ω_7	3.973	3.787	3.330
	(2)	(1)	(1)

4. REFERENCES.

1 Banichuk,N.V.:Optimization of anisotropic properties of deformable media in the framework of tho-dimensional theory of elasticity. Izv. Akad.Nauk SSSR,MTT,1,(1979) p.71-77.

2 Banichuk,N.V.: Problems and methods of optimal structural design. Plenum Press, New-York.(1983)

3 Landriani,G.S.; Rovati,M.: Optimal design for 2-D structures made of composite materials. ASME J.Engng. Mat. Techn.(to appear).(1991)

4 Pedersen,P.:On optimal orientation of orthotropic materials. Struct. Optim. 1,(1989) p. 101-106.

5 Pedersen,P.:Bounds on elastic energy in solids of orthotropic materials. Struct. Optim. 2,(1990) p. 55-63.

6 Pedersen, P.:On thickness and orientational design with orthotropic materials. Struct. Optim. 3,(1991) p. 69-78.

7 Seregin,G.A.;Troitskii,V.A. On the best position of elastic symmetry planes in an orthotropic body. Prikl. Matem.Mekhan.,45, 1,(1981) p.185-189.

8 Tomsen,J.: Optimization of composite discs. Struct. Optim.3,(1991) p. 89-98.

Optimal design based on power–law non–linear elasticity [1]

Pauli Pedersen[a] and John E. Taylor[b]

[a]Department of Solid Mechanics, The Technical University of Denmark, Denmark

[b]Department of Aerospace Engineering, University of Michigan, Ann Arbor, USA

Abstract

Many optimal design problems based on anisotropic elasticity have been solved in the recent years. However, like most of the results based on isotropic elasticity, linearity is assumed in these solutions. In the present paper we also treat the anisotropic models and furthermore extend to the non–linearities which can be modelled by the well–known power law.

Primarily we shall see, that these models return proportionality between strain energy density and stress energy density. This implies localized sensitivity analysis for the total strain energy and thus for a number of practical optimization objectives.

With localized sensitivity analysis we can extend the validity of the optimization criterion, known as uniform energy density. The optimal design will for these problems be a design with the same constitutive matrix at all points, and thus easy to analyze. The proven optimality criterion for the power–law non–linear elasticity "bridges" the now classical known solutions for linear elasticity and ideal plasticity. The result simply is, that the optimal design for this class of problems is independent of the power of non–linear elasticity.

1. INTRODUCTION

In contrast to the situation with linear systems, out of the various areas of interest in structural optimization relatively little is available in the form of general results for constitutively nonlinear systems. A most notable exception to this is the extensive set of classical work done in the area of optimal design relative to plastic collapse, dated mostly from the decade starting in the mid–1950s (the names Prager, Shield, and Drucker figure prominently in this subject; Martin (1975) provides an extensive listing for the era). Developments from this period were based on the specific model of a perfectly plastic solid material working in an isotropic and homogeneous system. (Modelling for structural optimization in fact reflects design for maximum collapse load). At the same time, clearly on practical grounds it would be useful to have a better understanding of analysis and design for more general anisotropic and nonlinear

---

[1] Dedicated to Professor Frithiof Niordson at his Seventieth anniversary.

materials. This is justified most simply on the basis that the behaviour of most ordinary engineering materials is distinctly nonlinear. Clearly knowledge of the means to predict optimal structural design in the face of material degradation nonlinearity would have immediate technical application as well.

As a step in the direction towards development of effective means for the treatment of constitutively nonlinear problems, we present results from a study of analysis and design related to a more rudimentary form of nonlinear material, namely materials with a 'power law' stress strain relation. Bell (1973) provides much information on the use since antiquity of this still common material model (identified there as 'Exponential Law'); his earliest citation is to work of James Bernoulli done in 1694! Relatively more contemporary applications of power law type models are given in Ramberg & Osgood (1943), Tvergaard (1983), and Ju and Kyriakides (1991), for example. The relation between this sort of modelling and reality is empirical, i.e., something realized essentially through curve–fitting, and it is a convenient form for such application. The work reported here is centered on the power law model for no better reason, i.e., it is used because the simplicity in its form provides conveniently for the kind of development undertaken in our study.

A number of independent, general results are obtained in connection with the modelling for optimal design of structures made of power law materials. In Section 2 the expressions for energy densities associated with this material are discussed, and a useful relation between strain energy density and complementary strain energy density is observed (this relates to earlier work on linear materials done by the first author (see e.g., Pedersen (1989), (1990), (1991)). The development of Section 3 provides for the evaluation of the design derivative of total strain energy in terms of local derivatives (sensitivities). These results are interpreted in the next section to express optimality conditions for certain single–purpose structural optimization problems. A recently developed extremum problem statement for the equilibrium analysis and design of constitutively nonlinear systems is extended to cover power law material; this is described in Section 5 and the results provide an independent confirmation of the optimality condition given earlier. Finally, results for several computational examples are given in Section 6.

2. CONSTITUTIVE MATRICES MODELLED BY POWER LAW NON–LINEARITY

The class of non–linear elastic problems that we shall treat is described by a power law stress–strain relation. In **two and three dimensional** problems we also need a scalar measure of the strain (or stress) state, termed the **effective strain**. To be specific let us first show the formulation in terms of strains.

With $[c]$ being a symmetric, positive definite and dimensionless matrix, the effective strain ϵ_e corresponding to the strain state $\{\epsilon\}$ (strain vector) is by definition

$$\epsilon_e^2 := \{\epsilon\}^T [c] \{\epsilon\} \tag{2.1}$$

The constitutive matrix that provides for the evaluation of the stress vector $\{\sigma\}$ is then

$$\{\sigma\} = \left[\frac{\epsilon_e}{\epsilon_0}\right]^{P-1} E_0[c]\{\epsilon\} = \epsilon_e^{P-1}E[c]\{\epsilon\} \tag{2.2}$$

where ϵ_0 , E_0 are strain and modulus for a **reference state** and to simplify the formulas we have defined $E := E_0/\epsilon_0^{P-1}$. The constitutive **secant matrix** that results thus is $\epsilon_e^{P-1}E[c]$.

The constitutive **tangent matrix** is obtained by differentials

$$\{d\sigma\} = (p{-}1)\epsilon_e^{P-2}E[c]\{\epsilon\}d\epsilon_e + \epsilon_e^{P-1}E[c]\{d\epsilon\} \tag{2.3}$$

and directly from (2.1)

$$\epsilon_e d\epsilon_e = \{\epsilon\}^T[c]\{d\epsilon\} \tag{2.4}$$

with $[c]$ being symmetric. Introducing (2.4) in (2.3) we have the differential relation

$$\{d\sigma\} = \epsilon_e^{P-1}E[c]\left[\frac{p-1}{\epsilon_e^2}\{\epsilon\}\{\epsilon\}^T[c] + [I]\right]\{d\epsilon\} \tag{2.5}$$

Now our primary interest is to determine the **strain energy density** u defined by its differential

$$du := \{\sigma\}^T\{d\epsilon\} \tag{2.6}$$

which by (2.2) and (2.4) is

$$du = \epsilon_e^{P-1}E\{\epsilon\}^T[c]\{d\epsilon\} = \epsilon_e^P E d\epsilon_e \tag{2.7}$$

This is easily integrated in terms of effective strain to find

$$u = \frac{E}{p+1}\,\epsilon_e^{P+1} \tag{2.8}$$

The **stress energy density** u^C is also defined by its differential

$$du^C := \{\epsilon\}^T\{d\sigma\} \tag{2.9}$$

and thus from (2.6) and (2.9) the total energy density is expressed as

$$u + u^C = \{\sigma\}^T\{\epsilon\} \tag{2.10}$$

This is written for our specific constitutive matrix (2.2) with (2.1) in the form

$$u + u^C = \epsilon_e^{P-1}E\{\epsilon\}^T[c]\{\epsilon\} = \epsilon_e^{P+1}E \tag{2.11}$$

which together with (2.8) leads to

$$u^C = \frac{pE}{p+1} \, \epsilon_e^{p+1} \qquad\qquad (2.12)$$

For the purpose of localized sensitivity analysis and for the interpretation later of an optimality criterion, **the important consequence** of the constitutive matrix is as read from (2.8) and (2.12), namely

$$\boxed{u^C = pu} \qquad\qquad (2.13)$$

i.e. the **ratio** between stress and strain energy densities is **constant** (independent of the energy level).

To complete the description for the present constitutive matrix, let us show the formulation in terms of effective stress. The power law is

$$\{\epsilon\} = \sigma_e^{n-1} \frac{1}{E^n} \, [c]^{-1}\{\sigma\} \qquad\qquad (2.14)$$

with the **effective stress** defined by

$$\sigma_e^2 := \{\sigma\}^T [c]^{-1}\{\sigma\} \qquad\qquad (2.15)$$

and thus the differential relation follows

$$\sigma_e d\sigma_e = \{\sigma\}^T [c]^{-1}\{d\sigma\} \qquad\qquad (2.16)$$

The differential of stress energy density by definition (2.9) is obtained using (2.14) and (2.16)

$$du^C = \sigma_e^{n-1} \frac{1}{E^n} \{\sigma\}^T [c]^{-1}\{d\sigma\} = \sigma_e^n \, d\sigma_e \frac{1}{E^n} \qquad\qquad (2.17)$$

and by integration the expression for complementary strain energy density is

$$u^C = \frac{1}{n+1} \sigma_e^{n+1} \frac{1}{E^n} \qquad\qquad (2.18)$$

Given that

$$n = 1/p \qquad\qquad (2.19)$$

the stress energy densities (2.12) and (2.18) agree, with the relation between effective stress and effective strain

$$\sigma_e = E \, \epsilon_e^p \qquad\qquad (2.20)$$

The reference stress in the formulation (2.14) is the modulus E. Assume that at a given stress level $\sigma_e = \sigma_0$ the constitutive secant matrix is given by

$$\{\epsilon\}_{\sigma_e=\sigma_0} = \frac{1}{E_0} [c]^{-1}\{\sigma\} \tag{2.21}$$

Then according to (2.14)

$$\sigma_0^{n-1}\frac{1}{E^n} = \frac{1}{E_0} => E = E_0^{1/n}\sigma_0^{(n-1)/n} = E_0^p\sigma_0^{1-p} \tag{2.22}$$

which together with the definition in (2.2) of $E = E_0\epsilon_0^{1-p}$ leads to the relations

$$\sigma_0 = E_0\epsilon_0 \tag{2.23}$$

3. LOCALIZED SENSITIVITY ANALYSIS

Our goal is to determine dU/dh, where U is the **total strain energy** and h is some design parameter. Even when the design parameter h_e is a **local design parameter**, related to design domain e, strain energy outside this domain is changing and thus one would expect an accumulative determination of dU/dh_e to be necessary. However, for the class of constitutive models described in section two we can prove that a localized calculation is possible.

Using the result (2.13) of constant ratio p between strain and stress energy densities the total strain energy U and complementary strain energy U^C satisfy

$$U + U^C = (1+p)U \tag{3.1}$$

Also, for a dead load system where the external potential is $-W$ we have

$$W = (1+p)U \tag{3.2}$$

Note that the argument is made without reference to a specific model and is thus valid for one–, two– and three–dimensional models, for analytical calculation. For numerical modelling it is valid independent of the numerical method chosen, say finite difference, finite element, or global (Galerkin) approaches.

Now, as (3.2) is valid also for the changed design it follows that

$$\frac{dW}{dh} = (1+p)\frac{dU}{dh} \tag{3.3}$$

which can be written with the "direct" and "indirect" terms separated as

$$\frac{\partial W}{\partial h} + \frac{\partial W}{\partial \epsilon}\frac{d\epsilon}{dh} = (1+p)\left[\frac{\partial U}{\partial h} + \frac{\partial U}{\partial \epsilon}\frac{d\epsilon}{dh}\right] \tag{3.4}$$

The strain symbol ϵ in (3.4) represents the **strain field in total**. Then using from the virtual work principle

$$\frac{\partial W}{\partial \epsilon} = \frac{\partial U}{\partial \epsilon} \tag{3.5}$$

and assuming **design independent loads** $\partial W/\partial h = 0$, we can obtain from (3.4)

$$\frac{\partial U}{\partial \epsilon} \frac{d\epsilon}{dh} = \frac{-(1+p)}{p} \frac{\partial U}{\partial h} \qquad (3.6)$$

Using this result to eliminate the "indirect" effect, the derivative dU/dh is expressed as

$$\frac{dU}{dh} = -\frac{1}{p} \left[\frac{\partial U}{\partial h}\right]_{\substack{\text{fixed} \\ \text{strains}}} \qquad (3.7)$$

which for linear elasticity (i.e., $p = 1$) reduces to the well–known result $dU/dh = -(\partial U/\partial h)_{\substack{\text{fixed} \\ \text{strains}}}$, see [6].

The result (3.7) is to be applied to the case of a local design variable h_e . The total strain energy is written as the sum of the domain strain energies U_i , i.e.

$$U = \sum_i U_i \qquad (3.8)$$

and so the derivative with respect to local change is stated

$$\frac{dU}{dh_e} = \frac{dU_e}{dh_e} + \sum_{i \neq e} \frac{dU_i}{dh_e} \qquad (3.9)$$

Also, (3.7) provides

$$\frac{dU}{dh_e} = -\frac{1}{p} \left[\frac{\partial U_e}{\partial h_e}\right]_{\substack{\text{fixed} \\ \text{strains}}} \qquad (3.10)$$

It is **important to note** that the last part of (3.9) is not zero so the **local physical change** in strain energy is not easily determined

$$\frac{dU_e}{dh_e} \neq -\frac{1}{p} \left[\frac{\partial U_e}{\partial h_e}\right]_{\substack{\text{fixed} \\ \text{strains}}} \qquad (3.11)$$

even though the change in total strain energy is available via (3.10).

The important result (3.10) is not intuitive understandable, and therefore some elaborating on its use may be justified. Often the strain energy will be expressed in terms of the strain energy density u_e and its corresponding volume V_e , i.e.

$$U_e = u_e V_e \qquad (3.12)$$

It is practical to treat two groups of design parameters, i.e. the ones without influence on V_e , say constitutive parameters, and the ones without **explicit** influence on u_e , say thickness or density parameters. Taking θ_e as representative of the first group, from (3.10) with (3.12) the derivatives with respect to local change is given by

$$\frac{dU}{d\theta_e} = \frac{-V_e}{p}\left[\frac{\partial u_e}{\partial\theta_e}\right]_{\substack{fixed \\ strains}} \tag{3.13}$$

For the second, with t_e as a representative design parameter the derivative is expressed as

$$\frac{dU}{dt_e} = \frac{-u_e}{p}\left[\frac{\partial V_e}{\partial t_e}\right] \tag{3.14}$$

with the last term often being equal to V_e/t_e (eventually with an integer constant).

4. SIMPLE OPTIMALITY CONDITIONS

Two classes of optimal design problems will result in simple optimality criteria. The first class is the unconstrained problems and the second class only involve a single constraint. Combining this with our local sensitivity analysis we obtain results that can serve directly as basis for an optimization procedure.

The **unconstrained** problems can be exemplified by the material orientation as design variable, say in domain e the parameter θ_e. The necessary condition for a stationary (optimal) total strain energy is then

$$dU/d\theta_e = 0 \text{ for all the domains e} \tag{4.1}$$

Applying the localized result (3.13) this is transformed to the much simpler **local criterion**

$$\partial u_e/\partial\theta_e = 0 \text{ for all the domains e} \tag{4.2}$$

and a iterative procedure can now be set up to find solutions that satisfy this condition. Details and discussion about local/global minimum/maximum are given in [7].

The **single constraint** problems, which is the main interest for this paper, are exemplified by thickness distribution as design variable, and material relative density can be treated similarly. The specific problem statement is to minimize the total strain energy for given structural volume $\bar{V}$:

$$\text{Minimize } U = U(t_e) \text{ for } V = \Sigma V_e(t_e) = \bar{V} \tag{4.3}$$

The well–known optimality criterion with a single constraint is a **constant ratio of the gradients** for all the design parameters t_e, i.e. with constant A

$$\frac{dU/dt_e}{dV/dt_e} = A \text{ for all } e \tag{4.4}$$

Using our localized result (3.14) this can be stated

$$\frac{-\frac{1}{p}\,u_e(\partial V_e/\partial t_e)}{(\partial V_e/\partial t_e)} = A \tag{4.5}$$

and therefore the result (well–known from linear elasticity and from ideal plasticity) of **constant energy density** equal to the mean energy density $\bar{u}$

$$u_e = \bar{u} \ \text{ for all } \ e \tag{4.6}$$

For linear elasticity we refer this result back to Wasiutynski (1960) and for ideal plasticity to Prager and Shield (1967) (see the discussion in Martin (1975)).

With uniform energy density (4.6), we get uniform effective strain as it follows from (2.8), and then by (2.2) uniform constitutive secant matrix. Thus **the optimal thickness distribution is independent of the power p of the constitutive matrix**. To state it in other terms: the optimal structure is equally loaded (in terms of strain energy density) at all points. The proven optimality criterion (4.6) "bridges" the classical solutions for linear elasticity and ideal plasticity.

Solutions which satisfy (4.6) may correspond to maximum or minimum or just to stationarity. Furthermore, the extremum may be local or global. Lastly, the existence of a design satisfying (4.6) is not proven, and a procedure for obtaining such a possible solution still has to be described. The procedure used normally is **iteratively to redesign** independently but simultaneously

$$(t_e)_{next} = t_e + \Delta t_e \tag{4.7}$$

The unknown optimal mean energy density $\bar{u}$ is approximated by the present mean energy density $\tilde{u}$. Furthermore we assume the domain total energy U_e to be constant through the redesign and then determine Δt_e from

$$\frac{U_e}{V_e(1+\Delta t_e/t_e)} = \bar{u} \ \text{ or } \ \Delta t_e = t_e(u_e-\tilde{u})/\tilde{u} \ \text{ or } \ (t_e)_{next} = t_e u_e/\tilde{u} \tag{4.8}$$

A relaxation power, say 0.8, is normally introduced in the procedure; that is important and works effectively especially in the first iterations.

5. OPTIMALITY CONDITIONS VIA AN ALTERNATIVE APPROACH

As indicated in the introduction, we seek through the developments described in this section to substantiate via an independent approach the form of the optimality conditions associated with the 'minimum compliance design' of structures made up of power law material. To facilitate the description of the design problem, the structural mechanics analysis is first cast in an unconventional way as an extremum problem expressed in terms of mixed stress and deformation variables. This statement of the analysis part of the problem comprises an extension of earlier works (Taylor (1992a), or for the continuum Taylor (1992b)) covering analysis of structures where a softening local or material constitutive character is represented to be arbitrary polygonal. Also, the analysis in the form given here is slightly more general than what is required for the simple power law material in that it accommodates degradation into an unstable state. The development is presented as a formalism; however, an interpretation within the context of results in the mathematics of nonlinear programming problems provides means to appreciate that the modelling is authentic according to familiar requirements for equilibrium analysis. This confirmation is covered partly in what follows.

For the sake of simplicity in the presentation, the development is described here as it applies to the analysis of arbitrary trussed structures (the counterpart modelling for analysis of continua is directly available in similar form). Total stress τ_i of the ith truss member is represented in terms of constituents ϵ_i and σ_i in a way that can be described in the form:

$$\tau_i = - E_i \epsilon_i + \sigma_i \quad (i = 1,2,...M) \tag{5.1}$$

where

$$|\sigma_i| = \begin{cases} C|\epsilon_i|^P & \text{for} \quad \sigma_i < \bar{\sigma}_i \ ; \ p \leq 1 \\ \bar{\sigma}_i & \text{otherwise} \end{cases}$$

and constants E_i, p, c, and $\bar{\sigma}_i$ represent material parameters. Given that these parameters are identified member by member, the model covers arbitrarily inhomogeneous structural systems. (In order that the construction (5.1) is admissible on physical grounds, certain restrictions apply, e.g., that for $\epsilon_i > 0$ and $\sigma_i > 0$, $\tau_i > 0$). The possibility of constitutive instability in this model is identified with the negative term in (5.1). Also, it is by virtue of the presence of this term that a 'mixed form' representation of the mechanics results. The qualitative character of the constituent stress σ_i is as shown in Figure 5.1a, and the typical form for total stress τ_i of (5.1) is given in Figure 5.1b. Reference is made later to the quality that in the case $E_i = 0$ and $\bar{\sigma}_i > \infty$ for all i, (5.1) reduces to the form of a simple power law.
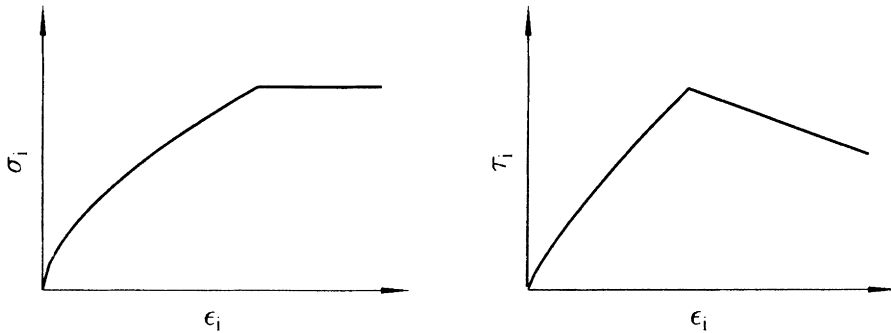
Figure 5.1. Typical form for stress constituent σ_i and total stress τ_i.

The issue of algebraic sign in the expression for constituent σ_i, left open in the statement of (5.1), is resolved by use of the notion of the positive part, say s_i, of the stress sigma defined as:

$$s_i := \max\{\sigma_i , 0\} \tag{5.2a}$$

With this term defined, the negative part, say t_i, of sigma is given by:

$$t_i := - (\sigma_i - s_i) \tag{5.2b}$$

and note that $s_i \geq 0$; $t_i \geq 0$; $s_i t_i = 0$ and $\sigma_i = s_i - t_i$. In other words, the original stress constituents σ_i is now represented by the two semi–definite components s_i and t_i , and this representation is particularly convenient for the expression of the extremum problem to be given below. The expression of complementary strain energy density associated with σ_i is needed for that purpose as well; it is from (2.18)

$$u_i^c = \hat{C}\left[s_i^{(1+1/p)} + t_i^{(1+1/p)}\right] \quad \text{where} \quad \hat{C} = \frac{p}{1+p}\left[\frac{1}{C}\right]^{1/p}$$

The method given in the references cited at the beginning of this section for the mathematical modelling of equilibrium problems for constitutively nonlinear systems is to be applied in the present case, i.e., for systems with the local constitutive properties associated with (5.1). This equilibrium analysis is covered by the nonlinear programming problem:

$$\max_{\alpha, s_i, t_i, \epsilon_i} \alpha \qquad\qquad [P]$$

subject to:

$$-\sum_{i=1}^{M} B_{\gamma i} A_i \ell_i (-E_i \epsilon_i + s_i - t_i) + \alpha q_\gamma = 0 \qquad (\gamma = 1,2,...N)$$

$$A_i \ell_i (s_i - \bar{\sigma}_i) \leq 0$$

$$A_i \ell_i (t_i - \bar{\sigma}_i) \leq 0$$

$$A_i \ell_i (-s_i) \leq 0 \qquad\qquad (i = 1,2,...M)$$

$$A_i \ell_i (-t_i) \leq 0$$

$$\sum_i A_i \ell_i \left\{ -E_i \epsilon_i^2/2 + \hat{C}\left[s_i^{(1+1/p)} + t_i^{(1+1/p)}\right]\right\} - \bar{U} \leq 0$$

$$-\sum_i A_i \ell_i \left\{ -E_i \epsilon_i^2/2 + \hat{C}\left[s_i^{(1+1/p)} + t_i^{(1+1/p)}\right]\right\} \leq 0$$

Load state is measured via the single load factor α , i.e., the equilibrium equation reflects proportional loading. Quantities $B_{\gamma i}$, A_i , E_i , q_γ , $\bar{\sigma}_i$, $\hat{C}$, p , and $\bar{U}$ in [P] are data. Note that the first constraint equations correctly reflect equilibrium requirements so long as $\sigma_i = s_i - t_i$ and so on per (5.2). In fact it is a novel aspect of the present type of formulation that the characteristics by which s_i , t_i are defined in (5.2) are implicit in the extremum problem statement [P] ; this is verified below.

In the interpretation of the Kurash–Kuhn–Tucker conditions that follows, vectors λ_γ , μ_i , ν_i , η_i and ζ_i represent Lagrange multipliers associated with the first five constraints respectively of [P] ; the multiplier on the next to last constraint is taken to have value unity, without loss of generality, and the one for the last constraint generally has value zero. The conditions for stationarity with respect to ϵ_i , s_i , and t_i

are in order:

$$\sum_\gamma B_{\gamma j}\lambda_\gamma - \epsilon_j = 0 \tag{5.3}$$

$$-\sum_\gamma B_{\gamma j}\lambda_\gamma + \mu_j - \eta_j + (s_j/C)^{1/p} = 0 \tag{5.4}$$

$$\sum_\gamma B_{\gamma j}\lambda_\gamma + \nu_j - \zeta_j + (t_j/C)^{1/p} = 0 \tag{5.5}$$

$$(j = 1,2,...M)$$

Using (5.3) to eliminate λ_γ from (5.4) and (5.5) produces

$$\mu_j - \eta_j + (s_j/C)^{1/p} = \epsilon_j \tag{5.6}$$

$$\nu_j - \zeta_j + (t_j/C)^{1/p} = -\epsilon_j \tag{5.7}$$

Considering the reduction from (5.6) and (5.7) for the case $(s_i, t_i < \bar{\sigma}_i) \rightarrow (\mu_i, \nu_i = 0)$, suppose that $s_j > 0$ which implies $\eta_j = 0$. Then from (5.6)

$$(s_j/C)^{1/p} = \epsilon_j$$

If at the same time $t_j > 0$ implying $\zeta_j = 0$, (5.7) requires

$$(t_j/C)^{1/p} = -\epsilon_j$$

which is a contradiction. Thus $s_j > 0 \rightarrow t_j = 0$. Of course the converse result follows by similar argument, i.e., $t_j > 0 \rightarrow s_j = 0$, so that the orthogonality $s_j t_j = 0$ is established. It follows as well once the orthogonality is available that $(s_j > 0) \rightarrow (\epsilon_j > 0)$ and $(t_j > 0) \rightarrow (\epsilon_j < 0)$. To complete this part of the interpretation, note that $(\mu_j > 0) \rightarrow (s_j = \bar{\sigma}_j) \rightarrow (\eta_j = 0)$ whence from (5.6)

$$\mu_j = \epsilon_j - (\bar{\sigma}_j/C)^{1/p}$$

This simply provides for the evaluation of multiplier μ_j; the expression for ν_j follows from (5.7) in the same way, for the case $(\nu_j > 0) \rightarrow (t_j = \bar{\sigma}_j)$. Before turning to treat the structural optimization problem, as an observation on the analysis represented via [P] note that for value $\bar{\sigma}_i$ specified sufficiently large while all other data are fixed, the stress bound constraints are not active. In this case the net constitutive character corresponds to a smooth curve such as the one shown in Figure 5.2. The characteristic value $\hat{\epsilon}$ at which the stress–strain curve turns downward is evaluated from the condition
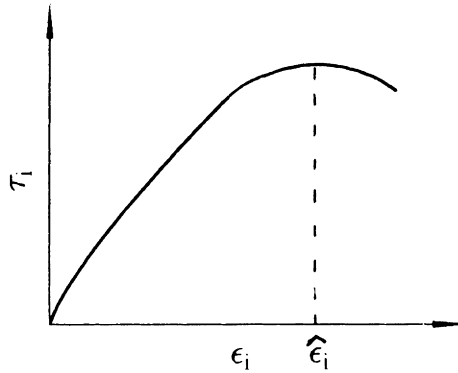
Figure 5.2. Total stress τ_i vs. strain/ $\bar{\sigma}_i$ large.

$$\text{Arg}\left[\frac{d\tau}{d\epsilon} = 0\right] = \hat{\epsilon} \quad \text{whereby} \quad (\text{for } \epsilon > 0) \quad \hat{\epsilon}_i = (E_i/pC)^{1/(p-1)} .$$

The design problem, which models the optimal material distribution for the single–purpose design of a truss of given layout, is expressed as a direct extension of the analysis problem $[P]$. The goal is to maximize load factor α with respect to the vector A_i of member section areas, within the (usual) design constraints that reflect a bound on total volume of structural material and a lower limit on section areas. The problem is stated:

$$\begin{array}{c} \max_{A_i} \ (\max \ \alpha) \\ < \text{constraints as in } [P] > \end{array} \qquad [D]$$

$$\ell_i(\underline{A} - A_i) \leq 0 \quad (i = 1,2,...)$$

$$\sum_{i=1}^{M} A_i\ell_i - R < 0$$

Values $\underline{A}$ and R are added to the list of data. Stationarity with respect to design requires

$$-\sum_{\gamma} B_{\gamma j}\left(-E_j\epsilon_j + s_j - t_j\right)\lambda_\gamma \tag{5.8}$$

$$+ \left\{-E_j\epsilon_j^2/2 + \hat{C}\left[s_j^{(1+1/p)} + t_j^{(1+1/p)}\right]\right\} = -\Gamma + \gamma_j$$

Complementarity conditions associated with the four stress constraints are already taken into account. The optimality condition is simply the reduced form of (5.8) for the subset, say J_D , of all members identified with $(A_j > \underline{A}) \to (\gamma_j = 0)$. With the further interpretation of this set into subsets J_+ and J_- of J_D , identified with tension and compression members respectively, after simplification using (5.3)–(5.5) the optimality conditions have the form:

$$- E_j \epsilon_j^2 / 2 + \left[\frac{1}{C}\right]^{1/p} \frac{1}{1+p} s_j^{(1+1/p)} = \Gamma \quad (j \in J_+) \qquad (5.9)$$

$$- E_j \epsilon_j^2 / 2 + \left[\frac{1}{C}\right]^{1/p} \frac{1}{1+p} t_j^{(1+1/p)} = \Gamma \quad (j \in J_-) \qquad (5.10)$$

For the special case $E_i = 0$ for all i, (5.9) and (5.10) in effect confirm the earlier optimality condition (4.6), namely that for the optimal design energy density has constant value over members (elements) in the design set. As noted in Section 4, it is striking to find that this simple result applies over the full range of mechanical behaviour.

A part of the construction of the nonlinear programming problem [P] , namely the superposition of constituents per (2.1) to form total stress, has appeared before in connection with different applications in the mechanics of nonlinear media (see e.g. the discussion by Besseling (1984)). It appears that there is significant potential for further development along the lines of the extremum problem formulation exemplified by the material of this section, within which use is made of this device. Also, there are several open questions remaining even in the context of the formulation given here. The challenging issue related to existence of a solution to (5.9)–(5.10) has not been considered, for example. Note also that with the introduction of local (i.e. material) instability as represented in the present model for analysis, issues of global stability of the structural system must be addressed. It is sufficient for the purposes of the above presentation to suppose that attention is limited to globally stable problems (this would be the case with values E_j sufficiently small, for example).

6. TWO–DIMENSIONAL EXAMPLES

Results from iterative analysis based on the constitutive relation (2.2) of section 2, and optimization based on the optimality criterion (4.6) of section 4 are presented for the three cases shown in Figure 6.1.

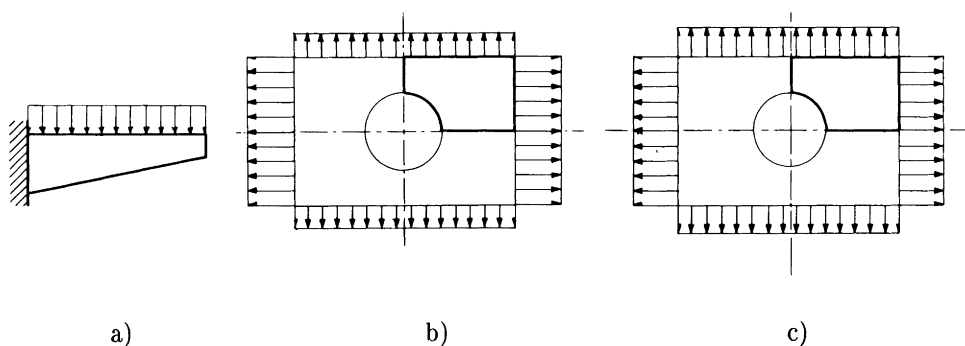a)   b)   c)

Figure 6.1: The three example cases: a) uniformly loaded cantilever of isotropic material. b) circular hole loaded biaxially 2:1 , isotropic material. c) optimal (see [8]) hole loaded biaxially 3:2 , orthotropic material.

The main result of section 4, is that the optimal thickness distribution is independent of the power p. Thus the results for the problems of Figure 6.1 mainly illustrates the influence from the power p on two given designs, i.e. the uniform thickness design and the optimal thickness design as obtained from linear elasticity, see [7] for a discussion of the optimization procedure, which is a simple recursive iteration procedure.

In terms of relative values table 6.1 gives the strain energy densities. Min., mean and max. values are related to the elements of the finite element models. The table clearly shows the different results from uniform and optimal thickness distribution. It is well known from optimization based on linear elasticity that certain areas in a model cannot be fully stresses (too little energy density). Thus the min. values are of minor interest, and the agreements of the max. values with the mean values better show the fulfillment of the optimality criterion (4.6).

The values of the objective function (work = compliance = $(1+p)$ × strain energy) are also given by the relative mean values in table 6.1, and shown in Figure 6.2. The factor between energy in uniform design and energy in optimal design is almost constant for the three cases, with a weak tendency to be more and more important with increasing

	Strain energy densities in % of reference energy density								
	cantilever, isotropic			circ. hole, isotropic			opt. hole, orthotropic		
	min	mean	max	min	mean	max	min	mean	max
$U_{1.0}$	0.5	**100**	577	4	**100**	677	47	**100**	387
$O_{1.0}$	14	**50**	**50**	81	**87**	**89**	59	**90**	92
$U_{0.9}$	0.7	163	935	4	140	951	60	138	528
$O_{0.9}$	23	**75**	**76**	112	**120**	**122**	63	**123**	**138**
$U_{0.8}$	0.9	280	1599	3	202	1391	79	196	737
$O_{0.8}$	39	**120**	**121**	159	**170**	**173**	69	**173**	**221**
$U_{0.7}$	1	512	2916	2	304	2127	108	288	1060
$O_{0.7}$	68	**201**	**202**	236	**251**	**256**	80	**253**	**369**
$U_{0.6}$	2	1005	5730	0.3	482	3430	153	445	1581
$O_{0.6}$	126	**357**	**359**	365	**387**	**394**	90	**385**	**641**
$U_{0.5}$	2	2151	12310	0.1	808	5891	227	722	2464
$O_{0.5}$	251	**683**	**686**	595	**630**	**640**	107	**618**	**1169**

Table 6.1: Table of relative results with uniform thickness U and with optimal thickness distribution O for linear elasticity $(p = 1)$ and for five models of non–linear elasticity modelled by the power $p < 1$. The three independent cases are shown in Figure 6.1.

non–linearity (decreasing p) . The stronger effect for the cantilever problem reflects the initial less uniform stress/strain distribution. Also the actual stress/strain level (higher for the cantilever problem) will have an influence, and thus the three cases should be read as individual cases. More detailed information are obtainable in stress/displacement/strain graphs, omitted in this short paper.

We note that the small difference between mean and maximum density (90 and 92) for the orthotropic case has a strong influence for the non–linear solutions (at p = 0.5 the values are 618 and 1169).
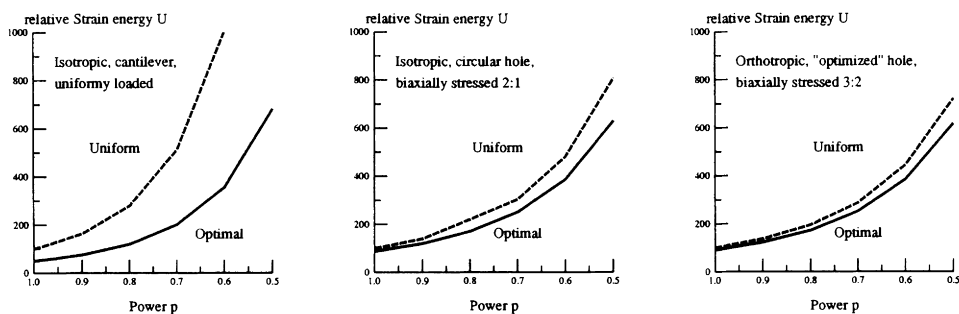

Figure 6.2: Resulting objectives with uniform thickness and with optimal thickness distribution for the three cases.

REFERENCES

1   Bell, James F. (1973),   Mechanics of Solids – Vol. I/The Experimental Foundations of Solid Mechanics, Springer–Verlag, Germany.

2   Besseling, J.F. (1984),   Models of Metal Plasticity: Theory and Experiment, in Plasticity Today, (A. Sawczuk and G. Bianchi, eds.), Elsevier–London & New York.

3   Ju, G.T. and Kyriakides, S. (1991),   Bifurcation Buckling Versus Limit Load Instabilities of Elastic–Plastic Tubes Under Bending and External Pressure, J. Offshore Mechanics and Arctic Engrg., Vol. 113, pp. 43–52.

4   Martin, J.B. (1975),   Plasticity: Fundamentals and General Results, The MIT Press, Cambridge, Massachusetts.

5   Pedersen, P. (1989),   On Optimal Orientation of Orthotropic Materials, Structural Optimization, Vol. 1, pp. 101–106.

6   Pedersen, P. (1990),   Bounds on Elastic Energy in Solids of Orthotropic Materials, Structural Optimization, Vol. 2, pp. 55–63.

7   Pedersen, P. (1991),   On Thickness and Orientational Design with Orthotropic Materials, Structural Optimization, Vol. 3, pp. 69–78.

8   Pedersen, P., Tobiesen, L. and Jensen, S.H. (1992), Shapes of Orthotropic Plates for Minimum Energy Concentration, Mechanics of Structures and Machines, Vol. 20, No. 4.

9   Prager, W. and Shield, R.T. (1967), A General Theory of Optimal Plastic Design, J. Appl. Mech., Vol. 34, 184.

10 Ramberg, W. and Osgood, W.R. (1943), Description of Stress–Strain Curves by Three Parameters, NACA Tech. Note 902.

11 Taylor, J.E. (1992a), Truss Topology Design for Elastic/Softening Materials, to appear in Proc. NATO Advanced Research Workshop: Topology Design of Structures, Sesimbra, Portugal, June 20–26, 1992, Kluwer Publishers.

12 Taylor. J.E. (1992b), A Global Extremum Principle for the Analysis of Solids Composed of Softening Material, publication pending.

13 Tvergaard, V. (1983), On the Transition From A Diamond Mode to An Axisymmetric Mode Collapse in Cylindrical Shells, Int. J. Solids Structures, Vol. 19, No. 10, pp. 845–856.

14 Wasiutynski, Z. (1960), On the Congruency of the Forming According to the Minimum Potential Energy with that According to Equal Strength, Bull. de L'Academie Polonaise des Sciences, Serie des sciences technique, Vol. VIII, No. 6, pp. 259–268.

OPTIMAL DESIGN WITH HIGHLY DEFORMABLE MATERIALS

Michał Życzkowski, Krzysztof Szuwalski
Cracow University of Technology - Poland

1. INTRODUCTION

Optimal design of structures is always a design on the edge of safety domain. Therefore, when large deformations may be expected, they must be taken into account. If not, it may turn out that construction designed as an optimal one, does not satisfy strength conditions after deformations. In such problems, we must resign of the rigidification principle (geometry changes must be allowed for), and finite strain theory must be applied.

Such an approach becomes necessary, when problem of ductile rupture in creep conditions is investigated. Discussing the optimal design of structures with respect to ductile creep rupture time, we must follow the whole creep process from its beginning till the rupture, understood, according to the Hoff's approach, as diminishing of transversal dimensions to zero.

The solution is much simpler, when as an objective, the time to brittle rupture is treated. Then the small strain theory is sufficient, and optimal shapes often coincide with shapes of uniform strength [4]. The review of various possible criteria in optimization of structures under creep conditions was given by Życzkowski [3].

Hoff's theory of ductile creep rupture describes fairly well the loss of carrying capacity for structural elements subject to uniaxial or biaxial tension, like bars, disks or shells in membrane state. So, these elements may be optimized for maximal ductile creep rupture time. In the present paper we show the problem, namely basic definitions, theorems and particular solutions, on the example of rotating disks.

The aim of present paper is to investigate whether shapes of uniform strength for rotating disks are optimal with respect to ductile creep rupture time. The results for bars under nonuniform tension [2] show, that

only in case of body forces depending on the material coordinate such a co-incidence exists. For body forces depending on the spatial coordinate (e.g. in rotating bars), the shape of uniform strength may be improved in order to obtain longer life-time to ductile rupture.

2. DISKS OF UNIFORM STRENGTH AND UNIFORM DEFORMABILITY

Discussing problem of uniform strength for disks made of material allowing for large deformations, we must distinguish several types of such disks. The definitions given below are formulated for full disks made of homogeneous material.

In these definitions, as in the whole paper, by capital letters are denoted parameters of undeformed disk (for t=0) and material (Lagrangean) coordinate, while all quantities connected with current configuration of already deformed disk and spatial (Eulerian) coordinate are denoted by small letters.

Def.1.The disks of uniform initial strength in a broader sense are the disks in which at the beginning of the creep process (t=0), the redu-ced stress calculated according to the chosen failure hypothesis, is the same for all radii.

$$\bigwedge R \in <0, R_o> \qquad \Sigma_{red}(R) = \text{const.} \qquad (1)$$

Def.2.The disks of uniform initial strength in a narrower sense are the disks in which at the beginning of the creep process, both: radial and circumferential stresses are equal, the same and independent of radius.

$$\bigwedge R \in <0, R_o> \qquad \Sigma_r = \Sigma_\vartheta = \text{const}(R) \qquad (2)$$

Def.3.The disks of uniform strength with respect to the ductile rupture time, are the disks in which the stage of ductile rupture (according to the Hoff's approach, i.e. diminishing of thickness to zero), is reached simultaneously in the whole disk.

$$\bigwedge R \in <0, R_o> \qquad\qquad h(R,t) \longrightarrow 0 \qquad\qquad (3)$$
$$t \rightarrow t_*$$

Def.4. *The disks of uniform deformability are the disks in which all strains are independent of radius, but changing in time.*

$$\bigwedge R \in <0, R_o> \qquad\qquad \varepsilon_i(R,t)=f(t) \qquad i=r,\vartheta,z \qquad (4)$$
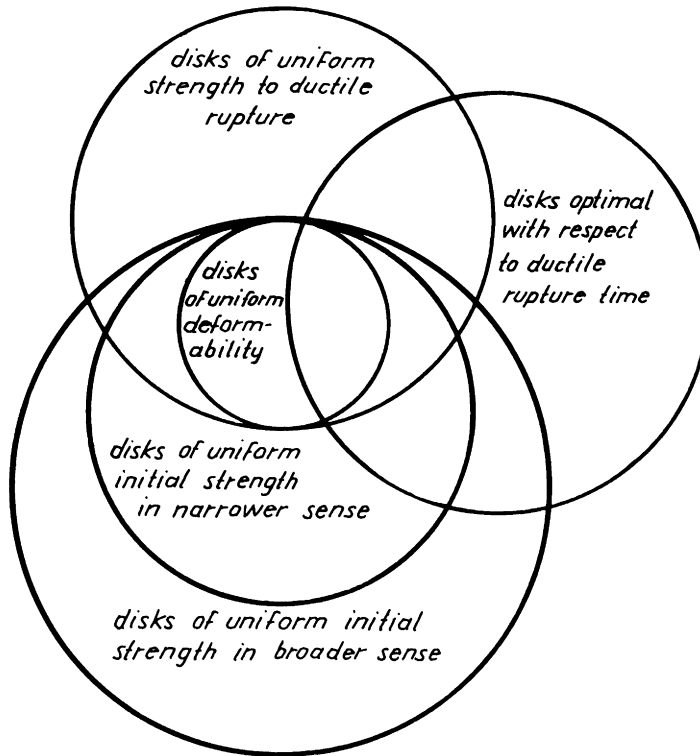
Fig. 1

Def.5.The optimal disk with respect to ductile rupture is the disk, which
for given volume of material V ensures the longest life-time to the
ductile creep rupture in Hoff's sense.

$$t_* \longrightarrow \max_{V = const} \qquad (5)$$

The relations among defined above disks are shown in Fig.1. The set of
disks optimal with respect to ductile creep rupture time may partially con-
tain all others above mentioned types of disks.

3.UNIFORM DEFORMABILITY OF DISKS OF UNIFORM STRENGTH

We shall closely investigate disks of uniform deformability, as they
are always disks of uniform strength with respect to the ductile rupture.
Therefore, they will not much differ from the optimal disks, and even some-
times may be optimal. We shall specify conditions, under which homogeneous,
isotropic, full disk will show the property of uniform deformability.

Thesis 1.The full disk of uniform initial strength in the narrower sense,
under assumptions:
    (1) material is incompressible;
    (2) body force in the disk is a homogeneous function of any degree
       m of spatial coordinate r (and/or any function of material
       coordinate R);
    (3) total radial force at the outer edge of disk is also a homoge-
       neous function of the same degree m, of Eulerian outer radius;
    (4) material is homogeneous and isotropic;
    is the disk of uniform deformability.

We shall prove this thesis, showing that assumption of uniform defor-
mability:

$$r = R \, \psi(t) \, , \qquad (6)$$

does not lead to any contradictions and fulfills all basic equations.

From the assumption *(1)*:

$$H\ R\ dR = h\ r\ dr \qquad (7)$$

where H stands for the initial and h for current thickness of the disk, taking into account (6) we find:

$$h(R,t) = \frac{H(R)}{\psi^2(t)} \qquad (8)$$

Relationship between the current and the initial radial body force, according to the assumption *(2)*, can be written:

$$b_r(r.R) = \psi^m\ B_r(R,R)\ . \qquad (9)$$

In the most frequent case of body forces - for the rotating disk, m = 1.

To the similar relation between current and initial values of total radial force at the outer edge leads the assumption *(3)*:

$$n_r(r) = \psi^m\ N_r(R)\ . \qquad (10)$$

For the homogeneous material (assumption *(4)*) in the disk of uniform initial strength in the narrower sense, radial and circumferential stresses are for t=0 the same in the whole disk

$$\Sigma_r = \Sigma_\vartheta = \Sigma = \text{const}(R)\ , \qquad (11)$$

The third stress, perpendicular to the middle surface of disk, is assumed to vanish thoughout the creep process.

From the condition of internal equilibrium for undeformed disk:

$$\frac{1}{H}\frac{d}{dR}\ (H\ \Sigma_r) + \frac{\Sigma_r - \Sigma_\vartheta}{R} + B_r(R,R) = 0\ , \qquad (12)$$

after substitution of (11), we can determine the shape of disk of uniform initial strength:

$$H(R) = C \exp \left[-\frac{1}{\Sigma} \int B(R,R) \, dR \right] \, .$$ (13)

The integration constant C results from the boundary condition:

$$H (R_o) = H_o \, ,$$ (14)

where H_o denotes the thickness of the disk at the outer radius R_o, depending on the value of the radial force at the outer edge:

$$H_o = \frac{N_r (R_o)}{2 \, \pi \, R_o \, \Sigma} \, .$$ (15)

Finally we obtain the formula for the initial profile of the disk:

$$H(R) = H_o \exp \left[-\frac{1}{\Sigma} \int_{R_o}^{R} B(\rho,\rho) \, d\rho \right] \, ,$$ (16)

where ρ is the formal integration variable.

Now we shall check up the behaviour of so shaped disk, during the creep process. The condition of internal equilibrium for already deformed disk:

$$\frac{1}{h} \frac{\partial}{\partial r} (h \, \sigma_r) + \frac{\sigma_r - \sigma_\vartheta}{r} + b_r (r, R) = 0 \, ,$$ (17)

may be rewritten, making use of the assumption (1) of incompressibility:

$$\frac{r}{R \, H} \frac{\partial}{\partial R} (h \, \sigma_r) + \frac{\sigma_r - \sigma_\vartheta}{r} + b_r (r, R) = 0 \, ,$$ (18)

where σ_r and σ_ϑ are true stresses, and b_r denotes the current radial body force.

Making use of the assumption of uniform deformability (6) and of (8) and taking into account assumption (2) we obtain:

$$\frac{\psi(t)}{H} \frac{\partial}{\partial R} \left[\frac{\sigma_r \, H}{\psi^2(t)} \right] + \frac{\sigma_r - \sigma_\vartheta}{R \, \psi(t)} + \psi^m(t) \, B(R,R) = 0 \, .$$ (19)

Putting into this equation the shape of the disk of uniform initial strength (10), we can calculate the function $\psi(t)$:

$$\psi^{m+1}(t) = \frac{\sigma_r(R,t)}{\Sigma} - \frac{\sigma_r'(R,t)}{B(R,R)} - \frac{\sigma_r(R,t) - \sigma_\vartheta(R,t)}{B(R,R)} \ . \tag{20}$$

Because on the left-hand side we have only the function of time, to satisfy this equation, on the right-hand side the function of material co-ordinate R must vanish. This is possible only if

$$\sigma_r(R,t) = \sigma_\vartheta(R,t) = \Sigma\,\varphi(t) \ , \tag{21}$$

what means, that the disk must show the property of uniform strength in the narrower sense during the whole creep process, and from (20) results:

$$\varphi(t) = \psi^{m+1}(t) \ . \tag{22}$$

The boundary condition at the external radius for the deformed disk, takes the form:

$$h(r_o) = \frac{n_r(r_o)}{2\,\pi\,r_o\,\Sigma\,\psi^{m+1}} \ , \tag{23}$$

where r_o denotes the current external radius, $n_o(r_o)$ - current value of to-tal radial force on the outer edge. Comparing it with the boundary condi-tion at the beginning of creep (15) and taking into account (6) and (8), we come to the conclusion that the only way to avoid contradictions is to satisfy assumption (3) and resulting from it (10). In case of different be-haviour of the external loadings, streses in disk of uniform initial strength will differ during the creep process.

We can state that, that disk of uniform initial strength in the narro-wer sense, satisfying assumptions (1)÷(4), will preserve this property till the end of the creep process. For homogeneous and isotropic disks it will be the disk of uniform deformability, and therefore the disk of uniform strength with respect to ductile rupture. These results are independent

from the physical law.

The physical law will decide on the form of the function $\psi(t)$ and in this way on the time of ductile rupture. Consider this law in general form:

$$F(\sigma_{red}, \dot{\sigma}_{red}, \varepsilon_{red}, \dot{\varepsilon}_{red}; \ t) = 0 \tag{24}$$

as a relation of the reduced true stress and its rate, and reduced logarithmic strain and its rate, calculated according to chosen failure hypothesis.

Logarithmic strains are defined:

$$
\begin{aligned}
\varepsilon_r &= \ln \frac{\partial r}{\partial R} = \ln r' \\
\varepsilon_\vartheta &= \ln \frac{r}{R} \\
\varepsilon_z &= \ln \frac{h}{H}
\end{aligned}
\tag{25}
$$

and their rates:

$$
\begin{aligned}
\dot{\varepsilon}_r &= \frac{\dot{r}'}{r'} \\
\dot{\varepsilon}_\vartheta &= \frac{\dot{r}}{r} \\
\dot{\varepsilon}_z &= \frac{\dot{h}}{h}
\end{aligned}
\tag{26}
$$

Applying the Huber-Mises-Hencky (HMH) hypothesis, we can replace the reduced quantities in (24) by: the effective stress:

$$\sigma_e = \sigma_r = \sigma_\vartheta = \Sigma \ \psi^{m+1}(t) \tag{27}$$

and effective logarithmic strain

$$\varepsilon_e = 2\varepsilon_r = 2\varepsilon_\vartheta = 2 \ \ln[\psi(t)] \ . \tag{28}$$

Finally we can rewrite (24) in form:

$$F \left\{ \Sigma\psi^{m+1}(t), \ (m+1)\Sigma\psi^m(t)\dot{\psi}(t), \ 2\ln[\psi(t)], \ 2\frac{\dot{\psi}(t)}{\psi(t)}, \ t \right\} = 0 \tag{29}$$

This equation, for the condition of ductile rupture:

$$\psi(t_*) \longrightarrow \infty \qquad (30)$$

enables calculation of the time of ductile rupture t_*.

4. DISK SUBJECT TO LOADING IN AXIAL DIRECTION

In this paragraph we shall discuss more general problem, resigning of the assumption of the plane stress in the disk. Besides the radial tension (in presence of radial body force) disk is subject to uniform compression in the axial direction (Fig.2).
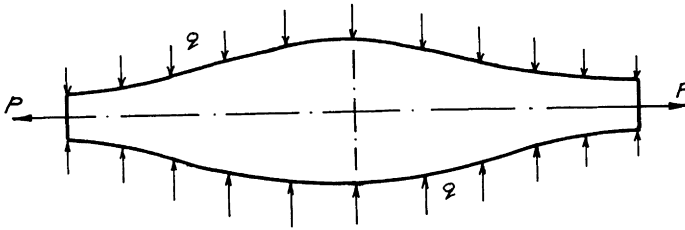
Fig. 2

In this disk we shall have the third, different from zero, stress:

$$\sigma_z = - q , \qquad (31)$$

independent of the radius.

In the problem under consideration we shall obtain identical results for fairly broad class of failure hypotheses, namely for hypotheses represented in the principal stress space by cylindrical limit states surfaces. All such hypotheses will be further called "cylindrical hypotheses" [5].

The above mentioned broad class of failure hypotheses containes e.g. Tresca-Guest hypothesis, the hypothesis of maximal deviatoric stress proposed by Schmidt-Ishlinski-Hill, "power" hypothesis by Hershey -Davis, and Huber-Mises-Hencky hypothesis. All of them assume independence of the

reduced stress from the mean stress σ_m. For any hypothesis, the reduced stress may be written as a function:

$$\sigma_{red} = f(\sigma_e, \omega_\sigma), \tag{32}$$

of effective stress, and angular invariant ω_σ, defined as:

$$\omega_\sigma = \text{arc sin } \frac{\sigma_2 - \sigma_3}{\sqrt{3}\ \sigma_e} \ . \tag{33}$$

In our case of the disk of uniform initial strength (3.15):

$$\sigma_e = |\sigma_r - \sigma_z|; \qquad \qquad \omega_\sigma = 0, \tag{34}$$

and for all cylindrical hypotheses we obtain

$$\sigma_{red} = \sigma_r + q. \tag{35}$$

Thesis 2. The full disk of uniform initial strength in the narrower sense,
under assumptions (1)÷(4) from thesis 1, and additional :
(5) pressure q acting normally to the middle surface of the disk,
is equal on the whole surface of the disk, but changing in
time,
is the disk of uniform deformability.

From the assumption *(5)* in the disk for t=0:

$$\Sigma_{red} = \Sigma_r + Q = const(R) \ , \tag{36}$$

where Q denotes the initial value of normal pressure. The profile of the disk of uniform initial strength (in the broader sense) is described by (16), where Σ should be substituted by Σ_r determined from (35):

$$H(R) = H_o \exp \left[- \frac{1}{\Sigma_{red} - Q} \int_{R_o}^{R} B(\rho,\rho) \ d\rho \right] \ , \tag{37}$$

and thickness at the outer radius H_o must be equal

$$H_o = \frac{N_r(R_o)}{2 \pi R_o (\Sigma_{red} - Q)} \tag{38}$$

Putting the initial profile of uniform strength (37) into equilibrium equation for the deformed disk (17), and assuming uniform deformability (6), we come to the equation:

$$\psi^{m+1}(t) = \frac{\sigma_r(R,t)}{\Sigma_{red} - Q} - \frac{\sigma_r'(R,t)}{B(R,R)} - \frac{\sigma_r(R,t) - \sigma_\vartheta(R,t)}{R \, B(R,R)} \ , \tag{39}$$

which may be satisfied, if

$$\sigma_r(R,t) = \sigma_\vartheta(R,t) = \Sigma_r(R) \ \psi^{m+1}(t) \ . \tag{40}$$

From (36) results, that at the assumption *(3)*, the initial radial stress Σ_r is independent of R, i.e. the stresses in the plane of disk will be all the time equal.

Also the reduced stress (35) will be at any moment the same in the whole disk, regardless whether the pressure q is related to the unit spatial area, when:

$$\sigma_{red} = (\Sigma_{red} - Q) \ \psi^{m+1}(t) + Q \ g(t) \ , \tag{41}$$

or it is related to the unit material area, then:

$$\sigma_{red} = (\Sigma_{red} - Q) \ \psi^{m+1}(t) - \frac{Q}{\psi^2(t)} \ g(t) \ , \tag{42}$$

In both cases the function g(t) may be taken arbitrarily.

Thus, assumption of uniform deformability (6) makes it possible, to satisfy all eqilibrium equations and boundary condition (22). Such a disk will be the disk of uniform strength in the narrower and in the broader sense, and consequently the disk of uniform deformability what means that also the disk of uniform strength with respect to the ductile rupture.

5. DISK OF UNIFORM DEFORMABILITY VS. OPTIMAL DISK

As it was proved in [1], for bars under nonuniform tension, only in case of body forces depending on the material coordinate the bar of uniform deformability is simultaneously the optimal one with respect to ductile creep rupture. Then the problem is a statically determine one, and distribution of stresses in deformed bar can be found regardless to the physical law, only from the statical equations.

For disks such a possibility does not exist. In order of determining of the true streses distribution, each time the set of equations must be solved: internal equilibrium condition and equation resulting from the compatibility condition for logarithmic strains [5]

$$\varepsilon_r = \varepsilon_\vartheta + \ln \left[1 + R \frac{\partial \varepsilon_\vartheta}{\partial R} \right] \tag{43}$$

in which strains must be replaced by true stresses, with help of the creep law combined with the law of similarity of deviators of true stresses and logarithmic strains rates. Moreover, the current geometry of deformed disk must be known, and it results also from the physical law.

Thus, we cannot say about the the statically determine disks, and consequently the time of ductile rupture cannot be written in form of infimum of certain expression, depending only on the thickness of the disk at given radius, as it was possible for bars [2]. For all these reasons, we come to the conclusion, that disks of uniform strength with respect to the ductile creep rupture, are generally not optimal with respect to the time to ductile rupture. This conclusion is independent of the type of body force in the disk, though only the case of rotating disk is the realistic one.

The shape of the rotating disk of uniform initial strength could be slightly changed (improved) in order to obtain longer life-time to the ductile rupture. The results of such improvements will be presented separately, here we shall quote only an example of corrected initial shape of optimal disk, compared with the shape of uniform initial strength (Fig. 3).
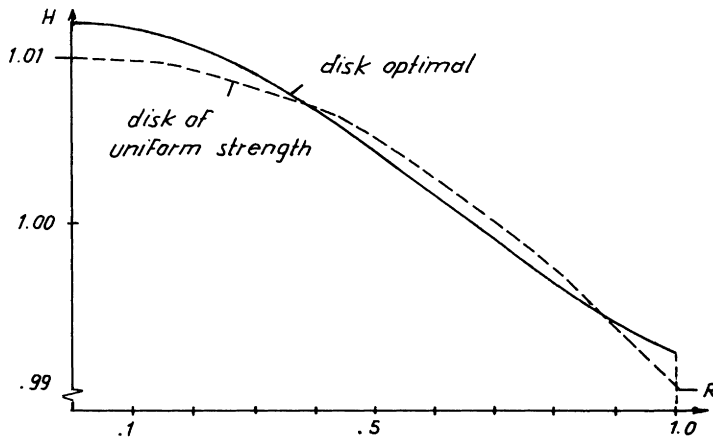
H

1.01

disk optimal

disk of
uniform strength

1.00

.99

R

.1   .5   1.0

Fig. 3

The differences are not very large and are, first of all, of qualitative importance. The shape of uniform initial strength may be treated as fairly good approximation, but only approximation of optimal solution with respect to ductile rupture time.

6. REFERENCES

1. K.Szuwalski, Optimal design of bars under nonuniform tension with respect to ductile creep rupture. *Mech. Struct. & Machines* 17 (1989), 3.

2. K.Szuwalski, Bars of uniform strength vs. optimal with respect to ductile creep rupture time. *Proc. IUTAM Symposium "Creep in Structures" Cracow 1990, Springer-Verlag Berlin 1991*, 637 - 643.

3. M.Życzkowski, Optimal structural design in rheology. *J. Appl. Mech. Trans. ASME* 38 (1971), 39 - 46.

4. M.Życzkowski, Optimal structural design under creep conditions. *Appl. Mech. Rev.* 41 (1988), 12, 453 - 461.

5. M.Życzkowski, Combined loadings in the theory of plasticity. *Polish Sc. Publ. Warszawa 1981*.

Stereological Quantification of the Microstructure Morphology for Composite Materials

Ryszard Pyrz

Institute of Mechanical Engineering, University of Aalborg, Denmark

Abstract

Methods of spatial statistics have been used to analyze the pattern of fibers' distribution in unidirectional composite materials. Several parameters and functions that characterize the spatial distribution of fibers are investigated with special emphasis on their ability to distinguish between different fibers' pattern. The analysis is performed for three different materials as well as for simulated distributions. A short discussion is devoted to characterization of the fracture profiles for investigated materials.

1. INTRODUCTION

It is recognized in all branches of materials science that there is a close relationship between global properties of materials and their microstructure. Although microstructures of materials usually display some typical feature by which they are recognized, an enormous variety in shape, size and arrangement of the parts within any one specimen is also obvious. This fact presents an obstacle to correlation with properties. There have been many attempts to trace a direct link between the macroscopic properties of materials and the microstructure. These attempts have generally rested upon the assumption of "unit cell" models where the microstructure is envisioned by some kind of repetitious structure composed of units of regular shape, size and spacing. In this sense few real microstructures are regular and moreover, seldom is a microstructure completely random either. In order to perceive the structure of materials as they really exist, rather than as described by some assumed model it is necessary to recognize that we have to deal with nonregular, nonrandom microstructures. It is true, however, that the geometric properties of the microstructure are capable of statistical repetition throughout the material provided that the following aspects in the quantitative evaluation of microstructures are considered:
- The microstructure of a material is, in general, an inhomogeneous, anisotropic union of isolated as well as multiconnected components. A descriptive framework that suitably characterizes such a multicomponent, spatially distributed aggregate has to be established.
- For most materials the investigation of an internal structure is only possible either on the internal surfaces generated by taking sections or on layers cut from the material that are sufficiently thin to be transparent. Thus the spatial characteristics of components must be evaluated from their planar sections and projections.

- Only a small part of the material can be thoroughly examined. Therefore the selection of samples for detailed investigation and a critical statistical assessment of the results obtained is of primary importance [1].

In the present analysis, an attempt has been made to address the problem encountered in the quantitative description of the arrangement of fibers in a unidirectionally reinforced composite material. The emphasis is placed on the selection of functions and parameters that sufficiently well describe and discriminate the microstructural features under study. The sampling techniques and statistical assessment of the results are left to further studies.

A multiphase material is by definition heterogeneous. Its local properties vary spatially. If the material is statistically homogeneous, which means that the local material properties are constant when averaged over a representative volume element, then it is possible to replace the real disordered material by a homogeneous one, where the local material properties are the averages over the representative volume elements in the original material. Several approximate micromechanical analyses of effective medium methods were proposed to calculate those averages [2-4]. It is necessary to note that effective medium methods are valid for dilute or at most moderate concentrations of the second phase since they do not depend on the geometrical configuration of a composite microstructure.

Thus the only statistical information involved in those methods is related solely to the volume concentration of each phase which is merely a statement of the overall composition of the material rather than of its dispersion characteristics. The geometrical arrangement of fibers is known to influence the overall properties [5,6]. Moreover, the interaction between fibers can not be neglected for higher volume concentrations and the dispersion pattern of fibers becomes a crucial issue. The relative positions of fibers in given configuration are described by the n-point correlation function where the symbol n denotes the correlation between n fibers. Field quantities are calculated as an ensemble averages rather than volume averages where the n-point correlation function plays a central role [7-9]. Distribution of fibers is very important in studying the fracture phenomenon due to the heterogeneity of the stress field that results from the complex geometrical arrangement of fibers and microcracks [10-12]. Both analytical and experimental evaluation of n-point correlation function is by no means a simple task even for lower order correlations [13]. However, recent developments in evaluation of correlation functions for nontrivial model microstructures [14,15] and the progress in experimental techniques [16] have made it possible to estimate the correlation functions with the reasonable effort.

In what follows several parameters that discriminate the dispersion of fibers are investigated. The discussion is based upon the statistical analysis of spatial point patterns and the construction of Dirichlet tessellations. The first-order properties of a spatial point pattern are described by an intensity function i.e. number of fiber centres in an observation area which corresponds to fibers' volume fraction. The second-order properties are characterized by the function that is directly related to the 2-point correlation function of fibers' pattern. Utilization of the modern image analysis technique is illustrated throughout the paper.

2. THEORETICAL BACKGROUND

Let us first assume that the centres of finite-sized fibers can be regarded in the same light as the infinitesimal points.

It is rudimentary to conclude that the distribution of fibers is random if it is not regular. However such a description is not precise as the spectrum of all possible arrangements of fibers lies between two extremes: regular and completely random.

The completely random point set (Poisson process) represents the simplest possible stochastic mechanism for the generation of point patterns and serves as an idealized standard of examination how far the observed pattern of points depart from the complete randomness in their distribution. The point set is Poisson if N points are placed in a region where each possible location for a point is equally likely to be chosen and the location of each point is independent of the location of any other point. Although strictly unattainable in a physical world the Poisson process of points is theoretically one of the best understood and sometimes provides a useful approximate description of an observed pattern [17].

Interaction between a pair of fibers depends upon their distance thus the distribution of nearest neighbour distances is of particular interest. Naturally the distribution of fibers' positions in the matrix governs the distribution of nearest neighbours. Under the Poisson hypothesis the frequency distribution function for the nearest neighbour distance is

$$f(d) = 2\pi d N_A \exp(-\pi d^2 N_A) \tag{1}$$

where d is the radial distance from a point to its nearest neighbour, and N_A is the estimator for a point pattern intensity i.e. a number of points N within an observation area A. The expected average mean distance E(d) is found by substituting Eq. (1) to the following integral

$$E(d) = \int_0^\infty r f(r) dr = 0.5 N_A^{-\frac{1}{2}} \tag{2}$$

It is easy to conclude that the nearest neighbour distance for a quadratic pattern is equal to

$$d_q = N_A^{-\frac{1}{2}} \tag{3}$$

and for a hexagonal pattern of points.

$$d_h = \left[\frac{2}{\sqrt{3}} \right]^{\frac{1}{2}} N_A^{-\frac{1}{2}} \tag{4}$$

There is of course no frequency function of the nearest neighbour distances for those patterns. The expected variance of nearest neighbour distances for the Poisson point set $E(s^2)$ is calculated using the second moment of the distance distribution function f(d) yielding

$$E(s^2) = \frac{4-\pi}{4\pi} \frac{1}{N_A} \tag{5}$$

In order to be able to use above formulas in micromechanical modelling the complete randomness of the observed pattern must be confirmed. From the multitude of possible test methods and parameters that discriminate "non-randomness" [18,19], the most simple

parameters are the ratio of observed and expected mean of nearest neighbour distances, Q, and the ratio of observed and expected variance of nearest neighbour distances, R, i.e.

$$Q = \frac{\bar{d}}{E(d)} \quad , \quad R = \frac{s^2}{E(s^2)} \tag{6}$$

where

$$\bar{d} = \frac{1}{N} \sum_{i=1}^{N} d_i \quad and \quad s^2 = \frac{1}{N} \sum_{i=1}^{N} d_i^2 - (\frac{1}{N} \sum_{i=1}^{N} d_i)^2$$

Deviations from unity indicate deviations from randomness and the discrimination between patterns is set up in the following way: $Q \approx 1$, $R \approx 1$ for the Poisson pattern, $Q > 1$, $R < 1$ for short range ordered sets, $Q < 1$, $R < 1$ for clustered sets.

An alternative characterization of different classes of point sets is provided by the function K(r), one definition of which is, [20]

$$K(r) = N_A^{-1} \cdot \: (\: \textit{number of further points within the distance r} \tag{7}$$
$$\textit{of an arbitrary point })$$

The practical way of estimation of the function K(r) is shown in [21]. The function K(r) discriminates different point patterns and more importantly it may be related directly to the 2-point correlation function in micromechanical modelling [22]. The K(r) function attached to the Poisson point set has value πr^2.

The assumption that the centres of finite-sized fibers may be regarded as points introduces an error into the calculation of nearest neighbour distances. This situation can be still simulated by the point set in which the points are forbidden to lie closer together than a certain minimum "hard-core" distance. It will be shown that the K(r) function is able to detect this type of pattern as well.

Determination of nearest neighbour distribution is significantly enhanced by the construction of the Dirichlet tessellation based upon the point pattern under consideration. The Dirichlet network is a set of polygons, each of which contains one of the set's points as nucleus. The sides of the enclosing polygon are created by the perpendicular bisectors of the line segments that join the nucleus with neighbouring points of the set. This procedure assignes a unique area to each point of the set and determines the "zone of influence" for each point. Moreover, the near neighbour points are determined by the sides of the polygon and the distribution of near neighbour distances may be calculated as well.

The coefficient of variation of the Dirichlet cells V_A is a useful counterpart to tests based on nearest neighbour distances. The coefficient of variation V_A is defined as the ratio of standard deviation of cell areas to the mean cell area

$$V_A = \frac{[\frac{1}{N} \sum_{i=1}^{N} A_i^2 - (\frac{1}{N} \sum_{i=1}^{N} A_i)^2]^{\frac{1}{2}}}{\frac{1}{N} \sum_{i=1}^{N} A_i} \tag{8}$$

where A_i is the area of the i-th cell.

The values larger than V_A for the Poisson point pattern suggest clustering of points and existence of cell areas significantly greater than mean area whereas the value smaller than V_A for the Poisson set indicates tendency for regularity in the point pattern. The construction of the Dirichlet tessellation provides more useful information that is discussed elsewhere [21].

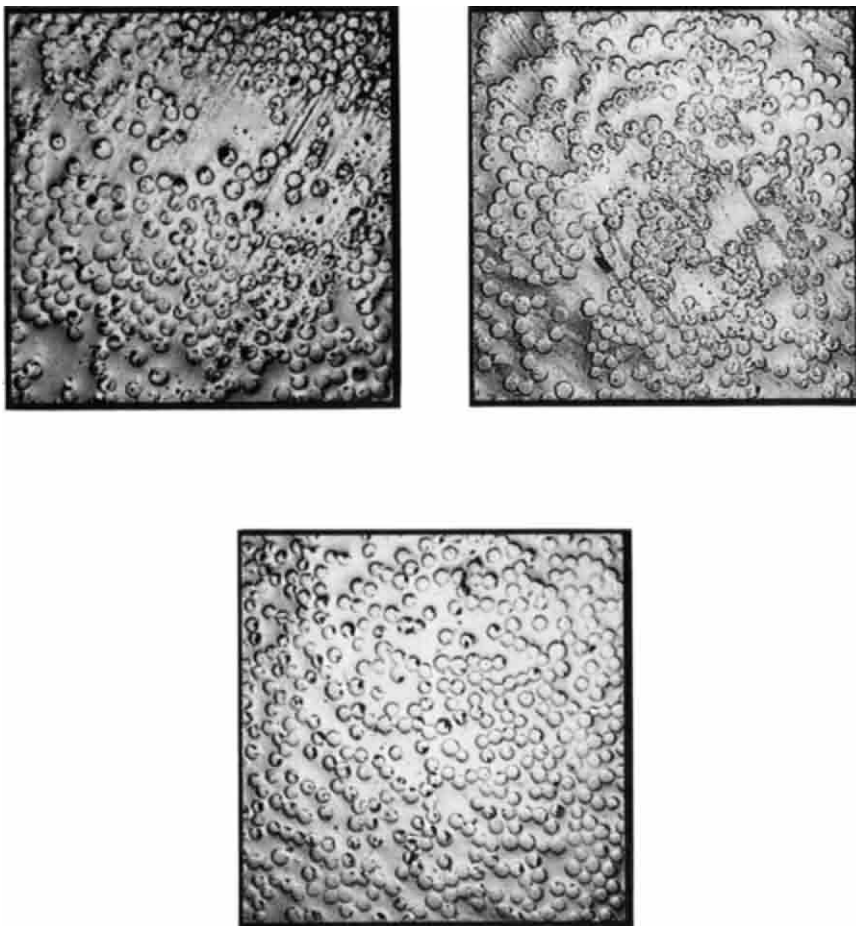## 3. EXPERIMENTAL PROCEDURE

Figure 1. Microstructures of three materials at x 410 magnification. Above: material 1 with zero pressure and material 2 with half pressure. Below: material 3 with maximum pressure.

The material analyzed in this study was glass fiber-epoxy composite with continuous fibers. The specimens were manufactured from prepregs of thickness 0.125 mm that were layered in the sequence of 8 unidirectional layers and processed in the autoclave. In order to obtain different arrangement of reinforcing fibers processing scheme was carried out along three different routes. While keeping the curing temperature constant during the manufacture the pressure applied to three batches of specimens was set to zero, half maximum and the maximum recommended by the supplier.

The microstructures obtained by these processing techniques are shown in Fig. 1. The diversity of fiber arrangements is apparent. Material 1 clearly exhibits clustering areas with large, matrix rich zones. These zones diminish with increasing pressure for materials 2 and 3, resulting in more regular distribution of fibers.
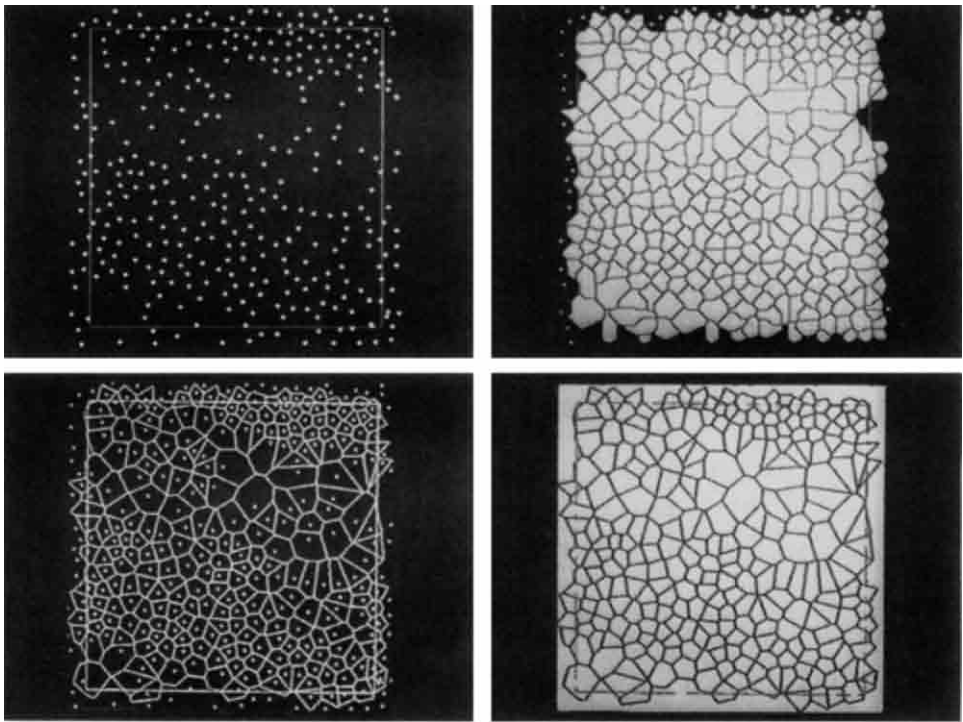

Figure 2. Detected fibers and their zone of influence for the material 1. Below: the Dirichlet tessellation for the material 1.

Position of fibers was detected by the image analysis system QUANTIMET 570. After several grey-tone morphological transformations performed on the original image of microstructure, the image analysis system created the zones of influence of fibers. Figure 2 illustrates the position of detected fibers and corresponding zones of influence for the image of the material 1 together with the Dirichlet tessellation constructed upon the actual distribution of fibers.

The Dirichlet tessellation and the zone of influence differ slightly due to the fact that the image analysis system creates the zone of influence based upon the grey tone morphology of the image rather than spacing distances between cells' nuclei. A statistical analysis of cells areas, size, shape and perimeters is built in the system. However, an automatic measurement of interpoint distances might be obtained only indirectly by the construction of the Dirichlet tessellation. The Dirichlet tessellations were computed by the Green-Sibson algorithm [23]. The position of fibers and corresponding Dirichlet tessellations for the material 2 and the material 3 are shown in Fig. 3.
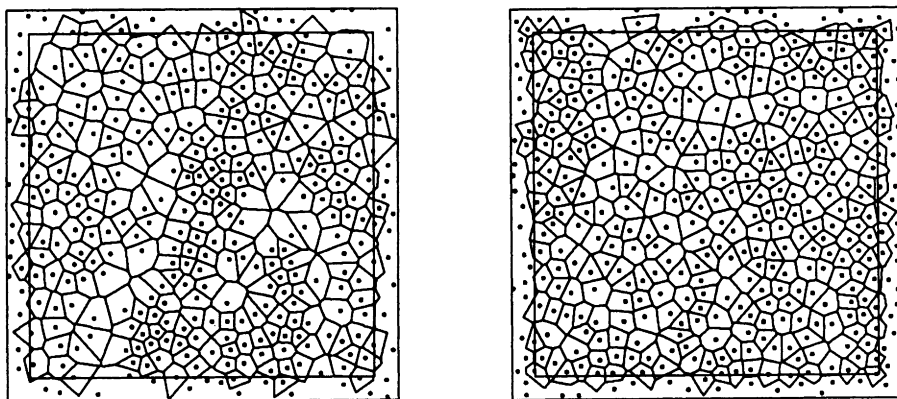

Figure 3. Detected fibers and tessellations for the materials 2 and 3.

The measurements of distances were performed within the inner, measure frame in order to minimize the edge effect. The side of a quadratic measure frame corresponds to 385 μm on the microscale.

4. RESULTS AND DISCUSSION

Table 1 summarizes the data for the discrimination parameters of three materials investigated.

For each material the simulation of the Poisson distribution and the simulation of the hard-core model were performed with exactly the same number of fibers as measured on images. The results are also shown in Table 1.

Table 1

	Q	R	V_A	Fracture stress
Material 1	1.481	0.386	0.510	15.8 [MPa]
Poisson set 1	1.097	0.991	0.489	
Hard-core 1	1.579	0.104	0.199	
Material 2	1.443	0.231	0.360	33.2 [MPa]
Poisson set 2	1.108	1.096	0.510	
Hard core 2	1.639	0.128	0.173	
Material 3	1.496	0.154	0.251	52.8 [MPa]
Poisson set 3	1.085	1.156	0.487	
Hard-core 3	1.686	0.072	0.147	

According to the classification, Q's and R's for all three materials take values that correspond to short range ordered sets, yet we would expect the value of Q to be smaller than one for the material 1. It would indicate apparent clustering. Nevertheless the remaining values of R and Q parameters show correct tendencies. Coefficient of variation V_A clearly indicates clustering for the material 1 and the strong ordering for the material 3.

Spacing parameters that can be measured from the Dirichlet tessellation are shown in Fig. 4.

Both the nearest- and near neighbour spacing histograms become taller and narrower as the pattern of points tends to more regular distribution. This tendency is seen in Fig. 4 where the structure of material 3 is closest to the ordered distribution. Material 1 inclines to the random distribution with clustering as indicated by certain number of points with near neighbour distances 3 times as large as the mean near neighbour distance.

Similar conclusions may be drawn from Fig. 5 where the distribution of cell areas is shown. The distribution of cell areas for the material 1 exhibits characteristic tail towards larger areas indicating the existence of matrix rich regions, which is the sign of clustering in other areas. On the contrary, the distribution of cell areas for the material 3 is approximately symmetric around the mean resulting in a certain order and uniformity of cell areas.

The simulations' results for the Poisson point pattern and the hard-core model with the same number of fibers as detected for the material 2 are shown in Fig. 6.

Simulations with the hard-core model were performed with the inhibition distance 9 μm which corresponded to the mean radius of fibers. The hard-core model seems to reproduce the distances of the material 2 reasonably well, at least as far as the nearest neighbour distances are concerned. Distribution of distances from the Poisson simulation does not match the distances for the material 2, at all. This is because the Poisson point process is related to a set of mathematical points instead of fibers that have a finite dimension. The situation could be improved by recording the position of fibers at magnification that allows to treat fibers as points. In such a case, matching of the Poisson and material's distances allows to use the equation 1 in the micromechanical modelling. Unfortunately, this may be achieved only with a significant decrease in accuracy of distances' measurements due to a fractal character of

distances. On the other hand the hard-core model provides more realistic description of fibers' distribution, however, the theoretical distribution of distances for this model is not known.
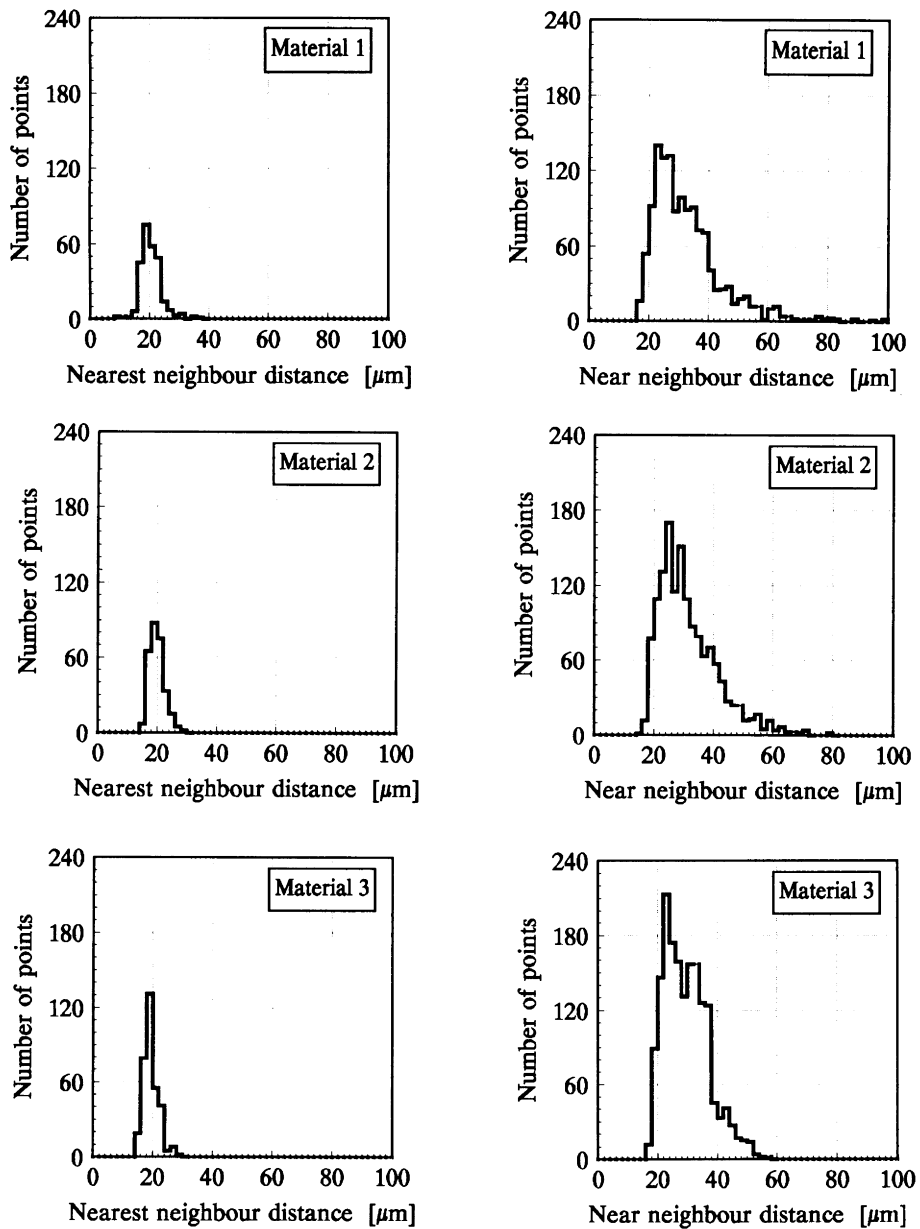

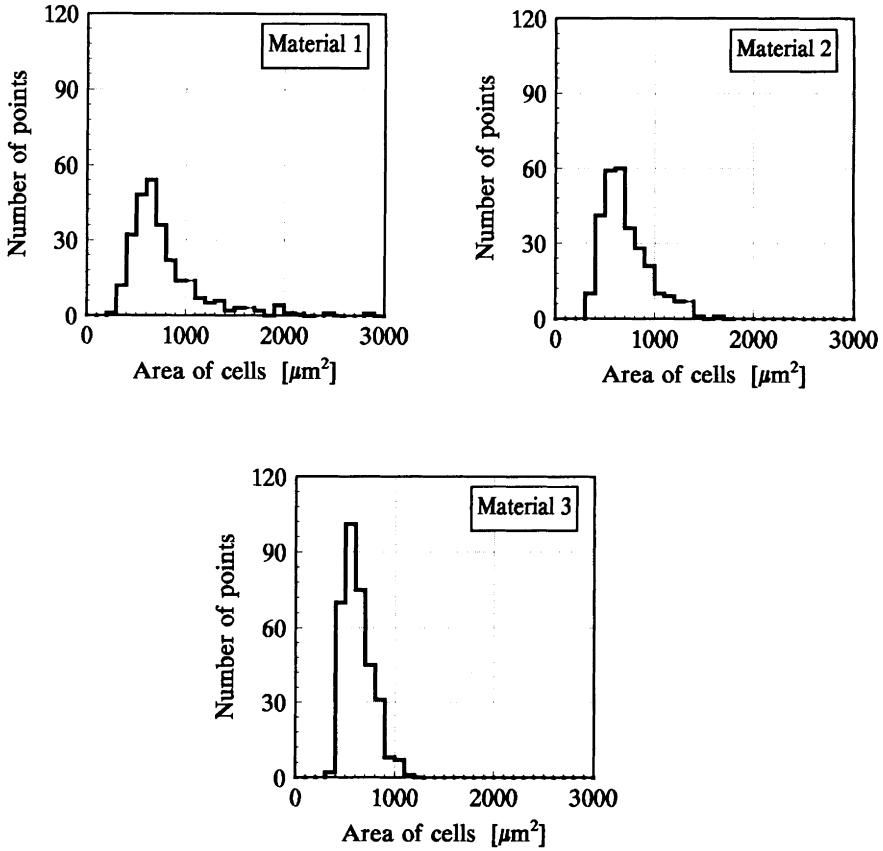Figure 4. Histograms of nearest- and near neighbour distances.

Figure 5. Histograms of cell areas.

Figures 7, 8 and 9 illustrate the distinction of point patterns based upon the behaviour of the K(r) function. The function K(r) for any random hard-core model lies always below the K(r) function of the Poisson distribution with the same intensity. Values of the function K(r) that lie above the Poisson curve suggest the distribution with clustering tendency. All tested materials exhibit a hard-core behaviour for small distances which is of course a physical necessity.

Material 1 shows both short-range and long-range clustering as the K(r) function remains above the Poisson curve for larger r as well. Material 2 is characterized by random distribution for longer distances where both curves almost coincide. The function K(r) for material 3 exits the random hard-core curve at r=30 μm which means more ordered distribution at these particular distances. For increasing r the fibers' distribution is less

regular than the hard-core model. Calculations performed for very long distances, approximately 3 times as large as shown in the Fig. 9, allow to detect slight clustering at r = 150 μm. The analysis of the K(r) function indicates that its discrimination ability is in accordance with other descriptors, particulary the coefficient of variation V_A. Moreover, the use of the K(r) leads to a more informative classification of patterns and as mentioned previously permits the calculation of the 2-point correlation function for further micromechanical modelling [22].
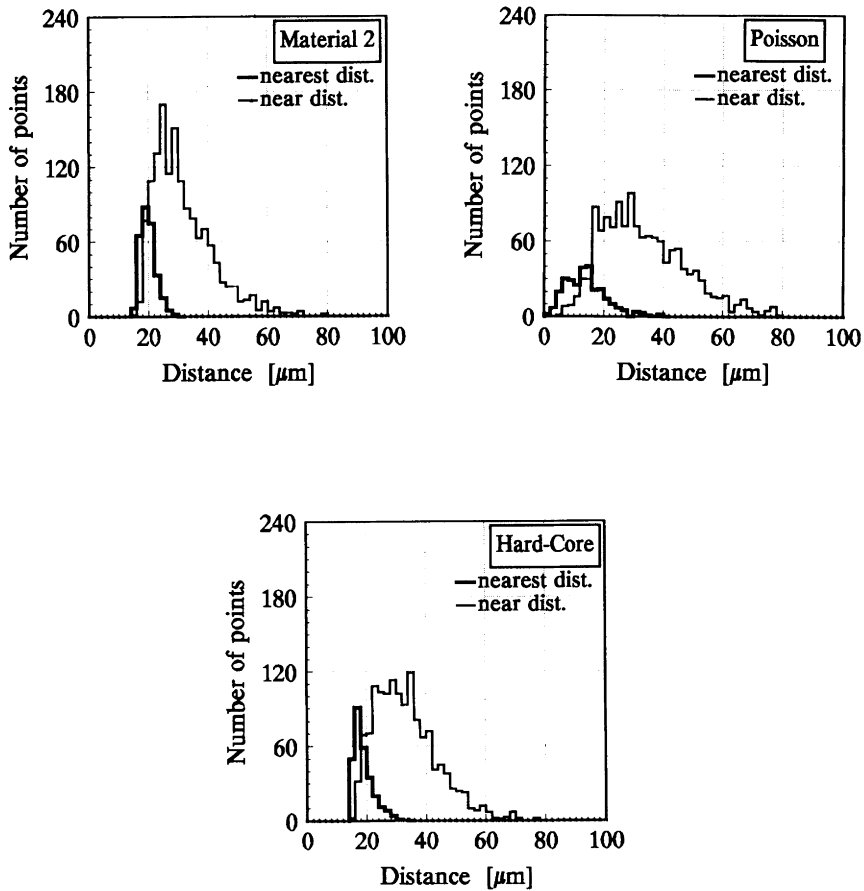
Figure 6. Distances for the material 2, the Poisson pattern and the hard-core model.
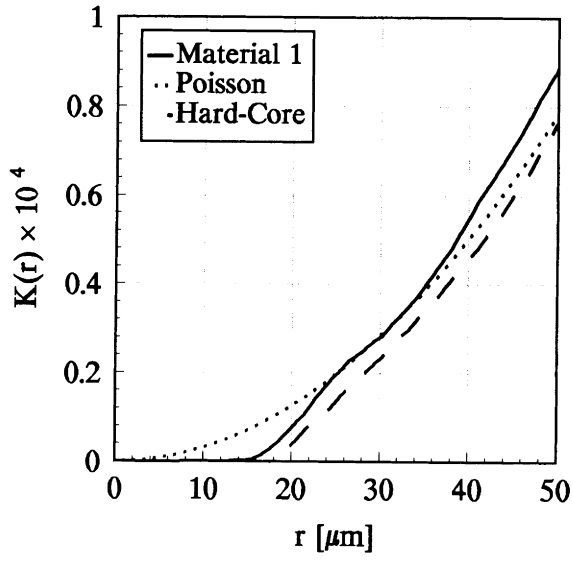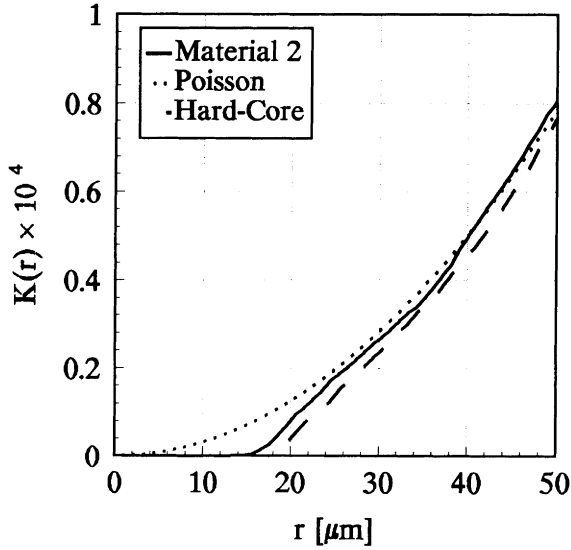
Figure 7. The K(r) function for the material 1.
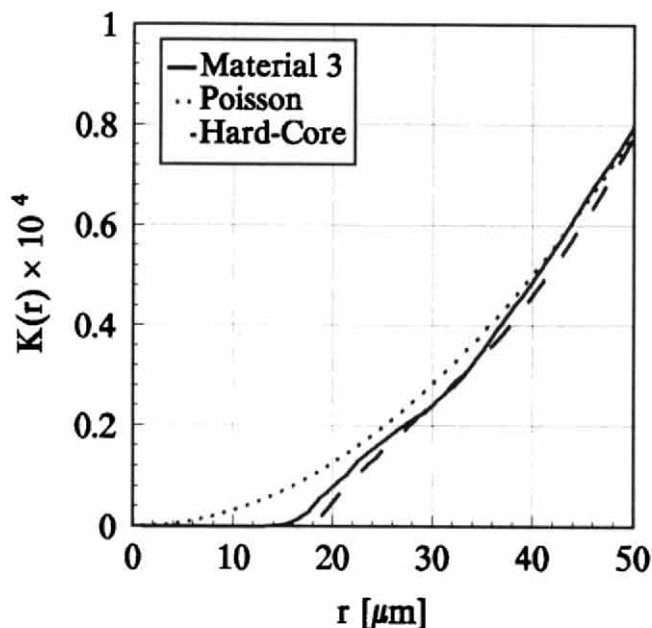

Figure 8. The K(r) function for the material 2.

Figure 9. The K(r) function for the material 3.

The study of descriptors that quantify a distribution of fibers as presented herein, is far from exhaustive. Further simulations for model distributions are necessary in order to provide, for comparative studies, a broad spectrum of patterns ranging from completely random to regular. For example, simulation of the Poisson set with varied intensity, pattern of points clumped in bands of different width, anisotropic distribution of points are of particular interest. Simulations to quantify these patterns are currently under way.

It is worth to mention that discriminators of the fiber's pattern presented in this contribution are also related to fracture surfaces and cracks' morphology in unidirectional composites. Significant differences in mean fracture stresses for three materials, listed in Table 1, result from the distribution of fibers. Observation of the fracture surfaces and their profiles revealed considerably longer fracture profiles for the material 3 as compared to materials 1 and 2, which consequently demanded a higher amount of accessible energy to be spent in creating the fracture surfaces. Figure 10 shows the fracture profiles for investigated materials at the same magnification as in Fig. 1. The fracture profile for the material 1 is much shorter than the fracture profile for the material 3. The fracture front of material 1 propagates along the boundary between fibers and matrix rich areas and does not need to kink around the fibers as it is the case for the material 3.

The length of the fracture profiles was measured by the image analysis system. The fracture profile detected and prepared for a measurement is shown in Fig. 11.
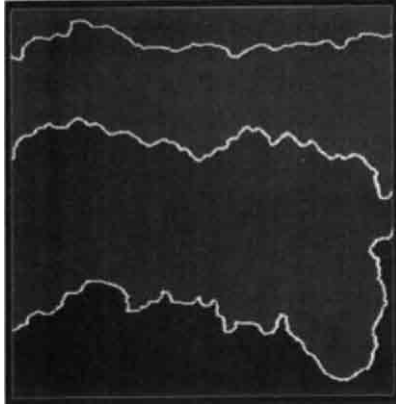
Figure 10. Fracture profiles at x410 magnification for the material 1 (top), the material 2 (middle) and the material 3 (bottom).
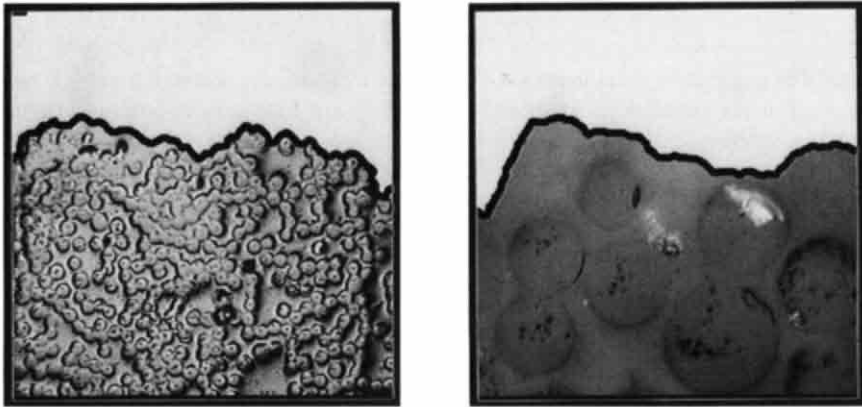

Figure 11. Detected fracture profile for the material 2 at x410 magnification (left) and at x2350 magnification (right).

For each material the fracture profile length was evaluated at different magnifications in order to take into account a fractal character of the fracture surface. The length of the fracture profile grows with increasing magnification and levels off at the magnification x410. The lengths of profiles from Fig. 11 are almost the same. Thus there exists a critical magnification beyond which the length measurements do not change. This critical magnification happens to be the same as the one used for the detection of fibers' distribution. It significantly enhances the correlation analysis between the pattern of fibers and the fracture profile. An influence of the fibers' distribution on the fracture surface is discussed elsewhere [24].

Acknowledgement

5. REFERENCES

1   E.R. Weibel, Stereological Methods, 1, 2, Academic Press, London (1980).
2   Z. Hashin, J. Appl. Mech., 50 (1983) 481.
3   S. Nemat-Nasser, T. Iwakuma and M. Hejazi, Mech. Mat., 1 (1982) 239.
4   J.R. Willis, J. Mech. Phys. Solids, 25 (1977) 185.
5   D.F. Adams and S.W. Tsai, J. Comp. Mat., 3 (1969) 368.
6   J.R. Brockenbrough, S. Suresh and H.A. Wienecke, Acta Metall. Mater., 39 (1991) 735.
7   H-S. Chen and A. Acrivos, Int. J. Solids Structures, 14 (1978) 349.
8   M.J. Beran and J.J. McCoy, Int. J. Solids Structures, 6 (1970) 1035.
9   A.K. Sen, F. Lado and S. Torquato, J. Appl. Phys., 62 (1987) 3503.
10 E.E. Gdoutos, Fib. Sci. Techn., 15 (1981) 173.
11 F. Pijanudier-Cabot and Z.P. Bazant, J. Engng. Mech., 117 (1991) 1611.
12 H. Zhu, and J.D. Achenbach, J. Comp. Mat., 25 (1991) 224.
13 P.B. Corson, J. Appl. Phys., 45 (1974) 3159.
14 S. Torquato, and G. Stell, J. Chem. Phys., 77 (1982) 2071.
15 S. Torquato, and G. Stell, J. Chem. Phys., 82 (1985) 980.
16 J.G. Berryman, J. Appl. Phys., 57 (1985) 2374.
17 A. Getis, and B. Boots, Models of Spatial Processes, Cambridge Univ. Press, Cambridge, 1978.
18 B.D. Ripley, J. Roy. Statist. Soc., Ser.B, 41 (1979) 368.
19 P.J. Diggle, J. Besag, and J.T. Gleaves, Biometrics, 32 (1976) 659.
20 B.D. Ripley, J. Roy. Statist. Soc., Ser.B., 39 (1977) 172.
21 R. Pyrz, J. Comp. Sci. Techn., (submitted).
22 R. Pyrz, J. Comp. Sci. Engng., (to appear).
23 P.J. Green. and R. Sibson, Compt. J., 21 (1978) 168.
24 R. Pyrz, J. Comp. Sci. Techn., (submitted).

Tensile Properties of Whisker Reinforced Metals: Variations with Grain Size*

V. Tvergaard[a] and A. Needleman[b]

[a]Department of Solid Mechanics, The Technical University of Denmark, Lyngby, Denmark

[b]Division of Engineering, Brown University, Providence, RI 02912, U.S.A.

Abstract

In SiC whisker reinforced aluminum the matrix grain size is typically comparable to the whisker dimensions. Planar crystal plasticity with three slip systems is used in numerical cell-model analyses to study the effect of different grain-sizes, and different misorientations between crystal axes in neighboring grains. The plane strain analyses focus on materials containing a periodic array of aligned whiskers with a fiber volume fraction of 30%. Comparison is made with predictions based on a single crystal matrix and with a corresponding flow theory of plasticity with isotropic hardening. It is found that the multi-grain model gives rise to shear localization induced by the high strain concentrations at the sharp whisker edges.

1. Introduction

Significantly improved mechanical properties of metallic materials can be obtained by reinforcement with brittle fibers, whiskers or particulates. Both the overall stiffness and the strength of the composite are substantially increased by the reinforcements, and metals reinforced by short fibers or particulates still have the advantage of being machinable and workable using conventional processing techniques. However, the reinforcement also results in poor ductility and low fracture toughness due to early debonding of the fiber-matrix interface or fiber breakage (Divecha *et al.*, 1981; McDanels, 1985; Nutt and Needleman, 1987; Zok *et al.*, 1988). Micromechanical studies are an important tool for obtaining a parametric understanding of the effects of material variables such as the volume fraction, the shape and the distribution of particulates or fibers.

A number of numerical micromechanical studies have been carried out for metals reinforced with perfectly bonded short fibers. Thus, Christman *et al.* (1989) and Tvergaard (1990) have used axisymmetric cell-model analyses, representing periodic arrays of aligned whiskers, to investigate the uniaxial tensile stress-strain behavior of a 2124 Al-SiC whisker composite, and Levy and Papazian (1990) have studied similar materials

---

* Dedicated to Professor Frithof Niordson on the occasion of his 70th birthday.

by a full 3D numerical analysis. Also Bao *et al.* (1991) have used full 3D numerical analyses to study metals reinforced by periodic arrays of particulates, short fibers or platelets. Planar models have been used by Christman *et al.* (1989) to study the effect of whisker clustering on the overall properties. Furthermore, some studies have focused on the effect of matrix-fiber debonding (Nutt and Needleman, 1987; Povirk *et al.*, 1991; Tvergaard, 1991). A common feature of all these studies is that the elastic-plastic matrix material behavior has been described by a phenomenological flow theory of plasticity.

The use of simple phenomenological plasticity theories is justified as long as the reinforcement size/spacing is large compared to the characteristic microstructural size scale, such as grain size or dislocation cell size. Otherwise, more detailed constitutive models may be needed, accounting for anisotropic crystal plasticity or even for specific rules of dislocation motion. The diameter of SiC whiskers is about 0.5 μm, and the aluminum matrix grain size in the powder compacted whisker composites is typically 2-3 μm, so here the details of crystallographic slip could play a significant role. Such effects have been studied by Needleman and Tvergaard (1991) for a periodic array of aligned whiskers in a single crystal matrix, and it has been found that the most pronounced effect of the crystal constitutive description is associated with strongly localized flow induced by the high strain concentrations at the sharp whisker edge. Needleman, Suresh and Tvergaard (1992) have used the same type of approach to study the effect of whisker clustering in a single crystal matrix.

In the present paper the crystal size scale is incorporated by analyzing composites with a few grains adjacent to each whisker, thus accounting for the effect of different crystal lattice orientations in the different grains. Some insight has been gained by the studies of McHugh *et al.* (1989, 1990), who considered a rigid hexagonal particle interacting with a number of neighboring crystalline grains, but fiber aspect ratio and shape play a significant role, and the focus here is on metals reinforced by aligned short fibers.

2. Problem Formulation

2.1 Field Equations

The formulation of the boundary value problem and the numerical procedure follow that in Needleman and Tvergaard (1991) and Needleman, Suresh and Tvergaard (1992), where further details and references can be found. A Lagrangian formulation of the field equations is used with all field quantities considered to be functions of convected coordinates, y^i, and time, t. The rate form of the principle of virtual work is written as

$$\Delta t \int_V [\dot{\tau}^{ij} \delta E_{ij} + \tau^{ij} \dot{u}^k_{,i} \delta u_{k,j}] \, dV = \Delta t \int_S \dot{T}^i \delta u_i \, dS - \left[\int_V \tau^{ij} \delta E_{ij} \, dV - \int_S T^i \delta u_i \, dS \right] \quad (1)$$

where V and S are the volume and surface, respectively, of the body in the reference configuration and $(\dot{\ }) = \partial()/\partial t$ at fixed y^i. The quantities τ^{ij} are the contravariant

components of the Kirchhoff stress ($\tau = J\sigma$, where σ is the Cauchy stress and J is the ratio of current to reference volume of a material element) on the deformed convected coordinate net. The second term on the right hand side is an equilibrium correction term that is used in the numerical procedure to reduce drift from the equilibrium path due to the discrete time step.

The nominal traction components, T^i, and the Lagrangian strain components, E_{ij}, are given by

$$T^i = (\tau^{ij} + \tau^{kj} u^i_{,k})\nu_j \tag{2}$$

$$E_{ij} = \frac{1}{2}(u_{i,j} + u_{j,i} + u^k_{,i} u_{k,j}) \tag{3}$$

where u_j are the components of the displacement vector on base vectors in the reference configuration, ( ),$_i$ denotes covariant differentiation in the reference frame and $\boldsymbol{\upsilon}$ is the surface normal in the reference configuration.

A doubly periodic array of identical cells is subject to plane strain tension, with y^2 being the tensile axis. Each cell contains a single rigid whisker, perfectly bonded to the matrix and aligned with the tensile axis. The cell dimensions are $2w_0$ along the y^1 direction and $2L_0$ along the y^2 direction. Consideration is restricted to deformations for which the straight lines bounding each cell remain straight after deformation and to deformations that preserve the mirror symmetry of the array so that straight lines connecting the centers of the cells remain straight. With these symmetries, the boundary conditions for the quadrant analyzed numerically are

$$\dot{u}^2 = 0 \qquad \dot{T}^1 = 0 \qquad \text{on} \qquad y^2 = 0 \tag{4}$$

$$\dot{u}^2 = \dot{U}_2 = \dot{\epsilon}_{ave}(L_0 + U_2) \qquad \dot{T}^1 = 0 \qquad \text{on} \quad y^2 = L_0 \tag{5}$$

$$\dot{u}^1 = \dot{U}_1 \qquad \dot{T}^2 = 0 \qquad \text{on} \quad y^1 = w_0 \tag{6}$$

Here, $\dot{\epsilon}_{ave}$ is a prescribed constant while $\dot{U}_1$ is determined from the condition that the average lateral traction rate vanishes, i.e.,

$$\int_0^{L_0} \dot{T}^1 dy^2 = 0 \qquad \text{on} \quad y^1 = w_0 \tag{7}$$

Since the matrix material remains perfectly bonded to the rigid whisker, $u_1 = u_2 = 0$ along the whisker-matrix interface.

2.2 Constitutive Relations

The constitutive formulation here follows that in Peirce *et al.* (1983), and falls within the general framework described in Rice (1971), Hill and Rice (1972) and Havner (1982). The numerical calculations are based on the planar crystal model of Asaro (1979), but with three slip systems, as used for composite materials in McHugh *et al.*

(1989, 1991), Needleman and Tvergaard (1991) and Needleman, Suresh and Tvergaard (1992). As in Lee (1969), the deformation gradient is written as

$$\mathbf{F} = \mathbf{F}^*\mathbf{F}^p \tag{8}$$

The deformation $\mathbf{F}^p$ consists solely of crystallographic slipping along specific slip systems $(\mathbf{s}^{(\alpha)}, \mathbf{m}^{(\alpha)})$, where $\mathbf{s}^{(\alpha)}$ is the slip direction and $\mathbf{m}^{(\alpha)}$ is the slip plane normal for slip system α (α=1, 2, 3), and the elastic deformation and any rigid body rotation are included in $\mathbf{F}^*$. The vectors $\mathbf{s}^{(\alpha)}$ and $\mathbf{m}^{(\alpha)}$ stretch and rotate according to

$$\mathbf{s}^{(\alpha)*} = \mathbf{F}^* \cdot \mathbf{s}^{(\alpha)} \qquad \mathbf{m}^{(\alpha)*} = \mathbf{m}^{(\alpha)} \cdot \mathbf{F}^{*-1} \tag{9}$$

Differentiating (8) with respect to time and grouping terms gives

$$\mathbf{D}^* + \mathbf{\Omega}^* = \dot{\mathbf{F}}^* \cdot \mathbf{F}^{*-1} \qquad \mathbf{D}^p + \mathbf{\Omega}^p = \mathbf{F}^* \cdot \dot{\mathbf{F}}^p \cdot \mathbf{F}^{p-1} \cdot \mathbf{F}^{*-1} \tag{10}$$

The plastic part of the rate of deformation tensor, $\mathbf{D}^p$, and the plastic part of the spin tensor, $\mathbf{\Omega}^p$, are given by

$$\mathbf{D}^p = \sum_\alpha \dot{\gamma}^{(\alpha)}\mathbf{P}^{(\alpha)} \qquad \mathbf{\Omega}^p = \sum_\alpha \dot{\gamma}^{(\alpha)}\mathbf{W}^{(\alpha)} \tag{11}$$

with

$$\mathbf{P}^{(\alpha)} = \frac{1}{2}(\mathbf{s}^{(\alpha)*}\mathbf{m}^{(\alpha)*} + \mathbf{m}^{(\alpha)*}\mathbf{s}^{(\alpha)*}) \qquad \mathbf{W}^{(\alpha)} = \frac{1}{2}(\mathbf{s}^{(\alpha)*}\mathbf{m}^{(\alpha)*} - \mathbf{m}^{(\alpha)*}\mathbf{s}^{(\alpha)*}) \tag{12}$$

and $\dot{\gamma}^{(\alpha)}$ is the rate of shearing on slip system α.

The lattice Jaumann rate of Kirchhoff stress, $\hat{\boldsymbol{\tau}}^*$, and $\mathbf{D}^*$ are related by

$$\hat{\boldsymbol{\tau}}^* = \dot{\boldsymbol{\tau}} + \boldsymbol{\tau} \cdot \mathbf{\Omega}^* - \mathbf{\Omega}^* \cdot \boldsymbol{\tau} = \mathbf{L} : \mathbf{D}^* \tag{13}$$

where $\mathbf{L}$ is the tensor of elastic moduli.

For use in (1), expressing (13) in terms of the material convected rate of Kirchhoff stress, $\dot{\boldsymbol{\tau}}^c$, and the rate of deformation tensor, $\mathbf{D}$, gives

$$\dot{\boldsymbol{\tau}}^c = \mathbf{L} : \mathbf{D} - \sum_\alpha \dot{\gamma}^{(\alpha)}\mathbf{R}^{(\alpha)} - \mathbf{D} \cdot \boldsymbol{\tau} - \boldsymbol{\tau} \cdot \mathbf{D} \tag{14}$$

with

$$\mathbf{R}^{(\alpha)} = \mathbf{L} : \mathbf{P}^{(\alpha)} + \mathbf{W}^{(\alpha)} \cdot \boldsymbol{\tau} - \boldsymbol{\tau} \cdot \mathbf{W}^{(\alpha)} \tag{15}$$

Slip system hardening is described by the power law relation, so that

$$\dot{\gamma}^{(\alpha)} = \dot{a}\left[\frac{\tau^{(\alpha)}}{g^{(\alpha)}}\right]\left[\left|\frac{\tau^{(\alpha)}}{g^{(\alpha)}}\right|\right]^{(1/m)-1} \tag{16}$$

Here, $\dot{a}$ is a reference strain rate, m is the strain rate hardening exponent, $g^{(\alpha)}$ is the slip system hardness, and the slip system resolved shear stress, $\tau^{(\alpha)}$, is given by

$$\tau^{(\alpha)} = \mathbf{s}^{(\alpha)*} \cdot \boldsymbol{\tau} \cdot \mathbf{m}^{(\alpha)*} \tag{17}$$

The evolution law for the hardness $g^{(\alpha)}$ is specified by

$$\dot{g}^{(\alpha)}(\gamma) = \sum_{\beta} h_{\alpha\beta}|\dot{\gamma}^{(\beta)}| \qquad g^{(\alpha)}(0) = \tau_0^{(\alpha)} \tag{18}$$

$$h_{\alpha\beta} = qh(\gamma) + (1-q)h(\gamma)\delta_{\alpha\beta} \qquad \gamma = \sum_{\alpha}|\gamma^{(\alpha)}| \tag{19}$$

with

$$h(\gamma) = h_0(\gamma/\gamma_0 + 1)^{N-1} \tag{20}$$

where h_0 is the initial slip system hardening rate, γ_0 is a reference strain, N is the strain hardening exponent and τ_0 is a reference strength. For the nearly rate independent behavior considered here, τ_0 effectively acts as the initial slip system flow strength.

2.3 Numerical Modelling

The finite element discretization of (1) is based on linear displacement triangles arranged into "crossed" triangle quadrilaterals. The unit cell quadrants analyzed numerically are shown in Fig. 1, where the same 304 quadrilateral finite element mesh is used in all three cases and each quadrilateral consists of four triangular finite elements. In Fig. 1a, the fiber is embedded in a single crystal, as in Needleman and Tvergaard (1991). In Fig. 1b the quadrant is divided into two grains, while in Fig. 1c it is divided into five grains. Subsequently, these will be referred to as the large grain and the small grain cases, respectively. Since no material length scale is present in the boundary value problem formulation, geometric lengths enter the formulation through their ratios, e.g. the fiber aspect ratio and the ratio of fiber spacing to size. Thus, grain size relative to the fiber size is what enters the analyses here. The effect of varying the grain size is to change the distribution of slip system orientations. The slip system orientations are uniform within a grain and differ from grain to grain.

With the orientation of the three slip systems specified by $\mathbf{s}^{(\alpha)} = (\cos\theta^{(\alpha)}, \sin\theta^{(\alpha)})$, where $\theta^{(\alpha)}$ is measured from the y^1 axis, the slip systems in a grain are oriented at $\theta^{(1)} = 60$ deg $+\Delta\theta$, $\theta^{(2)} = 120$ deg $+\Delta\theta$ and $\theta^{(3)} = 180$ deg $+\Delta\theta$. Figure 2 shows the three orientation distributions analyzed in the large grain calculations, while Fig. 3 shows those used for the small grain calculations. In both figures the orientation of
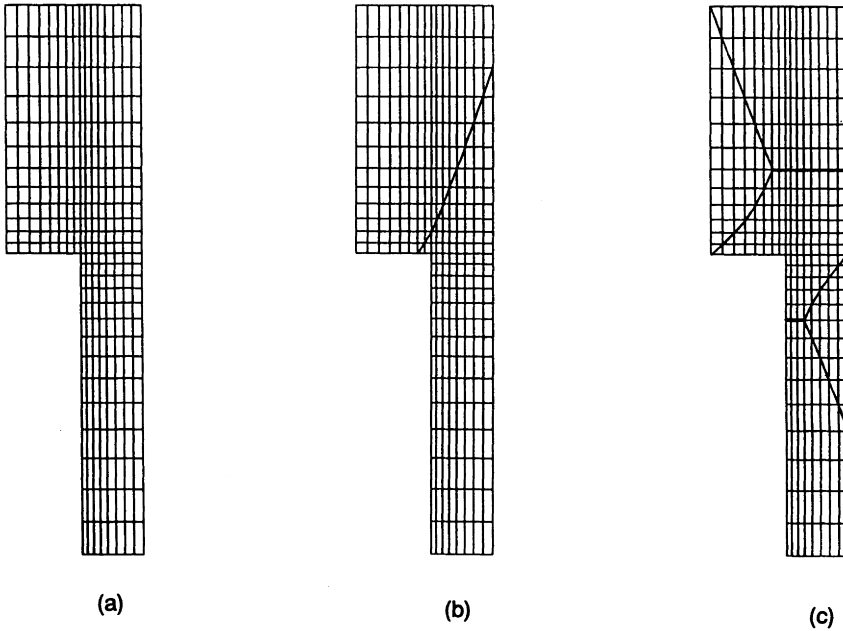
Figure 1. Grain distributions in the unit cell quadrant analyzed numerically shown on the finite element mesh. Each quadrilateral consists of four "crossed" triangular linear displacement elements. (a) a single grain; (b) two grains (large grains); (c) five grains (small grains). In all cases, the fiber volume fraction is 30% and the fiber and cell aspect ratios are 4.

slip direction 1 is shown and one slip plane direction is plotted per quadrilateral. For a quadrilateral in the interior of a grain, the slip plane orientations are identical in all four triangles within the quadrilateral. However, when the boundary between grains is along a quadrilateral diagonal, only one of the two orientations within the quadrilateral is shown.

In Fig. 2a, $\Delta\theta = 0$ deg in the upper grain and $\Delta\theta = 30$ deg in the lower crystal. Both these orientations correspond to symmetric double slip for a homogeneous crystal; with $\Delta\theta = 0$ deg the two slip systems with non-zero resolved shear stress are ± 30 deg from the tensile axis, while with $\Delta\theta = 30$ deg the two slip systems with non-zero resolved shear stress are ± 60 deg from the tensile axis. In Fig. 2b the orientations of the upper and lower grains are reversed, while in Fig. 2c $\Delta\theta = 15$ deg in the upper grain and $\Delta\theta = -15$ deg in the lower grain. Thus, in all three cases in Fig. 2 the magnitude of the misorientation across the grain boundary is 30 deg. Because of the 60 deg symmetry of the slip systems, this is the maximum misorientation. For the small grain cases in Fig. 3, values of $\Delta\theta$ are arbitrarily assigned that give rise to misorientations across grain boundaries ranging from 5 deg to 30 deg.
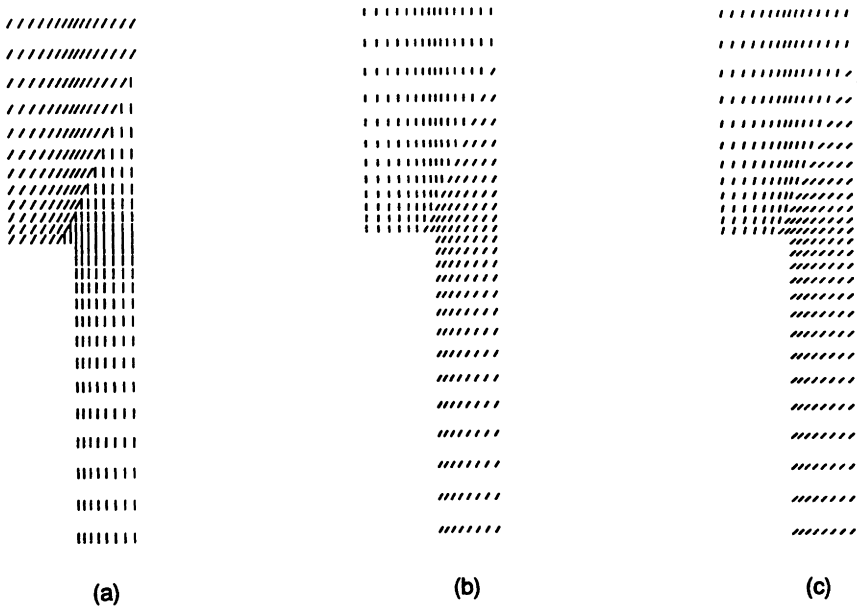
Figure 2. The direction of one slip plane showing the orientation distributions analyzed in the large grain calculations.
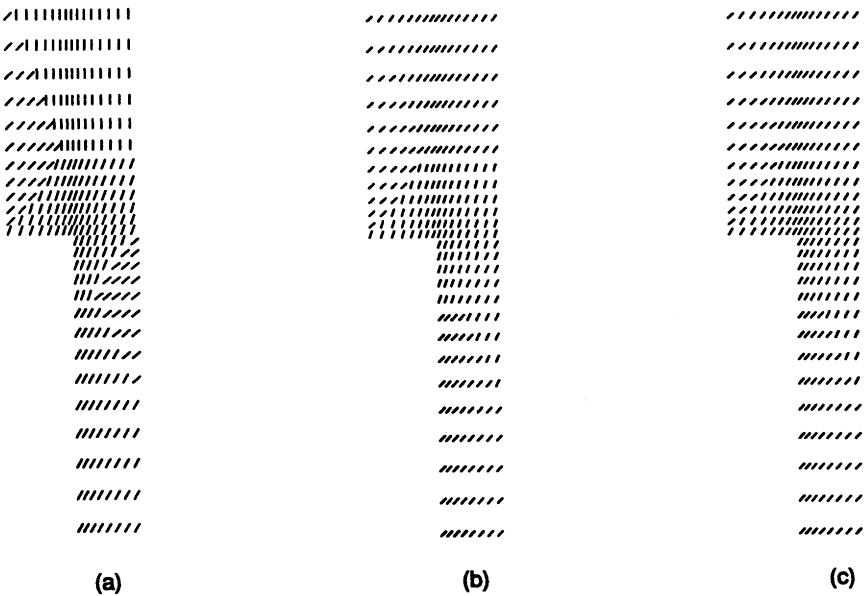

Figure 3. The direction of one slip plane showing the orientation distributions analyzed in the small grain calculations.

The material properties are taken to be uniform throughout the matrix and, unless stated otherwise, the geometric and material parameters have the following values. The fiber area fraction is 30%, the fiber and cell aspect ratios are 4, the matrix elasticity is isotropic with $\nu = 1/3$, $N = 0.1$, $m = 0.005$, $\gamma_0 = 0.01$, $\tau^{(1)} = \tau^{(2)} = \tau^{(3)} = \tau_0$, $E/\tau_0 = 496.67$ and $h_0/\tau_0 = 10$. The incremental boundary value problem is solved using a combined finite element-Galerkin method, which is the finite element-Rayleigh-Ritz method of Tvergaard (1976) for circumstances where the stiffness matrix is unsymmetric. An imposed strain rate $\dot{\epsilon}_{ave} = \dot{a}$ is prescribed and the deformation history is calculated in a linear incremental manner. In order to increase the stable time step, a rate tangent modulus method, as described in Peirce et $al.$ (1983), is used.

3. Results

The overall stress-strain response for two differently oriented whisker reinforced single crystals is shown in Fig. 4. Here, and subsequently, $\epsilon_{ave} = \ln(1 + U_2/L_0)$ and

$$\sigma_{ave} = \frac{1}{w_0 + U_1} \int_0^{w_0} T^2 dy^1 \ . \tag{21}$$

For the homogeneous matrix material in plane strain tension, the response in these two orientations coincides because the ratio of tensile stress to slip plane resolved shear stress, $2/\sin 2\theta^{(\alpha)}$, on the two active systems ($\tau^{(\alpha)} \equiv 0$ for one of the three slip systems) is the same for $\Delta\theta = 0$ deg and $\Delta\theta = 30$ deg. Since the elasticity is isotropic, the metal matrix composite response in the elastic range is independent of crystal orientation. Even in the initial stages of loading the overall stress-strain curves for the two fiber reinforced crystals in Fig. 4 essentially coincide. However, once lattice rotation effects become significant, the response of these two orientations differs somewhat, so that the maximum stress point and the onset of localization depend on initial orientation. For example, with $\Delta\theta = 0$ deg the sharp stress drop in Fig. 4 is at $\epsilon_{ave} = 0.0107$, while with $\Delta\theta = 30$ deg it is at $\epsilon_{ave} = 0.0103$. The stress drop is a consequence of the strain concentration at the fiber corner promoting very localized deformations.

Figure 5 shows the overall stress-strain response for the three large grain orientation distributions. There is very little difference between the curves in Fig. 5 and the single crystal stress-strain curves in Fig. 4. The sharp stress drops for the three large grain cases occur between $\epsilon_{ave} = 0.0103$ and $\epsilon_{ave} = 0.0105$. For the calculation based on the orientation distribution in Fig. 2b, a plot of the current lattice orientation and contours of accumulated slip, γ, and normalized hydrostatic tension, $\tau : \mathbf{I}/3\tau_0$, are shown in Fig. 6 at a stage following the stress drop. Figure 6a shows the orientation, in the current configuration, of the slip planes in Fig. 2b. The large rotations toward the tensile axis in the vicinity of the fiber corner are evident in this figure. There are also significant lattice rotations in this direction above the fiber. Figures 6b and 6c show the strain concentration at the fiber corner and the high tensile hydrostatic stresses that develop above the fiber. The distributions in Figs. 6b and 6c are very similar to those for a single crystal, Needleman and Tvergaard (1991).
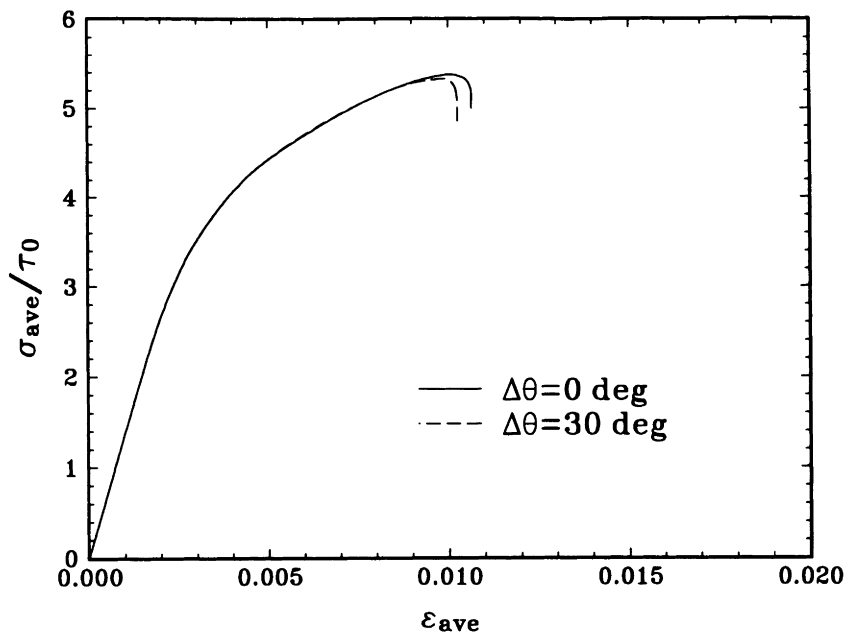
Figure 4. Stress versus strain in plane strain tension for two differently oriented planar single crystals.
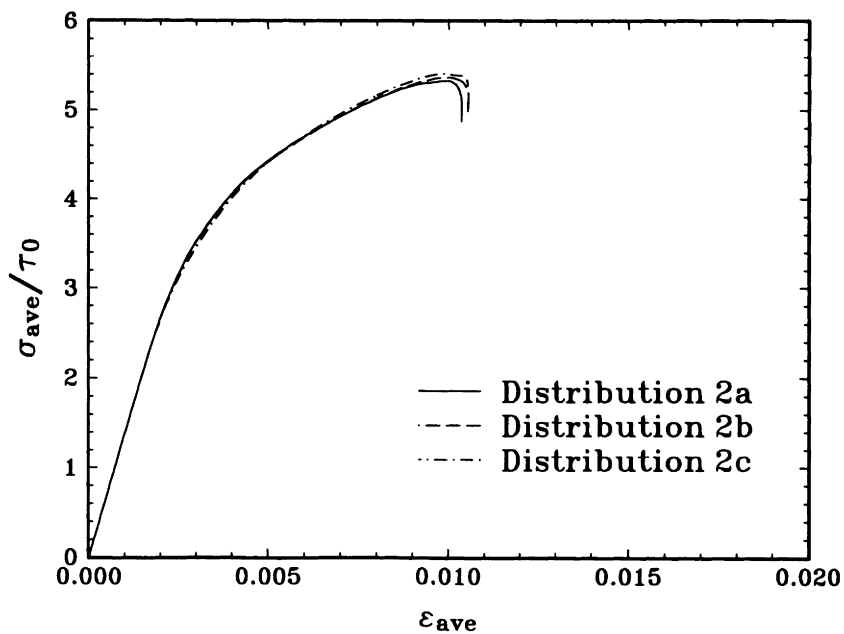

Figure 5. Stress versus strain in plane strain tension for the three large grain calculations. Distributions 2a, 2b and 2c correspond to Figs. 2a, 2b and 2c, respectively.
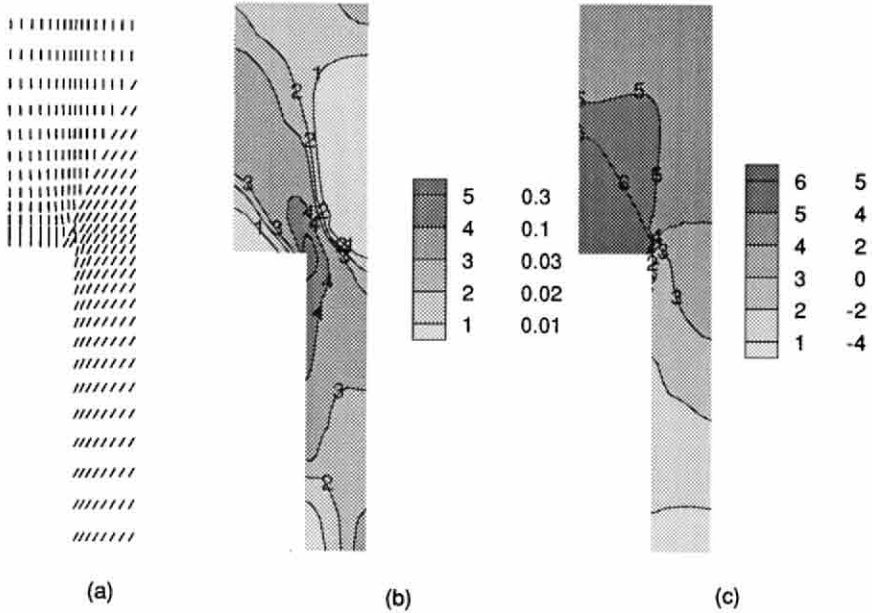
Figure 6. Current slip plane orientation (a) and contours of constant (b) accumulated shear strain, γ, and (c) normalized hydrostatic tension, $\tau : \mathbf{I}/3\tau_0$, for the large grain distribution of Fig. 2b at $\epsilon_{ave} = 0.0105$.

The overall stress-strain response for the three small grain orientation distributions are shown in Fig. 7. For comparison purposes, the corresponding curve for a composite with an isotropically hardening Mises matrix is also plotted. The results for the Mises and crystal matrices are essentially the same in the early stages of deformation. However, as in Needleman and Tvergaard (1991) and Needleman, Suresh and Tvergaard (1992), the stress-strain curves for the crystal matrices eventually soften, because of localization, relative to that for the composite with the Mises matrix. The stress drops in Fig. 7 occur between $\epsilon_{ave} = 0.0103$ and $\epsilon_{ave} = 0.0106$. Figures 4, 5 and 7 show that the overall stress-strain behavior, including the onset of localization, is relatively insensitive to the distribution of initial orientations.

Figure 8 shows the current lattice orientation and contours of accumulated slip, γ, and normalized hydrostatic tension, $\tau : \mathbf{I}/3\tau_0$, for the small grain orientation distribution in Fig. 3c at a stage of deformation after the stress drop. The qualitative features are as seen for the large grain case in Fig. 6. There is even generally good quantitative agreement between the contour plots in Figs. 8b and 8c and the corresponding plots in Figs. 6b and 6c. One feature in Fig. 8c that is not present in Fig. 6c is the elevation in hydrostatic stress in the upper right hand corner of the unit cell. This arises because the lattice there is not oriented for symmetric double slip.
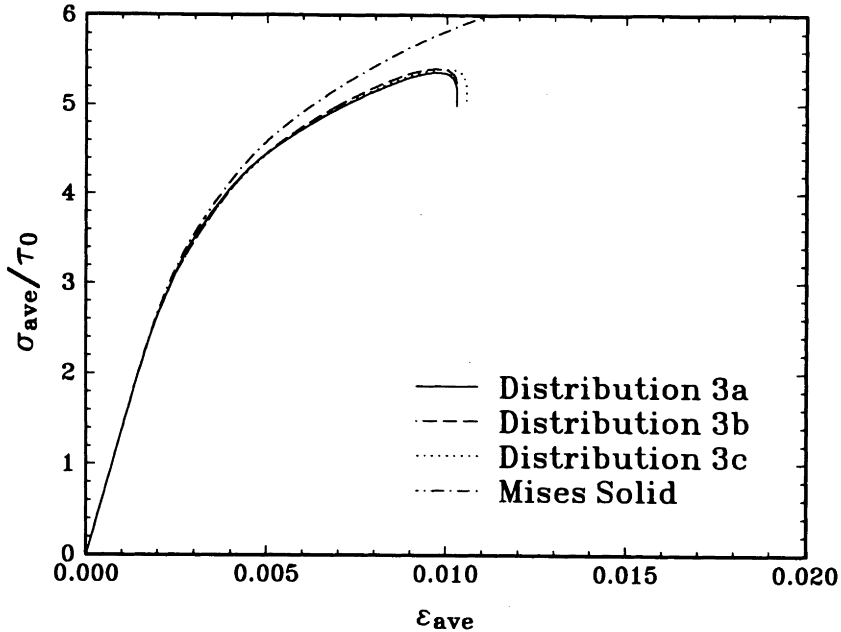
Figure 7. Stress versus strain in plane strain tension for the three small grain calculations. Distributions 3a, 3b and 3c correspond to Figs. 3a, 3b and 3c, respectively. For comparison purposes, the corresponding stress-strain curve for a Mises solid is shown.

Although in all the calculations the value of ϵ_{ave} remains small, Figs. 6 and 8 show that the local strains and lattice rotations are large. Nevertheless, it is found that the overall stress-strain response, including the onset of localization, is rather insensitive to the change in orientation distribution that occurs when the grain size is varied. The overall stress-strain response and the onset of localization do depend on fiber volume fraction and fiber distribution (Needleman and Tvergaard, 1991; Needleman, Suresh and Tvergaard, 1992), which have been kept fixed in the present investigation. The response also depends on fiber and cell aspect ratio. A calculation, not shown here, was carried out for a single crystal having $\Delta\theta = 0$ deg and with a fiber and cell aspect ratio of 2. The maximum value of σ_{ave} is reduced by about 20% and ϵ_{ave} at localization is increased to ≈ 0.02.

In the calculations so far it has been presumed that the material properties are independent of grain size. However, the single crystal flow strength can vary with grain size through a Hall-Petch type relation and changes in grain size can affect the whole stress-strain curve, see e.g. Honeycombe (1968). While the crystal model here does not incorporate any size effect, this effect can be explored by varying the slip system response. In order to illustrate the consequences of a variation in τ_0, with all other parameters fixed, Fig. 9 shows the results of two calculations; one is repeated from Fig. 7, while the other uses the same matrix characterization except that the reference strength of each of the three slip systems is taken to be $1.5\tau_0$ rather than τ_0. The change
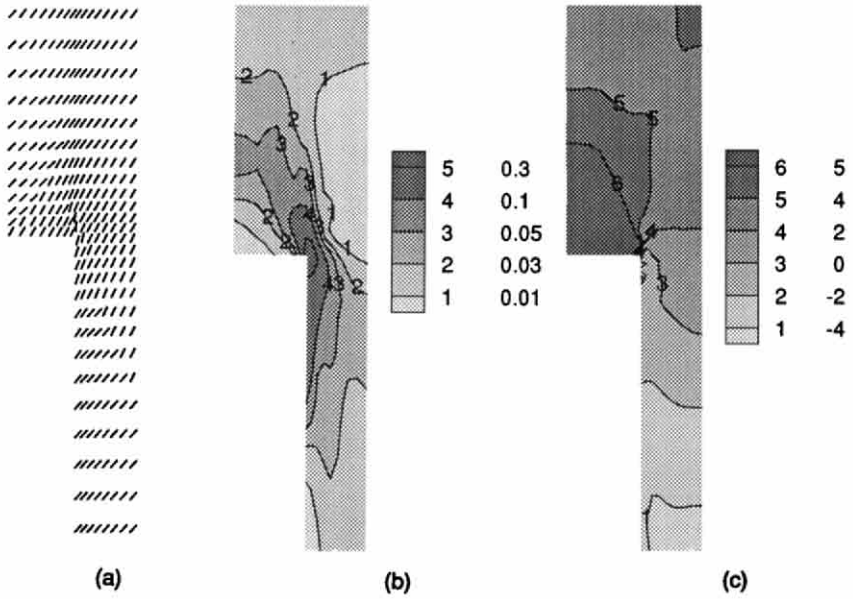
Figure 8. Current slip plane orientation (a) and contours of constant (b) accumulated shear strain, γ, and (c) normalized hydrostatic tension, $\tau : \mathbf{I}/3\tau_0$, for the small grain distribution of Fig. 3c at $\epsilon_{ave} = 0.0106$.
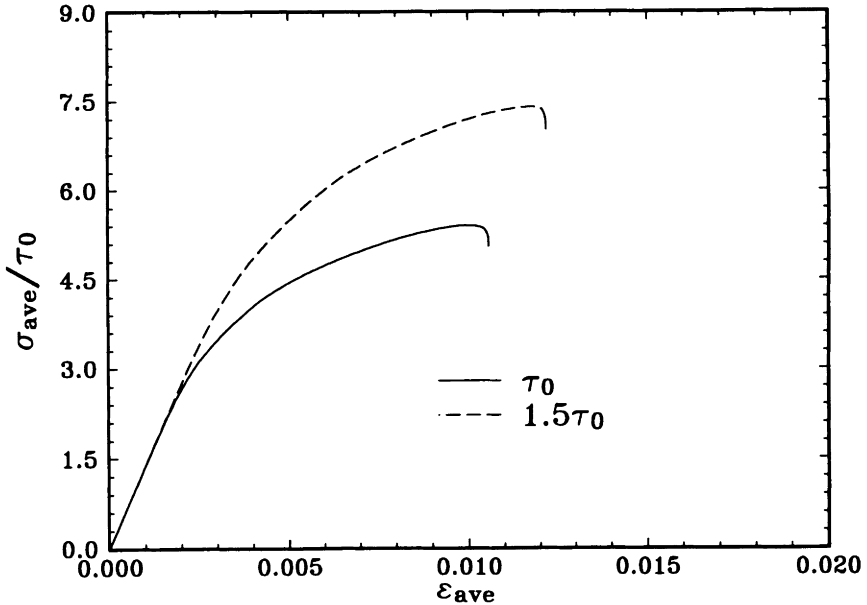
Figure 9. Stress versus strain in plane strain tension for the small grain distribution in Fig. 3c. The curve corresponding to τ_0 is repeated from Fig. 7, while the curve having $1.5\tau_0$ illustrates the effect of an increased flow strength with all other parameters fixed.

in the composite stress-strain curve seen in Fig. 9 reflects the change in τ_0. Because the value of h_0 is fixed at $10\tau_0$ in both calculations in Fig. 9, the strain hardening rate does not increase in proportion to the increase in strength and this somewhat delays the stress drop associated with localization. The results in Fig. 9 indicate that a grain size dependent response may arise from grain size variations in slip system hardening.

All the results in this investigation have been obtained using the 304 quadrilateral finite element mesh in Fig. 1. The strain concentration at the fiber corner plays an important role in precipating localization and, at least in part for this reason, the onset of the stress drop accompaning localization can be sensitive to the degree of mesh refinement. Mesh sensitivity analyses in Needleman and Tvergaard (1991) show that the value of ϵ_{ave} at which the stress maximum is attained decreases with increasing mesh refinement, but that prior to the localization induced stress decrease, the overall behavior obtained from more refined meshes essentially coincides with the predictions based on a mesh similar to the one used here.

4. Discussion

The previous investigations for aligned whiskers embedded in a single crystal matrix (Needleman and Tvergaard, 1991; Needleman, Suresh and Tvergaard, 1992) have shown that strongly localized flow induced by the high strain concentrations at sharp whisker edges is the main effect of crystal plasticity. In those studies the localization strain was found to depend on the whisker volume fraction and on the whisker distribution. In an aggregate of grains with random orientations of the crystal axes (Harren, Deve and Asaro; 1988) the tendency towards localization is less clear, and this could affect the predictions for a grain size of the order of magnitude of the fiber dimensions, where a shear band would have to cross a number of grains. However, the present computations show that the localization behavior predicted for short fibers surrounded by a number of grains is very similar to that predicted for a single crystal matrix, in spite of the crystal axis misorientation between neighboring grains. In fact, the localization strains predicted for a number of different multi-grain distributions and orientations are all bounded by the localization strains predicted for the two extreme crystal orientations in a single crystal matrix. The computations were terminated with the load dropping and localization continuing. One possibility for the subsequent behavior is the continued accumulation of localized straining. Another possibility is that the localized straining eventually saturates, due to material strain hardening and limits on textural softening, as seen in Tvergaard and Needleman (1992).

Comparison has been made with a Mises solid (Fig. 7), for which the response in homogeneous plane strain tension is essentially identical to that of a homogeneous single crytal oriented for symmetric double slip. Figure 7 shows that the composite with the planar multi-grain crystal matrix progressively softens relative to the composite with the Mises matrix, in agreement with the results of Needleman and Tvergaard (1991) for a single crystal matrix. Also, for the Mises matrix no load drop is predicted, associated with localized straining at the sharp whisker edges. It is noted that the assumptions of a phenomenological theory of plasticity should become a better approximation the smaller

the grain size relative to the fiber dimensions. However, it is also known (Hutchinson, 1970) that an aggregate of many grains shows the development of a vertex on the overall yield surface. Thus, in the limit of many small grains the predictions of crystal plasticity would not converge towards those of a solid with a smooth Mises yield surface, particularly in cases involving plastic flow localization, where the onset of localization is highly sensitive to details of the constitutive description.

The small difference found here between composites with a single grain matrix or a multi-grain matrix has focussed on the effect of misorientation, with all other material properties identical in the grains. However, in cases where the crytal flow strength varies with the grain size through a Hall-Petch type relation the whole stress-strain curve is changed for the grain aggregate, and this can also affect the onset of localization (Fig. 9).

The planar models used for the present studies do not allow for a realistic representation of the whisker geometry. Axiymmetric cell-model analyses have been used in a number of studies with a Mises material matrix, but in the case of crystals the slip systems do not have axisymmetric properties, so this would require a full three-dimensional numerical analysis. For a three-dimensional material subject to average plane strain conditions, the effect of localization is expected to be much like that found in the present studies, presuming that the planar model gives a response representative of the actual 3D crystal, but under axisymmetric-type conditions this effect would be less dominant, since materials are generally more resistant to localization under such circumstances (Needleman and Rice, 1978). Additionally, for actual 3D crystals there are orientations that are expected to be more resistant to localization than those represented by the three slip-system planar crystal model.

Acknowledgments

References

Asaro, R.J., 1979, "Geometrical Effects in the Inhomogeneous Deformation of Ductile Single Crystals," *Acta. Metall.*, **27**, 445-453.

Bao, G., Hutchinson, J.W. and McMeeking, R.M., 1991, "Particle Reinforcement of Ductile Matrices Against Plastic Flow and Creep," *Acta. Metall. Mater.*, **39**, 1871-1882.

Christman, T., Needleman, A. and Suresh, S., 1989, "An Experimental and Numerical Study of Deformation in Metal-Matrix Composites," *Acta Metall.*, 37, 3029-3050. See also Corrigendum, 1990, *Acta Metall. Mater.*, **38**, p. 879.

Divecha, A.P., Fishman, S.G. and Karmarker, S.D., 1981, "Silicon Carbide Reinforced Aluminum – A Formable Composite," *J. Metals*, **33**, 12-17.

Harren, S.V., Deve, H.E. and Asaro, R.J., 1988, "Shear Band Formation in Plane Strain Compression," *Acta Metall.*, **36**, 2435-2480.

Havner, K.S., 1982, "The Theory of Finite Plastic Deformation of Crystalline Solids," in: Mechanics of Solids, The Rodney Hill 60th Anniversary Volume, (ed. by. H.G. Hopkins and M.J. Sewell), Pergamon Press, Oxford, 265-302.

Hill, R. and Rice, J.R., 1972, "Constitutive Analysis of Elastic-Plastic Crystals at Arbitrary Strain," *J. Mech. Phys. Solids*, **20**, 401-413.

Honeycombe, R.W.K., 1968, *The Plastic Deformation of Metals*, Edward Arnold, London.

Hutchinson, J.W., 1970, "Elastic-Plastic Behavior of Polycrystalline Metals and Composites," *Proc. R. Soc. London*, **A318**, 249-276.

Lee, E.H., 1969, "Elastic-Plastic Deformation at Finite Strains," *J. Appl. Mech.*, **36**, 1-6.

Levy, A. and Papazian, J.M., 1990, "Tensile Properties of Short Fiber Reinforced SiC/Al Composites: Part II Finite Element Analysis," *Metall. Trans.*, **21A**, 411-420.

McDanels, D.L., 1985, "Analysis of Stress-Strain, Fracture, and Ductility Behavior of Aluminum Matrix Composites Containing Discontinuous Silicon Carbide Reinforcement, " *Metall. Trans.*, **16A**, 1105-1115.

McHugh, P.E., Asaro, R.J. and Shih, C.F., 1991, "Computational Modeling of Metal Matrix Composite Materials," in: *Proceedings of the 1991 TMS Annual Meeting*, to be published.

McHugh, P.E., Varias, A.G., Asaro, R.J. and Shih, C.F., 1989, "Computational Modeling of Microstructures," *Fut. Gen. Comp. Systems*, **5**, 295-318.

Needleman, A. and Rice, J.R., 1978, "Limits to Ductility Set by Plastic Flow Localization," in: *Mechanics of Sheet Metal Forming*, (ed. by D.P. Koistinen and N.-M. Wang), Plenum Press, New York, 237-265.

Needleman, A., Suresh, S. and Tvergaard, V., 1992, "Deformation of a Metal-Ceramic Composite with a Crystal Matrix: Reinforcement Distribution Effects," in: *Local Mechanics Concepts for Composite Material Systems*, (ed. by J.N. Reddy and K.L. Reifsnider), Springer-Verlag, Berlin, 199-213

Needleman, A. and Tvergaard, V., 1991, "Comparison of Crystal Plasticity and Isotropic Hardening Predictions for Metal-Matrix Composites," *J. Appl. Mech.*, to be published.

Nutt, S.R. and Needleman, A., 1987, "Void Nucleation at Fiber Ends in Al-SiC Composites," *Scripta Metall.*, **21**, 705-710.

Peirce, D., Asaro, R.J. and Needleman, A., 1983, "Material Rate Dependence and Localized Deformation in Crystalline Solids," *Acta Metall.*, **31**, 1951-1976.

Povirk, G.L., Needleman, A. and Nutt, S.R., 1991, "An Analysis of the Effect of Residual Stresses on Deformation and Damage Mechanisms in Al-SiC Composites," *Mater. Sci. Eng.*, **A132**, 31-38.

Rice, J.R., 1971, "Inelastic Constitutive Relations for Solids: An Internal Variable Theory and Its Application to Metal Plasticity," *J. Mech. Phys. Solids*, **19**, 433-455.

Tvergaard, V., 1976, "Effect of Thickness Inhomogeneities in Internally Pressurized Elastic-Plastic Spherical Shells," *J. Mech. Phys. Solids*, **24**, 291-304.

Tvergaard, V., 1990, "Analysis of Tensile Properties for a Whisker Reinforced Metal Matrix Composite," *Acta Metall. Mater.*, **38**, 185-194.

Tvergaard, V., 1991, "Effect of Thermally Induced Residual Stresses on the Failure of a Whisker-Reinforced Metal," *Mech. Mater.*, **11** 149-161.

Tvergaard, V. and Needleman, A., 1992, "Shear Band Development in Polycrystals," DCAMM Report No. 447, The Technical University of Denmark.

Zok, F., Embury, J.D., Ashby, M.F. and Richmond, O., 1988, "The Influence of Pressure on Damage Evolution and Fracture in Metal-Matrix Composites," in: *Mechanical and Physical Behavior of Metallic and Ceramic Composites*, (ed. by S.I. Andersen *et al.*), Risø National Laboratory, Denmark, 517-526.

Optimal Design with Advanced Materials
P. Pedersen (Editor)
1993 Elsevier Science Publishers B.V.

113

Parameter Identification for Nonlinear Constitutive Models:
Finite Element Simulation – Optimization – Nontrivial Experiments

Vassili V. Toropov[a] and Erik van der Giessen[b]

[a]Department of Solid Mechanics, Faculty of Mechanics and Mathematics, Nizhny Novgorod University, 23 Gagarin Avenue, 603600 Nizhny Novgorod, Russian Federation

[b]Lab. for Engineering Mechanics, Faculty of Mechanical Engineering and Marine Technology, Delft University of Technology, P.O. Box 5033, 2600 GA Delft, The Netherlands

Summary

An identification technique is presented which allows to obtain phenomenological coefficients of constitutive models describing nonlinear mechanical behaviour of engineering materials. The identification problem is considered as the following optimization problem: to obtain the set of material parameters by minimizing the difference between the experimental data and the computed response of the specimen under consideration. The focus is on so-called nontrivial experiments, i.e. experiments where inhomogeneous and multiaxial strain/stress fields within the specimen may be observed, which require numerical simulation of the same experiment by means of a nonlinear FE procedure incorporating the constitutive model to be identified.

Special attention is paid to reduce the number of calls for highly computationally expensive objective function evaluations needed to solve the optimization problem. The implemented optimization technique is based on an iterative approximation of the original objective function by computationally less expensive expressions, obtained by a weighted least-squares method.

The procedure is illustrated by the determination of parameters of large deformation plasticity models from solid bar torsion tests.

1. INTRODUCTION

There seems to be an irreversible tendency for the application of more and more complex materials under more and more severe external conditions, while subjected to increasing reliability requirements. Much work is and will be devoted in the future to developing constitutive models for the description of the nonlinear mechanical behaviour of modern materials. Ultimately, all such models contain a number of material parameters (phenomenological coefficients) which are to be determined from laboratory experiments. Traditionally, relatively simple tests are used where the stress and strain fields inside the specimen are to a high degree uniform (e.g. the tensile test). The material parameters for a chosen material model can be derived then from the test data immediately and, in many cases, analytically. However, when looking into more complex features of nonlinear material behaviour, one sooner or later runs into the limita-

tions of such tests in the sense that the actual stress/strain fields are no longer uniform in the range under consideration, leading to e.g. premature failure at inherent stress concentrations, strain localization in necks etc. The traditional attempts of minimizing the inhomogeneity face serious difficulties especially in the case of advanced materials (polymers, composites etc.).

Thus, it seems inevitable to carry out nontrivial experiments, i.e. experiments where the specimen to be used for model parameter assessment will involve inhomogeneous and multiaxial stress and strain fields. There are some more reasons in carrying out of nontrivial experiments, such as insensitivity to strain localization (e.g. the torsion test of solid bars), ease of manufacturing (e.g. in the case of composites), or the possibility to use structural elements from direct engineering practice as specimens. The price to be paid for this, however, is that the values of pertinent quantities cannot be derived from the experiment immediately. In contrast, a nonlinear FE analysis will usually be necessary to numerically simulate the actual experiment; however, this requires that the values of the material parameters are known. Thus, an iterative procedure is necessary (see, e.g., [1]–[5]). Here, the identification problem is formulated as an optimization problem where the function to be minimized is some error function that expresses the difference between numerical simulation results and experimental data. Analogous formulations have been considered in [6], [7] for the identification of linear orthotropic material parameters and in [8], [9] for viscoelastic material parameters.

2. FORMULATION OF OPTIMIZATION PROBLEM

Let us consider the material parameters to be identified as components of the vector $\mathbf{x} \in R^N$. Then the optimization problem can be formulated as follows:

Find the vector $\mathbf{x}$ that minimizes the objective function

$$F(\mathbf{x}) = \sum_{\alpha = 1}^{M} \Theta^{\alpha} F^{\alpha}(\mathbf{x}) \tag{1}$$

subject to

$$A_j \leq x_j \leq B_j \quad (j = 1, ..., N) , \tag{2}$$

where:

M is the total number of individual specific response quantities (denoted by a Greek index α) which can be measured in the course of experiments and then obtained as a result of the FE simulation;

$F^{\alpha}(\mathbf{x})$ is the dimensionless function

$$F^{\alpha}(\mathbf{x}) = \left(\sum_{s = 1}^{S_{\alpha}} [R_s^{\alpha} - R^{\alpha}(\mathbf{x}, \tau_s^{\alpha})]^2 \right) \Big/ \left(\sum_{s = 1}^{S_{\alpha}} [R_s^{\alpha}]^2 \right), \tag{3}$$

which measures the deviation between the computed α-th individual response and the observed one from the experiment;

τ^{α} is a parameter which defines the history of the process in the course of the experiment (e.g. the loading parameter), and the value τ_s^{α} ($\alpha = 1, ..., M$, $s = 1, ..., S_{\alpha}$) define the discrete set of S_{α} experimental data points;

R_s^{α} ($\alpha = 1, ..., M$, $s = 1, ..., S_{\alpha}$) is the value of the α-th measured response quantity corresponding to the value of the experiment history parameter τ_s^{α};

$R^{\alpha}(\mathbf{x}, \tau_s^{\alpha})$ is the value of the same response quantity obtained from the numerical simulation;

Θ^{α} is the weight coefficient which determines the relative contribution of information yielded by the α-th set of experimental data,

A_j, B_j are side constraints, stipulated by some additional physical considerations, which define a search region in the space R^N of optimization parameters.

Figure 1 shows an illustration of the idea of experimental and simulated response quantities R^{α} corresponding to various values of the experiment history parameter τ_s^{α} ($s = 1, ..., S_{\alpha}$).
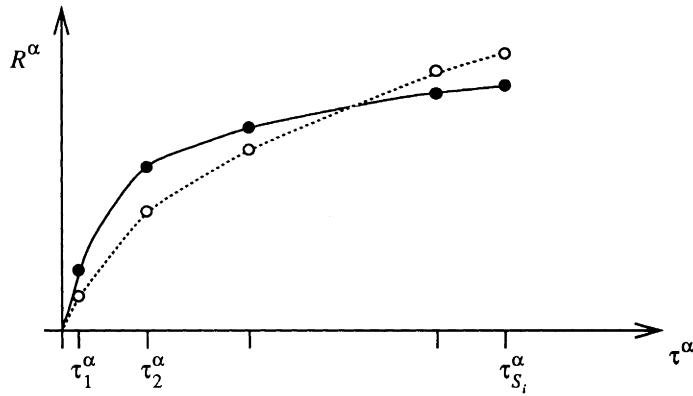

Figure 1. A response quantity R^{α} at various values of the history parameter τ_s^{α} ($s = 1, ..., S_{\alpha}$) as obtained from experiments (●) and from numerical simulations (○).

3. MULTIPOINT APPROXIMATION TECHNIQUE

The optimization problem (1), (2) has the following characteristic features:
- an objective function is an implicit function of parameters $\mathbf{x}$;
- to calculate values of this function for the specific set of parameters $\mathbf{x}$ means to use a nonlinear numerical (i.e. finite element) simulation of the process under consideration, which usually involves a large amount of computer time;
- function values present some noise, i.e. can only be estimated with a finite accuracy.

The direct implementation of any usual nonlinear mathematical programming technique would involve too large amount of computer time and, moreover, the convergence of a method cannot be guaranteed. To solve the problem, the iterative multipoint approximation concept [10], [11] was therefore borrowed from the field of structural optimization.

The technique is based upon the iterative approximation of computationally expensive functions $F^\alpha(\mathbf{x})$ by simplified functions. The initial optimization problem (1), (2) is replaced then with the succession of simpler subproblems as follows:

Find the vector $\mathbf{x}_k^*$ that minimizes the objective function

$$\tilde{F}_k(\mathbf{x}) = \sum_{\alpha = 1}^{M} \Theta^\alpha \tilde{F}_k^\alpha(\mathbf{x}) \tag{4}$$

subject to constraints

$$A_j^k \leq x_j \leq B_j^k \; ; \; A_j^k \geq A_j \, , \, B_j^k \leq B_j \quad (j = 1, \ldots, N) \tag{5}$$

where k is the current iteration number. The current move limits A_j^k and B_j^k define a subregion of the original search region where simplified functions $\tilde{F}_k^\alpha(\mathbf{x})$ are considered as current approximations of the initial implicit functions $F^\alpha(\mathbf{x})$. To estimate their accuracy, the error parameter

$$r_k = \left| \left[F(\mathbf{x}_k^*) - \tilde{F}_k(\mathbf{x}_k^*) \right] / F(\mathbf{x}_k^*) \right| \tag{6}$$

is evaluated.

To construct analytical expressions for the $\tilde{F}_k^\alpha(\mathbf{x})$ in (4), we shall implement methods of regression analysis. They are intended for obtaining analytical expressions that reflect the behaviour of an object considered as a function of its parameters, based on a set of experimental results. Note that here and in the remainder of this section, an *experiment* means a computational experiment using the FE model of the process under consideration. Also, it is essential to note that we do not intend to construct simplified expressions that are adequate in the whole of the search region (2) because it takes too large number of numerical experiments in case of real-life multiparameter problems. Therefore we construct such expressions iteratively only for separate search subregions; i.e. functions $\tilde{F}_k^\alpha(\mathbf{x})$ $\alpha = 1, \ldots, M$ give the piece-wise approximation of the actual functions $F^\alpha(\mathbf{x})$.

Let us now consider the problem of formulating the functions $\tilde{F}_k^\alpha(\mathbf{x})$. Assume that the function (3) is expressed in the following general form:

$$\tilde{F}_k^\alpha = \tilde{F}_k^\alpha(\mathbf{x}, \mathbf{a}^\alpha) \, . \tag{7}$$

The vector $\mathbf{a}^\alpha = (a_1^\alpha, \ldots, a_L^\alpha)$ in expression (7) consists of so-called *tuning parameters*; that is, free parameters the value of which is determined on the basis of numerical experiments at points located in the design variable space R^N in accordance with some design (plan) of experiments. Then the weighted least-squares method leads to the following problem:

Find the vector $\mathbf{a}^\alpha$ that minimizes the function

$$G_k^\alpha(\mathbf{a}^\alpha) = \sum_{p = 1}^{P} w_p^\alpha [F^\alpha(\mathbf{x}_p) - \tilde{F}_k^\alpha(\mathbf{x}_p, \mathbf{a}^\alpha)]^2 \tag{8}$$

where

P   is the total number of points in the plan of experiments;

x_p is the vector of design variables that defines the current point;

$F^\alpha(x_p)$, $\tilde{F}^\alpha_k(x_p, a^\alpha)$ are the values at the point x_p of the original function in (3) and of the approximate function in (7), respectively;

w^α_p is the weight coefficient that characterizes the relative contribution of the p-th experiment's information.

The solution of the optimization problem (8) is the vector **a** which makes up the simplified function (7). The weight coefficients w^α_p, ($p = 1, ..., P$) in (8) reflect the inequality of data obtained in different design points. The correct choice of these weights can substantially improve the properties of the functions $\tilde{F}^\alpha_k(x)$. In our optimization problem (1), (2) where no behavioural constraints are imposed, weights can reflect the difference in the contribution of data given by different numerical experiments depending on the objective function value at individual points in R^N. Then the maximum value of the weight coefficients corresponds to the optimization space point with the minimum value of the objective function.

After formulation of the simplified functions (7), the current mathematical programming problem (4), (5) is solved and the error parameter r_k in (6) for the point x^*_k is estimated. Next, the task is to identify the size and location of the next search region (i.e. to determine the move limits A^k_j and B^k_j for the next iteration). First the condition

$$r_k \leq e_k \tag{9}$$

is checked, where e_k is a small positive number which defines the feasible accuracy of approximation of the function $F^\alpha(x)$ by function $\tilde{F}^\alpha_k(x)$. If it is not satisfied (i.e. approximations are inaccurate), then the size of the search subregion of the $(k + 1)$-th step must be reduced. When the condition (9) is satisfied, we must decide upon the movement of the search subregion. If the point obtained, x^*_k, is located inside the k-th search subregion (none of the move limits is active), then the point x^*_k can be considered as the current approximation of the solution x^*. In that case, the next search subregion should be reduced and the other conditions of the search termination should be checked. Otherwise, if some of the conditions (5) are satisfied as equalities, the search must be continued. This means that the search subregion must be moved in the direction $x^*_k - x^*_{k-1}$ without changing its size. Depending on the accuracy of the approximations (i.e. values of the error parameters r_k), either a new plan of experiments in the next search subregion should be chosen or the approximations can be used once again in the new search subregion. The search process is terminated when (i) the condition (9) is satisfied, (ii) none of move limits is active and (iii) the subregion has reached a required small size.

Let us now consider the problem of formulating the simplified functions $\tilde{F}^\alpha_k(x, a^\alpha)$. Apparently, the efficiency of the optimization technique depends greatly on the accuracy of such expressions. Note that properly chosen expressions in our case of the optimization problem (1), (2) with no behavioural constraints imposed, must allow for an internal minimum point inside the search region defined by side constraints (2), for otherwise the convergency of the method can be slow; i.e., the number of steps of the algorithm and, correspondingly, the number of calls for the evaluation of the functions $F^\alpha(x)$ would be very large. Therefore, the simplest possible choice of a linear expression in **x** for all of the functions $\tilde{F}^\alpha_k(x, a^\alpha)$ ($\alpha = 1, ..., M$) will be inap-

propriate.

The simplest form of an expression which does satisfy the above requirement, is a full quadratic polynomial. If there are no other considerations available, then it can be considered as a reasonable choice. However, it requires at least $N(N+1)/2 + N + 1$ calls for the evaluation of the functions $F^\alpha(\mathbf{x})$ in (3), which can be a very large number in the case of a multiparameter identification problem where N can easily be of the order of 10.

There is an alternative approach based on so-called *mechanistic models*, which finds increasing application in empirical model-building [12]. The parameter estimation of such models requires the implementation of the most general (nonlinear) form of the least-squares method. These models are constructed on the basis of physical considerations, which can sometimes provide clues to the nature of a phenomena under consideration. The designer of such a mechanistic model can typically use *a priori* information, such as analytical solutions for simplified geometrical shape, loading or boundary conditions of the specimen under consideration. Clearly, in this approach, the researcher's experience and engineering judgement is essential to create high-quality approximations. Typically, the available information presents the description of the process under consideration as a function of the experiment history parameter τ^α. Such information can be used for the formulation of a simplified model in the following form:

$$\tilde{F}^\alpha_k(\mathbf{x}, \mathbf{a}^\alpha) = \left(\sum_{s=1}^{S_\alpha} \left[R^\alpha_s - \tilde{R}^\alpha_k(\mathbf{x}, \mathbf{a}^\alpha, \tau^\alpha_s) \right]^2 \right) \bigg/ \left(\sum_{s=1}^{S_\alpha} [R^\alpha_s]^2 \right), \tag{10}$$

where $\tilde{R}^\alpha_k(\mathbf{x}, \mathbf{a}^\alpha, \tau^\alpha_s)$ is a simplified model of the process under consideration.

It should be noted that the simplified functions $\tilde{F}^\alpha_k(\mathbf{x}, \mathbf{a}^\alpha)$ need not necessarily be explicit. There can be some numerical procedures involved in their formulation, such as numerical integration or even finite element modelling of the simplified process. But, the basic requirements to such models are:

- its description of the simplified process must depend on the same parameters $\mathbf{x}$ as the initial numerical model, presented by functions $R^\alpha_s(\mathbf{x})$ in (3);
- they have to contain some tuning parameters $\mathbf{a}^\alpha$ which are to be obtained by solving the optimization problem (8);
- they have to be simple enough to be used in numerous repeating calculations;
- in order to achieve fast convergency of the identification procedure, they have to be accurate enough in comparison with original functions (3).
- they have to be noiseless or, at least, the level of noise must not cause problems with convergence of an algorithm used to solve the optimization problems (4), (5) and (8).

4. APPLICATION TO LARGE STRAIN ELASTOPLASTIC TORSION

As a first relatively simple example of the above procedure, we shall discuss the identification of material parameters in a class of constitutive models for large elastoplastic deformations. In particular, we will focus on phenomenological models that include deformation-induced anisotropy, as it occurs in engineering metals under large strains. Such models find potential application in for instance the simulation of industrial forming processes, so as to be able to optimize

the process control. The inherent physical nonlinearity of such models is further complicated by the complex history dependence of the deformation-induced anisotropy. The simplest possible experiment —the uniaxial tensile test— poses two major difficulties for the parameter identification in large deformation plasticity models: (*i*) for models that include deformation-induced anisotropy, the uniaxial response need not depend on all material parameters, and (*ii*) at large strains, necking intervenes and leads to a complicated three-dimensional stress and strain state. A large strain torsion test does not lead to such instabilities, and does provide a means to identify all pertinent parameters for the class of models considered here. The parameter identification from the torsion test, however, is rather involved because of the inherent radially inhomogeneous and path dependent stress and strain state, thus requiring a numerical approach as suggested here. After discussing the typical experimental results of a large strain torsion test, we present the class of constitutive models that we are going to consider, the finite element approach to simulating the test and, finally, a highly approximate model to be used in the multipoint approximation technique.

4.1. Experimental Results

The torsion tests to be considered here employ solid circular bars with a cylindrical section of 150 mm length and an initial radius of $R_0 = 7.5$ mm. The angle of twist φ is measured over a gauge section of initial length $L_0 = 100$ mm which is believed to be sufficiently far away from the ends to exclude any end effects, so that it can be assumed with high accuracy that plane cross-sections remain plane (see Fig. 2). In addition to that, the axial displacement $U = L - L_0$
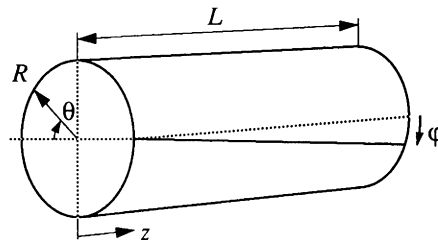

Figure 2. Torsion of a circular cylindrical solid bar

over the same gauge section is monitored by means of a special axial-torsional extensometer. The reason for doing that is that for large torsional strains, the specimen will tend to elongate when it is left free in the axial direction. This was first discovered by Swift [13] in 1947, and has been conclusively attributed to deformation-induced anisotropy due to texture (see, e.g., [14], [15]). Thus, the quantitative experimental determination of this Swift effect is an important source of information for the identification of material parameters in the constitutive description of the evolving anisotropy; but it should be realized that it is a second-order effect. Figure 3 shows typical results of such a torsion test on 304 stainless steel in terms of the torque T and the
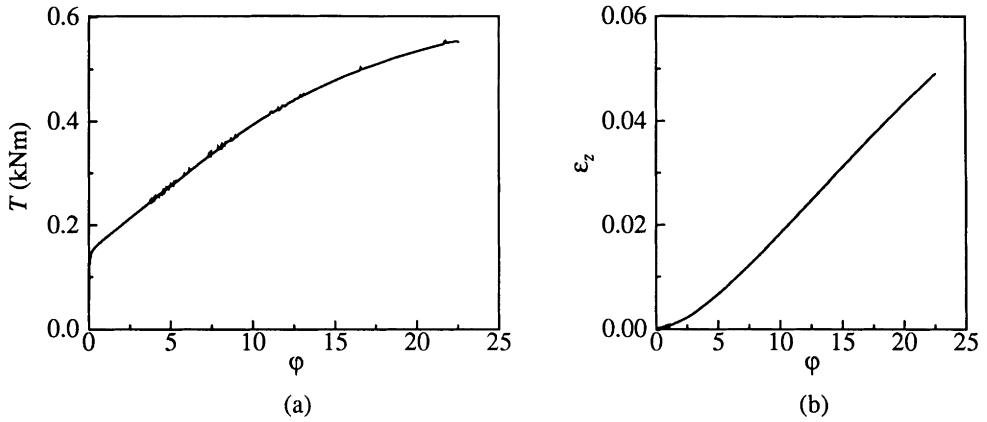
Figure 3. Torque response (a) and axial strain development (b) during free-end torsion of solid SS 304 bars.

(engineering) axial strain $\varepsilon_z = L/L_0 - 1$ as a function of twist φ [16]. The particular tests were carried out at room temperature and at a twist rate of $\dot{\varphi} = 1.1 \times 10^{-3}$ rad/s.

4.2. Constitutive Equations

Several phenomenological constitutive equations for large strain elastoplasticity may be found in the literature that have been used to study large strain torsion, or rather the significantly simpler problem of simple shear (see, e.g., [15], [17]–[19]). The referenced constitutive equations are of a kinematic hardening type, possibly coupled with isotropic hardening, incorporating the notion of plastic spin. Here, we will consider only one of them, which is a combined kinematic-isotropic hardening model —referred to as the DL model in [19])— with the plastic spin constitutive equation based on propositions of Dafalias [17] and Loret [18]. This particular model features the gradual fading of kinematic hardening at large strains, based on the experimental observation that typically at strains larger than several ten percents no Bauschinger effect is observed; evidence for that in large strain torsion may be found in [13], [16].

A summary of the constitutive equations is given in Table 1. Here, **D** and **W** are generic for strain-rate tensors and spin tensors, respectively, tr denotes the trace and : is the double dot product ($(\mathcal{L} : \mathbf{D})_{ij} = \mathcal{L}_{ijkl} D_{kl}$). Further, $\boldsymbol{\sigma}$ and **s** are the Cauchy stress tensor and its deviator, **a** is the back stress tensor which specifies the translation of the yield surface's centre in $\boldsymbol{\sigma}$-space and H specifies its isotropic expansion. The relative contributions of kinematic and isotropic hardening to strain hardening are governed by the parameter b. Purely isotropic behaviour is obtained for $b = 1$ while pure kinematic hardening corresponds to $b = 0$. Without going into further details, we note that this model incorporates the following material parameters:

E, ν Young's modulus and Poisson's ratio;
σ_y the initial von Mises yield stress;
$\Delta\sigma_y^{(i)}$, $\varepsilon_0^{(i)}$ parameters in the expression

$$\sigma_e = \sigma_y + \sum_{i=1}^{K} \Delta\sigma_y^{(i)} \left[1 - \exp(-\varepsilon_p/\varepsilon_0^{(i)})\right] \tag{11}$$

for the description of the uniaxial response in terms of the effective von Mises stress σ_e and the accumulated effective plastic strain ε_p;

ε_b the evolution parameter in the evolution of b (the initial value b_0 is taken to be 0);

ρ the (constant) plastic spin parameter.

With only one exponential term in (11), i.e. $K = 1$, a reasonable fit can be obtained to either the small strain or the large strain response; but in order to describe both ranges well, at least two terms will be necessary (see [19]).

Table 1

kinematics:	$\mathbf{D} = \mathbf{D}^e + \mathbf{D}^p , \quad \mathbf{W} = \mathbf{W}^e + \mathbf{W}^p$
(hypo-) elasticity:	$\overset{\vee}{\boldsymbol{\sigma}} = \dot{\boldsymbol{\sigma}} - \mathbf{W}^e\boldsymbol{\sigma} + \boldsymbol{\sigma}\mathbf{W}^e = \mathcal{L} : \mathbf{D}^e ,$ $\mathcal{L}_{ijkl} = \dfrac{E}{1+v}\left[\dfrac{1}{2}(\delta_{ik}\delta_{jl} + \delta_{il}\delta_{jk}) + \dfrac{v}{1-2v}\delta_{ij}\delta_{kl}\right]$
yield condition:	$\varphi(\bar{\mathbf{s}}) \equiv \dfrac{1}{2}\mathrm{tr}\,\bar{\mathbf{s}}^2 - \dfrac{1}{3}\sigma_y^2 , \quad \bar{\mathbf{s}} = \dfrac{1}{H}(\mathbf{s} - \mathbf{a})$
hardening evolution:	$\sigma_F \equiv H\sigma_y = (1-b)\sigma_y + b\sigma_e , \quad \sigma_e = \sqrt{3\,\mathrm{tr}\,\mathbf{s}^2/2} ,$ $\dot{b} = (1-b)\dot{\varepsilon}_p/\varepsilon_b , \quad \dot{\varepsilon}_p = \sqrt{\dfrac{2}{3}\mathrm{tr}\,\mathbf{D}^{p^2}}$
flow rule:	$\mathbf{D}^p = \lambda\dfrac{\partial\varphi}{\partial\bar{\mathbf{s}}} = \lambda\bar{\mathbf{s}} , \quad \mathbf{W}^p = \lambda\dfrac{1}{2}\rho\,(a\bar{\mathbf{s}} - \bar{\mathbf{s}}a)$
back stress evolution:	$\overset{\vee}{\mathbf{a}} \equiv \dot{\mathbf{a}} - \mathbf{W}^e\mathbf{a} + \mathbf{a}\mathbf{W}^e = \mu\mathbf{D}^p$

4.3. Finite Element Simulations

Since cross-sections of the bar can be considered to remain plane and the behaviour during large strain torsion remains axisymmetric, the state of stress and strain inside the bar are uniform in the axial and circumferential directions; but, there remains an inherent dependency on the radial coordinate. It has been demonstrated ([15], [19]) that this problem of free-end torsion can be efficiently solved by means the special purpose finite elements presented in [20]. Each element effectively is a circular cylindrical tube, but computationally it is considered to be one-dimensional along the r–axis, with two nodes at $r = r_1$ and $r = r_2$, respectively, and with two material sampling points. The degrees of freedom of the entire finite element model of the bar consisting of, say, n elements then comprise $n + 1$ radial nodal displacements along with the axial displace-
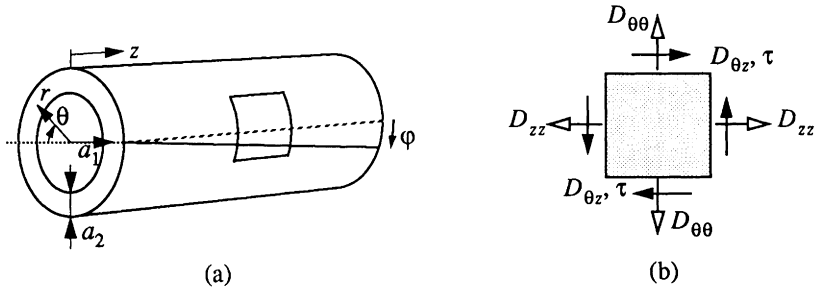
Figure 4. Approximate model based on a tube with mean radius a_1 and wall thickness a_2 (a). An element out of the tube, showing the skewsymmetric state of stress and rate of deformation such that $D_{\theta\theta} = -D_{zz}$ (b).

ment U and the angle of twist φ. It was found that highly accurate results are obtained for the solid bar problem by using only $n = 5$ elements.

4.4. Approximate Model

Let us now consider now the formulation of a much simpler mechanistic model of this free-end torsion problem to be used in the multipoint approximation technique. Since the torque response and the elongation response are the two response quantities of interest here, we will need approximate expressions for these quantities in function of the angle of twist. We recall that the approximate model needs only to inherit a functional dependence on the material parameters similar to the actual one, while suitable tuning parameters should allow for a numerically accurate representation of the response functions locally, i.e. within a relatively small neighbourhood of chosen material constants.

A possible approximate model that satisfies the requirements put forward earlier is based on a tubular specimen instead of a solid bar with a mean radius a_1 and a wall thickness a_2 (see Fig. 4a). If it is assumed that the shear stress τ is uniform in the radial direction and neglecting any geometric changes, the torque can be written as $T = 2\pi a_1^2 a_2 \tau$. On the other hand, if all stress components but the shear stress and the associated back stress are neglected, so that $\sigma_{\theta z} = \tau$, $\sigma_{ij} \equiv 0$ otherwise in a cylindrical (r, θ, z) coordinate system, we simply find from the yield condition that $\tau = a_{\theta z} + \sigma_F / \sqrt{3}$ once plastic deformation has started. The current value of the flow stress σ_F is determined through H by the current values of σ_e and b, both depending on the accumulated plastic strain ε_p. Neglecting elastic deformations, $\mathbf{D} = \mathbf{D}^p$, the accumulated plastic strain ε_p in the expression (11) for σ_e can be approximated as $\varepsilon_p = \gamma / \sqrt{3}$ where $\gamma = (a_1/L) \varphi$ is the mean shear strain in the tube. Furthermore, the evolution equation for b in Table 1 can be integrated at once to give

$$b = 1 - \exp\left(-\frac{1}{\sqrt{3}} \frac{\gamma}{\varepsilon_b}\right).$$

Combining these expressions and presupposing that we can give the shear back stress $a_{\theta z}$ as a function of the $\gamma = (a_1/L)\varphi$, we find the following approximate torque–twist expression in the plastic regime:

$$T(\varphi) = \frac{2}{\sqrt{3}}\pi a_1^2 a_2 \left(\sqrt{3} a_{\theta z}(\gamma) + \sigma_y + b \sum_{i=1}^{K} \Delta \sigma_y^i \left[1 - \exp(-\frac{1}{\sqrt{3}}\frac{\gamma}{\varepsilon_0^i}) \right] \right). \tag{12}$$

A similar relationship in the elastic regime is readily obtained from elementary considerations.

Let us now consider the specification of the back stress $a_{\theta z}$. According to the constitutive equations listed in Table 1, this back stress is determined by a rate equation that is coupled strongly with the plastic flow rule. To the authors' knowledge, there is no exact solution available; therefore we reside here in a 'phenomenological' approach, where we approximate the actual evolution of $a_{\theta z}$ as a function of γ by means of a functional expression based on the numerical results obtained in [19] and on known simple shear solutions [17], [18]. First, we note that the numerical results in [19] for a constitutive model that has a rapidly disappearing contribution of kinematic hardening, $b \approx 1$, can be approximated rather well by a function of the type $a_{\theta z}(\gamma) = a_3 \gamma^{a_4} \exp(-a_5 \gamma)$ with coefficients $a_3 > 0$, $a_4 > 1$, $a_5 > 0$. Secondly, we recall that if we use a purely kinematic hardening model, $b = 0$, the shear back stress exhibits an oscillatory $\sin\gamma$ response to simple shear if there is no plastic spin, $\rho = 0$, while with increasing value of ρ the response becomes more and more of the type $1 - \exp(-a_8 \gamma)$. We combine these responses for $b = 0$ into the expression $a_{\theta z}(\gamma) = a_6 \exp(-\rho \sigma_y)\sin\gamma + a_7 \rho \sigma_y [1 - \exp(-a_8 \gamma)]$, where we have nondimensionalized ρ by σ_y and where the coefficients a^α ($\alpha = 6, 7, 8$) are positive. Finally, we obtain the desired functional expression to be substituted into (12) by a linear combination of the above expressions for $b \approx 1$ and $b = 0$, respectively:

$$a_{\theta z}(\gamma) = b a_3 \gamma^{a_4} \exp(-a_5 \gamma) + (1 - b)\{a_6 \exp(-\rho \sigma_y)\sin\gamma + a_7 \rho \sigma_y [1 - \exp(-a_8 \gamma)]\}. \tag{13}$$

The simplified torque model thus obtained contains 8 tuning parameters a_l, $l = 1, ..., 8$.

An approximate expression for the axial strain response can be obtained in the following way. It follows from the skewsymmetric nature of the state of stress and deformation (see Fig. 4b) that $D_{\theta\theta} = -D_{zz}$, so that from plastic incompressibility $D_{rr} = 0$. Since $D_{zz} = \dot{\varepsilon}_z$ for small axial deformations, it is concluded from the flow rule listed in Table 1 that $\dot{\varepsilon}_z/\dot{\gamma} = \bar{s}_{zz}/2\bar{s}_{\theta z}$, while $\bar{s}_{rr} = 0$ and $\bar{s}_{\theta\theta} = -\bar{s}_{zz}$. Using then the yield condition —where all stress components are taken into consideration now— to eliminate $\bar{s}_{zz}$, we obtain

$$\frac{\dot{\varepsilon}_z}{\dot{\gamma}} = \pm\frac{1}{2}a_9\sqrt{\frac{1}{3}\left(\frac{\sigma_y}{\bar{s}_{\theta z}}\right)^2 - 1}\,, \tag{14}$$

where we have introduced the parameter a_9 as a tuning parameter to compensate for the approximations involved, especially to correct for the fact that the Swift effect in the actual solid bar will be less prominent than in a thin-walled tube because of constraints imposed by the core material. The stress dependent term in (14) can be written as $\sigma_y/\bar{s}_{\theta z} = \sigma_F/(\tau - a_{\theta z})$ which we shall further approximate by

$$\sigma_y / \bar{s}_{\theta z} = \sqrt{3} / (1 - \sqrt{3} a_{\theta z} / \sigma_e) \,,$$

with σ_e being given by (11). Finally, eq. (14) can be rewritten as an ordinary differential equation for $\varepsilon_z(\varphi)$ which has to be solved numerically. Just like the approximate torque model, this simplified model for the axial strain response also contains 8 tuning parameters a_l, $l = 1, 3, ..., 9$; but it should be noted that the two models will be considered as separate models, each with their own set of tuning parameters.

5. ILLUSTRATIVE EXAMPLE

To illustrate the implementation of the presented approach, let us consider in some detail the identification problem of the material parameters in the isotropic hardening model, $b = 1$ with $K = 1$, based on the comparison of measured and simulated values of the torque in the free-end solid bar torsion test. In this case, the angle of twist φ is considered as the experiment history parameter. The response quantity R_s^α for $\alpha = 1$ presents now the torque values ($s = 1, ..., 127$) obtained in the course of the experiment [16]; the simulated response $R^\alpha(x, \varphi)$ describes the torque as a function of the three parameters to be identified:

$$x_1 = \sigma_y \,, \quad x_2 = \Delta\sigma_y \,, \quad x_3 = \varepsilon_0 \,,$$

and the twist angle φ. The imposed side constraints are given in Table 2 In order to eliminate the effect of the large difference in values of the search region sizes, the optimization variables have been scaled by the linear transformation to new dimensionless values $\tilde{x}_1$, $\tilde{x}_2$, $\tilde{x}_3$, which correspond to the following scaled values of the side constraints: $\tilde{A}_j = 1.0$, $\tilde{B}_j = 11.0$ ($j = 1, 2, 3$)..

Table 2
Side constraints on material parameters for isotropic model

	$x_1 = \sigma_y$ (MPa)	$x_2 = \Delta\sigma_y$ (MPa)	$x_3 = \varepsilon_0$
A_j	1.	1.	0.001
B_j	1000.	4000.	2.0

To give some insight into the problem formulation, the search region has been scanned by repeated calls for the nonlinear FE simulation procedure. Every call required about 4.5 minutes of CPU time on a Sun SPARCstation 1. Figures 2,3 and 4 present two-dimensional slices of the dependence of the function $F(x)$ on the material parameters at the point $\tilde{x}_1^0 = 3.5$, $\tilde{x}_2^0 = 6.0$, $\tilde{x}_3^0 = 6.0$, which corresponds to the minimum value of the objective function $F(\tilde{x}^0) = 0.1146 \times 10^{-3}$, as obtained by a straightforward scanning procedure.

To solve the optimization problem, the simplified model was constructed in the form (10) by the procedure described in the previous section. For the purely isotropic model, where $b = 1$ and

the back stress must vanish identically, there remain only two tuning parameters in the simplified model (12), namely the radius a_1 and the wall thickness a_2 of the tube specimen, which are introduced artificially in order to construct the simplified expression.

Let us consider in detail the first step of the optimization procedure. The plan of numerical experiments corresponds to the starting point $\tilde{x}_1$, which is located in the centre of the search region, and points $\tilde{x}_p$ ($p = 2, 3, 4$), which are obtained by the steps in each x_j-coordinate direction. As the initial step length the value $0.25\,(\tilde{A}_j - \tilde{B}_j)$ has been chosen. It makes the plan of experiments as follows: $\tilde{x}_1 = (6.0, 6.0, 6.0)$, $\tilde{x}_1 = (3.5, 6.0, 6.0)$, $\tilde{x}_1 = (6.0, 3.5, 6.0)$, $\tilde{x}_1 = (6.0, 6.0, 3.5)$. The value of the objective function at the starting point is $F(\tilde{x}_1) = 0.2131$. The first search subregion is determined then by the move limits $\tilde{A}_j^{-1} = 2.0$, $\tilde{B}_j^{-1} = 7.5$ ($i = 1, 2, 3$). The location of the plan points and the search subregion is shown in Figures 5 a through c by numbered circles and rectangles, respectively. Figures 5 d through f present the behaviour of the simplified function $\tilde{F}(\tilde{x})$, using the following values of the tuning parameters $a_1 = 5.493$ mm, $a_2 = 4.609$ mm, as obtained from the optimization problem (8). Their comparison shows that with properly tuned parameters a_1, a_2 the simplified model presents a very good approximation of the actual function $F(\tilde{x})$.

The solution of the first step optimization problem (4), (5) gives the following values of the optimization variables: $\tilde{x}_1^* = 3.729$, $\tilde{x}_2^* = 4.711$, $\tilde{x}_3^* = 4.844$, which corresponds to the material parameters listed in Table 3 The obtained point $\tilde{x}_1^*$ is internal for the first search subregion; therefore the size of the second search subregion has been reduced by halve and the search process was continued from the obtained point. The process was stopped after the third iteration when the search subregion was reduced to 15% of its initial size. The obtained point $\tilde{x}_1^* = 3.763$, $\tilde{x}_2^* = 4.633$, $\tilde{x}_3^* = 4.897$ corresponds to the final value of material parameters listed in Table 3. Figure 6 presents the comparison of the simulated torque function using the identified material parameters with the measured values from the experiment [16].

Table 3
Material parameters for isotropic model from optimization problem (4), (5).

	$x_1 = \sigma_y$ (MPa)	$x_2 = \Delta\sigma_y$ (MPa)	$x_3 = \varepsilon_0$	$F(\tilde{x})$
first iteration	273.7	1485.0	0.7693	0.3057×10^{-3}
last iteration	277.0	1454.0	0.780	0.1513×10^{-3}

6. THE MATERIAL PARAMETERS IDENTIFICATION

Let us consider the identification problem of material parameters in the full mixed isotropic-kinematic hardening model shown in Table 1 with the two-term exponential fit in (11), $K = 2$, based on the comparison of measured and simulated values of both torque and axial strain in the solid bar torsion test described above. Again, the twist angle φ is considered as the experiment history parameter. The response quantity R_s^1 presents the torque values ($s = 1, ..., 158$) and R_s^2 corresponds to the axial strain values ($s = 1, ..., 24$) obtained in the course of the experiment
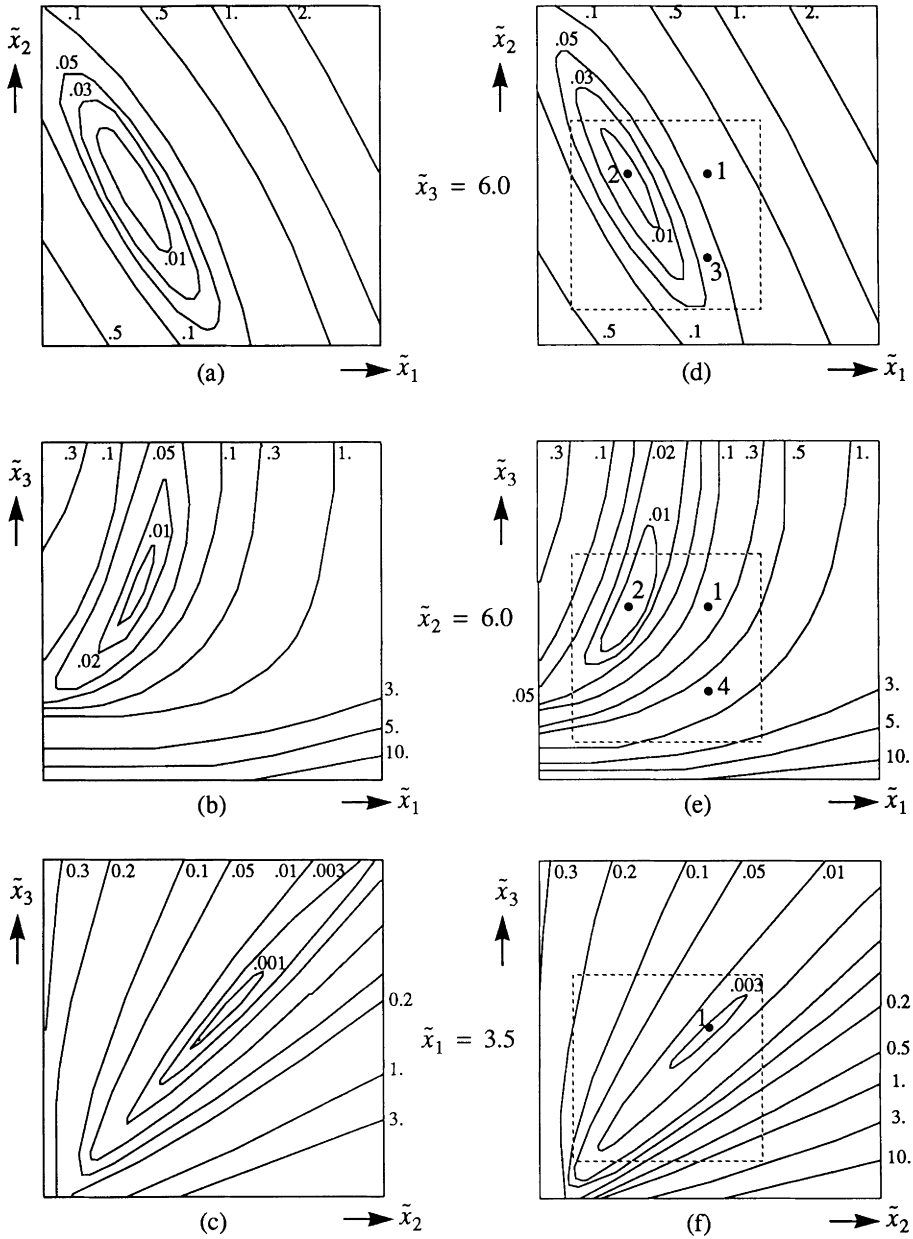
Figure 5. Contour plots of the objective function $F(\tilde{x})$ (left-hand side, figures a, b, c) and the simplified function $\tilde{F}(\tilde{x})$ (right-hand side, figures d, e, f) for the three-parameter problem. All nondimensional parameters $\tilde{x}_i$ are in the range $[\tilde{A}_j, \tilde{B}_j] = [1.0, 11.0]$. Numbered points indicate plan points and dashed boxes indicate the search subregion of the first iteration.
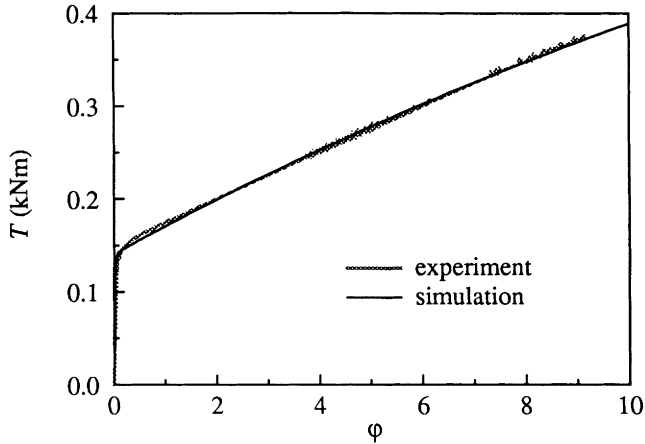
Figure 6. Comparison of experimental and simulated torque–twist curves according to the isotropic hardening model with the material parameters from Table 3.

[16]. The simulated response quantities $R^\alpha(\mathbf{x}, \tau_s^\alpha)$ describe the torque ($\alpha = 1$) and the axial strain ($\alpha = 2$) as functions of seven material parameters to be identified,

$$x_1 = \varepsilon_b \,, \quad x_2 = \sigma_y \,, \quad x_3 = \Delta\sigma_y^{(1)} \,, \quad x_4 = \varepsilon_0^{(1)} \,, \quad x_5 = \Delta\sigma_y^{(2)} \,, \quad x_6 = \varepsilon_0^{(2)} \,, \quad x_7 = \rho \,,$$

and the twist angle φ. Both response quantities are considered as being equally important for the material parameters identification, which means that the weight coefficients Θ^α are equal: $\Theta^1 = \Theta^2 = 1$. The imposed side constraints are given in the Table 4.

Table 4
Side constraints on material parameters

	ε_b	σ_y (MPa)	$\Delta\sigma_y^{(1)}$ (MPa)	$\varepsilon_0^{(1)}$	$\Delta\sigma_y^{(2)}$ (MPa)	$\varepsilon_0^{(1)}$	ρ
A_j	0.001	1.0	1.0	0.001	1.0	0.001	0.0
B_j	0.5	500	4000	2.0	400	0.01	0.01

As in the previous example, the optimization variables have been scaled to dimensionless values $\tilde{x}_j$, which correspond to the scaled values of the side constraints: $\tilde{A}_j = 1.0$, $\tilde{B}_j = 11.0$ ($j = 1, \ldots, 7$). The simplified models, used in the optimization procedure, have been constructed in the form (10) where the function $\tilde{R}_k^\alpha(\mathbf{x}, \mathbf{a}^\alpha, \tau_s^\alpha)$ corresponds to the simplified torque function T given by the expression (12) when $\alpha = 1$, and to the function ε_z derived from the

numerical solution of the differential equation (14) when $\alpha = 2$.

As the starting point for the optimization procedure, the set of material parameters suggested in [19] has been chosen, as listed in Table 5. The values of the individual response functions at the starting point, $F^1(\mathbf{x}_1) = 0.103\times10^{-1}$, $F^2(\mathbf{x}_1) = 0.860\times10^{-3}$ indicate that the discrepancy between the simulated and measured values of torque is much greater than the one of axial strain, as is clearly seen in Figures 4 and 5 in [19]. The total value of the objective function at the starting point is $F(\mathbf{x}_1) = 0.112\times10^{-1}$.

Table 5
Material parameters for mixed isotropic-kinematic hardening model.

	x_1	x_2	x_3	x_4	x_5	x_6	x_7
	ε_b	σ_y (MPa)	$\Delta\sigma_y^{(1)}$ (MPa)	$\varepsilon_0^{(1)}$	$\Delta\sigma_y^{(2)}$ (MPa)	$\varepsilon_0^{(1)}$	ρ
initial set	0.185	175.0	3200	1.5	100.0	0.003	0.0036
final set	0.185	175.1	2810	1.576	102.1	0.0027	0.00288

After two iterations of the optimization algorithm, the size of the search subregion was reduced to 5% of the initial search region size. The set of obtained material parameters is also presented in Table 5. The values of the individual response functions at the obtained point are as follows: $F^1(\mathbf{x}^*) = 0.302\times10^{-3}$, $F^2(\mathbf{x}^*) = 0.659\times10^{-3}$, and the total value of the objective function is $F(\mathbf{x}^*) = 0.961\times10^{-3}$. The figures 7a and b show the comparison of the measured values of torque and axial strain, respectively, and the simulated ones obtained with the obtained set of material parameters.

7. CONCLUDING REMARKS

- The approach presented in this paper allows for the determination of the phenomenological coefficients in nonlinear constitutive models for engineering materials by minimizing the difference between certain response quantities measured by means of laboratory experiments and obtained by numerical simulation.
- The error functions (3) are shown to be able to quantify correctly the difference between simulated and measured response.
- The implementation of the approach shows that there is a direct relationship between the quality of the (physically based) simplified functions, which are used in the optimization process instead of the actual ones, and the rate of convergence of the algorithm.
- Special attention must be paid to avoid numerical problems which may arise during the solution of the optimization problem (8), by for instance proper scaling, elimination of low sensitivity to some tuning parameters and high sensitivity to others, etc.
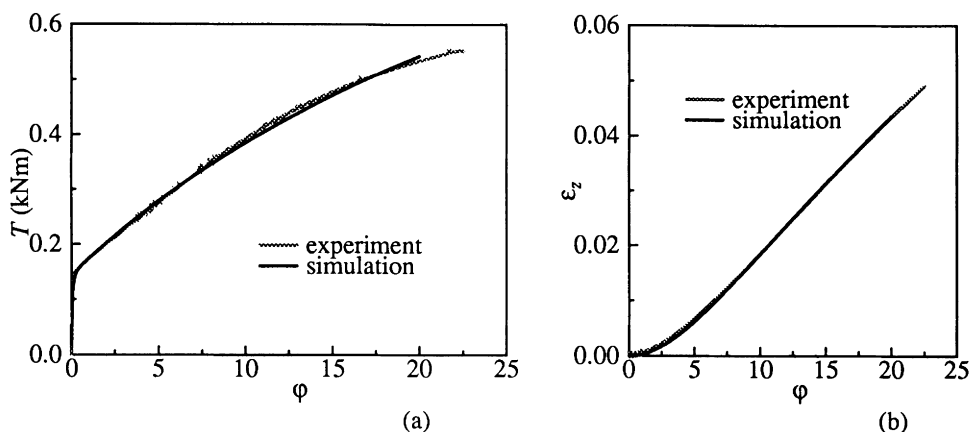
Figure 7. Comparison of experimental and simulated torque–twist curves (a) and axial strain development (b) during free-end torsion of a solid SS 304 bar.

- In principle, the present approach is applicable to any nonlinear constitutive model and is capable of handling an almost unlimited variety of (nontrivial) experiments, allowing for inhomogeneous material response, the use of structural components as specimens, etc.

Acknowledgement

8. REFERENCES

1. Distéfano, N.: On the identification problem in linear viscoelasticity. *ZAMM* **50** (1970) 683–690.
2. Kavanagh, K.T.; Clough, R.W.: Finite element applications in the characterization of elastic solids. *Int. J. Solids Structures* **7** (1971) 11–23.
3. Iding, R.H.; Pister, K.S., Taylor, R.L.: Identification of nonlinear elastic solids by a finite element method. *Comput. Meth. Appl. Mech. Engrg.* **5** (1974) 121–142.
4. Nappi, A.: Structural identification of nonlinear systems subjected to quasistatic loading. *Application of System Identification in Engineering* (ed. by H.G. Natke), Springer, 1988.
5. Hendrix, M.: *Identification of the mechanical behaviour of solid materials.* Ph.D. Thesis, Eindhoven University of Technology, The Netherlands, 1991.
6. Pedersen P.: Optimization methods applied to identification of material parameters. *Proceedings of the GAMM seminar on Discretization Methods and structural optimization*, Lecture Notes in Engineering 42, Springer, 1989.
7. Pedersen, P., Frederiksen, P.S.: Sensitivity analysis for identification of material parameters. *Proceedings of the 9th Int. Conf. on Experimental Mechanics*, Copenhagen, 1990, 545-551.

8. Lin, E.I.-H.; Sackman, J.L.: Identification of dynamic properties of nonlinear viscoelastic materials and the associated wave propagation problem. *Int. J. Solids Structures* **11** (1975) 1145–1159.

9. Vestergaard B.: Experimentation and identification for models of visco-elastic materials. *Proceedings of the 9th Int. Conf. on Experimental Mechanics*, Copenhagen, 1990, 601-608.

10. Toropov, V.V.: Simulation approach to structural optimization. *Structural Optimization* **1** (1989) 37-46.

11. Toropov, V.V.: Multipoint approximation method in optimization problems with expensive function values. *Proceedings of 4th Int. Symposium on Systems Analysis and Simulation*, Berlin 1992 (to appear).

12. Box, G.E.P.; Draper, N.R.: *Empirical model-building and response surfaces*. John Wiley & Sons, 1987.

13. Swift, H.W.: Length changes in metals under torsional overstrain. *Engineering* **163** (1947), 253–257.

14. Gil-Sevillano, J.; Van Houtte, P.; Aernoudt, E.: Deutung der Schertexturen mit Hilfe der Taylor-Analyse. *Z. Metallkunde* **66** (1975) 367–373.

15. Van der Giessen, E.; Wu, P.D.; Neale, K.W.: On the effect of plastic spin on large strain elastic-plastic torsion of solid bars. Delft Univ. of Techn., Lab. for Engrg. Mech. Report no. 942 (1991). *Int. J. Plasticity* (to be published).

16. Delhage, L.: Strain-rate and axial effects during reversed large strain torsion of solid circular bars. Delft Univ. of Techn., Lab. for Engrg. Mech. Report no. 924 (1991).

17. Dafalias, Y.F.: Corotational rates for kinematic hardening at large plastic deformation. *J. Appl. Mech.* **50** (1983) 561-565.

18. Loret, B.: On the effects of plastic rotation in the finite deformation of anisotropic elastoplastic materials. *Mech. Mater.* **2** (1983) 287-304.

19. Van der Giessen,E.; Wu, P.D.; Neale, K.W.: Effect of plastic spin and deformation-induced anisotropy on large strain torsion of solid bars. *Proceedings of IUTAM symposium on Constitutive Relations for Finite Deformation of Polycrystalline Metals*, Beijing 1991 (in press).

20. Wu, P.D.; Van der Giessen, E.: Analysis of elastic-plastic torsion of circular bars at large strains. *Arch. Appl. Mech.* **61** (1991) 89–103.

Natural vibrations of free thick plates and identification of transverse shear moduli

Per S. Frederiksen

Department of Solid Mechanics
The Technical University of Denmark, Lyngby, Denmark

Abstract

The first part of the paper presents a Ritz model which is applicable to the investigation of natural vibrations of thick laminated plates with all edges free. The model is based on a higher-order shear deformation theory, which accounts for parabolic distribution of the transverse shear strains through the thickness of the plate. A special family of functions related to the free/free beam mode shapes is used in the Ritz series, which provides very accurate results with a small number of degrees of freedom. Results obtained by a commercial 3-D finite element program are compared with the results obtained by the Ritz model.

In the second part the Ritz model is combined with optimization techniques with the goal of identifying material constants on the basis of experimentally determined natural frequencies for a thick plate. The unknown material constants are determined as those resulting in minimum error between model and experiment. The technique allows identification of six material constants: the two transverse shear moduli and the four in-plane constants (two Young's moduli, the shear modulus and Poisson's ratio).

The method has been implemented in a PC based integrated set-up providing fast and reliable determination of the material constants on the basis of a non-destructive and simple test. In practical experiments excellent agreement between measured and calculated natural frequencies have been obtained. Results for a rolled aluminium plate and a carbon/epoxy plate are shown.

1. INTRODUCTION

The constantly increasing use of advanced composite materials and the possibilities of designing these materials with optimized performances requires reliable knowledge of the material parameters. Determination of such parameters by traditional testing is destructive,

cumbersome and time-consuming. The present paper deals with the determination of elastic material constants by a combined numerical/experimental method, often known as "identification method". In the present approach natural frequencies of plates are measured and computer calculations are used to determine the unknown parameters in order to obtain optimum agreement between model and experiment. As structural frequencies are integrated quantities we obtain material parameters valid in the mean for the entire structure.

Some work has been done in the framework of the classical laminated plate theory. See e.g. Fälström and Jonsson [1], Deobald and Gibson [2], Sol [3] and Frederiksen [4], who used various techniques based on plate vibrations to determine elastic constants in thin plates. Apparently, the identification of transverse properties of plates has been neglected. Transverse properties of laminates are probably the most restrictive structural parameter in practice and transverse shear properties of laminated plates have to be assessed.

The object of the present paper is twofold. Firstly, to develop an accurate numerical model of natural vibrations of fully free thick plates. The model should be suitable for implementation on a PC due to integration with modal software and hardware and to assure later development of a portable technique. Secondly, to integrate the model with optimization techniques with the goal of determining material constants, including the two transverse shear moduli, on the basis of measured natural frequencies of thick plates.

The fully free plate was chosen because other boundary conditions such as the clamped or simply supported boundary condition are very difficult to realize experimentally.

A highly accurate modelling of the dynamic behaviour of a rectangular thick plate which accounts for transverse shear deformation is crucial for the reliability of the identification results. Finite element analysis was rejected because sufficiently accurate FEM solutions usually require a large number of degrees of freedom in the model. This would lead to considerable consumption of memory and computer time. Instead, a Ritz model based on a higher-order plate theory has been developed.

Several theories incorporating shear deformation have been proposed over the years. The first such theory for laminated anisotropic plates was advanced by Yang et al. [5], who extended Mindlin's theory for isotropic plates, Mindlin [6]. In this type of theory it is necessary to introduce a shear correction factor into the shear stress resultant to account for the fact that the theory predicts a uniform shear stress through the thickness of the plate, which is obviously not correct.

Several theories have been proposed which are more advanced than the Mindlin type theory. These theories are often known as higher-order theories. An n'th-order theory is one in which the displacements (often, the in-plane displacements) are expanded in terms of the thickness coordinate up to the n'th power. See Lo et al. [7] for a review.

The basis for this work is a refined third-order shear deformation theory proposed by Reddy [8]. A similar theory has been presented by Levinson [9]. The theory uses a displacement approach. The displacement field allows for distortion of third order of normals to the midplane of the undeformed plate, while the transverse deflection is assumed to be constant through the thickness. The displacement field chosen is of a special form satisfying the condition of stress-free plate surfaces. The theory involves the same number of dependent unknowns as the first-order Mindlin type shear deformation theory, but there is no need for shear correction coefficients because the theory accounts for parabolic variation of the

transverse shear stresses. Thus, the theory is an advanced two-dimensional theory which accurately describes the global behaviour of the plate.

For the fully free plate problem, exact closed-form solutions do not exist and a numerical discretization is necessary. A Ritz model based on the displacement field given in [8] and [9] is developed for this purpose. By proper choice of the functions, approximating the displacement field, very accurate results can be obtained with relatively few terms in the series, i.e. a small number of degrees of freedom. Thus, the model is suitable for implementation on a PC and yet a fast analysis is assured.

The general technique for identification of material parameters involving sensitivity analysis and optimization has previously been reported in [4] with the technique based on thin test plates and classical plate theory, whereby only the four in-plane material constants (two Young's moduli, the shear modulus and Poisson's ratio) have been determined. The present work thus forms a natural extension of the technique reported in [4] with the additional identification of the two transverse shear moduli. In the work [4] the number of frequencies involved in the identification was 7 to 10, but to asses the transverse shear properties it is necessary to increase the number of frequencies and/or the thickness of the test plate. The number of frequencies is typically 10 to 15.

2. DISPLACEMENT FIELD

Consider a rectangular plate of constant thickness h , length a and width b . A Cartesian coordinate system x-y-z is located at the middle plane with the z axis normal to this plane. The shear deformation theory proposed in [8] is based on a displacement field in which the displacements in the x and y directions are expanded as cubic functions of the thickness coordinate, and the transverse deflection is assumed to be constant over the thickness. The present analysis is limited to symmetric laminates, in which case the in-plane displacements of the midplane are zero due to the absence of in-plane loads. The applied simplified displacement field thus has the form

$$u(x, y, z) = z\,\psi_x(x, y) + z^2\,\varphi_x(x, y) + z^3\,\zeta_x(x, y)$$

$$v(x, y, z) = z\,\psi_y(x, y) + z^2\,\varphi_y(x, y) + z^3\,\zeta_y(x, y) \tag{1}$$

$$w(x, y, z) = w(x, y)$$

u, v and w are the displacement components in the x, y and z directions and ψ_x , ψ_y , φ_x , φ_y , ζ_x and ζ_y are unknown expansion functions. The Mindlin theory, (i.e. a first-order theory) is obtained for $\varphi_x = \varphi_y = \zeta_x = \zeta_y = 0$ and is parallel to the Timoshenko beam theory. For the present higher-order theory, the functions φ_x , φ_y , ζ_x and ζ_y can be determined using the condition that the transverse shear stresses σ_{13} and σ_{23} vanish on the top and bottom surfaces of the plate. The displacement field in (1) then becomes

$$u(x, y, z) = z\left[\psi_x - \frac{4}{3}\left[\frac{z}{h}\right]^2\left[\frac{\partial w}{\partial x} + \psi_x\right]\right]$$

$$v(x, y, z) = z\left[\psi_y - \frac{4}{3}\left[\frac{z}{h}\right]^2\left[\frac{\partial w}{\partial y} + \psi_y\right]\right] \quad (2)$$

$$w(x, y, z) = w(x, y)$$

Although distortion of third order of the in-plane displacements is taken into account, the displacement field (2) contains the same number of dependent unknowns as in the first-order Mindlin theory.

3. CONSTITUTIVE RELATIONS

It is assumed that a number of orthotropic plane sheets (plies) are stacked to form a plate. An orthotropic material has three mutually orthogonal planes of elastic symmetry. The three principal material directions will be denoted by a 1-2-3 coordinate system with the 3 axis normal to the plane of the ply (coincident with the z axis). In agreement with PEDERSEN [10] we choose the larger modulus direction of the two in-plane orthogonal directions as a reference axis. This axis is chosen as the 1 axis. For plies consisting of a unidirectional fibre-reinforced composite material, the direction notation thus has the specific meaning of 1 being the axis parallel to the fibres and 2 and 3 being the axes normal to the fibre direction, in-plane and out-of-plane, respectively.

If the analysis is limited to plates of moderate thickness, the orders of magnitude for the stresses, see Reddy [11], justify an assumption of a plane state with

$$\sigma_{33} = 0 \quad (3)$$

and the general constitutive stress-strain relations for the ply reduce to, see e.g. Whitney [12]

$$\left\{\begin{matrix}\sigma_{11}\\\sigma_{22}\\\sigma_{12}\end{matrix}\right\}_{12} = \frac{E_1}{\alpha_0}\begin{bmatrix} 1 & \nu_{12}E_2/E_1 & 0 \\ \nu_{12}E_2/E_1 & E_2/E_1 & 0 \\ 0 & 0 & \alpha_0 G_{12}/E_1 \end{bmatrix}_{12}\left\{\begin{matrix}\varepsilon_{11}\\\varepsilon_{22}\\2\varepsilon_{12}\end{matrix}\right\}_{12} \quad (a)$$

$$\left\{\begin{matrix}\sigma_{13}\\\sigma_{23}\end{matrix}\right\}_{12} = \frac{E_1}{\alpha_0}\begin{bmatrix} \alpha_0 G_{13}/E_1 & 0 \\ 0 & \alpha_0 G_{23}/E_1 \end{bmatrix}_{12}\left\{\begin{matrix}2\varepsilon_{13}\\2\varepsilon_{23}\end{matrix}\right\}_{12} \quad (b)$$

(4)

where

$$\alpha_0 = 1 - v_{12}^2 \, E_2/E_1 \tag{5}$$

and (4 b) is written in consistency with (4 a).

The engineering constants are

E_1 , E_2	: Young's modulus in the 1 and 2 directions, respectively
G_{12} , G_{13} , G_{23}	: Shear modulus in the 1-2 , 1-3 and 2-3 planes, respectively
v_{12}	: Poisson's ratio as determined from contraction in 2 direction under uniaxial tension in 1 direction

With the assumption of (3), the influence of E_3 , v_{13} and v_{23} is eliminated and a total of 6 independent engineering constants remains for the analysis.

The ply properties have to be added in a common (global) reference system which is geometrically natural to the solution of the problem, say the x-y-z coordinate system, so rotational transformations are of vital importance. These transformations can be found in most textbooks on composite material, e.g. Vinson and Sierakowski [13].
According to Pedersen [14] it is convenient to define practical non-dimensional material parameters based on the relative quantities of the orthotropic constitutive matrix from (4).

$$\alpha_2 = 4 - 4 \, E_2/E_1$$
$$\alpha_3 = 1 + (1 - 2v_{12}) \, E_2/E_1 \; - \; 4 \, \alpha_0 \, G_{12}/E_1$$
$$\alpha_4 = 1 + (1 + 6v_{12}) \, E_2/E_1 \; - \; 4 \, \alpha_0 \, G_{12}/E_1$$
$$\alpha_8 = 4(G_{13} + G_{23})\alpha_0 \, /E_1 \tag{6}$$
$$\alpha_9 = 4(G_{13} - G_{23})\alpha_0 \, /E_1$$

$$\alpha_0 = 1 - v_{12}^2 \, E_2/E_1 \; = \; 1 - (\alpha_4 - \alpha_3)^2 / \big(16(4 - \alpha_2)\big)$$

Upon transformation, the ply constitutive relations in the x-y-z coordinate system can be expressed as

$$\begin{Bmatrix} \sigma_{11} \\ \sigma_{22} \\ \sigma_{12} \end{Bmatrix}_{xy} = \frac{E_1}{8\alpha_0} \begin{bmatrix} c_{11} & c_{12} & c_{13} \\ c_{12} & c_{22} & c_{23} \\ c_{13} & c_{23} & c_{33} \end{bmatrix}_{xy} \begin{Bmatrix} \varepsilon_{11} \\ \varepsilon_{22} \\ 2\varepsilon_{12} \end{Bmatrix}_{xy} \qquad \text{(a)}$$

$$\tag{7}$$

$$\begin{Bmatrix} \sigma_{13} \\ \sigma_{23} \end{Bmatrix}_{xy} = \frac{E_1}{8\alpha_0} \begin{bmatrix} c_{44} & c_{45} \\ c_{45} & c_{55} \end{bmatrix}_{xy} \begin{Bmatrix} 2\varepsilon_{13} \\ 2\varepsilon_{23} \end{Bmatrix}_{xy} \qquad \text{(b)}$$

where the components c_{ij} of the non-dimensional constitutive matrix depend on the parameters α_2, α_3, α_4, α_8, α_9 and the angle γ relating the material coordinate system 1-2-3 and the reference coordinate system x-y-z .

4. THE RITZ MODEL

The displacement field (2) contains the three unknown functions w, ψ_x and ψ_y . Following the Ritz procedure, we assume the solution for the three functions to be in the form of finite series with undetermined coefficients. Each series is composed of multiplications of admissible functions

$$w(x,y) = \sum_{m,n}^{N} Z_{mn} W_m \left(\frac{2}{a} x\right) W_n \left(\frac{2}{b} y\right)$$

$$\psi_x(x,y) = \sum_{m,n}^{N} X_{mn} \Psi_m \left(\frac{2}{a} x\right) W_n \left(\frac{2}{b} y\right) \qquad (8)$$

$$\psi_y(x,y) = \sum_{m,n}^{N} Y_{mn} W_m \left(\frac{2}{a} x\right) \Psi_n \left(\frac{2}{b} y\right)$$

with the notation $\displaystyle\sum_{m,n}^{N} = \sum_{m=0}^{p-1} \sum_{n=0}^{p-1}$, $N = p^2$

i.e. we choose to deal with the same number of functions in the x and y directions and W_m and Ψ_m are functions of the non-dimensional variable ξ varying between ± 1 .

The arbitrary coefficients in the series are determined by minimizing an energy functional, thereby obtaining a best approximation to satisfy the equation of motion for the plate. The time variable is eliminated by assuming the harmonic time dependence $e^{i\omega t}$, considering w , u and v as the time-independent displacement amplitudes.

With a constant specific mass ρ , the maximum kinetic energy is

$$T = \tfrac{1}{2}\omega^2\rho \int_\Omega \int_{-h/2}^{h/2} (u^2 + v^2 + w^2)\, dz\,dx\,dy \tag{9}$$

where Ω denote the middle plane of the plate.
By substituting the displacement field (2) into (9) and performing the integration with respect to z , the maximum kinetic energy can be expressed in terms of the displacement and slope functions.

$$T = \tfrac{1}{2}\omega^2\rho \int_\Omega \left[\; w^2 h \; + \tfrac{17}{315}h^3\left(\psi_x^2 + \psi_y^2 \right) - \tfrac{8}{315}h^3\left(\frac{\partial w}{\partial x}\,\psi_x + \frac{\partial w}{\partial y}\,\psi_y \right) \right.$$
$$\left. + \tfrac{1}{252}h^3\left(\left[\frac{\partial w}{\partial x}\right]^2 + \left[\frac{\partial w}{\partial y}\right]^2 \right) \; \right] dx\,dy \tag{10}$$

The total strain energy is given by

$$U = \tfrac{1}{2} \int_\Omega \int_{-h/2}^{h/2} \sigma_{ij}\, \varepsilon_{ij}\, dz\,dx\,dy \tag{11}$$

The stresses can be eliminated from the strain energy using the constitutive relations (4), remembering the plane state condition, $\sigma_{33} = 0$. The maximum strain energy can be expressed in terms of the displacement and slope functions and the laminate stiffnesses by substituting the strains which can be derived from the displacement field (2) into (11) and performing the integration with respect to z .

Now, let $\overline{T}$ be the specific kinetic energy amplitude such that $T = \omega^2\,\overline{T}$ is the kinetic energy amplitude. For a conservative system, the total energy is constant, i.e.

$$U - \omega^2\overline{T} = 0 \tag{12}$$

Stationarity of the energy difference with respect to the constants Z_{kl} , X_{kl} and Y_{kl} results in

$$\frac{\partial U}{\partial Z_{kl}} - \lambda_i \frac{\partial \overline{T}}{\partial Z_{kl}} = 0 \quad \text{for } k, l = 0, 1, \dots, p\text{-}1$$
$$\frac{\partial U}{\partial X_{kl}} - \lambda_i \frac{\partial \overline{T}}{\partial X_{kl}} = 0 \quad \text{for } k, l = 0, 1, \dots, p\text{-}1 \tag{13}$$
$$\frac{\partial U}{\partial Y_{kl}} - \lambda_i \frac{\partial \overline{T}}{\partial Y_{kl}} = 0 \quad \text{for } k, l = 0, 1, \dots, p\text{-}1$$

U and $\overline{T}$ are always quadratic in the undetermined coefficients Z_{mn}, X_{mn} and Y_{mn} ; (13) thus represents a set of $3 \times p \times p$ linear homogeneous equations, i.e. a classical eigenvalue problem with the eigenvalue λ_i related to eigenfrequency ω_i by $\lambda_i = \omega_i^2$.

The partial derivatives of the strain energy are involved and extensive and will not be given in this presentation. However, it turns out that the derivatives involve 15 distinct integrals which are characteristic non-dimensional integrals of the assumed functions. These are listed below in an abbreviated form.

$$G_{mn}^{(r,s)} = \int_{-1}^{1} \frac{d^r w_m}{d\xi^r} \frac{d^s w_n}{d\xi^s} \, d\xi \quad \text{for } r, s = 0, 1, 2 \tag{14}$$

$$I_{mn}^{(r,s)} = \int_{-1}^{1} \frac{d^r \Psi_m}{d\xi^r} \frac{d^s \Psi_n}{d\xi^s} \, d\xi \quad \text{for } r, s = 0, 1 \tag{15}$$

$$J_{mn}^{(r,s)} = \int_{-1}^{1} \frac{d^r \Psi_m}{d\xi^r} \frac{d^s w_n}{d\xi^s} \, d\xi \quad \text{for } r = 0, 1 \text{ and } s = 0, 1, 2 \tag{16}$$

where $m, n = 0, 1, \ldots , p\text{-}1$

The partial derivatives for the specific kinetic energy $\overline{T}$ which are obtained from equation (10) are more tractable. The three expressions are given below using the above notation for the integrals.

$$\frac{\partial \overline{T}}{\partial Z_{kl}} = \sum_{m,n}^{N} \left\{ \frac{1}{4} abh\rho \, Z_{mn} G_{km}^{(0,0)} G_{ln}^{(0,0)} + \frac{1}{252} \rho h^3 \, Z_{mn} \left[\frac{b}{a} G_{km}^{(1,1)} G_{ln}^{(0,0)} + \frac{a}{b} G_{ln}^{(1,1)} G_{km}^{(0,0)} \right] \right.$$

$$\left. - \frac{2}{315} \rho h^3 \left[b \, X_{ml} J_{mk}^{(0,1)} G_{ln}^{(0,0)} + a \, Y_{kn} J_{nl}^{(0,1)} G_{km}^{(0,0)} \right] \right\} \tag{17}$$

$$\frac{\partial \overline{T}}{\partial X_{kl}} = \frac{\rho h^3}{315} \sum_{m,n}^{N} \left\{ \frac{17}{4} ab \, X_{mn} G_{ln}^{(0,0)} I_{km}^{(0,0)} - 2b \, Z_{mn} J_{km}^{(0,1)} G_{ln}^{(0,0)} \right\} \tag{18}$$

$$\frac{\partial \overline{T}}{\partial Y_{kl}} = \frac{\rho h^3}{315} \sum_{m,n}^{N} \left\{ \frac{17}{4} ab \, Y_{mn} G_{km}^{(0,0)} I_{ln}^{(0,0)} - 2b \, Z_{mn} J_{ln}^{(0,1)} G_{km}^{(0,0)} \right\} \tag{19}$$

Now, we may choose to write the eigenvalue problem (13) in the form

$$[\nabla U]\{\Delta_i\} = \lambda_i [\nabla \overline{T}]\{\Delta_i\} \qquad \text{for } i = 1,2,...,3N = 3p^2 \tag{20}$$

where $\{\Delta_i\}$ denotes the eigenvector corresponding to the eigenvalue λ_i , i.e. $\{\Delta_i\}$ is a vector which contains the $3p^2$ coefficients Z_{mn} , X_{mn} and Y_{mn}

$$\{\Delta\}^T = \{Z_{00}, Z_{01}, ..., Z_{p-1p-1}, X_{00}, X_{01}, ..., X_{p-1p-1}, Y_{00}, Y_{01}, ..., Y_{p-1p-1}\} \tag{21}$$

$[\nabla \overline{T}]$ is the coefficient matrix for the partial derivatives of the maximum specific kinetic energy and $[\nabla U]$ is the coefficient matrix for the partial derivatives of the maximum strain energy.

Once the assumed functions have been chosen, the integrals (14) to (16) are evaluated. The evaluations are performed only once as the integrals are dimensionless. The number of evaluations is $N = p^2$ for each of the 15 distinct integrals. The integrations were performed numerically.

A variety of numerical methods exists for solution of an eigenvalue problem. For this research, the subspace iteration was chosen. The technique is described in detail by Bathe and Wilson [15].

5. CHOICE OF ASSUMED FUNCTIONS

In applying the Ritz procedure to plate problems involving free edges, numerous researchers have used series of multiplications of free/free beam vibration mode shapes (ordinary beam functions) to approximate the deflection form, e.g. Ritz [16] and Leissa [17].

In the paper by Bassily and Dickinson [18] the inadequacy of the ordinary beam functions when used in the Ritz method for plate problems involving free edges was demonstrated. A new set of functions, related to the beam mode shapes, was postulated which allows considerably more accurate treatment of such plates. This family of functions known as "degenerated beam functions" is used in the present thick plate formulation. The function set for the free/free plate is

$$w_0(\xi) = 1$$

$$w_1(\xi) = \xi$$

$$w_m(\xi) = \cos(k_{(m+2)/2} \, \xi) \quad \text{for} \quad m = 2, 6, 10, \ldots$$

$$w_m(\xi) = \cosh(k_{(m+1)/2} \, \xi) \quad \text{for} \quad m = 3, 7, 11, \ldots \tag{22}$$

$$w_m(\xi) = \sin(k_{(m+2)/2} \, \xi) \quad \text{for} \quad m = 4, 8, 12, \ldots$$

$$w_m(\xi) = \sinh(k_{(m+1)/2} \, \xi) \quad \text{for} \quad m = 5, 9, 13, \ldots$$

where k_m is determined by

$$\tan k_m + (-1)^m \tanh k_m = 0 \quad \text{for} \quad m = 2, 3, 4, \ldots \tag{23}$$

The hyperbolic functions mainly assure an accurate deflection form near the edges, while the circular functions determine the overall deflection form.

It remains to choose the functions Ψ_m which are part of the series approximating the rotations ψ_x and ψ_y. With the special relations for the case of classical plate theory in mind, the following choice is made

$$\Psi_{m-1}(\xi) = \frac{\partial w_m}{\partial \xi} \quad \text{for} \quad m = 1, 2, 3, \ldots \tag{24}$$

Consistency with the classical plate theory in the limit of thin plates is thereby assured.

6. NUMERICAL RESULTS

When the degenerated beam functions are employed, a very rapid convergence is achieved, so highly accurate solutions can be obtained using relatively few terms in the series. Convergence tests have shown that a number of 10×10 equal 100 terms in each of the three series provides sufficiently accurate results for the first 15 natural frequencies for different plate configurations. Thus, the Ritz model with a total of 300 degrees of freedom is used. The computational time for the calculation of 10 natural frequencies with this model varies (depending on the starting vectors) from 1 to 2 minutes on a standard 486 33MHz PC.

The present Ritz model based on the higher-order shear deformation theory (HSDT) is verified by comparison with 3-D finite element results. Table 1 contains the first 8 natural frequencies of a thick isotropic plate calculated by the HSDT Ritz model and a 3-D finite element model. The finite element mesh consisted of 4 layers of 12×8 elements. A 20-node

brick element providing a parabolic displacement field was used. This element had three translational degrees of freedom assigned to each node, resulting in a total of 6339 degrees of freedom in the model. The finite element calculations were performed at Risø National Laboratory with the Solvia package.

When comparing the results it should be emphasized that the Ritz model is a two-dimensional model, which do not take transverse normal stress/strain into account. Despite this simplification the agreement with the 3-D finite element solution is very good and indicates that the Ritz model yields highly accurate results.

Table 1

Comparison of non-dimensional natural frequencies $\overline{\omega} = \omega a^2 \sqrt{\rho/(Eh^2)}$ for a fully free isotropic plate, with $\nu = 0.3$. Aspect ratio $a/b = 1.5$. Length-to-thickness ratio $a/h = 10$.

Freq. no.	Present HSDT Ritz Solution	3-D FEM SOLVIA	Difference relative to HSDT (%)
1	5.630	5.637	0.12
2	6.247	6.253	0.10
3	12.542	12.566	0.19
4	13.977	14.006	0.21
5	15.699	15.741	0.27
6	18.065	18.126	0.34
7	22.153	22.231	0.35
8	24.944	25.035	0.36

7. THE IDENTIFICATION PROBLEM

Assuming the plate dimensions, the plate mass and the stacking sequence to be known, we seek values for the five non-dimensional material parameters α_m that will provide agreement between the eigenfrequencies obtained through the numerical model and by experimental measurements.

With I being the number of eigenvalues involved in the identification, the experimentally obtained eigenvalues are

$$\overline{\lambda}_1 \ , \ \overline{\lambda}_2 \ , \ \overline{\lambda}_3 \ , \ \ldots \ , \ \overline{\lambda}_I \qquad (25)$$

The numerically calculated eigenvalues obtained by solving the matrix eigenvalue problem

(20) for a given plate with assumed material data α_m are

$$C\lambda_1 \ , \ C\lambda_2 \ , \ C\lambda_3 \ , \ \ldots \ , \ C\lambda_I \tag{26}$$

where the scaling factor C is defined by the mean value

$$C = \frac{1}{I} \sum_{i=1}^{I} \bar{\lambda}_i / \lambda_i \tag{27}$$

The influence of quantities which just scale the eigenvalue spectrum is thereby eliminated. From (25) to (27) we can define the error functional Φ. We choose the frequently used sum of squares function but alternatives are possible

$$\Phi = \sum_{i=1}^{I} (\bar{\lambda}_i - C\lambda_i)^2 / \bar{\lambda}_i^2 \tag{28}$$

The identification problem can now be formulated as an optimization problem, i.e. identification of the set of non-dimensional material parameters α_m that minimizes the error functional Φ :

Minimize $\Phi(\alpha_2, \alpha_3, \alpha_4, \alpha_8, \alpha_9) \geq 0$ (29)

From the optimal solution $(\alpha_2, \alpha_3, \alpha_4, \alpha_8, \alpha_9)$, the relative material moduli and α_0 are evaluated through the inverse relations of (6). As will be seen from (4), the constitutive matrix $[C]$ is proportional to E_1 , from which it follows that the system eigenvalues are proportional to E_1 as well. Thus, the eigenvalue scaling factor C is a direct measure of E_1 and provides the conversion from relative to absolute material parameters.

The identification/optimization technique, including the analytical sensitivity analysis which is fundamental for the speed of the method, is in principle as described in [4] and Pedersen and Frederiksen [19], although the references only treat the case of classical plate theory involving three parameters.

Experimentally, the plate natural frequencies are determined by the impulse technique, see Halvorsen and Brown [20]. Some details regarding application of the technique to free plates and the test set-up are given in [4].

8. RESULTS

An aluminium plate and a laminated carbon/epoxy plate are investigated. The identified parameters are the four in-plane engineering constants, E_1 , E_2 , G_{12} and v_{12} plus the two transverse shear moduli G_{13} and G_{23} .

The first example is a rolled aluminium plate. The mass was 841.6 g and the plate dimensions were as follows

$$\text{length} = 220.0 \text{ mm} , \text{width} = 140.0 \text{ mm} , \text{thickness} = 10.17 \text{ mm}$$

11 natural frequencies were accurately measured (in Hz) :

1037.3 , 1108.3 , 2363.2 , 2808.4 , 2955.0 , 3579.3 , 4312.1 , 5052.7 , 6033.6 , 6935.8 , 7366.3

The identified engineering constants were

$$E_1 = 71.2 \text{ GPa} , E_2 = 70.8 \text{ GPa} , G_{12} = 25.9 \text{ GPa} , v_{12} = 0.334 ,$$
$$G_{13} = 26.9 \text{ GPa} , G_{23} = 24.5 \text{ GPa}$$

The resulting relative differences between measured and calculated frequencies were (in %) :

$$0.08 , 0.09 , -0.14 , 0.02 , -0.08 , -0.04 , -0.01 , 0.01 , 0.00 , 0.01 , 0.06$$

Note that the frequency residuals are extremely small. Only for frequency number three does the difference exceed 0.1% . This confirms that both the experimental technique and the numerical model provide very accurate values for the plate natural frequencies.

The values for the material constants obtained by the identification method are in good agreement with values commonly known for aluminium and the material is observed to be nearly isotropic. For comparison, the in-plane isotropic Young's modulus is $E = 2G_{12}(1+v_{12})$ = 69.1 GPa . The rolling process seems to have a more significant effect on the transverse shear moduli than on the two Young's moduli.

The iteration history in terms of the non-dimensional material parameters defined by (6) as encountered during the optimization is shown in figure 1. The initial guess is (0.5, 0.5, 2, 1, 0) and the optimum solution is (0.02, 0.04, 2.70, 2.57, 0.12) .
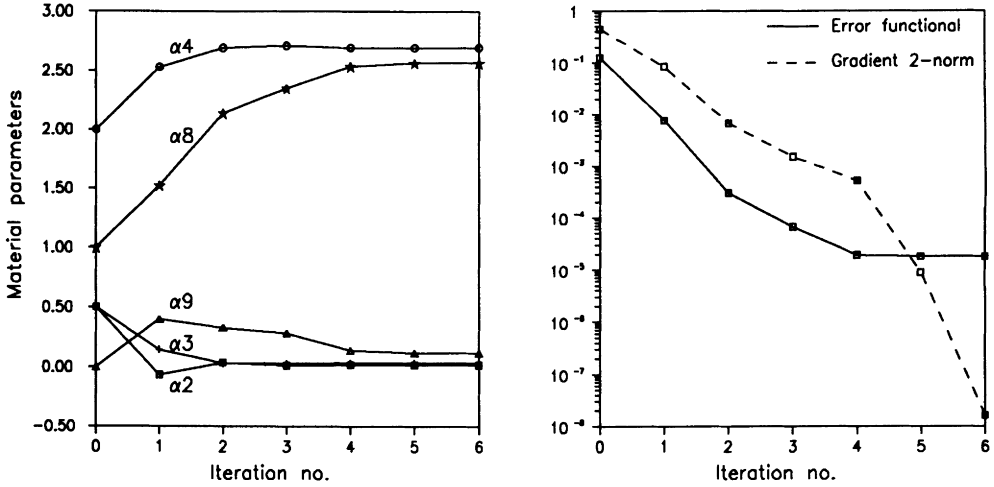
Figure 1. Iteration history for non-dimensional material parameters (left) and the corresponding error functional and its gradient 2-norm defined by $\|\{\partial\Phi/\partial\alpha_2 , \partial\Phi/\partial\alpha_3 , \partial\Phi/\partial\alpha_4 , \partial\Phi/\partial\alpha_8 , \partial\Phi/\partial\alpha_9\}\|_2$ (right).

The second example is a carbon fibre reinforced epoxy plate.
The plate was stacked by eight plies with fibres interwoven at right angles. The layout was $[(0°,90°)_8]$. The following parameters were measured

length = 170.6 mm , width = 147.0 mm , thickness = 2.63 mm , mass = 99.9 g

10 frequencies were measured (in Hz) :

176.16 , 516.90 , 628.95 , 775.71 , 851.59 , 1180.3 , 1414.5 , 1511.0 , 1943.4 , 2113.8

The identified engineering constants were

$E_1 = 56.6 \, GPa , E_2 = 52.1 \, GPa , G_{12} = 3.82 \, GPa , \nu_{12} = 0.074 ,$
$G_{13} = 3.04 \, GPa , G_{23} = 2.68 \, GPa$

with the resulting relative differences between measured and calculated frequencies (in %) :

-0.07 , -0.03 , 0.14 , -0.03 , 0.08 , -0.05 , -0.22 , 0.16 , 0.05 , 0.03

Again the agreement between measured and calculated frequencies is very good.
With respect to the identified quantities it is observed that the transverse shear moduli are significantly smaller than the in-plane shear modulus.

In the following some consideration will be given to the number of natural frequencies involved in the identification.

A large number of frequencies reduces, or even eliminates, the possibility of multiple optimal solutions, or a non-physical solution in combination with good agreement between calculated and measured frequencies. Furthermore, identification based on many frequencies presumably results in better averaged values than identification based on a few frequencies. However, the numerical work increases with the number of frequencies and the numerical model predicts the higher frequencies less accurately. In addition, the experimental determination of higher frequencies tends to become more complicated. For instance, higher modes are generally more closely spaced and care must be taken not to overlook resonance peaks in the frequency spectrum.

From a theoretical point of view, where perfect agreement between model and experiment exists, the identification result does not depend on the number of frequencies. However, in a practical experiment some variations may occur. To illustrate this effect table 2 shows the engineering constants for the carbon/epoxy plate identified on the basis of a varying number of frequencies. As many as 15 natural frequencies have been determined experimentally.

Very stable values of the in-plane engineering constants are found. Even the shear modulus G_{23} is only slightly affected by the number of frequencies. On the other hand, the estimated value of G_{13} is useless when the identification is based on 8 and 9 frequencies. When frequency number 10 is introduced, a reasonable estimate is obtained and the value is stable as more frequencies are added. The reason for this is that the effect of transverse shear may be significant only for higher modes of vibration. In addition the thickness of the plate and the ratio of elastic modulus to shear modulus has a strong impact on the transverse shear effect. In this respect the investigation of the frequency sensitivities with respect to the two transverse shear moduli plays an important role. Figure 2 shows the frequency sensitivities with respect to G_{13} and G_{23} for the carbon/epoxy plate. Frequency number 10 is seen to be the first frequency which provides a sufficiently high sensitivity with respect to G_{13} and its importance to the identification of G_{13} is obvious. Fairly high sensitivities with respect to G_{23} are provided by frequency numbers 7, 8 and 9, and this is the reason why G_{23} behaves well over the investigated range of frequencies. The overall stable values obtained when the number of frequency ranges from 10 to 15 confirms the reliability of the test.

Table 2
Identification results for various numbers of frequencies. Carbon/epoxy plate with woven fibres.

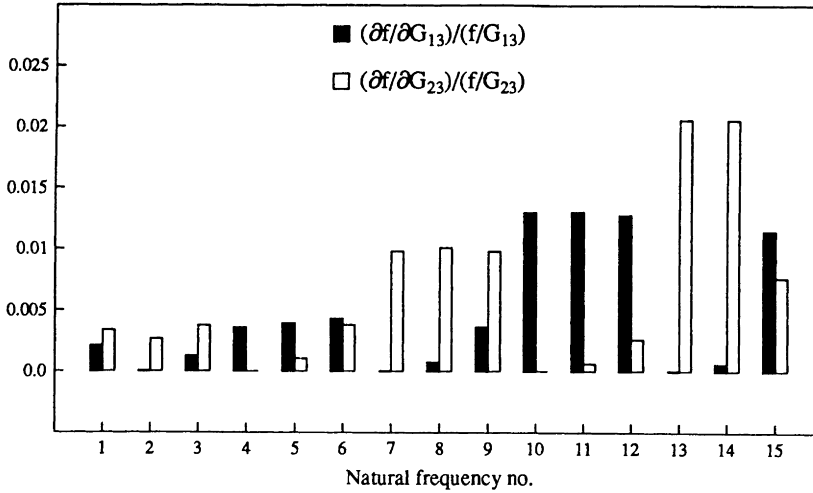| No. of freq.	E_1 (GPa)	E_2 (GPa)	G_{12} (GPa)	v_{12}	G_{13} (GPa)	G_{23} (GPa)
8	56.33	52.09	3.80	0.056	35.28	2.71
9	56.29	52.07	3.80	0.059	56.98	2.75
10	56.63	52.09	3.82	0.074	3.04	2.68
11	56.62	52.09	3.82	0.074	3.09	2.68
12	56.60	52.09	3.82	0.074	3.13	2.67
13	56.58	52.16	3.82	0.078	3.14	2.37
14	56.58	52.12	3.82	0.077	3.13	2.52
15	56.59	52.12	3.82	0.077	3.12	2.52

Non-dimensional
frequency sensitivity

Figure 2. Sensitivities for non-dimensional natural frequency with respect to the two transverse shear moduli for a carbon/epoxy plate with woven fibres.

9. CONCLUSION

A method for determination of elastic material parameters (engineering constants) of anisotropic plates with attention focused on the transverse shear moduli has been presented. The method takes advantage of the identification approach, which is an experimental strategy in which the experiment is designed to give results with a high level of reliability without forcing the desired quantities to be among the directly measured quantities. The quantities wanted can then be identified by computer calculations. As many as six elastic constants are determined simultaneously on the basis of experimental data from a single experiment.

The method is in contrast to the traditional testing idea and offers new possibilities for investigation of the material constants because it is non-destructive and very fast.

The technique provides outstanding possibilities for investigating the influence of different environmental conditions on the material constants. As an example, temperature dependence for in-plane constants for different materials obtained by the present approach can be found in [4].

The advantages of the method are obvious, but the approach inevitably raises new problems. Interpretation of the experiment is complicated because the desired quantities appear in a most indirect way. The analysis of the experiment is involved and can only be done in a numerical way with a computer. The close cooperation between experimental work and

numerical work implies a possibility of an additional error source compared with traditional testing, i.e. errors in the form of an inaccurate or erroneous numerical model. The importance of an accurate model to the reliability of the test must be emphasized. With this demand fulfilled, successful and reliable identification depends on the quality of the test plate, which is assumed to be flat and with uniform properties. In general, extremely good agreement between calculated and measured plate natural frequencies have been found.

The speed of the test is an important feature. With up-to-date high performance PC equipment (486 processor) the calculation time required for the identification is about 10 minutes.

The potential time savings and versatility of the technique combined with the promising results indicates that the method deserves further consideration. With further development, it is believed that the present technique for determination of elastic constants will become a valuable non-destructive test.

Although computer time and memory requirements limit the complexity of the numerical model, future developments in computer technology with constantly increasing capabilities will undoubtedly considerably increase the possibilities for more complex applications in the field of identification.

ACKNOWLEDGEMENT

REFERENCES

1   K.E. Fällström and M. Jonsson, A Nondestructive Method to Determine Material Properties in Anisotropic Plates, Polym. Compos., Vol. 12, No. 5, 1991, pp. 293-305.

2   L.R. Deobald and R.F. Gibson, Determination of Elastic Constants of Orthotropic Plates by a Modal Analysis/Rayleigh-Ritz Technique, J. Sound Vib., Vol. 124, 1988, pp. 269-283.

3   H. Sol, Identification of Anisotropic Plate Rigidities using Free Vibration Data, Doctoral Thesis, Free University of Brussels, 1986, p. 251.

4   P.S. Frederiksen, Identification of Temperature Dependence for Orthotropic Material Moduli, Mech. Mater., Vol. 13, 1992, pp. 79-90.

5   P.C. Yang, C.H. Norris and Y. Stavsky, Elastic Wave Propagation in Heterogeneous Plates, Int. J. Solids Struct., Vol. 2, 1966, pp. 665-684.

6   R.D. Mindlin, Influence of Rotary Inertia and Shear on Flexural Motions of Isotropic, Elastic Plates, J. Appl. Mech., Vol. 18, 1951, pp. 31-38.

7   K.H. Lo, R.M. Christensen and E.M. Wu, A Higher-Order Theory of Plate Deformation, J. Appl. Mech., Vol. 44, 1977, pp. 662-676.

8   J.N. Reddy, A Simple Higher Order Theory for Laminated Composite Plates, J. Appl. Mech., Vol. 51, 1984, pp. 745-752.

9   M. Levinson, An Accurate, Simple Theory of The Statics and Dynamics of Elastic Plates, Mech. Res. Commun., Vol. 7, 1981, pp. 81-87.

10 P. Pedersen, Concurrent Engineering Design of and with Advanced Materials, DCAMM Report No. S 56, The Technical University of Denmark, 1991, p. 45.

11 J.N. Reddy, Energy and Variational Methods in Applied Mechanics, Wiley, New York, 1984, p. 545.

12 J.M. Whitney, Structural Analysis of Laminated Anisotropic Plates, Technomic Publishing Co., Inc., Lancaster, 1987, p. 342.

13 J.R. Vinson and R.L. Sierakowski, The Behaviour of Structures Composed of Composite Materials, Nijhoff, Dordrecht, 1986, p. 323.

14 P. Pedersen, Notes for Lectures on Laminates − Analysis − Sensitivity Analysis − Optimal Design − Identification of Material Parameters, Department of Solid Mechanics, DTH, 1988, p. 140.

15 K.J. Bathe and E.L. Wilson, Numerical Methods in Finite Element Analysis, Prentice-Hall, Englewood Cliffs, 1976, p. 528.

16 W. Ritz, Theorie der Transversalscwingungen einer Quadratischen Platten mit Freien Randem, Annalen der Physik, Viente Folge, Vol. 28, 1909, pp. 737-786.

17 A.W. Leissa, The Free Vibration of Rectangular Plates, J. Sound Vib., Vol. 31, 1973, pp. 257-293.

18 S.F. Bassily and S.M. Dickinson, On the Use of Beam Functions for Problems of Plates Involving Free Edges, J. Appl. Mech., Vol. 42, 1975, pp. 858-864.

19 P. Pedersen and P.S. Frederiksen, Sensitivity Analysis for Identification of Material Parameters, Proceedings of the 9th international conference on experimental mechanics, Vol. 2, pp. 545-551, 1990, ed. V. Askegaard, Aaby Tryk, Copenhagen.

20 W.G. Halvorsen and D.L. Brown, Impulse Technique for Structural Frequency Response Testing, Sound and Vibration, November 1977, pp. 8-21.

Elaboration of Optimal Design Models for Objects from Data of Experiments

R. Rikards*

* CAD Centre, Riga Technical University, 1 Kalku St., LV–1047, Riga, Latvia

Abstract

The program systems to design composite materials with predicted properties are presented. For this purpose there are three main programs: program for evaluation of plans of experiments, approximation program and program for nonlinear programming problems. Approximation program gives regression models from data of experiment. These approxmate functions are used as control functions for optimization problems. Numerical examples of optimal design of composite materials with glass, carbon and aramid fibre fabrics are presented.

1. INTRODUCTION

The aim of investigation is to develop methods and program systems to design composite materials with predicted properties. Such properties are weight, price, modulus of elasticity, strength, damping properties etc. It is necessary to satisfy simultaneously several quality indeces, which, as a rule, are mutually contradictory: improvement of one index is attained only by impairing another.

For composite materials such problems are multiparameter and multiextremal, since there are many input or control parameters: Young' s modulus of fibre and matrix, fibre volume fraction, fibre orientation, layers stacking sequence etc. The solution of this problem is deviced into the following six stages: choice of control parameters and establishment of the domain of search, elaboration of informative plan of the experiment for the chosen number of reference points, execution of the experiments (physical experiment or computer simulation, for example, FEM analysis), determination of mathematical models for each quality index from the experimental data, optimization on the basis of discovered mathematical models and at the end verification experiments at the point of optimal solutions.

In each of these stages it is possible to solve a problem by various methods. So, there are many ways to get the plans of experiment (see, for example, handbook Ref. I). In the present investigation we use a new approach for planing out of experiments (see Ref. 2). The details of this approach shall be discussed later.

The mathematical models using data of multifactorial experiment can also be obtained by various methods. In this case a widely used method is polynominal approximation. In the present investigation we use another method to find out the equation of regression with program RESINT (see Ref. 3).

Also, there are various methods for optimization (see, for example, Refs. 4, 5). In the present investigation we use the penalty function method with random search and self training (see Ref. 6). The corresponding program SUPEX on the basis of this efficient method is widely used to solve various nonlinear programming problems.

All the methods mentioned above are used to design composite materials with predicted properties. Some numerical examples for glass, carbon and aramid fibre fabrics reinforced composites are discussed.

2. ELABORATION OF INFORMATIVE PLANS OF EXPERIMENT

Most of criteria for optimal plans of experiments are connected with the predicted mathematical model of designing object or process. Most of mathematical models are polinominal models and the corresponding plans of experiment are optimal only for these polinominal models. However, in most cases we don't know what is the best mathematical model.

Let us consider a criterion for elaboration of plans of experiment which is independent on mathematical model of the designing object or process. Such approach was at first suggested by P. Audze and V. Eglais (see Ref. 2). The initial information for elaboration of plan is number of factors n and number of experiments k. The main principles in this new approach are as follows:

1) the number of levels for each factor is equal to the number of experiments and for each level is only one experiment;

2) the points of experiments in the domain of variables (factors) are distributed as regular as possible. To realize the second principle it is suggested to use a criterion

$$\min \Phi = \sum_{i=1}^{k} \sum_{j=i+1}^{k} \frac{1}{l_{ij}^2} \qquad (1)$$

where l_{ij} is the distance between the points having numbers i and j $(i \neq j)$. Minimum of this criterion are being defined. Physically it is equal to minimum of potential energy of repulsive forces for the points with unity mass, if the magnitude of these repulse forces is inversely proportional to the distance between the points. The problem to minimize the criterion (1) together with the first principle leads to the solving a nonlinear integer programming problem. This problem is solved by program PLANEX. For each number of factors n and number of experiments k it is possible to elaborate a plan of experiment. But it needs much computer time, therfore each plan of experiment is elaborated only once and it can be used for various designing cases. The plan of experiment is characterized by the matrix of plan B_{ij}. Such matrices were calculated by program PLANEX for number of factors (space dimension) $n = 2 + 15$ and for the number of experiments $K = 2 \dots 25$. For example, we represent 9 point plan of experiment $(K = 9)$ for two $(n = 2)$ and three $(n = 3)$ factors

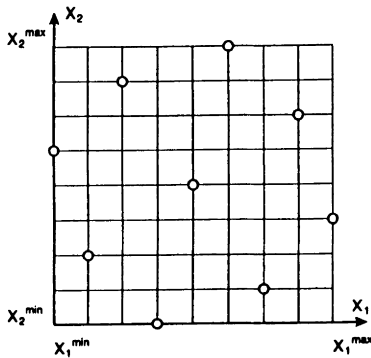Fig. 1 Plan of experiment for 2 factors ($n=2$) and 9 experiments ($k=9$)

$$B^T = \begin{vmatrix} 7\,1\,2\,5\,4\,9\,6\,8\,3 \\ 2\,6\,3\,5\,1\,4\,9\,7\,8 \end{vmatrix}$$

$$B^T = \begin{vmatrix} 1\,6\,9\,3\,4\,5\,2\,8\,7 \\ 4\,7\,6\,5\,1\,9\,8\,3\,2 \\ 7\,9\,4\,1\,5\,3\,6\,8\,2 \end{vmatrix} \qquad (2)$$

The points of experiment for the first matrix of plan ($n = 2$) are represented in Fig. 1.

We determine the domain of variables (factors) as $x_j \in [x_j^{min}; x_j^{max}]$. So, in this domain the points of experiments are calculated by the expression

$$x_j^{(I)} = x_j^{min} + \frac{1}{k}(x_j^{max} - x_{jmin}) \, B_{ij}$$

$$i = 1,2,...,k \; ; \qquad j = 1,2,...,n \qquad (3)$$

Since the matrices of plan B_{ij} are universal, these may be used for various design and optimization problems.

3. APPROXIMATION OF TABLE DATA BY EQUATION OF REGRESSION

Physical experiment or computer simulation gives an information about the object or process. This information may be respresented as table of data. Some of these data are parameters of the object $x_1, x_2, ..., x_n$, which are in connection with the parameter of response or control function y. Our aim is to express this relation in mathematical from as the equation of regression. The existing methods of regression analysis are based on the principle, that the form of the equation is known and the problem is to find the coefficients of the equation. However, in most cases the form of the equation is also unknown.

Let us consider a method which was suggested by V. Eglais (see Ref. 3), and in which the form of the equation of regression previously is unknown. There are two requirements for the equation of regression: accuracy and reliability. Accuracy is characterized as minimum of standard deviation of table data from the values given by the equation of regression. Increasing the number of terms in the equation of regression it is possible to obtain a complete agreement between the table data and the values given by the equation of regression. Moreover, in this case it may be any form of equation of regression and at the intervals between the table points prediction is not good. Reliability of the equation of regression may be characterized by meaning that standard deviations for the table points and for any other point are approximately the same. Obviously that for the smaller number of terms of the equation of regression the reliability is greater.

Let us consider the equation of regression in the form

$$y = \sum_{i=1}^{m} A_i \, f_i \, (x_j) \qquad (4)$$

where A_i are coefficients of the equation of regression, $f_i(x_j)$ are the functions from the bank of simple functions ϕ_1, ϕ_2,..., ϕ_n. These functions are assumed to be in the form

$$\varphi_k(x_j) = \prod_{i=1}^{n} x_j^{\alpha\,ki} \qquad (5)$$

where n is a number of parameter of the object, α_{ki} - positive or negative integer including zero.

Synthesis of the equation from the bank of simple functions is carried out in two stages: selection from the bank the perspective functions and then step by step elimination of the selected functions.

Selection of the perspective functions is carried out in the following manner. For all functions from the bank with the least square method the coefficients A_i und B_i of simple equations of regression are determined

$$y_i = A_i + B_i\,\phi_i\,(x_j) \qquad (6)$$

The sum of deviations also is calculated

$$S_i = \sum_{j=1}^{k} [A_i + B_i\,\varphi_i\,(x_j) - y_j\,]^2 \qquad (7)$$

where k is a number of points. Simple functions with minimum S_i are selected as perspective. After that we find out the most perspective function for the differences

$$\Delta_j = A_0 + \sum_{i=1}^{p} A_i\,f_i\,(x_j) - y_j\,; \quad j = 1,2,...,k \qquad (8)$$

where p is a number of the selected perspective funtions, $f_i\,(x_j)$ are the selected perspective functions, A_0 and A_i are the coefficients found by the least square method. After selection of the predicted number of the perspective functions the elimination is carried out.

Let us assume that the number of the selected perspective functions is p. So, the number of variants for the elimination of one function is p. All variants are checked out with the least square method and the function, which leads to the minimum S_i (7), is eliminated. The standard deviation is determined by the formula

$$\sigma_0 = \sqrt{\frac{S}{k-p+1}} \qquad (9)$$

In the same manner the next selected functions are eliminated. The last selection is from elimination diagram $\sigma = \sigma\,(p)$ (see Fig. 2a). If from the equation of regression insignificant functions are eliminated the increasing of the standard deviation is negligible. If in the equation of regression only significant functions are presented, then the elimination of them leads to important increasing of the stan-

dard deviation. There is a characteristic knee on the diagram of elimination (see Fig. 2a).
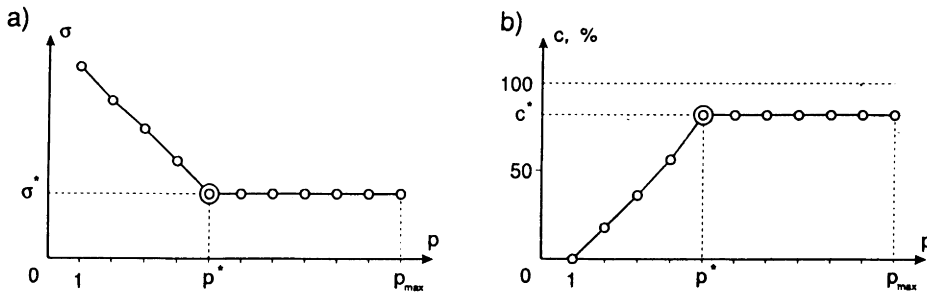
Fig. 2 Diagram of elimination: a – for standard deviation σ;
b – for coefficient of correlation c

It is convenient to characterize accuracy of the equation of regression by the coefficient of correlation c

$$c = \left(1 - \frac{\sigma}{\sigma_0}\right) \cdot 100\% \qquad (10)$$

where σ_0 is the standard deviation from the mean value of response

$$\sigma_0 = \sqrt{\frac{1}{k-1} \sum_{i=1}^{k} \left(y_i - \frac{1}{k} \sum_{j=1}^{k} y_j\right)^2} \qquad (11)$$

In this case the elimination diagram $c = c\,(p)$ has more universal scale.

The method of appoximation of the table data, examined above, has been as base to create the program RESINT. This program was widely used for elaboration of mathematical models in different field: biotechnology, robotics, composite material design and thin walled structure optimization.

4. NEW VERSION OF RANDOM SEARCH METHOD

There are many versions of the random search method. Let us consider a version, suggested by V. Eglais (see Ref. 6). We have constrained nonlinear programming problem

$$\min F(x); \quad H_i\,(x) \geq 0, \quad G_j\,(x) = 0$$
$$i = 1,2,...,I; \quad j = 1,2,...,J \qquad (12)$$

where I is a number of inequality constrains, J is a number of equality constrains. We use penalty functions and special procedure to minimize the unconstrained function. The initial data for algorithm is only the start point of search (see the flow chart in Fig. 3).

The constrained minimization problem (12) is replaced to the unconstrained minimization problem in which constrains are taken into account with the penalty functions

$$F_s(x) = F(x) + \sum_{i=1}^{I} S_{Ni}(x) + \sum_{j=1}^{J} S_{vj}(x) \qquad (13)$$

where F_s is the function with penalty, $S_{Ni}(x)$ is the penalty function for the inequality constrain i, $S_{vj}(x)$ is the penalty function for the equality constrain j. Penalty function for the inequality constrains has the form

$$S_{Ni(x)} = \alpha [H_i(x) - \varepsilon_i]^2, \quad \text{if } H_i(x) < \varepsilon_i \qquad (14)$$
$$S_{Ni}(x) = 0, \quad \text{if } H_i(x) \geq \varepsilon_i$$
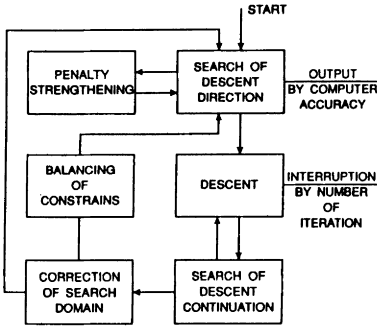
Fig. 3 Flow chart of algorithm

where $H_i(x)$ is the inequality constrain i, α is the coefficient of penalty power, ε_i is the balancing parameter with the ability to adapt for the constrain i. The penalty function for the equality constrains has the form

$$S_{vj}(x) = \alpha [Gj(x) - \varepsilon_j]^2 \qquad (15)$$

where $G_j(x)$ is the equality constrain j. The two types of the constrains in each stage of search has the same value of the coefficient α. The initial value of the coefficient is $\alpha = 1$. This coefficient is changed only in conclusion stage of search «penalty strengthening» (see Fig. 3).

Each constrain has different balancing parameters ε_i. The aim of these parameters with the ability to adapt is to determine a minimum of the penalty function at the active constrains with maximum accuracy. For all constrains the initial value of the balancing parameter $\varepsilon_i = 0$. Correction of these parameters is at the stage «balancing of constrains» (see Fig. 3).

At the first stage «search of descent direction» we search for the point, where the value of penalty function is smaller than at the initial point. For this in the search domain (12) we cut out a multidimension parallelepiped with centre at the initial point and with the length of edges d_i. The initial values for all d_i are equal ($d_i = 1$). For the uniform distribution of random numbers at each edge of parallelepiped we determine a random point and a value of penalty function (13) at this point. If at this test point the value is smaller than initial one then we transit to the stage «descent» (see Fig. 3). In contrary, a new test point we select in the opposite direction at a distance, which we determine from the value of previous unsuccesful step multiplied by the coefficient K_I

$$S_i = S_{i-1} K_I \qquad (16)$$

where S_i is the length of step for test i.

Also, if at the new test point the value of penalty function is greater than the initial value, then we decrease the step. For this we diminish the length of edges of the parallelepiped. The length of edges is multiplied by the coefficient K_2 and

we continue search in decreasing parallelepiped. It continues while we find a point with smaller value of penalty function or the value of penalty function is the same as initial one. In the first case we transit to the stage «descent», in the second case – to the stage «penalty strengthening» (see Fig. 3). It is possible that after step the test point is the same as the initial. In this case we suppose that the computer accuracy is achieved and further search is useless. Let us consider the stage «descent». In the direction which has been found above we make a step. The step length we obtain multiplying the previous step length by the coefficient K_3. If this step is successful then the step length is multiplied by the coefficient K_4 and at the next step – by the coefficient K_5.

If the step is unsuccessful then we transit to the stage "search of descent continuation" (see Fig. 3).

Let us consider the stage "search of descent continuation". This is the most complex stage. The relations for search consist of 13 coefficients and the information about the previous search. At this stage we also use random numbers with uniform distribution. If the step is successful then we transit to the stage «descent". In contrary, we transit to the stages «correction of search domain» and "balancing of constrains». It should be noted that the relations at the stage «correction of search domain» consist of 2 heuristical coefficients.

The aim of balancing is determination of the parameters ε_i for penalty function (14) and (15) to provide the best agreement of minimum of penalty function (13) with solution of the problem (12). At the stage «balancing of constrains» new values of the parameters ε_i are calculated. For this we use the previous values, the estimated values of constrains at the actual step and parameters with the ability to adapt R_i. These parameters take into account changing in signs for constrains at the previous balancing steps. Balancing of constrains is controlled by 6 coefficients.

When the actual point is in the vicinity of the solution of the problem, the improved value is found out at the stage «penalty strengthening», altering the coefficient of the penalty power α. At the same time the parameters of the penalty functions also are changed. After penalty strengthening the final stage of search begins, without returning to the stage «balancing of constrains». With repeated penalty strengthening it is possible to obtain solution with great accuracy. This algorithm provides only potential efficiency. The real efficiency of the method depends on values of coefficients. We chose some difficult problems of nonlinear programming (see Refs. 4 and 5) to find the optimal values of coefficients. For example, we solve Rosenbrock's and other problems to adapt the best coefficients. Moreover, informative plans of experiment, considered above, are used for optimization of coefficients. The most difficult was the stage «balancing of constrains». The number of coefficients for control of algorithm is about 30.

With this program of optimization SUPEX many difficult test problems (see Refs. 4 and 5) were successfully solved. One of these solutions see later. Some examples of optimization are represented in Refs. 6 and 7. In the investigation (Ref. 7) the program SUPEX was used together with the informative plans of experiment (program PLANEX) and the program of approximation RESINT. The

optimal design problems of complex structures from composite materials were solved. This shows efficiency of the new approach in optimization of structure. Further we shall illustrate some examples of composite materials design using the programs RESINT and SUPEX and standard example of nonlinear programming problem.

5. NUMERICAL EXAMPLES

Example 1. For testing the program SUPEX let us consider a standard problem of nonlinear programming (see example 16 in Ref. 5)

$$\min F(x) = -0.5 \ (x_1x_4 - x_2x_3 + x_3x_9 - x_5x_9 + x_5x_8 - x_6x_7) \tag{17}$$

under constrains

$$
\begin{aligned}
1 - x_3^2 - x_4^2 &\geq 0 & 1 - (x_3 - x_7)^2 - (x_4 - x_8)^2 &\geq 0 \\
1 - x_9^2 &\geq 0 & 1 - x_7^2 - (x_8 - x_9)^2 &\geq 0 \\
1 - x_5^2 - x_6^2 &\geq 0 & x_1 \ x_4 - x_2 \ x_3 &\geq 0 \\
1 - x_1^2 - (x_2 - x_9)^2 &\geq 0 & x_3 \ x_9 &\geq 0 \\
1 - (x_1 - x_5)^2 - x_2 - x_6)^2 &\geq 0 & -x_5 \ x_9 &\geq 0 \\
& & x_5 \ x_8 - x_6x_7 &\geq 0 \\
& & x_9 &\geq 0
\end{aligned} \tag{18}
$$

So, we have the problem with 9 variables, one linear and 13 nonlinear inequality constrains. As the initial we select the point $x_i = 1 \ (i = 1,2,...,9)$, where $F(x) = 0$. We find out that this problem has many optimal solutions, where at the optimum point from 6 to 9 constrains are active. In the program SUPEX about 5000 calculations of function with double precision are needed. For all optimal solutions the value of function is the same: $F(x) = -0.8660025403784438$. The active constrains are satisfied with the accuracy 10^{-15}. Also, the local solution with $F(x) = -0.6749$ was found out. Comparison study of various nonlinear programming codes shows (see Ref. 5), that only with one program from seven it is possible to solve the above problem.

Example 2. Further we consider the optimal design of expanding epoxy laminating systems. These special types of composite materials and processing technology were described in Ref. 8. An expanding agent is added to epoxy resin in order to get more light weight material of microcellular structure (voids) of matrix. Experimental investigation on these composite materials with various kinds of glass and carbon fiber reinforcement were carried out. Table 1 shows the results of experiments of glass fibre fabrics composite in static bending. Each result is a mean of 5 experiments. For this material the mean glass fiber volume fraction is $\mu_f = 42.5\%$.

The control (design) parameter is content of special expanding agent (wp in %). The last row shows the experimental results of standart composite material without expanding agent ($wp = 0$). The volume content of voids is $\mu_{voids}* 100\%$. This parameter may be the function y_5 of $wp \rightarrow x_1$. Also, μ_{voids} may be the argument x_2 of function. The control functions are: modulus of elasticity of composite material

$E \to y_1$, bending strength $\sigma_{max} \to y_2$, maximum of bending deformation $\varepsilon \to y_3$ and also material density $\rho \to y_4$

TABLE 1.
Experimental results for glass fibre fabrics composite in static bending

No	y_1 E N/mm^2	y_2 σ_{max} N/mm^2	y_3 ε %	y_4 ρ g/cm^3	x_1 wp [weight part}	x_2 or y_5 μ_{voids} %
1	13993	216	1,96	1,4231	2,0	27,4
2	14801	215	1,90	1,4356	1,5	25,4
3	16488	254	1,92	1,4996	1,0	20,7
4	15855	283	2,11	1,5497	0,5	16,8
5	16803	312	2,16	1,6156	0,2	11,4
6	17306	426	2,84	1,7185	0,0	0,0

In this example we have only one control parameter wp. Therefore, we find out the equations of regression $y_i(x_1)$ $(i = 1,2,3,4)$. In this case of approximation for one dimension we use a version of the programm RESINT, where the bank of simple functions contains also trigonometric functions. As control functions for optimal design we select modulus of elasticity of composite material $E \to y_1$, the bending strength $\sigma_{max} \to y_2$ and the material density $\rho \to y_4$. The version of the program RESINT gives the following equations of regression

$$y_1 (x_1) = 18280 + 4302 \sin 6 (z_1) - 1295 \cos 6 (z_1) - 2216 \cos 12 (z_1);$$
$$y_2 (x_1) = 336 - 232 z_2 + 109 z_2^2 + 0,0092 z_2^{-2} \qquad (19)$$
$$y_4 (x_1) = 1,613 - 0,2915 z_3 + 0,09125 z_3^2 + 0,006354 z_3^{-2}$$

where for each function we have different coefficients of normalization

$$z_1 = 0,52 + 0,24 x_1;$$
$$z_2 = 0,01 + 0,495 x_1; \qquad (20)$$
$$z_3 = 0,2 + 0,4 x_1$$

It should be noticed, that the equations of regression (19) could be used only for the domain, where we have information, i.e.

$$0 \geq wp \geq 2 ; \qquad 200 \geq \sigma_{max} \geq 450$$
$$14000 \geq E \geq 17300 ; \qquad 1,42 \geq \rho \geq 1,72 \qquad (21)$$

Let us consider optimal desgin problem: find out the volume content of the expanding agent $x_1 = wp$ to minimize the composite material weight ρ for the fixed values of modulus of elasticity of composite material E * and bending strength σ_{max}*

$$\min y_4 (x_1) \qquad (22)$$

under constrains

$$y_1(x_1) = E^* ; \qquad y_2(x_1) = \sigma_{max} ; \qquad 0 \le x_1 \le 2 \qquad (23)$$

Table 2 contains the results of optimization with program SUPEX for various values of the predicted modulus of elasticity E^* (in N/mm^2) and the bending strenght σ_{max}^* (in N/mm^2). In numerator we have the optimal part of weight of expanding agent (wp), while in denominator the weight ζ for optimal composite.

TABLE 2.

Results of optimal design of glass fibre fabrics composite with voids

E^* $\quad \sigma_{max}$*	200	250	300	350	450
14000	2,009 / 1,416	1,546 / 1,445	0,392 / 1,570	0,226 / 1,611	0 / 1.718
15000	2,055 / 1,416	1,220 / 1,469	0,377 / 1,575	0,145 / 1,636	0 / 1,718
16000	2,110 / 1,413	0,961 / 1,492	0,335 / 1,580	0,031 / 1,690	0 / 1,718
17000	2,180 / 1,410	0,938 / 1,495	0,281 / 1,595	0,025 / 1,700	0 / 1,718

From Table 2 it is possible to select a material with predicted properties. For example, if we need a composite material with modulus of elasticity $E^* = 16000$ N/mm^2 and bending strength not less than $\sigma_{max}^* = 250$ N/mm^2, then for minimum weight composite ($\rho = 1,49$ g/cm^3) the content of special expanding agent is: $wp = 0,96$ %.

Example 3. The next example is optimal design for price criterion of composite material with glass, carbon and aramid fibre fabrics reinforcement. Table 3 contains the results of experiment (see Ref. 9) for glass, carbon and aramid fibre composite materials with various fibre volume fraction $\mu_f \rightarrow x_5$, matrix modulus of elasticity $E_m \rightarrow x_3$ and Poisson's ration $\nu_m \rightarrow x_4$, number of plies $K \rightarrow x_6$, fibre modulus of elasticity $E_f \rightarrow x_7$ and maximum angle (in radians) of differences from the straight line for woven fabrics in warp direction x_1 and in fill direction x_2. Table 3 contains also control function: price of composite material y_1 and modulus of elasticity of composite material $E \rightarrow y_2$, where $E = 0,5 (E_x + E_y)$ (E_x is modulus of elasticity of composite material in warp direction, E_y is the same in fill direction). All these quantities were measured in the experiment. Only the price of composite material y_1 is determined as relative quantity and is approximate. We

get it from the price of glass fibre fabrics (approximately 20 DM/kg), carbon fibre fabrics (214 DM/kg) and aramid fibre fabrics (173 DM/kg) – these values multiplied by fibre volume fraction μ_f.

The program RESINT gives the following expressions for control functions: relative price of composite material $y_1(x_i)$ and modulus of elasticity of composite material $y_2(x_i)$

$$y_1(x_i) = 68,91 - 35,6\ z_3 + 11,578\ z_7 + 15,27\ z_5 + 7,042\ z_4 - $$
$$- 20,43\ z_3^2 - 14,65\ z_3\ z_5 + 4,96\ z_4\ z_5\ ; \qquad (24)$$

$$y_2(x_i) = 25,89 + 8,21\ z_7 + 5,596\ z_5 - 2,262\ z_3\ z_5 - 2,257\ z_5^2 - $$
$$- 1,776\ z_2\ z_5 - 2,577\ z_6^2 - 0,974\ z_3 \qquad (25)$$

where the coefficients of normalization for independent variables x_i are

$$z_3 = -2,79 + 0,94\ x_3\ ;$$
$$z_4 = 27,66 + 66,66\ x_4\ ;$$
$$z_5 = -3,07 + 0,074\ x_5\ ; \qquad (26)$$
$$z_6 = -1,28 + 0,28\ x_6\ ;$$
$$z_7 = -1,91 + 0,012\ x_7$$

Fig. 4 shows the diagram of elimination for the control function y_1 (price). We see, that the best approximation is for the function (24) with 8 terms. The corresponding value of coefficient of correlation is $C = 93,1\%$ and standard deviation is $\sigma = 1,96$. Let us consider the optimal design problem: minimize the price of composite material
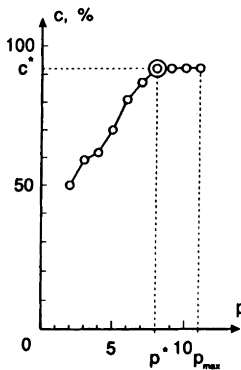
$$min\ y_1(x_i) \qquad (27)$$

under constrains

$$y_2\ (x_i) = E.\ ; \qquad 0,4 \le x_4 \le 0,43$$
$$0,044 \le x_1 \le 0,309 \qquad 27,96 \le x_5 \le 54,9 \qquad (28)$$
$$0,14 \le x_2 \le 0,22\ ; \qquad 1 \le x_6 \le 8$$
$$1,905 \le x_3 \le 4,032\ ; \qquad 73,5 \le x_7 \le 234$$

Fig. 4 Diagram of elimination for control function y_1

where the functions $y_1(x_i)$ and $y_2(x_i)$ are given by the expressions (24), (25) and E^* is the designing modulus of elasticity of composite material.With the program SUPEX we find out some local minimum. For the designing modulus of elasticity of composite material $E^* = 30$ kN/mm^2 the best local solution y_1^* and the coresponding opimal parameters are

$$\Omega_1 = 0,131;\quad \Omega_2 = 0,139;\quad E_m = 3,35\ kN/mm^{2.}\ ;$$
$$\nu = 0,4;\qquad \mu_f = 47,2\%;\quad K = 4,55; \qquad (29)$$
$$E_f = 1,71\ kN/mm^2;\qquad y_1^* = 50,8$$

It should be noticed, that the mean valne of fibres modulus of elasticity $E_f = 171$ kN/mm^2

TABLE 3.
Results of experiment for composite materials with glass, carbon and aramid fibre fabrics reinforcement

No.	x_1 Ω_1 rad	x_2 Ω_2 rad	x_3 E_m kN/mm^2	x_4 v_m	x_5 μ_f *100%	x_6 K	x_7 E_f kN/mm^2	y_1 Price	y_2 E kN/mm^2
	Glass fibre fabrics								
1	0,137	0,159	4,032	0,43	32,27	1	73,5	7,04	11,0
2	0,137	0,159	4,032	0,43	33,48	2		7,30	12,2
3	0,196	0,196	4,032	0,43	40,36	1		7,78	14,3
4	0,196	0,196	4,032	0,43	48,15	2		9,51	17,4
5	0,309	0,199	4,032	0,43	40,52	1		8,19	14,25
6	0,087	0,157	3,794	0,4	44,32	1		8,86	14,13
7	0,087	0,157	3,794	0,4	47,52	2		9,50	16,7
8	0,044	0,176	3,794	0,4	36,38	1		7,28	11,1
9	0,044	0,176	3,794	0,4	39,56	2		7,91	16,15
10	0,148	0,148	3,797	0,4	54,90	1		10,98	16,5
11	0,148	0,148	3,797	0,4	53,57	2		10,71	19,93
	Carbon fibre fabrics								
12	0,14	0,14	2,900	0,4	32,90	3	234	70,4	28,8
13	0,163	0,163	2,900	0,4	32,50	3		69,6	28,65
14	0,14	0,14	1,905	0,4	33,66	3		72,03	24,46
15	0,14	0,14	1,905	0,4	46,29	6		99,06	36,47
16	0,14	0,14	3,005	0,4	27,96	2		59,83	23,68
17	0,14	0,14	1,905	0,4	41,02	4		87,78	33,53
18	0,14	0,14	1,905	0,4	39,49	3		84,51	30,36
	Aramid fibre fabrics								
19	0,22	0,22	2,902	0,43	28,5	2	120	49,31	14,19
20			2,902	0,43	53,8	4		93,07	24,53
21			1,905	0,4	28,94	3		50,06	12,57
22			1,905	0,4	48,74	6		84,32	22,15
23			3,005	0,4	29,90	2		51,73	16,30
24			1,905	0,4	29,90	2		51,73	14,43
25			1,905	0,4	36,15	8		62,54	17,37
26			1,905	0,4	35,50	4		61,42	18,15

could be obtained only by combination of 60% carbon fibres and 40% glass fibres ($234 \times 0,6 + 73,5 \times 0,4 = 171$). So, in this case we have a hybrid composite

material with carbon fibre volume fraction μ_f^{carbon} = $47{,}2 \times 0{,}6$ = $28{,}3\%$ and glass fibre volume fraction μ_f^{glass} = $47{,}2 \times 0{,}4$ = $18{,}9\%$. (μ_f = μ_f^{carbon} + μ_f^{glass}). Actually the price of this hybrid composite material is y_1 = $0{,}472$ $(214 \times 0{,}6$ + $20 \times 0{,}4)$ = $64{,}4$. The price $(y_1$ = $64{,}4)$ of optimal hybrid composite material with the same modulus of elasticity is 24% less than the price $(y_1$ = $84{,}5)$ of carbon fibre composite (see material No. 18 in the Table 3).

Similar optimal design could be obtained also for the weight criterion under constrains for price and modulus of elasticity.

6. CONCLUSION

It is possible to solve various optimal design problems of composite materials, using the program of approximation RESINT and the program of nonlinear programming SUPEX. The control functions may be stiffness, strength, damping and thermal properties of composite material. The criterion may be the weight or price of the material. The control parameters may be fibre volume fraction, void content, fibre and matrix modulus of elasticity, number of plies and other variables. It should be noted, that for approximation of control functions with the program RESINT it is possible to use as information not only the results of physical experiments, but also the results from theoretical models or computer simulation.

7. REFERENCES

1. Tables of plans of experiments. Handbook, Moscow, Metallurgy Publishing House, 1982 (in Russian).
2. Audze, P.; Eglais, V.: New approach for planing out of experiments. Problems of Dynamics and Strengths, Vol. 35, 1977, Riga, Zinatne Publishing House, pp. 104-107 (in Russian).
3. Eglais, V.: Approximation of table data by multivariable equation of regression. Problems of Dynamics and Strength, Vol. 39, 1981, Riga, Zinatne Publishing House, pp. 120-125 (in Russian).
4. Bazarra, M.S.; Shetty, C.M.: Nonlinear Programming, Theory and Algorithms. John Wiley and Sons, New York - Chichester - Brisbaine - Toronto, 1979.
5. Himmelblau, D.M.: Applied Nonlinear Programming. Mc Graw-Hill, New York, 1972
6. Eglais, V.: Intuitive search - an effective version of random search method. Problems of Random Search, Riga, Zinatne Publishing House, 1988, Vol. II, pp. 53-62 (in Russian).
7. Rikards, R.; Eglais, V.; Goldmanis, M.: Optimization of Composite Conical Shells with Ring Frames under External Pressure. Soviet Applied Mechanics. Vol. 19, 1983, No. 12, pp. 44-51 (in Russian).
8. Kurek, K.; Fuhrmann, U.; Bledzki, A.K.: EXEPO-Systeme-Werkstoffe für den Leichtbau, Conference book of XVI-conference "Reinforced Plastics", Karlsbad, 14.-15. May, 1991

9. Kurek, K., Ehrenstein G.: Bericht zum Forschungsantrag "Einfluß der Fadenwelligkeit auf die mechanischen Kennwerte von mit Gewebe verstärkten Polymerwerkstoffen"; DFG Eh 6032-1, Kassel, 1989.

Optimal Design with Advanced Materials
P. Pedersen (Editor)
1993 Elsevier Science Publishers B.V.

163

Fundamental aspects of selecting materials based on NDI for delamination

K. Sekiguchi, M. Saka and H. Abé

Department of Mechanical Engineering, Tohoku University, Sendai 980, Japan

Abstract

Selecting materials is discussed based on nondestructive inspection (NDI) of delamination by ultrasonic testing. A simple example of laminated materials which is composed of two layers of different materials is considered. Two surfaces happened by delamination at the interface may contact each other. Also pressure for the contact may exist in some cases. By considering these circumstances it is concluded that the selecting materials, in which $Z_1 \geq Z_2$ and Z_1 and Z_2 are not much different, is fit for easy NDI of the delamination, where Z_1 is acoustic impedance of the material from whose side ultrasonic wave is incident and Z_2 is impedance of another material. Also in order to identify the wave in a time domain, it is easily found that one should design the thickness of the layer being greater than $c_1/2f$, where c_1 is the wave velocity in the layer and f is the ultrasonic frequency.

1. INTRODUCTION

Laminated materials are recently interested by many researchers and becoming to be used increasingly in industries. Interface in the materials plays a key role of determining properties of the materials. Many investigations have been done for evaluating strength and fracture of the interface, see Refs. [1] and [2] for examples.

Integrity assessment of materials requires detection and sizing of the delamination occurring at the interface. If the materials are selected optimally in designing not only for increasing strength but also for easy NDI of delamination, reliability of the integrity assessment is highly expected to increase. From the point of view stated, fundamental aspects are discussed for selecting materials based on NDI of delamination by treating ultrasonic testing as an example of NDI methods.

2. ULTRASONIC NDI FOR DELAMINATION

Well-known idea for detecting the delamination by using ultrasonics has been to compare intensity of sound waves reflected from bonded area and delaminated one which is modeled by a layer of air. To demonstrate the usual method Figure 1 shows a simple example which treats sinusoidal ultrasonic waves. Water is usually used as medium to transmit the wave from a probe to the surface of material inspected. The ultrasonic wave is incident perpendicularly from the side
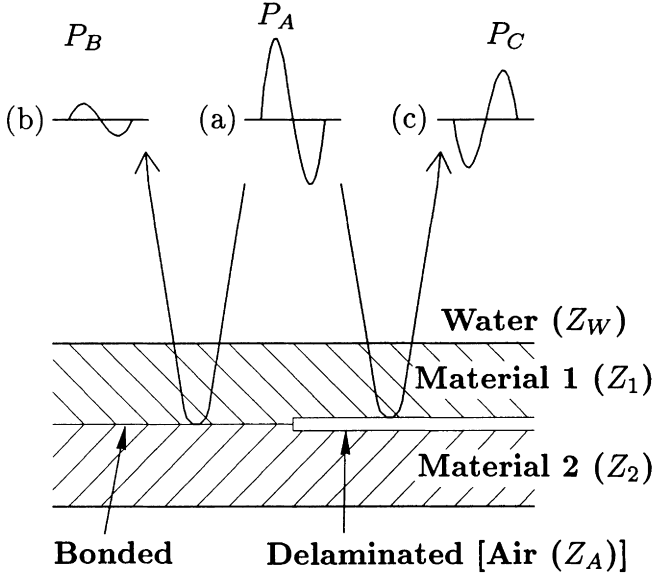
Figure 1. Well-known model of delaminated area.

of material 1 which has acoustic impedance Z_1. From theoretical analysis assuming plane harmonic wave [3], the intensity of the wave reflected from the bonded area, P_B, and the intensity of the wave reflected from the delaminated one, P_C, are related with the intensity of the incident wave, P_A, as

$$P_B = \frac{4Z_W Z_1}{(Z_W + Z_1)^2} \frac{|Z_2 - Z_1|}{Z_1 + Z_2} P_A \tag{1}$$

and

$$P_C = \frac{4Z_W Z_1}{(Z_W + Z_1)^2} \frac{|Z_A - Z_1|}{Z_1 + Z_A} P_A \tag{2}$$

where Z_W, Z_A and Z_2 are acoustic impedance of water, air and material 2, respectively. Generally Z_A is regarded as zero. Hence we obtain from Eq.(2)

$$P_C = \frac{4Z_W Z_1}{(Z_W + Z_1)^2} P_A \tag{3}$$

Equations (1) and (3) show that P_C is greater than P_B.

The modeling of the delamination by the layer of air is not always right. Two surfaces happened by the delamination may contact each other. Also pressure for the contact may exist in some cases. Because of these reasons, the method stated above leads to misjudgement in some cases.

It is needed to develop a method which considers not only perfectly delaminated area modeled by the layer of air but also imperfectly bonded one as delamination. Also easy inspection is favorable for NDI of the delamination. Easy NDI method is that uses only intensity to judge perfectly bonded area correctly without using additional information of the wave. By considering imperfectly bonded area, let us investigate the conditions for selecting optimally materials to use the method.

3. SELECTING MATERIALS

3.1. On materials character

Consider a laminated material as shown in Figure 2. The interface contains bonded and delaminated areas where in a part of the delaminated area two surfaces are contacting (imperfectly bonded). The contact of two surfaces is modeled by introducing an imaginary material of which acoustic impedance is Z^*, see Figure 3. The impedance Z^* is expressed as

$$Z^* = \alpha Z_2 \qquad (4)$$
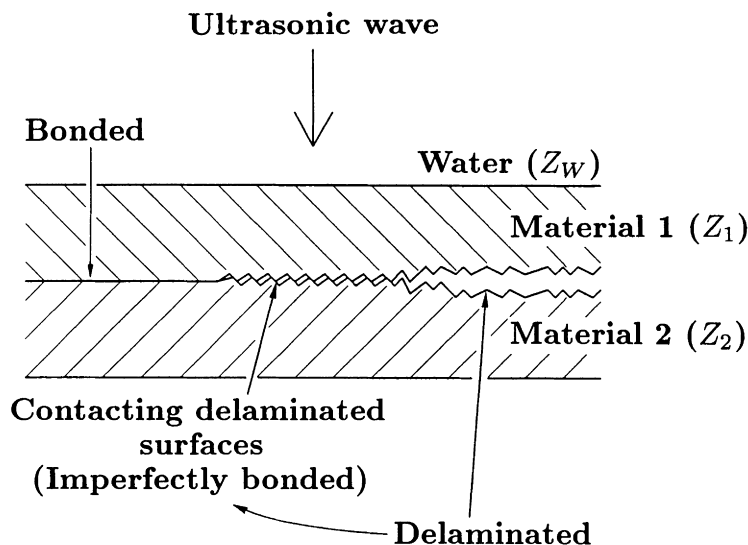
Figure 2. Simple example of laminated materials composed of two layers.
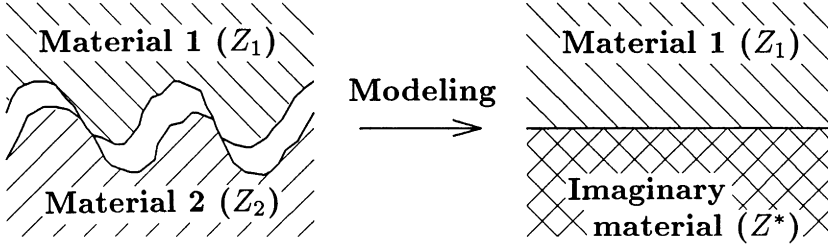
Figure 3. Modeling of the contacting delaminated area at the interface.

where coefficient α takes the value in the range of $0 \leq \alpha \leq 1$. The impedance Z^* is considered to take higher value for strong contact. The case of $\alpha = 1$ represents perfectly bonded interface.

The intensity of the wave reflected from the delaminated interface is obtained as

$$P_D = \frac{|Z^* - Z_1|}{Z_1 + Z^*} P_C \tag{5}$$

where P_C is given by Eq.(3). From Eqs.(1) and (3), on the other hand, the intensity of the wave reflected from the perfectly bonded interface is given by

$$P_B = \frac{|Z_2 - Z_1|}{Z_1 + Z_2} P_C \tag{6}$$

Whether P_D is smaller than P_B or not depends on the relation among Z_1, Z_2 and Z^*. When P_D is equal to P_B, we obtain from Eqs.(4) to (6)

$$\frac{|\alpha - \beta|}{\beta + \alpha} = \frac{|1 - \beta|}{\beta + 1} \tag{7}$$

where

$$\beta = \frac{Z_1}{Z_2} \tag{8}$$

and β takes the value in the range of $\beta > 0$. One can get from Eq.(7)

$$\alpha = \beta^2 \tag{9}$$

In a similar way, when P_D is smaller than P_B we obtain

$$\alpha > \beta^2 \qquad\qquad (10)$$

When P_D is greater than P_B, on the other hand, we obtain

$$\alpha < \beta^2 \qquad\qquad (11)$$

The relation between α and β given by Eqs.(9), (10) and (11) is shown in Figure 4. Generally we cannot know the value of α. It is found from Figure 4 that if we select materials of which β is greater than or equal to 1, the delaminated area can be detected independently of α by using only intensity of the wave. While if we select materials of which β is smaller than 1, the detection of the delamination by using only intensity is impossible in the case that α takes the value being equal to β^2. In other words, in this selection, perfectly bonded area cannot be judged correctly by using only intensity.
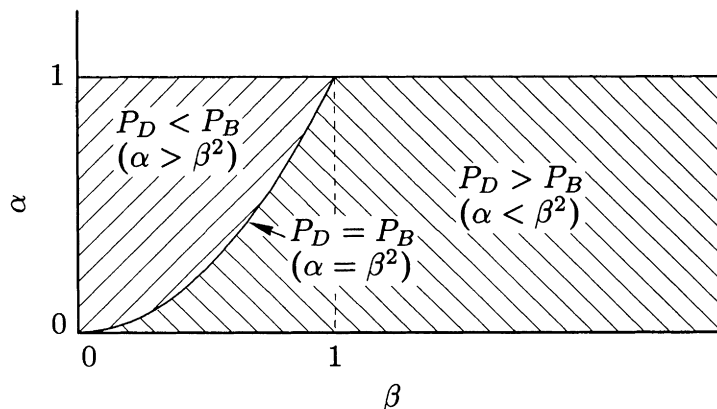
Figure 4. Intensity of the wave in the relation with α and β.

By the way, let us consider the phase of the wave reflected from the interface. Denote the quantity, which is obtained by removing the symbol ($|\ |$) for absolute value on the right hand side of Eq.(5), by P'_D as

$$P'_D = \frac{Z^* - Z_1}{Z_1 + Z^*}\, P_C \qquad\qquad (12)$$

Similarly define the quantity P'_B based on Eq.(6) as

$$P'_B = \frac{Z_2 - Z_1}{Z_1 + Z_2} P_C \tag{13}$$

Compare the signs of P'_D/P_C and P'_B/P_C. If the sign of P'_D/P_C does not equal to that of P'_B/P_C, the phase of the wave reflected from the delaminated area is different from one of the wave reflected from the bonded area. By using Eqs.(4), (8), (12) and (13) one can get Figure 5, which shows phase information in the relation with α and β. By combining Figures 4 and 5, we get Figure 6. It is found for the case of $0 < \beta < 1$ that the delaminated area can be detected by using both the intensity and the phase of the wave.

Phase of the wave reflected from the delaminated area <u>is the same as</u> one of the wave reflected from the bonded area.

Phase of the wave reflected from the delaminated area <u>is different from</u> one of the wave reflected from the bonded area.
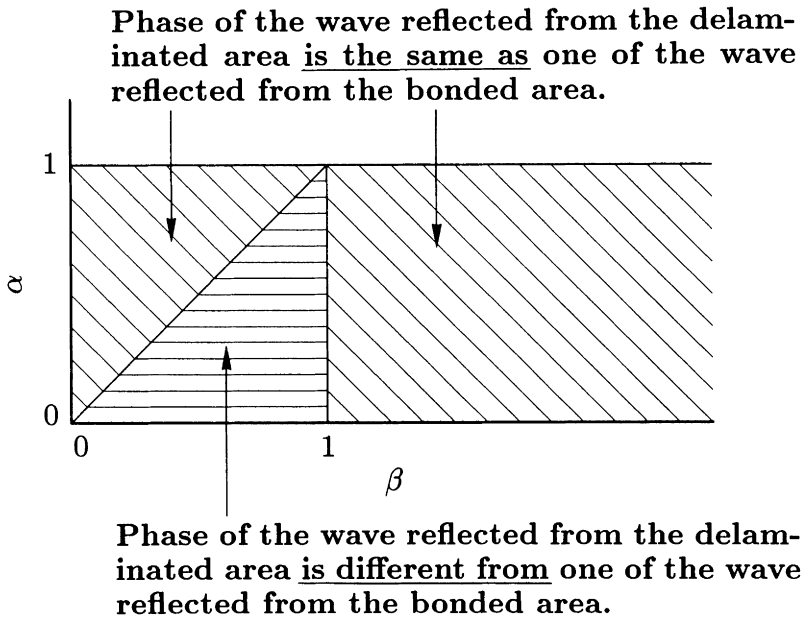
Figure 5. Phase information in the relation with α and β.

Table 1 summarizes how to detect delamination, where P_B is assumed to be known in advance as a reference. It is noted that P_B can be obtained by doing the measurement for the perfectly bonded specimen or it can also be evaluated through Eq.(6) by knowing the value of P_C from the measurement for material 1. In the case of $0 < \beta < 1$, additional information such as phase of the wave is necessary to judge perfect bonding, because the same intensity as that for the perfect bonding can be observed for imperfect bonding of $\alpha = \beta^2$. Since easy NDI is that judges perfect bonding correctly by using only intensity, it is led that we should select materials of which β is greater than or equal to 1.
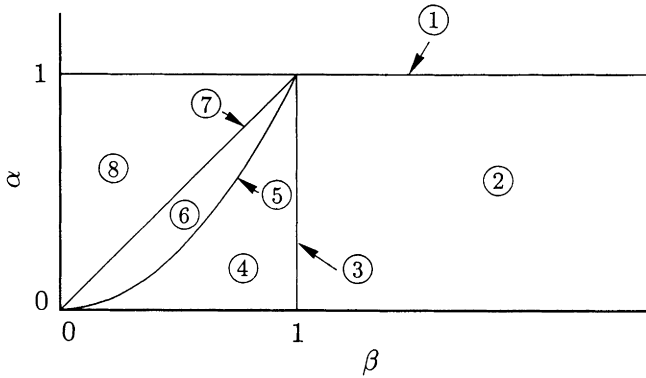
Case	Intensity	Phase	Interface
①	P_B(Standard)	Standard	Perfect bonding
②	$P_D > P_B$	Same*	
③	$P_D > P_B (= 0)$	——	
④	$P_D > P_B$	Different**	Perfect delamination
⑤	$P_D = P_B$	Different	&
⑥	$P_D < P_B$	Different	Imperfect bonding
⑦	$P_D (= 0) < P_B$	——	
⑧	$P_D < P_B$	Same	

*)   Same   : Phase of the wave reflected from the delaminated area is the same as one of the wave reflected from the perfectly bonded area.

**) Different : Phase of the wave reflected from the delaminated area is different from one of the wave reflected from the perfectly bonded area.

Figure 6. Intensity and phase information in the relation with α and β.

Next, let us consider a difference in the intensity of the waves reflected from the bonded interface and the delaminated one. Define the difference, ΔP, as

$$\Delta P = P_D - P_B \tag{14}$$

Figure 7 shows the relation of ΔP with β for some values of α. In the case that $\beta \geq 1$, the difference ΔP takes its maximum value at $\beta = 1$. From the viewpoint of inspection, the difference ΔP is favorable to be as large as possible.

Table 1
How to detect delamination

β	Perfect delamination & Imperfect bonding $(P = P_D)$		Perfect bonding
$0 < \beta < 1$	$P \neq P_B \ (\alpha \neq \beta^2)$		$P = P_B \ (\alpha = 1)$ Additional information (such as phase of the wave) is necessary.
	$P = P_B \ (\alpha = \beta^2)$ Additional information (such as phase of the wave) is necessary.		
$\beta \geq 1$	$P > P_B \ (\alpha < \beta^2)$		$P = P_B \ (\alpha = 1)$

P : Measuring intensity of the wave reflected from the interface
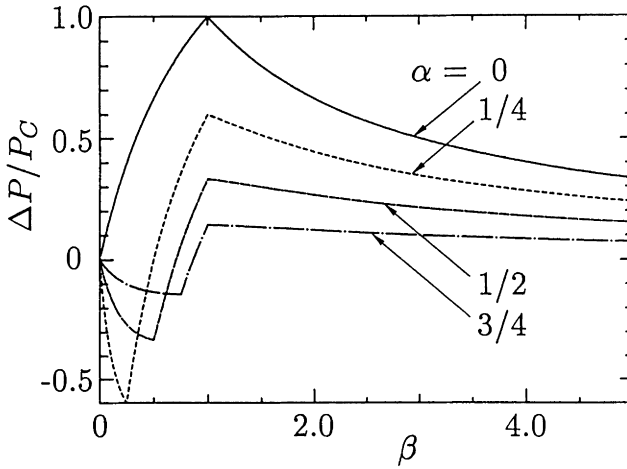
Figure 7. Difference in the intensity of the waves reflected from the bonded area and the delaminated one.

Hence one can conclude that the selecting materials, of which Z_1 and Z_2 are in the relation $Z_1 \geq Z_2$ and are not much different, is fit for the easy NDI of delamination. Table 2 summarizes applicability of easy NDI in terms of β.

Table 2
Applicability of easy NDI in terms of β

β	Applicability of easy NDI
$0 < \beta < 1$	**Not good** (**Applicability depends on α. Phase of the wave is needed to be considered in addition to the wave intensity.**)
β equals to 1 or is not very large	**Good**
β is very large	**Not good (ΔP is small.)**

3.2. On thickness of materials

It is important that the wave to be measured can be identified in a time domain. A simple illustration to explain how to deal with this problem is shown in Figure 8. The thickness and the wave velocity of the layer from the side of which
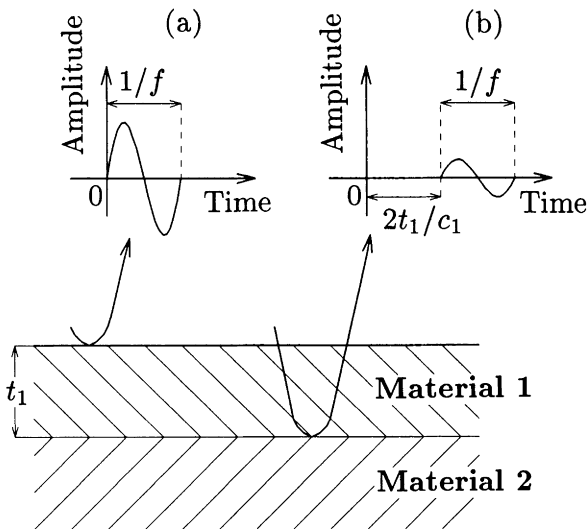
Figure 8. Waves in a time domain.

the ultrasonic pulse wave is incident are given by t_1 and c_1, respectively. Also the ultrasonic frequency is denoted by f. If the waves which are reflected from the surface of material 1 and reflected from the interface between material 1 and material 2 overlap, it is difficult to detect the delamination. In order to identify the wave reflected from the interface we need to design the thickness of the layer as

$$t_1 > \frac{c_1}{2f} \tag{15}$$

4. CONCLUSION

A method for selecting materials has been discussed based on easy NDI of delamination by ultrasonic testing. The ultrasonic technique treated uses only the intensity of the wave to judge perfectly bonded area correctly. By considering a simple example of laminated materials which is composed of two layers of different materials the following results have been obtained:

1. The selecting materials, in which $Z_1 \geq Z_2$ and Z_1 and Z_2 are not much different, is fit for the easy NDI of the delamination, where Z_1 and Z_2 are acoustic impedance of upper and lower materials, respectively.
2. It is shown that for materials in which $Z_1 < Z_2$, the phase information of the wave reflected from the interface is necessary for detection of the delamination.
3. In order to identify the wave in a time domain, one should design the thickness of the layer being greater than $c_1/2f$, where c_1 is the wave velocity in the layer and f is the ultrasonic frequency.

ACKNOWLEDGEMENT

REFERENCES

1 K.L. Reifsnider(ed.), Damage in Composite Materials, STP 775, ASTM, Philadelphia, 1980.
2 J.K. Kim and Y.W. Mai, Composites Science and Technology, 41 (1991) 333.
3 J. Krautkrämer and H. Krautkrämer, Ultrasonic Testing of Materials, Springer-Verlag, Berlin, (1990) 15.

Convex and fuzzy modelling of uncertainties in the optimal design of composite structures

S. Adali

Department of Mechanical Engineering, University of Natal, Durban 4001, Republic of South Africa

Abstract

The optimal design of a laminated panel under in–plane loads is obtained subject to uncertainties in the magnitude of the loads. Laminates are to be designed for minimum thickness taking the fibre orientations as the design variables. A suitable strength criterion is imposed to identify the failure condition. The uncertainties in the loading parameters are modelled using non–probabilistic theories of convex analysis and the fuzzy sets. In the convex modelling, the loads are allowed to vary arbitrarily around their average values subject to a bound on the sum of the squares of the variations which are assumed to be small. The minimum thickness of laminate is determined under the least favourable loading configuration.

In the fuzzy modelling, membership functions are introduced with the magnitude of the loads determined by their degree of membership which indicates the level of uncertainty. Minimum thickness is determined as a function of the degree of membership of the loads. In particular, the vertex method is used to calculate the least favourable loading condition under fuzzy load data. Both models lead to minmax problems and give comparable numerical results.

1. INTRODUCTION

In a structural design problem, it is often the case that the loads on the structure are not known in a precise manner. This leaves the designer with the task of designing the structure for the worst case of loading, i.e., the structure needs to be designed for the

least favourable loading condition. In the present study, two approaches are given to optimally designing a laminated structure under uncertain loading conditions. The first approach involves the convex model of uncertainty presented in [1]. In this approach, the loading parameters are allowed to have small and arbitrary but bounded variations around their average values. The method of Lagrange multipliers combined with Taylor series approximation is used to determine the least favourable loading condition. The second approach involves the fuzzy set theory in which the loading parameters are assigned membership functions [2]. The degree of membership of a loading parameter reflects the level of uncertainty associated with that load. The optimal design is obtained by computing the worst case of loading by the vertex method [3].

The above techniques of dealing with the uncertainties involve non–probabilistic approaches to the modelling of imprecise load data. Convex modelling has been previously applied to shell imperfections [4], vehicle response [5], diagnosis of blockage in fluid flow [6], stress concentration at an irregular hole [7], scatter in material properties [8] and vibrating beams under uncertain excitations [9]. The present study seems to be employing the convex modelling for the first time in an optimal design problem.

The use of the fuzzy logic to model uncertain behaviour of structures is described in [10]. The reader is referred to references [2,11–13] for examples of the application of the fuzzy set theory to optimal design problems.

The specific problem treated in the present study involves the minimum thickness design of a laminated panel under uncertain in–plane loads. The design variables of the problem are the fibre orientations. The least favourable loading condition refers to the set of loading parameters which produces the thickest optimal laminate. Hence the minimum thickness design under uncertain loading involves the solution of a minmax problem in which the laminate thickness is maximized over loading parameters and minimized over fibre orientations. Convex analysis and fuzzy set theory are employed in determining the least favourable loading conditions. Deterministic approaches to the optimal design of laminated panels under in–plane loads have been given in references [14–18].

2. LAMINATED PANEL UNDER IN–PLANE LOADS

We consider a symmetrically laminated panel of thickness H under in–plane loads N_1, N_2 and N_{12} as shown in Figure 1. The laminate consists of an even number of orthotropic layers of thickness H_k, k=1,2,...,n where $H_k = H_{n+1-k}$ due to symmetry

and n is the total number of layers. The fibre orientations θ_k with $\theta_k = \theta_{n+1-k}$ are defined as the angle between the fibre direction and the x axis (Figure 1).
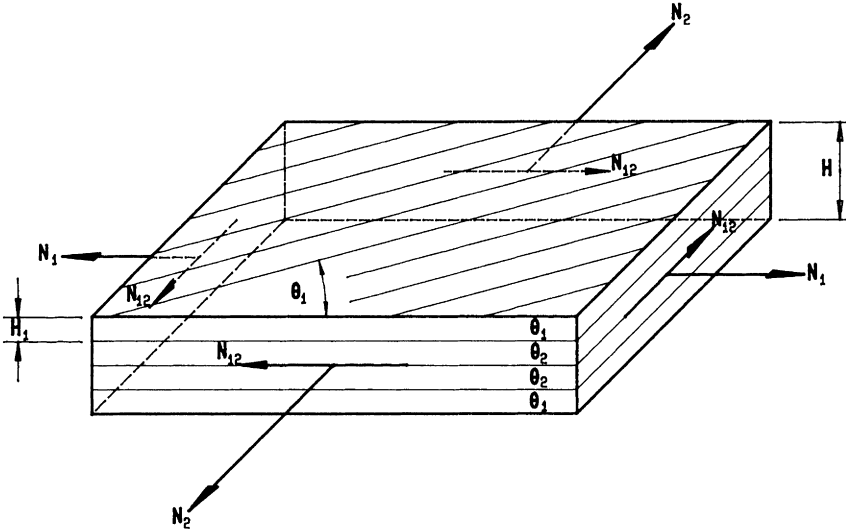
Figure 1. The geometry of the laminated panel and the loading

For symmetric laminates, the force resultants are given by

$$[N] = [A]\,[\epsilon] \tag{1}$$

where

$$[N] = \begin{bmatrix} N_1 \\ N_2 \\ N_{12} \end{bmatrix}, \quad [A] = \begin{bmatrix} A_{11} & A_{12} & A_{16} \\ A_{12} & A_{22} & A_{26} \\ A_{16} & A_{26} & A_{66} \end{bmatrix}, \quad [\epsilon] = \begin{bmatrix} \epsilon_x \\ \epsilon_y \\ \gamma_{xy} \end{bmatrix} \tag{2}$$

with A_{ij} denoting the extensional stiffnesses given by

$$A_{ij} = 2\,H \sum_{k=1}^{n/2} h_k\, \overline{Q}_{ij}(\theta_k) \tag{3}$$

where $h_k = H_k / H$. In equation (1), ϵ_x, ϵ_y and γ_{xy} denote the normal and shear

strains in the xy plane. The stress—strain relations for the k—th layer are given by

$$[s^{(k)}] = [\overline{Q}^{(k)}] [\epsilon] \tag{4}$$

where $[s^{(k)}] = [\ \sigma_x^{(k)}\ \sigma_y^{(k)}\ \tau_{xy}^{(k)}\ ]^{tr}$ is the transpose of the vector of stress components in the xy plane and $[\overline{Q}^{(k)}]$ denotes the matrix with components $\overline{Q}_{ij}(\theta_k)$.

The stress components in the material coordinate system, denoted by $[\sigma^{(k)}] = [\ \sigma_1^{(k)}\ \sigma_2^{(k)}\ \tau_{12}^{(k)}\ ]^{tr}$, are obtained from

$$[\sigma^{(k)}] = [T^{(k)}] [s^{(k)}] \tag{5}$$

where $[T^{(k)}]$ denotes the transformation matrix for the k—th layer. From equations (1), (4) and (5), it follows that

$$[\sigma^{(k)}] = [T^{(k)}] [\overline{Q}^{(k)}] [A]^{-1} [N] \tag{6}$$

Noting that $[T^{(k)}] [\overline{Q}^{(k)}] = [Q] [[T(k)]^{-1}]^{tr}$ (see reference [19]), $[\sigma^{(k)}]$ is given by

$$[\sigma^{(k)}] = [Q] [[T^{(k)}]^{-1}]^{tr} [A]^{-1} [N] \tag{7}$$

where

$$[Q] = \begin{bmatrix} Q_{11} & Q_{12} & 0 \\ Q_{12} & Q_{22} & 0 \\ 0 & 0 & Q_{66} \end{bmatrix} \tag{8}$$

with $Q_{11} = E_{11} / (1 - \nu_{12} \nu_{21})$, $Q_{12} = \nu_{12} E_{22} / (1 - \nu_{12} \nu_{21})$, $Q_{22} = E_{22} / (1 - \nu_{12} \nu_{21})$ and $Q_{66} = G_{12}$.

Design against failure is obtained by employing a suitable failure criterion. In this study, Tsai—Hill theory of failure, expressed by the inequality

$$\{(\sigma_1^{(k)})^2 - \sigma_1^{(k)} \sigma_2^{(k)}) X^{-2} + (\sigma_2^{(k)})^2 Y^{-2} + (\tau_{12}^{(k)})^2 S^{-2}\} \leq 1 \tag{9}$$

is used to determine the material failure. In equation (9), X and Y are the material strengths in the fibre and transverse directions and S is the in—plane shear strength.

3. MINIMUM THICKNESS DESIGN

The laminate is to be designed for minimum thickness subject to the failure criterion (9) by determining the fibre orientations optimally. We define

$$A_{ij} = H\, a_{ij}, \quad [a] = H^{-1}\, [A] \tag{10}$$

where a_{ij} is obtained from equation (3) as $a_{ij} = 2 \sum\limits_{k=1}^{n/2} h_k\, \overline{Q}_{ij}(\theta_k)$. From equation (7) it follows that

$$[\sigma^{(k)}] = H^{-1}\, [\sigma_h^{(k)}] \tag{11}$$

where

$$[\sigma_h^{(k)}] = [Q]\, [[T^{(k)}]^{-1}]^{tr}\, [a]^{-1}\, [N] \tag{12}$$

Substituting the stresses from equation (11) into the failure criterion (9), we obtain

$$H^2 \geq F(\theta_k;\, N_1,\, N_2,\, N_{12}) \tag{13}$$

for non—failure where

$$F(\theta_k;\, N_1,\, N_2,\, N_{12}) = (\sigma_{h1}^{(k)})^2 - \sigma_{h1}^{(k)}\, \sigma_{h2}^{(k)})\, X^{-2} + (\sigma_{h2}^{(k)})^2\, Y^{-2} + (\tau_{h12}^{(k)})^2\, S^{-2} \tag{14}$$

For the laminate not to fail, the inequality (13) needs to be satisfied for all layers, i.e., for $k = 1, 2, \ldots, n/2$.

The deterministic design problem can be stated in the following form:

$$H_{min} \equiv \min_{\theta_k}\ H(\theta_k;\, N_1,\, N_2,\, N_{12}) \tag{15}$$

subject to the constraint (13) for given values of h_k, N_1, N_2 and N_{12}.

4. CONVEX MODELLING

The minimum laminate thickness H_{min} depends on the loading parameters N_1, N_2, and N_{12} applied on the panel and satisfies the failure criterion. Thus we have

$$H^2_{min} \geq F(\theta_k; x_i) \tag{16}$$

where $x_1 = N_1$, $x_2 = N_2$ and, $x_3 = N_{12}$. The effect of uncertainties in x_i on the minimum thickness can be investigated by means of convex or fuzzy modelling.

In the case of convex modelling, the values of the uncertain parameters are allowed to vary arbitrarily around their average values x_{oi} such that $x_i = x_{oi} + \tilde{x}_i$. These variations, denoted by $\tilde{x}_i$, are assumed to be small and bounded such that

$$\tilde{x}_1^2 + \tilde{x}_2^2 + \tilde{x}_3^2 \leq R^2 \tag{17}$$

where R denotes the specified measure of maximum allowable uncertainty. The convex modelling problem involves the determination of the least favourable response of the system under the condition (17) on arbitrary and small variations of x_i around x_{oi}. In the present problem, the least favourable response corresponds to the minimum thickness H_{min} for non—failure with the uncertainties in the loading parameters producing the least favourable loading configuration subject to the inequality (17). From condition (17), it follows that in the present problem the region of uncertainty is a 3 dimensional sphere, and R denotes the radius of the uncertainty region.

The uncertainty problem consists of determining the minimum laminate thickness H_{min} needed for non—failure as the uncertain loading parameters vary arbitrarily in the spherical region defined by inequality (17). Thus the convex model of the optimization problem involves solving the following minmax problem

$$H^2_{min} = \min_{\theta_k} \ \max_{\tilde{x}_i} F(\theta_k; \tilde{x}_i) \tag{18}$$

subject to (17) to determine the least favourable response of the system. In the present problem the least favourable response corresponds to the loading parameter variations

which produce the thickest laminate.

The variations of uncertain parameters around their average values are assumed to be small. As such, the value of H_{min} needs to be evaluated only in a small neighbourhood of the average parameters. This observation allows us to approximate H_{min}^2 with a linear function by expanding $H_{min}^2 = F(\theta_k; \tilde{x}_i)$ in a Taylor series around the average values x_{oi} and retaining the first order terms only. The Taylor series expansion of H_{min} at x_{oi} is given by

$$H_{min}^2(\theta_k) = F(\theta_k; \tilde{x}_i) \cong F(\theta_k; x_{oi}) + [\nabla F(\theta_k; x_{oi})]^{tr} [\delta x] \tag{19}$$

where $[\delta x]$ denotes the difference vector

$$[\delta x] = [x_1 - x_{01} \quad x_2 - x_{02} \quad x_3 - x_{03}]^{tr} = [\tilde{x}_1 \quad \tilde{x}_2 \quad \tilde{x}_3]^{tr} \tag{20}$$

Since the domain of uncertainty is a convex region by virtue of the variations lying in a spherical region and H_{min} can be approximated by a linear function in this region, the maximum value of H_{min} lies on the boundary of the spherical domain defined by inequality (17). This result follows from the theory of convex sets [1, 4, 8]. The boundary can be represented as

$$C(R) = \{ \tilde{x}_1, \tilde{x}_2, \tilde{x}_3 \mid \tilde{x}_1^2 + \tilde{x}_2^2 + \tilde{x}_3^2 = R^2 \} \tag{21}$$

The problem of finding the maximum value of H_{min} on the spherical boundary is an equality constrained optimization problem and can be solved by the method of Lagrange multipliers. The Lagrangean of the problem is given by

$$L = F(\theta_k; x_{oi}) + [\nabla F(\theta_k; x_{oi})]^{tr} [\delta x] + \lambda (\tilde{x}_1^2 + \tilde{x}_2^2 + \tilde{x}_3^2 - R^2) \tag{22}$$

where λ is the unknown Lagrange multiplier. The optimality condition gives

$$\frac{\partial L}{\partial \tilde{x}_i} = \frac{\partial F(\theta_k; x_{oi})}{\partial \tilde{x}_i} + 2 \lambda \tilde{x}_i = 0 \tag{23}$$

From equation (23), we obtain the maximizing values of $\tilde{x}_i$, viz.

$$\tilde{x}_i = -(2\lambda)^{-1} \frac{\partial F(\theta_k; x_{oi})}{\partial \tilde{x}_i} \qquad (24)$$

The value of λ is computed from (21) as

$$\lambda = \mp (2R)^{-1} ([\nabla F]^{tr} [\nabla F])^{1/2} \qquad (25)$$

The variations producing the least favourable response are obtained from equations (24) and (25) as

$$x_i = \mp R ([\nabla F]^{tr} [\nabla F])^{-1/2} \frac{\partial F(\theta_k; x_{oi})}{\partial x_i} \qquad (26)$$

where the plus and the minus signs are associated with the maximum and the minimum of the thickness function $F(\theta_k; \tilde{x}_i)$. The non—deterministic design problem in the convex model can be stated as

$$H_{min} = \min_{\theta_k} \max_{\tilde{N}_i} H(\theta_k; N_1 + \tilde{N}_1, N_2 + \tilde{N}_2, N_{12} + \tilde{N}_{12}) \qquad (27)$$

subject to the constraint (13) with the values of $\tilde{N}_1$, $\tilde{N}_2$ and $\tilde{N}_{12}$ given by equation (26).

5. FUZZY MODELLING

In the fuzzy model of uncertainty, the problem parameters x_i are assigned membership functions. The degree of membership of a given parameter reflects the level of uncertainty in the information available for that parameter. Let the membership function for x_i be given by $\mu_i(x_i)$ as shown in Figure 2, viz.

$$\mu_i(x_i) = \begin{cases} 0 & \text{for } x_i \leq x_{ia} \text{ and } x_i \geq x_{id} \\ f_i(x_i) & \text{for } x_{ia} \leq x_i \leq x_{ib} \\ g_i(x_i) & \text{for } x_{ic} \leq x_i \leq x_{id} \\ 1 & \text{for } x_{ib} \leq x_i \leq x_{ic} \end{cases} \tag{28}$$

where $0 \leq f_i(x_i) \leq 1$ and $0 \leq g_i(x_i) \leq 1$ are functions representing the boundaries of the membership function. Thus, the membership function $\mu_i(x_i)$ can be considered as a mapping from the real number set $\mathbb{R}$ to the closed interval $[0, 1]$.
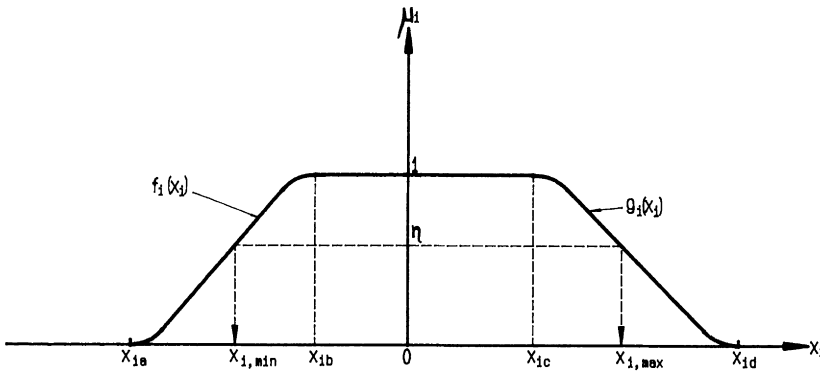
Figure 2. Membership function $\mu(x_i)$ for the loading parameter x_i

The degree of membership $\mu(\mathbf{x})$ of the parameter vector $\mathbf{x}$ is defined as

$$\mu(\mathbf{x}) = \min_i \{ \mu_i(x_i) \} , \quad i = 1, 2, 3 \tag{29}$$

A number of methods is available to compute the response of a fuzzy system. Among these, the vertex method presented in [3] provides a convenient method of obtaining the numerical answers. As the vertex method is explained in detail in [3], only an outline of the method is given here.

Let $\eta \in [0, 1]$ denote the degree of membership of the solution. Define the set

$$S_i = \{ x_{i,min} , x_{i,max} \mid \mu_i(x_{i,min}) = \mu_i(x_{i,max}) = \eta \} \tag{30}$$

where $x_{i,min}$ and $x_{i,max}$ are computed by determining the extreme points of the expression $\mu_i(x_i)$ satisfying $\mu_i(x_i) = \eta$. These values are shown in Figure 2. With each η and the fuzzy variable x_i, an interval $I_{\eta i}$ given by

$$I_{\eta i} = [x_{i,min}, \ x_{i,max}] \tag{31}$$

is associated. A function Y_η of the interval variable $I_{\eta i}$ associated with the thickness function $F(\theta_k; x_i)$ is defined as

$$Y_\eta = Y(I_{\eta i}) = \{ \ F(\theta_k; x_i) \ | \ x_i \in I_{\eta i} \ , i = 1, 2, 3 \ \} \tag{32}$$

whose value will be an interval number. When $F(\theta_k; x_i)$ is continuous and monotonic on $x_i \in I_{\eta i}$, Y_η is computed from

$$Y_\eta = [\min \{F(\theta_k; x_{i,min}), F(\theta_k; x_{i,max})\}, \ \max \{F(\theta_k; x_{i,min}), F(\theta_k; x_{i,max})\}] \tag{33}$$

The interval variables form a 3 dimensional rectangular $x_1 \times x_2 \times x_3$ with 2^3 vertices. The coordinates c_i of the vertices are given by a combination of the end points of this cube, viz.

$$c_1 = (x_{1,min}, x_{2,min}, x_{3,min}), \qquad c_2 = (x_{1,min}, x_{2,min}, x_{3,max})$$

$$c_3 = (x_{1,min}, x_{2,max}, x_{3,min}), \qquad c_4 = (x_{1,min}, x_{2,max}, x_{3,max})$$

$$c_5 = (x_{1,max}, x_{2,min}, x_{3,min}), \qquad c_6 = (x_{1,max}, x_{2,min}, x_{3,max}) \tag{34}$$

$$c_7 = (x_{1,max}, x_{2,max}, x_{3,min}), \qquad c_8 = (x_{1,max}, x_{2,max}, x_{3,max})$$

Y_η, for a given θ_k, is computed from

$$Y_\eta = [\ Y_{\eta,min}, \ Y_{\eta,max}] \tag{35}$$

where

$$Y_{\eta,min} = \min_{j} F(\theta_k; c_j), \qquad Y_{\eta,max} = \max_{j} F(\theta_k; c_j) \qquad (36)$$

with $j = 1, 2, \ldots, 8$. $Y_{\eta,min}$ and $Y_{\eta,max}$ correspond to the most and least favourable loading conditions and produce the smallest and the largest thicknesses of the laminate subject to the failure criterion (13). Let $c^* = (N_1^*, N_2^*, N_{12}^*)$ denote the coordinates of the vertex corresponding to $Y_{\eta,max}$, i.e., the least favourable load configuration computed from equation (36). The non–deterministic design problem in the fuzzy model can be stated as

$$H_{min} = \min_{\theta_k} H(\theta_k; c^*) \qquad (37)$$

subject to the constraint (13) with c^* determined from equation (36).

6. NUMERICAL EXAMPLE

The optimization techniques for laminates subject to uncertain loading data are illustrated by considering a numerical example. In particular, the optimization of a single layer panel under normal and shear loads N_1, N_2 and N_{12} is studied.

The stresses for an orthotropic lamina in the material coordinates are obtained from equation (12) by noting that for a single layer panel

$$[a]^{-1} = [\overline{Q}]^{-1} = [\overline{S}] = [T]^{tr} [S] [T] \qquad (38)$$

where $[\overline{S}]$ is the plane stress transformed compliance matrix and $[S] = [Q]^{-1}$ defined in equation (8). The index k denoting the layer numbers is omitted from the equations as k=1 for a single layer structure. Substituting $[a]^{-1}$ from equation (38) into (12), we obtain

$$[\sigma_h] = [T] [N] \qquad (39)$$

Thus the failure criterion (13) becomes

$$H^2 \geq F(\theta; N_1, N_2, N_{12}) = (\sigma_{h1}^2 - \sigma_{h1}\ \sigma_{h2})\ X^{-2} + \sigma_{h2}^2\ Y^{-2} + \tau_{h12}^2\ S^{-2} \tag{40}$$

By carrying out the convex analysis outlined in equations (18)–(26), the least favourable loading condition is determined and substituted into (40) to express the uncertain thickness function H in terms of θ. The results of the optimization for $N_1 = 3$ MN/m, $N_2 = 2$ MN/m, $N_{12} = 2$ MN/m and R=0.5 MN/m are shown in Figure 3 where the curves correspond to the least favourable, deterministic and the most favourable loading conditions. The corresponding optimal values are $H_{min} = 26.2$ mm at $\theta_{opt} = 37.16°$, $H_{min} = 11.3$ mm at $\theta_{opt} = 37.98°$ and $H_{min} = 5.3$ mm at $\theta_{opt} = 38.84°$.
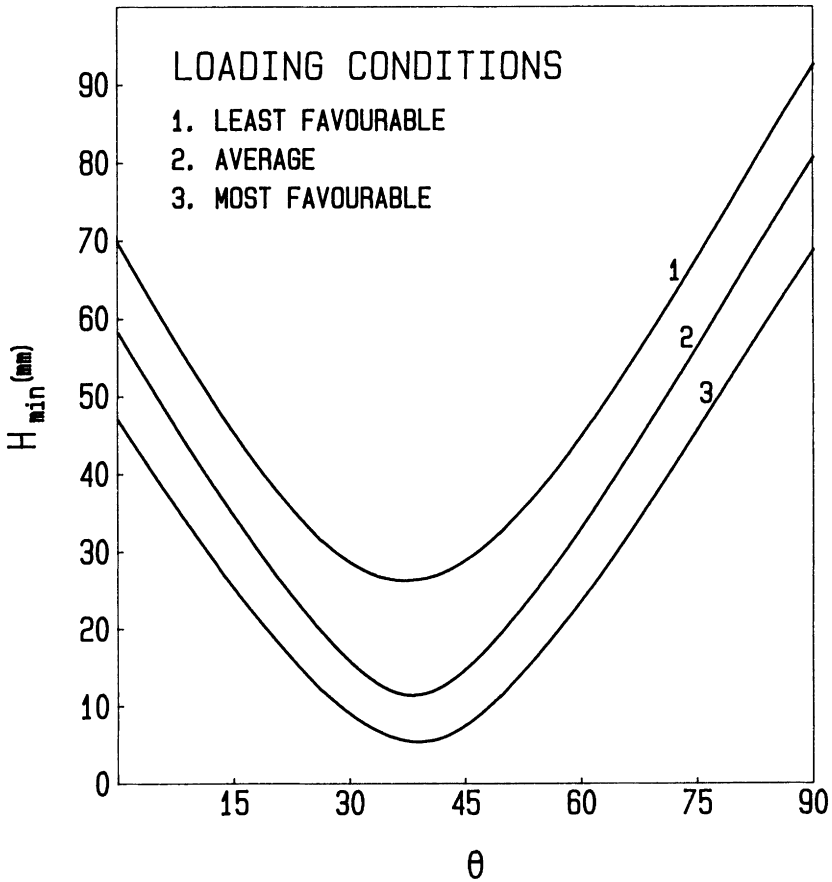
Figure 3. Curves of the minimum thickness versus the fibre orientations under the least favourable, average and the most favourable loading conditions

Thus the minimum thickness of the laminate for the least favourable case of loading with the uncertainty radius R=0.5 is 26.2 mm at the optimal fibre orientation of $37.16°$. The corresponding loading configuration is given by $N_1 = 3.14$ MN/m, $N_2 = 2.28$ MN/m, $N_{12} = 1.61$ MN/m.

Next we consider the fuzzy modelling of the optimization problem. The membership functions for the loading parameters are chosen in the following way:

$$\mu_1(N_1) = \begin{cases} 0 & \text{for } 2 \leq N_1 \text{ and } N_1 \geq 3.6 \\ N_1-2 & \text{for } 2 \leq N_1 \leq 3 \\ 6-5N_1/3 & \text{for } 3 \leq N_1 \leq 3.6 \end{cases} \tag{41}$$

$$\mu_2(N_2) = \begin{cases} 0 & \text{for } 1 \leq N_2 \text{ and } N_2 \geq 2.4 \\ N_2-1 & \text{for } 1 \leq N_2 \leq 2 \\ 6-5N_2/2 & \text{for } 2 \leq N_2 \leq 2.4 \end{cases} \tag{42}$$

$$\mu_3(N_{12}) = \begin{cases} 0 & \text{for } 1 \leq N_{12} \text{ and } N_{12} \geq 3 \\ N_{12}-1 & \text{for } 1 \leq N_{12} \leq 2 \\ 3-N_{12} & \text{for } 2 \leq N_{12} \leq 3 \end{cases} \tag{43}$$

All units are in MN/m. The average values of the load parameters are as in the previous case. Choosing the level of uncertainty $\eta = 0.5$, the extreme points of the expressions $\mu_i(N_i) = 0.5$ are determined as $I_{\eta 1} = [2.5, 3.3]$, $I_{\eta 2} = [1.5, 2.2]$, $I_{\eta 3} = [1.5, 2.5]$. The coordinates of the vertex points are determined from equations (34). The thickness is minimized for each vertex point to determine the least favourable loading condition. The results of this computation are given in Table 1.

The last row of Table 1 shows the results for the average loading parameters for which $\mu(x) = 1.0$. The least favourable loading is given by $N_1 = 3.3$ MN/m, $N_2 = 2.2$ MN/m, $N_{12} = 1.5$ MN/m with the corresponding minimum thickness being $H_{min} = 28.9$ mm at the optimal angle of $\theta_{opt} = 34.93°$. A comparison of the results for the convex and the fuzzy models indicates that the least favourable loading condition occurs at $(\tilde{N}_1, \tilde{N}_2, \tilde{N}_{12}) = (0.14, 0.28, -0.39)$ MN/m in the convex modelling corresponding

to an uncertainty radius of $R = 0.5$ MN/m with $H_{min} = 26.2$ mm. The corresponding figures in the fuzzy modelling are $(\tilde{N}_1, \tilde{N}_2, \tilde{N}_{12}) = (0.30, 0.20, -0.50)$ MN/m, $R = 0.62$ MN/m and $H_{min} = 28.9$ mm.

Table 1
The values of the loading parameters (MN/m), minimum thickness and the optimal fibre orientation

N_1	N_2	N_{12}	H_{min}(mm)	θ_{opt}
2.5	1.5	2.5	14.1	39.78°
2.5	2.2	1.5	21.2	42.14°
2.5	2.2	2.5	5.1	43.28°
3.3	1.5	1.5	16.5	29.52°
3.3	1.5	2.5	7.3	35.10°
3.3	2.2	1.5	28.9	34.93°
3.3	2.2	2.5	5.9	38.80°
3.0	2.0	2.0	11.3	37.98°

7. CONCLUSIONS

The problem of finding the minimum thickness of a laminated panel with imprecise information on the loading is studied. The minimum thickness is computed subject to Tsai–Hill failure criterion taking the fibre orientations as the design variables. Two approaches are employed in determining the least favourable loading configuration. In the first approach, called the convex modelling of uncertainty, the values of the loading parameters are allowed to vary around their average values subject to a bound on the sum of their squares. The method of Lagrange multipliers is used to compute the least favourable loading condition. In the second approach, the fuzzy set theory is used in modelling the uncertainties. This approach involves assigning membership functions to each loading parameter with the degree of membership reflecting the level of uncertainty

in the data. The vertex method is used in identifying the least favourable loading condition.

Both approaches lead to a minmax design problem in computing the minimum thickness. Comparative numerical results are given for a single layer composite panel the minimum thickness of which is determined under uncertain load data. It is observed that both methods yield similar results for the least and most favourable load conditions. The choice of a suitable method depends on the nature of available load data. If variations around average load values can be estimated, the convex model can be employed for design. If the membership functions can be estimated, the fuzzy model provides a suitable framework for design.

8. REFERENCES

[1]   Y. Ben–Haim and I. Elishakoff, *Convex Models of Uncertainty in Applied Mechanics*. Elsevier Science Publishers, Amsterdam, 1990.

[2]   S. Adali, Fuzzy optimization of laminated cylindrical pressure vessels. In *Composite Structures 6*. Edited by I.H. Marshall, Elsevier Applied science, London (1991) pp. 249–259.

[3]   V. Dong and H.C. Shah, Vertex method for computing functions of fuzzy variables. *Fuzzy Sets and Systems*, V. 4, (1987) 65–78.

[4]   I. Elishakoff and Y. Ben–Haim, Dynamics of a thin cylindrical shell under impact with limited deterministic information on its initial imperfections. *J. Structural Safety*, V. 8, (1990) 103–112.

[5]   Y. Ben–Haim and I. Elishakoff, Convex models of vehicle response to unknown but bounded terrain. *ASME J. of Applied Mechanics*, V. 58, (1991) 354–361.

[6]   Y. Ben—Haim, Convex models for optimizing diagnosis of uncertain slender obstacles on surfaces. *J. Sound and Vibration*, V. 152, (1992) 327—341.

[7]   D. Givoli and I. Elishakoff, Stress concentration at a nearly circular hole with uncertain irregularities. *ASME J. of Applied Mechanics*, V. 59, (1992) S65—S71.

[8]   I. Elishakoff, P. Elisseeff and S.A.L. Glegg, Non—probabilistic modelling of scatter in material properties for vibration analysis of viscoelastic structures. To appear in *AIAA Journal*.

[9]   I.S. Sadek, J.M. Sloss, S. Adali and J.C. Bruch Jr., Forced vibration of beams under uncertain excitations. In preparation.

[10]   D.I. Blockley, *The Nature of Structural Design and Safety*. Ellis Horwood, Chichester, 1980.

[11]   S.U. Mohandas, T.A. Phelp and K.M. Ragsdell, Structural optimization using a fuzzy goal programming approach. *Computers and Structures*, V. 37, (1990) 1—8.

[12]   Y—C. Yeh and D—S. Hsu, Structural optimization with fuzzy parameters. *Computers and Structures*, V. 37, (1990) 917—924.

[13]   A.K. Dhingra and S.S. Rao, An integrated kinematic—kinetostatic approach to optimal design of planar mechanisms using fuzzy theories. *ASME J. Mechanical Design*, V. 113, (1991) 306—311.

[14]   I.F. Obraztsov and V.V. Vasilev, Optimal design of composite structures. In *Structures and Design*. Edited by C.T. Herakovich and Y.M. Tarnopolskii, North Holland, Amsterdam, 1989, pp. 3—84.

[15]   A.A. Krikanov, Design of composite panels of minimum weight with several cases of loading. *Mechanics of Composite Structures*, V. 21, (1984) 599—602.

[16]   G. Flanagan and A.N. Palazotto, Composite laminate optimization program suitable for microcomputers. *Computers and Structures*, V. 22, (1986) 995—1009.

[17] A.M. Spencer, Simple design for reliable high–performance laminates. *Composites Science and Technology*, V. 28, (1987) 57–77.

[18] O. Ishai, S. Krishnamachari and L.J. Broutman, Structural design optimization of composite laminates. *J. Reinforced Plastics and Composites*, V. 7, (1988) 459–474.

[19] L.N. Phillips, *Design With Advanced Composite Materials*. Springer Verlag, Berlin, 1989.

Topology optimization of bi-material structures[1]

Niels Olhoff, Jan Thomsen and John Rasmussen

Institute of Mechanical Engineering, Aalborg University, DK-9220 Aalborg East, Denmark

Abstract

This paper deals with the problem of determining optimum topologies of linearly elastic structures composed of two different materials with given moduli of elasticity. Within a given admissible design domain, the structural topology is determined from the condition of maximum integral stiffness (minimum compliance) subject to given amounts of the two available materials. It is assumed that the structures are in plane stress and that geometric boundary conditions and static edge loading are specified.

The structures of optimum topologies obtained within the initial formulation are mainly composites. As this may be undesirable in certain cases, a formulation is also presented that penalizes formation of composite and yields structures which entirely consist of the isotropic base materials without small-scale mixing. Numerical examples pertaining to generation of optimum topologies of joints and assemblies of sandwich panels and beams, and optimum reinforcement against concentrated loads, are presented.

1. INTRODUCTION

Topology optimization of structures as introduced by Bendsøe and Kikuchi (1988), is performed as an optimum material distribution problem where the material is modelled as a porous, periodic microstructure of variable density (concentration) and orientation. This problem may be conceived a direct extension of the problem of optimizing mutually orthogonal fiber fields of variable concentration and orientation in composites, which was originally posed by Niordson and solved by Rasmussen (1979) in a PhD thesis in Danish (an account in English is available in Niordson and Olhoff 1979). The connection becomes obvious if we consider the fiber and matrix materials of the composite to represent the solid material and void, respectively, that ultimately define the structural topology.

The present paper deals with topology optimization of plane structures composed of two different elastic materials. By generalization of a technique available for single material structures, the mathematical formulation of the current bi-material topology optimization problem is based on derivation of the effective constitutive matrix of a layered second-rank porous, periodic microstructure by a homogenization (or smear-out) procedure. Each cell of the periodic microstructure is constructed from layers of the two materials and void, and

---

[1]Dedicated to Frithiof Niordson at his Seventieth anniversary

admits each of the relative densities of the two materials and void to cover the complete range from zero to unity. The constitutive matrix of the microstructure is expressed in terms of these densities and the cell orientation, which play the role as continuous functions of design variables over the admissible design domain for the structure.

The purpose of adopting a layered second rank microstructure is not only to work with a convenient, continuous material model which admits us to obtain analytical expressions for the elastic moduli. Thus, if the problem had been stated as an integer optimization problem such that only either "solid material 1", "solid material 2" or "no material" could be generated at any given point of the design domain, then the formulation would, in general, have been *ill-posed* and the existence of a solution (an optimum design) would not be obvious, see Olhoff *et al* (1981); Lurie and Cherkaev (1984); and Strang and Kohn (1986). The key would then be to regularize the formulation of the optimization problem by introducing a family of composites constructed from the base materials. This process is termed *relaxation* and has been studied in various connections by, e.g., Lurie *et al* (1982); Cheng and Olhoff (1982); Gibianski and Cherkaev (1984); Murat and Tatar (1985); Lurie and Cherkaev (1986); Kohn and Strang (1986); Thomsen and Olhoff (1990); and Thomsen (1991). Relaxation implies enlarging of the design space and tends to remove local optima (Kohn 1990). Traditionally, it was thought that one must consider the totality of all possible composites assembled from the set of originally given materials, an approach called *full relaxation*. However, recent investigations have shown that only the set of finite rank laminate composites need to be considered for many optimization problems (Avellaneda 1987; Kohn 1988a; Kohn and Lipton 1988b). This technique is termed *partial relaxation* and is performed by introducing some convenient, finite-parameter micro structure.

The micro structure adopted in this study is of the latter type. The solution of our bi-material structural topology optimization problem is based on a finite element discretization of the admissible design domain, and the optimum values of the design variables, which determine the optimum topology of the structure, are determined iteratively by a two-level procedure consisting of a global optimality criterion approach for the cell orientation as developed by Pedersen (1989, 1990), and a usual mathematical programming technique for the densities.

2. MATERIAL MODEL

We now develop the microstructural material model to be used for topology optimization of plane bi-material structures. In the literature dealing with topology optimization of structures consisting of only *one* relatively stiff material several numerical and analytical material models have been used. In all models integer optimization is avoided by using a continuous parameter material model, which is also defined for intermediate values between the limits of "material" and "no material" and implies that essentially the optimization can be performed as a sizing problem. Bendsøe and Kikuchi (1988); Suzuki and Kikuchi (1989); and Diaz and Bendsøe (1992) are using a numerically determined material model based on a micro structure consisting of an isotropic material with rectangular holes, and they use the orientation and the size of the holes as design variables of the optimization problem.

In this paper we adopt an analytical material model consisting of a layered, second rank composite material made up of two isotropic materials of different, relatively large

stiffnesses, and a very soft material which represents void. The composite is constructed in three micro levels. In the first level we model a layered composite consisting of "material 1" and "material 2", see Figure 1a. The densities (concentrations) of the two materials are given in terms of the dimensions δ_1 and $1-\delta_1$ shown in Figure 1a.
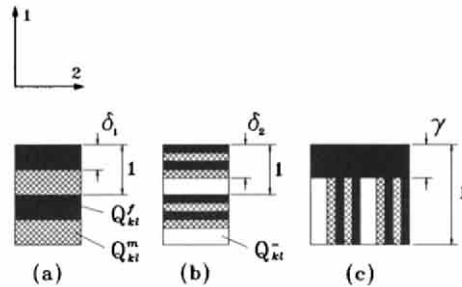
Figure 1. Construction of composite materials. (a) First level. (b) Second level. (c) Third level

In the second level we construct a layered composite from the material just obtained (Figure 1a) and the "very soft material", where the densities are defined through the dimensions δ_2 and $1-\delta_2$, see Figure 1b. Finally, in the third level we construct a composite consisting of layers of "material 1" and the composite in Figure 1b, with the concentrations given by the dimensions γ and $1-\gamma$, see Figure 1c. The three base materials used in the resulting material model in Figure 1c are isotropic and have the the stiffness matrices:

Q_{kl}^f : Material 1

Q_{kl}^m : Material 2

Q_{kl}^- : Very soft material

If all the design variables of the material model in Figure 1c are allowed to vary between 0 and 1, the model covers pure "material 1", pure "material 2", "no material" and composite combinations thereof when the full range of admissible values of γ, δ_1 and δ_2 are considered. We shall assume that the relatively simple material model in Figure 1c is general enough for our bi-material topology optimization problem. In any point of the design domain, in addition to $\gamma(x)$, $\delta_1(x)$ and $\delta_2(x)$, we shall also apply the material orientation $\theta(x)$ as a design variable. Notice that the material model admits creation of structures solely composed of the isotropic materials, but that it is possible as well that parts of the structure may become anisotropic as mixtures of the materials may be formed.

3. OPTIMIZATION PROBLEM

We consider maximization the integral stiffness of linearly elastic bi-material structures

in plane stress. The structures are analyzed by means of orthotropic finite elements in a fixed mesh, and the boundary conditions and in-plane loading are assumed to be given. Maximization of the integral stiffness is equivalent to minimization of the total elastic strain energy U of the structure which is given by

$$U = \sum_{i=1}^{n} \left\{ \left\{ \frac{1}{8}A_{11}\left[(\epsilon_I + \epsilon_{II}) + (\epsilon_I - \epsilon_{II})\cos 2\psi\right]^2 + \frac{1}{8}A_{22}\left[(\epsilon_I + \epsilon_{II}) - (\epsilon_I - \epsilon_{II})\cos 2\psi\right]^2 \right. \right.$$

$$\left. \left. + \frac{1}{4}A_{12}\left[(\epsilon_I + \epsilon_{II})^2 - (\epsilon_I - \epsilon_{II})^2\cos^2 2\psi\right] + \frac{1}{2}A_{66}(\epsilon_I - \epsilon_{II})^2\sin^2 2\psi \right\} S \right\}_i \tag{1}$$

for a fine finite element discretization. In (1), ϵ_I and ϵ_{II} denote the principal strains, [A] the matrix of in-plane stiffnesses, ψ the angle from the direction corresponding to the numerically largest principal strain ϵ_I to the direction associated with the largest stiffness A_{11}, and S is the finite element area. The design variables of the optimization problem are the densities and the orientation of "material" within each finite element. Thus, in topology optimization of structures with two materials of large stiffnesses, we apply γ, δ_1, δ_2 (see Figure 1c) and θ as design variables for the minimization of U, and we specify that the total amounts C_1 of "material 1" and C_2 of "material 2" must be less than or equal to given values $\overline{M_1}$ and $\overline{M_2}$, respectively,

Minimize $\quad U$
$\gamma_i, \delta_{1i}, \delta_{2i}, \theta_i$ $\tag{2a}$

$$0 \leq \gamma_i \leq 1 \quad ; \quad 0 \leq \delta_{1i} \leq 1 \quad ; \quad 0 \leq \delta_{2i} \leq 1 \quad ; \quad i=1,\ldots,n \tag{2b}$$

$$C_1 = \sum_{i=1}^{n} \left[\gamma_i + (1-\gamma_i)\delta_{2i}\delta_{1i}\right]S_i \leq \overline{M_1} \quad ; \quad C_2 = \sum_{i=1}^{n} \left[(1-\gamma_i)(1-\delta_{1i})\delta_{2i}\right]S_i \leq \overline{M_2} \tag{2c}$$

4. STIFFNESS MATRIX IN TERMS OF DESIGN VARIABLES

The stiffness matrix of the material shown in Figure 1c can be determined by a smear-out technique, see, e.g., Thomsen (1992), or we can use the homogenization technique in three steps. Bendsøe (1989) presents the formulas in (3) for determining the components Q_{kl}^H of the constitutive matrix of an orthotropic composite by homogenization. In (3), $M(f)$ denotes the average value of a function $f(y)$ in the interval Y as defined by (4), and Q_{kl} are the so-called reduced stiffnesses, which for an isotropic material with the Young's modulus E, Poisson's ratio ν and plane stress conditions are given by (5).

$$Q_{11}^H = \left[M\left(\frac{1}{Q_{11}} \right) \right]^{-1} \quad , \quad Q_{22}^H = M(Q_{22}) - M\left(\frac{Q_{12}^2}{Q_{11}} \right) + \left[M\left(\frac{Q_{12}}{Q_{11}} \right) \right]^2 \left[M\left(\frac{1}{Q_{11}} \right) \right]^{-1}$$

$$Q_{12}^H = M\left(\frac{Q_{12}}{Q_{11}} \right) \left[M\left(\frac{1}{Q_{11}} \right) \right]^{-1} \quad , \quad Q_{66}^H = \left[M\left(\frac{1}{Q_{66}} \right) \right]^{-1} \tag{3}$$

$$M(f) = \frac{1}{|Y|} \int_Y f(y)\,dy \tag{4}$$

$$Q_{11} = Q_{22} = \frac{E}{1-\nu^2} \quad ; \quad Q_{12} = \frac{\nu E}{1-\nu^2} \quad ; \quad Q_{66} = \frac{E}{2(1+\nu)} \tag{5}$$

We first consider the composite material composed of the two isotropic materials with the stiffnesses Q_{kl}^f and Q_{kl}^m, see Figure 1a. To simplify the calculations the materials are presumed to have the same Poisson's ratio. From (3)-(5) the elasticity constants Q_{kl}^{HI} of this composite are found to be

$$Q_{11}^{HI} = J_1 \quad ; \quad Q_{22}^{HI} = J_3 \quad ; \quad Q_{12}^{HI} = \nu J_1 \quad ; \quad Q_{66}^{HI} = \frac{1-\nu}{2} J_1 \tag{6}$$

where Q_{11}^{HI} and Q_{22}^{HI} are the stiffnesses corresponding to the orientation of the 1- and 2- axes shown in Figure 1, and

$$J_1 = \left[\frac{\delta_1}{Q_{11}^f} + \frac{1-\delta_1}{Q_{11}^m} \right]^{-1} \quad , \quad J_2 = \delta_1 Q_{11}^f + (1-\delta_1)Q_{11}^m \quad , \quad J_3 = J_2(1-\nu^2) + \nu^2 J_1 \tag{7}$$

The constitutive matrix Q_{kl}^{H3} of our second rank composite in Figure 1c can now be determined by repeating twice the use of (3) and (4), and we obtain the result given in (8), where J_1, J_3, Q_{11}^{H2} and Q_{22}^{H2} are given by (7) and (9). Finally, we determine by (10) the components A_{kl} of the stiffness matrix of our plane orthotropic bi-material structure that has variable micro structure of the type shown in Figure 1c, and a constant thickness denoted by h.

$$Q_{11}^{H3} = \left[\frac{\gamma}{Q_{11}^f} + \frac{1-\gamma}{Q_{22}^{H2}} \right]^{-1}$$

$$Q_{22}^{H3} = \gamma Q_{11}^f + (1-\gamma) Q_{11}^{H2} - \nu^2 \left[\gamma Q_{11}^f + \left(Q_{11}^{H2} \right)^2 \frac{1-\gamma}{Q_{22}^{H2}} - Q_{11}^{H3} \left(\gamma + Q_{11}^{H2} \frac{1-\gamma}{Q_{22}^{H2}} \right)^2 \right] \tag{8}$$

$$Q_{12}^{H3} = \nu \left[\gamma + Q_{11}^{H2} \frac{1-\gamma}{Q_{22}^{H2}} \right] Q_{11}^{H3} \,, \quad Q_{66}^{H3} = \frac{1-\nu}{2} \left[\frac{\gamma}{Q_{11}^f} + \frac{1-\gamma}{Q_{11}^{H2}} \right]^{-1}$$

$$Q_{11}^{H2} = \left[\frac{\delta_2}{J_1} + \frac{1-\delta_2}{Q_{11}^-} \right]^{-1}$$

$$Q_{22}^{H2} = \delta_2 J_3 + (1-\delta_2) Q_{11}^- - \nu^2 \left[\delta_2 J_1 + (1-\delta_2) Q_{11}^- \right] + \nu^2 Q_{11}^{H2} \tag{9}$$

$$A_{kl} = \int_{-h/2}^{h/2} Q_{kl}^{H3} dz = h Q_{kl}^{H3} \tag{10}$$

5. OPTIMIZATION TECHNIQUE

The optimization problem is solved iteratively by a two-level procedure of redesign. In each loop of redesign, the stress-strain field is initially determined by finite element analysis whereupon in the first level improved orientations θ_i ($i=1,...,n$) of the axes of anisotropy of the composite are determined by means of an analytic optimality criterion approach. In the second level of redesign the material densities δ_{1i}, δ_{2i} and γ_i are improved by a method of mathematical programming and analytic sensitivity analysis.

A notable feature of the present problem is that a usual gradient method may fail in determining the optimal orientation of the composite because local optima normally exist. To circumvent this inherent difficulty, we use the results obtained by Pedersen (1989, 1990), who performed an analytical investigation of the first and second derivative of the total strain energy with respect to the orientation of the composite. The results of the investigation are summarized in a table in Pedersen (1990). In an optimization problem where the stiffness of a structure is maximized using the material orthotropy directions as design variables, we may either orient the composite material relative to the principal stress or strain directions (Pedersen et al. 1991). However, numerical examples have shown that the best convergence properties are obtained for the optimization problem if the axes of orthotropy are rotated relative to the principal stress directions. Coincidence between the largest principal stress and strain directions is always found to be a result of the orientation

optimization, and normally these directions will coincide with the material direction associated with the largest stiffness (unless the material has a relatively high shear stiffness, see Pedersen 1990).

The second stage of the loop of redesign consists in determining an improved distribution of the amounts of material, i.e., to obtain improved values of the design variables δ_{1i}, δ_{2i} and γ_i, (i=1,...,n) governing the material densities. We apply a dual method of mathematical programming using mixed variables as developed by Svanberg (1987) and implemented in the computer code MMA (Method of Moving Asymptotes). To this end we need the sensitivities of the total elastic energy and the constraints with respect to the above mentioned design variables.

The total elastic energy of a linear elastic material is given by the finite element form

$$U = \frac{1}{2}\{d\}^T[K]\{d\} \tag{11}$$

where $\{d\}$ is the nodal displacement vector, and $[K]$ is the global stiffness matrix.

The change in the total elastic energy U due to a change in a design variable a_i consists of two parts,

$$\frac{dU}{da_i} = \frac{\partial U}{\partial a_i} + \frac{\partial U}{\partial \epsilon}\frac{\partial \epsilon}{\partial a_i} \tag{12}$$

where the first part is the change in U due to the change in the stiffness matrix in the domain related to the design variable a_i, and the second part is the change in U due to the change in the displacement field of the whole structure, i.e.,

$$\frac{\partial U}{\partial a_i} = \frac{1}{2}\{d\}^T\frac{\partial[K]}{\partial a_i}\{d\} \qquad , \qquad \frac{\partial U}{\partial \epsilon}\frac{\partial \epsilon}{\partial a_i} = \frac{1}{2}\left[\frac{\partial \{d\}^T}{\partial a_i}[K]\{d\} + \{d\}^T[K]\frac{\partial \{d\}}{\partial a_i}\right] \tag{13}$$

Let us now consider the global finite element equilibrium equation $[K]\{d\} = \{p\}$ where $\{p\}$ is the vector of external loads. Differentiation of this equation gives, if we assume design independent loads,

$$[K]\frac{\partial \{d\}}{\partial a_i} = -\frac{\partial[K]}{\partial a_i}\{d\} \tag{14}$$

If (14) and its transposed form is substituted into second of Eqs.(13) we get the following expression for the change in U due to the change in the displacement field:

$$\frac{\partial U}{\partial \epsilon} \frac{\partial \epsilon}{\partial a_i} = -\{d\}^T \frac{\partial [K]}{\partial a_i} \{d\} \tag{15}$$

This implies in view of (13) that the two parts of the sensitivity in (12) are related by the simple equation

$$\frac{\partial U}{\partial \epsilon} \frac{\partial \epsilon}{\partial a_i} = -2 \frac{\partial U}{\partial a_i} \tag{16}$$

that leads to the important result

$$\frac{dU}{da_i} = -\frac{\partial U}{\partial a_i} = -\frac{1}{2} \{d\}^T \frac{\partial [K]}{\partial a_i} \{d\} \tag{17}$$

which implies that, if the external loads are design independent, then the sensitivity of the total elastic energy with respect to a design variable a_i can be simply determined without a computation of the change in the displacement field due to the change of the design variable. This result was originally etablished by Pedersen (1990) by using Clayperon's theorem and the principle of virtual displacements.

Now, for a finite element discretized structure the total elastic energy U is equal to the sum of the element energies U_i, where the index i refers to the i-th element,

$$U = \sum_i U_i \tag{18}$$

Denoting by a_i a design variable referring to the i-th element, and assuming a fine discretization, it follows from (18) and (19) that the sensitivity of the total elastic energy can be simply obtained from the sensitivity of the specific strain energy u_i of the i'th element according to the formula

$$\frac{dU}{da_i} = -\frac{\partial U_i}{\partial a_i} = -\frac{\partial u_i}{\partial a_i} S_i \tag{19}$$

Here a_i denotes any of the design variables δ_{1i}, δ_{2i} or γ_i (i=1,...,n). Thus, the sensitivities of the total strain energy U with respect to δ_{1i}, δ_{2i} and γ_i can be simply determined by means of (1) and (19), assuming the strain field to be fixed, and restricting variation to the stiffness matrix [A]. Hence, for the i-th element of the discretized geometry we obtain the following expression for sensitivities with respect to the design variables a_i:

$$U,_{a_i} = -\left\{\left\{\frac{1}{8}A_{11}'\left[(\epsilon_I+\epsilon_{II})+(\epsilon_I-\epsilon_{II})\cos 2\psi\right]^2 + \frac{1}{8}A_{22}'\left[(\epsilon_I+\epsilon_{II})-(\epsilon_I-\epsilon_{II})\cos 2\psi\right]^2\right.\right.$$

$$\left.\left. + \frac{1}{4}A_{12}'\left[(\epsilon_I+\epsilon_{II})^2-(\epsilon_I-\epsilon_{II})^2\cos^2 2\psi\right] + \frac{1}{2}A_{66}'(\epsilon_I-\epsilon_{II})^2\sin^2 2\psi\right\}S\right\}_i , \quad i = 1,\dots,n \tag{20}$$

Here A_{kl}' is a shorthand notation for the derivatives dA_{kl}/da_i of the components of the stiffness matrix [A]. These sensitivities are derived analytically by Thomsen (1992), and results are available therein. Sensitivities of the constraints in (2) are readily derived analytically, and we thus have all the necessary sensitivity information for the optimization at the second level of redesign.

5.1 Example: Problem of force introduction solved via the original formulation

We now consider an optimization problem, where void and material is modeled by a composite composed of one very soft material (representing void) and two materials of large stiffnesses. A plane design domain which is subjected to concentrated forces and supported as shown in Figure 2 is considered. The available amounts of "material 1" and "material 2" are taken to be 30% and 60% of the design domain volume, respectively, and the stiffness ratio between these materials (Q_{kl}^f/Q_{kl}^m) is set to be 10. We discretize the design domain in Figure 2 into 22x66 orthotropic four-node rectangular elements.
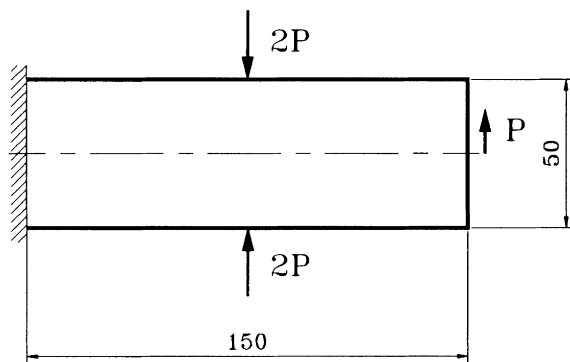
Figure 2. Design domain, load and boundary conditions.

Figure 3a shows the optimized structure which mainly consists of orthotropic material. The densities of the hatching shown in two perpendicular directions are proportional to the elastic moduli A_{11} and A_{22}, and the orientation of the hatching indicates the corresponding principal directions of the material. The material is distributed in such a way that the larger normal stresses are carried by relatively stiff material, while the shear stresses are carried by softer orthotropic material, the stiffnesses of which are almost equal in the two principal material directions. No material is distributed in sub-domains which have small strain energy density due to the applied load and boundary conditions.

(a)

(b)
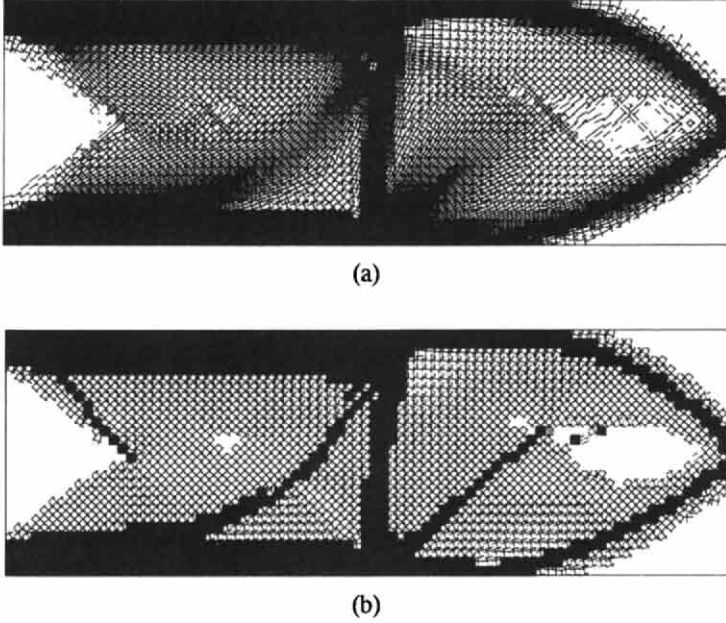
Figure 3. (a) Optimum topology. Structure is mainly composite. Hatching density is proportional to stiffness. White sub-domains represent void. (b) Optimum topology obtained by penalization of composite material. Here, black and hatched sub-domains represent purely isotropic "material 1" and "material 2", respectively. The compliance of the solution is only 5% higher than that of the anisotropic solution in Figure 3a.

6. PENALIZATION TECHNIQUE FOR REMOVAL OF SUB-DOMAINS WITH COMPOSITE MATERIALS

From a manufacturing point of view it would be preferable if a bi-material structure is only composed of the isotropic base materials. We now demonstrate how the optimization problem can be reformulated such that anisotropic characteristics of a solution to the original problem formulation are removed.

Let us construct the following non-negative function G that depends on the total amount of anisotropic material in the discretized structure:

$$G = \sum_{i=1}^{n} \left(\gamma_i (1 - \gamma_i) + \delta_{1i}(1 - \delta_{1i}) + \delta_{2i}(1 - \delta_{2i}) \right) S_i \tag{21}$$

Clearly, G only will be equal to zero, if γ_i, δ_{1i} and δ_{2i} attain their limiting values 0 or 1 everywhere. We now formulate the optimization problem with a view to minimize the total elastic energy U and simultaneously penalize presence of anisotropic material:

Minimize $\quad \tilde{F} = U + RG$
$\gamma_i, \delta_{1i}, \delta_{2i}, \theta_i$

$$(22)$$

Side constraints (2*b*)

Constraints (2*c*) *on amounts of materials*

Here $\tilde{F}$ is the original objective function augmented with the penalty term RG where $R=0,1,10,\ldots$ is a penalty parameter, the value of which we gradually increase during the optimization procedure.

By this formulation G is rendered equal to zero and structural topologies are obtained which are only composed of isotropic "material 1", isotropic "material 2" and "void".

6.1 Example: Removal of anisotropic sub-domains in previous example problem

If we apply the above penalization technique for the topology optimization problem in Section 5.1, and use the topology in Figure 3a as an initial design, we obtain the new topology solution in Figure 3b where the distribution of isotropic pure "material 1" and pure "material 2" is illustrated by black and hatched domains, respectively, and white domains represent void. The compliance of the isotropic bi-material topology in Figure 3b is 5% higher than for the anisotropic topology in Figure 3a.

7. ADDITIONAL EXAMPLES OF TOPOLOGY OPTIMIZATION OF BI-MATERIAL STRUCTURES

In both of the previous examples, it is noticed that a domain without material has been generated along the left, fully clamped boundary of the structures, see Figures 3a and 3b. Thus, at this boundary the two stiff "skin" materials will both transfer the bending and the shear stresses caused by the loading, which is not typical for a sandwich-like structure.

Consider now the example in Figure 4, where we shall perform an adaption for "sandwich beam" characteristics at the left boundary. Thus, we let the middle part of the left boundary offer full fixation against displacements, whereas we take the upper and lover parts to be simply supported only in those sub-regions where "skin" material is created. Thus the shear forces can be only transferred by the middle part of the boundary.
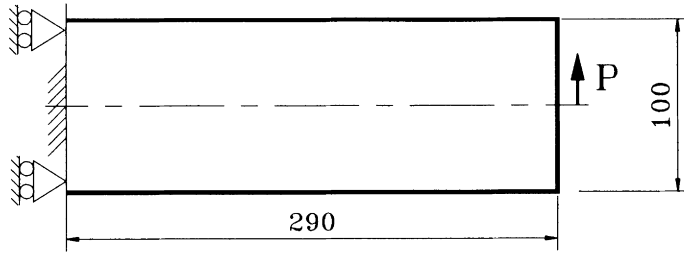
Figure 4. Design domain, load and boundary conditions.

The available amounts of "material 1" and "material 2" are taken to be 25% and 65% of the design domain volume, and using the symmetry conditions we only analyze the upper half of the structure. Minimizing total elastic energy U and the augmented objective function $\bar{F}$, respectively, we obtain the optimal topologies in Figures 5a and b. Again the structure is composed of anisotropic material if U is minimized, whereas we obtain an isotropic bi-material structure when $\bar{F}$ is minimized. The compliance of the solution in Figure 5b is 5% higher than for that in Figure 5a. In these examples the shear forces along the left boundary are carried by lower stiffness "core" material and the relatively stiff "skin" materials only transfer the bending normal stresses, as is the case for sandwich beams. Notice also that the thickness of the stiff "skin" material decreases nearly linearly from the left to the right end of the structure in accordance with the load situation.
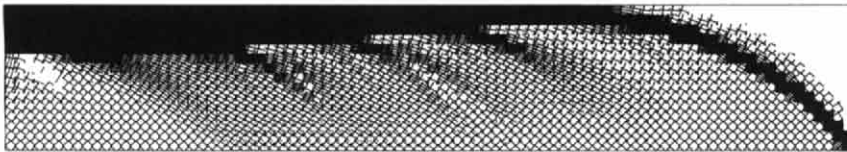
(a)
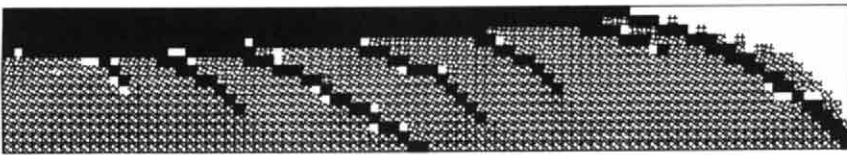
(b)

Figure 5. (a) Optimum topology. Structure is mainly composite. Hatching density is proportional to stiffness. White sub-domains represent void. (b) Optimum topology of isotropic bi-material structure. Here black and hatched sub-domains represent purely isotropic "material 1" and "material 2", respectively.

In the next example we investigate how the joining of two sandwich beams can be reinforced. The sandwich beams are mutually connected via a "T-joint", and the vertical beam is loaded in tension while the horizontal beam is subjected to combined bending and shear, see Figure 6.
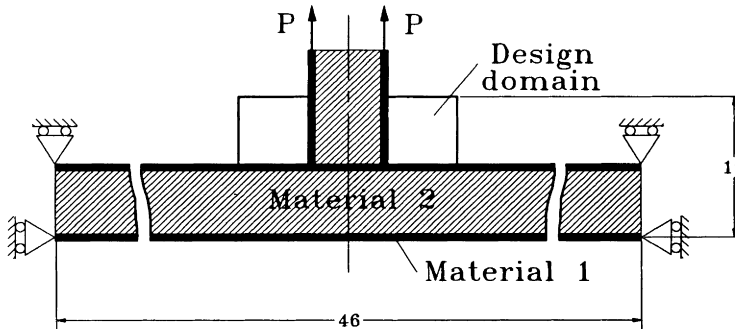
Figure 6. Design domain, load and boundary conditions.

By the optimization given amounts of the relatively stiff materials are distributed in the design domains. The available amounts of "material 1" and "material 2" are set to be 10% and 40% of the total design domain volume, respectively, and using the symmetry we only analyze the left part of the structure. The structure is optimized using the penalty formulation (22), and the result is seen in Figure 7. The stiffest "material 1" principally forms a straight "tension beam" which connects the sandwich beams, and the tension beam is reinforced by the softer "material 2".
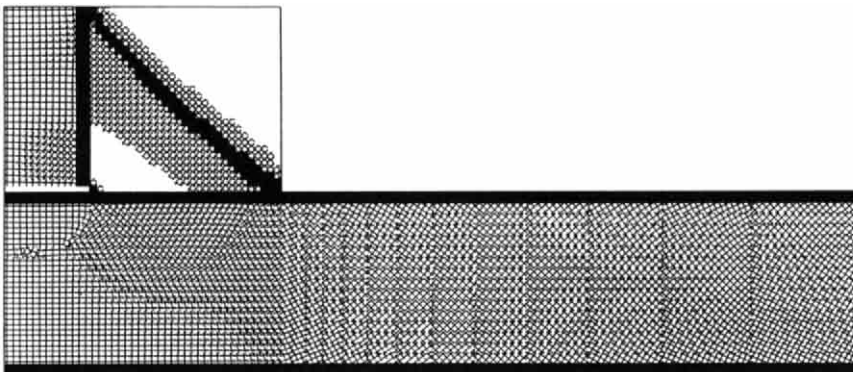
Figure 7. Optimized topology of isotropic bi-material joint.

As a final example we consider the structures in Figure 8. These are symbolizing two different joinings of "beams", which are assumed to be build up as sandwich structures. The available amounts of "material 1" and "material 2" are taken to be 35% and 50% of the total design domain volume in Figure 8a, respectively, and 30% and 50% of the design domain volume in Figure 8b.
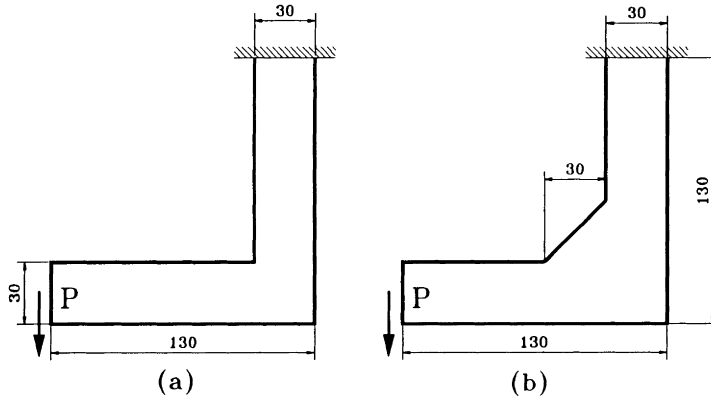
Figure 8. Design domain, load and boundary conditions.

By minimizing $\tilde{F}$ with arbitrarily large penalty factor R the topologies in Figure 9 are obtained. The vertical beams are mainly subjected to bending, and have no material distributed near the neutral axis. The horizontal beams are loaded by combined bending and shear, and in these beams the available amount of the relatively soft "material 2" is used to carry the shear forces.
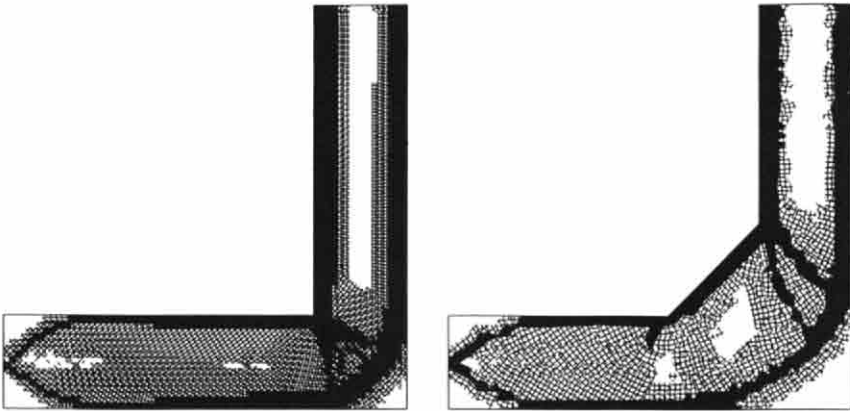
Figure 9. Optimum topologies of isotropic bi-material joinings.

8. REFERENCES

Avellaneda, M. 1987: Optimal Bounds and Microgeometries for Elastic Two-phase Composites. SIAM J. Appl. Math. 47, 1216-1228.

Bendsøe, M.P.; Kikuchi, N. 1988: Generating Optimal Topologies in Structural Design using a Homogenization Method. Comp. Meth. Appl. Mech. Eng., 71, 197-224.

Bendsøe, M.P. 1989: Optimal Shape Design as a Material Distribution Problem. Structural Optimization, 1, 193-202.

Cheng, G.; Olhoff, N. 1982: Regularized Formulation for Optimal Design of Axisymmetric Plates, Int. J. Solids Structures, 18, 153-169.

Diaz, A.R.; Bendsøe, M.P. 1992: Shape Optimization of Multipurpose Structures by a Homogenization Method. Structural Optimization, 4, 17-22.

Gibianski, L.V.; Cherkaev, A.V. 1984: Design of Composite Plates of Extremal Rigidity (in Russian). Preprint No. 914, A.F. Ioffe Institute, Leningrad.

Kohn, R.; Strang, G. 1986: Optimal Design and Relaxation of Variational Problems I-III. Comm. Pure Appl. Math. 39, 113-138, 139-182, 353-377.

Kohn, R. 1988a: Recent Progress in the Mathematical Modelling of Composite Materials. In: Composite Material Response: Constitutive Relations and Damage Mechanisms, G. Sih et. al. eds, Elsevier, 155-177.

Kohn, R.; Lipton, R. 1988b: Optimal Bounds for the Effective Energy of a Mixture of Two Incompressible Materials. Arch. Rat. Mech. Anal. 102, 331-350.

Kohn, R. 1990: Composite Materials and Structural Optimization. Proc. Workshop on Smart/Intelligent Materials and Systems. Honolulu, March 1990, (Thechonomic Press).

Lurie, K.A.; Fedorov, A.V.; Cherkaev, A.V. 1982: Regularization of Optimal Design Problems for Bars and Plates, Parts 1 and 2, 37, 499-521, and 37, 523-543.

Lurie, K.A.; Cherkaev, A.V. 1984: G-Closure of a Set of Anisotropically Conducting Media in the Two-dimensional Case. JOTA, 42, 283-304.

Lurie, K.A.; Cherkaev, A.V. 1986: Effective Characteristics of Composites and Problems of Optimum Structural Design (in Russian). Uspekhi Mekhaniki 9, 1-81.

Murat, F.; Tartar, L. 1985: Calcul des Variations et Homogenization. Le Methodes de l'Homogeneisation: Theorie et Applications en Physique, Coll. de la Dir. des Etudes et Recherche d'Electricite de France, Eyrolles, 319-369.

Niordson, F.I.; Olhoff, N. 1979: Variational Methods in Optimization of Structures. In: Trends in Solid Mechanics, Proc. W.T. Koiter Anniversary Symp. 1979, J.F. Besseling and

A.M.A. van der Heijden eds, Sijthoff & Noordhoff, 177-194.

Olhoff, N.; Lurie, K.A.; Cherkaev, A.V.; Fedorov, A.V. 1981: Sliding Regimes and Anisotropy in Optimal Design of Vibrating Axisymmetric Plates. Int. J. Solids Structures, 17, 931-948.

Pedersen, P. 1989: On Optimal Orientation of Orthotropic Materials. Structural Optimization, 1, 101-106.

Pedersen, P. 1990: Bounds on Elastic Energy in Solids of Orthotropic Materials, Structural Optimization, 2, 55-63.

Pedersen, P.; Bendsøe, M.P.; Nagendra, S. 1991: Note on the 2D-Match of Coaligned Principal Stresses and Strains. Dept. Solid Mechanics, Technical University of Denmark, Lyngby, Denmark.

Rasmussen, S.H. 1979: Optimization of Fiber Reinforced Structures (in Danish). Ph.D. Thesis. DCAMM Report No. S 12. Dept. Solid Mechanics, Technical University of Denmark, Lyngby, Denmark.

Strang, G.; Kohn, R.V. 1986: Optimal Design in Elasticity and Plasticity. Int. J. Num. Meth. in Eng., 22, 183-188.

Suzuki, K.; Kikuchi, N. 1989: A Homogenization Method for Shape and Topology Optimization. Department of Mechanical Engineering and Applied Mechanics, The University of Michigan, Ann Arbor, Michigan 48109, USA.

Svanberg, K. 1987: The Method of Moving Asymptotes - a New Method for Structural Optimization. Int. J. Num. Meth. Eng., 24, 359-373.

Thomsen, J.; Olhoff, N. 1990: Optimization of Fiber Orientation and Concentration in Composites. Control and Cybernetics, 19, 327-341.

Thomsen, J. 1991: Optimization of Composite Discs. Structural Optimization, 3, 89-98.

Thomsen, J. 1992: Optimization of Properties of Anisotropic Materials and Topologies of Structures (in Danish). Ph.D. Thesis, Special Report No. 14, Institute of Mechanical Engineering, Aalborg University, Denmark.

Design of crack-insensitive composite laminates

J. Wang and B. L. Karihaloo

School of Civil and Mining Engineering, University of Sydney, NSW 2006, Australia

Abstract

In $[\pm\theta^0/90^0/\mp\theta^0]$ fibre-reinforced composites, the outer θ^0 plies are known to act as crack arrestors, i.e. to reduce the stress intensity factors at the tips of a crack in the central 90^0 ply in all three modes of loading. The degree of reduction depends on the stiffness of the plies, the ply angle θ and the thickness of the outer plies. However, whilst the stress intensity factor decreases, the crack-induced interfacial von Mises stress increases. The situation is particularly severe under transverse mode II loading, inevitably resulting in interfacial delamination.

The aim of this paper is to choose the design variables of the laminate, viz. the ply angle θ, relative ply stiffness and thickness, in such a way as to minimize the stress intensity factor at a crack tip in the 90^0 ply without exceeding the interfacial von Mises bond strength. A constraint is also placed on the minimum flexural stiffness of the laminate. An alternative optimization problem in which the von Mises stress is minimized subject to a limit on the stress intensity factor is also formulated and solved.

1. INTRODUCTION

Most of the fibre-reinforced composite materials are used in the form of laminates composed of plies with different fibre directions. The most common and fatal form of failure in laminates resulting in loss of both their strength and stiffness is delamination between constituent laminae. Under compression, the delaminated sublaminates may buckle leading to overall failure of the laminate. The mechanism of delamination has been widely investigated both theoretically and experimentally (Chatterjee *et al.*, 1984; Crossman and Wang, 1982; Fish and Lee, 1990). The delamination often occurs at the free-edges of laminates and at the interface in front of a transverse lamina crack. On the other hand, it is known (Bailey *et al.*, 1979; Fan *et al.*, 1989) that crack propagation in the 90^0 ply in angle-ply laminates is constrained by the adjacent plies. This constraint effect results in the observed higher *in situ* strength of laminae in laminates (Fan *et al.*, 1989). Since this kind of lamination effect varies with the configuration of laminates, it may be expected that the risk of interfacial delamination can be reduced to a certain extent by varying the configuration of laminates.

It is the aim of this paper to explore this possibility. To this end, we will calculate the stress intensity factor for a transverse crack in the 90^0 ply of a $[\pm\theta^0/90^0/\mp\theta^0]$

antisymmetric laminate and also the *crack-induced* interfacial stresses between the 90^0 and θ^0 plies under transverse shear loading. These fracture mechanics results will then be used to optimize the configuration, so as to minimize the tendency of crack growth in the 90^0 ply and therefore of delamination between 90^0 and θ^0 plies under flexural loading. The optimization problem is posed as a non-linear programming problem whose solution is sought by several techniques. The results confirm the possibility of minimizing the crack driving force in the 90^0 ply and of avoiding the risk of delamination by a judicious choice of ply angle θ and relative ply thickness.

2. MODEL AND MATHEMATICAL SOLUTION

The model being studied in this paper is shown in Fig 1. It consists of a central ply in which the fibres are oriented normal to the plane of the paper (90^0 ply) and two outer plies which are composed of an equal number of $+\theta^0$ and $-\theta^0$ angle plies. The 90^0 ply of thickness $2d$ is transversely isotropic (in xy plane) and is assumed to contain a flaw in the form of a central transverse crack of length $2a$. Each outer ply of thickness b is treated as being homogeneous orthotropic with average elastic properties of $[\pm\theta^0]_s$ laminate, consistent with the classical lamination theory.

It is assumed that the composite laminate is subjected remotely to self-equilibrating shear stress $\tau_{xy} = \tau$, so that from a mathematical point of view one needs only to solve the problem of cancellation of this stress over the crack faces. Because of symmetry, it is enough to consider a quarter of the laminate, say $x \geq 0, y \geq 0$.

Since the 90^0 ply is isotropic in xy plane, the Airy stress function $\varphi(x,y)$ satisfies the biharmonic equation

$$\nabla^4 \varphi(x,y) = 0 \tag{1}$$

On the other hand, the θ^0 ply is orthotropic, so the equilibrium equations in the xy plane problem are

$$c_{11}u_{,xx} + c_{66}u_{,yy} + (c_{12} + c_{66})v_{,xy} = 0 \tag{2}$$

$$c_{66}v_{,xx} + c_{22}v_{,yy} + (c_{12} + c_{66})u_{,xy} = 0 \tag{3}$$

in which c_{ij} ($i,j = 1, 2, 6$) are the stiffness coefficients under plane strain which can be calculated following the procedures of lamination theory (Tsai and Hahn, 1980; Vinson and Chow, 1975); u and v are the displacement components in x and y directions, respectively.

The solutions of eqns (1)–(3) must satisfy the following boundary and continuity conditions:

$$\tau_{xy}^{90}(x,0) = -\tau; \quad 0 \leq x < a \tag{4}$$

$$u^{90}(x,0) = 0; \quad x \geq a \tag{5}$$
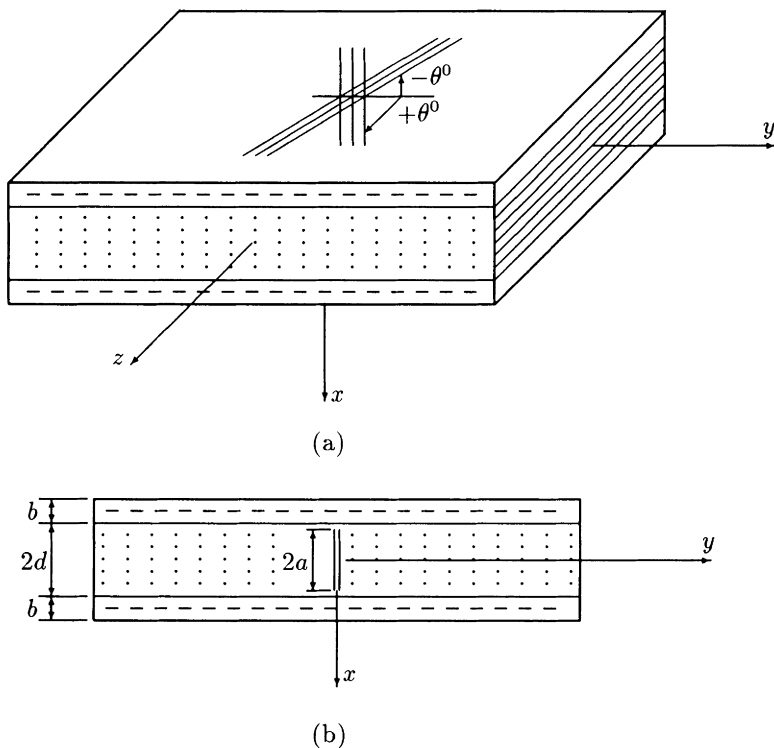
Fig 1. The composite laminate and co-ordinate axes

For $0 \leq y < +\infty$

$$\tau_{xy}^{90}(d,y) = \tau_{xy}^{\theta}(d,y) \tag{6}$$

$$\sigma_{xx}^{90}(d,y) = \sigma_{xx}^{\theta}(d,y) \tag{7}$$

$$u^{90}(d,y) = u^{\theta}(d,y) \tag{8}$$

$$v^{90}(d,y) = v^{\theta}(d,y) \tag{9}$$

$$\sigma_{xx}^{\theta}(d+b,y) = 0 \tag{10}$$

$$\tau_{xy}^{\theta}(d+b,y) = 0 \tag{11}$$

The solutions of (1), and (2)–(3) obtained using Fourier transforms will not be reproduced here. Satisfaction of the boundary conditions by the solution to (1) gives

$$\int_0^\infty E(s)\cos(sx)ds = -\left[\frac{\pi}{2}\tau - \int_0^\infty \{[A(s)+B(s)]\cosh(sx) + \right.$$
$$\left. +s\,A(s)x\sinh(sx)\}\,ds\right]; \quad 0 \leq x < a \tag{12}$$

$$\int_0^\infty \frac{1}{s} E(s) \cos(sx)\, ds = 0; \qquad x \ge a \tag{13}$$

Denoting $r = x/a$ and

$$F(s) = (\frac{\pi}{2s})^{\frac{1}{2}} E(\frac{s}{a}) \tag{14}$$

and noting

$$\cos(sx) \equiv (\frac{\pi sx}{2})^{\frac{1}{2}} J_{-\frac{1}{2}}(sx), \tag{15}$$

where $J_{-1/2}$ is the Bessel function of the first kind, the dual integral eqns (12)–(13) can be written in a form that has been studied by Copson (1961)

$$\int_0^\infty s\, F(s) J_{-\frac{1}{2}}(sr)\, ds = -\frac{1}{\sqrt{r}} \Big[\frac{\pi a}{2} \tau - \int_0^\infty \{ A(\frac{s}{a})[\cosh(sr) + s\,r \sinh(sr)] +$$

$$+ B(\frac{s}{a}) \cosh(sr)\} \, ds \Big]; \qquad 0 \le r < 1 \tag{16}$$

$$\int_0^\infty F(s)\, J_{-\frac{1}{2}}(sr)\, ds = 0; \qquad r \ge 1 \tag{17}$$

The functions $A(s/a)$ and $B(s/a)$ are determined from eqns (6)–(11).

Following the procedure of Copson (1961), Sih and Chen (1981) for solving dual integral equations, it can be shown that

$$E(s) = -\frac{\pi a}{2} \tau \left\{ \Phi(1)\, J_1(sa) - \int_0^1 \xi\, J_1(sa\xi) \frac{d}{d\xi}[\frac{\Phi(\xi)}{\sqrt{\xi}}]\, d\xi \right\}, \tag{18}$$

where $\Phi(\xi)$ is the solution of the following Fredholm integral equation

$$\Phi(\xi) + \int_0^1 K(\xi, \eta)\, \Phi(\eta)\, d\eta = \sqrt{\xi} \tag{19}$$

The kernel $K(\xi, \eta)$ in eqn (19) is

$$K(\xi, \eta) = -\sqrt{\xi\eta} \int_0^\infty \frac{s\, e^{-s\frac{d}{a}}}{\Delta(s)} \Big\{ [(K_{11} + K_{21})E_1 + (K_{12} + K_{22})E_2 +$$

$$+ (K_{13} + K_{23})E_3 + (K_{14} + K_{24})E_4]I_0(s\xi) +$$

$$+ [K_{11}E_1 + K_{12}E_2 + K_{13}E_3 + K_{14}E_4]\, s\xi\, I_1(s\xi) \Big\}\, ds, \tag{20}$$

where

$$E_1 = \Big[(a_{11} + a_{12}) - (a_{12} - a_{11})\, s\frac{d}{a} \Big] I_0(s\eta) + (a_{12} - a_{11})\, s\eta\, I_1(s\eta)$$

$$E_2 = \Big[2a_{11} + (a_{12} - a_{11})\, s\frac{d}{a} \Big] I_0(s\eta) - (a_{12} - a_{11})\, s\eta\, I_1(s\eta)$$

$$E_3 = s\frac{d}{a} I_0(s\eta) - s\eta\, I_1(s\eta)$$

$$E_4 = (1 - s\frac{d}{a})\, I_0(s\eta) + s\eta\, I_1(s\eta)$$

$I_0()$ and $I_1()$ are the modified Bessel functions of the first kind. a_{ij} $(i,j = 1,2)$ are the plane strain compliance coefficients of 90^0 ply, and $K_{11}, K_{12}, ..., K_{24}$ are functions of s related to a_{ij} and c_{ij} $(i,j = 1,2)$.

The stress and displacement components can be obtained after solving for $E(s)$ from eqns (18), (19) and (20).

The relevant shear stress component around the crack tip is

$$\tau_{xy}^{90}(x,0) = \frac{2}{\pi} \int_0^\infty E(s) \cos(sx) \, ds -$$
$$-\frac{2}{\pi} \int_0^\infty \left\{ [A(s) + B(s)] \cosh(sx) + A(s) \, s \, x \sinh(sx) \right\} ds \qquad (21)$$

Substituting eqn (18) into eqn (21) gives

$$\tau_{xy}^{90}(x,0) = -a\,\tau \int_0^\infty \left\{ \Phi(1) \, J_1(sa) - \int_0^1 \xi \, J_1(sa\xi) \frac{d}{d\xi}[\frac{\Phi(\xi)}{\sqrt{\xi}}] \, d\xi \right\} \cos(sx) \, ds -$$
$$-\frac{2}{\pi} \int_0^\infty \left\{ [A(s) + B(s)] \cosh(sx) + s \, A(s) \sinh(sx) \right\} ds \qquad (22)$$

The mode II stress intensity factor at the crack tip is

$$K_{II} = \lim_{x \to a^+} \sqrt{2(x-a)} \, \tau_{xy}^{90}(x,0) = \Phi(1) \, \tau \, \sqrt{a} \qquad (23)$$

If the θ^0 plies on the two sides are absent then the stress intensity factor is

$$K_{II} = F(\frac{a}{d}) \, \tau \, \sqrt{a} \qquad (24)$$

Table 1
Material properties

Properties & Material	E_L (GPa)	E_T (GPa)	G_{LT} (GPa)	G_{TT} (GPa)	ν_{LT} -	ν_{TT} -	Ply thickness(mm)
T300/934	138	11.7	4.56	4.18	0.29	0.40	0.132

For the graphite/epoxy material properties (in the notation of Tsai and Hahn, 1980) listed in Table 1 (Tan and Nuismer, 1989), the variation of $\Phi(1)$ with a/d is shown in Fig 2. Also shown is the value of $F(a/d)$. $\Phi(1)$ is equal to $F[a/(b+d)]$ when $\theta = 90^0$.

It is seen that the magnitude of $\Phi(1)$ and its variation with a/d are different from those of F – the geometry factor for an isotropic material. $\Phi(1)$ is not only related to the geometry a/d and b/d, but is also influenced by the stiffness of the 90^0 and θ^0 plies. Obviously, $\Phi(1) \leq F$, otherwise there would be no point in using composite materials. It is also for this reason that the θ^0 plies are regarded as constraints for central ply. It is noted that the degree of this constraint can be expressed solely in terms of $\Phi(1)$.
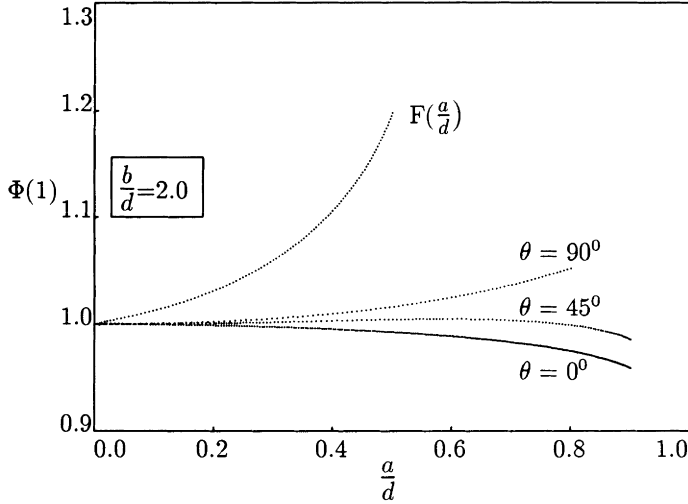
Fig 2. Values of $\Phi(1)$ and $F(\frac{a}{d})$

The non-dimensional normal and the shear stresses at the interface between the 90^0 and θ^0 plies are

$$\frac{\sigma_{xx}(d,y)}{\tau} = \int_0^\infty \frac{se^{-s\frac{d}{a}}}{\Delta(s)}\Big\{ [K_{11}G_1 + K_{12}G_2 + K_{13}G_3 + K_{14}G_4]s\frac{d}{a}\cosh(s\frac{d}{a}) +$$

$$+ [K_{21}G_1 + K_{22}G_2 + K_{23}G_3 + K_{24}G_4]\sinh(s\frac{d}{a})\Big\}\sin(s\frac{y}{a})\,ds -$$

$$- \int_0^\infty e^{-s\frac{y}{a}}K_5\,G_5\,ds \qquad (25)$$

$$\frac{\sigma_{yy}(d,y)}{\tau} = \int_0^\infty (-1)\frac{se^{-s\frac{d}{a}}}{\Delta(s)}\Big\{ [K_{11}G_1 + K_{12}G_2 + K_{13}G_3 +$$

$$+ K_{14}G_4][2\sinh(s\frac{d}{a}) + s\frac{d}{a}\cosh(s\frac{d}{a}] +$$

$$+ [K_{21}G_1 + K_{22}G_2 + K_{23}G_3 + K_{24}G_4]\sinh(s\frac{d}{a})\Big\}\sin(s\frac{y}{a})\,ds -$$

$$- \int_0^\infty e^{-s\frac{y}{a}}K_6\,G_6\,ds \qquad (26)$$

$$\frac{\tau_{xy}(d,y)}{\tau} = \int_0^\infty \frac{se^{-s\frac{d}{a}}}{\Delta(s)}\Big\{ [K_{11}G_1 + K_{12}G_2 + K_{13}G_3 +$$

$$+ K_{14}G_4][\cosh(s\frac{d}{a}) + s\frac{d}{a}\sinh(s\frac{d}{a})] +$$

$$+ [K_{21}G_1 + K_{22}G_2 + K_{23}G_3 + K_{24}G_4]\cosh(s\frac{d}{a})\Big\}\cos(s\frac{y}{a})\,ds -$$

$$- \int_0^\infty e^{-s\frac{y}{a}}K_7\,G_7\,ds \qquad (27)$$
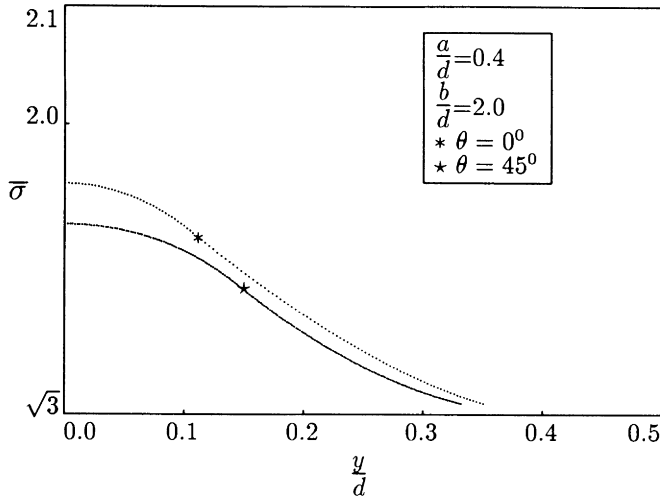
(a)
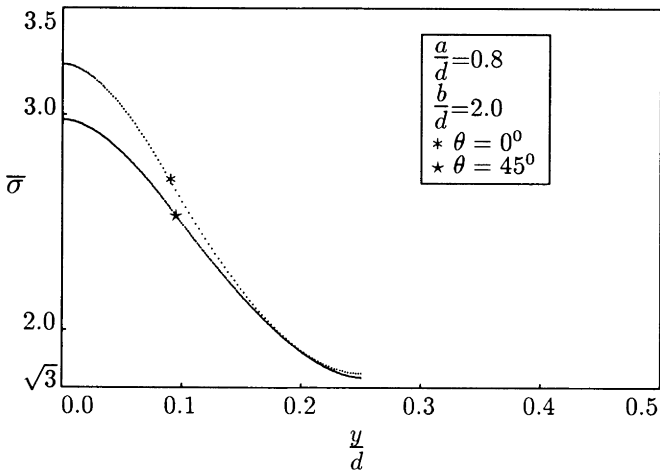
(b)

Fig 3. Crack-induced interfacial von Mises stress normalized by τ

At the interfacial point right in front of the crack tip, where $y = 0, x = d$, the non-vanishing stress is

$$\frac{\tau_{xy}(d,0)}{\tau} = \int_0^\infty \frac{se^{-s\frac{d}{a}}}{\Delta(s)}\Big\{[K_{11}G_1 + K_{12}G_2 + K_{13}G_3 +$$

214

$$+K_{14}G_4][\cosh(s\frac{d}{a}) + s\frac{d}{a}\sinh(s\frac{d}{a})] +$$

$$+[K_{21}G_1 + K_{22}G_2 + K_{23}G_3 + K_{24}G_4]\cosh(s\frac{d}{a})\Big\} ds +$$

$$+\int_0^1 \Phi(\xi)\,G_8(\xi)\,d\xi \tag{28}$$

In eqns (25)–(28)

$$G_i = \int_0^1 \sqrt{\eta}\,\Phi(\eta)\,E_i(s,\eta)\,d\eta \quad (i = 1,..,4)$$

$$G_5 = G_6 = G_7 = \int_0^1 \sqrt{\eta}\,\Phi(\eta)\,J_0(s\eta)\,d\eta$$

$$G_8 = (\frac{a}{d})^2 \frac{\sqrt{\xi}}{\sqrt{1-(\frac{a}{d}\xi)^2}\,\left[1+\sqrt{1-(\frac{a}{d}\xi)^2}\right]} \left\{ 2 + \frac{(\frac{a}{d}\xi)^2[1 + 2\sqrt{1-(\frac{a}{d}\xi)^2}]}{[1-(\frac{a}{d}\xi)^2][1+\sqrt{1-(\frac{a}{d}\xi)^2}]} \right\}$$

$$K_5 = s(2 - s\frac{y}{a})\sin(s\frac{d}{a})$$

$$K_6 = s^2\frac{y}{a}\sin(s\frac{d}{a})$$

$$K_7 = s(1 - s\frac{y}{a})\cos(s\frac{d}{a})$$
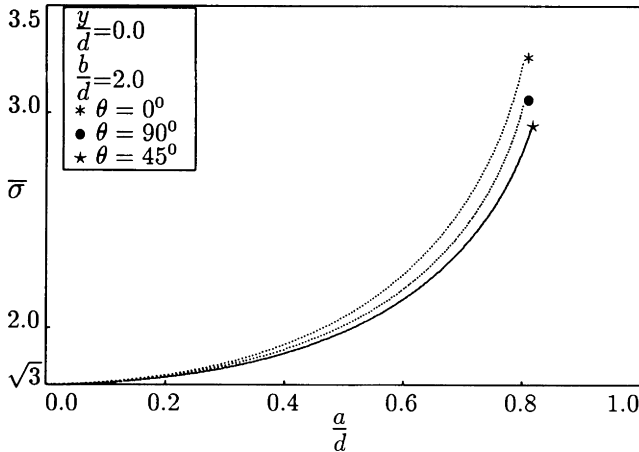
Fig 4. Largest interfacial von Mises stress normalized by τ

The variation of *crack-induced* von Mises stress with y/d and a/d for $\theta = 0^0$ and $\theta = 45^0$ is shown in Fig 3. It is seen that the largest von Mises stress (normalized by τ) occurs at $y/d = 0$ for different θ^0 and a/d. This largest stress is depicted in Fig 4, for $\theta = 0^0$, $\theta = 90^0$ and $\theta = 45^0$. As the crack tip approaches the interface

(a/d increases), the interfacial von Mises stress increases rapidly for all θ. For small cracks, the interfacial von Mises stress is fairly insensitive to changes in θ, but as a/d increases so also does its sensitivity to outer ply angle θ. An examination of Figs 2 and 4 shows that for all a/d, the crack driving force takes on its minimum value, but the largest interfacial von Mises stress (at $y/d = 0$) its maximum value when $\theta = 0^0$. There is thus a need for a compromise design which would ensure minimization of the crack driving force in the central ply without exceeding the von Mises interfacial strength of the laminate.

3. OPTIMIZATION PROBLEM AND SOLUTION

To obtain the compromise design, we formulate the following minimization problem

$$\operatorname*{Min}_{c_{ij}^\theta, \frac{b}{d}, \theta} \quad \Phi(1)[c_{ij}^\theta, \tfrac{b}{d}, \theta; \tfrac{a}{d}] \tag{29}$$

subject to

$$\bar{\sigma} \le \sigma_0 = (1 + \alpha)\sqrt{3} \tag{30}$$

$$\overline{D} \ge (1 - \gamma)D_0 \tag{31}$$

$$\underline{b} \le \frac{b}{d} \le \overline{b} \tag{32}$$

$$0^0 \le \theta \le \frac{\pi}{2} \tag{33}$$

Here, $\bar{\sigma}$ is the largest interfacial von Mises stress, normalized by τ

$$\bar{\sigma} = \sqrt{\frac{1}{2}\Big[(\sigma_{xx} - \sigma_{yy})^2 + (\sigma_{yy} - \sigma_{zz})^2 + (\sigma_{zz} - \sigma_{xx})^2 + 6\,\tau_{xy}^2\Big]} \tag{34}$$

$\bar{\sigma}$ is equal to $\sqrt{3}$ in the absence of a crack. $\overline{D}$ is the normalized laminate modulus. For the transverse loading case, $\overline{D}$ is the normalized flexural modulus

$$\overline{D} = \frac{\big[(1 + \frac{b}{d})^3 - 1\big]\, c_{22}^\theta + c_{22}^{90}}{(1 + \frac{b}{d})^3} \tag{35}$$

σ_0 is the specified interfacial von Mises strength and D_0 is the value of $\overline{D}$ when $\theta = 0^0$. α and γ are tolerance factors on the stress gain and stiffness loss, respectively.

Since the expressions relating $\Phi(1)$ and the interfacial von Mises stress to the geometry and stiffness properties of the plies are quite complicated, sensitivity of the objective with respect to design variables is calculated by a mixed analytical/numerical procedure. The integral equation (19) is discretized into a set of linear equations

$$[A][\Phi] = [B], \tag{36}$$

where $[A] = [a_{ij}]$, $[\Phi] = [\Phi(\xi_j)]^T$, $[B] = [\sqrt{\xi_i}]^T$, $(i, j = 1, ..., n)$. $n = 10$ resulted in sufficient accuracy. Then the sensitivity with respect to the design variables x_i is given by

$$\frac{\partial[\Phi]}{\partial x_i} = -[A]^{-1} \frac{\partial[A]}{\partial x_i} [\Phi], \tag{37}$$

where, x_i stands for c_{ij}^θ $(i, j = 1, 2)$, θ and b/d.

The sensitivity of the constraint (30) is calculated numerically, whereas that of (31) is calculated analytically.

The above minimization problem is solved by non-linear mathematical programming techniques, viz. sequential linear programming with move-limits (Pedersen, 1981), sequential quadratic programming (Powell, 1977) and sequential convex programming (Fleury and Braibant, 1986) which are available in the general purpose structural optimization package ADS (Vanderplaats, 1987). The numbers of functional and gradient evaluations for the above problem, and an alternative formulation to be considered below, are given in Table 2. It was found that among the three strategies, SLP and SCP terminated with fewer functional evaluations but more gradient calculations than SQP. However, when the objective function was somewhat flat near the optimum point, the SLP and SQP could sometimes terminate prematurely. It seems therefore for the present problem SQP produces the most precise results with fewer gradient calculations, but more functional evaluations.

Table 2
Functional (FE) and gradient (GE) evaluations

Method	Min $\Phi(1)$		Min $\overline{\sigma}$	
	FE	GE	FE	GE
SLP	7	7	10	10
SQP	12	3	26	6
SCP	7	7	8	8

4. NUMERICAL RESULTS AND CONCLUSIONS

The results of the optimization design problem for the laminate properties of Table 1 are shown in Fig 5.

It was found that for small a/d, the active constraints were the lower limit on θ and the upper limit on b/d. When $\theta = 0^0$, the outer plies have the strongest effect on the arrest of central ply crack. The minimum of $\Phi(1)$ always occurs at $\theta = 0^0$, no matter what initial θ is chosen. This agrees with the in-plane tensile experimental results (Flaggs and Kural, 1982) which show that when $\theta = 0^0$, the *in situ* transverse tensile strength of the 90^0 plies in $[\pm\theta^0/90_n^0]_s$ laminates has the largest value.

The relative thickness of the outer plies also plays an important role in arresting the crack growth. The relatively thicker the constraint plies, the smaller the crack driving force and hence the stronger the 90^0 ply.
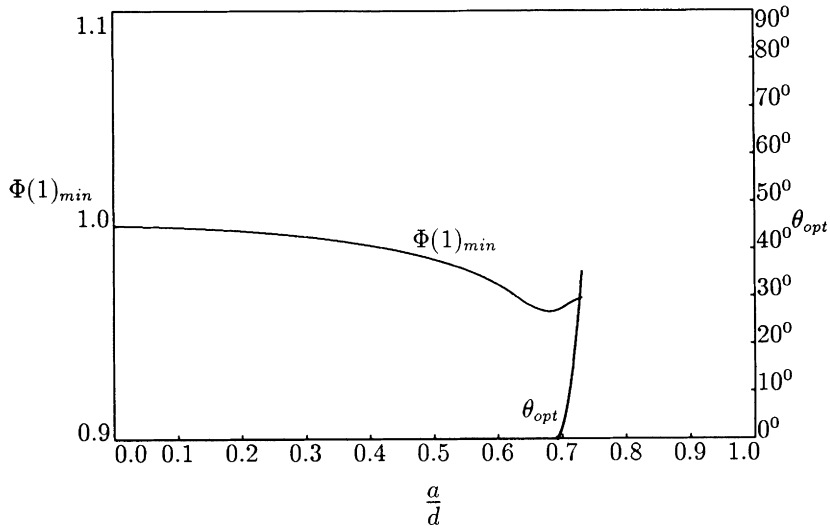
Fig 5. Minimization of $\Phi(1)$: $\left(\frac{b}{d}\right)_{opt} = \overline{b}$

When a/d is large, the interfacial stress constraint becomes critical to the design. For the satisfaction of this constraint the design angle θ takes a non-zero value. It was found that for $\alpha = 0.5$, $\gamma = 0.15$ and $\overline{b} = 4.0$, when a/d is greater than 0.7$\underline{3}$, no optimum design is possible because of the violation of the constraint on interfacial strength. For this reason an alternative formulation of the optimization problem was considered in which the interfacial von Mises stress was minimized subject to the constraint that $\Phi(1)$ not exceed 1.0 and that the flexural stiffness be adequate. The corresponding minimization problem is as follows:

$$\underset{c_{ij}^\theta, \frac{b}{d}, \theta}{\text{Min}} \quad \overline{\sigma}(c_{ij}^\theta, \tfrac{b}{d}, \theta; \tfrac{a}{d}) \tag{38}$$

subject to

$$\Phi(1) < 1.0 \tag{39}$$

$$\overline{D} \geq (1 - \gamma) D_0 \tag{40}$$

$$\underline{b} \leq \tfrac{b}{d} \leq \overline{b} \tag{41}$$

$$0^0 \leq \theta \leq \frac{\pi}{2} \tag{42}$$

The results of the above minimization problem are shown in Fig 6. In this case, $\overline{\sigma}$ reaches its minimum when $\theta = 50^0$ and $b/d = \overline{b}$. The reason that the laminate has sufficient flexural stiffness at such large θ is the high value of the transverse in-plane Poisson's ratio of the $\pm \theta^0$ plies and the use of plane strain stiffness parameters.

Besides the intralamina crack problem under out-of-plane (with respect to laminate, but in-plane with respect to crack) shear loading, analyses for in-plane (with respect to laminate) tensile and shear loadings are needed for a more comprehensive understanding of laminate strength and delamination characteristics. Likewise, the lamination effect on the stress singularity when the crack tip touches the interface needs to be investigated. These problems are currently being studied.
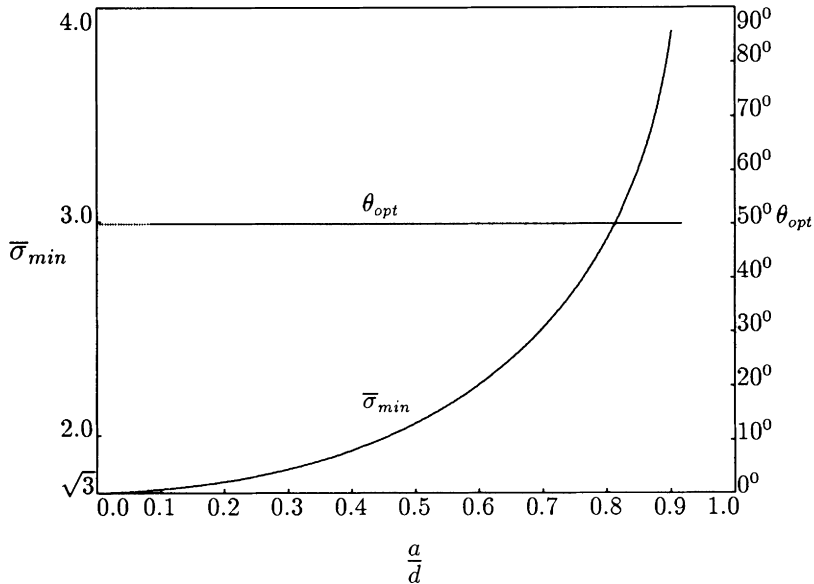
Fig 6.   Minimization of $\overline{\sigma}$: $\left(\frac{b}{d}\right)_{opt} = \overline{b}$

REFERENCES

1 J. E. Bailey, P. T. Curtis and A. Parvizi, Proc. R. Soc. London, 366 (1979) 599.

2 S. N. Chatterjee, R. B. Pipes and R. A. Blake Jr, ASTM STP, 836 (1984) 161.

3 E. T. Copson, Proc. Glasgow Math. Assoc., 5 (1961) 19.

4 F. W. Crossman and A. S. D. Wang, ASTM STP, 775 (1982) 118.

5 F. Fan, W. Dong and J. Wang, Acta Mechanica Sinica, 21 (1989) 450.

6 J. C. Fish and S. W. Lee, ASTM STP, 1059 (1990) 271.

7 D. L. Flaggs and M. H. Kural, J. Comp. Mat., 16 (1982) 103.

8 C. Fleury and V. Braibant, Int. J. Num. Meth. Eng., 23 (1986) 409.

9 P. Pedersen, In Optimization of Distributed Parameter Systems, E. J. Haug and J. Cea (eds.), Vol I 739, Sijthoff & Noordhoff, The Netherlands, 1981.

10 M. J. D. Powell, Report DAMTP77/NA2, University of Cambridge, (1977).

11 G. C. Sih and E. P. Chen, Mechanics of Fracture–Cracks in Composite Materials, Martinus Nijhoff, The Hague, 1981.

12 S. C. Tan and R. J. Nuismer, J. Comp. Mat., 23 (1989) 1029.

13 S. W. Tsai and H. T. Hahn, Introduction to Composite Materials, TECHNOMIC Publishing Co Inc, Westport, 1980.

14 G. N. Vanderplaats, ADS-A FORTRAN Program for Automated Design Synthesis, Engineering Design Optimization Inc, Santa Barbara, 1987.

15 J. R. Vinson and T. W. Chow, Composite Materials and Their Use in Structures, Applied Science Publishers Ltd, London, 1975.

OPTIMUM DESIGN OF LAMINATED PLATES WITH RESPECT TO
EIGENVALUES

Gengdong Cheng and Jun Tang
Dalian University of Technology, Dalian, China,P.R.

Abstract
The paper summarizes studies on features of optimum design of laminated plates with
respect to eigenvalues under various specific conditions. For bidirectional reinforced laminated
plates under shear load and/or biaxial compression load it is shown that the coupling effect
between extension and bending reduces buckling load, the optimum laminate with maximum
value of buckling load must be a symmetric one. For laminated plates under biaxial
compression load we further studied single buckling mode optimization, bimodal buckling
mode optimization and the related optimality condition. It is shown that the bimodal optimal
solution is possibly missed if one applies the normal numerical optimization algorithms
without careful consideration. By making use of the optimality criterion, the number of
possible optimal angles is determined for rectangular plate and more general cases. All these
features of optimum designs of laminated plates provide the guideline for numerical
optimization of laminate plates with respect to eigenvalues.

1. INTRODUCTION

Laminated composite plates are finding a wide range of applications in structural design
because they have superior mechanical properties such as high in-plane stiffness to weight
ratio and high in-plane strength to weight ratio. If the size of the plate is large its out-plane
performance such as lateral deformation under pressure, vibration frequency and buckling load
needs special consideration for its proper usage. Research on optimization and analysis of
vibration and buckling of laminated composite plates has been one of the interesting areas in
composite structural mechanics. Research topics include numerical method for optimum
design, sensitivity analysis and a number of important issues related to the characters of
optimum design of laminated plates, i.e., effect of coupling between extension and bending
on buckling load, symmetricity of laminate, number of design variables and bimodality of
optimum design.

As early as in 1973, Schmit,L.A. and Farshi,B.[1] studied optimum laminate design and
included the elastic stability constraints in the problem formulation. The thicknesses of
individual layers in a laminate are the design variables.

Bert,C.W. (1977,1978) [2,3] pioneered study on optimum design of rectangular plate to maximize its fundamental frequency with the ply angles of individual layers being design variables, but a priori knowledge of the eigenfrequency in terms of the laminate stiffness was assumed.

S.Adali(1983)[4] studied multi-objective optimum design of antisymmetric angle-ply laminate plate. The objectives of optimization are to minimize the maximum dynamic deflection and to maximize the eigenfrequency of a given mode. For a simply supported rectangular plate the first order sensitivity to the fiber orientation of individual layers is derived. Nonlinear programming technique is applied to determine the optimum design. The study has been further extended to design sensitivity analysis of an antisymmetric angle-ply laminate[5].

J.Tang(1984)[6] studied the effect of coupling between extension and bending on the buckling load of a rectangular plate, which is simply supported along all the four edges, made of bi-directional laminates and under the axial compression. It is proved in the paper that the optimum design is a symmetric laminate and the number of design variables is thus reduced to one half. And the single and bimodal optimum design is also discussed. In case of single modal optimum design the derivation further shows that the number of design variables is actually one.

Based on a special functional which is derived from harmonic displacement distributions and is valid for the vibration frequency, buckling load and bending deflection of simply supported plates, Pedersen(1987)[7] optimized the lamination parameters and reached the interesting conclusions for harmonic displacement distributions, that is, the optimal fiber orientation is less dependent on the actual material but strongly dependent on the displacement mode, The optimal orientation is the same, independent of the position of the layer in the laminate, and thus the same for all layers. By numerical computation, Pedersen further shows that the three angles correspond to local maximum and local minimum, respectively and presents the corresponding conditions.

Miki(1986)[8] and Grenestedt(1989)[9] used the lamination parameters to derive their results concerning buckling and vibration optimization, respectively, and they reached the conclusion from a large number of numerical test that only one relevant parameter for the optimization problems is necessary.

J.Tang(1987)[10] studied the conditions of single mode and bimodal optimum design for a rectangular plate under bidirectional axial compression to maximize buckling load. Bimodality of buckling modes in two directions is studied.

Muc(1988)[11] studied optimal fiber orientation for rectangular simply-supported angle-ply plate to maximize buckling load under the biaxial compression. With the series solution of buckling modes the effect of coupling between the bending and extension is studied. Bimodal optimum design under uniaxial compression was studied in the paper.

J.Tang(1989)[12] presented study on optimum design for a rectangular plate under shear. It was proved that the coupling between extension and bending reduces the buckling load of the plate for shear load. The paper also pointed out that for the type of plate the maximum buckling load design has an identical angle for all the layers as long as they are made of the same material. The direct consequence of the study is that the number of the design variables, i.e. the number of ply angles of individual layers in an optimum laminate reduces to one and only the one-dimensional search is necessary to determine the optimal angle.

Most of the above mentioned work limited their study to simply supported rectangular plate because a series solution of the governing plate equation is available. In case of general

shaped laminate composite plates[13,14,15], numerical methods such as mathematical programming technique are dominate. In addition to the ply thickness, the ply angles are the design variables to be optimized. Due to lack of deep understanding of characters of optimum design the number of design variables as many as the number of plys were introduced in literatures. Since the computational cost increases with the number of design variables rapidly, examples with no more than 6 layers were given in literatures.

Cheng (1986)[16] derived expressions for design derivatives for minimum compliance with respect to the ply angles and come to the conclusion that for any orthotopic plate with minimum compliance under rather general condition there are never more than four layup angles necessary. The results are applicable to the maximum frequency design or maximum buckling load design too.

2. EFFECT OF COUPLING BETWEEN EXTENSION AND BENDING, SYMMETRICITY OF OPTIMUM PLATE

Let us consider the optimization problem of bidirectional reinforced laminate plates. It is assumed that the laminate is composed of L layers and each layer of the plate has an equal number of the same fibers in the Θ_k and $-\Theta_k$ direction with respect to the x-axis. The subscript k denotes the k-th layer. Taking R=a/b which represents the length-to-width ratio of the rectangular plate simply supported along the four edges, the plate deflections are assumed as

$U = \Sigma\Sigma\ U_{mn}\ \cos(m\pi x/a)\sin(n\pi y/b)$
$V = \Sigma\Sigma\ V_{mn}\ \sin(m\pi x/a)\cos(n\pi y/b)\ \ (m=1,2..,M;\ n=1,2,..N;)$
$W = \Sigma\Sigma\ W_{mn}\ \sin(m\pi x/a)\sin(n\pi y/b)$

Let us consider a plate under biaxial compressive load N_x, N_y and denote $\alpha = N_y/N_x$ By applying the plate governing equation, the buckling load for plate under biaxial compressive load can be written as

$$\Phi = \frac{12N_x b^2}{\pi^2 t^3 Q_{22}},$$

$$\Phi = \frac{12}{t^3 R^2 Q_{22}(m^2 + \alpha n^2 R^2)}\ [T_{33} + \frac{2T_{12}T_{13}T_{23} - T_{22}T_{13}^2 - T_{11}T_{23}^2}{T_{11}T_{22} - T_{12}^2}]$$

(1)

where

$$T_{11} = A_{11}m^2 + A_{66}n^2R^2, \quad T_{22} = A_{66}m^2 + A_{22}n^2R^2, \quad T_{12} = (A_{12} + A_{66})mnR, \tag{2}$$
$$T_{33} = D_{11}m^4 + 2(D_{12} + 2D_{66})m^2n^2R^2 + D_{22}n^4R^4,$$
$$T_{13} = B_{11}m^3 + (B_{12} + 2B_{66})mn^2R^2, \quad T_{23} = (B_{12} + 2B_{66})m^2nR + B_{22}n^3R^3$$

and A_{ij}, B_{ij}, D_{ij} are extensional, coupling and bending stiffnesses of laminated plate, respectively, t is thickness of plate and Q_{ij} is stiffness of laminate. It is known from theory of composite laminate plate that for bidirectional reinforced laminate plates all the coupling terms $A_{16}, A_{26}, D_{16}, D_{26}$ vanish.
By introducing T_n, T_d, T_c,

$$T_n = T_{11}T_{23}^2 + T_{22}T_{13}^2 - 2T_{12}T_{13}T_{23}$$
$$T_d = T_{11}T_{22} - T_{12}^2, \quad T_c = -T_n / T_d \tag{3}$$

Eq.1 can be rewritten as

$$\Phi = \frac{12}{t^3R^2Q_{22}(m^2 + \alpha n^2R^2)}(T_{33} + T_c) \tag{4}$$

It can be shown that $T_d > 0$, $T_n > 0$, which leads to negative T_c or implies the fact that the effect of coupling between bending and extension lows the buckling load.
   For plate under shear load, explicit formula for buckling load is not available. By making use of Galerkin method and the governing equation for buckling, the coefficients W_{mn} satisfy

$$[T_{33} + T_c]W_{pq} - \lambda \sum_m \sum_n \frac{mnpq}{(m^2 - p^2)(n^2 - q^2)}W_{mn} = 0 \tag{5}$$
$$(p = 1, 2, ..., M, \quad q = 1, 2, ..., N, \quad m+p \text{ and } n+q \text{ are odd})$$

where p and q are the number of half waves in the x and y directions, respectively, and

$$\lambda = \frac{32abR^2}{\pi^4}N_{xy} \tag{6}$$

The Eq.(5) can be rewritten using matrix notation

$$[K - C]\{W\} - \lambda[G]\{W\} = 0 \tag{7}$$

where the elements of the diagonal matrix [K] and [C] are

$$K_{ii} = T_{33}, \quad C_{ii} = -T_c \tag{8}$$

the elements of matrix [G] are

$$G_{ii} = 0,$$

$$G_{il} = 0, \qquad\qquad \text{when m+p or n+q is even}$$

$$G_{il} = mnpq/((m^2-p^2)(n^2-q^2)), \quad \text{when m+p and n+q are odd} \tag{9}$$
$$\text{and}$$
$$l = (m-1)N+n, \quad i=(p-1)N+q$$

The minimum eigenvalue λ_1 of Eq.(7) is given by the well-known Rayleigh Quotient

$$\lambda_1 = \min\frac{\{W\}^T[K-C]\{W\}}{\{W\}^T[G]\{W\}}, \tag{10}$$

Let

$$\beta_1 = \min\frac{\{W\}^T[K]\{W\}}{\{W\}^T[G]\{W\}} \ , \quad \mu_1 = \min\frac{\{W\}^T[C]\{W\}}{\{W\}^T[G]\{W\}} \tag{11}$$

both [K] and [C] are positive definite, so we have

$$\beta_1 \geq \lambda_1 + \mu_1 \tag{12}$$

which represents the fact that the matrix [C], i.e., the effect of coupling between bending and extension lows the buckling load of the laminated plate under shear. For plate under combined axial compression N_x, $N_y=\alpha N_x$ and shear load $N_{xy}=\beta N_x$, the coefficients W_{mn} satisfy

$$[T_{33}+T_c]W_{pq} -\lambda\{ \sum_m \sum_n \frac{mnpq}{(m^2-p^2)(n^2-q^2)}W_{mn} +\frac{\pi^2}{32R\beta}(p^2+\alpha q^2R^2)W_{pq} \}= 0, \qquad (13)$$

$$(p=1,2,...,M, \quad q=1,2,...,N, \quad m+p \text{ and } n+q \text{ are odd})$$

which can also be rewritten into the form of Eq.(7) with

$$G_{ii} = \frac{\pi^2}{32R\beta}(p^2+\alpha q^2R^2),$$

$$G_{il} = \frac{mnpq}{(m^2-p^2)(n^2-q^2)}, \quad \text{when } m+p \text{ and } n+q \text{ are odd}, \qquad (14)$$

$$G_{il} = 0, \quad \text{when } m+p \text{ or } n+q \text{ is even},$$
$$l = (m-1)N+n, \quad i=(p-1)N+q$$

By means of similar derivation, one can prove the fact that the effect of coupling between bending and extension lows the buckling load for combined shear and biaxial compression load too. So the optimum laminate must be symmetric one and the Eqs.(4) and (7) can be simplified as

$$\Phi = \frac{12}{t^3R^2Q_{22}(m^2+\alpha n^2R^2)}T_{33} , \qquad (15)$$

$$[K]\{W\} - \lambda[G]\{W\} = 0$$

For square plate simply supported along its four edges by defining

$$\Phi= \omega^2 b^4 \frac{\rho}{Q_{22}t^3}$$

where ω is the natural vibration frequency of laminated plate, ρ is the density of plate, then the expression of the objective function can be written as

$$\Phi = \frac{1}{Q_{22}t^3R^4}(T_{33}+T_c)$$

By applying the same argument as before, we can reach the same conclusion for the optimum design of the natural frequency of laminated plate, the optimum laminate must be symmetric one.

3. BIMODAL BUCKLING UNDER COMPRESSION

For a laminate plate under bidirectional compression, the bimodal buckling modes are not limited in one direction. Bimodal buckling may happen in any of the two directions. If the two buckling modes (m+1,n) and (m,n) associate with the same buckling load we have bimodal buckling in x-direction and the condition for bimodal buckling is

$$\frac{m^2(m+1)^2+\alpha n^2 R^2[(m+1)^2+m^2]}{n^4 R^4} = \frac{D_{22}-2\alpha(D_{12}+2D_{66})}{D_{11}} \tag{16}$$

In the case that the buckling modes (m,n+1) and (m,n) have the same buckling load, we have bimodal buckling in y-direction and the condition for bimodality in y-direction is given by

$$\frac{m^2 R^2[(n+1)^2+n^2]+\alpha n^2(n+1)^2 R^4}{m^4} = \frac{\alpha D_{11}-2(D_{12}+2D_{66})}{D_{22}} \tag{17}$$

If the compression is only uniaxial, for example in the x-direction, the n equals to 1 and the Eq.(16) can be simplified as

$$\frac{D_{22}}{D_{11}}R^4 = m^2(m+1)^2 \tag{18}$$

For optimum design problem of maximization of buckling load, the single buckling mode optimization and the bimodal mode optimization must be distiguished. The former can be calculated from the stationary values of objective function Φ, but the latter, the buckling mode conditions eqs.(16),(17),(18) must be considered in its optimization.

4. THE NUMBER OF OPTIMUM PLY ORIENTATION

Let us consider the single mode optimization for maximum buckling load design of

laminated plates under bidirectional compression. The optimality condition for maximum buckling load is given by

$$\frac{\partial \Phi}{\partial \Theta_k} = 0 \tag{19}$$

By substituting Eqs.(15) and (2) into Eq.(19), we obtain a system of equations each of which has the same form and is independent of the layer number k,

$$sin2\Theta_k(4Fcos2\Theta_k - J) = 0 \tag{20}$$

where

$$F = U_3(6m^2n^2R^2 - m^4 - n^4R^4), \quad J = U_2(m^4 - n^4R^4) \tag{21}$$

and U_i are linear combinations of the plate stiffness

$$U_2 = \frac{Q_{11} - Q_{22}}{2}, \quad U_3 = \frac{Q_{11} + Q_{22} - 2Q_{12} - 4Q_{66}}{8} \tag{22}$$

The solutions of Eq.(20) are the ply angles for extremum of the objective fuction Φ. It can be proved that for maximum of Φ the optimum ply angle is

$$\Theta_k = 90^0 \quad \text{when} \quad \frac{m}{nR} \leq [\frac{3 - \sqrt{8 + (U_2/4U_3)^2}}{1 - (U_2/4U_3)}]^{1/2} \tag{23}$$

the optimum ply angle is

$$\Theta_k = 0^0, \quad \text{when} \quad \frac{m}{nR} \geq [\frac{3 + \sqrt{8 + (U_2/4U_3)^2}}{1 - (U_2/4U_3)}]^{1/2} \tag{24}$$

the optimum ply angle is

$$\Theta_k = \frac{1}{2}cos^{-1}(J/4F) \quad \text{when} \quad [\frac{3 - \sqrt{8 + (U_2/4U_3)^2}}{1 - (U_2/4U_3)}]^{1/2} \leq \frac{m}{nR} \leq [\frac{3 + \sqrt{8 + (U_2/4U_3)^2}}{1 - (U_2/4U_3)}]^{1/2} \tag{25}$$

The Eqs. (23),(24) and (25) are all independent of k, so, for the laminate under bidirectional compression, if the optimum buckling mode is single one, the optimum ply angles of each layer are all equal to each other. However, it is noted that the objective function is a family of curved surfaces corresponding to the different values of m and n in the space of Θ_k-Φ. The result of Eq.(20) is only the result of extremum $\Phi_{m,n}$ of one specific curved surface associated with given n and m, i.e.,

$$\Phi^{\bullet}_{m,n} = \max_{\Theta_k} \Phi_{m,n} \tag{26}$$

The optimum Φ_{op} of the objective function Φ under bidirectional compression is

$$\Phi_{op} = \min_{m,n} \Phi^{\bullet}_{m,n} = \min_{m,n} \max_{\Theta_k} \Phi_{m,n} \tag{27}$$

To obtain the minimum of $\Phi_{m,n}$ with respect to m and n, we substitute m+1,m and m-1 together with given n into Eq.(15) and obtain $\Phi_{m-1,n},\Phi_{m,n}$ and $\Phi_{m+1,n}$, the condition

$$\Phi^{\bullet}_{m-1,n} \geq \Phi^{\bullet}_{m,n} \leq \Phi^{\bullet}_{m+1,n} \tag{28}$$

leads to the discriminate

$$\frac{m^2(m+1)^2+\alpha n^2 R^2[(m+1)^2+m^2]}{n^4 R^4} \geq \frac{D_{22}-2\alpha(D_{12}+2D_{66})}{D_{11}}$$
$$\geq \frac{m^2(m-1)^2+\alpha n^2 R^2[(m-1)^2+m^2]}{n^4 R^4} \tag{29}$$

Similarly, by substituting n-1,n,n+1 together with given m into Eq.(15) and compare the $\Phi_{m,n-1}$, $\Phi_{m,n}$ and $\Phi_{m,n+1}$, we obtain another discriminate

$$\frac{m^2R^2[(n+1)^2+n^2]+\alpha n^2(n+1)^2R^4}{m^4} \geq \frac{\alpha D_{11}-2(D_{12}+2D_{66})}{D_{22}}$$
$$\geq \frac{m^2R^2[(n-1)^2+n^2]+\alpha n^2(n-1)^2R^4}{m^4} \tag{30}$$

If the two discriminates (29) and (30) are all satisfied by the optimum angle Θ_k, the optimum design is obtained.

For the bimodal buckling, the condition of bimodal buckling must be taken into consideration. For example, if the laminate is under unidirectional compressive load along the x direction, by substituting Eq.(18) into Eq.(2), we get

$$T_{33} = D_{11}[m^4+m^2(m+1)^2]+2(D_{12}+2D_{66})m^2R^2 \tag{31}$$

By substituting Eq.(31) into Eq.(19), a system of equations independent of k is obtained as follows

$$sin2\Theta_k\{[m^2+(m+1)^2]U_2-[6R^2-m^2-(m+1)^2]4U_3cos2\Theta_k\} = 0 \tag{32}$$

the extreme points are the solutions of the equation, i.e., $\Theta_k=0^0$, $\Theta_k=90^0$ or

$$\Theta_k = \frac{1}{2}cos^{-1}[\frac{m^2+(m+1)^2}{6R^2-m^2-(m+1)^2}\frac{U_2}{4U_3}] \tag{33}$$

It can be shown that the three different values of ply angle are the optimum design under different aspect ratio of plate and different buckling modes. The optimum ply angles of each layer are still all equal to each other, i.e., the number of design variables is only one.

For the laminate under shear load the gradient of objective function λ with respect to design variable Θ_k are

$$\frac{\partial\lambda}{\partial\Theta_k} = \frac{\{W\}^T\frac{\partial[K]}{\partial\Theta_k}\{W\}}{\{W\}^T[G]\{W\}} \tag{34}$$

By setting the Eq.(34) equal to zero, we obtain the optimality condition,

$$\{W\}^T \frac{\partial [K]}{\partial \Theta_k} \{W\} = 0 \tag{35}$$

where the elements of the diagonal matrix $\dfrac{\partial [K]}{\partial \Theta_k}$ are

$$\frac{\partial T_{33}}{\partial \Theta_k} = 4[\frac{h^3}{12} + h(\frac{Z_{k+1} + Z_k}{2})^2] \ sin2\Theta_k (4F \ cos2\Theta_k - J) \tag{36}$$

By substituting Eq.(36) into Eq.(35) we obtain the extremum value of λ at ply angles $\Theta_k = 0^0$, $\Theta_k = 90^0$ or another one, which satisfies

$$\{W\}^T [4F \ cos2\Theta_k - J \ ]\{W\} = 0 \tag{37}$$

Furthermore, it can be proved that the optimization of laminated plate under shear can be simplified to a single variable optimization, i.e., the optimum ply angles of each layer are still equal to each other too.

5. GENERAL CASE

For buckling and vibration of laminated plate under rather general condition, the eigenvalue, i.e., the buckling load or the vibration frequency can be given by the Rayleigh Quotient

$$\lambda = \min_{w} \frac{C(W, \Theta_k)}{F(W)} \tag{38}$$

where the $C(W, \Theta_k)$ is proportional to the elastic strain energy of the laminate plate, $F(W)$ is proportional to the work done by the external load for buckling or the kinematic energy for vibration. Because the functional $F(W)$ is not explicitly dependent of the ply angles, the condition of optimum ply angle can be obtained from

$$\delta C = 0 \tag{39}$$

Let us consider the symmetric laminate plates under rather general condition and assume that no work is done by external moment or shear force along the plate boundaries, the functional C is given by

$$C = \int\int_{\Omega} [D_{11}W^2_{,xx} + D_{22}W^2_{,yy} + 4D_{66}W^2_{,xy} + 2D_{12}W_{,xx}W_{,yy} + 4D_{16}W_{,xx}W_{,xy} + 4D_{26}W_{,yy}W_{,xy}]d\Omega \quad (40)$$

By substituting Eq.(40) into Eq.(39) and introducing the transformation

$$\chi_k = \tan\Theta_k \quad (41)$$

it is not difficult to find the optimality condition for new variables X_k

$$a_k\chi_k^4 + b_k\chi_k^3 + c_k\chi_k^2 + d_k\chi_k + e_k = 0,$$
$$(k = 1, 2,..., N/2) \quad (42)$$

where the coefficients a_k, b_k, c_k, d_k and e_k are independent of k. When the laminate is made of the same material, i.e., the Eq.(42) is a system of equation independent of k and have the same form for all layers, the solutions of Eq.42 is no more than 4. In this way we come to the conclusion that for symmetric laminate under rather general plate configuration, loading and boundary conditions, the number of different optimum ply angles in the laminate is no more than 4. The above conclusion can be further specilized for specific problem. And the conclusion is very useful for numerical optimization.

6. REFERENCES

[1] Schmit,L A & Farshi B, Optimum Laminate Design for Strength and Stiffness, Int. J. Num. Meth. Eng.,7, 519-536, 1973.
[2] Bert C W, Optimal Design of a Composite-Material Plate to Maximize its Fundamental Frequency, J. Sound and Vibration, 50(2), 229-237.
[3] Bert C W, Design of Clamped Composite-Material Plate to Maximize Fundamental Frequency, J.Mech. Design 100, 274-278, 1978.
[4] Adali S, Multiobjective Design of an Antisymmetric Angle-Ply Laminate by Nonlinear Programming,ASME J. Mechanisms, Transmissions and Automation in Design, 105,214-219,1983.
[5] Adali S, Design Sensitivity Analysis of an Antisymmetric Angle-Ply Laminate,Eng. Opt., Vol.7, No.1,69-82, 1983.
[6] Tang J, On Optimum Design of Laminated Plates and the Effect of Coupling between Bending and Extension, Comp. Struct. Mech. and Appl., Vol.1, No.2, 75-84, 1984 (in Chinese).
[7] Pedersen P, On Sensitivity Analysis and Optimal Design of Specially Orthotropic Laminates, Engg. Opt., 11, 305-316, 1986.

[8] Miki M, Optimum Design of Laminated Composite Plates Subject to Axial Compression, Proc. Japan-US, CCM-III, Tokoyo, 673-680,1986.

[9] Grenestedt J L, Layup Optimization and Sensitivity Analysis of the Fundamental Eigenfrequency of Composite Plates, Comp. Struct., 12,193-209, 1989.

[10] Tang J, On Optimum Design of Laminated Plates under Bidirectional Axial Compression, ACTA Mechanica Sinica, Vol.19, sup. issue, 268-272, 1987.(in Chinese)

[11] Muc A, Optimal Fiber Orientation for Simply-Supported Angle-Ply Plates under Biaxial Compression, Comp. Struct., 9,161-172, 1988.

[12] Tang J, On Optimum Analysis of Laminated Plates under Shear, ACTA Materal Composite Sinica, Vol.6, No.4, 48-55, 1989. (in Chinese)

[13] Hirano Y, Optimum Design of Laminated Plates under Shear, J.Composite Materials, Oct., 329-334,1979.

[14] Jiang Y Q ,Optimum Design of Fiber Reinfoced Composite Laminated Plates, Comp. Struct. Mech. Appl., Vol.1, No.1, 39-46, 1984.(in Chinese)

[15] Tauchert T R & Adibhatla S, Design of Laminated Plates for Maximum Stiffness, J. Composite Materials, 18, Jan.,1984.

[16] Cheng G D, Sensitivity Analysis and a Mixed Approach to the Optimization of Symmetric Layered Composite Plates, Engg. Opt.,9,233-248, 1986.

Optimal Design with Damping Materials for Vibration Reduction

H. Eschenauer and H.-W. Wodtke

Research Center for Multidisziplinary Analyses and Applied Structural Optimization (FOMAAS), Institute of Mechanics and Control Engineering, University of Siegen, D-W 5900 Siegen, Germany

Abstract

In this paper the problem of optimal design of unconstrained damping layer distribution on thin walled structures subject to broadband excitation is considered. The objective is to minimize structural resonance responses in a given frequency band with a fixed amount of damping material. The min-max-problem resulting from this task can be formulated as a parameter optimization problem which is treated using an approximation method based on damped single degree of freedom-responses. The method will be applied to coated beams, circular plates and shallow spherical shells.

1. INTRODUCTION

Damping layers are extensively used to reduce bending vibrations of thin walled structures. Their main field of application is noise reduction (automotive parts, machine coverings etc.), but they are also applied for service-life enhancement (e.g. aircraft panels). The damping layers are basically made of amorphous materials exhibiting a high degree of internal losses, such as bitumen, polymers or vitreous enamels. Caused by vibrations of the base structure these materials are subject to alternating strains, and subsequently they dissipate some amount of the vibrational energy.

Surface damping treatments are usually applied to one side of the structure. There are two different common layer damping types, namely the so-called constrained layer, where the damping material is forced into shear deformation between two metal sheets, and the single or unconstrained damping layer which is subject to tension and compression [8] (Fig. 1). The latter can be easily shaped and is for that reason used here for optimization. However, the method presented in this paper can also be applied to constrained damping treatments.

The performance of damping layers not only depends on their material properties (Youngs modulus, loss factor) which are strongly influenced by temperature and frequency [9], but also on their distribution with respect to the vibration modes and the loading. It can be improved firstly by increasing the thickness of the viscoelastic layer and secondly by concentrating the damping material at such places where the vibration mode of the base structure shows its maximum curvatures [7]. In general, the arrangement of the damping layer considerably influences the mass distribution and in case of modern damping materials (Youngs modulus in the order

of magnitude of 1000 N/mm²) also the stiffness distribution of the structure and subsequently its vibration shapes. Since these correlations are quite complicated the optimal design of layer damping treatments requires the numerical methods of structural optimization.
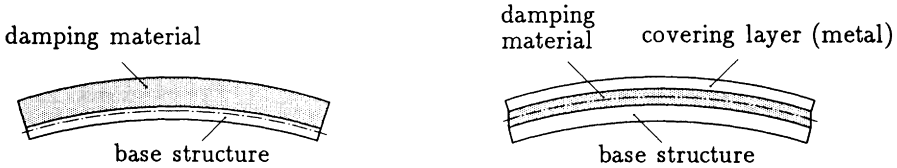
Fig. 1: Single (left) and constrained (right) damping layer (deformed)

In principle there are two different approaches for the optimization of damping distribution. One method is to maximize the loss factors of selected modes of the structure [11] which has the advantage that the objective function is easily formulated. The essential drawbacks of this approach arise from the necessary eigenvalue analyses and from the fact that neither the structural stiffness nor the kind of loading has any influence on the objective function.

These disadvantages can be avoided by directly minimizing the vibration response of the system or by establishing it as a constraint. If the excitation frequencies are prescribed [3,4] then first of all the shift of system eigenfrequencies caused by changes of mass- and stiffness distribution is responsible for the decrease in response. Therefore, in order to exploit the damping in response minimization it is necessary to consider the resonances where damping takes full effect. Following this, the optimum solution is defined as the one which minimizes the resonance responses in a given frequency interval [5,6]. By using this formulation, however, one obtains a min-max-problem, the treatment of which is much more difficult than solving a pure minimization problem. Nevertheless, this approach will be used here to find optimal damping layer distributions on beams, plates and shells. Considering the min-max-problem as a parameter optimization problem [2], we attempt to perform the expensive resonance tracking as effective as possible by means of an approximation method.

2. STRUCTURAL ANALYSIS

For the optimization of damping layer distributions with the aim of minimum resonance responses a structural analysis method is required which permits the calculation of vibration responses of non-homogeneous, viscoelastic components having arbitrary geometries. Because of its universality the finite element method is employed here. The beams are modeled by means of two layer structural elements including shear-compliance of the damping layer. For the circular plates and spherical shells we use an axisymmetric 4-node solid element with additional incompatible shape functions. According to the correspondence principle of linear viscoelasticity, damping is introduced into the equations of motion through a com-

plex and frequency-dependent stiffness matrix:

$$[\tilde{K}(\omega) - \omega^2 M]\,\tilde{u} = \tilde{f} \tag{1}$$

where $\tilde{u}$ complex vector of nodal displacements,

$\tilde{f}$ complex vector of excitation forces,

$\tilde{K}(\omega) = K_{Re}(\omega) + i K_{Im}(\omega)$ complex, frequency-dependent stiffness matrix,

M mass matrix,

ω angular frequency of excitation.

The imaginary part of the stiffness matrix is obtained by integration over the volume of the viscoleastic material only. While the base structures are made of steel, which is assumed to be pure elastic, (E_S = 210000 N/mm^2, ϱ_S = 7.85 kg/dm^3, ν_S = 0.3, η_S = 0), we take experimental data for Youngs modulus and loss factor from [10] for the damping material (Fig. 2), and set Poissons ratio to ν_D = 0.45.
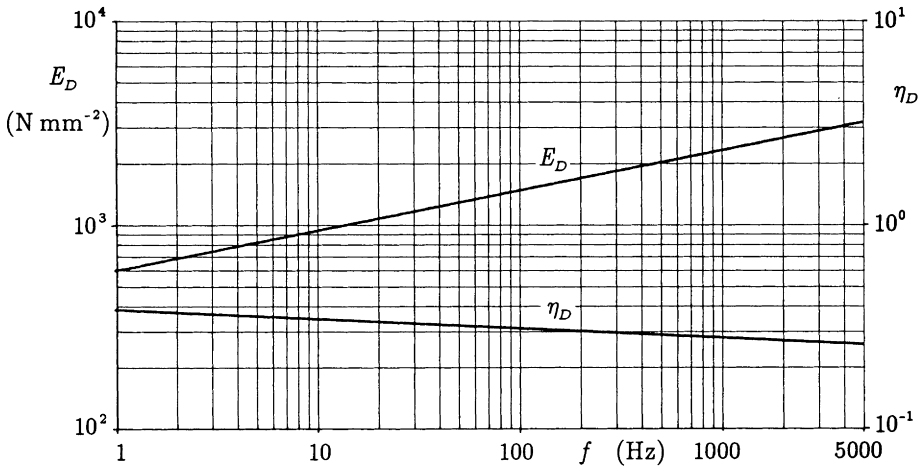
Fig. 2: Youngs modulus and loss factor of the damping material measured at 20 °C

Those parts of the stiffness matrix which are only geometry-dependent are kept in the computer memory separately for each material in order to avoid re-integration of element matrices (solid element) if just the frequency is changed. Regardless of this fact the equation system (1) must be solved for every given excitation frequency. In order to maintain the band shape of the equation system, this is performed by means of a Gauss-algorithm with complex arithmetic.

The presented structural model has been proven to give very good results by comparing the theoretical data with experimentally determined vibration shapes and frequency response curves of partially covered beams, circular plates and spherical caps [10].

3. OPTIMIZATION PROBLEM

As mentioned before, the minimization of resonance responses leads to a so-called min-max-problem, which shall be clarified with an example. In Fig. 3 the response (magnitude of compliance) of a partially damped circular plate around its first resonance is given for varying arrangements of the damping material. There is only one design variable in this problem namely the thickness of the damping layer. The volume of the damping material is kept constant by changing the diameter of the damped region.
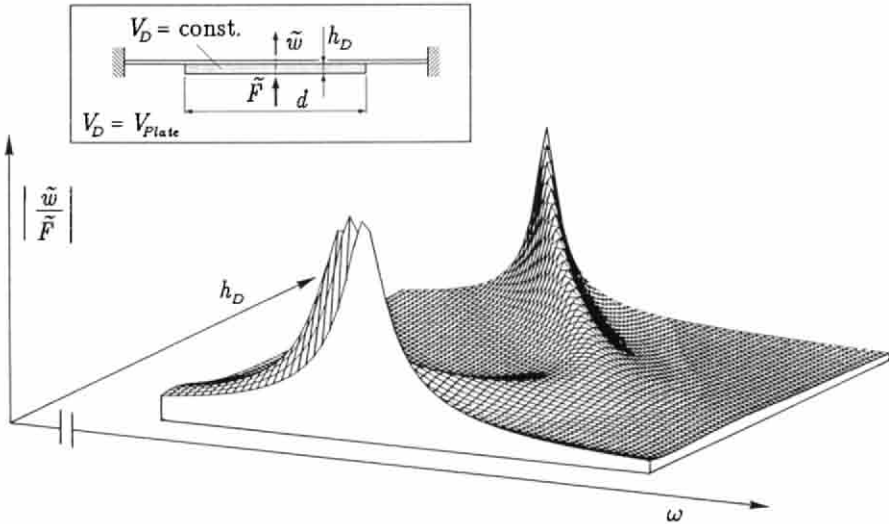
Fig. 3: Vibration response of a circular plate for varying damping layer distribution

From Fig. 3 it can be seen that a certain damping layer thickness exists which minimizes the resonance response. This is the wanted optimum which corresponds to the saddle point of the 3D-surface. Due to the variation of the layer thickness not only the magnitude of the resonance changes but also its frequency. For that reason the resonance frequency must be continuously updated during the optimization. This is called the *inner problem* which is solved by maximizing the vibration response with respect to the excitation frequency. The inner problem causes the main difficulties of the optimization task.

Mathematically, the inner problem can be formulated as a search of an auxiliary objective function f^*:

$$f^*(\boldsymbol{x}) := \max_{\omega} \left\{ f(\boldsymbol{x},\omega) \mid \omega \in [\omega_l, \omega_u] \right\} , \tag{2}$$

where f is a valuation function based on the vibration response (e.g. mean square velocity) and $\boldsymbol{x}$ the vector of design variables. If there are several resonances in the

frequency band of interest, one may form a preference function out of the maximum values f_j^* [1].

Using (2), the complete optimization problem reads as follows:

$$\underset{\boldsymbol{x}}{\text{Min}}\ \underset{\omega}{\text{max}}\ f(\boldsymbol{x},\omega) \qquad\qquad (3)$$

under the conditions: $\boldsymbol{g}(\boldsymbol{x}) \le \boldsymbol{0}$, $\omega \in [\omega_l,\ \omega_u]$. Written in such a hierarchical form it is called a parameter optimization problem [2] where the excitation frequency ω is the parameter here.

In Fig. 4 a float chart of the whole optimization procedure is given. From this figure it becomes particularly evident that the total computational effort of the optimization strongly depends on how effective the inner problem can be solved, i.e. how few structural evaluations are required to determine the resonance response.
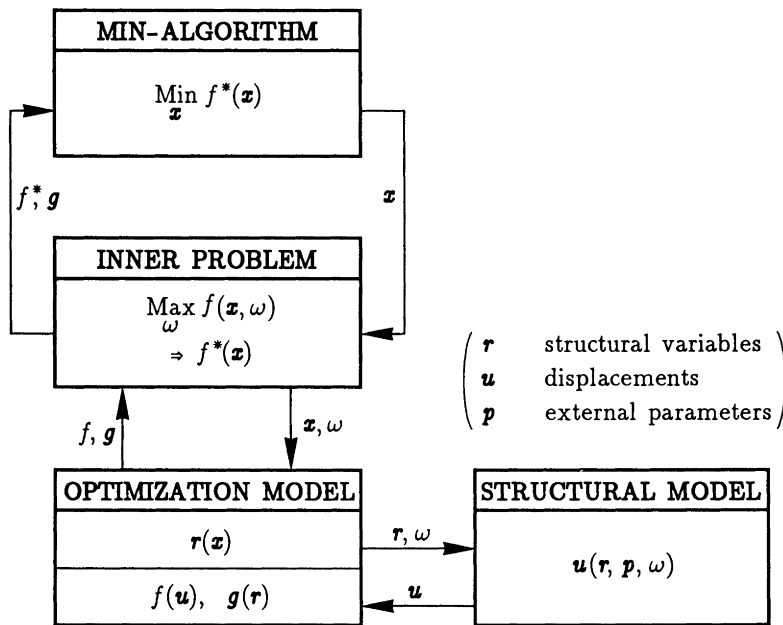
Fig. 4: Optimization loop with inner problem

The easiest way of solving the inner problem is to subdivide the frequency interval and to pick out the maximum of say n discrete response values. Obviously a lot of unnecessary structural analyses must be performed in this method, especially in case of sharp resonance peaks (low damping) where a fine discretization is needed. A much more effective way of finding the resonances can be achieved by means of iterative search algorithms. This method was proposed by McMunn and Plunkett [6] who employed a Newton-Raphson-procedure for the optimization of

multi-body-systems, but it is also possible to use any one-dimensional maximization algorithm (line search). The main drawback of using an algorithmic search method is that the convergence behavior of the procedure strongly depends on whether the search parameters (e.g. initial values, step size factors, break-off criteria) are well chosen. Therefore, another method for solving the inner problem has been developed and is presented in the next section.

4. APPROXIMATION METHOD

This method is based on the fact that the response of linear vibration systems can be written as a sum of modal contributions. The basic idea stems from the theory of modal testing where some curve fitting methods are used for extracting modal parameters from a set of measured response values. The simplest approach of this theory is to approximate each resonance by taking the frequency response function of a single degree of freedom (SDOF) system. In [12] undamped SDOF responses are assumed to estimate resonance frequencies, whereas, if damping is included into the SDOF response-function, not only the frequencies but also the amplitudes of the resonances can be estimated from just two complex response values which may be arranged at arbitrary positions close to the resonance.

Starting point of the method is the modal representation of the structural response written in complex form:

$$\tilde{\boldsymbol{u}}(\omega) = \sum_j \tilde{\boldsymbol{\varphi}}_j \frac{\tilde{\alpha}_j}{1 - (\omega/\Omega_j)^2 + i\eta_j} \tag{4}$$

where Ω_j, η_j j-th natural frequency and corresponding loss factor,

$\tilde{\boldsymbol{\varphi}}_j$ j-th eigenvector (mode),

$\tilde{\alpha}_j = \alpha_j + i\beta_j$ participation factor of the j-th mode.

Provided that the vicinity of a resonance is considered and the damping is "weak enough", one may combine all parts which do not belong to this resonance to a constant value. As a further simplification this constant part is also neglected. Thus, we have:

$$\tilde{\boldsymbol{u}}(\omega) \approx \tilde{\boldsymbol{\varphi}}_j \frac{\tilde{\alpha}_j}{1 - (\omega/\Omega_j)^2 + i\eta_j} := \tilde{\boldsymbol{q}}_j(\omega) \tag{5}$$

Since the mode shapes $\tilde{\boldsymbol{\varphi}}_j$ change only very little near resonance, there are just four unknowns remaining in this expression, namely the modal parameters $\tilde{\alpha}_j$ (real and imaginary part), Ω_j and η_j. In order to determine these parameters, we need four pieces of information which can be obtained from the complex response of the structural model taken at two different frequencies $(\omega_k, \tilde{\boldsymbol{u}}_k)$, $k = 1, 2$ close to the resonance. For that, it is sufficient to consider a single degree of freedom $\tilde{u}_k$ which is suitably selected (e.g. the one with the largest amplitude). Setting the approximation equal to the true response and splitting the resulting equations into real and imaginary part yields:

$$\alpha_j \; + \; \eta_j \, \mathrm{Im}(\tilde{u}_k) \; + \; \frac{\omega_k^2}{\Omega_j^2} \, \mathrm{Re}(\tilde{u}_k) \; = \; \mathrm{Re}(\tilde{u}_k) \; , \tag{6a}$$

$$\beta_j \; - \; \eta_j \, \mathrm{Re}(\tilde{u}_k) \; + \; \frac{\omega_k^2}{\Omega_j^2} \, \mathrm{Im}(\tilde{u}_k) \; = \; \mathrm{Im}(\tilde{u}_k) \; . \tag{6b}$$

In (6) the eigenvector $\tilde{\varphi}_j$ has been scaled in such a way that the part belonging to the chosen degree of freedom $\tilde{u}_k$ equals the real value one. The solution of (6) can be easily expressed in a closed form. When the solution is known, the resonance response is calculated from (5) by setting $\omega_j = \Omega_j$. It should be mentioned that it is also possible to perform the approximation in a very similar way, based on both, the structural response and its frequency derivative at a single frequency, or based on three magnitude values [10].

Fig. 5 shows the approximations of the first two resonances of a partially damped circular plate. It can be seen that the peak amplitudes are well estimated, even if the supporting frequencies are chosen relatively far from the resonances. Additionally, it has to be remarked that in this example the material properties of the damping layer are frequency-dependent (cf. Fig. 2).
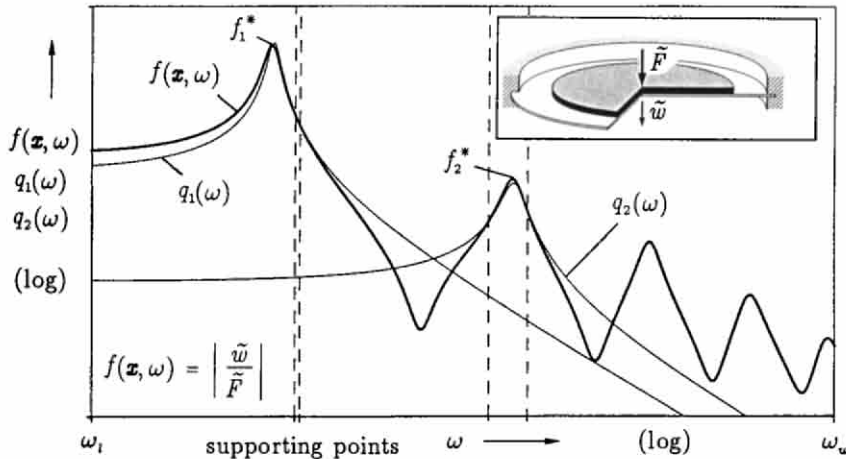
Fig. 5: Approximations of the first two resonances of a partially damped plate

In order to set up a complete optimization procedure, the method described above and also the discrete and the iterative method have been integrated into the program system SAPOP [1]. A test of the methods with a simple example (simply supported beam, one design variable) has shown that, by using the approximation method, considerable savings of computing time can be achieved (50 – 70%, even in comparison with the iterative resonance search) [10]. The approximation method is therefore employed for the following examples.

5. APPLICATION EXAMPLES

The optimization of the damping layer distribution will be applied to three different examples, namely a beam, a circular plate and a shallow spherical shell which all have clamped boundaries. The minimization is carried out for the first (lowest) resonance. All three base structures consist of steel and have evenly applied damping layers in the initial design. An upper bound for the volume V_D of the damping material is introduced by means of the constraint:

$$g_1 := \frac{V_D}{V_{D_{max}}} - 1 \tag{7}$$

where $V_{D_{max}}$ is the maximum allowed damping layer volume.

a) Clamped Beam

The dimensions of the beam are: length 300 mm, thickness 1 mm. The broadband force excitation is applied to the middle of the beam and the driving point compliance is chosen to be the objective function:

$$f := |\tilde{w}/\tilde{F}| \cdot \mathrm{N\,mm^{-1}} . \tag{8}$$

The beam is subdivided into 40 finite elements assigning the thickness of the damping layer of each element to a design variable.

Fig. 6 shows the optimum damping material distributions for two different layer volumes. In Fig. 7 the frequency response curves of the initial design and the optimum design are given for the case of the smaller layer volume.

V_D/V_B	f_{ini}/f_{ref}	f_{opt}/f_{ini}
1.0	1.0	0.187
2.0	0.209	0.331
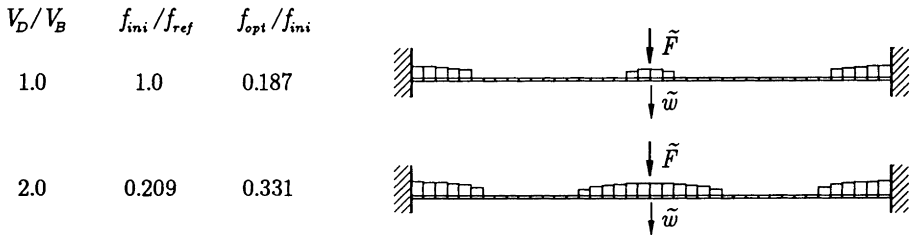
Fig. 6: Optimum designs for a clamped beam with two different layer volumes (V_B beam volume; f_{ini}, f_{opt} initial, optimum values; f_{ref} reference value)

Fig. 6 shows that the damping material concentrates at those points, where the first mode has its strongest curvatures. The tendency towards local concentration decreases, if more damping material is applied. The same counts for the improvements which can be gained by optimization. From the quasi-static responses in Fig. 7 it is obvious that the reduction of the resonance amplitudes does not only result from the increase of damping but also from an increased stiffness. It is furthermore remarkable that, although only the first resonance is minimized, the
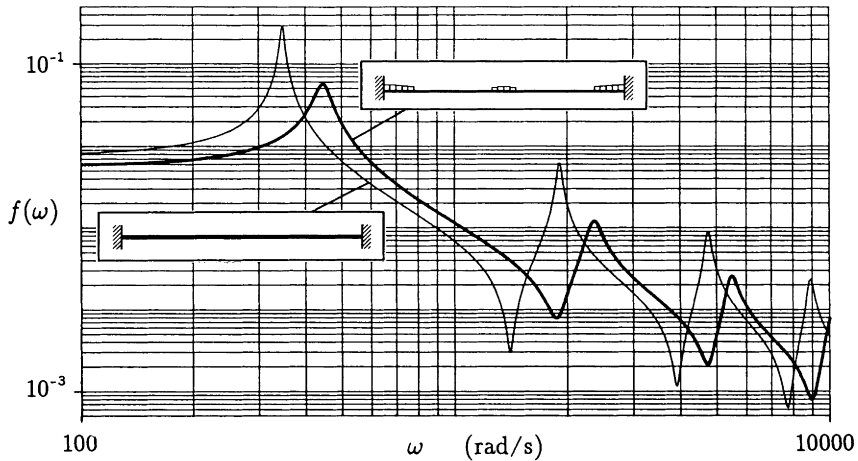
Fig. 7: Frequency response curves of initial and optimum design $(V_D = V_B)$

higher resonances are also substantially reduced in the optimization. This, however, does not apply to all cases (cf. example c). The situation, for instance, may change if unsymmetrical modes are excited at the same time.

b) Clamped Circular Plate

The diameter of the circular plate is 300 mm, the thickness is 1 mm as before. The excitation force is applied to the centre of the plate. The objective function

$$f := \frac{1}{|\tilde{F}|^2} \, \omega^2 \int_A |\tilde{w}|^2 \, dA \, \cdot \, \mathrm{N^2 s^2 mm^{-4}} \tag{9}$$

is chosen as a measure of the radiated sound power (above coincidence). In this expression, $\tilde{w}$ denotes the complex displacement amplitude perpendicular to the surface A of the structure (one side). The layer volume is limited to the volume of the plate.

Two different design models will be employed. The first is characterized by a single design variable which defines the thickness of the rectangularly shaped layer distribution. The second model contains a piecewise linear description of the thickness distribution with 5 design variables which are assigned to the thicknesses at the corner points of the polygon. 40 finite elements are used for the plate and for the damping layer as well. For numerical reasons, a minimum thickness (1% of the plate thickness) is introduced for the elements of the damping layer.

In Fig. 8 the optimal solutions and the corresponding frequeny response curves are shown. It can be seen that the response curves of both optimal solutions differ only very slightly. In both cases, the reduction of the sound power in the first resonance is about 14 to 15 dB. For the practical application of damping layers this small difference is very advantageous, since layers of constant thickness can be realized much more easily. It must be taken into account, however, that jump-shaped

boundaries may cause high delamination stresses. These should be avoided by tapering the edges of the damping layer. Like in the first example, the higher resonances are diminished so strongly that they do not have to be included into the objective function. In contrast to the clamped beam, the damping material is concentrated at the centre of the plate only. This is due to the quadratic dependence of the layer volume on the radial coordinate.
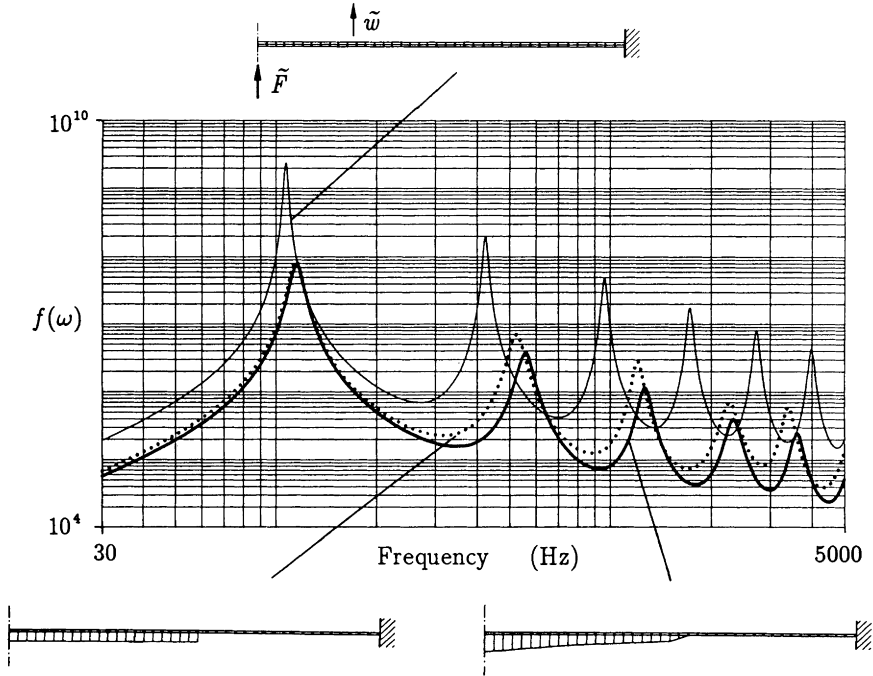
Fig. 8: Damping material distributions and frequency response curves of a clamped circular plate; initial and optimum design of two different design models

c) Clamped Spherical Cap

The cap is chosen to have a spherical radius of 300 mm and a base diameter of 300 mm too (opening angle 60°). In this example, the number of design variables for the piecewise linear design model is 10. Both, the shell and the damping layer are represented by 50 finite elements. All other specifications remain the same as before.

Fig. 9 shows the initial design and the optimal solutions as well as the frequency response curves. Although, in this example, the optimal layer distributions and the corresponding response curves of the two design models differ substantially, the improvements achieved are of about the same degree. It should be noticed that in case of the piecewise linear design model the reduction of the objective function is

somewhat higher than in the plate example. This is a result of the fact that the variation of the damping layer distribution not only decreases the amplitudes of the displacements, but also considerably changes the vibration shape in a positive manner. Through the latter, firstly the portion of bending energy is increased and secondly the shell is made a weak radiator.
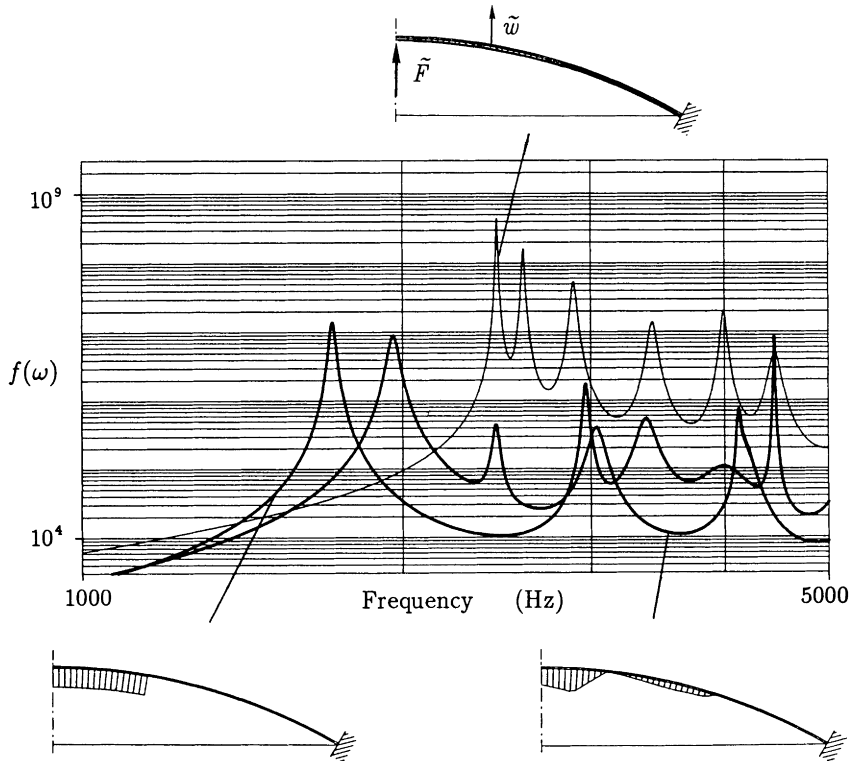
Fig. 9: Damping material distributions and frequency response curves of a clamped spherical shell; initial and optimum design of two different design models

6. CONCLUSIONS

The aim of the present paper was to find optimal distributions of unconstrained damping layers in such a way that the resonance amplitudes of thin walled structures under broadband excitation are minimized. Damped beams, circular plates, and shallow spherical shells are considered as examples. The driving point compliance or the radiated sound power (mean square velocity) of the structure have been taken as objective functions. For structural analysis, the finite element method

has been used where damping was introduced via a complex, frequency-dependent stiffness matrix.

The minimization of resonance responses leads to a parameter optimization problem the major difficulty of which is caused by the task of finding and following the resonances during optimization. An approximation method has been presented which is based upon modal identification and which permits a very effective solution of this problem. The given examples have shown that the optimization of damping layer distributions is worthwhile even if very simple design models are used. Especially in case of curved structures this is not only a result of damping improvement but also of changing the shapes of vibration.

7. REFERENCES

1 Eschenauer, H.; Koski, J.; Osyczka, A.: Multicriteria Design Optimization. Springer-Verlag, Berlin Heidelberg New York, 1990.
2 Haug, E.J.; Arora, J.S.: Applied Optimal Design. John Wiley & Sons, New York Chichester Brisbane Toronto, 1979.
3 Lekszycki, T.; Olhoff, N.: Optimal Design of Viscoelastic Structures under Forced Steady State Vibration. Danish Centre for Applied Mathematics and Mechanics, DCAMM Report No. 195, November 1980.
4 Lin, T.-C.; Scott, R.A.: Shape Optimization of Damping Layers. US/National Aeronautics and Space Administr., NASA Conference Publications 2488, Proc. 58th Symp. on Shock and Vibration, Huntsville Al, Oct 13-15, 1 (1987), 395-409.
5 Lunden, R.: Optimum Distribution of Additive Damping for Vibrating Frames. Journal of Sound and Vibration 72 (1980) 3, 391-402.
6 McMunn, J.C.; Plunkett, R.: Multi-Parameter Optimum in Linear Dynamical Systems. ASME, Vibration Conf., Philadelphia, March 1969, 69-VIBR-42, 2-8.
7 Mead, D.J.; Pearce, T.G.: The Optimum Use of Unconstrained Layer Damping Treatments. University of Southampton, Department of Aeronautics and Astronautics, A.A.S.U. Report 126, July 1961.
8 Nashif, A.D.; Jones, D.I.G.; Henderson, J.P.: Vibration Damping. John Wiley & Sons, New York Chichester Brisbane Toronto Singapore, 1985.
9 Oberst, H.: Schwingungsdämpfende Copolymerisate mit optimierten akustischen Eigenschaften in der Lärmbekämpfung. Hoechst AG, G 10 78 (7035), 1975.
10 Wodtke, H.-W.: Optimale Auslegung von Dämpfungsbelägen zur Schwingungsreduzierung. Dissertation, Universität-Gesamthochschule Siegen, FOMAAS, TIM-Bericht T01-09.92, 1992.
11 Yildiz, A.; Stevens, K.: Optimum Thickness Distribution of Unconstrained Viscoelastic Damping Layer Treatments for Plates. Journal of Sound and Vibration, 103 (1985) 2, 183-199.
12 Yoshimura, M.: Analysis and Optimisation of Structural Dynamics of Machine Tools by a Synthesis of Dynamic Rigidity Program System. Proceedings of the 16th International Machine Tool Design and Research Conference, Manchester, 1975, 209-215.

Topology and Shape Optimization Methods for Structural Dynamic Problems

Zheng-Dong Ma[a], Noboru Kikuchi[a], Hsien-Chie Cheng[a], and Ichiro Hagiwara[b]

[a]Computational Mechanics Laboratory, Department of Mechanical Engineering and Applied Mechanics, The University of Michigan, Ann Arbor, MI 48109-2215, U.S.A.

[b]Vihecle Research Laboratory, Nissan Research Center, Nissan Motor Co., LTD, Natsushima 1-Chome, Yokosuka-shi, 237, Japan

ABSTRACT

A topology and shape optimization technique using the homogenization method is presented for structural dynamic problems. A new objective function using multi-eigenvalues is introduced for improving solvability of the eigenvalue optimization problem. An improved optimization algorithm is then applied to solve the problems, which is derived using a new convex generalized-linearization approach and the dual method. Finally, applications are presented to substantiate feasibility of the present approach.

1. INTRODUCTION

A most actively studied subject in structural optimization in recent years is related to topology optimization. Even though the use of existing techniques which have developed for the sizing and shape optimization problems has made it possible to obtain the optimal size and shape of a structure, significant improvement of design could not be achieved without including topology optimization. In many cases, if a structure has been well designed through an experienced design practice, then just about 5% weight reduction can be obtained by changing the sizes, while about 15% reduction can be obtain by changing the shape of a structure for minimum weight design. In order to obtain further weight reduction, we have to modify the topology and make a brand-new structure.

Optimization of the topology of a continuum structure was hardly solved before Bendsøe and Kikuchi [1] presented their method that is based on a simple idea of transforming the problem to find the ODM (Optimal Distribution of Material) within a specified design domain. It is assumed that the material is not homogeneous, but instead has a variable solid-cavity microstructure. By using the homogenization method (to define the effective homogenized elasticity constants) and mathematical tools of optimization, a mathematical formulation of ODM can be obtained for a given set of loads and boundary conditions . That gives the optimum layout of a structure involving topology, shape and size at the same time.

This idea has been successfully applied to the problems of maximizing the stiffness of a static structure (e.g., Bendsøe and Kikuchi [1], Suzuki and Kikuchi [2,3], Olhoff et al.[4]). In structural dynamic problems, a solution for the eigenvalue optimization has been obtained by Diaz and Kikuchi [5] using a direct application of the method for the stiffness problem. Recently, Ma et al. [6] have extended this method for solving the frequency response optimization problem. However, a dynamic problem is quite different from the static one. It was shown in Ma et al. [6] that even though the original optimization algorithm, which uses a scaling based resizing technique in Bendsøe and Kikuchi [1], is well-convergent in the static problem, it does not work well in the dynamic case, especially when exciting frequency

becomes high. Therefore, an improved algorithm had to be developed (see Ma et al. [6]) in order to overcome the difficulty mentioned above. The basic idea in the modification is to make a convex generalized linearization using a shift parameter which corresponds to the Lagrange multiplier, and employs the dual method to separate a multi-variables minimization problem to several one-dimensional problems. Then an improved resizing rule can be obtained, which has much better convergence property and can be reduced to the previous one if choosing a zero value as the shift parameter. The concept of the convex linearization with the use of duality is also the basis of widely used optimization methods CONLIN (Fleury and Braibant [7], Fleury [8]) and MMA (Svanberg [9]), but the new algorithm can be more efficient and suitable for the present problem. It has been shown that the new algorithm has the simplicity as the scaling based resizing technique, and it has good convergence property in the frequency response problem. Since several examples for the frequency response problem, have been solved in Ma et al. [10] we shall further develop a new additional technique to improve the solution of eigenvalue optimization problem, which has been first discussed by Diaz and Kikuchi [5].

As shown in this paper, in the eigenvalue optimization problem, if one follows a specified mode of the structure to optimize (usually maximize) its corresponding eigenvalue, then the number of this mode may be changed during the optimization process. For example, if k is the original number of order of the mode, then it may change to $k+p$ finally, where $p>0$. In contrast, if we follow the number of modal order, e. g., to optimize k-th eigenvalue, then the mode being the object of optimization process may be changed to another one. In this case, the sensitivities of the objective function become discontinuous, and oscillation may be caused in the objective function within optimization process. In order to avoid this problem, a new objective function is suggested in this paper, which is correspond to a specified multi-eigenvalue optimization problem. It will be shown that the use of this objective function and the improved optimization algorithm mentioned in above can greatly improve the solution, and to optimize not only a single eigenvalue but also multi-eigenvalues by choosing the weighting functions and shift parameter properly.

First, the structural optimization problem is transformed to an ODM problem using a specified 2-D microstructure. Then, a new objective function is proposed for improving the solution of the eigenvalue optimization problem. Based on the sensitivity analyses given in Ma and Hagiwara [11,12], an improved optimization algorithm is presented for solving the problem. Finally, examples are described to substantiate the feasibility of the present approach.

2. OPTIMUM MATERIAL DISTRIBUTION PROBLEM

A minimum weight problem which is subject to the constraint on the specified stiffness can be transformed to a dual problem that maximizes the stiffness subject to the constraint on the specified amount of the material. In general, a structural optimization problem can be conceived as an ODM problem within a prescribed admissible structural domain assuming the loading and boundary conditions to be given (Bendsøe and Kikuchi [1]). As shown in Fig.1, it is considered that the structural domain is filled by a nonhomogeneous material that has variable microstructures. Despite of arbitrary choice of microstructure for perforation of a structure that defines the so-called relaxed design problem, we assume the microstructure is formed by microscale rectangular holes inside a structure in plane elasticity problem that is characterized by the unit cell shown in Fig. 1. Where, the distributed functions a, b (define the relative size of a rectangular hole in the unit cell, and then the density of microscale holes) and θ (angle of rotation of a rectangular hole) are regarded as the design variables in the ODM formulation. Inside cavity of the microstructure is variable along with the design variables, a and b, while the microstructure becomes a complete void when $a=b=0$ and a complete solid when $a=b=1$.
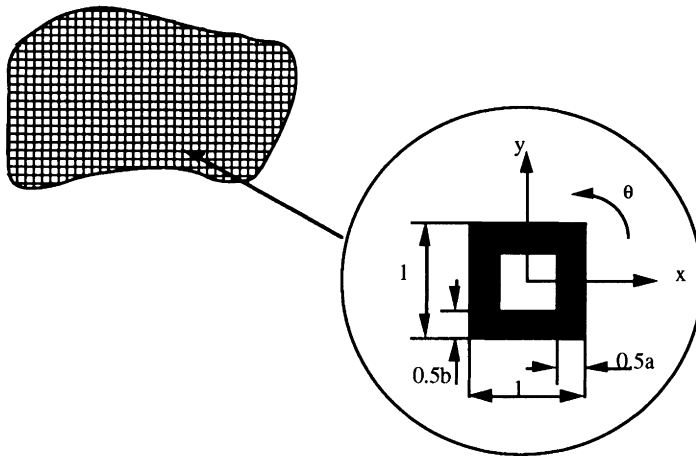
Figure.1 Microstructure in a Structural Domain

In the optimization process, the microstructures are changed from empty to solid or from solid to empty. Therefore, if assuming the total amount of the material of the structure is constant, then the pieces of the material are moved from a part of the structure to another part while the optimization process is progressed. By moving the material for the aim of reducing the objective function, finally we can obtain an ODM that gives the optimal structure.

The linearly elastic coefficients E_{ijkl} and mass density ρ can be also utilized to characterize the problem. Here, in general, E_{ijkl} and ρ are functions of the spatial coordinate. It is assumed:

$$E_{ijkl} = \begin{cases} E_{ijkl}^0 & \text{in solid} \\ 0 & \text{in cavity} \end{cases}, \qquad \rho = \begin{cases} \rho_0 & \text{in solid} \\ 0 & \text{in cavity} \end{cases}$$

where, E_{ijkl}^0 and ρ_0 are elasticity tensor and mass density of the solid portion in the structural domain, respectively.

Since we have assumed the existence of microstructure, a homogenized effective macroscoptic elasticity constants must be obtained to define the equilibrium of a structure using , for example, the homogenization method. The homogenized elastic constants E_{ijkl}^h and mass density ρ^h, which are corresponding to an un-rotated cell, can be obtained as follows :

$$E_{ijkl}^h = \frac{1}{|Y|}\int_Y (E_{ijkl} - E_{ijpq}\frac{\partial \chi_p^{kl}}{\partial y_q})dy \quad , \qquad \rho^h = \frac{1}{|Y|}\int_Y \rho\ dy$$

where, Y is the domain of the cell, and χ_p^{kl} is the solution of the microstructural problem, that characterized micromechanical behavior of the microstructure (Bensøe and Kikuchi [1]).

Finite-element discretization can also be employed to solve the problem. Assuming the system is damped with the viscous damping, the fundamental finite-element equation can be written as

$$\mathbf{M\ddot{u} + C\dot{u} + Ku = f} \tag{1}$$

where $\mathbf{u}$, $\mathbf{M, C, K}$ and $\mathbf{f}$ stand for the nodal displacement vector, mass matrix, damping matrix, stiffness matrix and force vector, respectively. Here we assume $\mathbf{C} = \alpha\mathbf{K} + \beta\mathbf{M}$ for given parameters α and β.

$$\mathbf{K} = \overset{n_{el}}{\underset{e=1}{A}} \mathbf{k}_e \quad , \qquad \mathbf{M} = \overset{n_{el}}{\underset{e=1}{A}} \mathbf{m}_e$$

where, $\overset{n_{el}}{\underset{e=1}{A}}$ stands for the finite element assembly operator, and, $\mathbf{k}_e$ and $\mathbf{m}_e$ are the element stiffness and mass matrices obtained by

$$\mathbf{k}_e = \int_{\Omega_e} \mathbf{B}_e^T \mathbf{D}_e \mathbf{B}_e d\Omega \quad \text{and} \quad \mathbf{m}_e = \int_{\Omega_e} \rho_e \, \mathbf{N}_e^T \mathbf{N}_e d\Omega$$

where $\mathbf{B}_e$ and $\mathbf{N}_e$ stand for the strain shape function and chape function, respectively. $\mathbf{D}_e = \mathbf{T}_e^T \mathbf{D}^h \mathbf{T}_e$ and $\rho_e = \rho^h$ are the rotated homogenized stiffness and mass density, where $\mathbf{T_e} = \mathbf{T_e}(\theta)$ is the transformation matrix for the e-th element. In the plane elasticity problem using the microstructure shown in Fig.1, we have (Ma et al.[10])

$$\mathbf{D}^h = \begin{bmatrix} E_{1111}^h & E_{1122}^h & 0 \\ E_{1122}^h & E_{2222}^h & 0 \\ 0 & 0 & E_{1212}^h \end{bmatrix}$$

Assuming the design variables with respect to an arbitrary finite element Ω_e are a_e, b_e and θ_e, then the element stiffness matrix $\mathbf{k}_e$ and mass matrix $\mathbf{m}_e$ are the functions of a_e, b_e and θ_e, i.e.,

$$\mathbf{k}_e = \mathbf{k}_e(a_e, b_e, \theta_e) \, , \quad \mathbf{m}_e = \mathbf{m}_e(a_e, b_e)$$

3. EIGENVALUE OPTIMIZATION PROBLEM

In the eigenvalue problem, the state equation is written by

$$(\mathbf{K} - \lambda_n \mathbf{M}) \, \phi_n = 0 \tag{2}$$

where, λ_n stands for the n-th eigenvalue of the structure ($n=1,2,...$), ϕ_n the corresponding eigenvector.

Maximizing a chosen eigenvalue of the system is usually used as the object in an eigenvalue optimization problem. However, in the eigenvalue optimization problem, when one maximizes a lower eigenvalue, higher eigenvalus may fall down to the lower values. It means that if the optimization process is to follow a specified mode of the structure, then the order number of this mode may be changed within the optimization process. For example, at beginning, we consider to optimize the k-th eigenvalue, finally the optimal solution obtained may correspond to the $k+p$ th mode, where $p>0$. Thus the problem is changed to an unexpected one. In constrast, if one follows the number of modal order, e. g., to optimize the k-th eigenvalue, then the mode being optimized may change to another one. In this case, the

sensitivities of the objective function become discontinuous, and it probably cause oscillation and divergence in the iterative process for optimization. In order to overcome this problem, a specified multi-eigenvalue optimization problem is suggested. To do this, let us define a mean eigenvalue λ^* by

$$\lambda^* = \begin{cases} \lambda_0 + \left\{ \dfrac{\displaystyle\sum_{i=1}^{m} w_i}{\displaystyle\sum_{i=1}^{m} \dfrac{w_i}{\left(\lambda_{n_i} - \lambda_{0_i}\right)^n}} \right\}^{\frac{1}{n}} & n \neq 0 \\[4em] \lambda_0 + \exp\left\{ \dfrac{\displaystyle\sum_{i=1}^{m} w_i \ln\left|\lambda_{n_i} - \lambda_{0_i}\right|}{\displaystyle\sum_{i=1}^{m} w_i} \right\} & n = 0 \end{cases} \tag{3}$$

where λ_{n_i} are chosen eigenvalues defining the eigenvalue optimization problem, λ_{0_i} are specified desired eigenvalues, λ_0 is a constant shift parameter, w_i are the weights, m is the number of eigenvalues to define a mutiple eigenvalue optimization problem, and n is an appropriately chosen parameter to specify objective of optimization. The mean eigenvalue is introduced to define the optimization problem not only for maximizing a chosen eigenvalue but also for maximizing the distance of two prescribed neighboring eigenvalues as well as for determining a structure that possesses the desired eigenvalues. By choosing parameters appropriately, the mean eigenvalue defined in above can yield various optimization problems. It is also noted that this quantity is introduced as an analogy to the multi-purpose optimization problem with a weighted sum of objectives.

a) Maximize the chosen eigenvalues of a structure

Minimize $f_1 = -\lambda^*$ (4)

where $n = 0, \pm 1, \pm 2, \pm 3, \ldots\ldots$ and $\lambda_0 = \lambda_{0_1} = \lambda_{0_2} = \lambda_{0_3} = \ldots\ldots = \lambda_{0_m} = 0$.

b) Maximize the gap of any arbitrary given two eigenvalues of a structure

Minimize $f = -\lambda^*$ (5)

where $n = 0, \pm 1, \pm 2, \pm 3, \ldots\ldots$ and $\lambda_{0_i} = \lambda_{n_j} (i \neq j)$.

c) Optimum design to impose the desired eigenvalues

Minimize $f = -\lambda^*$ (6a)

where $n = 0, \pm 1, \pm 3, \pm 5, \ldots\ldots$, λ_0 is a given constant, and λ_{0_i} are the desired eigenvalues. If $n = 0, \pm 2, \pm 4, \pm 6, \ldots\ldots$ are assumed, we must change the objective function as

$$\text{Minimize } f = \lambda^* \qquad\qquad\qquad (6b)$$

In general, we assume $\displaystyle\sum_{i=1}^{m} w_i = 1$. If $m = 1$ and $n \neq 0$, the mean eigenvalue in (4) is reduced to $\lambda^* = \lambda_0 + \left(\lambda_{n_1} - \lambda_{0_1}\right)$, and then the optimization problem becomes so as to maximize the n_1-th eigenvalue λ_{n_1}. If $n \neq 0$ and $w_i = 1/m$, the mean eigenvalue in (4) becomes $\lambda^* = \lambda_0 + \sqrt[n]{m \Big/ \displaystyle\sum_{i=1}^{m} \left(\lambda_{n_i}\right)^{-n}}$. Thus, if $n > 0$ is assumed, contribution of the maximum eigenvalue of the set $\left\{\lambda_{n_i}\right\}$ of eigenvalues considered to the objective function becomes considerably small, and then the structure would be designed so as to possess larger values of the smaller eigenvalues of the set $\left\{\lambda_{n_i}\right\}$. Conversely, if $n < 0$, then the optimization problem yields increase of the larger eigenvalues of the set $\left\{\lambda_{n_i}\right\}$, while the smaller ones might not be changed much. If $n \neq 0$, $w_i = 1/m$, and $\lambda_{0_i} = \lambda_{n_{i-1}}$ $(i = 2,...,m)$, the mean eigenvalue in (5) becomes $\lambda^* = \lambda_0 + \sqrt[n]{m \Big/ \displaystyle\sum_{i=2}^{m} \left(\lambda_{n_i} - \lambda_{n_{i-1}}\right)^{-n}}$. Thus the distance of the second and the first eigenvalues will be maximized when $n > 0$, while the difference between two largest eigenvalues will be maximized for $n < 0$.

4. OPTIMIZATION ALGORITHM

In the general case, the optimization problem, which is corresponding to either eigenvalue problem and frequency response problem, can be written as

$$\underset{\mathbf{X}, \Theta}{\text{Minimize}} \quad f \qquad\qquad\qquad (7)$$

$$\text{Subject to state equation (2) ,} \qquad\qquad (8a)$$

$$h(\mathbf{X}) \leq 0 , \qquad\qquad (8b)$$

$$\underline{x}_i \leq x_i \leq \overline{x}_i , \qquad (i = 1,2,\cdots,N) \qquad (8c)$$

where $\mathbf{X} = \text{col}\{x_i\}$ $(x_i \in A \cup B)$, $\Theta = \text{col}\{\theta_i\}$ are vectors of the design variables, A and B stand for the sets of the design variables a_i and b_i, respectively; $\underline{x}_i$ and $\overline{x}_i$ are the minimum and maximum values of the design variables x_i, respectively; and $N = 2n_{el}$. The objective function f can be any one of that we defined previously.

The Lagrangian function of the optimization problem is defined as

$$L = f + \lambda h + \sum_{i=1}^{N} [\alpha_{-i} \, (\underline{x}_i - x_i) + \alpha_{+i}(x_i - \overline{x}_i)] \qquad (9)$$

where, λ, α_{-i} and α_{+i} are the Lagrange multipliers. If assuming (8b) to be active, then we have $\lambda > 0$. Making a new objective function $f^* = f - \mu h$, where μ is a given shift parameter, (9) can be rewritten as

$$L = f^* + \lambda^* h + \sum_{i=1}^{N} [\alpha_{-i} (\underline{x}_i - x_i) + \alpha_{+i}(x_i - \bar{x}_i)] \tag{10}$$

where $\lambda^* = \lambda + \mu$. Now we have a new optimization problem, this problem is completely equivalent to the original one (Ma et al. [10]).

The Kuhn-Tucker conditions of the problem become

$$\frac{\partial f^*}{\partial x_i} + \lambda^* \frac{\partial h}{\partial x_i} = \alpha_{-i} - \alpha_{+i} \quad (i = 1, 2, \cdots, N)$$

$$\frac{\partial f^*}{\partial \theta_i} = 0, \quad (i = 1, 2, \cdots, N)$$

$$(\lambda^* - \mu)h = 0 \; ; \; \alpha_{-i} (\underline{x}_i - x_i) = 0 \; , \; \alpha_{+i}(x_i - \bar{x}_i) = 0 \; ,$$

$$\lambda^* \geq \mu \; , \; \alpha_{-i} \geq 0 \; , \; \alpha_{+i} \geq 0 \; (i = 1, 2, \cdots, N)$$

and it is assumed that the state equation , i.e., (2) is always satisfied.

Using a generalized reciprocal approximation, we assume intermediate linearization variables as $y_i = (1/x_i)^{\xi_i}$, where ξ_i are parameters, which can be determined by the known property of the objective function. For example, if f is an almost linear function of $1/x_i$, $\xi_i = 1$ is a proper choose. Here we assume $\xi_1 = \xi_2 = \cdots = \xi_N = \xi$. Then f^* can be linearly approximated in the space of y_i at $y_i = y_i^k = (x_i^k)^{-\xi}$ as $f^k = f_0^k + \sum_{i=1}^{N} a_i^k x_i^{-\xi}$, where x_i^k are the k-th approximations of the design variables obtained in last iteration step of the optimization process, and f_0^k is a constant,

$$a_i^k = \frac{\partial f^*}{\partial y_i}|_{y_i = y_i^k} = -\frac{1}{\xi}\left(\frac{\partial f}{\partial x_i} - \mu \frac{\partial h}{\partial x_i}\right)_{x_i = x_i^k} (x_i^k)^{\xi+1} \; , \; (i = 1, 2, \cdots, N)$$

If we choose the shift parameter μ in the k-th iteration step as $\mu^k \geq [\frac{\partial f}{\partial x_i} / \frac{\partial h}{\partial x_i}]|_{x_i = x_i^k}$ then, we have $a_i^k \geq 0$, and the approximation of objective function f^k is convex as $\xi > 0$ and $x_i^k \geq 0$.

In this problem, the constraint function h is a linear function with respect to an individual design variable x_i, therefore it can be linearly approximated as $h^k = h_0^k + \sum_{i=1}^{N} b_i^k x_i$ where $h_0^k < 0$ is a constant, and $b_i^k = \frac{\partial h}{\partial x_i}|_{x_i = x_i^k} \geq 0$. Assuming I_-^k and I_+^k are the sets of number of

the design variables which arrive the minimum and maximum values, respectively, and I^k is the set of number of the other design variables, i. e., $I_-^k = \{i \mid x_i = \underline{x}_i\}$, $I_+^k = \{i \mid x_i = \overline{x}_i\}$, and $I^k = \{i \mid \underline{x}_i < x_i < \overline{x}_i\}$. Then the Lagrangian function in the k-th iteration, (10) can be approximated as

$$L^k(\mathbf{X}, \lambda, \mathbf{a}) = l_0^k + \sum_{i \in I^k} l_i^k + \sum_{i \in I_-^k} l_{-i}^k + \sum_{i \in I_+^k} l_{+i}^k \tag{11}$$

where, $\mathbf{a}$ stands for the vector of the Lagrange multipliers α_{-i} ($i \in I_-^k$) and α_{+i} ($i \in I_+^k$).

$$l_0^k = f_0^k + \lambda\, h_0^k + \sum_{i \in I_-^k} \alpha_{-i} \underline{x}_i - \sum_{i \in I_+^k} \alpha_{+i} \overline{x}_i \tag{12a}$$

$$l_i^k = a_i^k x_i^{-\xi} + \lambda\, b_i^k x_i , \qquad \text{(for } i \in I^k) \tag{12b}$$

$$l_{-i}^k = a_i^k x_i^{-\xi} + \lambda\, b_i^k x_i - \alpha_{-i} x_i \quad \text{(for } i \in I_-^k) \tag{12c}$$

$$l_{+i}^k = a_i^k x_i^{-\xi} + \lambda\, b_i^k x_i + \alpha_{+i} x_i \quad \text{(for } i \in I_+^k) \tag{12d}$$

and for simplicity, the index "*" on λ is omitted.

Since the approximated Lagrangian function $L^k(\mathbf{X}, \lambda, \mathbf{a})$ is convex, we can use the dual method to solve the problem (Haftka and Gurdal [13]). The dual problem is defined by

$$\max_{\lambda,\, \mathbf{a}} \ L_m^k(\lambda, \mathbf{a})$$

$$\text{subject to } \lambda \geq 0, \ \mathbf{a} \geq 0$$

where

$$L_m^k(\lambda, \mathbf{a}) = \min_{\mathbf{X}} L^k(\mathbf{X}, \lambda, \mathbf{a}) \tag{13}$$

Because the minimization problem (13) is separable, it can be replaced with N one-dimensional minimization problems as follows.

a) For design variable x_i ($i \in I^k$):

$$\min_{x_i (i \in I^k)} \ l_i^k(x_i) = a_i^k x_i^{-\xi} + \lambda\, b_i^k x_i \tag{14a}$$

b) For design variable x_i ($i \in I_-^k$):

$$\min_{x_i (i \in I_-^k)} \ l_{-i}^k(x_i) = a_i^k x_i^{-\xi} + \lambda\, b_i^k x_i - \alpha_{-i} x_i \tag{14b}$$

c) For design variable x_i ($i \in I_+^k$):

$$\min_{x_i (i \in I_+^k)} \ l_{+i}^k(x_i) = a_i^k x_i^{-\xi} + \lambda\, b_i^k x_i + \alpha_{+i} x_i \tag{14-c}$$

where $a_i^k \geq 0$, $b_i^k \geq 0$ and $\underline{x}_i < x_i < \bar{x}_i$ $(i = 1, 2, \cdots, N)$.

Solving (14a), we can obtain its solution as

$$x_i^* = \lambda^{-\eta} e_i^k, \quad (\text{for } \underline{x}_i < \lambda^{-\eta} e_i^k < \bar{x}_i) \tag{15}$$

where $\eta = \dfrac{1}{\xi + 1}$, and $e_i^k = \left(\dfrac{\xi a_i^k}{b_i^k}\right)^{\eta} = \left[\mu^k - \left(\dfrac{\partial f / \partial x_i}{\partial h / \partial x_i}\right)\Big|_{x_i = x_i^k}\right]^{\eta} x_i^k$.

To solve (14b), we have

$$\frac{\partial l_{-i}^k}{\partial x_i} = -\xi a_i^k x_i^{-(\xi+1)} + \lambda\, b_i^k - \alpha_{-i} = 0 \tag{16}$$

Since $x_i = \underline{x}_i$ when $i \in I_-^k$, then from (16) we can obtain

$$\alpha_{-i} = -\xi a_i^k \underline{x}_i^{-(\xi+1)} + \lambda\, b_i^k = b_i^k[\lambda - (e_i^k / \underline{x}_i)^{\frac{1}{\eta}}] \quad \text{for } \lambda^{-\eta} e_i^k \leq \underline{x}_i \tag{17}$$

Same way, solving (14c), we can obtain

$$\alpha_{+i} = b_i^k[(e_i^k / \bar{x}_i)^{\frac{1}{\eta}} - \lambda], \quad (\text{for } \lambda^{-\eta} e_i^k \geq \bar{x}_i) \tag{18}$$

Substituting {(15), (17),(18)} into {(12),(11)} yields

$$L^k = \tilde{f}_0^k + \lambda\, \tilde{h}_0^k + \lambda^{1-\eta}(1-\eta)^{-1}\sum_{i \in I^k} b_i^k e_i^k$$

where $\tilde{f}_0^k = f_0^k + \sum_{i \in I_-^k} a_i^k \underline{x}_i^{-\xi} + \sum_{i \in I_+^k} a_i^k \bar{x}_i^{-\xi}$ and $\tilde{h}_0^k = h_0^k + \sum_{i \in I_-^k} b_i^k \underline{x}_i + \sum_{i \in I_+^k} b_i^k \bar{x}_i$. To solve the

maximization problem (13), we have $\dfrac{\partial L^k}{\partial \lambda} = \tilde{h}_0^k + \lambda^{-\eta}\sum_{i \in I^k} b_i^k e_i^k = 0$, then the Lagrange

multiplier can be obtained as

$$\lambda^* = \left(\frac{-1}{\tilde{h}_0^k}\sum_{i \in I^k} b_i e_i^k\right)^{\frac{1}{\eta}} \tag{19}$$

It should be noted that because the sets I_-^k, I^k and I_+^k are dependent on the solution of Lagrange multiplier λ^*, an iterative calculation is required for obtaining λ^*.

In summary, the improved optimization algorithm can be described by

    a) Give the initial value of the design variables, x_i^k and θ_i^k for $k = 0$.

    b) Find the solution of state equation (2) with respect to $x_i = x_i^k$, $\theta_i = \theta_i^k$

c) Calculate $\partial f/\partial x_i$ and $\partial h/\partial x_i$ with respect to $x_i = x_i^k$, $\theta_i = \theta_i^k$.

d) Calculate μ^k using

$$\mu^k = \max_{1 \le i \le N} \left\{ \left| \left(\frac{\partial f/\partial x_i}{\partial h/\partial x_i} \right) \right|_{x_i = x_i^k} \right\} \tag{20}$$

e) Calculate

$$e_i^k = \hat{D}_i^k x_i^k, \quad (i = 1, 2, \cdots, N) \tag{21}$$

where

$$\hat{D}_i^k = \left(\mu^k - \left(\frac{\partial f/\partial x_i}{\partial h/\partial x_i} \right) |_{x_i = x_i^k} \right)^{\eta} \tag{22}$$

f) Determine the Lagrange multiplier by a inner iteration loop using

$$\tilde{\lambda}^k = \frac{-1}{\tilde{h}_0^k} \sum_{i \in I^k} b_i e_i^k \tag{23}$$

where $\tilde{\lambda}^k = (\lambda^k)^{\eta}$, $\tilde{h}_0^k = h_0^k + \sum_{i \in I_-^k} b_i^k \underline{x}_i + \sum_{i \in I_+^k} b_i^k \overline{x}_i$, $I_-^k = \{ i \mid e_i^k/\tilde{\lambda}^k \le \underline{x}_i \}$,

$$I^k = \{ i \mid \underline{x}_i < e_i^k/\tilde{\lambda}^k < \overline{x}_i \}, \text{and } I_+^k = \{ i \mid e_i^k/\tilde{\lambda}^k \ge \overline{x}_i \}$$

g) Modify the design variables as follows:

$$x_i^{k+1} = \begin{cases} \underline{x}_i & \text{if } i \in I_-^k \\ e_i^k/\tilde{\lambda}^k & \text{if } i \in I^k \\ \overline{x}_i & \text{If } i \in I_+^k \end{cases}, \qquad (i = 1, 2, \cdots, N) \tag{24}$$

h) Determine θ_i^{k+1} using (34) or its equivalent form (Suzuki and Kikuchi [2]).

i) Let $k = k + 1$, and repeat b) to h) until $|f^{k+1} - f^k| < \delta$, where δ is a given error limit.

Obviously, this algorithm can also be extended to deal with the optimization problem with multi-constraints instead of (8b), but the discussions about this development will be left to a separate report.

5. EXAMPLE 1 : Layout optimization of a simple supported column

In the optimal layout problem, only a design domain and boundary conditions are given. As shown in Fig.2, the design domain is specified as a rectangle, 14.0cm in horizontal length and 2.0cm in vertical height with two simple supported boundaries at the left and right ends. This problem is similar to the shape optimization problem of a simple supported column (see Olhoff [14]). Here, the finite-element model is made by 700 (70×10) finite elements with 781 nodes. This yields 1,582 D.O.F. for the structural domain and 2,100 design variables for

the optimization process in this problem. As shown in Fig. 2, the lowest-five eigenfrequencies of the initial structure (that is the uniformly perforated thin elastic plate with the volume 17cm^2 for a solid material) were 19.8 Hz, 60.8 Hz, 94.1 Hz, 106.0 Hz and 151.4 Hz.

Two cases were considered for the constraint of the total mass being $V_0 = 17.0 \times \rho_0$ (the area of whole domain is 28.0), and the shift parameter λ_0 is assumed to be zero. Figures 3 and 4 show the optimal layouts obtained by using the technique presented in this paper to maximize the first and second eigenvalues by choosing the parameter $n=2$ in the mean eigenvalue. Figure 3 shows the result corresponding to the first eigenvalue optimization, where Fig.3 (a), (b) and (c) are obtained by using (a)the first mode only, (b)modes 1 and 2, and (c)modes 1, 2, 3 and 4, respectively. As shown in Fig.3, the all of three cases have the same layout of the outside, but the interior topology is different. It is shown that when higher modes are used in the optimization process, the final structures seemed to be stiffer (Fig.3 (b) and (c)) because the higher eigenvalues are also enlarged. Therefore, using the multi-eigenvalue optimization technique makes it possible to obtain a better structure.

Figure 4 shows the result corresponding to the second eigenvalue maximization, where Fig.4 (a), (b) and (c) are obtained by using (a)the second mode only, (b)modes 2 and 3, and (c)modes 2, 3, 4 and 5, respectively. Same tendency can be observed as for the first eigenvalue.

In order to show the improvement in convergence of the optimization process, Figs.5 (a) and (b) are given with the history of change in four lower eigenvalues by tracing their modes within first 20 iterations. Figure 5 (a) shows the history corresponding to Fig.4 (a), which used only second mode for optimizing second eigenvalue. Thus it is a single eigenvalue optimization (SEO) problem. Figure 5 (b) gives the convergence history corresponding to Fig.4 (c), which used second, third, fourth, and fifth modes. Thus, it is a multi-eigenvalue optimization (MEO) problem. It is clear that monotone convergence can be obtained by using multiple eigenmodes, while the single eigenvalue problem attains a slightly better result than the case of multiple eigenvalues with non-monotone convergence. It is also noted that the single eigenvalue case may yield significant decrease of the adjacent larger eigenvalues, but controlling multiple eigenvalues always implies increase of the values by design optimization. In this sense, the multiple eigenvalue optimization might provide far more realist design than the case of single eigenvalue optimization.

6. EXAMPLE 2 : Layout optimization of a clumped plate (in plane motion)

We shall now solve the optimum layout problem in a rectangular domain, both left and right sides of which are clumped. A non-structured concentrated mass ($m_0 = 5 \times 10^{-6}$) is also attached at the center of the domain. The structure is formed with solid material whose mass density is $\rho=1 \times 10^{-6}$kg with Young's modulus E=100MPa and Poisson's ratio ν=0.3. The size of the rectangular domain in which we shall layout a structure is 14cm x 2cm as in the first example. Using 700 (70×10) finite elements, the domain is discretized, the single eigenvalue optimization that maximizes the lowest frequency is solved for the volume constraint 9 cm^2 to form a structure. If a solid material is uniformly distributed to form a homogeneous perforated thin elastic plate, the lowest three frequencies are 16.31Hz, 51.56Hz, and 63.80Hz, respectively. Application of the ODM algorithm yields the optimum layout shown in Fig.6(a) that does not have any perforation, but forms more or less framed structure whose lowest three frequencies are 62.95Hz, 75.13Hz, and 106.59Hz, respectively by using the single lowest frequency for optimization. About 286% improvement is achieved by the layout optimization. In order to make comparison to the usual sizing problem, we shall solve a similar problem by determining the optimum height of a solid beam spanned on the interval (0, 14cm). Restricting the maximum and minimum height of the beam into 0.1cm $\leq h \leq$ 2.0cm, the configuration of the shape is defined by a linear function in each finite element, and its optimum is determined by maximizing the lowest frequency derived
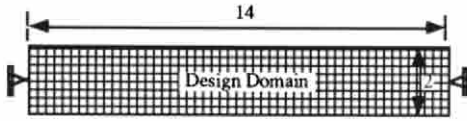
Fig. 2. Initial Structure

f1	f2	f3	f4	f5
19.8	60.8	94.1	106.0	151.4

(a) One Mode Utilized(1)

w1	w2	w3	w4	w5
1.0	--	--	--	--
f1	f2	f3	f4	f5
54.6	59.1	135.8	186.2	240.5

(b) Two Modes Utilized(1-2)

w1	w2	w3	w4	w5
1.0	1.0	--	--	--
f1	f2	f3	f4	f5
52.2	141.9	235.1	262.4	262.8

(c) Four Modes Utilized(1- 4)

w1	w2	w3	w4	w5
1.0	1.0	1.0	1.0	--
f1	f2	f3	f4	f5
52.4	145.9	248.4	279.7	317.7

Fig 3. Optimization for the 1st Eigenvalue

(a) One Mode Utilized(2)

w1	w2	w3	w4	w5
--	1.0	--	--	--
f1	f2	f3	f4	f5
35.6	179.5	191.5	200.4	207.5

(b) Two Modes Utilized(2-3)

w1	w2	w3	w4	w5
--	1.0	1.0	--	--
f1	f2	f3	f4	f5
29.7	185.1	254.2	257.2	294.2

(c) Four Modes Utilized(2-5)

w1	w2	w3	w4	w5
--	1.0	1.0	1.0	1.0
f1	f2	f3	f4	f5
27.8	175.0	274.0	279.9	409.8

Fig 4. Optimization for the 2nd Eigenvalue
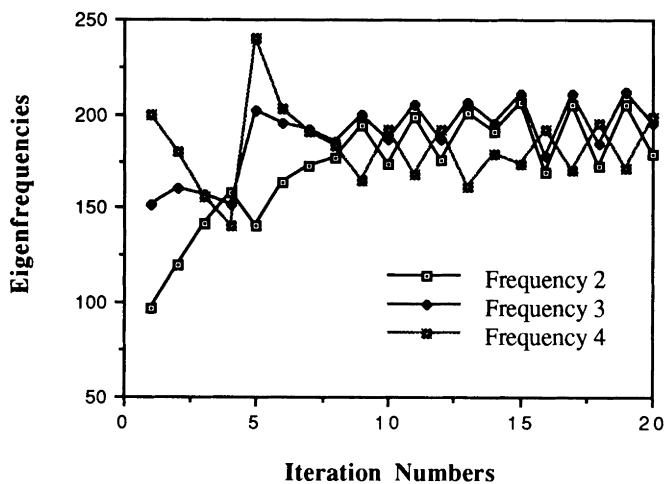
(a) Using Single Eigenvalue as Objective Function(SEO)
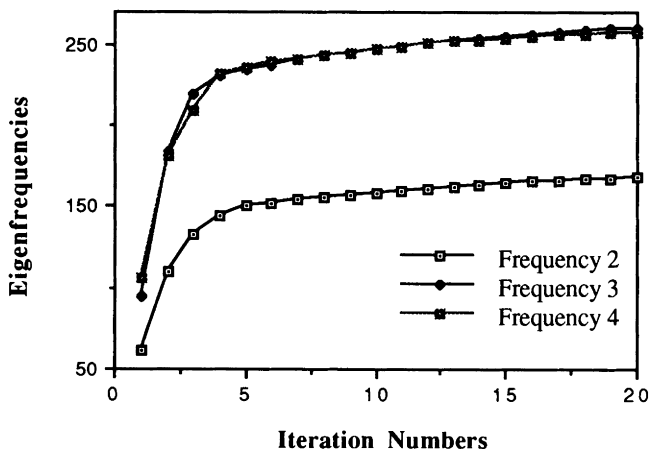
(b) Using Multi-Eigenvalue as Objective Function(MEO)

Fig.5 The Changes of Eigenfrequencies by Using SEO and MEO
(by Tracing the Modes)

from the Euler beam theory using 224 finite elements. Constraining the volume of the beam to be the same for the layout optimization, the optimum shape is obtained as shown in Fig.6(b) with improvement of the lowest three frequencies, 28.27Hz, 96.02Hz, and 171.52Hz, respectively, from the initial constant height beam, 21.59Hz, 92.81Hz, and 149.37Hz, respectively. Improvement is only about 31% for this shape (sizing) optimization. It is clear that the layout design provides much larger improvement.

(a) Homogenization Method (Volume = 9)

(b) Sizing Optimization of a Beam
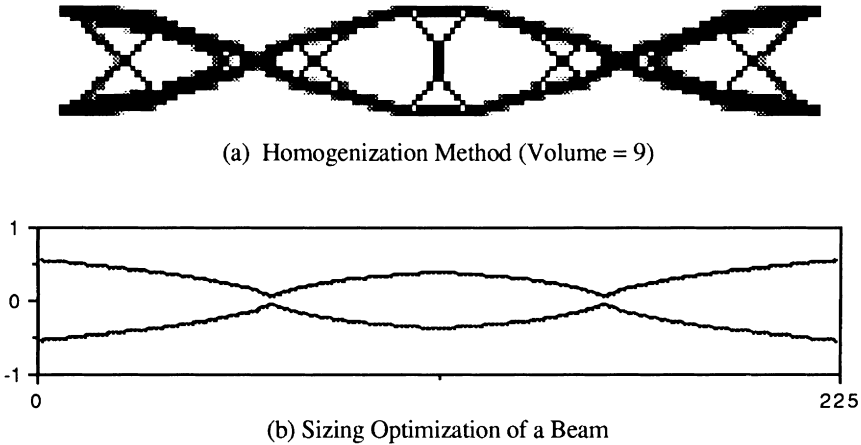
Fig.6 The Optimal Structures by the Homogenization Method and the Sizing (height of the beam) Optimization

7. CONCLUSION

A new objective function corresponding to the multi-eigenvalue is introduced for improving the solution of the eigenvalue optimization problem defined by the homogenization method. An improved optimization algorithm is then applied to solve the problem. It is shown that the use of the multi-eigenvalue optimization technique and the new updating algorithm can greatly improve the solution, and they optimize not only a single eigenvalue but also multi-eigenvalues by choosing the weighting functions and shift parameters appropriately. The feasibility of the present approache is demonstrated by an example.

An extended description of the present approach shall be published in [10], 1992 ASME Winter Annual Meeting, Recent Advances in Structural Mechanics, with many other numerical examples which show the effectiveness of the present method.

REFRENCES

[1] Bendsøe, M. P. and Kikuchi, N., 1988, "Generating optimal topologies in structural design using a homogenization method," Comput. Methods Appl. Mech. Energ., Vol. 71, pp. 197-24.

[2] Suzuki, K. and Kikuchi, N., 1990, "Generalized layout optimization of shape and topology in three-dimensional shell structures," Rept. No. 90-05, Dept. Mich. Engrg. and Appl. Mech., comp. Mech. Lab., University of Michigan, USA.

[3] Suzuki, K. and Kikuchi, N., 1991, "A homogenization method for shape and topology optimization," Comput. Methods Appl. Mech. Energ., to appear.

[4] Olhoff, N., Bendsøe, M., and Rasmussen, J., 1991, "On CAD-integrated structural topology and design optimization," Comput. Methods Appl. Mech. Energ., Vol. 89, pp. 259-279.

[5] Diaz, A. and Kikuchi, N., 1992, "Solution to shape and topology eigenvalue optimization problems using a homogenization method," International Journal for Numerical Methods in Engineering, to appear.

[6] Ma, Z.-D., Kikuchi, N. and Hagiwara, Y., 1992, "Structural topology/shape optimization for a frequency response problem," submitted to International Journal for Numerical Methods in Engineering.

[7] Fleury, C. and Braibant, V., 1986, "Structural optimization: a new dual method using mixed variables," International Journal for Numerical Methods in Engineering, Vol. 23, pp. 409-428.

[8] Fleury, C., 1989, "Efficient approximation concepts using second order information," International Journal for Numerical Methods in Engineering, Vol. 28, pp. 2041-2058.

[9] Svanberg, K., 1987, "The method of moving asymptotes-a new method for structural optimization," International Journal for Numerical Methods in Engineering, Vol. 24, pp. 359-373.

[10] Ma, Z.D., Kikuchi, N., Cheng, H.C., and Hagiwara, I., 1992, Structural topology / shape optimization technique for structural dynamic problems, Proceeding of ASME 1992 Winter Annual Meeting, to appear

[11] Ma, Z. D. and Hagiwara, I., 1991a, "Sensitivity analysis methods for coupled acoustic-structural systems, part 1: Modal sensitivities," AIAA Journal, Vol. 29, No.11, pp. 1787-1795.

[12] Ma, Z. D. and Hagiwara, I., 1992a, "Sensitivity calculation methods for conducting modal frequency response analysis of coupled acoustic-structural systems," JSME International Journal, Series III, Vol. 35, No. 1, pp. 14-21.

[13] Haftka, R. T. and Gurdal, Z., 1992, "Elements of structural optimization," Third revised and expanded edition, Kluwer Academic Publishers.

[14] Olhoff, N, 1981, "Optimization of transversely vibrating and rotating shafts" in Optimization of Distributed Parameter Structures (Ed. E. J. Haug and J. Cea), Sijthoff & Noordhoff, pp. 177-199.

Heuristic Optimisation of Composite Structural Components

S. K. Morton[a] and J. P. H. Webber[b]

[a]Department of Engineering Mathematics and [b]Department of Aerospace Engineering, University of Bristol, Bristol, England

Abstract
    In this paper we describe a knowledge-based system for the design of composite structural components for aerospace applications. The general approach is of initial approximate design followed by successive enhancements until a satisfactory design is obtained. Design enhancement is made by the user on the basis of suggestions generated by a a set of heuristic redesign rules which use the results of extensive analysis programs. The method is applied to the design of a single component in the form of a laminated plate and then to the integrated design of a configuration of two struts and a floorbeam.

1. NOTATION

t_θ	thickness of $\theta°$ plies
x, y, z	plate axes
L_B, L_S, L_P, L_Q, L_F, L_R	geometry of floorbeam/struts configuration (Figure 3)
$\underline{M}$, $\underline{N}$	moments and loads per unit length applied to plate
P, Q	vertical loads applied to beam
θ	ply fibre orientation
ψ	strut orientation

2. INTRODUCTION

   Despite their great potential, advanced composite materials have not been as fully exploited in the aerospace industry as their many advantages would imply. This is because the nature of such orthotropic materials entails limitations to the kinds of design that can be practicably put together, so that the design process is more tied up with the manufacturing process and non-structural operational aspects than for isotropic materials. Component development therefore becomes a problematic and expensive activity: this provides the incentive for a composites design expert system.
   The complexity of the design process itself arises from the theory of orthotropic materials' behaviour: a relatively straightforward analysis to find the amount of material required to withstand a given loading case is not possible as in the case of isotropic materials. In addition there are complications such as free edge effects, delamination and thermal residual stresses.
   There are several ways in which manufacture considerations influence the design procedure. Adequate transfer of the loads to and from other components requires suitable end fittings. Putting bolts or holes in the material produces stress concentrations leading to unpredictable effects. Thermal stresses are present since a laminated component has to be laid up and then cured at a high temperature until the material is set. In addition, qualitative

aspects apart from manufacturability, such as reparability and other operational factors, have to be considered during the design process.

Thus any computer-based expert system that would be of use to a designer using composite materials will firstly have to efficiently access and apply analysis programs implementing the mathematical theories as and when required; and secondly perform a systematic assessment of designs taking into account both quantitative and qualitative desiderata. Beyond that, in order to fulfil the role of adviser to the designer, a user-friendly and flexible man-machine interface is essential; particular features should include menus, dialogue boxes, an explanation facility, and graphics displays.

Various examples of this kind of system have been developed as aids to aerospace designers. Zumsteg and Flaggs [1] discuss the implementation of an expert system shell providing a versatile interface between a rule-based expert system and existing analysis programs for aerospace structures. Chehayeb et al. [2] discuss the knowledge and tools necessary to a knowledge-based design expert system. Zumsteg et al. [3] and Pecora et al. [4] describe an expert system using PROLOG for specific application to the design of sandwich panels using composites. Webber [5] presents some design optimisations for composite laminates using an interactive program written in BASIC. That work was developed by Burden and Lipton [6] to incorporate different failure criteria and ply degradation due to non-catastrophic ply failure. The predecessor of the work presented in this paper was an expert system called CODEX which is discussed in the next section, and details of which can be found in previous papers [7; 8; 9; 10; 11].

The approach discussed in this paper combines the methodologies of expert systems with theories from structural mechanics. Heuristics, or "rules of thumb", derived from human expert knowledge are linked up with extensive analysis programs in an iterative design-test-redesign strategy. Thus not only do we have the common-sense, high-level knowledge of the designer, but we also have the facilities to do complicated analysis very efficiently. Linking these together enables us to obtain a reasonable design in a short number of cycles. However this approach must be tempered by ensuring that the user has absolute control over the design procedure; therefore the inferences derived from the applications of the heuristics are not automatically implemented in the updated design (as in CODEX), but are instead presented as suggestions to the user, upon which he can act or not.

In the next section we expound the general approach of CODEX2 and in sections 4 and 5 we show how it is applied in modules for plate design and integrated struts and floorbeam configuration design respectively. Results are presented for the plate and compared to those obtained using an approach comprising an exhaustive search of the design variable space. The module for the integrated design is not fully implemented so few details and no results are presented.

3. GENERAL APPROACH

In this section we describe in broad terms an expert system for the design of composite structural components called CODEX2. CODEX (COmposites Design EXpert) is the name of the original version of the program; its successor, still under development, is intended as a revised version with much greater potential. Firstly though we describe CODEX.

Essentially CODEX is divided into three subsystems: laminated plate design, laminated strut design and design assessment. Plates are designed with a cyclic design-test-redesign procedure using heuristic redesign rules in the successive updating of intermediate designs to a quasi-optimal solution. The final design is termed "quasi-optimal" since there is no guarantee that it will in fact be optimal, as there would be if we were employing a mathematical programming/structural optimisation approach; however in the great majority of cases it has been found that the set of rules used leads to a design comparable to the true optimum [8; 10; 11].

Struts were designed initially by an analytical method that used simultaneous occurrence

of local and global buckling to derive a set of optimal dimensions for any of seven different cross-sectional shapes. These ideal designs were then modified so that the thicknesses were multiples of the available prepreg thickness, usually 0.125 mm [9; 12].

Assessment was performed on competing solutions to the same plate or strut design problem, i.e. solutions using different materials, ply lay-ups, cross-sectional shapes, etc. The assessment incorporated uncertainty using the formal methodology of support logic as implemented in the language FRIL [13]. A measure of how good designs were with respect to a number of design desiderata was obtained in the form of a support pair.

The new version of the system incorporates the facilities of CODEX, but has greater capability, flexibility and user-friendliness. Apart from plate and strut design, modules are incorporated for beam design, tapered plate design and an integrated struts and floorbeam design that utilises finite element analysis. As mentioned above the user has more control over the system, enabling him at each stage to be more flexible in his choice of operations. This is facilitated by the extensive use of menus and dialogue boxes in the user interface. Moreover the assessment module will have an extensive explanation and "what-if" facility.

The approach of CODEX2 is similar to that of the plate design module of CODEX in that we have an initial design procedure followed by a cyclic test-redesign-test methodology that uses heuristic rules. However it differs in that the inferences made by the rules are not automatically enacted in updating the design; instead they are given back to the user as suggestions, which he can either implement or not. He can also call on other options during the design process to perform analysis, display graphics etc. Thus the system is much more flexible, enabling the user to have greater control over its operation. The general scheme is as shown in Figure 1 and described below.
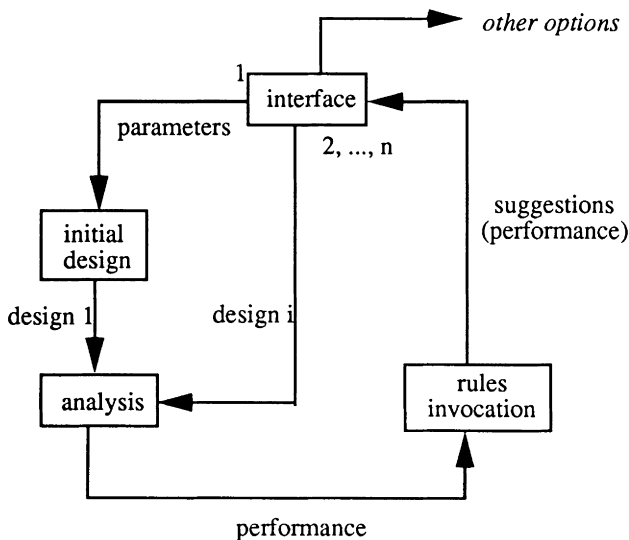
Figure 1. Operation of a CODEX2 design module.

1. The user defines design parameters which are used as input for an initial design module deriving an initial design$_1$ (i = 1).

2. Failure analysis, etc., is carried out by an analysis module, giving a number of factors

defining the design's performance.

2. There is no direct link between redesign rules and design definition: the user iteratively updates design$_i$ on the basis (or not) of suggestions arising from the firing of the rules until he is satisfied ($i = 2, ..., n$).

3. Other options include storing the design, evaluating design properties, sensitivity analyses, graphical display, etc.

In the next two main sections we show how this methodology has been applied to laminated plate design and how it is being adapted to the integrated design of a floorbeam with two struts respectively.

4. LAMINATED PLATE DESIGN

The nature of fibre-reinforced composite materials is such that they are extremely strong in the fibre direction but relatively weak in directions transverse to the fibre direction. The usual solution to this problem when designing a plate from such materials is to construct the plate as a laminate comprising layers of material with the fibres oriented at different angles. Thus, while each layer is weak in the transverse fibre direction, the laminate as a whole has all-round strength. Given a configuration of fibre orientations, i.e. the layers and their orientations, of a putative laminate, the design problem becomes that of finding the set of layer thicknesses that gives the laminate the strengths required for a particular set of multi-directional in-plane loads and moments. In addition the designer must select the most suitable material and also consider other lay-up configurations on the basis of weight, cost, plate stiffnesses, failure load factors and various qualitative criteria.

The complexity of the theory means that there is no practical analytical method, and so we take the rule-driven approach as outlined in section 3. We thus employ a netting analysis for initial design (section 4.1) followed by an heuristic design-test-redesign strategy. The main analysis (section 4.2) includes first ply failure analysis, free edge and interlaminar failure analysis, and ultimate failure analysis; it takes thermal effects into account throughout. The rules (section 4.3) consist of condition-action pairs relating a ply failure mode to the thickening of particular plies. Although an optimal design is not guaranteed using this method, as for instance in a structural optimisation approach, the rule-based approach is much more efficient and gives comparable results in most cases (section 4.4).

The plate design module was initially based on the work of Webber [5] and Burden and Lipton [6]. The plate design and analysis procedures of CODEX2 to be discussed are an extension of those described by Webber and Morton [8]. Throughout this section we assume that the only ply fibre orientations considered are 0°, 90° and ±45°, and that the plate is always balanced. The materials available to the system are :-

CFRPHS914	carbon fibres in 914 resin
CFRPHS913	carbon fibres in 913 resin
CFRPEEK	carbon fibres in PEEK resin
GFRPE913	E-glass fibres in 913 resin
KFRP49913	Kevlar 49 fibres in 913 resin
SCRAL	silicon carbide fibres in an aluminium matrix
AAL168	aluminium alloy.

The assumed values for the mechanical properties of these are given by Webber and Morton [8].

4.1. Initial design
The netting analysis is an approximate method which enables us to derive an initial design

in terms of a set of layer thicknesses, from which it is hoped a satisfactory design will be efficiently derived using the redesign rules of the design cycle. Although the netting analysis for in-plane loads is straightforward, that for applied moments is more complex due to the effect on the bending strains of a ply's distance from the neutral plane. We now present a brief summary of the method outlined by Morton and Webber [4].

4.1.1. In-plane loads

A netting analysis is a simplification of laminated plate theory where the individual plies are assumed to withstand the applied loads independently in their respective fibre directions. Thus the plies with fibres at 0° orientation withstand the load along the plate axis, and the plies with fibres at 90° orientation withstand the load transverse to the plate axis. Additionally since a pure shear load resolves into direct loads in the ±45° directions, the ±45° plies are deemed to withstand such a load. The thicknesses obtained from the analysis for each fibre orientation are such that the strain in the fibre direction at the given load equals the relevant (tensile or compressive) failure strain. In such an approach we are simplifying by ignoring the transverse and shear stiffness and strength of the material, and the mechanical dependence between the layers.

4.1.2. Moments

The situation with applied moments is somewhat more complicated than with applied loads, since the strain in any ply depends on its distance from the neutral plane of the laminate as well as on the magnitude of the moment(s). If we are given a prescribed configuration of ply orientations, the moment netting analysis can be performed in two stages. Firstly an initial thickness can be obtained for each of the 0°, 90° and ±45° plies by considering a single ply of that fibre orientation, assuming it is aligned with the neutral plane of the plate, and finding the thickness required for the relevant moment. Thus, in a manner similar to the load netting analysis, the 0° and 90° layers relate to the bending moments parallel and perpendicular to the plate axis respectively, and the ±45° layers to the twisting moment.

In general the thickness values derived from this procedure will, when assigned to the plies in the prescribed lay-up configuration, be too great; in other words the plate will have been over-designed. This is because the overall bending stiffness of the resulting lay-up is increased when the plies are further away from the neutral plane, rather than being aligned with it. Therefore we need to reduce the thicknesses so that taken together in the given lay-up, each of the applied moments will be resisted by the plies with fibre orientations in the corresponding direction. Since the thickness of one sort of ply determines the distance from the neutral plane of another sort of ply, an iterative procedure must be followed to derive the final moment netting analysis thicknesses.

The thicknesses for the 0°, 90° and ±45° layers derived in the first procedure are used as the initial values of this iteration. At each stage we use a simplification of the theory to derive three equations of the form $P(t_\theta) = 0$, for $\theta = 0°$, 90° or ±45°, where P is a cubic operator and t_θ is the corresponding thickness variable; the equation for one of 0°, 90° or ±45° is solved to give t_θ which is then substituted into the equations for the other two fibre orientations; these are solved in turn, and so on. When the iteration has converged the resulting total ply thicknesses for the respective fibre orientations are such that they will withstand the corresponding moments independently, i.e. in the fibre direction.

In order to achieve reasonable values the three equations are solved in the same order as the first ply of each fibre orientation in the lay-up, going from the outside to the inside. This is because the solution to the equation for the inner plies tends to be negative unless the outer

plies' thicknesses have been reduced first, i.e. the stiffness provided by the outer plies is sufficient. Thus for a [0°/+45°/-45°/90°/90°/-45°/+45°/0°] lay-up the equations at each stage are solved for the thicknesses of 0°, ±45°, and 90° plies in that order.

4.2. Analysis
4.2.1. First ply failure
When analysing an initial or intermediate design we must use the same prescribed failure criterion on each cycle. There are many such described in the literature: for example [14] provides a summary of the most plausible criteria for failure in a single ply of fibre-reinforced composite material. The criterion chosen would depend on the user's opinion on its relative validity, and also on which empirical strength constants are available.

The failure criteria currently available for first ply failure in CODEX2 are maximum strain, maximum stress, Tsai-Hill and Tsai-Wu. The first two assume that the failure modes are independent, i.e. failure occurs when the failure strains or stresses are exceeded in any direction. Thus, although five different tests must be made on the stresses for each ply, it is clear which mode has failed in both the maximum strain and maximum stress criteria. This is important for the purposes of the redesign heuristics since we need to know the failure mode in order to decide which layers to thicken (see section 4.3).

The Tsai-Hill and Tsai-Wu criteria (also referred to as quadratic criteria) assume that the strengths in the different modes are interdependent. An expression involving the ply stresses and failure stresses is evaluated and when this is greater than or equal to 1 failure is predicted, although the mode of failure is not. In order to find the failure mode for the purposes of the redesign heuristics we therefore make an assumption about the layer stresses, namely that the mode in which the proportion of the stress value to the failure stress is greatest is the failure mode.

The Tsai-Hill and Tsai-Wu criteria have the advantages that they are single-valued functions and are thus easy to use, and they produce a smooth failure surface, whereas the maximum strain and stress criteria produce parallelepiped surfaces in stress space. Moreover the maximum strain and stress criteria lead to cusps in the variation of uniaxial strength with fibre orientation due to changes in the failure mode.

4.2.2. Ultimate failure and plate stiffnesses
Having designed to first ply failure, the user may wish to find the plate's ultimate or catastrophic failure load; that is, when one of its plies fails in the fibre direction. Alternatively he may wish to design to ultimate failure in the first place. Material failure prior to ultimate failure will be in the matrix only and so it is necessary to have some idea of how the mechanical properties of the failing layers are degraded. It is usually assumed that the transverse Young's modulus and shear modulus in these layers are reduced by a certain factor, usually about 50%. Testing for ply failure subsequent to first ply failure can then take place on this basis. This process can be repeated, finding intermediate ply failures, until a set of layers fails in the fibre direction. We then have a value for the ultimate load factor.

The plate's apparent stiffnesses in the plate directions can be found by carrying out failure analyses for simple loads. Thus the direct moduli of the plate can be found by applying unidirectional loads parallel and transverse to the plate axis respectively, and the plate shear modulus by applying a pure shear load.

4.2.3. Free edge effects
Although the laminate analysis discussed so far assumes no out-of-plane stresses, it is well known that delamination sometimes occurs at a free edge due to interlaminar normal and shear stresses arising from a mismatch of elastic properties between plies. To predict the values of these stresses and hence the delamination initiation load, a finite element approach such as that of Herakovich [15] will supply detailed information about the stress distributions at and near the free edge. However this is a very time-consuming method, and in order to

provide a designer with a simple and efficient way of estimating these stresses, analytic approximations to the stress distributions have been devised.

A free edge analysis module has been implemented based on the model of Kassapoglou and Lagace [16]. This is a general solution which can cope with any number of plies efficiently to give estimates of the interlaminar stresses. The principal assumptions are that the functional dependences of the stresses on the y and z values can be separated, and that they can be written in a form involving two exponential parameters. Furthermore these functions are chosen so that they satisfy the overall equilibrium equations, the stress-free conditions at the free edge, and also stress continuity between adjacent plies. The parameters of these functions are then determined by minimising the plate complementary energy.

Having established the stress state in the boundary layer near the free edge the next task is to predict the applied load at which delamination initiation occurs. At the free edge itself the analytic approach predicts very high stresses which do not, in practice, occur. Instead average stresses, taken over an "averaging distance", measured from the free edge, are compared with certain empirical strength parameters using some failure criterion. In the CODEX2 free edge analysis module the averaging value is taken to be the same as the material's nominal thickness. The failure criterion used in the system is the quadratic stress criterion as proposed by Brewer and Lagace [17], for which it is necessary to use empirically-derived values for the interlaminar failure stresses. An alternative approach is that promulgated by O'Brien [18] where a simple formula involving the strain energy release rate is applied. This is used for delamination prediction at ply drop-offs in the tapered plate analysis module soon to be incorporated into CODEX2.

The user interface to the free edge analysis module allows the user to select the ply ordering on which to perform the analysis. This is useful since, for a given set of fibre orientations and corresponding ply thicknesses, the predicted delamination initiation load generally varies considerably with the order of the plies. On the other hand, the first ply failure, ultimate failure and plate stiffness analyses are unaffected by the swapping around of fibre orientations (as long as there are no applied moments).

4.3. Redesign rules
4.3.1. Thickening rules

In practice a design engineer will choose a material and a ply fibre orientation configuration and then use trial and error and stress analysis techniques to improve the design to the required load specification. Similarly, at each stage of the design-and-test procedure before a satisfactory design is obtained, the intermediate plate designs must be improved by a selective thickening of plies. The complexity of laminated plate theory does not allow for an analytic approach in the general case. Instead a number of rules derived from the subjective observations of human composite design "experts" are employed to decide on the layers to be thickened given a certain mode of failure, as shown in Table 1.

Each rule consists of an action and one or two conditions. In the "ACTION" column is shown the fibre orientation of the plies to be thickened if the corresponding conditions are met. In the "CONDITIONS" column are shown the condition relating to the fibre orientation and mode of failure of the failing plies, and the condition relating to the presence or absence in the laminate of certain other fibre orientations. For any combination of in-plane loads and bending moments that we have used a set of satisfactory ply thicknesses can be derived by the iterative application of these rules in under 11 cycles. The plate material can be any of the seven materials mentioned above, or any hybrid configuration, as long as the layers are balanced about the plate mid-plane.

As an example consider rule number 1A: here the failure condition is transverse failure in a 90° layer, and the subsidiary condition is existence of 0° plies; the action is to thicken those same 0° plies. Similarly rule 1B deals with the same failure situation when there are no 0° plies, when we instead thicken the 90° plies. Rules 2A and 2B deal with transverse failure in the 0° plies in an analogous manner. In rules 3A and 4A shear failure in the 0° and 90° plies

is dealt with by thickening the ±45° plies, if they are present. In rule 5 transverse failure in the ±45° plies is remedied by thickening the ±45° plies, so that in effect this kind of failure in the +45° is dealt with by thickening the -45° plies and vice versa. In rule 6A shear failure in the ±45° is handled by thickening both the 0° and 90° plies in a manner analogous to the thickening of the ±45° plies in rules 3A and 4A. Rules 7A, 7B and 7C are straightforward thickening of the same layers as fail in the fibre direction.

Table 1
Redesign heuristics

RULE #	ACTION	CONDITIONS	
	thicken ply	failing ply and mode	other plies present
1A	0°	90° transverse	0° layers
1B	90°	90° transverse	no 0° layers
2A	90°	0° transverse	90° layers
2B	0°	0° transverse	no 90° layers
3A	±45°	90° shear	±45° layers
3B	0°	90° shear	no ±45° layers
4A	±45°	0° shear	±45° layers
4B	0°	0° shear	no ±45° layers
5	±45°	±45° transverse	
6A	0°, 90°	±45° shear	0° & 90° layers
6B	±45°	±45° shear	no 0° or 90° layers
7A	0°	0° fibre	
7B	90°	90° fibre	
7C	±45°	±45° fibre	

The question remains as to how the thickening is carried out. After the netting analysis the resultant total thickness for each fibre orientation has two components: one from the in-plane load netting analysis and one from the moment netting analysis. These are treated differently in the redesign thickening. From the load netting analysis equations, the thickness obtained is proportional to the corresponding load. Therefore, for the redesign thickening, we can plausibly increase the load component of the thickness in the same proportion as the failure load is to the prescribed load, i.e. by one over the load factor. On the other hand from the initial moment netting analysis equations [10] the thickness obtained is proportional to the square root of each of the corresponding bending moments. Therefore we equally plausibly

increase the moment component of the thickness by a factor equal to the square root of one over the load factor in the redesign thickening.

The results obtained by successive application of these thickening heuristics generally justify this approach. For instance thickening the moment components of the thicknesses by one over the load factor rather than the square root thereof leads to plates which are too thick.

4.3.2. Rectifying over-thickening

In some load cases the ply thicknesses resulting from the netting analysis and the subsequent application of the above thickening heuristics may result in a plate that is over-designed, i.e. the failure loads are much higher than the prescribed loads. For example this occurs when we do the netting analysis for a $[0°/+45°/-45°/90°]_{sym}$ lay-up subjected to a load and moment acting in the fibre direction with zero transverse load and moment. This is because the thicknesses derived for the 0° plies are more than adequate to withstand the principal load and moment, and since there is no transverse load or moment there is no possibility of transverse failure in the top and bottom plies. Also the bending strain on the 90° plies is small since they are at the centre of the lay-up. Typically the ratio of first ply failure load factor for this kind of case is about 1.4 - 1.6 which is clearly not satisfactory; a load factor value after the netting analysis of less than 1.1 is deemed to be satisfactory. In such a situation the initial thicknesses are reduced by the value of the load factor, and the failure analysis is redone. This will generally result in a more reasonable initial design from which to begin the design-and-test procedure. The same remedy is suggested to the user if the application of the redesign rules leads to over-design.

4.4. Results

In Figure 2 are graphs showing the total plate thicknesses of designs obtained using CODEX for a wide range of complex loads (reproduced from [10]). In each case the material used is CFRPHS914, the lay-up is $[0°/+45°/-45°/90°]_{sym}$, and failure is predicted using the maximum strain criterion. Figures 2(a) and 2(b) show the effects of loading cases excluding applied moments: Figure 2(a) shows the effect of varying N_y while keeping N_x fixed and Figure 2(b) shows the effect of varying N_{xy} for different values of N_y while keeping N_x fixed. The approximately linear relationship between laminate thickness and applied load is evident from these graphs, as it is to a lesser extent when an M_x moment is added as shown in Figure 2(c) where N_x and N_{xy} are fixed and M_x and N_y are varied.

With more complex loads the situation is less straightforward as shown in Figure 2(d) where M_y and N_y are varied. The design thickness drops off as M_y is increased from 250 Nmm/mm to 500 Nmm/mm for a given value of N_y. This can be explained by the bending effect cancelling out the stretching effect at the bottom of the plate. In Figure 2(e) the effect of adding a twisting moment M_{xy} as well is shown for different values of N_y while keeping the other loads fixed. The variation in the thickness here has no apparent trend, except a convergence to a value of 5.3-5.4 mm when M_{xy} becomes large with respect to M_x. In Figure 2(f) the in-plane loads are set to zero and the unusual and unpredictable effect of varying the twisting moments for different values of M_y here is even more pronounced.

In Table 2 we show some results for the rule-based method compared with those obtained using a particular optimisation algorithm known as the COMPLEX algorithm of Box [19]. This algorithm performs a fairly exhaustive search of the design variable space, but usually takes about 200 iterations. As can be seen the total plate thicknesses obtained using the heuristic method compare very well, although they are slightly too high for the cross-ply plates. The number of iterations taken however is in each case less than 11.
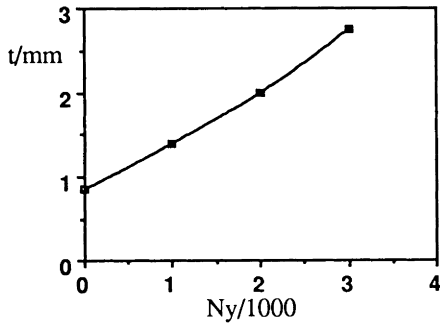
(a) $\underline{N} = [1000,Ny,0]$ N/mm;
$\underline{M} = \underline{0}$ Nmm/mm.
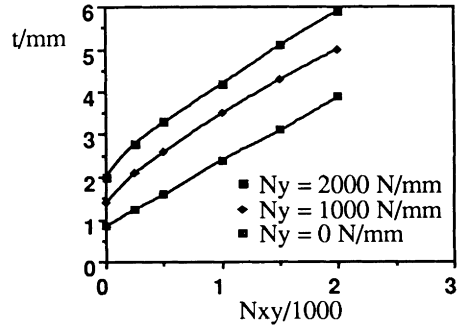
(b) $\underline{N} = [1000,Ny,Nxy]$ N/mm;
$\underline{M} = \underline{0}$ Nmm/mm.
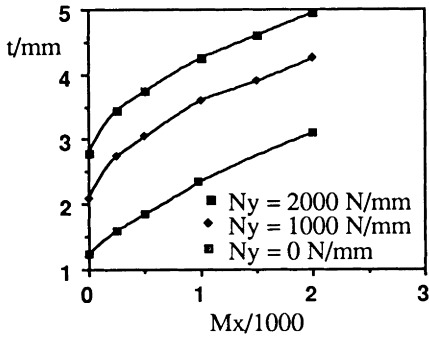
(c) $\underline{N} = [1000,Ny,250]$ N/mm;
$\underline{M} = [Mx,0,0]$ Nmm/mm.
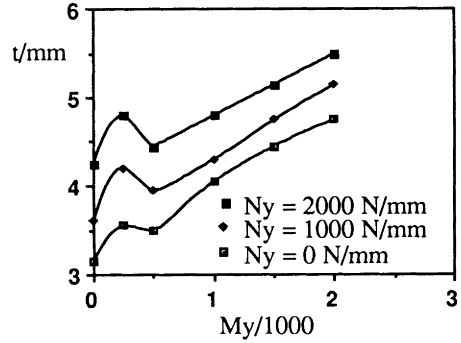
(c) $\underline{N} = [1000,Ny,250]$ N/mm;
$\underline{M} = [1000,My,0]$ Nmm/mm.
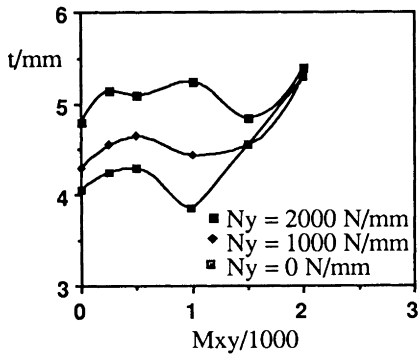
(e) $\underline{N} = [1000,Ny,250]$ N/mm;
$\underline{M} = [1000,1000,Mxy]$ Nmm/mm.
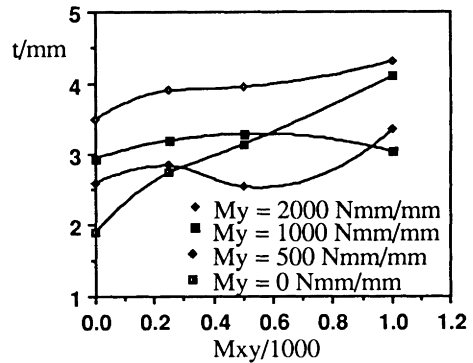
(f) $\underline{N} = \underline{0}$ N/mm;
$\underline{M} = [1000,My,Mxy]$ Nmm/mm.

Figure 2. Thickness of laminated plate designs derived using the heuristic method.

Table 2
CFRPHS914 laminates obtained using the CODEX and COMPLEX methods with the Tsai-Hill failure criterion

load/1000		lay-up	thickness (mm)	
$\underline{N}$ (N/mm)	$\underline{M}$ (Nmm/mm)		CODEX	COMPLEX
[2, -1, 0.5]	[0, 0, 0]	$[0°/90°]_{sym}$	8.95	6.7
[2, -1, 0.5]	[0, 0, 0]	$[45°/-45°]_{sym}$	18.8	18.9
[2, -1, 0.5]	[0, 0, 0]	$[0°/45°/-45°/90°]_{sym}$	3.7	3.65
[2, -1, 0.5]	[0, 0, 0]	$[0°/45°/-45°/0°/90°]_{sym}$	3.7	3.65
[2, -1, 0.5]	[0, 0, 0]	$[\{0°/45°/-45°/0°/90°\}_i, i=1, 2]_{sym}$	3.8	3.9
[0, 0, 0]	[2, -1, 0.5]	$[0°/90°]_{sym}$	7.35	6.35
[0, 0, 0]	[2, -1, 0.5]	$[45°/-45°]_{sym}$	10.7	10.7
[0, 0, 0]	[2, -1, 0.5]	$[0°/45°/-45°/90°]_{sym}$	4.8	4.7
[0, 0, 0]	[2, -1, 0.5]	$[0°/45°/-45°/0°/90°]_{sym}$	5.4	4.7
[0, 0, 0]	[2, -1, 0.5]	$[\{0°/45°/-45°/0°/90°\}_i, i=1, 2]_{sym}$	4.7	4.9
[1, 1, 0.25]	[1, 2, 0]	$[0°/90°]_{sym}$	6.7	6.5
[1, 1, 0.25]	[1, 2, 0]	$[45°/-45°]_{sym}$	8.4	8.1
[1, 1, 0.25]	[1, 2, 0]	$[0°/45°/-45°/90°]_{sym}$	6.2	6.15
[1, 1, 0.25]	[1, 2, 0]	$[0°/45°/-45°/0°/90°]_{sym}$	6.15	6.2
[1, 1, 0.25]	[1, 2, 0]	$[\{0°/45°/-45°/0°/90°\}_i, i=1, 2]_{sym}$	5.8	6.0

5. INTEGRATED DESIGN OF STRUTS AND FLOORBEAM

The CODEX2 approach is also used when we are dealing with a configuration of components and for which we need to do finite element analysis (FEA). In Figure 3 is shown a configuration of floorbeam and struts. Figure 4 shows a dataflow diagram for the integrated design of this based on the CODEX2 approach. The hatched areas correspond to the boxes in Figure 1, with the beam and strut design modules constituting the initial design procedure, and the FEA and failure analysis modules constituting the analysis.

The configuration parameters define the geometry of the structure as a whole, the points of application of the external loads and the maximum allowable deflection. From these can be derived the strut length and orientation, while the beam and strut end conditions, material and shape must be selected by the user. The beam shear load and bending moment and the strut compressive load are initially estimated from the external forces and the overall geometry.

The beam and strut parameters are then used in separate initial design programs to derive the respective approximate designs, leading to an initial design for the overall configuration. This is then formulated as a finite element problem and analysed giving the forces and

displacements at each node. From these we obtain the forces in the beam and struts and carry out stress analyses allowing us to calculate their respective failure and buckling factors; also for the beam we can derive a deflection factor, by comparing the maximum deflection with the prescribed maximum allowable deflection.

(a) beam and struts configuration   (b) variation of strut position
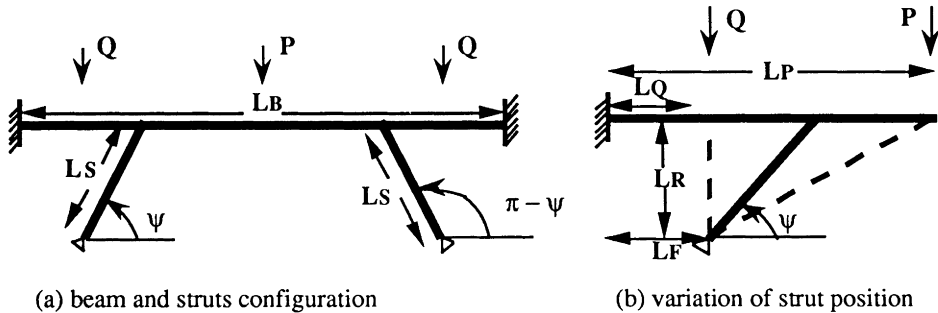
Figure 3. Geometry of floorbeam and struts.

These factors and the predicted modes of failure then become inputs to a set of redesign rules which infer the most effective design modifications. The user then updates the beam and strut geometries on the basis of these suggestions (or not) and a new finite element analysis is performed. The output from the new FEA is then used as the input to a further invocation of the redesign rules and the process continues cyclically until the failure factors reach some values satisfactory to the user.

5.1. Initial strut design
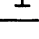
The initial design of the strut is based on the procedures developed by Wu and Webber [12] for the optimisation of the dimensions of any of the seven cross-sectional shapes shown in Table 3. The parameters for strut design are: the end conditions, i.e. simply supported at both ends, fixed at both ends, or one end fixed and the other simply supported; the material, which must be one of those used in the plate design module; the shape; the compressive end-load; and the length across which the strut is to span.

These are all specified directly by the user with the exception of the load and the length. The load is approximated from the magnitudes of the external loads applied to the beam: for example if the total vertical beam load were 4000 N, then the load in each strut (for the purposes of the initial design) would be assumed to be 2000 N. The strut spanning length is derived from the geometry of the overall configuration as specified by the user.

The criterion used for the optimisation is that of simultaneous occurrence of local and global buckling. For example in the I-section there are two possible modes of global buckling corresponding to the two axes perpendicular to the principal strut axis, and two modes of local buckling corresponding to the web and any of the half flanges. The global buckling equations relate the buckling load to the second moment of area

Table 3
Strut cross-sectional shapes

I-section	⊥
C/channel section	⊏
Modified I-section	⊥
Square section	☐
T-section	⊤
Circular tube section	◯
Modified T-section	⊤
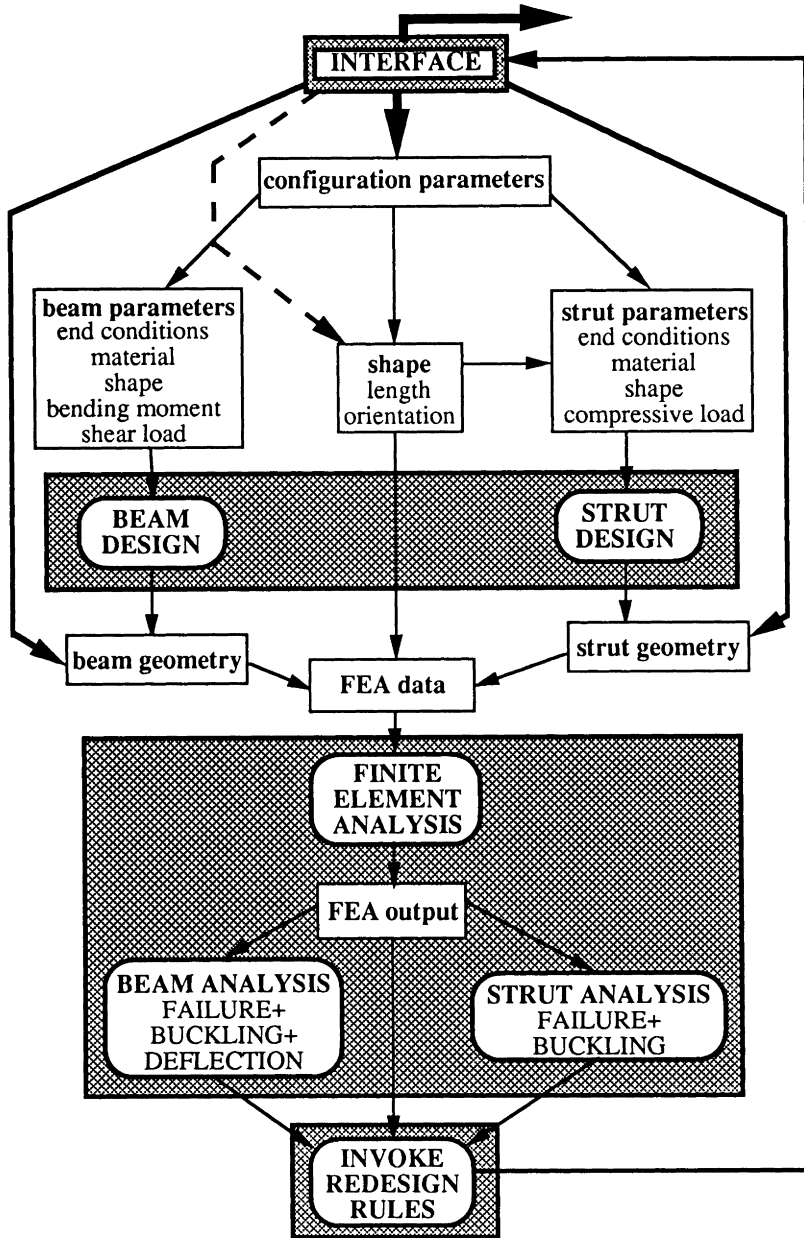
Figure 4. Dataflow graph for the design of a configuration of floorbeam and struts.

about the relevant axis and involve a buckling constant that depends on the end conditions.

The web is considered as a long flat plate simply supported on both sides: values for the buckling load for a composite plate of this type are obtained from [20]. The half flanges on the other hand have one side simply supported and the other side free: we must therefore employ the iterative method of [21] to evaluate the required buckling load.

Equating the buckling loads leads to four equations from which we can solve for the four unknowns denoting the widths and thicknesses of the web and flanges. The procedure is similar for the other shapes, although for the modified T-section there are six equations with seven unknowns for which we have to minimise the area using Lagrangian multipliers and solve using Newton-Raphson iteration.

The strut dimensions obtained using this method are then analysed for first ply failure using one of the four failure criteria available in the plate analysis module. If failure does occur then the strut cross-section is resized appropriately; generally however the buckling load is much lower than the first ply failure load.

The strut design procedure also allows the design of end fittings in the case of the I-section and tubular strut; however these are not yet considered in the overall design strategy.

5.2. Initial beam design

Initial design of the beam is based on the approximate method of Morton and Webber [22], which is similar to the approach used in the strut design above. Up to now it has only been fully developed for the I-beam, although the procedure would be very similar for any beam of constant cross-section. The method is summarised below.

The approximate beam design procedure results in a set of values for the six dimensions of an I-beam cross-section which will approximately minimise the cross-sectional area subject to certain design constraints. This procedure is iterative since we must begin with an initial set of flange dimensions in order to calculate a half-flange buckling coefficient using the method of [21].

To simplify the analysis we make a number of assumptions. We are concerned with a simply supported I-beam loaded at the midpoint. A maximum deflection is prescribed for the beam, and shear deformation is neglected. The bending moment is assumed to be taken by the flanges, so that the flanges' lay-up is $[0°/90°/0°]$ with t_{90} about 10% of t_0. The shear force is assumed to be taken by the web, so that the web's lay-up is $[45°/–45°/–45°/45°]$, with all plies of equal thickness.

We equate the expressions for local buckling loads in the web and flanges to the internal loads derived for the given maximum beam deflection. In order to algebraically equate the internal shear load in the web to the pure shear buckling load, this latter quantity is formulated by a linear approximation to the graphs in Figure 5 of [20]. For this purpose the plate length is taken to be equal to its width by assuming that internal stiffeners are built in at intervals along the web. We also assume for this initial design stage that the pure bending load along the beam axis can be ignored, since it varies from negative to positive across the depth of the web, and also varies along the length of the web, as it depends on the bending moment. We equate the local half-flange buckling loads to the internal loads when the deflection equals the prescribed maximum allowable.

The force and moment equilibrium equations are then formulated for given maximum allowable deflection. We assume that the two flanges are of equal size so that the force equilibrium equation simplifies to stating that the neutral axis is in the centre of the web. We are thus left with three equations for the four unknowns corresponding to the thickness and width of the flanges and the thickness and depth of the web. A minimisation of the cross-sectional area subject to these equations gives us the new cross-sectional dimensions. The flange dimensions are then updated and the above procedure is repeated until the flange dimensions converge. This usually requires about 40 iterations, but the evaluation at each iteration is straightforward.

5.3. Analysis

The analysis module has three main components: finite element analysis, strut analysis and beam analysis.

5.3.1. Finite element analysis

Parameters for the FEA are derived from the beam and strut geometries and mechanical properties. A simple FEA module has been implemented for the analysis of frames consisting of connected one-dimensional beam elements based on the the formulations of Ross [23] and Rao [24]. The elements may be either simply supported or fixed. For our analysis we assume that the beam ends are fixed and the strut ends are simply supported.

There are three different topologies that arise, depending on the relative values of L_Q and L_F and on where the struts join the beam. If the struts meet at the midpoint of the beam, then only 7 nodes and 6 elements are required. If the point of application of the Q-load is outside or inside the strut attachment, i.e. L_Q is less or greater than $(L_F + L_R/\tan \psi)$, respectively, then 9 nodes and 8 elements are required.

The analysis consists of evaluating the element stiffness matrices and global stiffness matrix, solving for the unknown displacements and forces and transforming them into local element co-ordinates. From these we obtain the loads important to the component analysis, namely the loads in the strut and the maximum shear force and bending moment in the beam.

5.3.2. Strut analysis

Even though there will usually be a bending moment and shear load in the strut, analytical tools are not currently available to determine the buckling loads in a composite strut under a multi-axial load, and so we have to assume a purely compressive load. We therefore apply the formulas for the buckling load used in section 5.1 for the strut initial design. We also perform a first ply failure analysis on the strut. We end up with a number of failure factors relating to the different failure modes. For example for the I-section we have two global buckling failure factors, two local buckling failure factors and two first ply failure factors.

5.3.3. Beam analysis

The compressive loads in the I-beam flanges and web are found from the shear force and bending moment using the analysis of [22]. Classical plate theory is then employed to derive the stresses and strains in the material directions of each ply. Since the axial load varies across the web from positive to negative, the ply stresses in the material directions will vary across the web accordingly. The maximum value of the first ply failure factor is found to occur at either the top or bottom of the web: these are therefore the only locations at which it is evaluated.

The internal compressive load in the upper (or lower) flange is compared with the theoretical buckling load to derive a flange buckling factor. The buckling load for the half flanges is found using the method of [21] and the formulas employed in the beam initial design procedure.

For the web we have a pure bending load and a shear load. Since the flanges may be asymmetric, the situation is not exactly one of pure bending; however if the flanges are of a similar size we can make the approximation of assuming a pure bending load equal to the average of the loads in the top and bottom of the web. The internal loads in the web are compared with the theoretical pure bending and shear buckling loads using a quadratic failure criterion for combined loads to derive a web buckling factor. The isotropic approximation used in the estimation of the buckling load due to pure bending is examined in [22].

The maximum deflection is calculated from the FEA results and compared with the prescribed maximum allowable deflection to derive a deflection factor.

5.4. Redesign rules

The analysis results in a number of failure factors relating to the different possible modes of failure in the strut and beam (including exceeding the maximum allowable deflection which is henceforth referred to as "deflection failure"). In the case of a first ply failure factor exceeding 1 in any of the component plates in the strut or beam similar redesign rules to those employed in the plate module can be applied. However in general failure is most likely to occur due to buckling or deflection failure.

For global buckling of the strut the buckling load depends on the second moment of area about the relevant axis. With the I-section, for example, global buckling parallel to the web will therefore depend on the square of the web width, while global buckling parallel to the flanges will similarly depend on the square of the flange width. Thus the appropriate resizing heuristics will be

IF strut buckles parallel to web

THEN widen web by (buckling factor)$^{1/2}$

IF strut buckles parallel to flanges

THEN widen flanges by (buckling factor)$^{1/2}$

For local flange and web buckling in the strut or beam, the buckling load is proportional to the cube of the plate thickness (see [22]). Therefore the rules thicken the plate by the cube root of the buckling load factor, viz

IF flange buckles

THEN thicken all plies in flange by (buckling factor)$^{1/3}$

IF web buckles

THEN thicken web by (buckling factor)$^{1/3}$

The deflection of the beam is proportional to the square of the web depth since it depends on the second moment of area of the cross-section. Therefore the rule for deflection failure deepens the web by the square root of the deflection factor, viz

IF maximum deflection of beam exceeded

THEN deepen beam web by (deflection factor)$^{1/2}$

The result of the application of these rules will be a set of modifications of the cross-sectional dimensions for the strut and the beam which the the user will be invited to implement.

6. CONCLUSIONS

The rule-based technique has been seen to be effective for the design of composite laminated plates. Extending the technique to the integrated design of a floorbeam and struts configuration has been shown to be feasible, although it has not been fully implemented.

7. ACKNOWLEDGEMENTS

8. REFERENCES

[1] Zumsteg, J.R., & Flaggs, D.L., "Knowledge-based analysis and design systems for aerospace structures", in Proc. Winter Annual Meeting ASME, Miami Beach, Florida, pp. 67-80, 1985.

[2] Chehayeb, F.S., Connor, J.J., & Slater, J.H., "An environment for building engineering knowledge based systems", in Proc. Winter Annual Meeting ASME, Miami Beach, Florida, pp. 9-28, 1985.

[3] Zumsteg, J.R., Pecora, D., & Pecora, V.J., "A prototype expert system for the design and analysis of composite material structures", in Proc. ASME International Computers in Engineering Conference, Boston, Massachusetts, pp. 137-143, 1985.

[4] Pecora, D., Zumsteg, J.R., & Crossman, F.W., "An application of expert systems to composite structural design and analysis", in Proc. Winter Annual Meeting ASME, Miami Beach, Florida, pp. 135-147, 1985.

[5] Webber, J.P.H., "Some laminated plate optimum design studies using an interactive computer programme", Aeronautical Journal of the Royal Aeronautical Society **92**, pp. 107-114, 1988.

[6] Burden, P.I., & Lipton, B.J., "An interactive computer program for the design of composite laminated plates", Department of Aerospace Engineering Report no. 368, University of Bristol, Bristol.

[7] Morton, S.K., & Webber, J.P.H., "Uncertainty reasoning applied to the assessment of composite materials for structural design", Engineering Optimization **16**, pp. 43-77, 1990.

[8] Webber, J.P.H., & Morton, S.K., "An expert system for laminated plate design using composite materials", Computers and Structures **37**, pp. 1051-1067, 1990.

[9] Wu, C.M.L., Webber, J.P.H., & Morton, S.K., "A knowledge based expert system for laminated composite strut design", The Aeronautical Journal **95**, pp. 1-20, 1991.

[10] Morton, S.K., & Webber, J.P.H., "Heuristic methods in the design of composite laminated plates", Composite Structures **19**, pp. 207-265, 1991.

[11] Morton, S.K., Webber, J.P.H, & Wu, C.M.L., "A Computer Expert System for Composite Plate and Strut Design", *in* Hernandez, S., & Brebbia, C.A. (Eds.), **Optimization of Structural Systems and Industrial Applications**, Proc. Second International Conference on Computer Aided Optimum Design of Structures (OPTI-91), Boston, Massachusetts, pp. 629-642, 1991.

[12] Wu, C.M.L., & Webber, J.P.H., "Minimum weight optimization of composite laminated struts", Engineering Optimization **17**, pp. 21-63, 1991.

[13] Baldwin, J.F., Martin, T.P., & Pilsworth, B.W., **FRIL manual**, FRIL Systems Ltd., Bristol, 1988.

[14] Engineering Sciences Data Unit, "Failure criteria for an individual layer of a fibre reinforced composite laminate under in-plane loading", ESDU Item no. 83014, 1986 *(private communication)*.

[15] Herakovich, C.T., "Free edge effects in laminated composites", *Chapter 4*, **Handbook of Composites 2** (Eds. Herakovich, C.T., & Tarnopol'skii, Y.M.), Elsevier, Amsterdam, 1989.

[16] Kassapoglou, C., & Lagace, P.A., "An efficient method for the calculation of interlaminar stresses in composite materials", Journal of Applied Mechanics **53**, pp. 744-750, 1986.

[17] Brewer, J.C., & Lagace, P.A., "Quadratic stress criterion for initiation of delamination", Journal of Composite Materials **22**, pp. 1141-1155, 1988.

[18] O'Brien, T.K., "Characterization of delamination onset and growth in a composite

laminate", in Damage in Composite Materials, ASTM STP 775 (Ed. Reifsnider, K.L.), American Society for Testing and Materials, pp. 140-167, 1982.

[19] Box, M.J., "A new method of constrained optimization and a comparison with other methods", The Computer Journal **8**, pp. 42-52, 1965.

[20] Engineering Sciences Data Unit, "Buckling of rectangular specially orthotropic plates", ESDU Item 80023, 1980 *(private communication)*.

[21] Webber, J.P.H., Holt, P.J., & Lee, D.A., "Instability of carbon fibre reinforced flanges of I section beams and columns", Composite Structures **4**, pp. 245-265, 1985.

[22] Morton, S.K., & Webber, J.P.H., "Optimal design of a composite I-beam" *(to appear)*, 1992.

[23] Ross, C.T.F., **Finite Element Methods in Structural Mechanics**, Ellis Horwood Ltd., Chichester, Sussex, 1985.

[24] Rao, S.S,. **The Finite Element Method in Engineering**, Pergamon Press, Oxford, Oxfordshire, 1982.

Composite structures preliminary design :
The satisfaction of mechanical requirements

S. QUILICI and O. DEBORDES

Institut Méditerranéen de Technologie, Technopole de Chateau-Gombert
13451 MARSEILLE CEDEX 13

Laboratoire de Mécanique et d'Acoustique, 31, Chemin Joseph Aiguier
13402 MARSEILLE CEDEX 9

Abstract

An original method, combining Artificial Intelligence type of algorithms with finite element analysis and optimization is proposed for the preliminary design of laminated composite structures. Design requirements taken into account are allowable stresses and displacements, lowest natural frequency and buckling load. The methodology proposed is based upon heuristic searches through families of solutions obtained by defining the total laminate as a repetition of sublaminates.

1. INTRODUCTION

One of the main drawbacks for the application of Artificial Intelligence to structural design of composite structures is the satisfaction of mechanical requirements.Indeed if part of the designer's knowledge can be described as logical rules in a knowledge base, it is difficult to model in such an easy way the process of determining the fibre angles, layer thicknesses and stacking sequence of a laminated structure to insure its mechanical integrity.In this study we propose a methodology, combining design rules written in PROLOG with Finite Element and Optimization procedures written in FORTRAN to determine the optimal laminate satisfying the following mechanical requirements :

Stiffness Requirement - bounds on deflections at different points of the structure
Strength Requirement - allowable stresses at each point
Stability Requirement - critical buckling load below the applied loading
Frequency Requirement - lowest natural frequency above a specified value

The type of structures involved are laminated thin shells under coupled in plane and bending loadings. Using a material database, families of solutions are constructed and explored by means of heuristic algorithms. For each composition one has to solve a simple unidimensional optimization problem.

Making use of these simple solutions the system can then generate "complex solutions" by solving more comprehensive optimization problems depending on the particular application. A solution to the preliminary design problem is thus found step by step and intermediate results are stored in an output database and used to control and accelerate ulterior optimization phases. In this basic structure could subsequently be integrated logical rules aimed at the satisfaction of non-mechanical requirements.

2. DETERMINATION OF SIMPLE SOLUTIONS

The problem is to find the minimum weight laminate to satisfy the different mechanical requirements under the following assumptions :

Assumption A1. The thin shell thickness is a constant over the structure.
Assumption A2. The laminate layers are all made of the same unidirectional.

Restricting fibre orientations to the dicrete set $\theta_1, \theta_2, \dots, \theta_d$, this problem can be written:

$$\text{Min} \left[\sum_{i=1}^{n} n_{\theta i} \right] \qquad \qquad \underline{\text{Problem } P_O}$$
$$(n_{\theta 1},\dots,n_{\theta d}) \in \mathbb{N}^d$$

$$\text{subject to}: \quad g_{jC}(\, \mathfrak{A}(n_{\theta 1},\dots,n_{\theta d})\,) \geq 0 \quad \text{generated by the mechanical requirements}$$

$$\mathfrak{A} \in \mathcal{E} \text{ set of allowable stacking sequences}$$

$$n_{\theta i} \in \mathbb{N} \text{ number of plies with orientation } \theta_i$$

Problem P_O is an integer non convex problem where the constraints $g_j(s)$ are implicit functions of the design variables $n_{\theta i}$.
Here rather then solving P_O directly we make the following additional assumption :
Assumption A3. The laminate is the repetition of n (unknown) times the same sublaminate (of unknown but simple composition).

Designing with sublaminates

This method of design was first introduced by Tsaï [1] as an alternative to conventional optimization for laminates under in-plane loadings. The laminate is defined as the repetition of n times (n being called the repeat index) a laminate of fixed composition called a "sublaminate". A sublaminate family $\mathcal{F}$ is defined by :
  - a number p of plies constant for all the family sublaminates
  - a number d of orientations constant (we will take d=4 in what follows)
  - the value of these orientations

A sublaminate $s \in \mathcal{F}$ is coded : $s = (\, c_{\theta 4}.c_{\theta 3}.c_{\theta 2}\, c_{\theta 1}\,)$ with $c_{\theta 1}+c_{\theta 2}+c_{\theta 3}+c_{\theta 4} = c$

(cθi number of plies with orientation θi)

We can generalize this approach to the case of bending loading, by fixing the stacking sequence at a sublaminate level. Furthermore, as a first order approximation, the effect of the core can be neglected, allowing to represent sandwich type of structures as shown on Figure 1 Configuration 2.

Figure 1
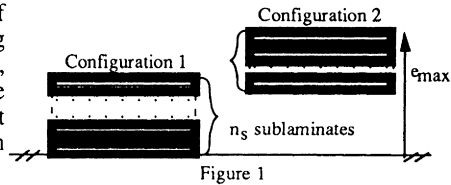
Decomposition of the initial optimization problem
Problem P_O is decomposed into the following two subproblems :
- An **inner subproblem** P_N solved numerically to find the repeat index of a given sublaminate e.g. the lowest number of times one has to repeat the sublaminate to satisfy the mechanical requirement:

$$\text{Find } r_C(s) = \underset{n_s \in \mathbb{N}}{\text{Min}} \left\{ n_s \text{ tel que } g_j(n_s.s) \geq 0 \right\} \qquad \underline{\text{Problem } P_N}$$
s a given sublaminate
g_j constraints generated by mechanical requirement C

- An **outer subproblem** P_L solved by means of an heuristic algorithm to find the sublaminate of lowest repeat index in family $\mathcal{F}$:

$$\text{Find } s^* \text{ such that } r_C(s^*) = \underset{s \in \mathcal{F}}{\text{Min}} \{ r_C(s) \} \qquad \underline{\text{Problem } P_L}$$

Ranking of the sublaminate family - Resolution of problem P_L

In simple cases where there is no need for finite element analyses, Tsaï resorts to an exhaustive search through family $\mathscr{F}$ to solve P_L. This method presents the advantage to yield not only the optimum but also a "ranking" of family $\mathscr{F}$ by increasing repeat index.

Such a ranking of solutions gives us the flexibility needed to include the optimization procedures within a conventional expert system to insure the satisfaction of non mechanical requirements; the optimum of P_L can be a poor solution of the global preliminary design problem, if particularly difficult to process in practice for example. In this case, using the ranking method, alternate solutions are available. Furthermore we benefit of a great flexibility with regards to multiple load cases and the satisfaction of each mechanical requirement regardless of the others, the final ranking being determined by simple comparison of elementary rankings obtained for each requirement under each load case.

The aim is here to find a "good solution" of problem P_L and avoid an exhaustive search.
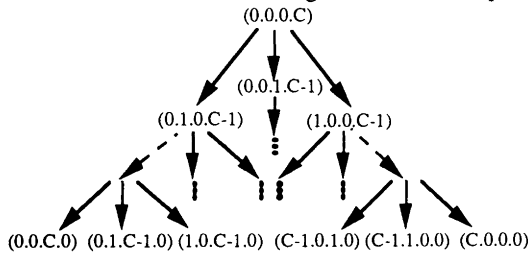
A tree-like representation is used to represent the sublaminate family by defining a particular direction as "descent direction". To each node of the tree are associated three sons by permuting a ply from the descent direction to one of the other three directions. The top of the tree is the sublaminate for which all plies are oriented in the descent direction.

Figure 2

The algorithm proposed simply amounts to choose a descent direction, to compute the repeat index of the sublaminate at the top of the tree and the ones of his three sons, to define the son with lowest repeat index as the new father and so on, until the best son's repeat index is greater then his father's one, in which case we stop the descent (Figure 3).

Initialization S_p^1 (0.0.0.C)
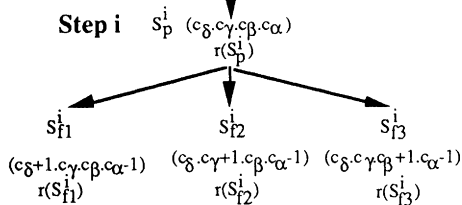
Descent algorithm

Let $S_{f\,opt}^i$ be the best son at step i:

$$r(S_{f\,opt}^i) = \text{Min } (\ r(S_{f1}^i)\ ,\ r(S_{f2}^i)\ ,\ r(S_{f3}^i)\ )$$

if $\ r(S_{f\,opt}^i) \leq r(S_p^i)\ $ then $\quad S_p^{i+1} = S_{f\,opt}^i$

else end

  optimal solution = S_p^i

Figure 3

The quality of the solution given by this algorithm strongly depends on the initialization, that is the descent direction. In practice we will use the following heuristic: compute all four unidirectional sublaminates (0.0.0.C), (0.0.C.0), (0.C.0.0), (C.0.0.0) and take as descent direction the direction giving the lowest repeat index.

To rank the family up to an order higher than one, we must modify the descent algorithm above to account for the case where one of the sons at step i has already been ranked. Denoting by S_p^i the solution at step i, we will carry on the descent from:

- sons of S_p^i ranked before step i, by setting $r(S_{f\,ranked}^i) = r(S_p^i)$
- the best son of S_p^i un-ranked at step i.

Finite Element Techniques

Let us consider the case of thin laminated shells under coupled in-plane and bending loading, extension of the classic Love Kirchhoff hypothesis where:
- each ply of the laminate is thin and transversely istropic or orthotropic,
- the ply is under a state of plane stress (no transverse shear effect).
The behavior law relating generalized stress and strain can be written as:

$$\begin{Bmatrix} N \\ M \end{Bmatrix} = \begin{bmatrix} A & B \\ B^t & D \end{bmatrix} \begin{Bmatrix} \varepsilon \\ \chi \end{Bmatrix} \quad \text{where}: \quad A_{ij} = \sum_k (Q_{ij})^k (h_k - h_{k-1}) \quad D_{ij} = \frac{1}{3} \sum_k (Q_{ij})^k (h_k^3 - h_{k-1}^3)$$

$$B_{ij} = \frac{1}{2} \sum_k (Q_{ij})^k (h_k^2 - h_{k-1}^2)$$

with $(Q_{ij})^k$ stiffness of ply k and h_k distance of ply k to the middle plane.

We limit ourselves to the case of symmetric laminates for which $B_{ij} = 0$. The laminate stiffness is then completely defined by 12 stiffness parameters, the coefficients of (3,3) symmetric matrices $[A]$ and $[D]$ (p_{i_m} i=1,6 for in plane behavior, p_{i_f} i=1,6 for bending).

The structure is discretized into thin shell DKT or DKQ elements [2]. To allow a straightforward calculation of the global stiffness matrix $[K_g]$ for different sublaminate compositions and repeat indexes n_s, we proceed to the assembly of 12 global stiffness matrices ($[K_m^i]$ et $[K_f^i]$, i=1,6) obtained by setting all stiffness parameters but one to zero so as to have the following simple linear relation:

$$[K_g(n_s,s)] = \sum_{i=1}^{6} (p_{i_m}(n_s,s) [K_m^i] + p_{i_f}(n_s,s) [K_f^i]) \tag{1}$$

We will need the first derivatives of behavioral quantities (displacements, stresses, ...) with respect to the repeat index n_s. Such sensitivity analysis can easily be performed using the first derivative of the global stiffness matrix obtained explicitly by:

$$\frac{\partial [K_g(n_s)]}{\partial n_s} = \sum_{i=1}^{6} \left[\frac{\partial p_{i_m}(n_s)}{\partial n_s} [K_i^m]_k + \frac{\partial p_{i_f}(n_s)}{\partial n_s} [K_i^f]_k \right]$$

Expression of the different mechanical constraints
For a given sublaminate, the constraints generated by the mechanical requirements are implicit functions of the repeat index.

Stiffness requirement. The corresponding constraints can be expressed as:

$$g_j(n_s) = 1 - \frac{u_j^2(n_s)}{u_{jb}^2} \geq 0 \qquad \text{for } j=1,...,n_b \tag{2}$$

with : n_b number of displacement bounds, u_{jb} bound on displacement j

Strength requirement. We will use the Tsaï-Wu criterion which is written for each ply k of the sublaminate: $C(\{\sigma^k\}) = F_{ij} \sigma_i^k \sigma_j^k + F_i \sigma_i^k \leq 1$, with $\{\sigma^k\}$ the stresses in the material orthotropy axes. The relations to be verified at each integration point for each orientation of the last sublaminate in the stacking sequence (for each "ipo") can be expressed as:

$$g_{pgo}(n_s) = 1 - C(\sigma^{pgo}(n_s)) \geq 0 \qquad \text{for each ipo} \tag{3}$$

Frequency requirement. The associated constraint is of the form:

$$g(n_s) = 1 - \frac{\omega^2}{z(n_s)} \geq 0 \tag{4}$$

where ω^2 is the square of the forcing frequency , $z(n_s)$ the lowest eigenvalue of :

$$\left[K_g(n_s)\right] \{U(n_s)\} = z(n_s) \left[M_g(n_s)\right] \{U(n_s)\} \tag{5}$$

with $\left[M_g(n_s)\right]$ the global mass matrix, $\{U(n_s)\}$ the eigenvector associated to $z(n_s)$.

Stability requirement.

Let $f(n_s)$ be the smallest positive eigenvalue of equation:

$$\left[K_g(n_s)\right] \{U(n_s)\} = f(n_s) \left[K_{geo}(n_s)\right] \{U(n_s)\} \tag{6}$$

where $\left[K_{geo}(n_s)\right]$ is the so-called geometrical stiffness matrix
The constraint to be satisfied to preclude elastic instability is of the form:

$$g(n_s) = 1 - \frac{1}{f(n_s)} \geq 0 \tag{7}$$

Resolution of P_N - Constraint approximation

The problem to be dealt with can be stated as:

$$\underset{n_s \in \mathbb{N}}{\text{Min}} \{ \ n_s \ , \ g_j(\ n_s \ ) \geq 0 \ \text{for} \ j=1,...,n_c \} \qquad \underline{\text{Problème } P_N}$$

n_c = number of constraints generated by the mechanical requirement C

An iterative procedure is used to solve this non-linear problem (n_s^i stands for the value of n_s at iteration i). Because of the constraints implicit dependence upon n_s, it is interesting to use explicit approximation forms proposed by Prasad ([3],[4]) as an extension of the mixed linearization methods introduced by Fleury ([5],[6]) and Schmit [7]:

$$g_j(n_s) \ \text{approximated by} \quad \widetilde{g}_j^i(n_s) = g_j(n_s^i) + (\ \gamma - \gamma^i) \ \frac{\partial g_j(n_s^i)}{\partial \gamma} \tag{8}$$

$$\text{with :} \quad \gamma = \frac{1}{p-1} \ n_s^{1-p} \qquad \text{for} \ p \neq 1$$

$$\gamma = -\ln(n_s) \qquad \text{for} \ p = 1 \ ,$$

a first order Taylor series expansion at point n_s^i in terms of the intermediate variable γ, where the tuning parameter p is chosen to best represent the dependence of a particular behavorial constraint upon the repeat index. Depending on the type of loading and the behavorial constraint we use the following values for exponent p (Table 1).

Requirement	Loading		Both	
	In-plane	Bending	Laminate	Sandwich
Stiffness	p=3	p=7	3≤p≤7	p=3
Strength	p=2	p=4	2≤p≤4	p=2
Frequency		p=3	1≤p≤3	
Stability			3≤p≤5	p=3

Table 1

(8) can be written : $\widetilde{g}_j^i(n_s) = g_j(n_s) - \dfrac{n_s^i}{p-1}\left(\dfrac{\partial g_j(n_s^i)}{\partial n_s}\right)(n_s^{1-p} - n_s^{i\,1-p})$ $p \neq 1$ (9)

We then replace the resolution of P_N by the resolution of a sequence of approximate problems $\widetilde{P}_N^i$ written at step i:

$$\underset{n_s \in \mathbb{N}}{\text{Min}} \{\ n_s\ ;\ \widetilde{g}_j^i(n_s) \geq 0 \quad \text{for } j=1,...,n_c\ \} \qquad\qquad \underline{\text{Problem } \widetilde{P}_N^i}$$

Always taking p > 1 in equation (8) according to Table 1, the solution n_s^{i+1} of $\widetilde{P}_N^i$ is:

$$n_s^{i+1} = \underset{j}{\text{Max}} \left\{ \left[\dfrac{n_s^{i\,p}\, \dfrac{\partial g_j(n_s^i)}{\partial n_s}}{(p-1)\, g_j(n_s^i) + n_s^i\, \dfrac{\partial g_j(n_s^i)}{\partial n_s}} \right]^{\frac{1}{p-1}} , \text{ for } j=1,...,n_c \right\} \qquad (10)$$

System architecture
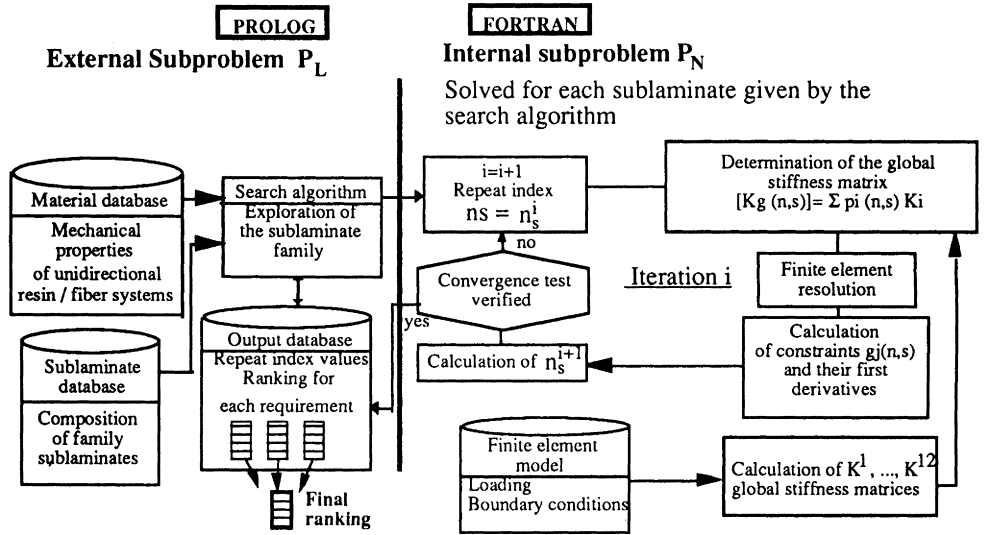
Figure 4

3 . DETERMINATION OF COMPLEX SOLUTIONS

We intend here to remove previous assumptions A1 and A2. Retaining a sublaminate type of decomposition, we are led to define the following problem obtained by removing A1:
Find the sublaminate giving the least weight thickness distribution over different regions of the structure and satisfying the mechanical requirements

$$\underset{s \in \mathcal{F}}{\text{Min}} \left(\mathcal{C}(s) = \sum_{i=1}^{n_r} r_i(s).a_i \right) \qquad\qquad \underline{\text{Problem } P_C}$$

subject to :   with : n_r total number of regions
    $g_j(\ s, r_1(s),...,r_{n_r}(s).) \geq 0$ a_i region i area
                                $r_i(s)$ sublaminate s repeat index over region i

As in the case of simple solutions we decompose problem P_{C_1} into two subproblems:

inner subproblem: Given a sublaminate s, find the optimal repeat index distribution $r_i(s)$

Find $(r_1(s),...,r_{n_z}(s)) \in \mathbb{R}^{n_z}$ such that: $\qquad$ Problem P_{CN}

$$\mathcal{C}(s) = \sum_{i=1}^{n_r} r_i(s).a_i = \underset{(n_{s1},...,n_{snr}) \in \mathbb{N}^{nr}}{\text{Min}} \left(\sum_{i=1}^{n_r} n_{si}.a_i \right)$$

subject to: $\qquad g_i(n_{si}.s_i) \geq 0$

outer subproblem : Find the optimal sublaminate composition in family $\mathscr{F}$

Find $s^* \in \mathscr{F}$ such that:

$\qquad$ Problem P_{CL}

$$\mathcal{C}(s^*) = \underset{s \in \mathscr{F}}{\text{Min}} \left(\mathcal{C}(s) = \sum_{i=1}^{n_z} r_i(s).a_i \right)$$

Outer subproblem P_{CL}

We look for a "good" solution of problem P_{CL} by making use of the simple solution S_{opts} obtained previously under the assumptions A1 and A2. To do this we need to define an ascent algorithm to allow a backtracking up the tree from solution S_{opts}.

Denoting by α the descent direction which gave solution $S_{opts} = (p_\delta.p_\gamma.p_\beta.p_\alpha)$, we calculate the cost (by solving P_{CN}) of the S_{opts} fathers obtained by permutation of a ply from directions β,γ,δ to α. If the best father has a lower cost than S_{opts} we carry on the ascent, else the best father is given as a result of the backtracking (Figure 5).
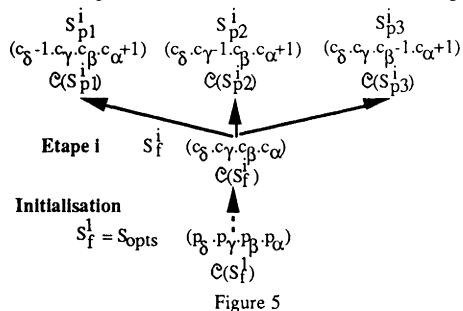
Ascent algorithm

Let $S_{f\ opt}^i$ be the best father at step i :

$$r(S_{f\ opt}^i) = \text{Min}(r(S_{f1}^i),\ r(S_{f2}^i)\ ,r(S_{f3}^i))$$

if $r(S_{f\ opt}^i) \leq r(S_f^i)$ then $S_f^{i+1} = S_{f\ opt}^i$
$\qquad\qquad\qquad\qquad\qquad\qquad\qquad i = i+1$

else end
$\qquad$ **bactracking point $S_a = S_{f\ opt}^i$**

Figure 5

The descent and ascent algorithms are then combined in the following way to avoid a complete search from the top of the tree:

Initialization $\quad s^0 = (c_\delta^0 . c_\gamma^0 . c_\beta^0 . c_\alpha^0) = s_s^*$ $\quad$ simple optimal solution

Step i $\qquad\quad$ Let $s^i = (c_\delta^i . c_\gamma^i . c_\beta^i . c_\alpha^i)$ be the sublaminate at step i

$\qquad\qquad\qquad$ Apply ascent algorithm on s^i to get s_a^i

$\qquad\qquad\qquad$ Apply descent algorithm on s_r^i to get s_d^i

$\qquad\qquad\qquad$ *if* $s_d^i \neq s^i$ $\qquad$ *then*
$\qquad\qquad\qquad\qquad$ $i = i+1$
$\qquad\qquad\qquad\qquad$ go back to step i
$\qquad\qquad\qquad\qquad\qquad\qquad$ *else*
$\qquad\qquad\qquad\qquad$ *end*
$\qquad\qquad\qquad\qquad$ result $s_c^* = s_d^i$

Inner subproblem - Determination of the optimal repeat index distribution for a given sublaminate

Consider problem P_{CN}:

$$\text{Min } (\mathcal{C}(n_1,...,n_r)) \qquad\qquad \underline{\text{Problème } P_{CI}}$$
$$(n_1,...,n_r)\in \mathbb{R}^r$$

subject to :   with : $\mathcal{C}(n_1,...,n_r)$ linear cost function

$g_j(n_1,...,n_r) \geq 0$ of repeat indexes n_i

From a design $n_o=(n_{1_o},...,n_{r_o})$ we define an approximate subproblem $\tilde{P}_{CN}$ by using the previous approximation forms (9) in the case of n_r variables:

$$\tilde{g}_j(n_1,...,n_r) = g_j(n_o) + \sum_{i=1}^{r} \frac{n_{io}}{p_{ji}-1} \left(\frac{\partial g_j}{\partial n_i}\right)_{no} (n_{io}^{\,1-p_{ji}} - n_i^{\,1-p_{ji}}) \qquad p_{ji} \neq 1 \qquad (11)$$

The approximate subproblem $\tilde{P}_{CN}$ is an explicit separable optimization problem with respect to design variables n_i. It is also a convex problem providing the following rule is verified when choosing the exponents p_{ji} depending on the sign of the derivative $\left(\frac{\partial g_j}{\partial n_i}\right)_{no}$:

If $\forall j,i$ $\text{Sign}(p_{ji}) = \text{Sign}(\frac{\partial g_j(n_i^0)}{\partial n_i})$ **then** $\tilde{P}_{CN}$ is convex

In general we obtain positive values of the first derivative of the mechanical constraint g_j with respect to the repeat indexes and exponents p_{ji} can be chosen according to the values given in Table 1. For negative values of $\frac{\partial g_j(n_i^0)}{\partial n_i}$ it is more tricky to guess an appropriate value for exponent p_{ji}. However one can show that we get a more conservative approximation for decreasing values of p_{ji} [3]. In that case we generally take $p_{ji}=-1$ (a more conservative approximation than a linear approximation obtained for $p_{ji}=0$).

$\tilde{P}_{CN}$ is solved by means of an interior point penalty method [8] which consists in the transformation of the initial problem into an unconstrained minimization of a function $\mathcal{F}(n,r)$ such that:

$$\mathcal{F}(n,r) = \mathcal{C}(n_1,...,n_r) + r \sum_j \Phi(\tilde{g}_j(n))$$

The interior penalty functions Φ are extended in the infeasible space by:

$$\Phi(g_j) = \frac{1}{g_j} \qquad\qquad \text{for } g_j \geq g_o, \text{ interior part of the penalty function}$$

$$\Phi(g_j) = \frac{1}{g_o} + A \left(1 - \frac{g_j}{g_o} \right)^3 \qquad \text{for } g_j < g_o, \text{ exterior part of the penalty function}$$

For a given value of the penalty parameter r (which tends to zero) the minimum of function $\mathcal{F}$ is found by application of Newton's method. This implies the calculation of the Hessian of function $\mathcal{F}$, which is straightforward because constraints $\tilde{g}_j$ are known explicitly.

Remark - We can use similar procedures to solve the following problem:
<u>Find the minimum weight laminate made of two different materials with thickness lower than a given value and satisfying the mechanical requirements</u>

Min ($C(s_1,s_2) = r(s_1).p_1 + r(s_2).p_2$) $s_1, s_2 \in \mathcal{F}^2$	Problem P_{C_2}
subject to : $g_j(r(s_1).s_1 + r(s_2).s_2) \geq 0$ $r(s_1).e_1 + r(s_2).e_2 \leq e_{max}$	with : p_1, p_2 cost of material 1 et 2 $r(s)$ sublaminate s repeat index e_i thickness of a sublaminate in material i

In this case, sublaminate the composition of both materials must vary simultaneously when solving the outer subproblem. We are thus led to define two levels in the tree structure:
- a main level where the only varying composition is the one for the sublaminate in the material determined from simple solutions as providing the major part of the laminate thickness.
- a secondary level where, the main level sublaminate composition being fixed, we look for the optimal sublaminate composition in secondary material.

SIMPLE SOLUTIONS EXAMPLE

Consider the structure represented on figure 6 with pressure loading of 0.1 MPa and nodal forces F of 0.05MN.
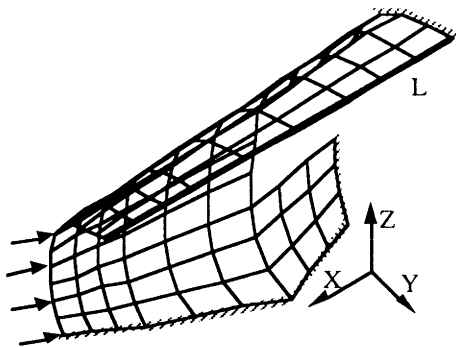
Mechanical requirements.

1. Stiffness: Deflection bounds of 1 mm in directions y et z on line L

2. Strength criterion: $C_{max}(\sigma) \leq 1$

3. Frequency: $\omega_{min}^2 \geq 10^5$

4. Stability: Critical load $f \geq 1$

We use a family with 8 plies and 4 fibre angles (-45°,45°,90°,0°) of 165 sublaminates. (coded ($c_{-45}.c_{45}.c_{90}.c_0$) in the following tables).

Ranking of this sublaminate family with respect to the different mechanical requirements up to an order of 5 is given in Table 2 and 3 for two different materials.

Glass-Epoxy solutions

Ranking	Stiffness		Strength		Frequency		Stability		All	
	s	n_s	s	n_s	s	n_s	s	n_s	s	n_s
1	1.2.4.1	16.6	2.0.6.0	17.0	1.1.6.0	7.60	0.2.6.0	8.24	3.0.5.0	17.7
2	1.3.3.1	16.6	1.0.7.0	17.6	0.1.6.1	7.60	0.3.5.0	8.25	2.0.6.0	18.1
3	0.2.4.2	16.7	3.0.5.0	17.7	1.0.6.1	7.62	1.2.5.0	8.28	4.0.4.0	18.9
4	1.4.2.1	16.8	1.1.6.0	18.2	1.1.5.1	7.62	0.4.4.0	8.30	1.0.7.0	19.0
5	3.3.2.0	16.8	2.1.5.0	18.5	1.0.7.0	7.63	1.3.4.0	8.32	3.1.4.0	19.2

Carbon-Epoxy solutions

Ranking	Stiffness		Stength		Frequency		Stability		All	
	s	n_s	s	n_s	s	n_s	s	n_s	s	n_s
1	1.2.4.1	12.2	2.1.5.0	3.48	1.0.6.1	3.12	0.4.4.0	6.02	1.2.4.1	12.2
2	0.2.4.2	12.3	0.1.5.2	3.50	1.1.5.1	3.12	0.3.5.0	6.12	0.2.4.2	12.3
3	1.3.3.1	12.3	0.2.4.2	3.58	0.1.6.1	3.12	0.1.6.1	6.13	1.3.3.1	12.3
4	1.1.5.1	12.3	1.0.6.1	3.61	1.1.6.0	3.12	1.2.5.0	6.19	1.1.5.1	12.3
5	2.4.2.0	12.3	1.1.5.1	3.61	1.0.7.0	3.17	0.2.5.1	6.19	2.4.2.0	12.3

```
┌─────────────────────────────────┐
│    EXAMPLE WITH THICKNESS       │
│         DISTRIBUTION            │
└─────────────────────────────────┘
```
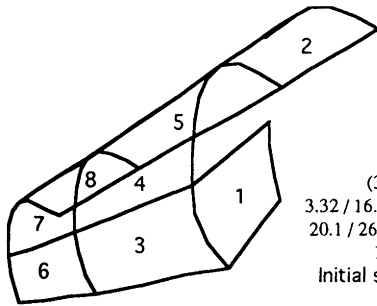
Glass-Epoxy solutions tree search

(2.0.6.0)
3.11 / 17.1 / 2.85 / 7.38 /
19.6 / 23.2 / 12.2 / 9.33
105.95

┌──────────────┐
│ Legend   │
│ (sublaminate)│
│ Rep. Ind. area i │
│ cost   │
└──────────────┘

(3.0.5.0)
3.32 / 16.2 / 2.56 / 8.18 /
20.1 / 26.2 / 4.89 / 10.2
104.45
Initial solution

(2.1.5.0)
2.95 / 16.0 / 2.78 / 7.54 /
19.1 / 26.5 / 4.70 / 9.14
100.55
Optimal solution

(2.0.5.1)
3.28 / 17.2 / 2.84 / 7.81 /
19.5 / 32.7 / 4.72 / 10.1
107.75

(3.1.4.0)
3.10 / 16.6 / 2.82 / 7.79 /
19.5 / 26.8 / 4.61 / 9.88
103.30

(2.2.4.0)
2.90 / 16.2 / 2.71 / 7.40 /
19.0 / 27.7 / 5.30 / 8.79
100.93

(2.1.4.1)
3.11 / 17.0 / 2.68 / 7.61 /
19.4 / 36.0 / 5.75 / 9.51
108.63
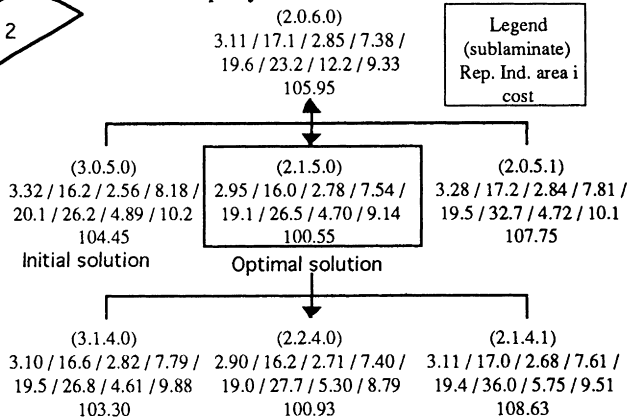
After using the ascent and descent algorithms from the initial solution (3.0.5.0) :

Optimal solution
(2.1.5.0)

Region 1	2	3	4	5	6	7	8
n_s 2.95	16.0	2.78	7.54	19.1	26.5	4.7	9.14

Cost = 100.55

Carbon-Epoxy solutions

(3.2.3.0)
0.76 / 13.3 / 2.55 / 6.43 /
14.9 / 9.26 / 6.32 / 7.63
3013.2

(3.1.4.0)
0.78 / 12.4 / 2.63 / 6.65 /
15.5 / 9.77 / 6.14 / 7.56
3028.1

(2.3.3.0)
0.64 / 15.3 / 2.43 / 5.69 /
12.5 / 7.62 / 5.50 / 7.13
2843.5

(2.2.4.0)
0.64 / 11.4 / 2.70 / 6.33 /
14.9 / 8.52 / 5.60 / 6.83
2840.8

(2.2.3.1)
0.77 / 16.0 / 2.43 / 5.95 /
13.5 / 8.17 / 6.16 / 8.23
3043.2

(2.1.4.1)
0.73 / 12.0 / 2.72 / 6.89 /
16.2 / 8.86 / 5.93 / 8.03
3057.2

(1.3.4.0)
0.60 / 10.6 / 2.64 / 5.94 /
14.3 / 6.99 / 4.92 / 6.07
2646.6
Optimal solution

(1.2.5.0)
0.59 / 11.2 / 2.49 / 5.70 /
13.8 / 7.67 / 5.36 / 6.11
2654.3

(1.2.4.1)
0.65 / 12.8 / 2.89 / 6.45 /
14.6 / 7.38 / 5.18 / 7.31
2909.0
Initial solution

(0.4.4.0)
1.36 / 10.6 / 2.48 / 4.66 /
13.3 / 19.0 / 22.5 / 15.3
3469.3

(0.3.5.0)
1.35 / 10.6 / 2.39 / 4.69 /
13.0 / 18.3 / 22.8 / 15.1
3431.9

(0.3.4.1)
0.63 / 10.6 / 2.89 / 6.13 /
14.6 / 5.77 / 4.19 / 6.37
2659.8

Hence the Carbon-Epoxy optimal solution:
Optimal solution
(1.3.4.0)

Region 1	2	3	4	5	6	7	8
n_s 0.6	10.6	2.64	5.94	14.3	6.99	4.92	6.07

Cost = 100.55

REFERENCES

[1] S. Tsaî,"Composites design",4th edition,1988
Think Composites,Dayton OHIO

[2] J. L. Batoz,K. J. Bathe, L. W. Ho,"A study of three-node triangular plate bending element",Int.J.Num.Meth.Engng.,15,1771-1812(1980)

[3] B. Prasad,"Explicit constraint approximation forms in structural optimization.
Part one : Analyses and projections",Comput.Meths.Appl.Mech.Engng.,40,1-26(1983)

[4] B. Prasad,"Explicit constraint approximation forms in structural optimization.
Part two : Numérical experiences",Comput.Meths.Appl.Mech.Engng.,46,15-38(1984)

[5] C. Fleury,"A unified approach to structural weigth minimization",
Comput.Meths.Appl.Mech.Engng.,20,17-38(1979)

[6] C. Fleury,V.Braibant,"Structural optimization: A new dual method using mixed variables",Int.J.Num.Meth.Engng,23,409-428(1986)

[7] L.A. Schmit,K.J. Chang,"Optimum design sensitivity basad on approximation concepts and dual methods",Int.J.Num.Meth.Engng.,20,39-75(1984)

[8] M.Minoux,"Programmation mathématique (2 tomes)",
C.N.E.T.-E.N.S.T.,Dunod (1983)

Optimal Design of Composite and Fibre-Reinforced Plates

G.I.N. Rozvany, O. Sigmund and T. Birker

FB 10, Essen University, D-4300 Essen 1, Germany

Abstract

Various mathematicians have shown that for two-material composite plates in plain stress or bending the optimal micro-structure consists of a so-called rank2 laminate, having ribs of first and second order infinitesimal width in the two principal directions. The first author, Olhoff, Bendsøe and others obtained some analytical solutions for the above class of problems. They have also found that if (i) the stiffness and specific cost of the second material tends to zero (i.e. we consider a perforated plate) and (ii) the prescribed compliance value tends to infinity (i.e. the volume fraction tends to zero) then the optimal solution becomes identical to that for Michell trusses or least weight grillages for plain stress and bending, respectively. This conclusion was confirmed recently by Kohn and Allaire. The optimal grillage theory, developed by the first author and Prager in the seventies, is also valid for plastically designed fibre-reinforced plates of minimum fibre volume.

Entirely new classes of optimal topologies for the fibre-reinforced plates (= grillage) problem will be discussed on the basis of (i) analytical solutions obtained by the first author and (ii) discretized solutions developed by the second author, which show a complete agreement with each other.

Moreover, generalized shape optimization methods for perforated plates, resulting in simultaneous optimization of the boundary shape and boundary topology, are discussed and methods for solid/empty (SE) type topologies presented.

1. INTRODUCTION

The aim of this paper is to review briefly earlier research, and to report a number of recent developments, in the field of least-weight design of composite plates and related subjects. In much of the literature, and also in this paper, the investigation is restricted to *composite plates* consisting of two materials, having either one or the other material along the entire length of any line segment normal to the plate surface (Fig. 1a). One material is usually stiffer, stronger, heavier (or dearer) and the other one less stiff, weaker, lighter (or cheaper). The distribution of the two materials is to be chosen in such a way that (i) total weight (total cost) of the plate is minimized, (ii) subject to behavioural constraints (e.g. on displacements, stresses, natural frequencies, etc.). A special case of composite plates is a *perforated plate*, in which one material has zero stiffness, zero strength and zero weight (zero cost).

Considering elastic perforated plates subject to a constraint on the *compliance* (i.e. total external work), it has been found that the solution in general consists of three

types of regions, namely
- *solid regions* (filled with material),
- *empty regions* (without material), and
- *porous regions* (some material, with cavities of infinitesimal size).

Moreover, it was shown by various mathematicians [1-3, 34] that one possible optimal microstructure in the porous regions consits of *rank-2 laminates*, with ribs of first and second order infinitesimal width, made out of the stiffer material, in the two principal directions (Fig. 1b). Using the above microstructure, *analytical solutions* were obtained by Rozvany, Olhoff, Bendsøe *et al.* [4, 5] for axisymmetric plates in bending. These indicated that in exact solutions a *high proportion* of the optimal design consists of *porous regions*. The same authors found that for *low volume fractions* (i.e. low ratio of material volume/available volume), the optimal solutions for perforated plates reduce to those for *least-weight trusses* or Michell-frames [6] (in the case of plane stress) or to those for *least-weight grillages* [7] (in the case of flexure). The same conclusion was confirmed using a rigorous proof by Kohn and Allaire [8], who also mentioned an *alternative optimal microstructure* by Vigdergauz [33], having the properties as follows. At very low volume fractions, the solution tends to a Michell frame (Fig. 1c, but theoretically infinite number of members). As the volume fraction increases, the microstructure develops roundings at the corners (Fig. 1d). Finally, at very high volume fractions, the microstructure consists of elliptic holes, with axes in the principal directions (Fig. 1e).

It has been shown [9, 10] that, for a single load condition, least-weight solutions for trusses and grillages are equally valid for plastic design and for elastic design with a stress, a compliance or a natural frequency constraint. The optimal layout of grillages is also valid for plastically designed fibre-reinforced plates with a minimum fibre-volume [9].

In Section 2, analytical solutions for perforated and composite plates are reviewed. New classes of analytical solutions for grillages and fibre-reinforced plates are discussed in Section 3. Discretized, numerical solutions for the same class of problems are presented in Section 4. Finally, discretized methods for least-weight perforated and composite plates are outlined in Section 5 and some concluding remarks are offered in Section 6.

2. REVIEW OF ANALYTICAL SOLUTIONS: LEAST-WEIGHT PERFORATED AND COMPOSITE PLATES

Using the optimal microstructure derived by others [1-3], Rozvany, Olhoff, Bendsøe *et al.* [4] and Ong, Rozvany and Szeto [5] arrived at the following conclusions.
- For rank-2 laminates (Fig. 1b), the normalized *specific cost* (weight) *function* ψ in terms of the normalized principal stiffnesses (s_1, s_2) can be stated for *zero Poisson's ratio* $(\nu = 0)$ as

$$\psi = \frac{s_1 - 2s_1 s_2 + s_2}{1 - s_1 s_2} , \tag{1}$$

where the relation between normalized principal stiffnesses and rib densities (d_1, d_2) is given by

$$s_1 = d_1 , \quad s_2 = \frac{d_2}{1 - d_1 + d_1 d_2} , \tag{2}$$
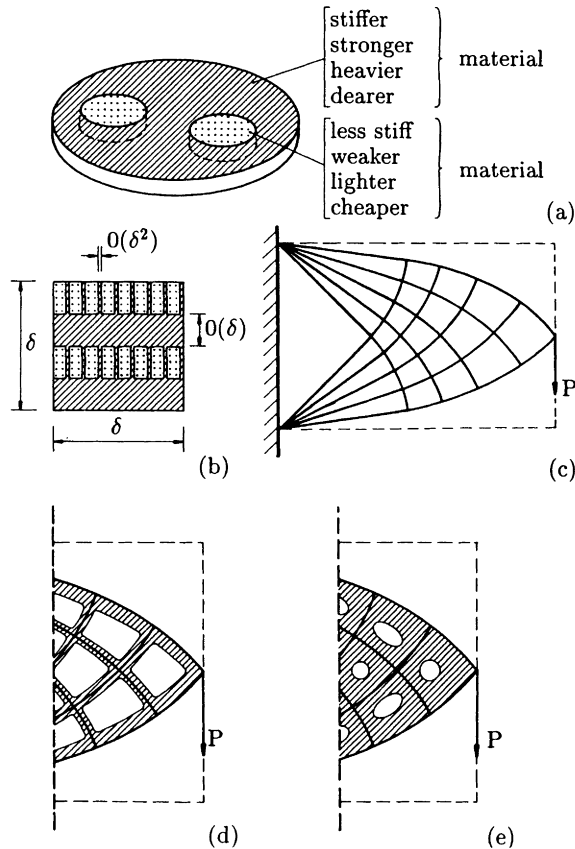
Fig. 1   Problem formulation and optimal microstructures for composite and perforated plates.

and the specific compliance (c) for plates under bending is furnished by

$$c = M_1^2/s_1 + M_2^2/s_2 . \tag{3}$$

For plane stress problems the principal moments M_1 and M_2 are replaced by the principal forces N_1 and N_2.

- Using optimality criteria based on (1) and a variational derivation, it can be shown that for axially symmetric plates only the following two types of non-empty *optimal regions* may occur in least-weight solutions:
  (i) unperforated (solid) regions;
  (ii) regions consisting of radial ribs only.
- Optimal solutions for various axisymmetric support and loading conditions were confirmed by independent numerical solutions using sequential quadratic programming and by a *comparison with intuitively selected designs*. In Fig. 2, for example, the structural volume of various partially optimized intuitive designs (A, B, C, E) for
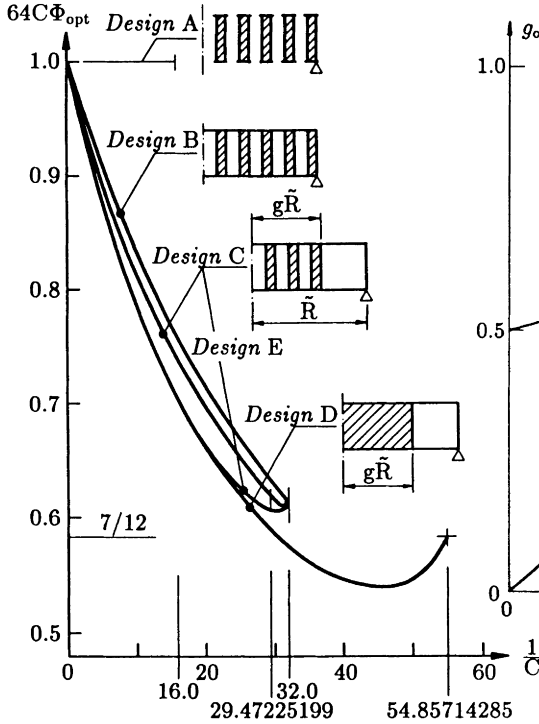
Fig. 2 A comparison of the structural volume of optimal and non-optimal solutions for uniformly loaded simply supported elastic perforated plates with a compliance constraint $(\nu = 0)$.
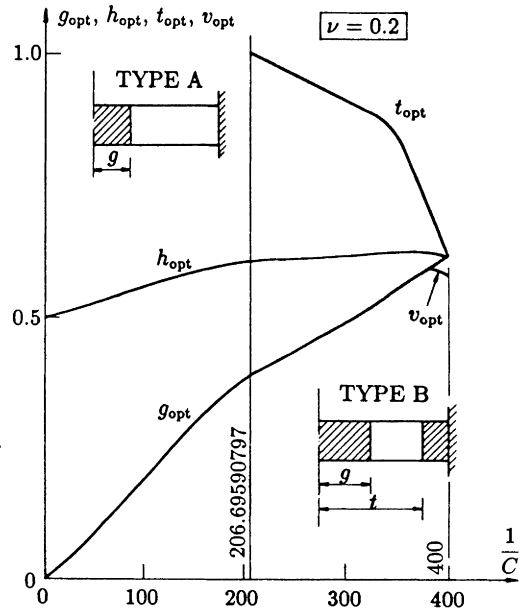
Fig. 3 Variation of radii of optimal region boundaries and of lines of contraflexure for uniformly loaded clamped perforated plates $(\nu = 0.2)$.

uniformly loaded simply supported circular plates is compared with that of the optimal design (D), in dependence of the reciprocal compliance $(1/C)$ value. Designs C and E are similar, except that the latter permits a different stiffness/moment ratio in the inner and outer regions. The radius $g\tilde{R}$ of the region boundary was optimized in all designs consisting of two regions. As predicted by the optimality criteria method, design D was found to have the lowest weight at all $1/C$ values.

- For *non-zero Poisson's ratio* $(\nu \neq 0)$, the specific cost function in (1) can be used [5] if s_1 and s_2 have the meaning defined in (2), where s_1 and s_2 do not represent the principal stiffnesses any more but the specific compliance is given by

$$c = M_1^2/s_1 + M_2^2/s_2 - \nu M_1 M_2 \tag{4}$$

for plates under bending, or the equivalent expression with N_1 and N_2 for plates under plane stress.

- Using the above formulation, solutions have been determined for various axisymmetric support and loading conditions. Figure 3, for example, shows that the solution

for clamped, uniformly loaded plates with $\nu = 0.2$ may take on two topologies, with either one or two solid regions and one region with radial ribs. The optimal radii (g, t) of the region boundaries and those (h, v) of the lines of contraflexure are also shown in Fig. 3. It is interesting that for solutions consisting almost entirely of solid regions, two lines of contraflexure appear in the optimal design.

- Further extensions of the above approach [11] dealt with *composite plates* with *zero Poisson's ratio* ($\nu = 0$) having stiffness and cost ratios of α and β, respectively. The specific cost ψ and principal stiffnesses (s_1 and s_2) for this class of problems are given by

$$\psi = \frac{(s_1 + s_2)(1 + \alpha) - 2(s_1 s_2 + \alpha)}{1 - s_1 s_2} \cdot \frac{1 - \beta}{1 + \beta} + \beta, \tag{5}$$

$$s_1 = \frac{d_1(1 - \alpha)(1 - d_2) + \alpha}{1 - d_2(1 - \alpha)}, \quad s_2 = \frac{d_2 + \alpha(1 - d_2)}{1 - (1 - \alpha)(d_1 - d_1 d_2)}. \tag{6}$$

- A variational formulation based on the relations (5) and (6) has shown that only the following regions may occur in the optimal solution for axisymmetric composite plates under flexure:
  (i) regions filled with the stiffer material (cross-hatched in Fig. 4),
  (ii) regions filled with the less stiff material (one-way hatching in Fig. 4), and
  (iii) radial ribs of the stiffer material, the gaps filled with the less stiff material (unhatched areas in Fig. 4).
  Optimal solutions for uniformly loaded simply supported circular plates have two possible topologies, one consisting of all three types of optimal regions and the other one of the first two regions listed above. In Fig. 4, where optimal radii of the region are shown, the broken line indicates the radii at which the single region boundary bifurcates into two boundaries for a given α value, as we vary the reciprocal compliance $1/C$.

- The formulation has also been generalized to *composite plates with non-zero Poisson's ratio* ($\nu \neq 0$) [12]. In that case the relations (5) and (6) can still be applied, but s_1 and s_2 do not represent actual stiffnesses and the specific compliance is given again by (4). Solutions based on a variational formulation and optimality criteria are given in Fig. 5 for a simply supported plate with a central point load and a stiffness ratio of $\alpha = 0.3$ for the two materials.

3. NEW CLASSES OF ANALYTICAL SOLUTIONS FOR GRILLAGES AND FIBRE-REINFORCED PLATES

It was already mentioned in the Introduction that the optimal layout of grillages is important in the present context, because they represent a *limiting case for least-weight perforated plates* with low volume fractions [4, 8].

Least-weight grillages (e.g. [7]) represent a very successful application of the *optimal layout theory* [13-17] developed in the seventies by Prager and the first author, and extended in the eighties by the latter. The optimal layout theory is based on two underlying principles, namely the *structural universe* (union of all potential members) and *continuum-based optimality criteria* (COC) expressed in terms of a fictitious system termed *adjoint structure*. For elastic grillages with a compliance constraint, the adjoint structure is identical with the real structure for the basic design problem (i.e. without
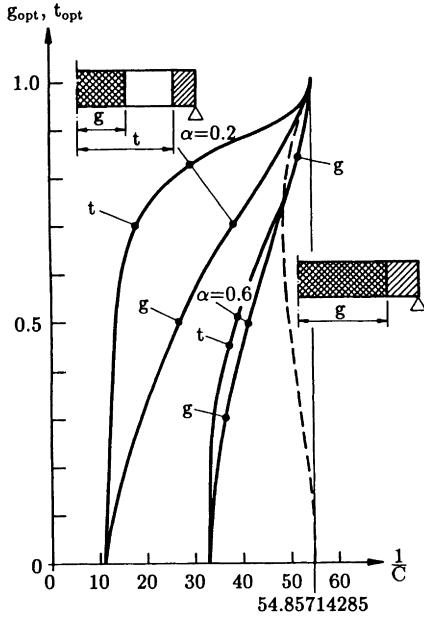
Fig. 4 Variation of the optimal radii of region boundaries for uniformly loaded simply supported composite plates with zero Poisson's ratio in dependence of the reciprocal compliance $(1/C)$ and stiffness ratio (α) for the two materials.
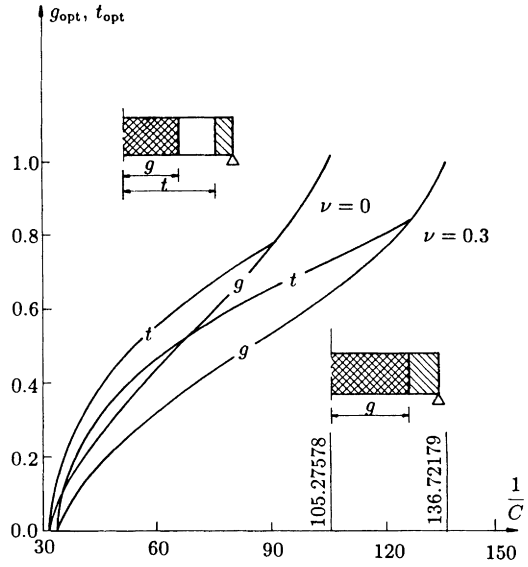
Fig. 5 Variation of the optimal radii of region boundaries for simply supported composite plates with a central point load: two different Poisson's ratios and a stiffness ratio of $\alpha = 0.3$.

allowance for cost of supports, selfweight etc.). Because we have adjoint strain requirements also for vanishing members, and since the grillage problem is convex, fulfilment of the optimality criteria for the entire structural universe ensures optimality of the layout *and* of the cross-sections for non-vanishing members.

Details of the grillage theory are given elsewhere [7, 9, 13-17] and therefore only the most important aspects are reviewed here briefly. The *adjoint displacement field for grillages* must be kinematically admissible, such that (i) at least one principal curvature takes on a constant absolute value (say k) and the other one has an absolute value which is smaller than or equal to k; (ii) the direction of all nonvanishing beams must match principal directions with an absolute curvature k, and (iii) all (statically admissible) beam moments must match the sign of the corresponding principal curvatures. This can be expressed mathematically as

$$\text{(for } M_i^S \neq 0) \quad \overline{\kappa}_i^K = k \, \text{sgn} \, M_i^S \,, \quad \text{(for } M_i^S = 0) \quad |\kappa_i^K| \leq k \,, \tag{7}$$

in which the superscripts S and K denote static and kinematic admissibility and $\overline{\kappa}_i = \partial^2 \overline{u}/\partial \xi_i^2$ the adjoint (small deflection) curvature, where $\overline{u}$ is the adjoint deflection and ξ_i is the spatial coordinate in the considered principal direction. The above optimality criteria admit five types of *optimal regions*. In R-type regions only one principal

$$R^+ \qquad R^- \qquad T \qquad S^+ \qquad S^-$$
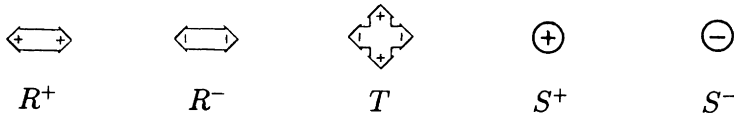
Fig. 6 Symbols representing various types of optimal regions in grillages.

curvature has the absolute value k and bemas may run only in that direction, whilst in S- and T-type regions both principal curvatures have the absolute value k, both having the same sign in S-regions and different signs in T-regions. It follows that the optimal regions for grillages are R^+, R^-, S^+, S^- and T, where superscripts denote the sign of the principal curvatures having an absolute value k (and the sign of the corresponding beam moment). Symbols representing the above optimal regions in grillage layouts are shown in Fig. 6.

The above optimality criteria mean that we have now replaced a rather complex non-smooth variational problem with the following geometrical problems. The structural domain (available space for grillage beams) must be covered with the above optimal regions, such that
- the adjoint displacements fulfil all kinematic boundary conditions,
- continuity and slope continuity of displacements is satisfied along region boundaries; and
- statically admissible beam moments match the direction and sign of the corresponding adjoint curvatures.

A unique feature of the optimal grillage theory is that *closed form analytical solutions are avialable for most boundary and loading conditions*. The few remaining gaps in this theory are being filled under a current project, which will be reviewed in the remainder of this section.

3.1 Combinations of Free Edges, Simple Supports and Clamped Edges

In general, along free edges the optimal grillage contains a so-called "beam-weave" [7], consisting of beams of infinitesimal length in negative bending and long beams in positive bending (Fig. 7a). Considering a combination of a *straight free edge and a straight simple support* [18], the general equation for the relation between the distance t along the edge and the angle enclosed by a long beam and the free edge is (Fig. 7b)

$$t/a = \exp \left[\int_{\alpha}^{\alpha_0} \frac{\sin \gamma \, d\alpha}{\sin(\alpha + \gamma) \cos(2\alpha + 2\gamma) \sin \alpha} \right] , \tag{8}$$

and the adjoint deflection $\bar{u}$ at a point A (Fig. 7c) of the free edge is given by

$$\bar{u}_A = \frac{\sin \gamma \sin(2\alpha_0 + \gamma)}{2 \sin^2(\alpha + \gamma)} (a - t_A) - \int_{t_A}^{a} \cos(2\alpha)(t - t_A) dt , \tag{9}$$

The above equations reduce to known analytical results [14] for $\alpha = 0°, 45°$ and $90°$.

For a *straight free edge* that is *parallel to a straight clamped edge* [18], we have the following governing equations (Fig. 8):

300
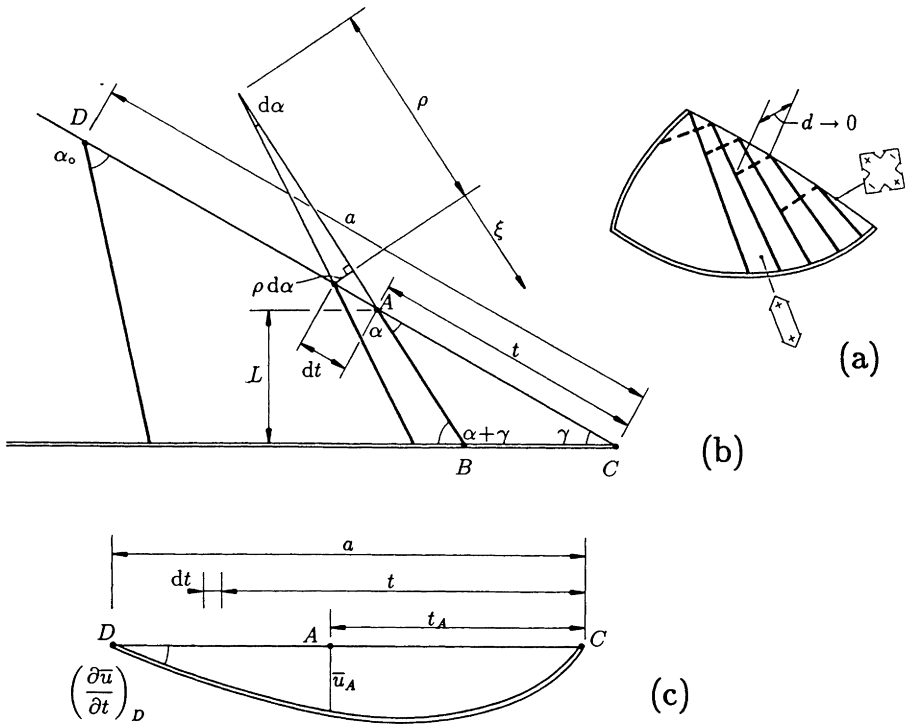
Fig. 7 Optimal grillage layout for a straight free edge and a straight simple support.
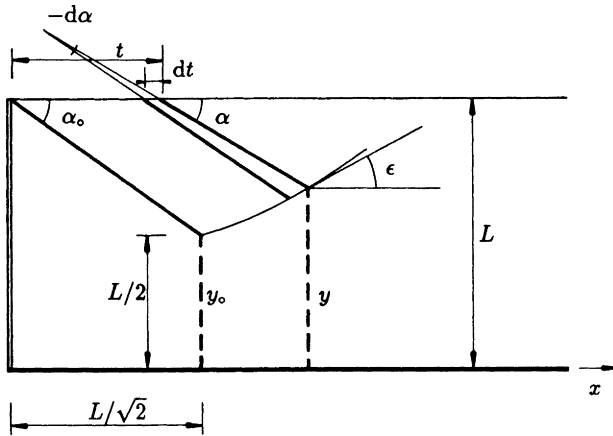
Fig. 8 Grillage layout for parallel free and clamped edges.

$$dt = \frac{L-y}{\sin^2 \alpha} \cdot \frac{1 + \sin^2 \varepsilon}{2 \sin^2(\alpha + \varepsilon) - 1 - \sin^2 \varepsilon} d\alpha, \quad \frac{d^2 u}{dt^2} = -\cos(2\alpha),$$
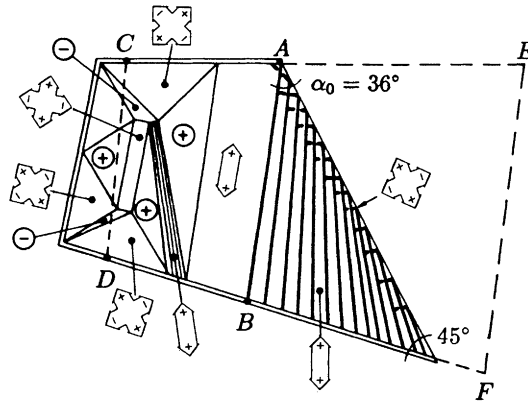
Fig. 9   Grillage layout for three simply supported edges and a free edge.

$$y = L - \sin\alpha\sqrt{(L^2 - 2\bar{u})/(1 + \sin^2\alpha)}, \quad \tan\varepsilon = \mathrm{d}y/\mathrm{d}x. \tag{10}$$

To demonstrate the complexity of optimal grillage layouts for even relatively simple boundary conditions, a least-weight solution for three simply supported edges and one free edge is shown in Fig. 9. Beams are indicated by thicker lines only in the free-edge region.

3.2. Partially Upward and Partially Downward Loads

Figure 10a shows a clamped edge with three upward and one downward load. The adjoint field for such problems can be constructed by assuming a fictitious supporting line (HG in Fig. 10b) with a non-zero deflection and using the construction described in Section 3.3 for allowance for cost of supports. The optimal beam layout, with beams in negative bending shown in broken line, is given in Fig. 10c.

3.3. Allowance for the Cost of Supports

Surprisingly simple, yet quite general constructions for optimal grillage layouts with allowance for the cost of supports were derived recently [19]. These are shown in Fig. 11a for two clamped supports and in Fig. 11b for a clamped and a simple support, in which, respectively,

$$a + ky^2 - c^2/2k = b + kx^2 - d^2/2k, \tag{11}$$

$$a + ky^2 - c^2/2k = b + kx^2/2. \tag{12}$$

The above constructions take care of both cost of clamping moments (M_C) and cost of vertical reactions (R). With $a = b = c = d = 0$, the constructions in Fig. 11 reduce to those for grillages with zero support cost [9].

An interesting feature of these solutions is that the real and adjoint displacement fields differ due to different kinematic boundary conditions.
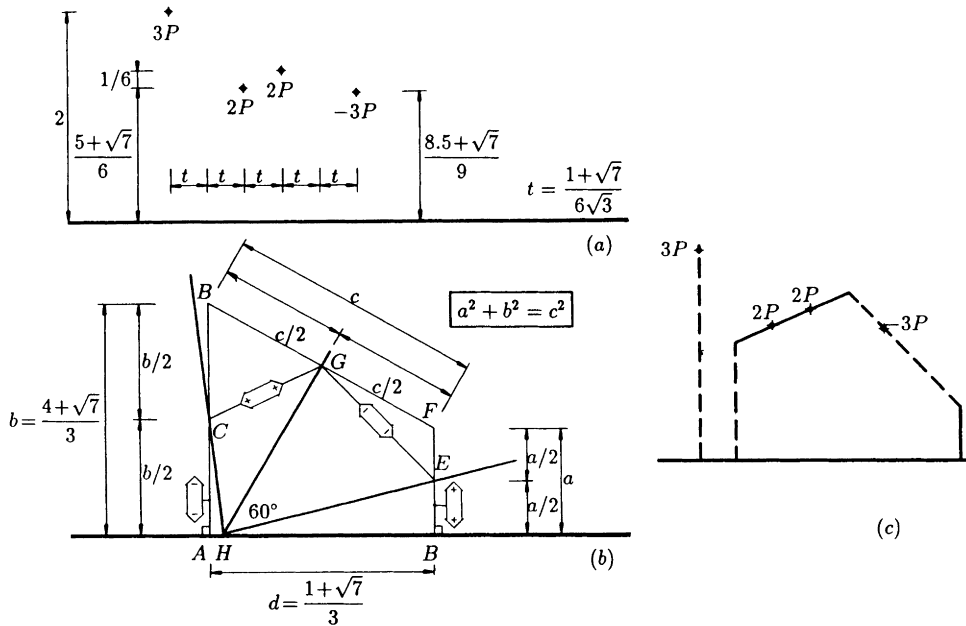
Fig. 10 Analytical solution for upward and downward loads

4. DISCRETIZED SOLUTIONS FOR LEAST-WEIGHT GRILLAGES US-ING OPTIMALITY CRITERIA

Toplogical optimization of grid-type systems usually involves a very large number of variables because for a reasonable accuracy one requires a structural universe (ground structure) with several thousand members. Moreover, for a realistic design, it is necessary to impose constraints at least on the stresses and displacements, resulting in a considerable number of active constraints. This means that usual optimization methods do not have a sufficient capability for handling such problems because so-called primal programming methods are restricted to about 10^2 variables and dual (and conventional discretized optimality criteria, DOC) methods to about 10^2 active constraints. This difficulty has been overcome by the introduction of new iterative continuum-type optimality criteria (COC) methods [20] and their discretized equivalent (DCOC) for finite element systems [21]. These methods are based on a general formulation of the analytical school for structural optimization (e.g. [22, 23]). The basic advantage of COC/DCOC methods is that their optimization capability is limited only in terms of the number of active *global* constraints because active stress constraints are handled by explicit equations at the element level, which requires only almost negligible computer time. Since the number of active global constraints is small for even very large structural systems, COC/DCOC have a several orders of magnitude greater optimization capability than traditional methods if structures with stress and displacement are to be optimized. Another advantage of COC/DCOC is the fact that sensitivity analysis is replaced by the analysis of the *adjoint structure*, involving the decomposed stiffness matrix which is already available from the analysis of the real system. It is to be noted that various mathematicians (e.g. [24, 25]) have optimized trusses with a large number
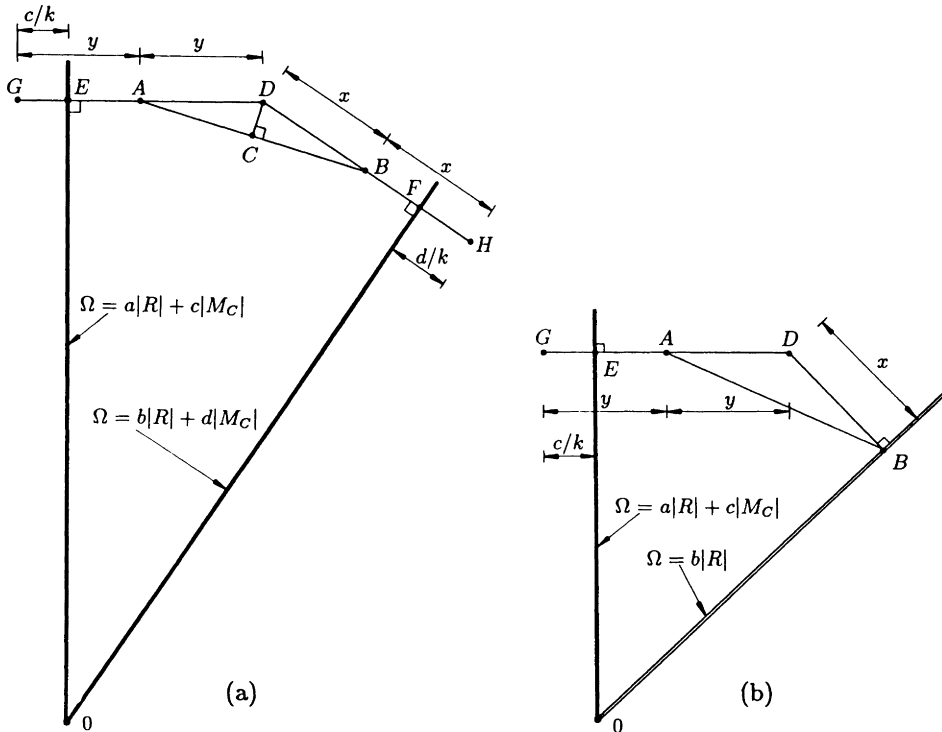
Fig. 11 Optimal grillage layouts with allowance for cost of supports.

of potential members but only for a complicance constraint with a single load condition, for which the dual problem has only one variable, making compliance design rather inexpensive even by conventional dual methods. Moreover, for compliance problems the real and adjoint structures are identical, which means a further simplification of the general problem discussed herein.

The considerable attractiveness of COC/DCOC for layout optimization will be demonstrated in this lecture on test examples involving grillages, an investigation carried out by Sigmund, who used some of the algorithms developed by Zhou and Rozvany.

The first test example concerns a *clamped square grillage* for which the analytical solution is shown in Fig. 12a, the structural universe with 624 beam elements in Fig. 12b, and the corresponding discretized COC solution for nine point loads in Figs. 12c and d. For this class of problems, Sigmund extended the COC method to linearly varying beam elements. The analytical and discretized solution gave almost the same nondimensionalized weight (0.234619 vs. 0.234620).

Figure 13a shows the structural universe and loading (solid circles upward load, empty circles downward load) for the second test example and Fig. 13b the discretized optimal solution by COC, which was used for verifying the recently developed theory for partially upward and partially downward loading (see Section 3.2).

Figures 14a and b show discretized COC solutions with 466 and 1892 elements for a grillage with one clamped edge, one simple support and a free edge. The topology shown
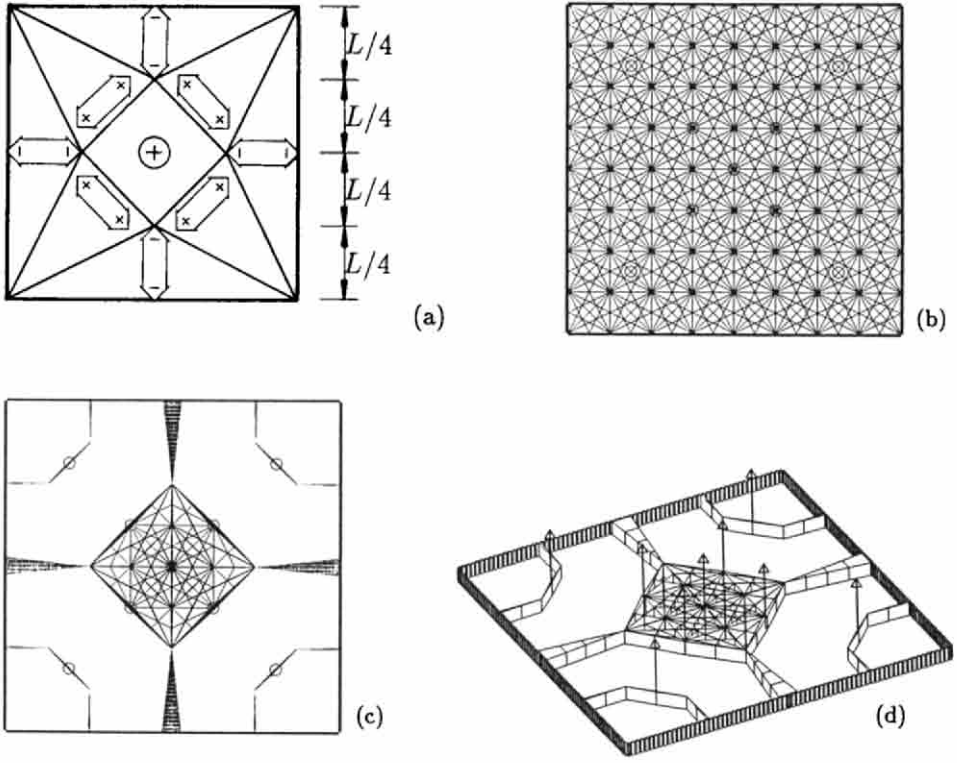
Fig. 12   First test example.
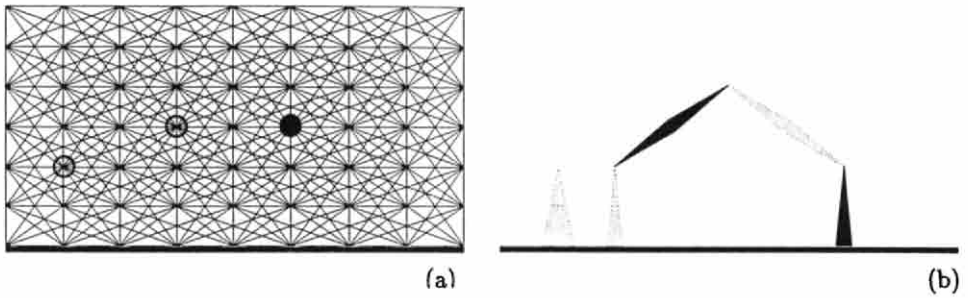
Fig. 13   Second test example.

by this numerical solution has lead to the exact analytical solution [(10) in Section 3.1], which is plotted in Fig. 14c.

Figure 15a shows the structural universe with 9312 beam elements and loading for a grillage with two clamped and two free edges, for which the analytical solution is not know to date. The discretized COC solution is shown in fig. 15b. This solution has a
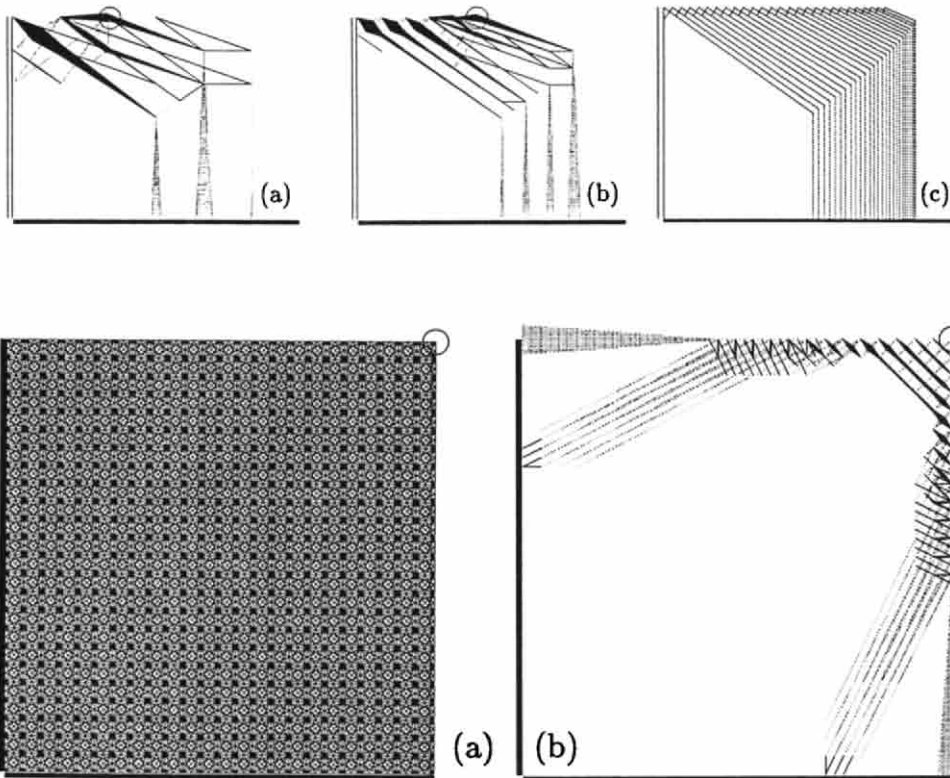
Fig. 15   Discretized solution for a problem for which the analytical solution is not yet
         known.

nondimensional weight of 0.1819, whereas a simple solution with two cantilevers along
the free edge would have a weight of 0.25, which is over 37 % heavier than the numerical
optimal solution.

Finally, Fig. 16 shows a series of solutions for a quarter of a clamped square plate
with various values of the permissible shear stress.

It is to be remarked that the same method has been used for several loading con-
ditions, and combinations of stress, deflection and natural frequency constraints, also
with allowance for structural mass and selfweight.

5. LEAST-WEIGHT PERFORATED PLATES CONSISTING OF SOLID AND EMPTY REGIONS ONLY

It was mentioned in the Introduction that exact analytical solutions [4, 5] for per-
forated plates consist of solid, empty and porous regions. Following the above de-
velopment, near-optimal solutions were derived *numerically* using both the optimal
microstructure (rank-2 laminates) and "suboptimal" microstructure (square and rect-

$\tau_{max} = 10.6$ (unconstrained)
Cost = 0.44580

$\tau_a = 3.0$
Cost = 0.50301

$\tau_a = 5.0$
Cost = 0.45667

$\tau_a = 2.0$
Cost = 0.64017
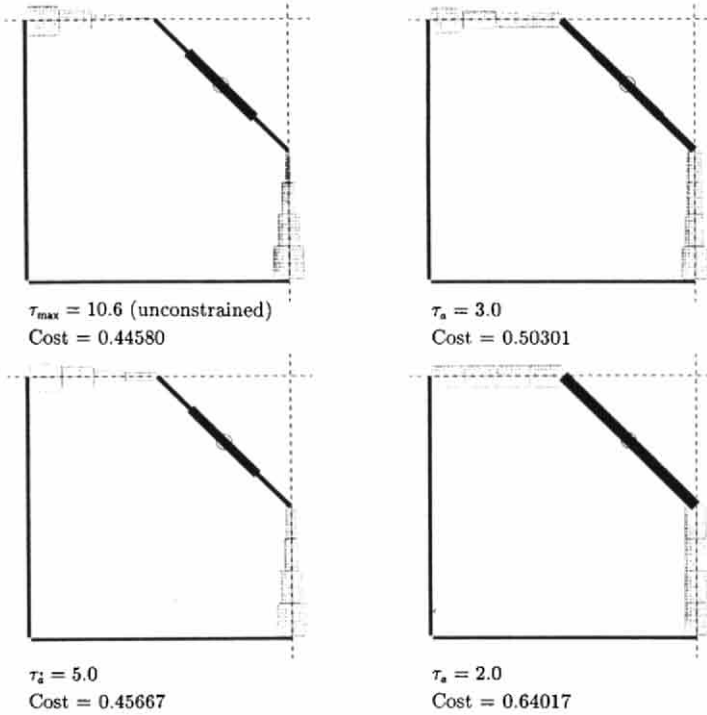
Fig. 16   Discretized solutions for a grillage with deflection and shear stress constraints

angular holes) by Bendsøe and his research associates [26-30]. This is an importan
development, because they represent useful results in generalized shape optimizatio
(i.e. in the simulations optimization of boundary topology and shape). However, solu
tions with rank-2 and similar microstructures are somewhat unpractical for the followin
reasons:
- a high proportion of the exact optimal design consists of porous regions with a dens
  system of holes. Even an approximated version of these regions would require hig
  manufacturing costs;
- rank-2 laminates for perforated plates in plane stress have zero shear stiffness in th
  direction normal to the ribs with second order width, which renders this solutio
  unstable if we change the loading; and
- solutions of this type are only available for a compliance constraint which does nc
  represent a real-world design condition in engineering. Moreover, it was shown b
  Haftka *et al.* [31] that even the optimal topology for compliance is not necessaril
  valid for other design constraints.

    For these reasons, it is desirable to find least-weight solutions for perforated plate
which consist of *solid and empty regions only*. This can be done by penalizing an
thereby suppressing porous regions in the solution. In order to achieve such solution
we can use *any* microstructure with an appropriate penalty for porous regions (or ir
termediate densities). In selecting the microstructure, the following objectives shoul
be kept in mind:
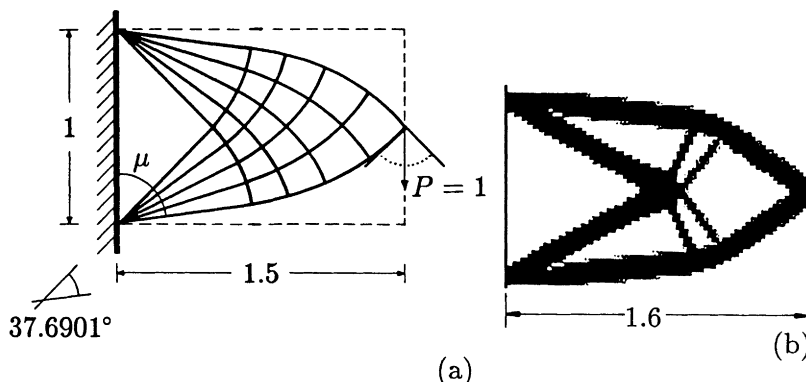
Fig. 17   Analytical solution and solution with suboptimal microstructure for a cantilever truss.

- simplicity of analysis and optimization,
- selective suppression of porous regions by adjustable penalty; and
- capability of handling a variety of design conditions.

It was shown by Rozvany and Zhou ([20], Part II) that a "solid" microstructure (filled with an isotropic material) with a concave cost function for penalizing intermediate densities is very efficient in locating least-weight solid-empty type topologies. A similar approach was mentioned earlier by Bendsøe [26]. Because of length limitations, only one test example is given in this paper which is due to T. Birker in the first author's department. The exact solution for a type of cantilever beam [32] is shown in Fig. 17a and a solution with a "suboptimal" microstructure by Kikuchi [30] in Fig. 17b. Figure 18a shows a series of solutions by Birker after various iteration numbers (n), starting with a plate of *uniform thickness*. In Fig. 18b, a starting design is used which was obtained *without penalty for intermediate densities*. This latter method, suggested to the first author by R. Kohn, gave a better topology and a lower weight.

6. CONCLUDING REMARKS

It will be seen that new continuum-type optimality criteria (COC) methods are highly suitable for deriving both exact analytical solutions and discretized numerical solutions for composite plates and related structures, such as perforated plates and grillages. Solutions in which porous regions are suppressed (Section 5) are currently being extended from perforated to composite plates.

7. REFERENCES

1. Lurie, K.A.; Cherkaev, A.V. 1984: G-closure for some particular set of admissible material characteristics for the problem of bending thin elastic plates. *JOTA*, **42**, 305–316

2. Murat, F.; Tartar, L. 1985: Calcul des variations et homogénéisation. In: *Les méthodes de l'homogénéisation: Théorie et applications en physique*, pp. 319–370. Eyrolles, Paris: Coll. de la Dir. des Etudes et Recherches de Elec. de France

3. Kohn, R.V.; Strang, G. 1986: Optimal design and relaxation of variational problems, I, II, and III.
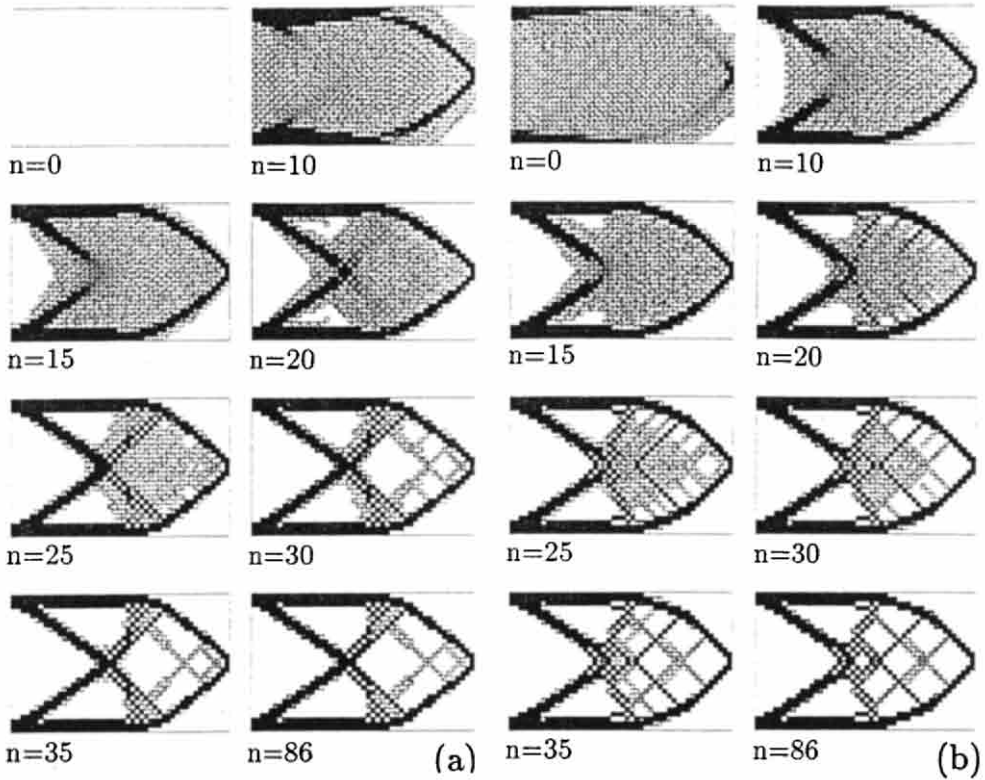
Fig. 18 Solutions with solid isotropic microstructure with penalty (SIMP) for intermediate densities.

Comm. Pure Appl. Math. **39**, 113–137, 139–182, 353–377

4. Rozvany, G.I.N.; Olhoff, N.; Bendsøe, M.P.; Ong, T.G.; Sandler, R.; Szeto, W.T. 1987: Least-weight design of perforated elastic plates I, II. *Int. J. Solids Struct.* **23**, 521–536, 537–550

5. Ong, T.G.; Rozvany, G.I.N.; Szeto, W.T. 1988: Least-weight design of perforated elastic plates for given compliance: non-zero Poisson's ratio. *Comp. Meth. Appl. Mech. Eng.* **66**, 301–322

6. Michell, A.G.M. 1904: The limits of economy of material in frame-structures. *Phil. Mag.* **8**, 589–597

7. Prager, W.; Rozvany, G.I.N. 1977: Optimal layout of grillages. *J. Struct. Mech.* **5**, 1–18

8. Kohn, R.V.; Allaire, G. 1992: Structural optimization using homogenization. *Proc. NATO ARW "Topology design of structures"* (held in Sesimbra, Portugal). Dordrecht: Kluwer

9. Rozvany, G.I.N. 1976: *Optimal Design of Flexural Systems.* Oxford: Pergamon (Russian version: Moscow, Stroiizdat, 1980)

10. Olhoff, N.; Rozvany, G.I.N. 1982: Optimal grillage layout for given natural frequency. *J. Eng. Mech. ASCE* **108**, 971–975

11. Ong, T.G. 1987: *Structural optimization via static-kinematic optimality criteria.* Ph.D. Thesis, Monash Univ. (Melbourne)

12. Szeto, W.T. 1989: *Microstructure studies and structural optimization.* PhD. Thesis, Monash Univ. (Melbourne)

13. Prager, W.; Rozvany, G.I.N. 1977: Optimization of structural geometry. In: Bednarek, A.R.;

Cesari, L. (Eds.) *Dynamical Systems*, pp. 265–293. Academic Press, New York

14. Rozvany, G.I.N. 1981: Optimality criteria for grids, shells and arches. In: Haug, E.J.; Cea, J. (Eds.) *Optimization of Distributed Parameter Structures* (Proc. NATO ASI held in Iowa City, 1980), pp. 112–151. Sijthoff and Noordhoff, Alphen aan der Rijn, The Netherlands

15. Rozvany, G.I.N.; Ong, T.G. 1987: Minimum-weight plate design via Prager's layout theory (Prager memorial lecture). In: Mota Soares, C.A. (Ed.) *Computer Aided Optimal Design: Structural and Mechanical Systems* (Proc. NATO ASI held in Troia, Portugal, 1986), pp. 165–179. Springer-Verlag, Berlin

16. Rozvany, G.I.N. 1992: Optimal layout theory (Chapter 6, see also Chapters 7–10). In: Rozvany, G.I.N. (Ed.) *Shape and Layout Optimization of Structural Systems and Optimality Criteria Methods* (CISM Course held in Udine 1990), pp. 75–163, Springer-Verlag, Vienna

17. Rozvany, G.I.N. 1992: Layout theory for grid-type structures. *Proc. NATO ARW "Topology Design of Structures"* (held in Sesimbra, Portugal), Dordrecht: Kluwer

18. Rozvany, G.I.N.; Gerdes, D. 1992: Optimal layout of grillages – Part I: free and simply supported edges
Rozvany, G.I.N.; Sigmund, O. 1992: Part II: free and clamped edges. *Struct. Optim.* (submitted)

19. Rozvany, G.I.N.; Gollub, W. 1992: Optimal layout theory – allowance for the cost of supports and optimization of support locations. *Mech. Struct. Mach.* (accepted)

20. Rozvany, G.I.N.; Zhou, M. 1991: The COC algorithm, Parts I and II. *Comp. Meth. Appl. Mech. Eng.* **89**, 281–308, 309–336

21. Zhou, M.; Rozvany, G.I.N. 1992: A new discretized optimality criteria method in structural optimization. *Proc. AIAA/ASME/ASCE/AHS/ASC Struct. Mat. Dyn. Conf.* (held in Dallas), pp. 2576–2585, Washington DC: AIAA

22. Prager, W.; Shield, R.T. 1967: A general theory of optimal plastic design. *J. Appl. Mech. ASME* **34**, 184–186

23. Rozvany, G.I.N. 1989: *Structural Design via Optimality Criteria*. Dordrecht: Kluwer

24. Ben-Tal, A.; Bendsøe, M.P. 1992: A new method for optimal truss topology design. *SIAM J. Optim.*, (to appear)

25. Zowe, J. 1992: A non-smooth approach to simultaneous topology and geometry design of trusses. *Proc. NATO ARW "Topology Design of Structures"* (held in Sesimbra), Dordrecht: KLuwer

26. Bendsøe, M.P. 1989: Optimal shape design as a material distribution problem. *Struct. Optim.* **1**, 193–202

27. Bendsøe, M.P.; Kikuchi, N. 1988: Generating optimal topologies in structural design using a homogenization method. *Comp. Meth. Appl. Mech. Eng.* **71**, 197–224

28. Díaz, A.R.; Bendsøe, M.P. 1992: Shape optimization of multipurpose structures by a homogenization method. *Struct. Optim.* **4**, 17–22

29. Olhoff, N.; Bendsøe, M.P.; Rasmussen, J. 1991: On CAD-integrated structural topology and design optimization. *Comp. Meth. Appl. Mech. Eng.* **89**, 259–29

30. Suzuki, K.; Kikuchi, N. 1991: A homogenization method for shape and topology optimization. *Comp. Meth. Appl. Mech. Eng.* **93**, 291–318

31. Sankaranarayanan, S.; Haftka, R.T.; Kapania, R.K. 1992: Truss topology optimization with simultaneous analysis and design. *Proc. 33rd AIAA/ASME/ASCE/AHS/ASC Struct. Dyn. Mat. Conf.* (held in Dallas), pp. 2576–2585. Washington DC: AIAA

32. Hemp, W.S. 1973: *Optimum structures*. Oxford: Clarendon

33. Vigdergauz, S. 1992: Two-dimensional grained composites of extreme rigidity. *18th Int. Congr. Theor. Appl. Mech.* (held in Haifa)

34. Avellaneda, M. 1987: Optimal bounds and microgeometries for elastic two-phase composites. *SIAM J. Appl. Math.* **27**, 1216–1228.

Layup Optimization of Composite Material Structures

J.L. Grenestedt[a] and P. Gudmundson[b]

[a]Department of Lightweight Structures, Royal Institute of Technology, S-100 44 Stockholm, Sweden

[b]Swedish Institute of Composites, Box 271, S-941 26 Piteå, Sweden

Abstract

Layup optimization of laminated composite structures is considered. Lamination parameters rather than layup angles and ply thicknesses are used as design parameters, thus any physically possible layup is included and the number of design variables is kept small; twelve for the most general layup. These twelve parameters are functions of the in-plane coordinates if the layup changes from point to point in the structure. It is shown that the feasible region of the parameters is convex, and the object functions to be maximized (stiffnesses, vibration frequencies, or buckling loads) are concave functions; local optima are therefore avoided and the optimization is accordingly significantly simplified. In order to use these parameters for optimization, their feasible region has to be known. The current knowledge is summarized, and some new results concerning the feasible region of the parameters of an orthotropic laminate are presented. When the feasible region of the lamination parameters is known, optimization of general composite material structures can efficiently be performed. A number of simple examples are included, such as flat in-plane homogeneous (same layup and thickness in every point) plates concerning deflections under uniform loads, vibration frequencies, and buckling under uni-axial or shearing loads.

1. INTRODUCTION

Tsai and Pagano [1] derived transformation properties of an orthotropic material - typically a lamina in a layered composite - during rotation in terms of multiple angles instead of the classical relations using powers of sines and cosines. The in-plane (A_{ij}), coupling (B_{ij}), and bending (D_{ij}) stiffnesses could then be expressed as linear combinations of so-called lamination parameters, with the coefficients being material constants, see eqs. (7) - (13) below. Simply stated, the lamination parameters are integrals through the thickness of the sines and cosines of the layup angles of the different plies constituting the laminate. Twelve lamination parameters suffice in describing the A_{ij}, B_{ij}, and D_{ij} stiffnesses of a general laminated composite. The lamination parameters are attractive for layup optimization of composite material structures for many reasons, e.g. there are few parameters and all physically possible layups of the considered material can be included. This is generally not the fact when layup angles and/or thicknesses of discrete plies are used as design variables. Lamination parameters have been used successfully in a number of design and optimization studies. In these studies, subsets of the twelve lamination parameters were used, mainly since the feasible region of all twelve parameters currently is not known. The feasible region is a purely mathematical limitation of the values of the lamination parameters. When one lamination parameter, e.g. the integral of sinus of the layup angles, is specified, other lamination parameters, e.g. the integral of cosinus of the layup angles, cannot take arbitrary values. Miki [2] determined the feasible region of the two lamination parameters needed to describe the in-plane stiffnesses of orthotropic laminates and, successively, Miki [3]

determined the allowable region of the two lamination parameters needed to describe the bending stiffnesses of orthotropic laminates, and performed some optimization. For symmetric laminates, Fukunaga [4] determined the feasible region of the four parameters needed to describe the in-plane stiffnesses and, separately, the feasible region of the four parameters for bending stiffnesses. Further, Fukunaga [5] made an effort to derive the feasible region of the four lamination parameters needed to describe both in-plane and bending stiffnesses of orthotropic laminates but, as will be shown below, only an "inner boundary" was obtained. In the present study the true feasible region of these parameters is derived. It is further shown that the feasible region of all twelve parameters is convex. The facts that the stiffnesses are linear in the lamination parameters and the feasible region is convex result in the desirable property that no local optima exist for e.g. maximization of potential energy (which is a sort of stiffness maximization), maximization of the lowest eigenfrequency, or maximization of buckling load. This result descends from Svanberg [6], who showed that stiffness optimization of a structure whose finite element structural stiffness matrix is linear in the design variables can be made convex. This is proved slightly differently below. Layup optimization using lamination parameters is a significant improvement over optimization using thicknesses and layup angles of discrete ply laminates as design variables, since in the latter case object functions such as buckling loads often show very complicated behaviour with many local optima.

2. CONSTITUTIVE PARAMETERS

In the following, Einstein's summation convention is used and repeated indices α, β, γ, δ range from 1 to 2. The constitutive equation for a ply under plane stress ($\sigma^{\alpha\beta}$) conditions is

$$\sigma^{\alpha\beta} = Q^{\alpha\beta\gamma\delta} \, \varepsilon_{\gamma\delta} \tag{1}$$

where $Q^{\alpha\beta\gamma\delta}(x_\alpha, z)$ is the stiffness tensor and $\varepsilon_{\gamma\delta}(x_\alpha, z)$ are membrane strains. x_α are coordinates in the middle surface of the structure, and z is the through-the-thickness coordinate. The Kirchhoff kinematics for a shell with small thickness-to-curvature ratio are

$$\varepsilon_{\gamma\delta} = \varepsilon_{\gamma\delta}^o + z \, \kappa_{\gamma\delta} \tag{2}$$

where $\varepsilon_{\gamma\delta}^o = \varepsilon_{\gamma\delta}^o(x_\alpha)$ are middle surface strains and $\kappa_{\gamma\delta} = \kappa_{\gamma\delta}(x_\alpha)$ is change of curvature. $u_\gamma(x_\alpha)$ are in-plane and $w(x_\alpha)$ is out-of-plane deformation. Different kinematic expressions relating deformations u_γ and w to strain measures $\varepsilon_{\gamma\delta}^o$ and $\kappa_{\gamma\delta}$ for shells exist. For flat plates

$$\varepsilon_{\gamma\delta}^o = \frac{1}{2}(u_\gamma\big|_\delta + u_\delta\big|_\gamma) \tag{3}$$

and

$$\kappa_{\gamma\delta} = -w\big|_{\gamma\delta} \, . \tag{4}$$

The strain energy per unit area, W (neglecting through-the-thickness stresses and strains)

$$W = \frac{1}{2} \int_{-h/2}^{h/2} \sigma^{\alpha\beta} \, \varepsilon_{\alpha\beta} \, \mathrm{d}z \tag{5}$$

where h is the local thickness of the shell, becomes

$$W = \frac{1}{2}(A^{\alpha\beta\gamma\delta}\varepsilon^o_{\alpha\beta}\varepsilon^o_{\gamma\delta} + 2B^{\alpha\beta\gamma\delta}\varepsilon^o_{\alpha\beta}\kappa_{\gamma\delta} + D^{\alpha\beta\gamma\delta}\kappa_{\alpha\beta}\kappa_{\gamma\delta}) \tag{6}$$

with the stiffnesses

$$\left\{A^{\alpha\beta\gamma\delta}, B^{\alpha\beta\gamma\delta}, D^{\alpha\beta\gamma\delta}\right\} = \int\limits_{-h/2}^{h/2}\left\{1, z, z^2\right\}Q^{\alpha\beta\gamma\delta}\,dz\ . \tag{7}$$

The strain energy is linear in the stiffnesses $A^{\alpha\beta\gamma\delta}$, $B^{\alpha\beta\gamma\delta}$, $D^{\alpha\beta\gamma\delta}$ if the deformation is fixed.

Using the expressions derived by Tsai and Pagano [1] for rotational transformation of stiffnesses of a ply from one orthogonal coordinate system to another

$$Q_{11} = U_1 + U_2\cos 2\theta + U_3\cos 4\theta,$$

$$Q_{22} = U_1 - U_2\cos 2\theta + U_3\cos 4\theta, \qquad Q^{1111} = Q_{11}, \qquad Q^{1212} = Q_{66},$$

$$Q_{12} = U_4 - U_3\cos 4\theta, \qquad\qquad\qquad\ Q^{1112} = Q_{16}, \qquad Q^{1222} = Q_{26},$$

$$Q_{66} = \tfrac{1}{2}(U_1 - U_4) - U_3\cos 4\theta, \qquad\ Q^{1122} = Q_{12}, \qquad Q^{2222} = Q_{22}, \tag{8}$$

$$Q_{16} = \tfrac{1}{2}U_2\sin 2\theta + U_3\sin 4\theta, \qquad\ Q^{ijkl} = Q^{ijlk} = Q^{klij},$$

$$Q_{26} = \tfrac{1}{2}U_2\sin 2\theta - U_3\sin 4\theta,$$

where θ is the off-axis angle and U_i are elastic stiffnesses of the ply, see e.g. Table 1, the normalized stiffnesses can be expressed as

$$A^*_{11} = U_1 + U_2\xi^A_1 + U_3\xi^A_2,$$

$$A^*_{22} = U_1 - U_2\xi^A_1 + U_3\xi^A_2, \qquad\qquad A^{1111} = A_{11}, \qquad A^{1212} = A_{66},$$

$$A^*_{12} = U_4 - U_3\xi^A_2, \qquad\qquad\qquad\quad A^{1112} = A_{16}, \qquad A^{1222} = A_{26},$$

$$A^*_{66} = \tfrac{1}{2}(U_1 - U_4) - U_3\xi^A_2, \qquad\quad A^{1122} = A_{12}, \qquad A^{2222} = A_{22}, \tag{9}$$

$$A^*_{16} = \tfrac{1}{2}U_2\xi^A_3 + U_3\xi^A_4, \qquad\qquad\quad A^{ijkl} = A^{ijlk} = A^{klij},$$

$$A^*_{26} = \tfrac{1}{2}U_2\xi^A_3 - U_3\xi^A_4,$$

$$B^*_{11} = U_2\xi^B_1 + U_3\xi^B_2,$$

$$B^*_{22} = -U_2\xi^B_1 + U_3\xi^B_2, \qquad\qquad\quad B^{1111} = B_{11}, \qquad B^{1212} = B_{66},$$

$$B^*_{12} = -U_3\xi^B_2, \qquad\qquad\qquad\qquad\ B^{1112} = B_{16}, \qquad B^{1222} = B_{26},$$

$$B^*_{66} = -U_3\xi^B_2, \qquad\qquad\qquad\qquad\ B^{1122} = B_{12}, \qquad B^{2222} = B_{22}, \tag{10}$$

$$B^*_{16} = \tfrac{1}{2}U_2\xi^B_3 + U_3\xi^B_4, \qquad\qquad\quad B^{ijkl} = B^{ijlk} = B^{klij},$$

$$B^*_{26} = \tfrac{1}{2}U_2\xi^B_3 - U_3\xi^B_4,$$

$$D_{11}^* = U_1 + U_2\xi_1^D + U_3\xi_2^D,$$

$$D_{22}^* = U_1 - U_2\xi_1^D + U_3\xi_2^D, \qquad\qquad D^{1111} = D_{11}, \qquad D^{1212} = D_{66},$$

$$D_{12}^* = U_4 - U_3\xi_2^D, \qquad\qquad\qquad D^{1112} = D_{16}, \qquad D^{1222} = D_{26},$$

$$D_{66}^* = \tfrac{1}{2}(U_1 - U_4) - U_3\xi_2^D, \qquad\qquad D^{1122} = D_{12}, \qquad D^{2222} = D_{22}, \qquad\qquad (11)$$

$$D_{16}^* = \tfrac{1}{2}U_2\xi_3^D + U_3\xi_4^D, \qquad\qquad\quad D^{ijkl} = D^{ijlk} = D^{klij}.$$

$$D_{26}^* = \tfrac{1}{2}U_2\xi_3^D - U_3\xi_4^D,$$

in an orthogonal curvilinear coordinate system. In eqs. (8) to (11), $Q^{\alpha\beta\gamma\delta}$, $A^{\alpha\beta\gamma\delta}$, $B^{\alpha\beta\gamma\delta}$, and $D^{\alpha\beta\gamma\delta}$ are the physical components of the corresponding tensors. The normalization is

$$A_{ij}^* = A_{ij}/h,$$

$$B_{ij}^* = 4\,B_{ij}/h^2, \qquad\qquad\qquad\qquad\qquad\qquad\qquad\qquad\qquad (12)$$

$$D_{ij}^* = 12\,D_{ij}/h^3.$$

$\xi_i{}^A$, $\xi_i{}^B$, $\xi_i{}^D$ are the lamination parameters

$$\xi_{[1,2,3,4]}^A = \frac{1}{2}\int_{-1}^1 [\cos 2\theta, \cos 4\theta, \sin 2\theta, \sin 4\theta]\,dz^*,$$

$$\xi_{[1,2,3,4]}^B = \int_{-1}^1 [\cos 2\theta, \cos 4\theta, \sin 2\theta, \sin 4\theta]\,z^*\,dz^*, \qquad\qquad (13)$$

$$\xi_{[1,2,3,4]}^D = \frac{3}{2}\int_{-1}^1 [\cos 2\theta, \cos 4\theta, \sin 2\theta, \sin 4\theta]\,z^{*2}\,dz^*,$$

where $z^* = 2z/h$ is the normalized through-the-thickness coordinate. The material in all plies must be the same (inter-laminar hybrids are not allowed, but intra-laminar are OK).

In this paper the lamination parameters $\xi_i{}^A$, $\xi_i{}^B$, $\xi_i{}^D$ are used as design variables for the layups of the structures. The stiffnesses are thus expressed as linear combinations of the twelve lamination parameters $\xi_i{}^X$ ($X=A,B,D$, $i=1,2,3,4$) according to eqs. (9)-(11), and consequently also the strain energy is a linear function of the lamination parameters (keeping the deformation fixed). This will later be used to show that the object functions are concave.

Table 1. Typical material constants [7]

Material	U_1 (GPa)	U_2 (GPa)	U_3 (GPa)	U_4 (GPa)
graphite/epoxy T300-5208	76.4	85.7	19.7	22.6

3. PROBLEM FORMULATION

The lamination parameters are chosen as design variables for the layup optimization. A major benefit of this approach is that all physically possible layups are included using a minimum number of design variables. This choice also leads to significant simplifications

during the optimization which are due to the fact that local optima are avoided. Below, the object functions are stated.

3.1. Static Deformation

The solution of a linear elastic static problem is obtained as the minimum of a functional of the deformation, the potential energy U. For plates,

$$U[u_\alpha, w] = \int_S W(u_\alpha, w) \, dS - \int_S p \, w \, dS - \int_{\partial S_V} V \, w \, d\eta + \int_{\partial S_M} M_{\xi\xi} \frac{\partial w}{\partial \xi} \, d\eta - \int_{\partial S_T} T^\beta \, u_\beta \, d\eta - \sum_{i=1}^{n} R w \quad (14)$$

where S is the plate surface, ∂S is the boundary of the plate, ∂S_V is the part of the boundary where V is specified, etc. (ξ, η) is a local coordinate system with η along the boundary of the plate and ξ along its outward normal. The loads are design independent and dead (deformation independent). p is load per unit area on the plate surface and it is defined positive in the positive z direction. V is the equivalent boundary shear force

$$V = Q^\alpha v_\alpha + \frac{\partial}{\partial \eta} (M^{\alpha\beta} v_\alpha e_\beta) \, , \tag{15}$$

$M_{\xi\xi}$ is the moment parallel to the plate boundary

$$M_{\xi\xi} = M^{\alpha\beta} v_\alpha v_\beta \, , \tag{16}$$

T^β is the membrane traction

$$T^\beta = N^{\alpha\beta} v_\alpha \tag{17}$$

and R is the equivalent corner force

$$R = \left[M^{\alpha\beta} v_\alpha e_\beta \right]_{\eta_c-}^{\eta_c+} \tag{18}$$

where η_c is the η coordinate of the corner. Above, the transverse shear loads Q^α are

$$Q^\alpha = \int_{-h/2}^{h/2} \sigma^{z\alpha} \, dz \, , \tag{19}$$

the bending moments $M^{\alpha\beta}$ are

$$M^{\alpha\beta} = \int_{-h/2}^{h/2} \sigma^{\alpha\beta} \, z \, dz \, , \tag{20}$$

and the in-plane loads $N^{\alpha\beta}$ are

$$N^{\alpha\beta} = \int_{-h/2}^{h/2} \sigma^{\alpha\beta} \, dz \tag{21}$$

and v_α and e_β are the components of the normal and tangent vectors, respectively, on the boundary of the plate. Observe that ∂S_V, ∂S_M, and ∂S_T may overlap. The strain energy W is expressed in displacements using some kinematic relations between displacements and strains and changes of curvatures. In the case there are springs, extensional or rotational, attached to the structure, their deformation energies should be added to the integral of the strain energy.

The object function to be maximized is

$$U_{\min} = \min_{u_\alpha, w} U[u_\alpha, w] \tag{22}$$

which is a measure of the stiffness of the structure, see below. $U_{\min}$ is a function of the layup, i.e. the lamination parameters. Because of the minimum of the potential energy for the true deformations u_α, w,

$$U\left[u_\alpha^*, w^*\right] \geq U_{\min} \tag{23}$$

for any test deformations u_α^*, w^* fulfilling the kinematic boundary conditions. Eq. (23) thus constitutes an upper bound for the object function. Observe that U is linear in the lamination parameters if the deformation is fixed.

Cases of practical interest are e.g.

(*i*) Prescribed concentrated load P (or moment). The object function is then

$$U_{\min} = -\frac{1}{2} P u_p \tag{24}$$

where u_p is the displacement corresponding to the concentrated load. Maximization of $U_{\min}$ is equivalent to minimization of the displacement u_p.

(*ii*) Pressure load on S, when

$$U_{\min} = -\frac{1}{2} \int_S p w \, dS \ . \tag{25}$$

Maximizing $U_{\min}$ equals minimizing the weighted average displacement

$$\int_S p w \, dS \ . \tag{26}$$

3.2. Vibration

The square of the lowest eigenfrequency, ω^2, is chosen as the object function for the vibration optimization task. The Rayleigh quotient for the vibration problem is

$$R_{vibr}\left[u_\alpha^*, w^*\right] = 2 \frac{\int_S W(u_\alpha^*, w^*) \, dS}{\int_S \rho \, (u_\alpha^* u_\alpha^* + w^{*2}) \, dS} \tag{27}$$

which is an upper bound for the object function, ω^2, for any test functions u_α^*, w^* fulfilling the kinematic boundary conditions. In case springs are present, their deformation energies should be added to the numerator of eq. (27). The Rayleigh quotient R_{vibr} may be considered as a

"potential" to be minimized for the vibration problem. R_{vibr} is linear in the lamination parameters if the deformation is fixed.

3.3. Buckling

For the buckling optimization, proportional loading independent of the layup is assumed

$$N^{\alpha\beta} = \gamma\, N'^{\alpha\beta} \tag{28}$$

where $N'^{\alpha\beta}$ are initial membrane loads for a reference state. The load factor γ when instability occurs is taken as the object function.

The Rayleigh quotient gives an upper bound for the object function. For plates,

$$R_{buck}\left[w^*\right] = 2\frac{\displaystyle\int_S W\left[w^*\right] dS}{\displaystyle\int_S N'^{ij}\, w^*_{,i}\, w^*_{,j}\, dS} \;. \tag{29}$$

when the denominator is positive definite and w^* fulfils the kinematic boundary conditions. R_{buck} may be considered as a "potential" to be minimized for the buckling problem. As for the vibration task, if springs are attached to the structure their deformation energies should be added to the numerator of eq. (29) and, further, R_{buck} is linear in the lamination parameters if the deformation is fixed.

4. CONVEXITY OF THE FEASIBLE REGION

Let the bold symbol $\boldsymbol{\xi}[\theta]$ represent a vector consisting of the twelve lamination parameters obtained with the layup $\theta(z^*)$. This vector might either be constant all over the structure, or it might be an arbitrary function of x_α, the coordinates in the middle surface of the structure, i.e. the layup is either the same in all points of the structure, or it changes. The feasible region of the lamination parameters is convex, i.e. there exists a vector $_\alpha\boldsymbol{\xi}$ in the region between any two vectors $_1\boldsymbol{\xi}$ and $_2\boldsymbol{\xi}$ in the region:

$$_\alpha\boldsymbol{\xi} = {}_1\boldsymbol{\xi}\,\alpha + {}_2\boldsymbol{\xi}\,(1-\alpha) \tag{30}$$

for any $\alpha \in \mathbf{R}[0,1]$, see Fig. 1. This is seen by dividing the z^* interval $[-1,\,1]$ into N infinitesimal intervals

$$\Delta z^*_i = z^*_{i+1} - z^*_i \tag{31}$$

such that both of the layup functions $_1\theta(z^*)$ and $_2\theta(z^*)$ (corresponding to $_1\boldsymbol{\xi}$ and $_2\boldsymbol{\xi}$, respectively) are continuos within each Δz_i^* . Within each Δz_i^* the layup $_\alpha\theta$ is chosen as a mixture of both $_1\theta$ and $_2\theta$:

$$_\alpha\theta(z^*) = \begin{cases} {}_1\theta(z^*) \text{ for } z^* \in (\,z^*_i\,,\, z^*_i + \alpha\,\Delta z^*_i\,) \\[2mm] {}_2\theta(z^*) \text{ for } z^* \in (\,z^*_i + \alpha\,\Delta z^*_i\,,\, z^*_{i+1}\,) \end{cases} \tag{32}$$

see Fig. 2. When the length of the largest $\Delta z_i{}^*$ approaches zero, $\xi[_\alpha\theta]$ approaches $_\alpha\xi$. Only the first component of $\xi[_\alpha\theta]$ will be studied to show this :

$$\xi_1^A\left[_\alpha\theta\right] = \frac{1}{2}\int_{-1}^{1}\cos(2\,_\alpha\theta(z^*))\,dz^* = \frac{1}{2}\sum_{i=0}^{N-1}\int_{z_i^*}^{z_i^*+\alpha\Delta z_i^*}\cos(2\,_1\theta(z^*))\,dz^*$$

$$+\frac{1}{2}\sum_{i=0}^{N-1}\int_{z_i^*+\alpha\Delta z_i^*}^{z_i^*+\Delta z_i^*}\cos(2\,_2\theta(z^*))\,dz^* = \alpha\frac{1}{2}\sum_{i=0}^{N-1}\Delta z_i^*\cos(2\,_1\theta(z_i^*+_1\zeta\alpha\Delta z_i^*))$$

$$+(1-\alpha)\frac{1}{2}\sum_{i=0}^{N-1}\Delta z_i^*\cos(2\,_2\theta(z_i^*+\alpha\Delta z_i^*+_2\zeta(1-\alpha)\Delta z_i^*)) \tag{33}$$

$$\to \alpha\xi_1^A\left[_1\theta\right] \;+\; (1-\alpha)\xi_1^A\left[_2\theta\right] \qquad \text{when} \quad \max_i\Delta z_i^* \to 0$$

where $_1\zeta$ and $_2\zeta \in \mathbf{R}[0,1]$ .The first equality is obtained using eq. (32), the second equality is due to continuity within each interval $\Delta z_i{}^*$. The remaining components of $\xi[_\alpha\theta]$ follow the same pattern, and the proof is thus considered completed.
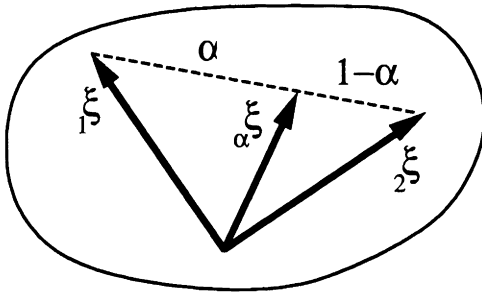
Fig. 1. The region of the lamination parameters is convex.
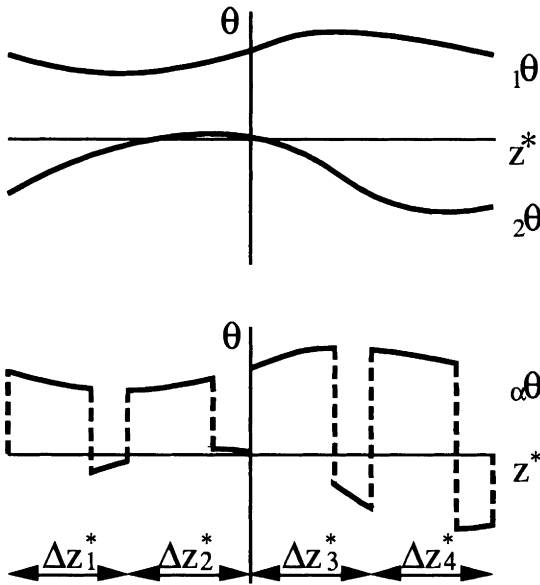
Fig. 2. Construction of $_\alpha\theta(z^*)$.

5. CONCAVITY OF THE OBJECT FUNCTIONS

Using the result that the strain energy is a linear function of the lamination parameters for a fixed deformation, it will be shown that the object functions to maximize (the potential energy for the static problem, the square of the eigenfrequency for the vibration problem, the load factor for buckling) are concave functions of the lamination parameters. This result is descending from Svanberg [6], who showed that "convex" optimization problems can be obtained when the structural stiffness matrix of a finite element discretization of a structure is linear in the design parameters. Concavity of the object functions is independent of whether the lamination parameters are constant or change from region to region in the structure. "Potentials" fulfilling minimum properties for the true deflection functions are used. These are U for the static problem, and the Rayleigh quotients R_{vibr} for the vibration and R_{buck} for the buckling problems; jointly they will be called R below. For simplicity, the in-plane and out-of-plane deformations are collectively denoted w. The object functions are thus $\min_w R$.

Now consider the object function $\min_w R$ with the solution $_\alpha w$ for the layup

$$_\alpha\xi = {}_1\xi\,\alpha + {}_2\xi\,(1-\alpha) \tag{34}$$

for any $\alpha \in \mathbf{R}[0,1]$. The object function $\min_w R$ is a concave function, Fig. 3, of the lamination parameters since

$$\min_w R\left(_\alpha\xi\right) = R\left(_\alpha\xi,\, _\alpha w\right) = \alpha R\left(_1\xi,\, _\alpha w\right) + (1-\alpha)R\left(_2\xi,\, _\alpha w\right)$$
$$\geq \alpha \min_w R\left(_1\xi\right) + (1-\alpha)\min_w R\left(_2\xi\right) \tag{35}$$

where the second equality is obtained because of the linear dependence of the strain energy on ξ. Observe that the result is valid independent of whether the layup is constant in the whole structure (in-plane homogeneous), or if it is different in a finite number of regions, each with a constant layup. It is thus valid for both cases schematically shown in Fig. 4.
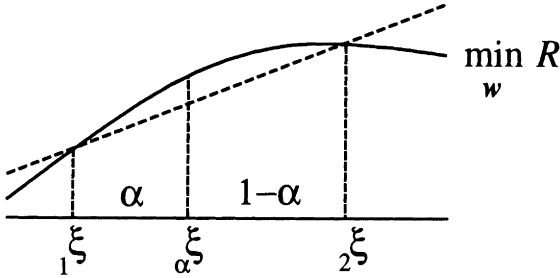
Fig. 3. R is a concave function of the lamination parameters.
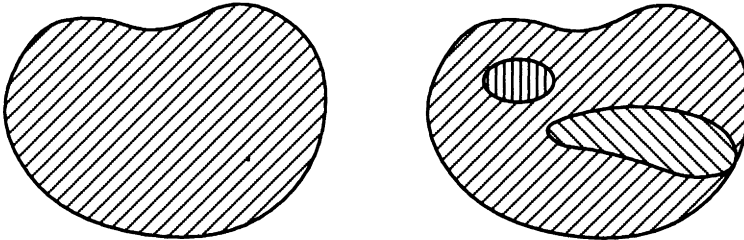
Fig. 4. Plate with in-plane homogeneous layup (left) and plate with in-plane non-homogeneous layup (right). The layup of the right plate is different in a finite number of regions, each with a constant layup. The line pattern symbolizes e.g. fiber directions.

The fact that the feasible region is convex and the object functions that should be maximized are concave considerably simplifies the optimization. Such optimization problems have no local optima but just one global optimum, e.g. [8]. Fig. 5 shows an example of problems arising when layup angles are used as design variables - lots of local optima [9].

If, for some reason, one would be interested in finding the layups that *minimizes* potential energies, *minimizes* eigenfrequencies or *minimizes* buckling loads, the optimal designs will be extreme points of the boundary of the feasible region [8].
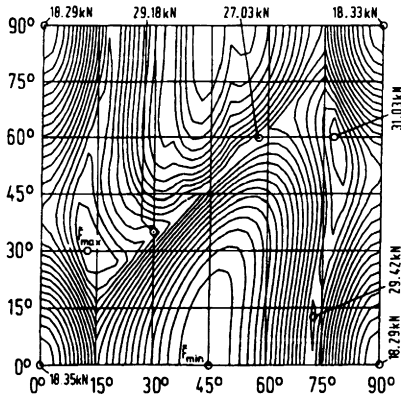
Fig. 5. Buckling load of a uni-axially compressed cylinder *versus* θ_1 and θ_2 in a $(+/-\theta_1, +/-\theta_2)$ layup, from Zimmermann [9].

6. FEASIBLE REGION, SOME SPECIAL CASES

The major problem with optimization using lamination parameters to describe the layup is that the feasible region of the twelve lamination parameters still is not fully known. Because of the normalization, all lamination parameters satisfy

$$\xi_i^x \in \mathbf{R}[-1,1] \ . \tag{36}$$

6.1. In-plane Problems

Some structures are completely determined by the in-plane stiffnesses A_{ij}, e.g. structures subject to in-plane stresses only and with no coupling between in-plane stresses and out-of-plane deformations, $B_{ij} = 0$. For the optimization of such structures only the four in-plane lamination parameters ξ_i^A are needed. If the structure further is orthotropic, only two parameters are needed, ξ_1^A and ξ_2^A. The feasible region of these two parameters was determined by Miki [2]. It is simply derived using Schwarz inequality

$$\int_{-1}^{1} f^2 \, dz^* \int_{-1}^{1} g^2 \, dz^* - \left(\int_{-1}^{1} fg \, dz^* \right)^2 \geq 0 \tag{37}$$

with

$$f = 1, g = \cos(2\theta(z^*)) \tag{38}$$

and thus

$$1 + \xi_2^A - 2\xi_1^{A^2} \geq 0 \ . \tag{39}$$

This, together with eq. (36), gives an "outer boundary" of the feasible region, but since it can be realized using a discrete layup where the layup angle θ is independent of its position through the

322

thickness z^*, this is together with eq. (36) the true feasible region of $\xi_1{}^A$ and $\xi_2{}^A$, see Fig. 6. The curved boundary of the feasible region is described by an off-axis uni-directional laminate $(+\theta_1)$ or, equivalently, by an angle-ply laminate $(+/-\theta_1)$.

Fukunaga [4] derived the feasible region of the four in-plane lamination parameters, and the result is, besides eqs. (36) and (39),

$$2\left(1 + \xi_2^A\right)\xi_3^{A2} - 4\xi_1^A\xi_3^A\xi_4^A + \xi_4^{A2} \leq \left(\xi_2^A - 2\xi_1^{A2} + 1\right)\left(1 - \xi_2^A\right) . \tag{40}$$

Any combination of these four lamination parameters can be realized with a small number of discrete plies [4].
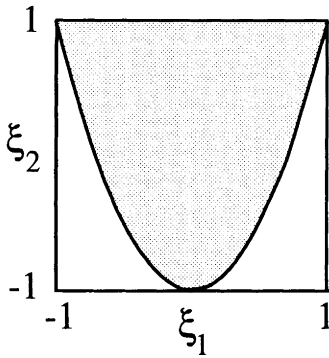
Fig. 6. Feasible region of $\xi_1{}^A$ and $\xi_2{}^A$ or, alternatively, of $\xi_1{}^D$ and $\xi_2{}^D$.

6.2. Out-of-plane Problems

It is quite common that the in-plane and out-of-plane equations for plates can be uncoupled. Examples are bending, vibration, and buckling of plates lacking coupling stiffnesses, $B_{ij} = 0$ (and statically determined in-plane loads in the case of buckling). To optimize for example deflections, vibration frequencies and/or buckling loads of such structures, only the four out-of-plane lamination parameters ξ_i^D are needed. If the structure further is orthotropic, only two parameters are needed, $\xi_1{}^D$ and $\xi_2{}^D$. The feasible region of these two parameters was determined by Miki [3]. It is besides eq. (36)

$$1 + \xi_2^D - 2\xi_1^{D2} \geq 0 \tag{41}$$

which is illustrated in Fig. 6. The boundary of the feasible region is described by an off-axis uni-directional laminate $(+\theta_1)$ or, equivalently, by an angle-ply laminate $(+/-\theta_1)$. Fukunaga [4] derived the feasible region of the four out-of-plane lamination parameters which, besides eqs. (36) and (41), is

$$2\left(1 + \xi_2^D\right)\xi_3^{D2} - 4\xi_1^D\xi_3^D\xi_4^D + \xi_4^{D2} \leq \left(\xi_2^D - 2\xi_1^{D2} + 1\right)\left(1 - \xi_2^D\right) . \tag{42}$$

Again, any combination of these four lamination parameters can be realized with a small number of discrete plies [4].

6.3. Orthotropic Laminate, Coupled Problems

The behaviour of for example shallow orthotropic shells generally depends on both in-plane, A_{ij}, and out-of-plane, D_{ij}, stiffnesses. ξ_1^A, ξ_2^A, ξ_1^D, and ξ_2^D describe the stiffnesses of a general orthotropic laminate; the other lamination parameters are zero. For optimization of orthotropic laminates, the feasible region of the four lamination parameters ξ_1^A, ξ_2^A, ξ_1^D, and ξ_2^D is therefore needed. The region is obtained by determining the layup function $\theta(z^*)$ which maximizes the functional

$$F\left[\theta(z^*)\right] = k_1 \xi_1^A\left[\theta(z^*)\right] + k_2 \xi_2^A\left[\theta(z^*)\right] + k_3 \xi_1^D\left[\theta(z^*)\right] + k_4 \xi_2^D\left[\theta(z^*)\right]$$

$$= \int_{-1}^{1}\left\{\left(\frac{k_1}{2} + \frac{3k_3}{2}z^{*2}\right)\cos\left(2\theta(z^*)\right) + \left(\frac{k_2}{2} + \frac{3k_4}{2}z^{*2}\right)\cos\left(4\theta(z^*)\right)\right\}dz^* \qquad (43)$$

$$\equiv \int_{-1}^{1} G\left(\theta(z^*)\right) dz^*$$

where the k_i are given numbers and G is defined by the last equality. Geometrically this is illustrated in Fig. 7. F is constant on a hyperplane whose normal is (k_1, k_2, k_3, k_4). By increasing F, the hyperplane is translated in the normal direction. The maximum of F for given k_i is obtained when the hyperplane is tangent to the feasible region of the lamination parameters. Thus, the layup obtained by extremizing F yields lamination parameters on the boundary of the feasible region. By determining the layups for all directions, i.e. for all k_i with $\sum k_i^2 = 1$, the feasible region is obtained.
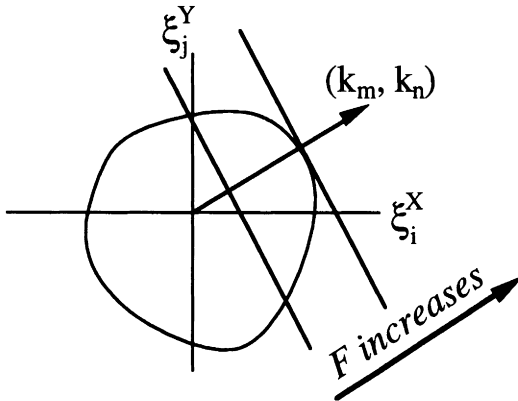
Fig. 7. The principle for determining extreme points of the feasible region.

Another interpretation of eq. (43) is that $k_1 \xi_1^A$ is extremized when the other lamination parameters, ξ_2^A, ξ_1^D, ξ_2^D, are constrained to certain values, i.e. a constrained optimization where k_2, k_3, and k_4 are Lagrange multipliers.

The functional F could be extremized using variational calculus, which results in the Euler equation

$$\frac{\partial G}{\partial \theta} = 0 \quad \Leftrightarrow \quad \sin 2\theta \left[(k_1 + 3k_3 z^{*2}) + 2(2k_2 + 6k_4 z^{*2}) \cos 2\theta \right] = 0 \qquad (44)$$

thus either

$$\sin 2\theta = 0, \text{ i.e. } \cos 2\theta = +/-1, \qquad (45)$$

or

$$(k_1 + 3k_3 z^{*2}) + 2(2k_2 + 6k_4 z^{*2}) \cos 2\theta = 0. \qquad (46)$$

These conditions are necessary but not sufficient since they do not determine the layup uniquely, i.e. where eq. (45) and where eq. (46) should be fulfilled. The Euler equation is not expected to yield a sufficient condition since θ not necessarily has to be a continuos function of z^*. A stronger requirement can though be obtained by requiring that

$$F\left[\theta(z^*)\right] - F\left[\theta(z^*) + \vartheta(z^*)\right] \geq 0 \qquad (47)$$

for, in the present case, any *piece wise* continuos test function $\vartheta(z^*)$. $\vartheta(z^*)$ is chosen as a narrow "peak" at z_0^* in order to get a requirement on θ locally :

$$\vartheta(z^*) = \Delta \left[H(z^* - z_0^*) - H(z^* - z_0^* - \varepsilon) \right] \qquad (48)$$

where H is the Heaviside step function, and ε and Δ are the width and height of the peak, see Fig. 8. ε is infinitesimal and positive, whereas Δ is arbitrary.
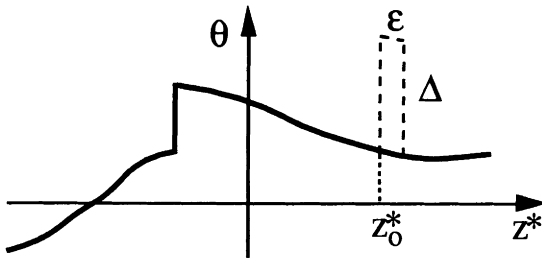
Fig. 8. $\theta(z^*)$ and the test function $\vartheta(z^*)$.

Eq. (48) in eq. (47) gives

$$F\left[\theta(z^*)\right] - F\left[\theta(z^*) + \vartheta(z^*)\right] = \int_{-1}^{1} \{G(\theta(z^*)) - G(\theta(z^*) + \vartheta(z^*))\} \, dz^*$$

$$= \int_{z_0^*}^{z_0^* + \varepsilon} \{G(\theta(z^*)) - G(\theta(z^*) + \Delta)\} \, dz^* \rightarrow \varepsilon \{G(\theta(z_0^*)) - G(\theta(z_0^*) + \Delta)\} \qquad (49)$$

$$\equiv \frac{1}{2} \varepsilon R$$

where R is defined by the last equality. R should be non-negative for arbitrary Δ, i.e.

$$R = 2\left(\frac{k_1}{2} + \frac{3k_3}{2}z_0^{*2}\right)\{\cos(2\theta(z_0^*)) - \cos(2\theta(z_0^*) + 2\Delta)\}$$
$$+ 2\left(\frac{k_2}{2} + \frac{3k_4}{2}z_0^{*2}\right)\{\cos(4\theta(z_0^*)) - \cos(4\theta(z_0^*) + 4\Delta)\} \tag{50}$$
$$= (c - c_\Delta)\{b_1 + b_2(c + c_\Delta)\} \geq 0$$

where

$$c = \cos(2\theta(z_0^*)),$$

$$c_\Delta = \cos(2\theta(z_0^*) + 2\Delta),$$

$$b_1 = k_1 + 3k_3 z_0^{*2}, \tag{51}$$

$$b_2 = 2k_2 + 6k_4 z_0^{*2}.$$

Eq. (50) should be fulfilled for all $c_\Delta \in \mathbf{R}[-1, 1]$ and, successively, for all $z_0^* \in \mathbf{R}(-1, 1)$ save for intervals of zero measure. This gives a layup function $\theta(z^*)$ which yields lamination parameters for a point on the boundary of the feasible region. Since eq. (50) should be fulfilled for any $z_0^* \in \mathbf{R}(-1, 1)$, the subscript 0 on z_0^* is from now on omitted. Eq. (50) is independent of the sign of z^* so the layup on the boundary will be symmetric. It is accordingly sufficient to study the interval $z^* \in \mathbf{R}(0, 1)$. How θ is determined is schematically explained in the algoritm in Fig. 9, and also explained below.

```
If b2 < 0 then
        If 1 cc > 1then
             c = 1
        elseif -1 ≤ cc ≤ 1 then
             c = cc
        elseif cc < -1 then
             c = -1
        endif
elseif b2 > 0 then
        if cc > 0 then
             c = -1
        elseif cc < 0 then
             c = 1
        elseif cc = 0 then
             c = +/-1      (see the text)
        endif
elseif b2 = 0 then
        if b1 > 0 then
             c = 1
        elseif b1 < 0 then
             c = -1
        elseif b1 = 0 then
             ! This will occur only on intervals of measure zero
        endif
endif
```

Fig. 9. Pseudo code for determination of $\cos 2\theta$.

To find the layup angle θ at a certain z^* for given k_i, c should be selected such that $R \geq 0$ for any $c_\Delta \in \mathbf{R}[-1, 1]$. All k_i are not allowed to be zero simultaneously since F then is identically zero, eq. (43). At a certain z^*, values of b_1 and b_2 are calculated according to eq. (51). First, assume that b_2 is non-zero at this point; that case will be dealt with later. In the c-c_Δ-plane, R is then zero only on the two crossing lines $c - c_\Delta = 0$ and $b_1 + b_2(c + c_\Delta) = 0$, Fig. 10. The value of c at the crossing is called c_c, and

$$c_c = -\frac{b_1}{2b_2} \; . \tag{52}$$
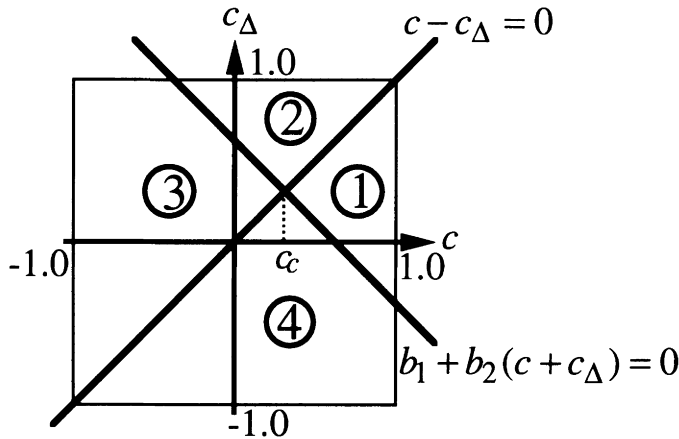
Fig. 10. The c - c_Δ - plane and its regions.

R is positive either in regions 1 and 3, or in regions 2 and 4. When $b_2 < 0$ then R is positive in regions 2 and 4, and the only value of c for which $R \geq 0$ for all $c_\Delta \in \mathbf{R}[-1, 1]$ is $c = c_c$ when $c_c \in [-1, 1]$. If $c_c \notin [-1, 1]$, then $c = 1$ for $c_c > 1$, and $c = -1$ for $c_c < -1$.

When R is positive in regions 1 and 3, i.e. when $b_2 > 0$, then $c = -1$ if $c_c > 0$, and $c = 1$ if $c_c < 0$, as seen in Fig. 10. When $c_c = 0$, then $c = +/-1$ i.e. the layup is not uniquely determined. If both k_1 and k_3 are zero, i.e. b_1 is identically zero ($b_1 = 0$ for all z^*), then the *layup* cannot be determined solely by the requirement that $R \geq 0$. If b_1 not is identically zero then there is no problem since the layup is indeterminate only in a point and thus the integrals for the lamination parameters are not affected. The case when b_1 is identically zero and $b_2 > 0$ will be dealt with later.

When b_2 is identically zero, b_1 is not identically zero since all k_i cannot vanish simultaneously. b_1 may vanish for certain z^* but the layups in these points are immaterial since these intervals are of measure zero. If $b_1 > 0$ then $c = 1$ is required for R to be positive for all $c_\Delta \in \mathbf{R}[-1, 1]$, and if $b_1 < 0$ then $c = -1$ is required, see Fig. 10.

The remaining case, $b_2 > 0$ and b_1 identically zero, will be dealt with now. b_1 is identically zero only when $k_1 = k_3 = 0$, i.e. the feasible region of only *two* of the lamination parameters, ξ_2^A and ξ_2^D, is determined. ξ_2^A and ξ_2^D depend only on $\cos 4\theta$. Above it was shown that $c = +/-1$, and since $\cos 4\theta = 2\cos^2 2\theta - 1 = 2c^2 - 1$, these lamination parameters are independent of the sign of c. Since $b_1 = 0$, $c_c = 0$ and the layup will be $\cos 4\theta = 1$ when $b_2 > 0$ and $\cos 4\theta = -1$ when $b_2 < 0$. b_2 is symmetric in z^* and changes sign at most once is the interval $z^* \geq 0$. Integrating ξ_2^A and ξ_2^D, their feasible region is readilly determined to

$$\frac{\left(\xi_2^A + 1\right)^3}{4} - 1 \leq \xi_2^D \leq \frac{\left(\xi_2^A - 1\right)^3}{4} + 1. \tag{53}$$

ξ_1^A and ξ_1^D are still undetermined. They cannot be determined from the requirement that $R \geq 0$ because the feasible region is locally non-strictly convex or, geometrically, it is "flat" locally, and thus uniqueness of the *layup* is lost. However, $c = 1$ or $c = -1$ is required. The remaining

problem is to determine where $c = 1$ and where $c = -1$. ξ_1^A depends only on the fraction, μ, of the z^* interval where $c = 1$ and $c = -1$, not the position through the thickness, whereas ξ_1^D does depend on the position through the thickness; see the definitions of the lamination parameters in eq. (13). Consider the following example where $k_2 = 4/5$ and $k_4 = -3/5$ apart from $k_1 = k_3 = 0$. Since the layup will be symmetric, only the region $z^* > 0$ is analysed. $b_2 > 0$ for $z^* < 2/3$, and otherwise $b_2 \leq 0$. $c = 0$ for $b_2 < 0$, i.e. $c = 0$ for $z^* > 2/3$. For $z^* < 2/3$, $c = 1$ or $c = -1$. Fixing ξ_1^A, the fraction μ is determined :

$$\xi_1^A = \int_0^1 \cos 2\theta \, dz^* = \int_0^{\mu 2/3} 1 \, dz^* + \int_{\mu 2/3}^{2/3} (-1) \, dz^* + \int_{2/3}^1 0 \, dz^* = \frac{2}{3}(2\mu - 1) \tag{54}$$

thus, in this example,

$$\mu = \frac{3}{4}\xi_1^A + \frac{1}{2} \tag{55}$$

ξ_1^D then varies between

$$\xi_1^D = 3\int_0^1 \cos 2\theta \, dz^* = 3\int_0^{\mu 2/3} z^{*2} \, dz^* + 3\int_{\mu 2/3}^{2/3} -z^{*2} \, dz^* + 3\int_{2/3}^1 0 \, dz^* = \left(\frac{2}{3}\right)^3 (2\mu^3 - 1)$$

$$= \frac{1}{4}\left(\xi_1^A + \frac{2}{3}\right)^3 - \left(\frac{2}{3}\right)^3 \tag{56}$$

which is obtained by placing all fraction of $c = 1$ closest to the middle of the laminate, and

$$\xi_1^D = 3\int_0^1 \cos 2\theta \, dz^* = 3\int_0^{(1-\mu)2/3} -z^{*2} \, dz^* + 3\int_{(1-\mu)2/3}^{2/3} z^{*2} \, dz^* + 3\int_{2/3}^1 0 \, dz^* = \left(\frac{2}{3}\right)^3 (1 - 2(1-\mu)^3)$$

$$= \frac{1}{4}\left(\xi_1^A - \frac{2}{3}\right)^3 + \left(\frac{2}{3}\right)^3 \tag{57}$$

which is obtained by placing all fraction of $c = 1$ as close to the surface of the laminate as possible. Any value of ξ_1^D between the values of eq. (56) and eq. (57) can be obtained. With this, the layup on the boundary of the feasible region of the four lamination parameters needed for an orthotropic composite is completely determined.

Now that the layup is known on the boundary of the feasible region, the feasible region is simply determined by integrating the lamination parameters. The four-dimensional region is naturally difficult to display visually, but fixing the two in-plane lamination parameters ξ_1^A and ξ_2^A, the feasible region of ξ_1^D and ξ_2^D can be displayed. An example is provided in Fig. 11 where $\xi_1^A = \xi_2^A = 0$. In this figure, the boundary according to Fukunaga [5] is also shown as well as an outer boundary which is derived in the Appendix. As clearly seen, the region of Fukunaga is too small, and it is thus not - contrary to what was stated in the paper [5] - the true boundary of the feasible region of those four lamination parameters.

For optimization it is easier and sometimes appropriate is to use either an outer boundary of the feasible region, obtained e.g. by Schwarz inequality in the Appendix, or the inner boundary obtained by Fukunaga [5].
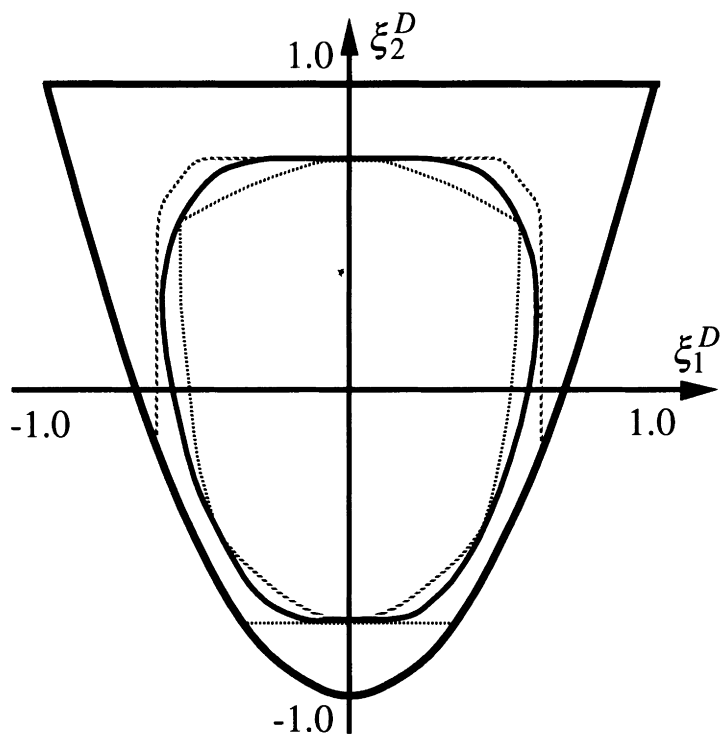
Fig. 11. The true feasible region of ξ_1^D and ξ_2^D (inner continuos line) when $\xi_1^A = \xi_2^A = 0$. Also, the inner boundary according to Fukunaga [5] (inner dashed curve), and an outer boundary derived in the Appendix (outer dashed curve).

7. SOME APPLICATIONS AND RESULTS OF OPTIMIZATION

7.1. In-plane Homogeneous Rectangular Plates

For in-plane homogeneous plates (thicknesses and stiffnesses independent of in-plane Cartesian coordinates) without bending-extension coupling stiffnesses B^{ijkl}, the equations for bending, vibration, and buckling are, respectively,

$$D^{\alpha\beta\gamma\delta}\,w|_{\alpha\beta\gamma\delta} = p\,,$$

$$D^{\alpha\beta\gamma\delta}\,w|_{\alpha\beta\gamma\delta} = \rho\omega^2\,,$$

$$D^{\alpha\beta\gamma\delta}\,w|_{\alpha\beta\gamma\delta} = (N^{ij}\,w|_i)\big|_j\,. \qquad (58)$$

Design independent loads are assumed. The expression

$$\phi = D_{11}\left(\frac{m}{a}\right)^4 + 2(D_{12} + 2D_{66})\left(\frac{m}{a}\right)^2\left(\frac{n}{b}\right)^2 + D_{22}\left(\frac{n}{b}\right)^4 \qquad (59)$$

where a and b are the in-plane dimensions of the plate, and m and n are integers, plays an important role for orthotropic simply supported plates concerning deflection, vibration, and buckling. This expression is linear in the bending stiffnesses D_{11}, D_{12}, D_{22}, and D_{66}, and these stiffnesses are linear in the lamination parameters. Accordingly, the maximum and minimum of ϕ will be found on the boundary of the feasible region, eq. (41). It is clear that the optimal fundamental eigenfrequency ($m=n=1$) of simply supported plates always will be located on this boundary, since $\omega^2 = \pi^4 \phi / \rho$; see also Fig. 12. The boundary of the feasible region is described by an angle-ply laminate, $\theta = (+/-\theta_1)$, i.e. there is only one remaining design variable, e.g. the layup angle θ_1. Analytical and numerical studies of rectangular orthotropic plates show that the optimum usually is located on the boundary of the feasible region, see Fig. 12 and e.g. Grenestedt [10,11].

When the deflection is symmetric for an orthotropic laminate, it can be shown that non-zero D_{16} and D_{26} terms never improve the performance of the laminate, e.g. Grenestedt [10,12,13].

Numerical studies of shear buckling of a rectangular non-orthotropic plate indicate that the optimum again is determined by a single parameter, this time the off-axis angle of a uni-directional laminate, Grenestedt [11].
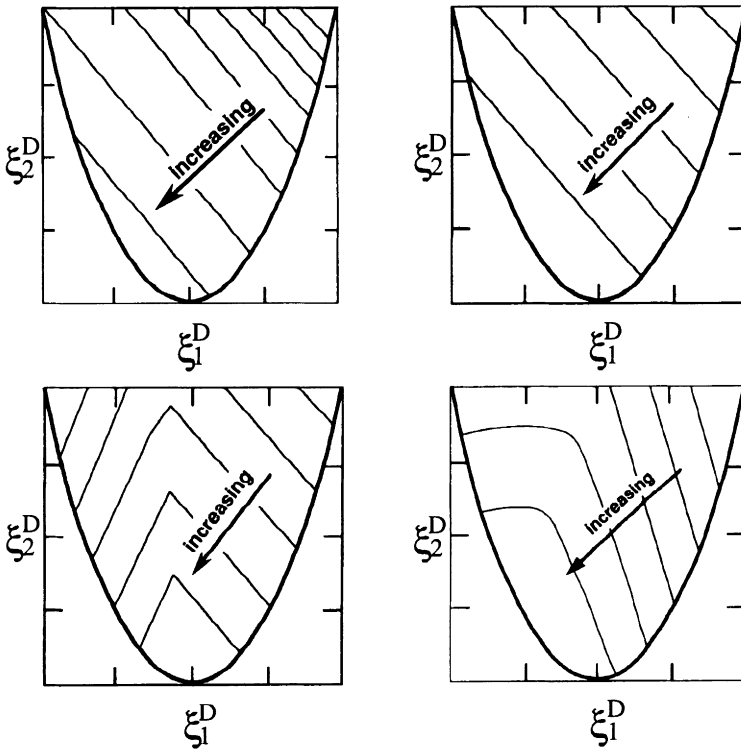
Fig. 12. Examples of object functions *versus* the lamination parameters ξ_1^D and ξ_2^D for simply supported orthotropic rectangular plates. From left to right and up to down: potential energy for static deformation (U_{min}) for $a/b=1.3$ and uniformly distributed surface load,

vibration frequency (ω^2) for a/b=1.3, buckling load during uniaxial compression (N^{11}) for a/b=1.3, and buckling load during shearing (N^{12}) for a/b=1.7. The maximum and minimum are found on the boundary of the feasible region.

7.2. In-plane Homogeneous Orthotropic Elliptical Plates

For a uniformly distributed load p_0 on an elliptical clamped plate with in-plane dimension a and b, the deflection is

$$w = \frac{a^4 p_0}{8\left(3D_{11} + 2\left(\frac{a}{b}\right)^2 (D_{12} + 2D_{66}) + 3\left(\frac{a}{b}\right)^4 D_{22}\right)} \left(1 - \frac{x_1^2}{a^2} - \frac{x_2^2}{b^2}\right)^2 . \tag{60}$$

Since the inverse of the deflection is linear in the lamination parameters, the optimal layup will apparently be an angle-ply (+/-θ_1), independent of whether the layup for maximum or minimum stiffness is sought. Interesting to note is that for a round plate (a=b), the deflection is independent of the lamination parameters, i.e. all layups are equivalent (even laminates with non-zero D_{16} and D_{26} stiffnesses).

8. STRENGTH OF MATERIAL

The strength of composite material plies strongly depend on the orientation of the plies relative the stress field. The longitudinal failure stress can be in the order of twenty times the transverse or shear failure stresses. The longitudinal failure strain is though usually in the same order as e.g. the transverse failure strain. A failure criteria based on strains is far less dependent on orientation of the plies than a failure criteria based on stresses. An approximate failure criteria can be based on the invariants of the strain tensor, thus the composite's strength would be independent of the rotation of the strain field. Tsai and Hahn [7] dwelled upon such a criteria which can be used as a conservative first-ply-failure approximation. For a failure criteria based on the invariants of the strain tensor, lamination parameters can be used.

9. CONCLUSIONS

It has been shown how layup optimization can be cast in a fully "convex" form, thus avoiding all troublesome local optima. All physically possible layups were included using a minimum of design variables. The feasible region of the four lamination parameters needed for an orthotropic laminate was determined. A number of simple examples of optimization were provided.

10. ACKNOWLEDGEMENTS

332

11. REFERENCES

1. Tsai, S.W., Pagano, N.J., "Invariant Properties of Composite Materials," *Composite Materials Workshop*, Technomic, Westport, CT, 1968, pp. 233-253.
2. Miki, M., "Material Design of Composite Laminates with Required In-Plane Elastic Properties," In: Hayashi,T., Kawata,K., Umekawa,S. (eds.), ICCM-IV, Tokyo, 1982, pp. 1725-1731.
3. Miki, M., "Design of Laminated Fibrous Composite Plates with Required Flexural Stiffness," In: Vinson,J.R., Taya,M. (eds.), ASTM STP 864, 1985, pp. 387-400.
4. Fukunaga, H., "Stiffness Design Method of Symmetric Laminates using Lamination Parameters," *private communication* .
5. Fukunaga, H., "Netting theory and its application to optimum design of laminated composite shells and plates," AIAA/ASME/ASCE/AHS 29th Structures, Structural Dynamics and Materials Conf., Williamsburg, 1988, pp. 983-991.
6. Svanberg, K., "On local and global minima in structural optimization," In: Atrek et al (ed.), *New directions in optimum structural design*, 1984, pp. 327-341.
7. Tsai, S.W., Hahn, H.T., *Introduction to Composite Materials* , Technomic, 1980.
8. Luenberger, D.G., *Linear and Nonlinear Programming*, 2nd ed., Addison-Wesley, 1984.
9. Zimmermann, R., "Optimization of axially compressed CFRP cylinders," *Proc. Spacecraft Structures*, CNES, Toulouse, 3-6 Dec., 1985.
10. Grenestedt, J.L., "Composite Plate Optimization Only Requires One Parameter," *Structural Optimization* **2**, 1990, pp. 29-37.
11. Grenestedt, J.L., "Layup Optimization against Buckling of Shear Panels," *Structural Optimization* **3**, 1991, pp. 115-120.
12. Grenestedt, J.L., "Layup Optimization and Sensitivity Analysis of the Fundamental Eigenfrequency of Composite Plates," *Composite Structures* **12**, 1989, pp. 193-209.
13. Grenestedt, J.L., "A Study on the Effect of Bending-Twisting Coupling on Buckling Strength," *Composite Structures* **12**, 1989, pp. 271-290.

APPENDIX

A1. Some Simple Constraints

The feasible region of pairs of lamination parameters can easilly be obtained with the approach of Section 6.3 above. The layup on the feasible region of e.g. ξ_1^A and ξ_1^D is found using eq. (50) with $k_2 = k_4 = 0$. Below, some scattered results are expressed :

$$\frac{\left(1+\xi_1^A\right)^3}{4}+1 \le \xi_1^D \le \frac{\left(\xi_1^A-1\right)^3}{4}+1 \tag{A.1}$$

$$\frac{\left(1+\xi_2^A\right)^3}{4}+1 \le \xi_2^D \le \frac{\left(\xi_2^A-1\right)^3}{4}+1 \tag{A.2}$$

$$\left|\xi_1^B\right|-1+\xi_1^{A^2} \le 0 \tag{A.3}$$

$$\left|\xi_2^B\right|-1+\xi_2^{A^2} \le 0 \tag{A.4}$$

$$\left|\xi_1^D\right|-1+\left|\xi_1^B\right|^{3/2} \le 0 \tag{A.5}$$

$$\left|\xi_2^D\right|-1+\left|\xi_2^B\right|^{3/2} \le 0 \tag{A.6}$$

A2. Outer Boundary of the Feasible Region

An outer boundary of the feasible region of the lamination parameters can be found using e.g. Schwarz inequality

$$\int f^2 \, dz^* \int g^2 \, dz^* - \left(\int fg \, dz^*\right)^2 \geq 0 \ . \tag{A.7}$$

Table A1 lists a number of constraints obtained in this way. The constants e, e_1, and e_2 are selected so that the left side of eq. (A.7) is minimized. In order to find a better boundary for the feasible region of ξ_1^A, ξ_2^A, ξ_1^D, ξ_2^D the results of eq. (45) and (46) must probably be incorporated.

Table A1.

f	g	constraint
1	$\cos 2\theta$	$-1 - \xi_2^A + 2\xi_1^{A2} <= 0$
1	$z^* \cos 2\theta$	$3\xi_1^{B2} - 2(1+\xi_2^D) <= 0$
1	$(z^*+e) \cos 2\theta$	$6\xi_1^{B2}(1+\xi_2^A) + 3(\xi_2^{B2} - 4\xi_1^A \xi_1^B \xi_2^B)$ $- 4(1+\xi_2^D)(1 + \xi_2^A - 2\xi_1^{A2}) <= 0$
z^*	$\cos 2\theta$	$3\xi_1^{B2} - 2(1+\xi_2^A) <= 0$
z^*	$z^* \cos 2\theta$	$-1 - \xi_2^D + 2\xi_1^{D2} <= 0$
z^*	$(z^*+e) \cos 2\theta$	$-2(1 + \xi_2^D - 2\xi_1^{D2})(-3\xi_1^{B2} + 2(1+\xi_2^A))$ $+ 3(\xi_2^B - 2\xi_1^B \xi_1^D)^2 <= 0$
z^*+e	$\cos 2\theta$	$3\xi_1^{B2} - 2(1 + \xi_2^A - 2\xi_1^{A2}) <= 0$
z^*+e	$z^* \cos 2\theta$	$3\xi_1^{B2} - 2(1 + \xi_2^D - 2\xi_1^{D2}) <= 0$
z^*+e_1	$(z^*+e_2)\cos 2\theta$	see below
$\cos \theta$	$z^* \cos \theta$	$3\xi_1^{B2} - 4(1+\xi_1^A)(1+\xi_1^D) <= 0$
$\cos 2\theta$	$z^* \cos 2\theta$	$3\xi_2^{B2} - 4(1+\xi_2^A)(1+\xi_2^D) <= 0$
$z^{*2}+e$	$\cos 2\theta$	$5(\xi_1^A - \xi_1^D)^2$ $- 2(1 + \xi_2^A - 2\xi_1^{A2}) <= 0$
$z^{*2}+e_1 z^*+e_2$	$\cos 2\theta$	$3\xi_1^{B2} + 5(\xi_1^A - \xi_1^D)^2$ $- 2(1 + \xi_2^A - 2\xi_1^{A2}) <= 0$
$z^{*2}+e_1$	$(z^{*2}+e_2) \cos 2\theta$	see below

A2.2 $f = z^*+e_1$, $g = (z^*+e_2)\cos 2\theta$

With

$$f = z^*+e_1, \ g = (z^*+e_2)\cos 2\theta \tag{A.8}$$

another constraint is obtained:

$$e_1{}^2 \left[\, e_2{}^2\, (\, 2 + 2\xi_2{}^A - 4\xi_1{}^{A2}\,) + e_2\, (\, 2\xi_2{}^B - 4\xi_1{}^A\xi_1{}^B\,) + (\, -\xi_1{}^{B2} + 2/3(1+\xi_2{}^D)\,)\,\right]$$

$$+ e_1 \left[\, e_2{}^2\, (\, -4\xi_1{}^A\xi_1{}^B) + e_2\, (\, -2\xi_1{}^{B2} - 8/3\xi_1{}^A\xi_1{}^D\,) + (\, -4/3\xi_1{}^B\xi_1{}^D\,)\,\right]$$

$$+ \left[\, e_2{}^2\, (\, -\xi_1{}^{B2} + 2/3(1+\xi_2{}^A)\,) + e_2\, (\, -4/3\xi_1{}^B\xi_1{}^D + 2/3\xi_2{}^B)\right.$$

$$\left. + (\, -4/9\xi_1{}^{D2} + 2/9(1+\xi_2{}^D)\,)\,\right]$$

$$= e_1{}^2\,[\chi_0] + e_1[\chi_1] + [\chi_2] >= \chi_2 - \chi_1{}^2\,/\,(4\chi_0) >= 0 \qquad\qquad (A.9)$$

where the functions χ_0 - χ_2 are defined by the first equality as the quantities within the square brackets. The first inequality is obtained by minimizing the expression *versus* e_1. The last expression is a function of e_2, and it is numerically minimized *versus* this variable.

A2.3 $f = z^{*2} + e_1$, $g = (z^{*2} + e_2)\cos\, 2\theta$

This constraint is appealing since it is zero when the layup angle θ fulfills eq. (46) which was derived using variational methods. It does though not incorporate the result of eq. (45) and the resulting constraint can thus not be expected to correspond to the true constraint in more than certain areas, whereas for most areas it will just constitute another outer boundary.

$$f = z^{*2} + e_1,\ \ g = (z^{*2} + e_2)\cos\, 2\theta \qquad\qquad (A.10)$$

makes the constraint, called C below,

$$C(e_1,e_2) = g_1(e_1,e_2;\xi) + g_2(e_1)\, t_2 - t_1 - g_3(e_1,e_2)\, t_3 >= 0 \qquad\qquad (A.11)$$

where

$$g_1(e_1,e_2;\xi) = (2/5 + 4/3e_1 + 2e_1{}^2)(2/3e_2(\xi_2{}^D + 1) + e_2{}^2(\xi_2{}^A + 1)) - (2/3(e_1 + e_2)\xi_1{}^D + 2e_1e_2\xi_1{}^A)^2$$

$$g_2(e_1) = 2/5 + 4/3e_1 + 2e_1{}^2$$

$$g_3(e_1,e_2) = 4/3(e_1 + e_2)\xi_1{}^D + 4e_1e_2\xi_1{}^A$$

$$t_1 = \left(\int_{-1}^{1} z^{*4}\cos 2\theta\ dz^*\right)^2$$

$$t_2 = \int_{-1}^{1} z^{*4}\cos^2 2\theta\ dz^*$$

$$t_3 = \int_{-1}^{1} z^{*4}\cos 2\theta\ dz^*$$

$C(e_1,e_2)$ is minimized vs. e_1 and e_2. The three integrals t_1, t_2, and t_3 can not be expressed with the lamination parameters, so bounds on them are used. An expression $C^*(e_1,e_2)$ which is always larger than or equal to $C(e_1,e_2)$ is thus constructed,

$$C^*(e_1,e_2) = g_1(e_1,e_2;\xi) + g_2(e_1)t_2{}^b - t_1{}^b - g_3(e_1,e_2)t_3{}^b >= 0 \qquad\qquad (A.12)$$

where t_i^b is the bound for the integral t_i, i=1,2,3.

$g_2(e_1)$ is positive for all e_1, and thus an upper bound for t_2 must be used. $g_3(e_1,e_2)$ can be either positive or negative. When $g_3(e_1,e_2)$ is positive a lower bound on t_3 must be used, and *vice versa*. t_1 is positive since it is a square of a real quantity. t_1 is preceded by a minus sign and therefore a lower bound has to be used. Bounds on t_1 - t_3 were obtained using the method of Section 6.3 and Schwarz inequality. The bounds are as follows :

t_1 : The lower bound of t_1 will be derived after the bound of t_3 is obtained, see below.

t_2 : Extremizing t_2 and fixing ξ_2^A leads to a layup with $\cos 4\theta = +/-1$, e.g. $\theta=0$ and $\theta=45$

deg. An upper bounds on t_2 is obtained by using a ($0_{(1-\alpha)}$, 45_α)$_s$ layup, where α is varied from 0 to 1, thus

$$t_2 \leq \frac{2}{5}\left\{1-\left(\frac{1-\xi_2^A}{2}\right)^5\right\} . \tag{A.13}$$

The same procedure but keeping ξ_1^D fixed leads to the bound

$$t_2 \leq \frac{2}{5}\left\{1-\left(\frac{1-\xi_2^D}{2}\right)^{5/3}\right\} . \tag{A.14}$$

The smallest of the two upper bounds is used.
t_3 : Schwarz inequality with

$$f=z^* \cos^2\theta \text{ and } g=z^{*3} \tag{A.15}$$

gives the bound

$$t_3 \leq \sqrt{\frac{2\left(\xi_2^D + 4\xi_1^D + 3\right)}{21}} - \frac{2}{5} \tag{A.16}$$

and with

$$f=z^* \cos 2\theta \text{ and } g=z^{*3} \tag{A.17}$$

the bound

$$|t_3| \leq \sqrt{\frac{2}{21}(\xi_2^D+1)} . \tag{A.18}$$

Extremizing t_3 using the method of Section 6.3 and constraining ξ_1^A shows that upper and lower bounds on t_3 are obtained by using ($90_{(1-\alpha)}$, 0_α)$_s$ and ($0_{(1-\alpha)}$, 90_α)$_s$ layups, respectively, where α is varied from 0 to 1:

$$\frac{2}{5}\left\{2\left(\frac{1+\xi_1^A}{2}\right)^5 - 1\right\} \leq t_3 \leq \frac{2}{5}\left\{-2\left(\frac{1-\xi_1^A}{2}\right)^5 + 1\right\} . \tag{A.19}$$

The same procedure but keeping $\xi_1{}^D$ fixed leads to the bounds

$$\frac{2}{5}\left\{2\left(\frac{1+\xi_1{}^D}{2}\right)^{5/3}-1\right\}\le t_3\le\frac{2}{5}\left\{-2\left(\frac{1-\xi_1{}^D}{2}\right)^{5/3}+1\right\}.$$

(A.20)

When $g_3(e_1,e_2)$ is positive a lower bound on t_3 must be used, and the largest of the three lower bounds is used. When $g_3(e_1,e_2)$ is negative an upper bound on t_3 must be used, and the smallest of the four upper bounds is used.

t_1 : Using the results above leads to the following bounds,

$$t_1 \ge \begin{cases} \left\{\dfrac{4}{25}\left\{2\left(\dfrac{1+\left|\xi_1{}^A\right|}{2}\right)^5-1\right\}\right\}^2, & \text{when} \quad \left|\xi_1{}^A\right| \ge 2^{4/5}-1 \\ 0, & \text{otherwise} \end{cases}$$

(A.21)

and

$$t_1 \ge \begin{cases} \left\{\dfrac{4}{25}\left\{2\left(\dfrac{1+\left|\xi_1{}^D\right|}{2}\right)^{5/3}-1\right\}\right\}^2, & \text{when} \quad \left|\xi_1{}^D\right| \ge 2^{2/5}-1 \\ 0, & \text{otherwise} \end{cases}$$

(A.22)

$C^*(e_1,e_2)$ shall be minimized versus e_1 and e_2. One variable, e.g. e_1, is easily reduced in the same way as in the last line of eq. (A9), thus resulting in a function $C^*(e_2)$. The minimum of $C^*(e_2)$ is then sought by numerical means. The minimization is carried out in three steps. First $g_3(e_1,e_2)$ is guessed to be positive, and C^* is minimized. If this minimum results in a negative $g_3(e_1,e_2)$ then the minimum is neglected. The same is then performed for a negative $g_3(e_1,e_2)$. In the third step $g_3(e_1,e_2)$ is set to zero, which yields an equation for e_1 and e_2. $C^*(e_1,e_2)$ is then minimized on the curve $g_3(e_1,e_2)=0$. The smallest of the non-neglected minimum values is the one used for the constraint.

A MODEL FOR LAYOUT OPTIMIZATION OF PLATE STRUCTURES

CIRO A. SOTO[1] and   ALEJANDRO R. DÍAZ[2]
Michigan State University
Department of Mechanical Engineering
East Lansing, MI 48824-1226, USA

Abstract
      In this paper we present a solution to the layout and shape optimization problem of plate structures using the Mindlin plate theory. The problem is stated as the determination of the optimum distribution of ribs symmetrically located above and below a central ply made by an isotropic material. We use a method based on homogenization techniques where the optimum shape problem is posed as a problem of optimization of material distribution. Numerical examples are presented to show the influence of different parameters on the optimum layout and shape of plates.

1.   INTRODUCTION

Homogenization techniques in layout and shape optimization problems have been successfully applied in two-dimensional elasticity ([BEN88, DIA92]) and three-dimensional elasticity [SUZ91].   This motivates the present study on shape optimization of plate structures. Bendsøe [BEN82] used homogenization techniques in plates with ribs in one direction and applied a "smear" out procedure to compute the homogenized properties of plates with ribs in two orthogonal directions. Suzuki and Kikuchi [SUZ92] introduced an approach to compute homogenized plate stiffness properties using the homogenized properties derived from two-dimensional elasticity. Their procedure was based on the assembly of three plies, two of them made using a homogenized material, to build a laminate that models ribbed plates. Our interest is in the application of homogenization techniques directly to the plate equation to obtain homogenized properties without using the smear out technique of Bendsøe or homogenized properties from two-dimensional elasticity. We present results following this line of inquiry here.

In this paper we use homogenized properties derived from the Mindlin plate equation, which enables us to consider transverse shear deformations.

---

[1]Graduate Student, [2]Associate Professor.

Homogenization techniques call for the use of microscopically pseudo-periodic materials. In this study we use layered material cells (Fig. 1) to describe the microstructure of the material. The advantage of using these cells is that they allow one to compute analytically the homogenized properties of plates. In this work we use a rank-2 cell (Fig. 1(b)) that can model ribs in two orthogonal directions with thickness 'a' and 'b', respectively. These two design variables will describe the shape of the plate cross section at each point of the domain. When 'a' or 'b' are unity, the plate has thickness $2h_2$; when 'a' and 'b' are both zero, the plate has thickness $2h_1$; and when 'a' and 'b' are between zero and one the plate has a very rapidly varying thickness between $2h_1$ and $2h_2$. There is a third design variable in this problem, the orientation of the principal axes of the material with respect to the global coordinate system.

The idea of assembling plies used in [SUZ92] is also valid when the homogenization procedure is performed directly on the plate equation . This is achieved also by assembling three plies, but this time the assembly is performed before the homogenization procedure is carried out on the plate equation.
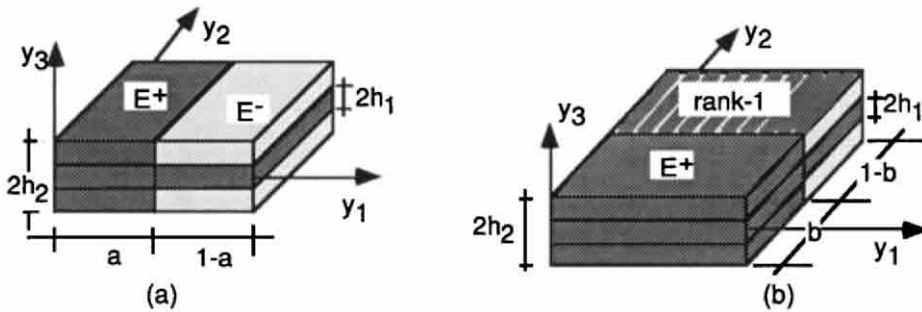
Fig. 1. Layered material plate cells: (a) rank-1, and (b) rank-2.

Figure 2 shows how the assembly of plies is done before the homogenization is performed. To simplify the exposition we use a rank-1 material to build a plate with ribs along only one direction. We start with two different isotropic materials, a strong one, E^+, and a weak one, E^-, which are used to build two plates made by three plies. We label the *strong plate* one built using the strong material in the three plies, as shown in Fig. 2 (a). Similarly, we label the *weak plate,* a plate built using weak material in the lower and upper plies and strong material in the central ply (Fig. 2 (b)). The stiffness properties of these two plates are computed using classical lamination theory [JON75], which yields the reduced stiffness matrix of each plate as a function of h_1, h_2, E^+ and E^-.

A small scale cell is built by cutting a very thin slice (of order ε) from the strong and weak plates and placing the slices next to each other, as illustrated in Fig. 2 (c). The result is a basic cell whose thickness is large ($2h_2$) in comparison with the other two dimensions. The strong plate slice represents the ribs and the weak

plate slice models the gap between the ribs. This cell is repeated in a domain $\Omega^o \subset \Re^2$ to build a large scale plate of dimensions $L_x \times L_y \times 2h_2$, as shown in Fig. 2 (d). The stiffness properties of this plate change rapidly in a small scale.

In order to build a plate made of a rank-2 material one combines a thin slice of the strong plate (Fig. 2 (a)) with a thin slice of the plate made of rank-1 material. This stacking process is made in a second direction, e.g., x_2. The resulting plate has two families of ribs, one running in the x_1 direction and the other in the x_2 direction.

A similar procedure may be followed to build plates with different cross section geometries. Depending on the type of material used in each ply of the weak plate it is possible to build plates with internal ribs (honeycomb) or perforated plates [SOT92].

The optimization algorithm used to solve the problem is based on the optimality criteria approach and the equations are derived in section 2. It is found that the optimality conditions of the orientations of the local material axes with respect to the global coordinate system reduces to the solution of a fourth order polynomial equation. The solution of the plate equation at each iteration step of the algorithm is based on the finite element method with a four noded isoparametric plate element.

In section 3 we review the homogenized plate model derived using Mindlin plate equations for cells made of layered materials (Fig. 1). Several examples of optimum shape of plates are presented in section 4 using the homogenized models shown in section 3. Results show that the homogenization technique used in plate problems is a powerful tool to obtain optimum layouts and shapes.

2. OPTIMIZATION PROBLEM STATEMENT

The objective function in the optimization problem is the mean compliance of the plate. This is minimized finding the best distribution of ribs symmetrically located above and below the central ply of the plate.

2.1 The Discretized Optimization Problem

The design domain Ω is discretized using N finite elements. We assume that the material properties are constant within each element but vary from element to element. Formally, the optimization problem to be solved is:

Given a prescribed amount of material $V \leq |\Omega|$, find the rib widths and angle orientations $\mathbf{a} = \{a_1, a_2, \cdots, a_N\}$, $\mathbf{b} = \{b_1, b_2, \cdots, b_N\}$ and $\boldsymbol{\theta} = \{\theta_1, \theta_2, \cdots, \theta_N\}$ that
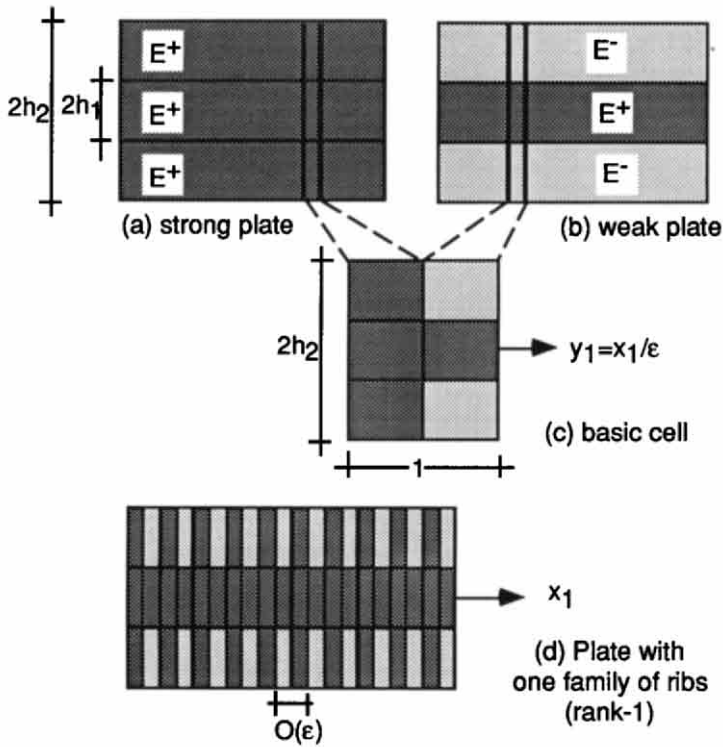
Fig. 2 Assembly of plies.

minimize

$$C = \sum_{i=1}^{3} \int_{\Omega} f_i \, u_i \, d\Omega \qquad (1.1)$$

subject to

$$2\int_{\Omega}(\rho(h_2 - h_1) + h_1) \, d\Omega = 2\sum_{e=1}^{N}((a_e + b_e - a_e b_e)(h_2 - h_1) + h_1)A_e \leq V \qquad (1.2)$$

$$0 \leq a_e \leq 1, \ 0 \leq b_e \leq 1, \ -\frac{\pi}{2} \leq \theta_e \leq \frac{\pi}{2} \qquad (1.3)$$

and equilibrium equations with appropriate boundary conditions. In (1) $\mathbf{u} = \{w, \theta_x, \theta_y\}^t$ is the vector of transverse displacements and angles, A_e the area of

each element, $2h_1$ and $2h_2$ are the heights of the core and ribs, respectively (Fig. 1) and $f = \{f_w, f_{\theta_x}, f_{\theta_y}\}^t$ is the generalized force vector.

2.2 Optimality Conditions

Here we derive necessary conditions for optimality of a, b and θ in problem (1). Introducing multipliers $\lambda > 0$, μ, r^+, r^-, s^+, s^-, the Lagrangian function L associated with (1) is:

$$L = \sum_{i=1}^{3} \int_{\Omega} f_i \, u_i \, d\Omega + \lambda \left(2 \sum_{e=1}^{N} ((a_e + b_e - a_e b_e)(h_2 - h_1) + h_1) A_e - V \right) +$$
$$\mu^t(f - Ku) + \sum_{e=1}^{N}(a_e - 1)r_e^+ - a_e r_e^- + \sum_{e=1}^{N}(b_e - 1)s_e^+ - b_e s_e^- \tag{2.1}$$

where K is the stiffness matrix of the whole structure.

2.2.1. Optimality Conditions for a_e and b_e

Stationarity of L with respect to a and b requires that

$$u_e^t \frac{\partial K_e}{\partial a_e} u_e = 2\lambda(1 - b_e)(h_2 - h_1)A_e + (r_e^+ - r_e^-) \tag{2.2}$$

$$u_e^t \frac{\partial K_e}{\partial b_e} u_e = 2\lambda(1 - a_e)(h_2 - h_1)A_e + (s_e^+ - s_e^-) \tag{2.3}$$

for e=1,2,...,N. K_e is the stiffness matrix for the finite element e. Also, complementarity conditions require that

$$s_e^+(a_e - 1) = 0 \qquad \text{and} \qquad s_e^- a_e = 0$$

and

$$r_e^+(b_e - 1) = 0 \quad \text{and} \quad r_e^- b_e = 0$$

with $s^+ \geq 0$, $s^- \geq 0$, $r^+ \geq 0$, $r^- \geq 0$ and
$$r_e^+ r_e^- = 0 \qquad \text{and} \qquad s_e^+ s_e^- = 0$$

2.2.2. Optimality Conditions for θ_e

Differentiation of L with respect to θ_e yields to

$$\frac{\partial}{\partial\theta_e}\left(u_e^t K u_e\right) = 0 \qquad\qquad e=1,2,...,N \qquad\qquad (2.4)$$

Using the strain-displacement relations, equation (2.4) can be expressed in terms of plate deformations in each element:

$$\frac{\partial}{\partial\theta_e}\left(u_e^t K u_e\right) = \kappa_e^t \frac{\partial H_2}{\partial\theta_e}\kappa_e + \gamma_e^t \frac{\partial H_S}{\partial\theta_e}\gamma_e = 0 \qquad\qquad e=1,2,...,N \qquad\qquad (3)$$

where H_2 and H_S are the homogenized stiffness matrices of the plate in bending and shear deformation, respectively. κ_e and γ_e are the curvature and the shear deformation vectors associated with the element e.

Equation (3) holds for any rotated system of coordinates since the energy term $(u_e^t K u_e)$ is invariant with respect to rotations. Therefore, using the standard formulas for properties in arbitrary orientation [JON75] it is possible to rewrite (3) as

$$\kappa_e^t \frac{\partial \overline{H}_2}{\partial\theta_e}\kappa_e + \gamma_e^t \frac{\partial \overline{H}_S}{\partial\theta_e}\gamma_e = 0 \qquad\qquad e=1,2,...,N \qquad\qquad (4)$$

where the bar in $\overline{H}_2$ and $\overline{H}_S$ indicates that the rotated system of coordinates is used. Each one of the N equations in (4) becomes a 4th order polynomial equation in $Sin(2\theta_e)$. If membrane-type deformations are considered, equation (4) has an extra term of the form $\varepsilon_e^t \frac{\partial \overline{H}_0}{\partial\theta_e}\varepsilon_e$, where ε_e is the vector of membrane deformations and $\overline{H}_0$ the corresponding rotated homogenized stiffness matrix. This extra term also produces a fourth order polynomial in $Sin(2\theta_e)$. Therefore, the computation of the optimum angle always reduces to the solution of a polynomial equation.

Equation (4) gives slightly different angles to those computed in two-dimensional elasticity, where the optimum angle often coincides with the direction of principal strains (see Pedersen [PED89]). This also differs from the method used in [SUZ92] where the angle is computed using principal stress directions and, if in-plane stresses are present, contributions from the top and bottom plies are weighted differently. Since the fourth order polynomial can be solved exactly, the computation of the optimum angles in each step of the algorithm to find the solution is very fast and accurate.

3. HOMOGENIZED PLATE MODEL

The following is a brief description of the homogenized plate model used here. Detailed derivations are found in [SOT92]. Formulas will be given in terms of the arithmetic average $(\overline{A})$ and the harmonic average $(\underline{A})$, whose definitions are given below.

Arithmetic average. For all $x \in [0,1]$, the *arithmetic average* $\overline{A}$ of two real numbers m_1 and m_2 is defined here as the function

$$\overline{A}(m_1, m_2, \xi) = \xi m_1 + (1-\xi) m_2 \tag{5.1}$$

Harmonic average. For all $x \in [0,1]$, the *harmonic average* $\underline{A}$ of two positive real numbers m_1 and m_2 is defined here as the function

$$\underline{A}(m_1, m_2, \xi) = \left[\xi (m_1)^{-1} + (1-\xi)(m_2)^{-1} \right]^{-1} = \frac{m_1 m_2}{\xi m_2 + (1-\xi) m_1} \tag{5.2}$$

For positive m_1 and m_2, $\overline{A} \geq \underline{A}$ and $\overline{A} = \underline{A}$ if and only if $m_1 = m_2$.

The average properties of the plate are obtained applying the homogenization procedure to the Mindlin plate equations [LEW91, SOT92]. The homogenized formulas in bending (H2) and shear (HS) for a plate made of rank-1 material (Fig. 1(a)) with rib thickness 'a' are

$$H_2^{R1}(1,1) = \frac{2}{3} \underline{A}(E_{1111}^+ h_2^3, \ E_{1111}^+ h_1^3 + E_{1111}^- (h_2^3 - h_1^3), \ a)$$

$$H_2^{R1}(1,2) = H_2^{R1}(2,1) = \frac{2}{3} \underline{A}(E_{1122}^+ h_2^3, \ E_{1122}^+ h_1^3 + E_{1122}^- (h_2^3 - h_1^3), \ a)$$

$$H_2^{R1}(2,2) = \frac{2}{3}((1-\upsilon^2)\overline{A}(E_{2222}^+ h_2^3, \ E_{2222}^+ h_1^3 + E_{2222}^-(h_2^3 - h_1^3), \ a) +$$
$$\upsilon^2 \underline{A}(E_{2222}^+ h_2^3, \ E_{2222}^+ h_1^3 + E_{2222}^-(h_2^3 - h_1^3), \ a))$$

$$H_2^{R1}(3,3) = \frac{2}{3} \underline{A}(E_{1212}^+ h_2^3, \ E_{1212}^+ h_1^3 + E_{1212}^-(h_2^3 - h_1^3), \ a)$$

$$H_S^{R1}(1,1) = 2\underline{A}\left(E_{1313}^+ h_2, \ E_{1313}^+ h_1 + E_{1313}^-(h_2 - h_1), \ a\right)$$
$$H_S^{R1}(2,2) = 2\overline{A}\left(E_{2323}^+ h_2, \ E_{2323}^+ h_1 + E_{2323}^-(h_2 - h_1), \ a\right) \tag{6}$$

The E_{ijkl}s are the entries of the fourth order tensor for isotropic elastic materials. The '+' and '-' superscripts denote the strong and weak material used in the layering construction. The superscript R1 denotes that the material is rank-1, i.e., the plate cross section has ribs along only one direction. The homogenized formulas for a Mindlin plate made of rank-2 material (Fig. 1(b)) are

$$H_2^{R2}(1,1) = \overline{A}\left(\frac{2}{3}h_2^3 E_{1111}^+, H_2^{R1}(1,1),b\right) - \overline{A}\left(\frac{2}{3}v^2 h_2^3 E_{2222}^+, \frac{H_2^{R1}(1,2)^2}{H_2^{R1}(2,2)},b\right) +$$

$$\overline{A}^2\left(v, \frac{H_2^{R1}(1,2)}{H_2^{R1}(2,2)},b\right)\underline{A}\left(\frac{2}{3}h_2^3 E_{2222}^+, H_2^{R1}(2,2),b\right)$$

$$H_2^{R2}(1,2) = H_2^{R2}(2,1) = \underline{A}\left(\frac{2}{3}h_2^3 E_{2222}^+, H_2^{R1}(2,2),b\right)\overline{A}\left(v, \frac{H_2^{R1}(1,2)}{H_2^{R1}(2,2)},b\right)$$

$$H_2^{R2}(2,2) = \underline{A}\left(\frac{2}{3}h_2^3 E_{2222}^+, H_2^{R1}(2,2),b\right)$$

$$H_2^{R2}(3,3) = \underline{A}\left(\frac{2}{3}h_2^3 E_{1212}^+, H_2^{R1}(3,3),b\right)$$

$$H_S^{R2}(1,1) = \overline{A}\left(2h_2 E_{1313}^+, H_S^{R1}(2,2),b\right)$$

$$H_S^{R2}(2,2) = \underline{A}\left(2h_2 E_{2323}^+, H_S^{R1}(1,1),b\right) \qquad (7)$$

All other entries of H_2 and H_S that do not appear in (6) and (7) are zero. This plate may have ribs along perpendicular directions.

When the thickness of the plate is relatively small in comparison with the in-plane dimensions of the plate it is possible to neglect the transverse shear deformation of the plate. A typical approach followed in practice is to view the transverse shear strain energy as a penalty contribution in the total strain energy that enforces Kirchhoff's assumptions ($\gamma = 0$), that is,

$$H_S = \frac{1}{\varepsilon}\begin{bmatrix} 1 & 0 \\ 0 & 1 \end{bmatrix} \qquad 0 < \varepsilon \ll 1 \qquad (8)$$

A variation of the homogenized Mindlin plate model to be used in thin plates may be made using this idea.

4.   EXAMPLES

These examples are designed to show the influence of some of the parameters involved in the shape optimization problem of plate structures. The amount of material available to build the ribs, the thickness ratio h_2/h_1, and the total plate thickness ($2h_2$) are studied here.

4.1.   Example 1.   Effect Of The Available Material

In this example we study the variation of the optimum shape as the volume fraction V (see eq. 1.2) used to build the reinforcing ribs is increased. We solved the shape optimization problem for a clamped thin rectangular plate subject to a uniform transverse load for four different amounts of material. The plate has external ribs (Fig. 3(a)) with thickness ratio $h_2/h_1 = 5$. The results are presented in a plan view where ribs (of thickness $2h_2=0.25$) are represented by dark areas, and the central ply (of thickness $2h_1=0.05$) by white areas. The value of the *normalized mean compliance* for the optimum shape, C^*/C_0, is also reported. These values are the ratio between the mean compliance of the optimum plate and the compliance of a uniform thickness plate made with the same amount of material   used in the optimization problem. The results are given in Figs. 3(b)-3(e) for area fractions 5%, 10%, 20% and 40% of the plate area (5x8), respectively. Gray areas in the results indicate the presence of microscopic ribs where the plate has rapidly varying thickness. When the available material increases, the optimum shape of the plate presents areas of 'full thickness' (indicated by black color) where the plate has a uniform thickness of $2h_2$.   The reinforcing ribs appear where the strains or the stresses are high in order to minimize the compliance, in this case, on the sides and around the center of the plate. The normalized mean compliance for the optimum shape is lower for small amount of available material V, ($C^*/C_0=0.18$ in Fig. 3(b)) than for large values of V ($C^*/C_0=0.28$ in Fig. 3(e)). This is consistent with the limit case when the area fraction is 100% that corresponds to $C^*/C_0=1$.

4.2.   Example 2.   Effect Of The Thickness Ratio h_2/h_1

In this example a simply supported rectangular thin plate is considered to study the effect of the thickness ratio on the optimum shape of the plate. The total thickness is fixed at $2h_2=0.25$ and the central ply thickness is varied such that four values of the thickness ratio can be studied, $h_2/h_1=1.5, 3, 5$, and 6 (Fig. 4(b)-4(e)). For a given amount of material, tall rib plates are stiffer than small rib plates. Therefore, plates with high thickness ratio usually have more areas with microscopic ribs (gray areas). This can be confirmed comparing Fig. 4(b) and 4(e). Concerning the compliance, notice that the higher the thickness ratio, the smaller is the normalized compliance.
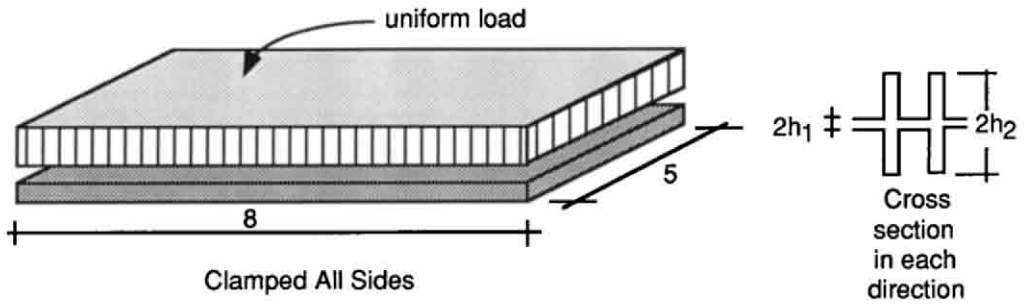
(a) Geometry
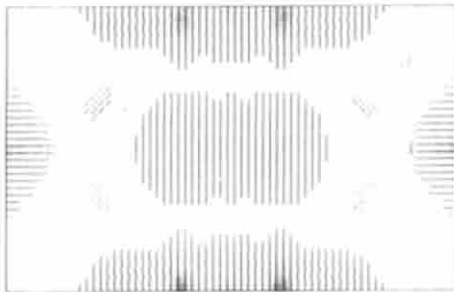
(b) C^*/C_0=0.18
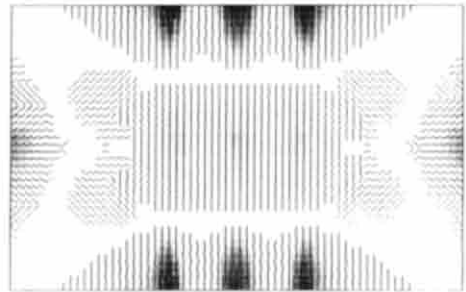
(c) C^*/C_0=0.18
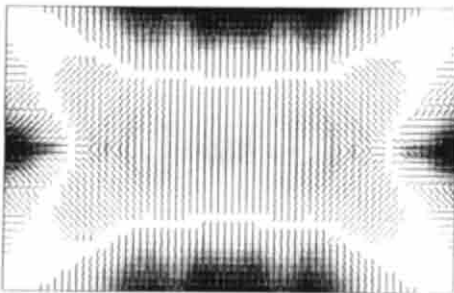
(d) C^*/C_0=0.19
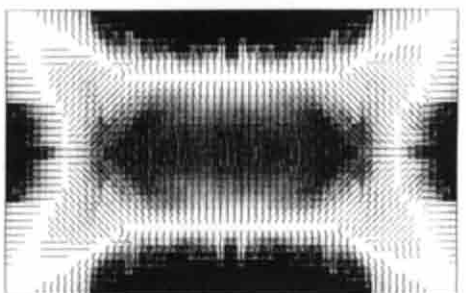
(e) C^*/C_0=0.28

Fig. 3 (a) Geometry of the plate. Area fraction: (b)5%, (c) 10%, (d) 20%, (e) 40%.

4.3. Example 3. Effect Of The Total Thickness

This example shows how the thickness of the plate affects the optimum shape. Two cases are considered, a simply supported and a clamped rectangular plate under uniform transverse load. For each one of these cases the optimum shape is determined for a thick plate ($L/(2h_2)$=5) and for a thin plate ($L/(2h_2)$=20), where L

denotes the smallest dimension of the plate, L=5 (Fig. 3(a)). The amount of material used to build ribs is fixed at 10%, and the thickness ratio h_2/h_1 at 5. The results are given in Figs. 5(a)-5(d). The effect of the transverse shear deformation in thick plates results in different optimum shapes and compliance.
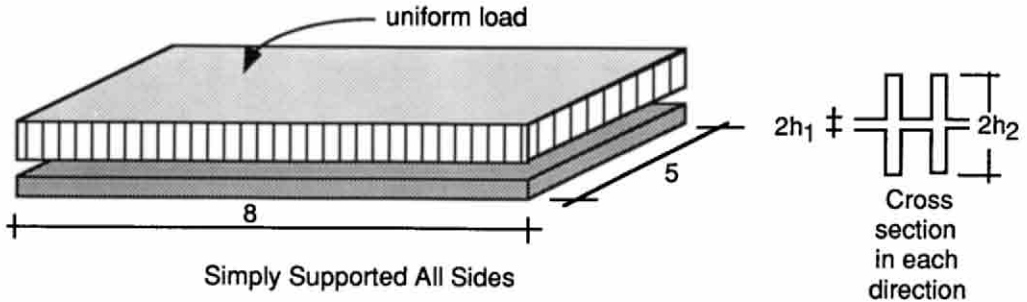
(a) Geometry
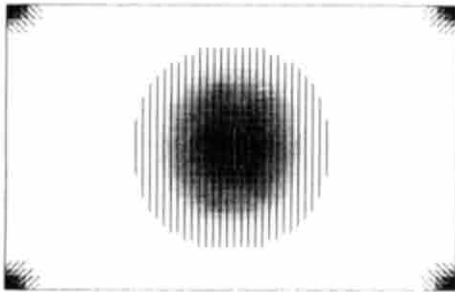
(b) $C^*/C_0=0.89$
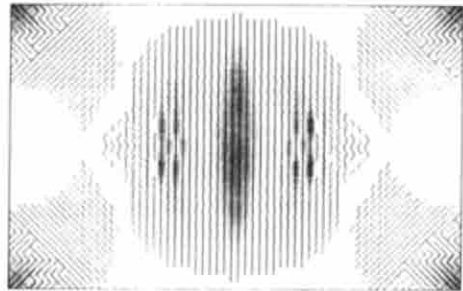
(c) $C^*/C_0=0.50$
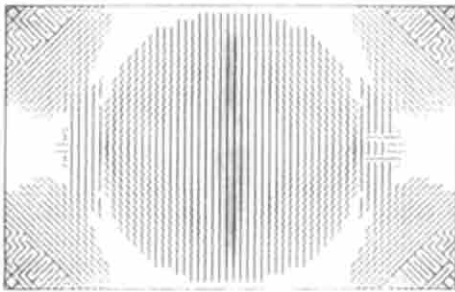
(d) $C^*/C_0=0.26$
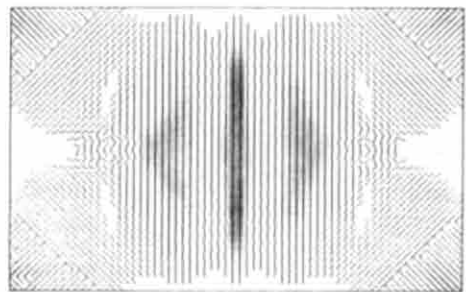
(e) $C^*/C_0=0.17$

Fig. 4 (a) Geometry of the plate. Thickness ratio h_2/h_1: (b) 1.5, (c) 3.0, (d) 5.0, (e) 6.0.

(a) $C^*/C_O=0.26$

(b) $C^*/C_O=0.28$

(c) $C^*/C_O=0.18$

(d) $C^*/C_O=0.23$
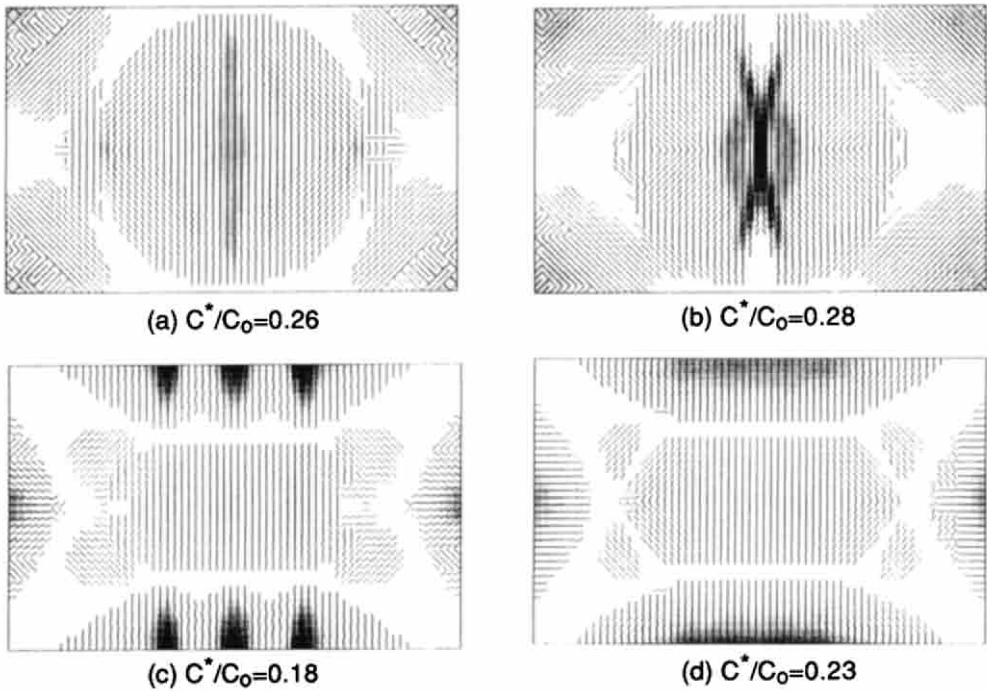
Fig. 5 (a) Simply supported and thin, (b) simply supported and thick, (c) clamped and thin, and (d) clamped and thick.

4.4 Example 4. Non Symmetric Problem

In this example the boundary conditions of the plate are not symmetric (Fig. 6(a)). Two sides of the plate are clamped (CL) and the other two simply supported (SS). The amount of material used to build the ribs varies from 5% to 40 %, and the thickness ratio h_2/h_1 is fixed at 6. The system of loads consists of three point loads as indicated in Fig. 5(a). The results show that there is a concentration of ribs below each point load in order to minimized the compliance. The behavior of the normalized compliance is similar to the example 1. The reduction of compliance (compared to uniform thickness plate) is more pronounced when only a small amount of material is used to build the ribs.

5. CONCLUSIONS

It has been shown that homogenization techniques are a powerful tool to solve the optimum layout and shape in plate structures subject to transverse loads. The use

(a) Geometry

2h₁ ... 2h₂

Cross section in each direction

CL=clamped
SS=simply supported
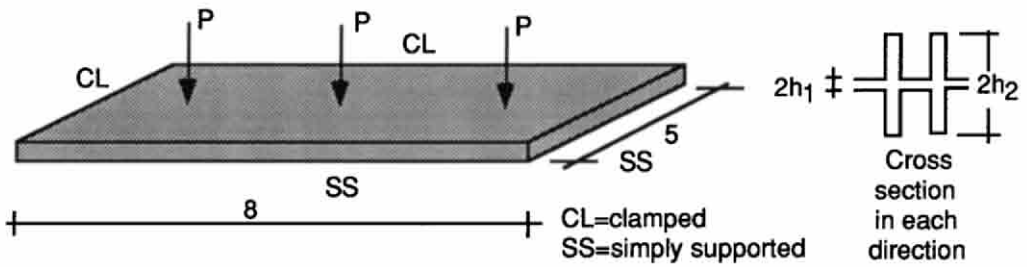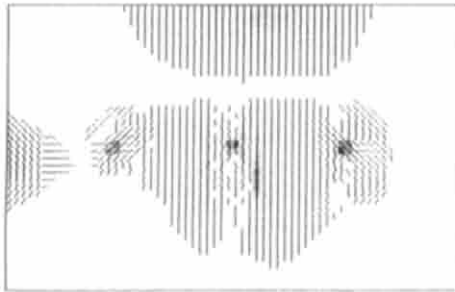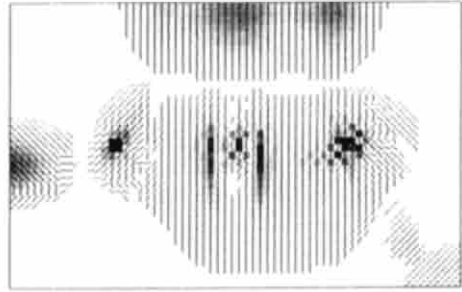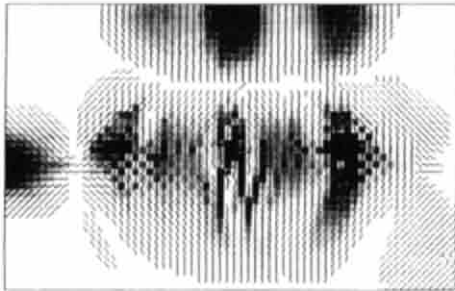
(b) C*/C₀=0.14

(c) C*/C₀=0.14

(b) C*/C₀=0.17
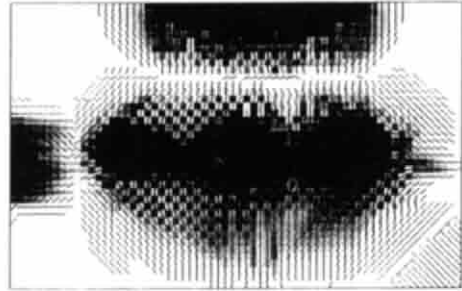
(c) C*/C₀=0.25

Fig. 6 (a) Geometry of the plate. Area fraction: (b)5%, (c) 10%, (d) 20%, (e) 40%.

of the Mindlin plate theory in shape optimization allows us to consider transverse shear deformations present in thick plates. The examples presented show that for low amounts of available material the optimum shapes present ribs in a microscopic scale (rapidly varying thickness plates). High values of thickness ratio give better reduction of the compliance of the plate. Different optimum shapes may be found for thick and thin plates under the same loads and displacement boundary conditions. For the examples studied, the reduction of the compliance (compared to plates of uniform thickness), was more pronounced for thin than for the thick plates.

350

REFERENCES

[BEN82] Bendsøe, M.P. (1982) "Some Smear-Out Models for Integrally Stiffened Plates with Applications to Optimal Design". In Proc. Int. Symp. Optimum Structural Design, Univ. Ariz., Tucson, Arizona. Pineridge Press Ltd., Swansea, pp 13-29 to 13-34.

[BEN88] Bendsøe, M.P. and Kikuchi, N. (1988) "Generating Optimal Topologies in Structural Design using a Homogenization Method", Comp. Meth. in Applied Mech and Engin, 71, 197-224.

[DIA92] Díaz, A. and Bendsøe, M. (1992) "Shape Optimization of Structures for Multiple Loading Conditions Using a Homogenization Method" Structural Optimization, 4,17-22.

[JON75] Jones, R. (1975) Mechanics of Composite Materials, McGraw Hill . New York.

[LEW91] Lewinski, T. (1991) "Effective Models of Composite Periodic Plates - III. Two-Dimensional Approaches", Int. J. Solids Structures, 27, 1185-1203.

[PED89] Pedersen, P. (1989) "On Optimal Orientation of Orthotropic Materials", Structural Optimization, 1, 101-106.

[SOT92] Soto, C. and A. Díaz. (1992) "On the Modeling of Ribbed Plates for Shape Optimization", Technical Report CDL-92-2, Computational Design Laboratory, Michigan State University, East Lansing, Michigan, USA.

[SUZ91] Suzuki, K. and Kikuchi, N. (1991) "A Homogenization Method for Shape and Topology Optimization" Comp. Meth. in Applied Mech in Engin, 93, 291-318.

[SUZ92] Suzuki, K. and Kikuchi, N. (1992) "Generalized Layout Optimization of Shape and Topology in Three-Dimensional Shell Structures", Comp. Meth. in Applied Mech in Engin, to appear.

OPTIMAL DESIGN OF ADVANCED MATERIALS

Daniel A. Tortorelli, Michael M. Tiller and Jonathan A. Dantzig

Department of Mechanical and Industrial Engineering,
University of Illinois, Urbana, Illinois 61801 USA

ABSTRACT
    A general framework is presented for the optimal design of nonlinear parabolic systems which govern the manufacture of advanced materials. The methodology combines the finite element method, design sensitivity analysis, and numerical optimization. The general methodology is then specialized to treat nonlinear transient conduction systems and then exemplified for the optimal manufacture of crystals.

1. INTRODUCTION

    Herein we are concerned with the design of advanced materials rather than the design with advanced materials. In particular, we focus our attention on the optimization of crystal solidification processes for the electronic components industry. The major contribution of this work is the development and computation of the design sensitivity expressions which drive the numerical optimization algorithm. The objective of a sensitivity analysis is to quantify the effects which design parameter variations have on the response. For example, in the forthcoming discussion of the crystal growth processing problem, changes in the crystal temperature field are determined with respect to changes in the process parameters. Once these sensitivities are computed, they are combined with numerical optimization strategies to systematically search the design space for an optimal design [1]. Again, referring to the crystal growth problem, one determines an optimal set of process parameters to give a desired temperature distribution which maximizes the product quality.
    Tortorelli, et al.[2] describe a Lagrange multiplier method for formulating the adjoint design sensitivities of nonlinear transient thermal systems. Dems [3] uses both the direct and adjoint approaches to derive sensitivities for thermal systems. An adjoint approach is also utilized by Meric [4] and Haftka [5] to compute analytical design sensitivities. In all cases, the variation of a general response functional is expressed in explicit form with respect to variations in the design parameters.
    In the following sections, a general approach for deriving both direct and adjoint sensitivities for nonlinear parabolic systems is presented. Then, the general methodology is specialized for nonlinear transient thermal systems. The last section discusses an example problem in which the solidification process for GaAs crystals in Bridgman furnaces is studied. An optimal furnace wall temperature distribution is determined

to obtain the desired temperature profile in the crystal. Obtaining the desired crystal temperature field reduces radial segregation, and thus produces a more desirable product. A similar problem is investigated by Dantzig and Chao [6], however their approach does not utilize efficient numerical optimization techniques.

2. GENERAL SENSITIVITY APPROACH

We commence to describe a general approach for the design sensitivity analysis of nonlinear parabolic systems. First, the parabolic problem is described, then the concept of a cost/constraint function is introduced and the sensitivity problem is defined. Finally, the direct and adjoint approaches for design sensitivity analysis are presented.

2.1. Nonlinear Parabolic Problem Statement

Consider the general form of the nonlinear parabolic differential equation [7]

$$L(u(x,t),x,t) = u_t(x,t) \quad \text{for} \quad (x,t) \in B \times I \tag{1}$$

which is subject to a set of prescribed initial conditions and boundary conditions. In the above, L is a nonlinear differential operator (in space), u is the response, t denotes time in the time domain $I = [0, t_f]$ with terminal time t_f, x denotes a point in the spatial domain B, and subscripts denote partial differentiation with respect to the indicated argument. A specific example of this equation is the nonlinear transient conduction system discussed in the following section in which u becomes the temperature field.

The above equation may be solved for the response u, via the Newton-Raphson process. In this procedure a residual is defined as

$$R(u(x,t),x,t) = 0 = L(u(x,t),x,t) - u_t(x,t) \quad \text{for} \quad (x,t) \in B \times I \tag{2}$$

If a given guess of the solution u, satisfies the above equation then we have a solution. On the other hand, if u does not satisfy this equation, the solution u, is updated via the Taylor series expansion about the current iterate u,

$$R(u(x,t) + \Delta u(x,t),x,t) = 0 = R(u(x,t),x,t) + R_u(u(x,t),x,t)\Delta u(x,t) \quad \text{for} \quad (x,t) \in B \times I \tag{3}$$

where

$$R_u(u(x,t),x,t)\Delta u(x,t) = L_u(u(x,t),x,t)\Delta u(x,t) - \Delta u_t(x,t) \quad \text{for} \quad (x,t) \in B \times I \tag{4}$$

The above may be used to evaluate the incremental response Δu, through

$$\Delta u(x,t) = -[R_u(u(x,t),x,t)]^{-1} R(u(x,t),x,t) \quad \text{for} \quad (x,t) \in B \times I \tag{5}$$

Once Δu is determined, the solution is updated according to $u^{I+1} = u^I + \Delta u$ where the superscript I, denotes the iteration number. This procedure of evaluating the residual R, determining the incremental response Δu, and updating the solution u^{I+1}, is repeated until the system converges.

In the finite element method, the above equations are discretized in both time and space where $R(u(x,t),x,t)$ forms the residual vector; $R_u(u(x,t),x,t)$ forms the tangent stiffness matrix; Δu forms the incremental response; and the time derivative u_t is approximated e.g. by implicit time integration $u_t(x,t) = (u(x,t) - u(x,t - \Delta t))/\Delta t$ where Δt is the time step. The above iterative process is repeated at each time step until convergence is obtained, which is determined when the norm of the residual vector is sufficiently small. Although the Newton-Raphson procedure exhibits quadratic convergence as it approaches the solution, it still requires numerous iterations, each of which requires computationally expensive tangent stiffness matrix formations and decompositions.

2.2. Sensitivity Problem

The above parabolic system governs many manufacturing design problems. For example, in the next section we discuss the design of a thermal processing system. Ultimately, the design is defined by some set of design parameters $\mathbf{b} \in \Re^n$ which are used to describe the material response, boundary conditions, and initial conditions. Additionally, the design parameters could describe the geometry of the domain, i.e. $B(\mathbf{b})$. However, to simplify the ensuing analysis, the domain is assumed to be independent of the design. In light of this design dependency, the above problem, Equation 2, is re-expressed as

$$R(u(x,t,\mathbf{b}),x,t,\mathbf{b}) = 0 = L(u(x,t,\mathbf{b}),x,t,\mathbf{b}) - u_t(x,t,\mathbf{b}) \quad \text{for} \quad (x,t,\mathbf{b}) \in B \times I \times \Re^n \quad (6)$$

Consequently, changes in the design $\mathbf{b}$, obviously affect the response u.

To gage the performance of the design, a generalized cost/constraint functional is defined as

$$G(\mathbf{b}) = \int_I \int_B g(u(x,t,\mathbf{b}),x,t,\mathbf{b}) dv\, dt \quad (7)$$

Although G is expressed in integral form, it may represent localized quantities by incorporating the appropriate weighting functions in g. For example, to examine the response at a distinct time t' and location x' we define g as $g(u(x,t,\mathbf{b}),x,t,\mathbf{b}) = u(x,t,\mathbf{b})\delta(x - x')\delta(t - t')$ where δ is the Dirac delta function.

After the system is analyzed for the given design $\mathbf{b}$, functions of the above form are evaluated to determine whether a proposed design is defective, in which case redesign is necessary, or acceptable, in which case prototyping may begin. We are concerned with the former, i.e. the redesign problem. Specifically, we must select the necessary design variation $\delta \mathbf{b}$, to reduce the cost and satisfy the constraints.[1] To this end, we evaluate the variation of G, i.e. $\delta G(\mathbf{b}; \delta \mathbf{b})$ for all possible design variations $\delta \mathbf{b}$, so as to select the best possible design modification. Assuming sufficient smoothness, the variation for any design perturbation may be evaluated through the gradient, indeed $\delta G(\mathbf{b}; \delta \mathbf{b}) = \nabla G(\mathbf{b}) \cdot \delta \mathbf{b}$. Thus, the objective of the sensitivity analysis is to evaluate the gradient $\nabla G(\mathbf{b})$

$$\nabla G = \int_I \int_B [g_u u_\mathbf{b} + g_\mathbf{b}] dv\, dt \quad (8)$$

---

[1] Problems of this type are generally ill-posed. Hence the existence of the solution is not in general guaranteed. Likewise, uniqueness of the solution is not guaranteed.

where the arguments have been suppressed for conciseness. The difficulty of evaluating the above is due the presence of the derivative u_b, as this term is implicitly defined on the design through the system equation, c.f. Equation 6.

Several means for evaluating the sensitivities have been proposed, namely the finite difference, the direct differentiation, and the adjoint methods cited earlier. The finite difference method is the easiest to implement, however it is computationally prohibitive for large problems and may suffer from round-off or truncation errors. For this reason, we restrict the present discussion to the direct and adjoint approaches.

2.3. Direct Differentiation

In the direct differentiation method, the system equation (Equation 6) is differentiated with respect to each of the design parameters b_α, $\alpha = 1, n$ to give

$$R_{b_\alpha}(u(x,t,\mathbf{b}), x, t, \mathbf{b}) + R_u(u(x,t,\mathbf{b}), x, t, \mathbf{b})u_{b_\alpha}(x,t,\mathbf{b}) = 0 \quad \text{for} \quad (x,t,\mathbf{b}) \in B \times I \times \Re^n \quad (9)$$

where, in light of Equation 6

$$R_{b_\alpha}(u(x,t,\mathbf{b}), x, t, \mathbf{b}) = L_{b_\alpha}(u(x,t,\mathbf{b}), x, t, \mathbf{b}) \quad \text{for} \quad (x,t,\mathbf{b}) \in B \times I \times \Re^n \quad (10)$$

This problem may be solved for the pseudo response u_{b_α} through

$$u_{b_\alpha}(x,t,\mathbf{b}) = -[R_u(u(x,t,\mathbf{b}), x, t, \mathbf{b})]^{-1} R_{b_\alpha}(u(x,t,\mathbf{b}), x, t, \mathbf{b}) \quad \text{for} \quad (x,t,\mathbf{b}) \in B \times I \times \Re^n \quad (11)$$

where we note that we must solve this system n times, once for each design parameter α and that each of the problems has the initial conditions $u_{b_\alpha}|_{t=0}$ which is the explicit derivative of the initial conditions.

Note that the above pseudo problem (Equation 11) resembles the incremental problem of Equation 3. Thus, in regard to finite element implementation, the pseudo response may be efficiently solved at each time step. Indeed, for each of the design parameters we merely form the pseudo load vector R_{b_α}, and perform a back substitution into the decomposed tangent stiffness matrix. Further note that if the convergence tolerance is sufficiently small, then the tangent stiffness that corresponds to the converged solution differs only slightly from the tangent stiffness matrix from the previous (next to last) iterate. Hence, the decomposed tangent stiffness matrix from the primal analysis (c.f. Equation 5) may be used to evaluate the pseudo response; so that in regard to Equation 11 the additional computationally expensive tangent stiffness matrix assembly and decomposition is avoided.

2.4. Adjoint Method

In the adjoint method, the response derivative u_b, is eliminated from the sensitivity equation (c.f. Equation 8) via the Lagrange multiplier method. Following the usual Lagrange multiplier formulation, we define the augmented functional $\hat{G}$ through Equations 7 and 6 as

$$
\begin{aligned}
\hat{G}(\mathbf{b}) &= \int_I \int_B g(u(x,t,\mathbf{b}), x, t, \mathbf{b}) dv\, dt + \int_I \int_B \lambda(x,t,\mathbf{b}) R(u(x,t,\mathbf{b}), x, t, \mathbf{b}) dv\, dt \\
&= \int_I \int_B g(u(x,t,\mathbf{b}), x, t, \mathbf{b}) dv\, dt + \int_I \int_B \lambda(x,t,\mathbf{b})[L(u(x,t,\mathbf{b}), x, t, \mathbf{b}) - u_t(x,t,\mathbf{b})] dv\, dt
\end{aligned}
\quad (12)
$$

where λ denotes the Lagrange multiplier field and we note the equality $G = \hat{G}$ since the augmented term is identically zero because $R = 0$. Differentiation of the above yields

$$\nabla \hat{G} = \int_I \int_B [g_u u_b + g_b] dv\, dt + \int_I \int_B \lambda [L_u u_b + L_b - u_{tb}] dv\, dt \tag{13}$$

and we again note the equality $\nabla G = \nabla \hat{G}$ since the design derivative of the augmented term (c.f. Equation 9) is identically zero. The contribution in the above equation due to the derivative λ_b is omitted, as this term gives a zero contribution because its coefficient $(L - u_t)$ equals zero. Integration by parts over time of λu_{tb} in Equation 13 is used to transform $\nabla \hat{G}$ to, after some rearrangement

$$\nabla \hat{G} = \int_I \int_B [\lambda L_b + g_b] dv\, dt \int_I \int_B u_b [L_u^T \lambda + \lambda_t + g_u] dv\, dt - \left[\int_B \lambda u_b dv \right]_{t=0}^{t=t_f} \tag{14}$$

where the superscript T denotes the transpose operator. In regard to the right most quantity of Equation 14 note that at time $t = 0$ the response derivative u_b, is known, as this is merely the design derivative of the initial conditions. The above is rearranged as the sum $\nabla \hat{G} = \hat{G}_b + \hat{G}_u$ of an explicit term $\hat{G}_b$ and an implicit term $\hat{G}_u$, respectively where

$$\hat{G}_b = \int_I \int_B [g_b + \lambda L_b] dv\, dt + \left[\int_B u_b \lambda dv \right]_{t=0} \tag{15}$$

and

$$\hat{G}_u = \int_I \int_B u_b [L_u^T \lambda + \lambda_t + g_u] dv\, dt - \left[\int_B u_b \lambda dv \right]_{t=t_f} \tag{16}$$

Note that once the Lagrange multiplier field λ, is determined, $\hat{G}_b$ may be readily evaluated. On the other hand, $\hat{G}_u$ contains response derivatives which are implicit quantities as discussed in the previous subsection.

To eliminate the implicit response derivatives in $\hat{G}_u$, we define the Lagrange multiplier to annihilate the implicit quantity, i.e. we define λ to obtain $\hat{G}_u = 0$. To this end, we introduce the time mapping and its inverse

$$\begin{aligned} s(\tau) = t_f - \tau = t \\ s^{-1}(t) = t_f - t = \tau \end{aligned} \tag{17}$$

and then the composite Lagrange multiplier field

$$\gamma(x, \tau, \mathbf{b}) = \lambda(x, s(\tau), \mathbf{b}) \tag{18}$$

Next, we apply the chain-rule to the above, i.e.

$$\gamma_\tau(x, \tau, \mathbf{b}) = \lambda_t(x, s(\tau), \mathbf{b}) s_\tau(\tau) = -\lambda_t(x, s(\tau), \mathbf{b}) \tag{19}$$

where we used

$$s_\tau(\tau) = -1 \tag{20}$$

Now, using the above Equations and $\frac{ds}{d\tau} = \frac{dt}{d\tau} = -1$, we apply the change of variable theorem to transform Equation 16 to

$$\hat{G}_u = \int_I \int_B u_b(x, s(\tau), b)\left[L_u^T(x, s(\tau), b)\gamma(x, \tau, b) - \gamma_\tau(x, \tau, b) + g_u(x, s(\tau), b)\right] dv\, d\tau -$$
$$\int_B u_b(x, t_f, b)\gamma(x, 0, b)dv \tag{21}$$

Note that the above time mappings may be avoided via the introduction of the convolution operator [8].

To annihilate $\hat{G}_u$ we define the following adjoint problem,

$$0 = L_u^T(x, s(\tau), b)\gamma(x, \tau, b) - \gamma_\tau(x, \tau, b) + g_u(x, s(\tau), b) \quad \text{for} \quad (x, t, b) \in B \times I \times \Re^n$$
$$= R_u^T(x, s(\tau), b)\gamma(x, \tau, b) + g_u(x, s(\tau), b) \qquad \text{for} \quad (x, t, b) \in B \times I \times \Re^n \tag{22}$$

with the homogeneous initial conditions $\gamma(x, 0, b) = 0$. The composite Lagrange multiplier may then be obtained from

$$\gamma(x, \tau, b) = -[R_u(x, s(\tau), b)]^{-T} g_u(x, s(\tau), b) \quad \text{for} \quad (x, t, b) \in B \times I \times \Re^n \tag{23}$$

which is similar to the incremental problem of Equation 5 where we replace the incremental response Δu and residual R with the composite Lagrange multiplier (or adjoint) response γ and functional derivative (or adjoint load) $-g_u$, respectively. Substituting the solution for γ into Equation 15 yields

$$\hat{G}_b(b) = \int_I \int_B \left[g_b(u(x, t, b), x, t, b) + \gamma(x, s^{-1}(t), b)L_b(u(x, t, b), x, t, b)\right] dv\, dt$$
$$+ \int_B u_b(x, 0, b)\gamma(x, t_f, b)dv \tag{24}$$

which is the desired explicit sensitivity expression.

There are some additional differences, however, between the adjoint and incremental problems that must be addressed. Note that we use the transposed operator that corresponds to the tangent stiffness matrix. Fortunately, this poses no computational limitations, as linear equation solvers can efficiently solve the above transposed problem from the one adjoint load vector assembly corresponding to $-g_u(u(x, t, b), x, t, b)$ followed by an inexpensive back substitution into the existing decomposed stiffness matrix. The issue which leads to cumbersome computations is the fact that the form of the adjoint load $-g_u$, will not, in general, be known until the primal solution u, is evaluated throughout the time history; and even if the adjoint load is known (which results if g is linear in u), the fact that we are solving for adjoint response γ, at time τ, and using the tangent operator R_u, corresponding to time $s(\tau) = T - \tau$, necessitates the completion of the entire primal analysis before the adjoint system may be evaluated. This requires that either the decomposed tangent stiffness for each time step be stored and later retrieved or that they be completely re-assembled and decomposed to solve the adjoint problem. Still further complications arise if variable time stepping algorithms are implemented into the analysis. For a more detailed discussion on the computational aspects of transient adjoint sensitivity analyses see [9] and [10]. The latter article [10] discusses the special cases of a linear analysis with constant time steps in which the computational complexities involving the storage or re-computation of the stiffness matrices are avoided as the tangent operator is constant.

3. DESIGN SENSITIVITY ANALYSIS FOR THERMAL SYSTEMS

In the following we specialize the results from the preceding analysis to the case of nonlinear transient thermal systems. We recall that to simplify the sensitivity analyses, parameters which describe the geometry of the physical domain are excluded, i.e. shape sensitivities are not discussed.

3.1. Nonlinear Transient Conduction Problem Statement

The residual of Equation 6 is formulated from the following initial-boundary value problem

$$
\begin{aligned}
\nabla \cdot \mathbf{q} + r &= \frac{dh}{dt} & &\text{in } B \times I \times \Re^n \\
\mathbf{q} &= \hat{\mathbf{q}} & &\text{in } B \times I \times \Re^n \\
\mathbf{g} &= \nabla T & &\text{in } B \times I \times \Re^n \\
T &= T^P & &\text{on } A_T \times I \times \Re^n \\
q^s &= q^p & &\text{on } A_q \times I \times \Re^n \\
h|_{t=0} &= h^0 & &\text{in } B \times \Re^n
\end{aligned}
\tag{25}
$$

where ∇ is the spatial gradient operator; $T(\mathbf{x}, t, \mathbf{b})$ is the temperature; $\mathbf{q}(\mathbf{x}, t, \mathbf{b})$ is the heat flux vector; $\mathbf{g}(\mathbf{x}, t, \mathbf{b})$ is the temperature gradient; and $q^s(\mathbf{x}, t, \mathbf{b}) \equiv \mathbf{q}(\mathbf{x}, t, \mathbf{b}) \cdot \mathbf{n}(\mathbf{x}, t, \mathbf{b})$ defines the surface heat flux. $h(T(\mathbf{x}, t, \mathbf{b}), \mathbf{x}, \mathbf{b})$ is the enthalpy which may be modeled as a nonlinear function of the temperature to simulate phase changes. Likewise $r(T(\mathbf{x}, t, \mathbf{b}), \mathbf{g}(\mathbf{x}, t, \mathbf{b}), \mathbf{x}, t, \mathbf{b})$ represents the internal heat generation which is expressed in a generalized form to enable the modeling of convective transport terms when fluid flow is present and phase changes. The constitutive relation $\hat{\mathbf{q}}(T(\mathbf{x}, t, \mathbf{b}), \mathbf{g}(\mathbf{x}, t, \mathbf{b}), \mathbf{x}, \mathbf{b})$ is also expressed as a general function and capable of modeling nonlinear material response; a common form of this relation is $\hat{\mathbf{q}}(T(\mathbf{x}, t, \mathbf{b}), \mathbf{g}(\mathbf{x}, t, \mathbf{b}), \mathbf{x}, \mathbf{b}) = \mathbf{K}(T(\mathbf{x}, t, \mathbf{b}), \mathbf{x}, \mathbf{b}) \mathbf{g}(\mathbf{x}, t, \mathbf{b})$ where $\mathbf{K}(T(\mathbf{x}, t, \mathbf{b}), \mathbf{x}, \mathbf{b})$ is the temperature dependent conductivity tensor. The initial enthalpy is given by $h^0(T^0(\mathbf{x}, \mathbf{b}), \mathbf{x}, \mathbf{b})$ and is an explicit function of the initial temperature field $T^0(\mathbf{x}, \mathbf{b})$ and the design $\mathbf{b}$. A_T and A_q are complementary subsurfaces of ∂B and correspond to surfaces with prescribed temperature $T^p(\mathbf{x}, t, \mathbf{b})$ and prescribed flux $q^p(T(\mathbf{x}, t, \mathbf{b}), \mathbf{x}, t, \mathbf{b})$, respectively; the latter quantity is represented by a generalized function of the temperature to allow for the modeling of convection and nonlinear conditions such as radiation.

The above equation is in the form of Equation 1. Indeed, the response field $u(\mathbf{x}, t, \mathbf{b})$ consists of the temperature $T(\mathbf{x}, t, \mathbf{b})$, temperature gradient $\mathbf{g}(\mathbf{x}, t, \mathbf{b})$, heat flux vector $\mathbf{q}(\mathbf{x}, t, \mathbf{b})$, and surface flux $q^s(\mathbf{x}, t, \mathbf{b})$. And we express $\frac{dh}{dt}(T(\mathbf{x}, t, \mathbf{b}), \mathbf{x}, \mathbf{b}) = h_T(T(\mathbf{x}, t, \mathbf{b}), \mathbf{x}, \mathbf{b}) T_t(\mathbf{x}, t, \mathbf{b})$ and then divide Equation 25_1 by $h_T(T(\mathbf{x}, t, \mathbf{b}), \mathbf{x}, \mathbf{b})$ to attain the form of Equation 1.

To solve the above boundary-value problem we make use of the usual displacement based formulation (commonly employed in the finite element method) in which we solve Equation 25 by determining the square integrable temperature field T which satisfies

Equations 25_{2-6} and zeroes the following residual

$$R = -\int_B \left\{ \nabla\lambda \cdot \hat{\mathbf{q}} - \lambda \left[r - \frac{dh}{dt} \right] \right\} dv + \int_{A_q} \lambda q^p da = 0 \qquad (26)$$

for all square integrable λ which equal zero on A_T. Here, λ plays the role of the weighting function. By resorting to the displacement based approach, the response field is reduced to the temperature field $T(\mathbf{x}, t, \mathbf{b})$. Once this field is determined, the other response fields may be determined via Equations 25_{2-3} and the surface flux definition. Solving the above with the Newton-Raphson process we evaluate the tangent stiffness operator, which is the linear function R_T

$$R_T(\Delta T) = -\int_B \left\{ \nabla\lambda \cdot \hat{\mathbf{q}}_T(\Delta T) + \nabla\lambda \cdot \hat{\mathbf{q}}_{\mathbf{g}} \nabla(\Delta T) - \lambda \left[r_T(\Delta T) + r_{\mathbf{g}} \nabla(\Delta T) - \frac{d}{dt}(h_T \Delta T) \right] \right\} dv$$
$$+ \int_{A_q} \lambda q_T^p(\Delta T) da \qquad (27)$$

that operates on the increment ΔT in the above equation. Upon securing the tangent operator, the response may be evaluated via the Newton-Raphson as seen through Equation 5 and the surrounding discussion.

For the thermal problem, the cost/constraint functional of Equation 7 takes the form

$$G(\mathbf{b}) = \int_I \left\{ \int_B f(T(\mathbf{x}, t, \mathbf{b}), \mathbf{g}(\mathbf{x}, t, \mathbf{b}), \mathbf{q}(\mathbf{x}, t, \mathbf{b}), \mathbf{x}, t, \mathbf{b}) dv + \right.$$
$$\left. \int_{\partial B} g(T(\mathbf{x}, t, \mathbf{b}), q^s(\mathbf{x}, t, \mathbf{b}), \mathbf{x}, t, \mathbf{b}) da \right\} dt \qquad (28)$$

An application of the chain rule to Equation 28 yields the sensitivity

$$\nabla G = \int_I \left\{ \int_B [f_T T_{\mathbf{b}} + f_{\mathbf{g}} \mathbf{g}_{\mathbf{b}} + f_{\mathbf{q}} \mathbf{q}_{\mathbf{b}} + f_{\mathbf{b}}] dv + \int_{\partial B} [g_T T_{\mathbf{b}} + g_{q} \cdot q_{\mathbf{b}}^s + g_{\mathbf{b}}] da \right\} dt \qquad (29)$$

where again we note the complications which arise due to the presence of the response derivatives in the above, namely $T_{\mathbf{b}}, \mathbf{g}_{\mathbf{b}}, \mathbf{q}_{\mathbf{b}}$ and $q_{\mathbf{b}}^s$. To evaluate the explicit sensitivities we rely on the direct and adjoint methods as discussed in the following.

3.2. Direct Differentiation Method

Recall that in the direct approach the response derivatives are evaluated and that in the displacement based method, the response field consists of only the temperature field. To evaluate the sensitivities of the other response fields we merely apply the chain rule to Equations 25_{2-3} and the surface flux definition,

$$\begin{aligned} \mathbf{g}_{\mathbf{b}} &= \nabla T_{\mathbf{b}} & \text{in} \quad & B \times I \times \Re^n \\ \mathbf{q}_{\mathbf{b}} &= \hat{\mathbf{q}}_{\mathbf{g}} \nabla T_{\mathbf{b}} + \hat{\mathbf{q}}_T T_{\mathbf{b}} + \hat{\mathbf{q}}_{\mathbf{b}} & \text{in} \quad & B \times I \times \Re^n \\ q_{\mathbf{b}}^s &= \mathbf{q}_{\mathbf{b}} \cdot \mathbf{n} & \text{on} \quad & \partial B \times I \times \Re^n \end{aligned} \qquad (30)$$

Following the approach of section 2.3 we differentiate Equation 26 with respect to each of the n design parameters b_α. Thus, in regard to the pseudo problem of Equation 9, $R_u u_{b_\alpha}$ is evaluate from Equation 27, where we replace ΔT with T_{b_α} and R_{b_α} is evaluated from Equation 26 after an application of the chain rule,

$$R_{b_\alpha} = -\int_B \left\{ \nabla\lambda \cdot \hat{q}_{b_\alpha} - \lambda\left[r_{b_\alpha} - \frac{d}{dt}(h_b)\right]\right\} dv + \int_{A_q} \lambda q^p_{b_\alpha}\, da \tag{31}$$

where we liken $\hat{q}_{b_\alpha}$ to an initial stress, $r_{b_\alpha} - h_{Tb_\alpha} T_t$ to a heat source, and $q^p_{b_\alpha}$ to a prescribed flux on the surface A_q. Essential boundary conditions of $T^p_{b_\alpha}$ are subjected to the surface A_T and the initial conditions are $T^0_{b_\alpha}$. Note that in this problem, λ still plays the role of a weighting function.

3.3. Adjoint Method

In the adjoint approach, recall that we use the Lagrange multiplier method to eliminate the temperature derivatives T_b from Equation 29. Using equations 28 and 26 we define the augmented functional G^*. Integrating $\lambda\frac{dh}{dt}$ by parts, differentiating with respect to the design, isolating the implicit and explicit derivatives, and incorporating the time mappings (c.f. Equations 17, 18, 19, and 20) gives

$$\begin{aligned}
G_b = \int_I \{ & \int_B \left[f_q|_t \hat{q}_b|_t + f_b|_t - \nabla\gamma|_{t_f - t}\hat{q}_b|_t + \gamma|_{t_f-t} r_b|_t - \gamma|_{t_f-t}\frac{d}{dt}(h_b|_t)\right] dv \\
& + \int_{\partial B} g_b|_t da + \int_{A_q} (g_{q^*}|_t + \gamma|_{t_f-t}) q^p_b|_t da + \int_{A_T} g_T|_t T^p_b|_t da\} dt + \int_B \gamma|_{t_f} h^0_T T^0_b dv
\end{aligned} \tag{32}$$

and

$$\begin{aligned}
G_u = \int_I \langle\{ & \int_B [f_T|_{t_f-\tau}(T_b|_{t_f-\tau}) + f_g|_{t_f-\tau}\nabla(T_b|_{t_f-\tau}) + f_q|_{t_f-\tau}[\hat{q}_g|_{t_f-\tau}(\nabla T_b|_{t_f-\tau}) + \\
& \hat{q}_T|_{t_f-\tau}(T_b|_{t_f-\tau})]] dv + \int_{A_q} [g_{q^*}|_{t_f-\tau}q^p_T|_{t_f-\tau} + g_T|_{t_f-\tau}](T_b|_{t_f-\tau}) da + \int_{A_T} g_{q^*}(q^s_b|_{t_f-\tau}) da\} \\
& - \{ \int_B [\nabla\gamma|_\tau \cdot \hat{q}_T|_{t_f-\tau}(T_b|_{t_f-\tau}) + \nabla\gamma|_\tau \cdot \hat{q}_g|_{t_f-\tau}\nabla(T_b|_{t_f-\tau}) - \gamma|_\tau[r_T|_{t_f-\tau}(T_b|_{t_f-\tau}) \\
& + r_g|_{t_f-\tau}\nabla(T_b|_{t_f-\tau})] + \gamma_\tau|_\tau h_T|_{t_f-\tau}(T_b|_{t_f-\tau})] dv \\
& + \int_{A_q} \gamma|_\tau q^p_T|_{t_f-\tau}(T_b|_{t_f-\tau}) da\}\rangle d\tau - \int_B \gamma|_0 h_T|_{t_f} T_b|_{t_f} dv
\end{aligned} \tag{33}$$

where the notation $|_a$ denotes that the respective quantity is evaluated at time a. The above adjoint problem $G_u = 0$, is identified by the adjoint load which is contained in the first set of braces and the incremental tangent operator of Equation 27 which is

contained in the second set of braces. For the adjoint problem, we of course determine γ and now treat T_b as the weighting function. The adjoint load is defined through a source term of $f_T + f_q q_T$, an initial stress type term of f_g, an initial strain type term of f_q, an essential boundary conditions of g_{q}. on A_T, a natural boundary conditions of $-g_T|_{t_f-\tau} + q_T^p|_{t_f-\tau}(\gamma|_\tau - g_{q}.|_{t_f-\tau})$ on A_q, and subject to the homogeneous initial conditions $\gamma|_{\tau=0} = 0$.

4. Results and Discussion

We are concerned with the specification of the furnace wall temperature distribution in a Bridgman furnace to control the position and shape of the liquid-solid interface during crystal growth process. Additional details of this problem appear in [11].
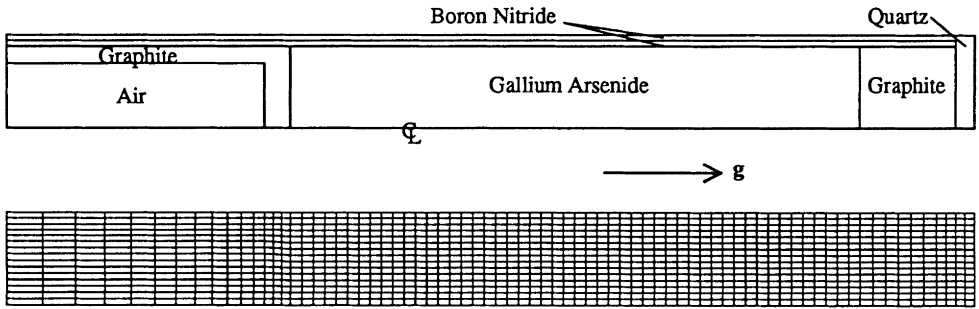
Fig. 1: Schematic view of the model for experimental apparatus to grow GaAs crystals, along with corresponding finite element mesh containing 1216 nodes and 1230 elements.

It is desired to grow a GaAs crystal in a Bridgman furnace under microgravity conditions. As shown in Fig. 1, heat is transferred from the furnace wall to the ampoule by radiation. When a constant temperature gradient boundary condition is imposed on the furnace wall, the resulting solid-liquid interface is nonplanar because of the difference between thermal conductivities of solid and liquid GaAs.[11] Non-planarity of this interface leads to buoyancy-driven convection, even under microgravity conditions, which results in radial segregation of the wafers sliced from the crystal. Any electronic chips produced from these wafers would then possess undesirable nonhomogeneous material properties. The objective of the optimization problem, then, is to generate a planar interface.

We quantify this objective in the function G by specifying a set of desired temperature distributions to be achieved over time within the crystal

$$G(\mathbf{b}) = \left(\frac{1}{J \cdot K} \sum_{j=1}^{J} \sum_{k=1}^{K} [T(\mathbf{x}_k, t_j, \mathbf{b}) - \bar{T}(\mathbf{x}_k, t_j)]^2 \right)^{\frac{1}{2}} \tag{34}$$

where $T(\mathbf{x}_k, t_j, \mathbf{b})$ are the computed (finite element) temperatures at location $\mathbf{x}_k$, time t_j, and design $\mathbf{b}$ and the $\bar{T}(\mathbf{x}_k, t_j)$ are the desired temperatures (to produce the flat interface)

at corresponding locations and times. Thus, our cost function is the rms error between the desired $\bar{T}$, and computed T, temperature fields.

The selection of the objective temperature distribution $\bar{T}(\mathbf{x}_k, t_j)$ was based on the following crystal growth considerations. A crystal grower would ideally enforce some prescribed temperature gradient in the crystal ahead of the liquid-solid interface, ∇T_L, as well as the speed at which the interface is to move, $\mathbf{V}$. To this end, we examine the Stefan condition at the interface,

$$k_S \nabla T_S \cdot \mathbf{n} - k_L \nabla T_L \cdot \mathbf{n} = \rho L_f \mathbf{V} \cdot \mathbf{n} \qquad (35)$$

In the above, k_S and k_L are the isotropic thermal conductivities of the solid and liquid phases, respectively; T_S and T_L refer to the temperature in the solid and liquid at the interface, respectively; $\mathbf{n}$ is the normal vector to the interface; ρ is the density and is assumed to be equal in the two phases; and L_f is the latent heat of fusion. Since the desired interface profile is flat, we align $\mathbf{n}$ with the axial direction and subsequently determine the ratio of the gradients at the liquid–solid interface

$$\frac{|\nabla T_S|}{|\nabla T_L|} = \frac{k_L}{k_S} + \frac{\rho L_f |\mathbf{V}|}{|\nabla T_L|} \qquad (36)$$

It is also desirable to bound the temperatures within the crystal to reduce thermostress and the temperature range of the furnace. Using these criteria as a guideline, the axial temperature profile was generated as illustrated in Fig. 2 and translated along the axis to generate the desired velocity of the interface. Selected locations and times from this graph we used to form G (c.f. Equation 34)

OPTIMAL AMPOULE TEMPERATURE PROFILES
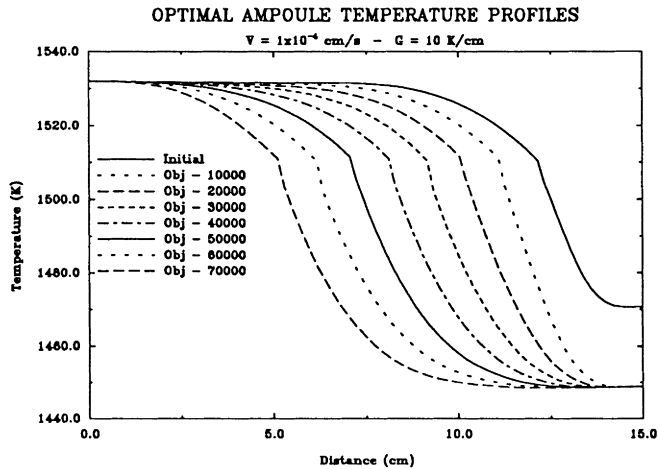
Fig. 2: Temperature distributions to be achieved in the crystal at a series of times. Note that the initial temperature distribution is compatible with Eq. (36) when $|\mathbf{V}| = 0$, *i.e.* at steady state.

The goal of the optimization is to determine the furnace wall temperature profile which yields the desired temperature field $\bar{T}$. The furnace wall temperatures were parameterized by a set of distinct control points in space and time; these parameters

then served as the design variables b. The temperature at any other point is linearly interpolated between the appropriate control points in space and time. We divide the furnace wall spatially into ten zones, equally spaced between eleven control points on the furnace wall, and we define a set of eight time points spanning the solidification time of the crystal. Thus, a total of 88 design parameters are used. The desired temperatures in the crystal $\bar{T}$, were used to define the initial design parameters for the optimization.

Radiation between the furnace wall and the ampoule was modeled as an effective heat transfer coefficient:

$$q^p = \underbrace{\sigma\varepsilon\left(T^2 + \theta^2\right)(T + \theta)}_{h_{eff}}(T - \theta) \tag{37}$$

where q^p is the radiative heat flux, σ is the Stefan-Boltzmann constant, ϵ is the emissivity, T is the local crystal temperature and $\theta(x, t, b)$ is the design dependent furnace wall temperature at the corresponding point. The value of $\theta(x, t, b)$ is determined through interpolation as described above. Radiative exchange was assumed to exist only between opposing points, *i.e.* no view factors were calculated. All of the material properties were modeled as temperature dependent and axisymmetry is assumed.

Sensitivities were computed using the direct differentiation method described earlier. In this case, the pseudo load was a flux on the furnace wall surface defined through

$$q^p_{b_\alpha} = 4\sigma\varepsilon\theta^3\theta_{b_\alpha} \tag{38}$$

where $\theta_{b_\alpha}(x, t, b)$ represents the explicit design derivative of the furnace wall temperature which is determined through the interpolation relations.

OPTIMAL AMPOULE TEMPERATURE PROFILES
$V = 1 \times 10^{-4}$ cm/s   –   G = 10 K/cm – Centerline of Crystal
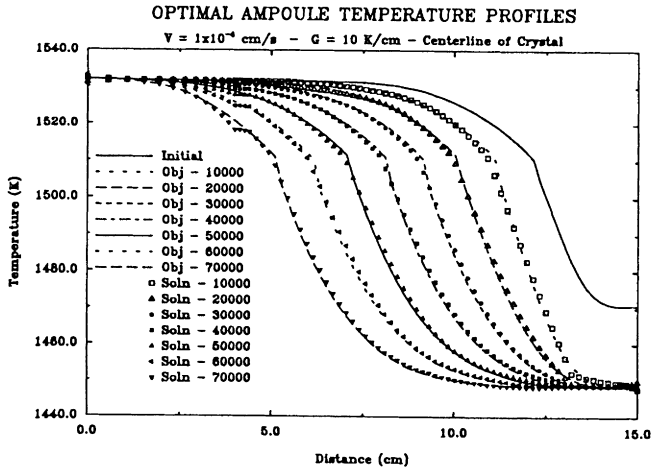
Fig. 3: Ampoule temperature profiles along centerline of the crystal under optimal processing conditions, compared with objectives.

The finite element analysis was performed using the commercial program FIDAP, with a number of enhancements to compute both the sensitivity and the full Newton-Raphson tangent stiffness matrix.[12] The Quasi-Newton (BFGS) scheme with a parabolic interpolation one-dimensional search strategy was employed to perform the optimization.[1] Optimal solutions were obtained after 10 to 12 line searches, corresponding

to a total of 35 to 45 function evaluations, depending on the initial design and optimization convergence tolerances. Temperature distributions along the centerline of the ampoule for a typical case (V = 1 μm/s and $|\nabla T|$ = 1 K/mm) are shown in Fig. 3 for the optimized design, along with the corresponding objective temperatures $\overline{T}$. Corresponding results for the periphery of the crystal are quite similar, but have been omitted for brevity. The optimized temperature contours conform closely to the desired profiles. In fact, the optimized rms error is just 0.77 K. (This amounts to a total error of 720 for 152 temperatures at eight time steps.)

PROGRESS OF OBJECTIVE AND SENSITIVITY
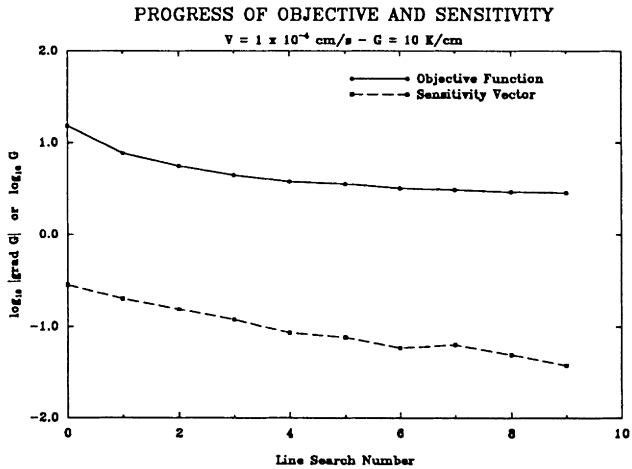
Fig. 4: Progress of the objective function and sensitivities during the optimization.
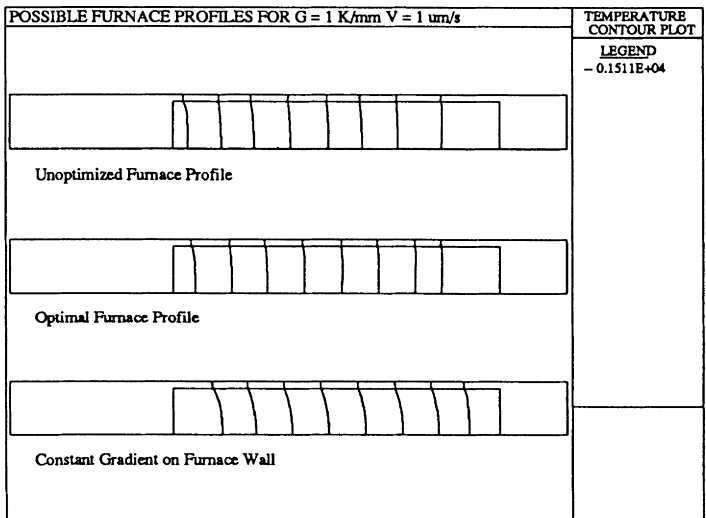
Fig. 5: Successive interface positions for initial, optimal, and constant gradient furnace profiles.

The progress of the objective function and the sensitivities during the simulation is shown in Fig. 4. We see that the optimization quickly converges, and that the sensitivities are reduced by nearly two orders of magnitude. Recall that a zero sensitivity value corresponds to the presence of a local extrema. In this case, the nine line searches corresponded to 45 function evaluations. The total clock time for the entire optimization process was about six hours on a Sun SPARCstation 2 with sufficient memory to solve in core.

Further insight of the results appear in Fig. 5, where a time series of computed liquid–solid interface locations is shown for three designs: the initial guess, the optimal solution, and a fixed gradient furnace, the latter shown for reference. We can see that the interfaces are somewhat flatter in the optimal case, but the differences are not significant. The need for optimization becomes more apparent when the crystal solidification velocity V, is increased. Figs. 6 and 7 illustrate the results of the optimization for a growth rate of 5 μm/s. Upon comparison to Figs. 3 and 6 we note that the primary difference between the two problems is the value of temperature gradient is much larger for the second problem (c.f. Equation 36). Upon observing Fig. 7 the benefits of the optimization become apparent. The optimal furnace wall temperature distributions for the latter case (V = 5 μm/s) are shown in Fig. 8, where one can see that the optimal solution is quite practical, giving a maximum temperature gradient of less than 100 K/cm throughout the cooling cycle.
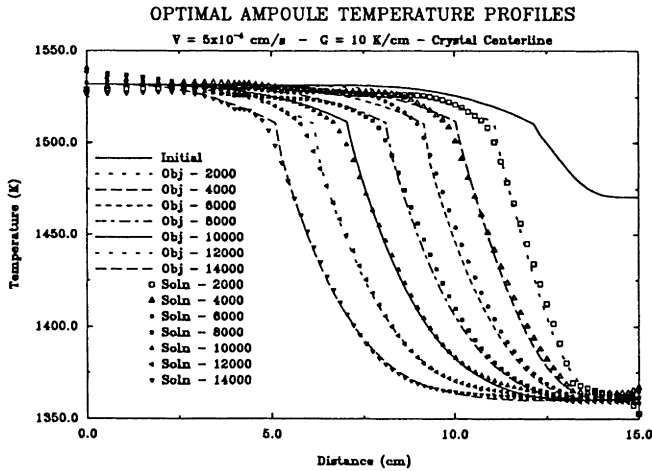
Fig. 6: Ampoule temperature profiles along centerline of the crystal under optimal processing conditions, compared with objectives for crystal growth at 1 μm/s at several times.

POSSIBLE FURNACE PROFILES FOR G = 1 K/mm V = 5 um/s	TEMPERATURE CONTOUR PLOT
	LEGEND — 0.1511E+04

Unoptimized Furnace Profile

Optimal Furnace Profile

Constant Gradient on Furnace Wall
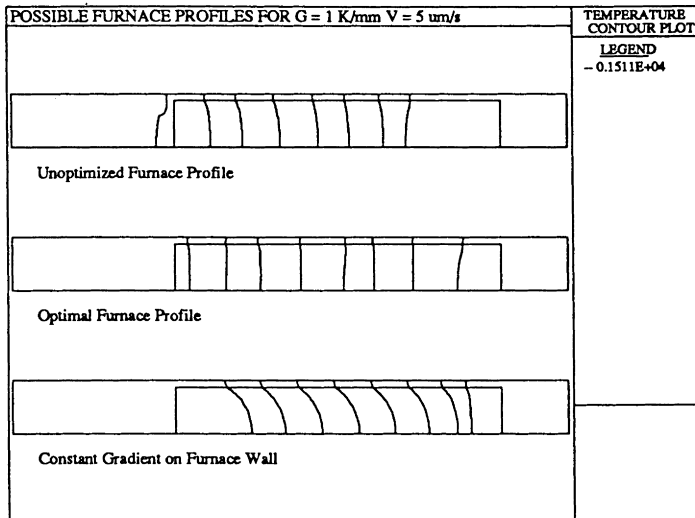
Fig. 7: Successive interface positions for initial, optimal, and constant gradient furnace profiles. Irregularities in the position of the interface are characteristic of enthalpy methods.[13]

OPTIMAL FURNACE TEMPERATURE PROFILES

V = 5x10⁻⁴ cm/s – G = 10 K/cm

Initial (Steady)
t = 2000 s
t = 4000 s
t = 6000 s
t = 8000 s
t = 10000 s
t = 12000 s
t = 14000 s
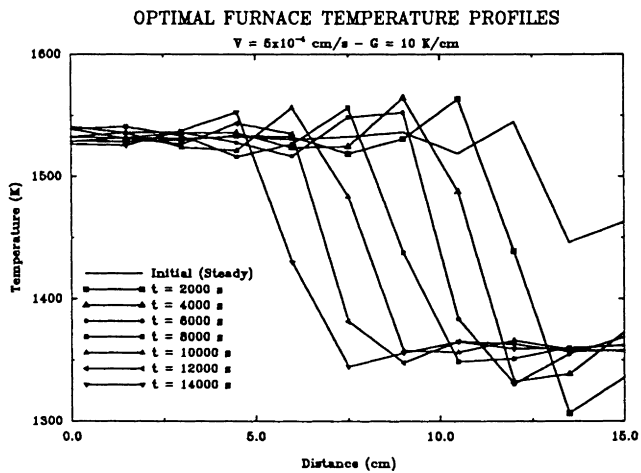
Fig. 8: Optimal temperature distributions to be applied to the furnace wall to achieve the objective temperatures for the case where crystal growth proceeds at 5 μm/s.

5. Conclusions

An algorithm for the design of advanced materials has been presented. The scheme combines finite element analysis, explicit design sensitivity analysis, and numerical optimization to design the manufacturing process for the advanced material. The methodology was exemplified for the optimal process parameter selection in a furnace that is used to grow crystals.

6. Acknowledgment

7. REFERENCES

[1] G. N. Vanderplaats. *Numerical Optimization Techniques for Engineering Design: with Applications*. McGraw-Hill, New York, 1984.

[2] D. A. Tortorelli, R. B. Haber, and S. C.-Y. Lu. Design Sensitivity Analysis for Nonlinear Transient Thermal Systems. *Computer Methods in Applied Mechanics and Engineering*, 75:61–78, 1990.

[3] K. Dems. Sensitivity in thermal problems i: Variation of material parameters within a fixed domain. *J. Therm. Stresses*, 9:303–324, 1986.

[4] R. Meric. Shape design sensitivity analysis for nonlinear anisotropic heat conducting solids and shape optimization using the bem. *Internat. J. Numer. Methods Engrg*, 26:109–120, 1988.

[5] R. Haftka. Techniques for thermal sensitivity analysis. *Internat. J. Numer. Methods Engrg*, 17:71–80, 1981.

[6] J. A. Dantzig and L. S. Chao. Interface shape control in bridgman crystal growth. In M. Rappaz and M. Ozgu, editors, *Modeling of Casting, Welding and Advanced Solidification Processes*, page in press, Warrendale, PA, 1991. TMS-AIME.

[7] E. Haug and K. Choi. *Methods of Engineering Mathematics*. University of Iowa, 1991.

[8] D. Tortorelli, S. C.-Y. Lu, and R. Haber. Design sensitivity analysis for elastodynamic systems. *Mechanics of Structures and Machines*, 18:1:77–105, 1990.

[9] E. Haug. *Design Sensitivity Analysis of Dynamic Systems,NATO ASI Series, Vol. F27, Computer-Aided Optimal Design: Structural and Mechanical Systems. Editied by C.A. Mota Soares*. Springer-Verlag, Heildelberg, 1987.

[10] D. Tortorelli and R. Haber. First order design sensitivities for transient conduction problems by an adjoint method. *International Journal for Numerical Methods in Engineering*, 28:4:61–78, 1989.

[11] J. A. Dantzig and D. A. Tortorelli. Optimal design for solidification processes. In G. S. Dulikravich, editor, *Third International Conference on Inverse Design Concepts and Optimization in Engineering Design*, pages 213–226, 1991.

[12] M. S. Engelman. *FIDAP Theoretical Manual*. Fluid Dynamics International, Evanston, IL, 1987.

[13] J. A. Dantzig. Modeling Liquid-Solid Phase Changes with Melt Convection. *International Journal of Numerical Methods in Engineering*, 28:1769–1785, 1989.

ON OPTIMAL END CLOSURES MADE FROM WOVEN CFRP

J. Blachut

Department of Mechanical Engineering, University of Liverpool, P.O. Box 147, Liverpool, L69 3BX, United Kingdom

Abstract
    Shape and variable wall stiffness are used as simultaneous design variables in externally pressurised carbon fibre reinforced plastic domes. The cost function is related to the Tsai-Wu failure index (FI). The minimum of the integrated failure index and min-max of the FI are sought for shells made from epoxy resin woven pre-preg. Meridionally variable stiffness is introduced through a number of differently stacked segments in each ply. These butt-jointed segments can also be of different lengths. Meridional shape is confined to generalized ellipses and only geometrically perfect models are considered. The numerical results are based on the Complex Method of Box [15].

1. INTRODUCTION

    Use of fibre reinforced plastic (FRP) shells has widely diversified during the last decades. The paper addresses one of the new application areas relevant to deep sea exploration. This activity has been hindered by the lack of an efficient pressure hull, since traditional materials cannot provide sufficient buoyancy. The depth of 6500 m is within reach when titanium alloys are used for the pressure hull [1]. Several research tasks have been carried out to evaluate the possibility of utilizing epoxy resin FRP as a potential new material to substitute for titanium alloys and to secure further increases in operational depth, payload and mission time [2-5].
    We will consider relatively thick domed end closures where a number of experimental and numerical feasibility studies have recently been carried out in Liverpool. They have shown that collapse of these composite shells is caused by brittle material failure rather than by buckling. Hemispherical, torispherical and ellipsoidal shapes have been studied [6-9]. The classical laminate theory has been used to correlate experimental data. The through thickness transverse shear was included in a case study and this had no effect on the collapse strength [8]. Manufacturing routes included vacuum bagging of petalled and unpetalled woven pre-preg CFRP and filament winding of carbon pre-preg tows [6, 9]. Most of the tested models had diameter 0.8 m and some of the collapse pressures were equivalent to about 1500 m diving depth. Problems, related to bifurcation buckling of thin closures, were analyzed numerically in Ref. [10].

While some experimental and theoretical issues are being further investigated, attempts have also been made to improve performance of the composite domed ends via optimisation [8, 11, 12]. An up to date review of recent activities in optimisation of shells in general can be found in [13].

Influence of meridional shaping on the collapse strength of FRP domes has been examined in Ref. [11]. Parabolic and cubic splines, circular arcs and generalized ellipses were used to approximate the meridional shape. Bifurcation buckling, axisymmetric collapse and first ply failure (FPF) were considered as possible mechanisms of a dome collapse. The objective was to maximise the lowest collapse pressure for constant wall thickness, given the material and lamination sequence. Strong dependence of the cost function on the meridional shape has emerged. In Ref. [12] optimal meridional shape (generalized ellipses) and the thickness distribution in a filament wound dome closure were investigated in order to increase the buckling strength. The variable thickness profile was obtained through the appropriate stacking sequence of continuously wound pre-preg carbon tows in polar mode. Large increases in the collapse strength were obtained for some configurations. The collapse strength of optimally wound domes was then compared with quasi-isotropic lay-up of woven and vacuum bagged closures having the same mass and meridional shape. The latter models were, in many cases, stronger than their wound counterparts.

The optimal configurations of vacuum bagged, [11], and wound shells, [12], lose their strength through the FPF mechanism. Experiments, [6, 9], show that damage in the FPF failed shells is very localised. A large portion of the shell wall is unaffected at the FPF load level.

The aim of this paper is to redistribute that local over-stressing, measured by the quadratic failure index (FI), through the meridional shaping and variable anisotropy. Some references are also made to experimental data in order to provide checks of adequacy of the analysis and highlight the existing scope for optimisation.

2. POST-MORTEM ANALYSIS OF FPF-COLLAPSED TORISPHERE

Let us consider a torisphere made from 30 plies of woven, 4x4 twill, 3k epoxy resin pre-preg carbon fibre under static external pressure (see Fig. 1). The best-fit geometry for the external surface and the measured wall thickness are given in Table 1. The stacking sequence was $[0/0/15/30/45/45/60/75/90/105/120/135/150/165/180]^{\circ}_s$. The torisphere was loaded up to the failure through quasi-static incremental loading. The catastrophic failure was accompanied by a detonation type loud bang. The view of the failed torisphere is depicted in Fig. 2 (from [9]). The through thickness crack visible in Fig. 2, extends circumferentially by about 210 deg.

Table 1

Dome [9]	R_s/D	r/D	L/D	D	t_{cap}	t_{tor}	t_{cyl}	t_{av}
				(mm)				
TVB30B	0.599	0.241	0.063	799.7	8.42	9.05	10.08	8.85

A narrow strip passing through the apex was then cut from the tested dome (Fig. 3). The wall of the shell was examined under the microscope at a number of points. All points which were then examined did not show any visible delamination or matrix cracking. The cracked area is confined to about 20 mm along the meridian. Fig. 4b depicts the wall in vicinity of the crack, i.e. near the point '6'. Fig. 4a shows a magnified cross-section at the opposite side and at the same latitude, i.e. near the point '2'.
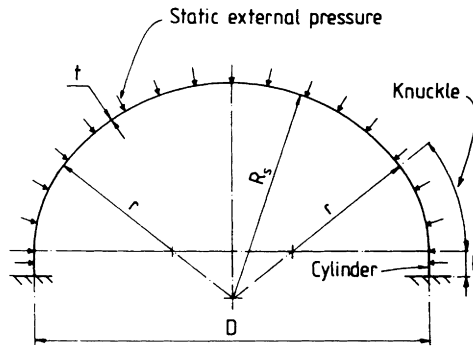
Fig. 1   Geometry of torispherical shell

The FPF pressure is determined numerically using the Tsai-Wu interactive failure criterion written in stress space:

$$\frac{\sigma_1^2}{X_t X_c} - \frac{\sigma_1 \sigma_2}{2\sqrt{X_c X_t Y_c Y_t}} + \frac{\sigma_2^2}{Y_t Y_c} + \frac{\sigma_s^2}{S^2} + \left(\frac{1}{X_t} - \frac{1}{X_c}\right)\sigma_1 + \left(\frac{1}{Y_t} - \frac{1}{Y_c}\right)\sigma_2 = FI. \qquad (1)$$

Direct and in-plane shear stresses (σ_1, σ_2, σ_s) are evaluated at the top and bottom of each ply in the material coordinates. The compressive strength constants (X_c, Y_c) correspond to the material axis 1 and 2, respectively. The same convention applies to the tensile strengths (X_t, Y_t). Finally, S denotes the in-plane shear strength.

Fig. 2 30-ply CFRP torisphere after a failure test
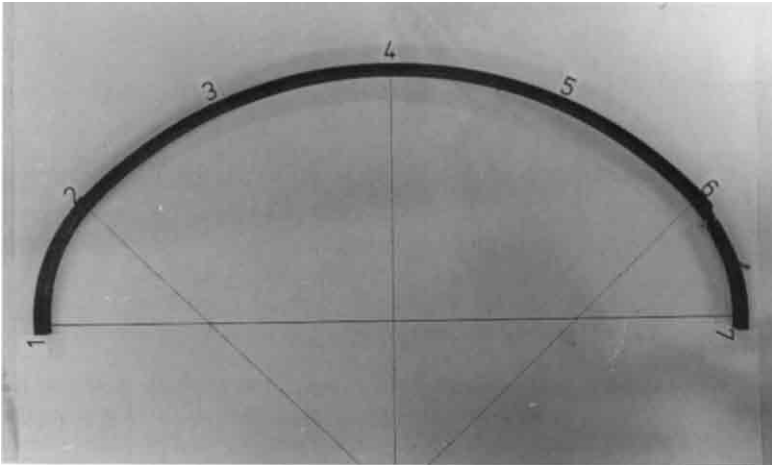
Fig. 3 Section through the tested dome

<div align="center">(a)   (b)</div>
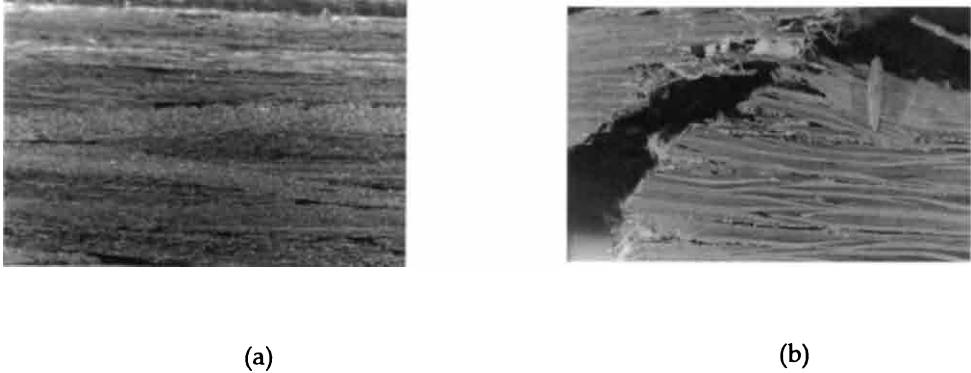
Fig. 4   Magnified view of the through thickness section

For each meridional node in the n-ply composite wall the FI index, given by Eq. (1), has n + 1 components chosen from 2n values (see Fig. 5):

$$FI \equiv \{FI^-(z_0), \; sup[FI^-(z_1), FI^+(z_1)], \; sup[FI^-(z_2), FI^+(z_2)], \; .... \tag{2}$$
$$...., \; sup[FI^-(z_{n-1}), FI^+(z_{n-1})], \; FI^+(z_n)\}$$
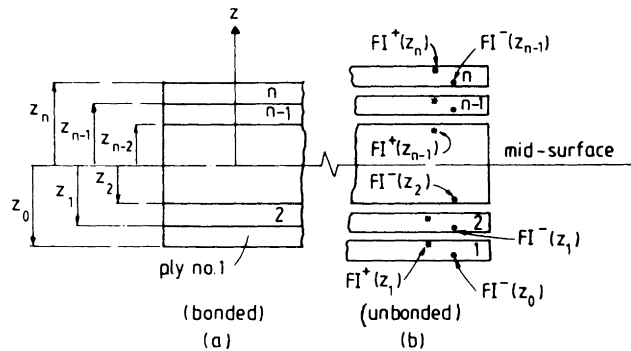
Fig. 5   Lamination convention and assignment of the FI indices

where '-' and '+' correspond to the bottom and top of the ply, respectively. An incremental technique is used to find such loading at which the failure index FI becomes unity, i.e. FI = 1 (see Ref. [7] for more details). In our case this loading is called the First Ply Failure (FPF) pressure. The following material properties are used in all calculations: $E_1 = E_2 = 70$ kN/mm^2; $G_{12} = 5$ kN/mm^2; $\nu_{12} = 0.1$; $X_c = Y_c = 570$ N/mm^2; $X_t = Y_t = 600$ N/mm^2 and S = 90 N/mm^2. The wall thickness of the TVB30B dome was measured along 18 equispaced meridians and at 20 mm meridional intervals. The thickness distribution was reasonably axisymmetric but

its magnitude varied along the meridional direction by about 25%. The numerical analysis was based on axisymmetric modelling. The meridionally variable thickness profile was generated from measured data using the cubic splines approximation. Appropriate adjustments were made in BOSOR 4 code [14], to allow for the variable meridional stiffness. Table 2 contains the experimental collapse pressure, the FPF pressure and bifurcation buckling pressure corresponding to 6 circumferential waves.

Table 2

Dome	Experiment	FPF	Bifurcation	fi from Eq. (6)
	(N/mm^2)			
TVB30B	8.83	8.70	16.01(6)	0.228

By examining Fig. 2 and results in Table 2 it becomes clear that FPF is the controlling mechanism of the dome's failure. The localised character of the FPF mechanism is illustrated in Fig. 6. It is an isometric view of the computed FI at 31 stations through the wall thickness along the full meridional length. There is sharp increase of the FI index on the inside side of the shell near the spherical cap/knuckle junction. This maximum corresponds to the location of the crack seen after the test - see Fig. 2. It is also seen that the FI index stays at about the 0.2 level in the larger portion of the spherical cap. It is worth noting here that there was no visible damage to the wall near the point '2' in Fig. 3, although it is likely that the area around that point was heavily stressed. This suggests that the shell is able to sustain loadings leading to the FI becoming close to unity and at the same time leaving the wall without traces of debonding or cracking. The above case shows how the FI surface could be used to influence the dome's level of stressing or magnitude of the collapse pressure.

The dome TVB30B was manufactured from 30 single pieces of woven cloth. These individual plies were continuous and not cut. There have also been tests on domes manufactured from petalled plies [6, 9]. Each ply was butt-jointed from a number of pieces cut to size and shape. No deterioration of performance was noted in these shells. The ability of composing the shell's wall from differently cut woven pieces will be explored in the next paragraphs and the effects on the shell's performance will be investigated.

3. PROBLEM FORMULATION

Let us consider an axisymmetric, n-ply composite shell of diameter D and variable meridional profile given by
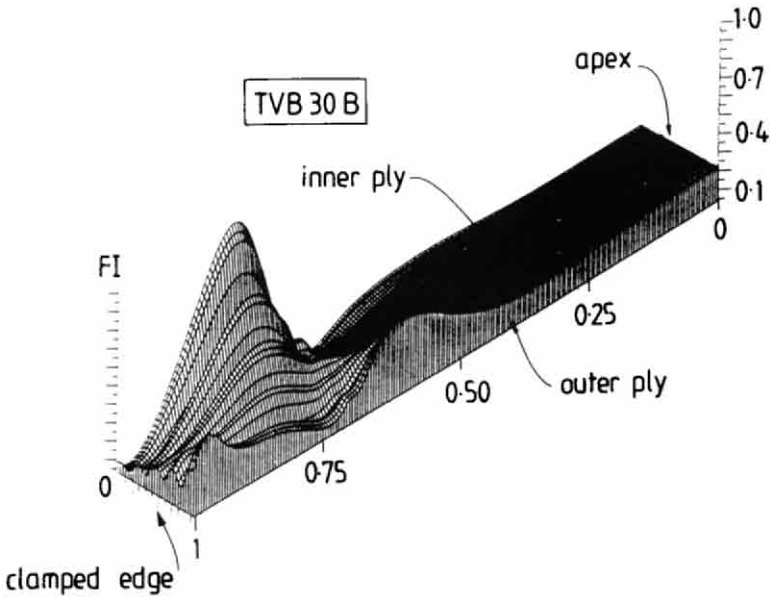
Fig. 6   Numerically simulated surface of the FI index at the first ply failure loading

$$\left[\frac{2x}{D}\right]^{k_1} + \left[\frac{y}{k_3}\right]^{k_2} = 1 \tag{3}$$

Let us also assume that the shell is under given static external pressure p, and it is fully clamped at the equator (Fig. 7a). Each ply is divided into N segments of different length L_{ij}, where i = 1, ..., n and j = 1, ..., N. Each segment can in turn be independently orientated with respect to the meridional direction. Let us denote this orientation by the angle θ_{ij}, where subscript 'i' refers to the layer number 'i' and the subscript 'j' denotes j^{th} material segment in the ith ply (see Fig. 7b). The design vector R is defined as follows:

$$R \equiv \{k_1,\ k_2,\ k_3,\ \theta_{ij},\ L_{ij}\} \tag{4}$$

and it contains the following 2nN + 3 components:

-       three shape variables k_1, k_2, and k_3,
-       nN anisotropy variables θ_{ij}.
-       nN explicit variables L_{ij} describing the length of individual segments.

Lengths L_{ij} (k_1, k_2, k_3) have to satisfy the following conditions:

$$\sum_{j=1}^{N} L_{ij} = L_{tot'} \qquad i = 1, \ldots, n \qquad (5)$$

where L_{tot} is the implicit, total meridional, length of each ply:

$$L_{tot} (k_1, k_2, k_3) = \int_0^{D/2} \sqrt{1 + (y')^2} \ dx. \qquad (6)$$
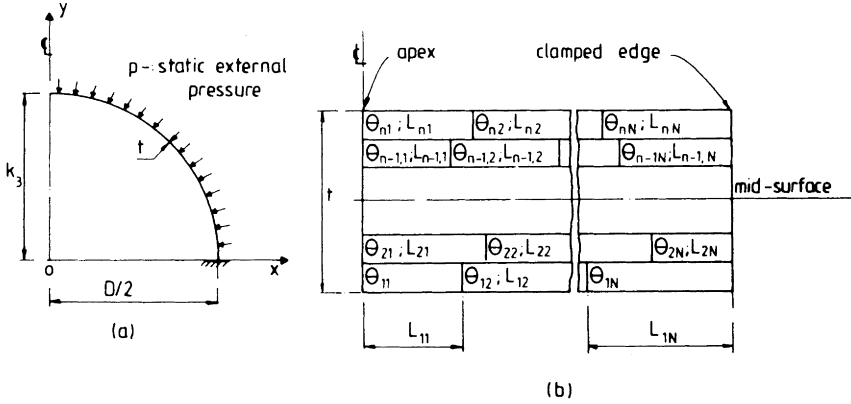
Fig. 7   Details of meridional shape and assignment of design variables

Performance of the considered dome will be assessed using two different cost functions, i.e. one local and one global. Both objective functions refer to magnitude of the FI index for a fixed level of loading and shell mass.

3.1   Global Performance

Let us introduce the following integrated and dimensionless cost function fi(R) related to the failure index FI given by Eq. (2):

$$fi(R) = \frac{\int FI(R;z,s) \ dzds}{\int dzds} \qquad (7)$$

and seek its minimum

$$fi^{opt} = \min_{R} fi(R) \qquad (8)$$

subject to the following imposed explicit and implicit conditions:
-        explicit constraints

$$1.3 \; < \; k_1 \; < \; 2.5 \tag{9}$$

$$1.3 \; < \; k_2 \; < \; 2.5 \tag{10}$$

$$0.1D \; < \; k_3 \; < \; D \tag{11}$$

$$0.05D \; < \; L_{ij} \; < \; L_{tot} \tag{12}$$

$$-90^\circ \; < \; \theta_{ij} \; < \; +90^\circ \tag{13}$$

where $i = 1, \ldots, n$ and $j = 1, \ldots, N$.
- implicit constraints

$$\sum_{j=1}^{N} L_{ij} = L_{tot} \; (k_1, k_2, k_3) \qquad i = 1, \ldots, n \tag{14}$$

$$FI(R; z,s) \leq SM \tag{15}$$

$$m = const \tag{16}$$

Conditions (9-13) are simple bounds on components of the design vector R. There are further n implicit equality conditions imposed on the total length of all segments within each ply (Eq. 14). The condition (15) prescribes the level of the safety margin in the structure. The first ply failure would correspond to SM = 1 at any single point in the shell. In the proposed approach we can adopt a required local safety margin and seek the minimum of a global quantity, i.e. the integrated failure index fi over the whole shell cross-section. However, within the considered class of the application, it is not clear at the moment what the level of the SM parameter should be used for design purposes.

3.2   Local Performance

This approach is based on minimisation of the maximal FI index encountered in the shell cross-section:

$$FI^{opt} = \min_{R} \max \; FI(R; z,s) \tag{17}$$

subject to constraints (9-14) and (16).

The need for this approach stems from observations made in paragraph 2, where local peaks in the FI values led to shell brittle collapse. In the examples which follow we include both shape only and shape and anisotropy components into the vector R.

4.   OUTLINE OF THE SOLUTION METHOD

The optimisation algorithm adopted in this paper is based on a sequential search technique developed in Ref. [15] and known as the Complex Method of Box. We start with an initial, feasible, vertex. The remaining complexes are randomly scattered throughout the feasible domain and therefore increasing the chances of the global rather than local minimum being reached. If a constraint is violated the point is moved inside the feasible region in a prescribed manner. The selected points must, at any time, satisfy both the explicit and implicit constraints. The objective function is formed utilizing the reference surface quantities outputted from the BOSOR 4 code [14]. Ref. [2] gives details how it is done.

Different starting points have been used to check for the global optimum. In most cases the optimum was reached at the same point regardless of the initial vertex.

5.   NUMERICAL STUDIES

5.1   Global Performance

This paragraph provides numerical results for the integrated failure index fi, as outlined in paragraph 3.1. Let us fix the number of layers to n = 6, assume a symmetric lay-up $[0/60/-60]^{\circ}_s$ and use non-petalled segments. This reduces variable components of the design vector R to k_1, k_2 and k_3. The optimisation problem given by Eq. (8) is subjected to constraints (9-11), (15) and (16). The assumed, constant mass, 'm' equals the mass of a hemisphere with the diameter-to-thickness ratio D/t_H = 100. The wall thickness in the optimised dome do not vary along the meridian and its value is obtained from Eq. (16) for every considered shape in the optimisation process. Calculations were performed for the safety margin parameter SM = 1. Table 3 contains optimal solutions for 5 pressure values, i.e. p = 5, 10, 12.5, 15 and 17.5 N/mm². It also gives thicknesses and maximum values of the FI index at the optima. The last column in Table 3 provides dimensionless values of the performance ratio γ defined as: γ = pressure * volume enclosed by shell/weight of shell. In our case the ratio γ^{opt}/γ_H reduces to the ratio of enclosed volume at the optimum to the volume of hemisphere due to Eq. (16). For all analysed pressures the optimal solutions result in 15% - 43% thicker shells than the mass equivalent hemisphere. Also, the resulting domes enclose from 52% to 78% volume of the mass equivalent hemisphere.

Ref. [11] examined the maximisation of the FPF pressures under constraints (9-11) and (16). It follows from Ref. [11] that the maximum FPF pressure for the above case is 18.44 N/mm² and it is attained at k_1 = 1.351, k_2 = 1.932 and k_3/D = 0.491. The integrated failure index fi = 0.657 and the wall thickness t/t_H = 1.091 are obtained for the maximum. Change of the R^{opt} as a function of external pressure is shown in Fig. 8 and the corresponding meridional profiles are shown in Fig. 9. The FI surfaces at the optimum are provided in Fig. 10 for the loading levels p = 5, 10 and 15 N/mm². Sharp increase in the FI appears on the inner surface, near the

clamped edge, for all three pressure levels. In general, the shape of the FI surface resembles that in Fig. 6 for the TVB30B torisphere. Use of the integrated failure index, fi, does not remove locally concentrated stressing.

Table 3

p (N/mm²)	fi^{opt}	R^{opt}			t/t$_H$	max FI	$\frac{\gamma^{opt}}{\gamma_H}$
		k_1	k_2	k_3/D			
5.0	0.046	1.853	1.300	0.314	1.428	0.113	0.52
10.0	0.154	1.871	1.301	0.314	1.427	0.417	0.52
12.5	0.232	1.898	1.301	0.317	1.426	0.643	0.53
15.0	0.327	1.903	1.301	0.317	1.408	0.937	0.53
17.5	0.524	1.852	1.759	0.416	1.153	1.000	0.78
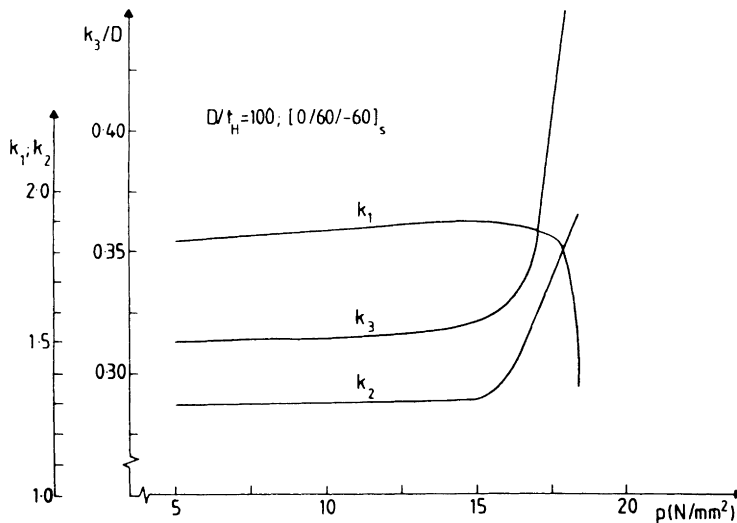
Fig. 8   Behaviour of design variables at optimum

5.2   Local Performance

In this paragraph we examine two cases. The first one illustrates the effect of meridional shaping only on the FI index for a prescribed loading. The problem itself is formulated in paragraph 3.2. The number of plies, design variables and stacking sequence are the same as in the previous paragraph, i.e. 5.1. The results are summarised in Table 4. The surfaces of FI(R^{opt};z,s) for some levels of loading are

depicted in Fig. 11. Variation of the FI surfaces is much smoother for the min-max approach. Comparison of results in Tables 3 and 4 indicates that the min-max approach offers the better choice for design purposes.
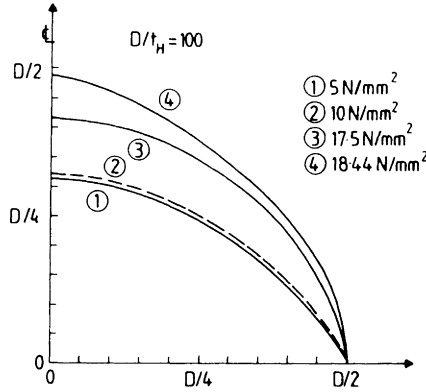
Fig. 9   Meridional profiles of some optimal solutions

Table 4

p (N/mm^2)	FI^{opt}	R^{opt}			t/t$_H$	fi	$\dfrac{\gamma^{opt}}{\gamma_H}$
		k_1	k_2	k_3/D			
5.0	0.097	2.173	1.303	0.272	1.468	0.055	0.48
10.0	0.258	1.817	1.977	0.412	1.133	0.204	0.80
15.0	0.560	1.854	1.975	0.410	1.132	0.445	0.80
17.5	0.768	1.727	1.984	0.424	1.123	0.574	0.81

In the second example we consider shape, anisotropy and variable length, simultaneously as design variables. In addition to constraints (9-11) and (16) we add constraints (12-14) and we assume N=3 segments of variable length within each ply. The stacking sequence is kept, as in previous cases, symmetric. Table 5 summarises results obtained for different pressures. Some further improvements in lowering the peak values of the FI have been obtained.

Finally, Table 6 provides values of the integrated failure index fi and local, maximal values of the FI for hemispheres with D/t$_H$ = 100. Optimal solutions given in Tables 3, 4 and 5 show how much both local and global measures of stress can be reduced.
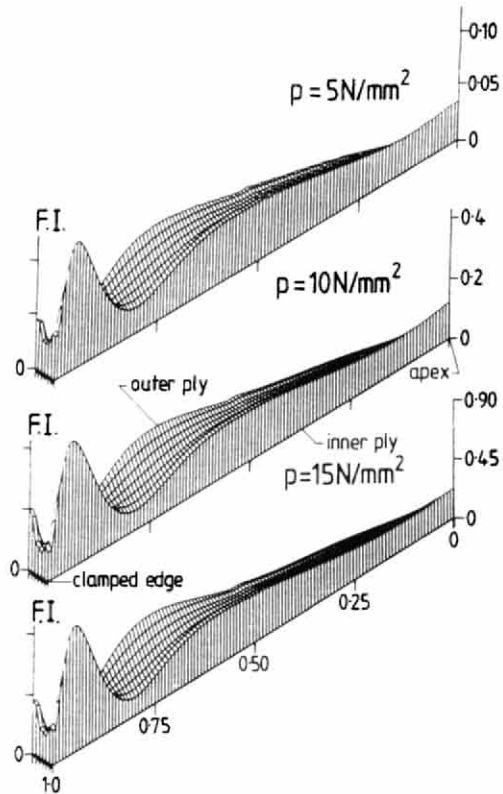
Fig. 10 View of the FI surface at optimum for some prescribed levels of loading [min(fi) case]

Table 5

p*)	FI^{opt}	N\n	θ_{ij} (deg)			L_{ij}/D			k_1	k_2	k_3/D
			1	2	3	1	2	3			
5	0.062	1	-76.9	-57.4	-71.8	0.264	0.061	0.370	1.94	1.74	0.40
		2	-1.9	-19.8	3.5	0.432	0.091	0.172			
		3	83.8	57.3	73.5	0.303	0.140	0.252			
10	0.231	1	-65.8	66.3	3.55	0.090	0.265	0.310	1.94	1.74	0.35
		2	-12.2	78.6	81.8	0.528	0.055	0.082			
		3	39.8	-70.1	89.9	0.286	0.061	0.318			

*)   pressure (N/mm^2)
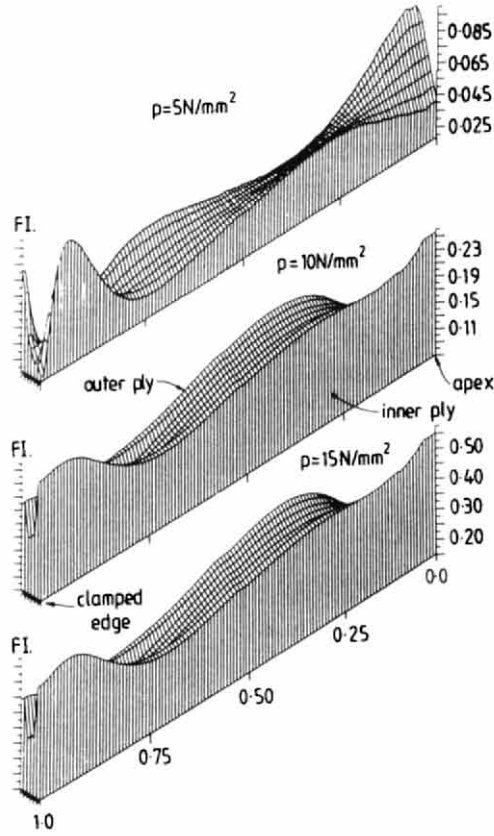
Fig. 11   The FI surfaces at optimum for fixed pressures [min-max (FI) case]

Table 6

p (N/mm²)	2.5	5.0	7.5	9.08
fi	0.022	0.068	0.138	0.199
FI	0.087	0.317	0.690	1.000

6.   CONCLUSIONS

Two ways of lowering the level of the interactive failure index have been investigated numerically. The min-max approach resulted in more acceptable

solutions from a practical point of view. In this approach each ply was made from a number of segments. Length of each segment and its orientation were the design variables. Every two adjacent segments were butt-jointed. This offers nominally constant wall thickness. Variable stacking sequence assures that material strength is fully utilised.

The above idea removes edge effects usually associated with ply drop-off in a variable wall thickness. This is particularly suitable for the woven fabric where some successful experiments have been carried out on petalled and butt-jointed closures.

In some winding techniques we cannot achieve the required strength of unidirectional fibres due to limitations on the stacking sequence. Basically, the idea presented in this paper should also be applicable to vacuum bagged domes made from unidirectional tapes. But there have been no experimental trials to assess butt-joints performance in domes made from unidirectional segments.

7. REFERENCES

1. N. Nanba et al, "Development of deep submergence research vehicle SHINKAI 6500", MHI Technical Rev., 3, Vol. 27, 1990, 157-168.
2. J. Blachut, G.D. Galletly and A.G. Gibson, "CFRP domes subjected to external pressure", J. Marine Struct., Vol. 3, 1990, 149-173.
3. R.E. Garvey, "Composite hull for full-ocean depth", MTS J., Vol. 24, 49-58, 1990.
4. C.S. Smith, "Design of submersible pressure hulls in composite materials", J. Marine Struct., Vol. 4, 141-182, 1991.
5. J.C. Hall et al, "Deep submergence design of intersecting composite spheres", in 'Composites - Design, Manufacture and Application', (eds.) S.W. Tsai and G.S. Springer, SAMPE, 1991, pp. 2F1-2F12.
6. J. Blachut and G.D. Galletly, "Externally-pressurised hemispherical fibre-reinforced plastic shells", Proc. Instn. Mech. Engrs., Vol. 206, 1992, 179-191.
7. J. Blachut and G.D. Galletly, "A numerical investigation of buckling/material failure modes in CFRP dome closures", in 'Composite Materials - Design and Analysis', (eds.) W.P. de Wilde and W.R. Blain, Springer Verlag, 1990, pp. 395-412.
8. J. Blachut, F. Levy-Neto and G.D. Galletly, "Towards optimum carbon-fibre-reinforced plastic end closures", Proc. Instn. Mech. Engrs., Vol. 205, 1991, 329-342.
9. G.D. Galletly and J. Blachut, "Collapse strength of composite domes under external pressure", in 'Advances in Marine Structures', (eds.) C.S. Smith and R.S. Dow, Elsevier Appl. Sci., 1991, pp. 708-732.
10. A. Muc, "Buckling analysis of laminated ellipsoidal shells subjected to external pressure", in 'Composite Structures', (ed.) I.H. Marshall, Elsevier Appl. Sci., 1991, pp. 307-323.
11. J. Blachut, "Influence of meridional shaping on the collapse strength of FRP domes", J. Eng. Opt., Vol. 19, 1992, 65-80.

12. J. Blachut, "Externally-pressurised filament wound domes - scope for optimisation", Computers Struct., (submitted), also presented at the NATO-ASI, Berchtesgaden, FRG, October 1991.

13. M. Zyczkowski, "Recent advances in optimal structural design of shells", European J. of Mechanics, ser. A (Solids), (submitted).

14. D. Bushnell, "BOSOR 4 - program for stress, stability and vibration of complex, branched shells of revolution", in 'Structural Analysis Systems', (ed.) A. Niku-Lari, Pergamon Press, Vol. 2, 1986, pp. 25-53.

15. M.J. Box, "A new method of constrained optimisation and a comparison with other methods", Computer J., 1, Vol. 8, 42-52, 1965.

DISCRETE AND CONTINUOUS REINFORCEMENT OF MATERIALS AND STRUCTURES

Z. Mróz[a]   and   K. Dems[b]

[a]Institute of Fundamental Technological Research, Warsaw, Poland

[b]Łódź Technical University, Łódź, Poland.

Abstract

The materials are usually reinforced by inclusions, fibers or constitute more types of multi laminate composites. The present paper discusses optimality conditions for the case of inclusion reinforcement, introduction of reinforcing curvilinear fibers, membranes or beam stiffeners, finally by softening interfaces representing displacement discontinuity and aimed at reducing maximal stress concentrations.

1. INTRODUCTION

In order to increase material stiffness, the reinforcement is usually introduced in a form of rigid or stiff particulates, whiskers or fibers. The resulting increase of stiffness depends much on shape and distribution of inclusions. Similarly, for fiber reinforcement, the orientation and density of rectilinear fibers are to be specified in order to maximize the element stiffness. For a curvilinear fiber layout, a more complex problem arises to specify the density and layout in particular material layers. Let us note that a curvilinear fiber layout introduces the traction discontinuity in the matrix material. A similar concept can be investigated for membrane-like reinforcing layers with a curvilinear fiber layout within the layer.

The stiffening action is usually considered for the case of specified loading conditions. However, for thermally induced initial strain action or under displacement control, the stiffest material structure will generate very high stresses and therefore is not optimal from the engineering point of view. For an elastic material, both stiffness and stress constraints should be introduced. When both loading and thermal gradients occur, then stiffness and stress constraints provide conflicting design requirements and an optimal solution corresponds to

a compromise design, cf. Garstecki and Mróz [1].

For an inelastic material response, the inclusion or fiber reinforcement is aimed at reducing the creep rate or increasing the limit load of a perfectly plastic matrix.

Some studies of the effect of inclusion shape on stiffness of linear and nonlinear power law materials indicate large sensitivity of stiffness with respect to shape parameters of ellipsoidal inclusions, cf. Lee and Mear [2], Duva [3]. A numerical study of the effect of rigid spherical inclusions on limit load of a ductile plastic matrix indicates a significant reinforcement effect for large volume concentrations, cf. Home and McMeeking [4].

In this paper, we shall discuss the relevant optimality conditions for three cases of interfaces, expressed in terms of local stress, strain or their discontinuities. Our analysis will follow previous derivations of optimality conditions for composite, reinforcing and softening interfaces, cf. Dems and Mróz [5,6,7]. For a periodic array of inclusions or dense distribution of reinforcing fibers, the representative element concept can be used and the effective material moduli are then optimized with respect to density and orientation of reinforcing inclusions. The optimality criteria for such case are considered and some illustrative examples are presented.

2. FORMULATION OF INTERFACE PROBLEMS

Numerous problems in material science are related to moving interphases, for instance, in grain boundary evolution, austenite – martensite transformation, etc. In the study of design modification, such interphase is varied in order to achieve an improved or optimal design. The interface can be regarded as surface on which some static or kinematic fields undergo discontinuities. Let us first discuss briefly three fundamental types of interfaces.

2.1. Inclusion interface S_i

Consider an inclusion of different (usually higher) elastic moduli from those of matrix material, Fig. 1. On the external boundary S_i of the inclusion, the displacement and surface traction are continuous, thus

$$[\![\underline{u}]\!] = 0 \quad , \quad [\![\underline{T}]\!] = [\![\underline{\sigma} \, \underline{n}]\!] \qquad \text{on } S_i \qquad (1)$$

where $\underline{u}$, $\underline{\varepsilon}$, $\underline{\sigma}$ denote displacement, strain and stress fields. $[\![\ ]\!]$ denotes the discontinuity of the enclosed quantity at the interface, thus $[\![\underline{u}]\!] = \underline{u}_2 - \underline{u}_1$ on S_i, where $\underline{u}_1$, $\underline{\varepsilon}_1$, $\underline{\sigma}_1$ and $\underline{u}_2$, $\underline{\varepsilon}_2$, $\underline{\sigma}_2$ denote state fields within the matrix and the inclusion, respectively. The displacement gradients, strain and stress

fields, however, undergo discontinuities satisfying (1), so that
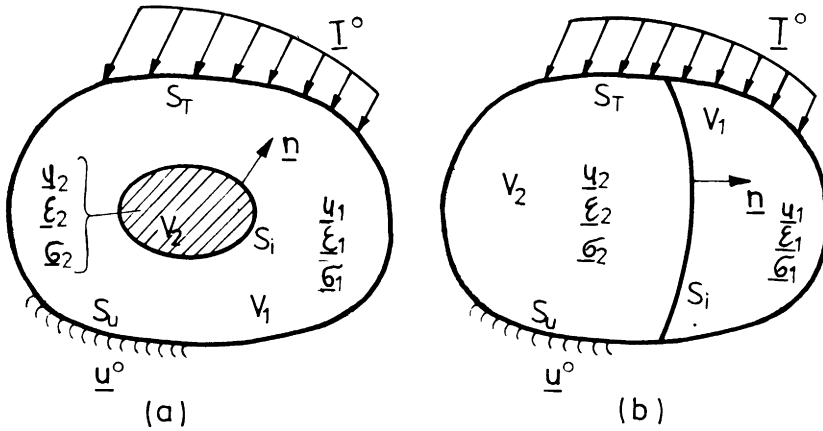
Figure 1. (a) Internal inclusion with closed interface;
(b) Interface penetraiting into external boundary.

$$[\![u_{i,j}]\!] = a_i n_j \quad \text{or} \quad [\![\nabla \underline{u}]\!] = \underline{a} \otimes \underline{n}$$

$$[\![\varepsilon_{ij}]\!] = \frac{1}{2}(a_i n_j + a_j n_i) \quad , \quad [\![\omega_{ij}]\!] = \frac{1}{2}(a_i n_j - a_j n_i) \tag{2}$$

Here $\underline{a}$ denotes the discontinuity vector and $\underline{n}$ is the unit normal vector to the interface S_i, directed into the exterior of the inclusion domain. The form of discontinuity (2) assures the continuity of deformation of material elements within the interface. Assume the inclusion and the matrix to satisfy the linear elasticity relations

$$\underline{\sigma}_1 = \underline{C}_1(\underline{\varepsilon}_1 - \underline{\varepsilon}_1^i) \quad , \quad \underline{\sigma}_2 = \underline{C}_2(\underline{\varepsilon}_2 - \underline{\varepsilon}_2^i) \tag{3}$$

where $\underline{C}_1$ and $\underline{C}_2$ are the elasticity matrices of inclusion and matrix, $\underline{\varepsilon}_1^i$, $\underline{\varepsilon}_2^i$ denote the initial strains. To preserve sufficient generality, we assume that the initial strains may exist in both portions, for instance, thermal and transformation strains. In view of (3), we have

$$[\![\underline{\sigma}]\!] = \underline{C}_2 \underline{\varepsilon}_2 - \underline{C}_1 \underline{\varepsilon}_1 - \underline{C}_2 \underline{\varepsilon}_2^i + \underline{C}_1 \underline{\varepsilon}_1^i = \underline{C}_2 [\![\underline{\varepsilon}]\!] + [\![\underline{C}]\!] \underline{\varepsilon}_1 +$$

$$\underline{C}_1 \underline{\varepsilon}_1^i - \underline{C}_2 \underline{\varepsilon}_2^i \tag{4}$$

From the condition $[\![\underline{\sigma}]\!] \underline{n} = 0$, (2) and (4), we obtain

$$(\underline{n}\ \underline{C}_2\ \underline{n})\underline{a} + \underline{n}[\![\ \underline{C}\ ]\!]\underline{\epsilon}_1 + \underline{n}\ \underline{C}_1\underline{\epsilon}_1^i - \underline{n}\ \underline{C}_2\underline{\epsilon}_2^i = 0 \qquad (5)$$

Denote by $\underline{A}$ the acoustic (or Christoffel) tensor

$$\underline{A} = \underline{n}\ \underline{C}\ \underline{n}\ \quad,\qquad A_{jk} = n_i C_{ijkl}n_l \qquad (6)$$

and by $\underline{b}$ the interface "force vector"

$$\underline{b} = -\ \underline{n}[\![\ \underline{C}\ ]\!]\underline{\epsilon}_1 - \underline{n}\ \underline{C}_1\underline{\epsilon}_1^i + \underline{n}\ \underline{C}_2\underline{\epsilon}_2^i \qquad (7)$$

Equation (5) now takes the form

$$\underline{A}_2\ \underline{a} = \underline{b} \qquad \text{or} \qquad A_{(2)jk}a_k = b_j \qquad (8)$$

Let us note that the acoustic tensor is familiar from plane wave propagation problems, and the vector $\underline{b}$ does not vanish when the stiffness moduli of inclusion and matrix are different or the initial stresses on both sides of the interface are different. In particular, when $\underline{C}_1 = \underline{C}_2 = \underline{C}$, then $\underline{b} = \underline{n}\ \underline{C}[\![\ \underline{\epsilon}^i\ ]\!]$. This is a typical case of a phase transformation process when the developing phase is associated with the specified transformation strain at the interface. Note that solution of (8) requires inversion of acoustic tensor $\underline{A}_2$, thus $\underline{a} = \underline{A}_2^{-1}\underline{b}$.

2.2. Reinforcing interface S_r

Assume now that the interface S_r constitutes an internal shell carrying forces and bending moments, thus inducing discontinuity in surface tractions on S_r. Such interface can be thought of as a thin reinforcing shell inclusion (or a beam in plane case) of different stiffness from the matrix material, or a thin layer of concentrated initial strains. This case can also correspond to a grain boundary with account for grain boundary energy or to an austenite – martensite interface.

The traction discontinuity is now related to interface generalized forces $\underline{N}$ through local equilibrium equations of the interface element, thus

$$[\![\ \underline{\sigma}\ \underline{n}\ ]\!] = [\![\ \underline{T}\ ]\!] = \underline{L}(\underline{N},\underline{q}) \qquad (9)$$

where $\underline{L}$ is in general a differential operator involving derivatives within the interface and $\underline{q}$ denotes the geometric variable of the interface (metric and curvature tensors). The displacement gradient discontinuity is expressed by (2) with $\underline{b}$ specified by (8), where now

$$\underline{b} = \underline{L}(\underline{N},\underline{q}) - \underline{n}[\![\ \underline{C}\ ]\!]\underline{\epsilon}_1 - \underline{n}\ \underline{C}_1\underline{\epsilon}_1^i + \underline{n}\ \underline{C}_2\epsilon_2^i \qquad (10)$$

In particular, when $\underline{C}_1 = \underline{C}_2$, $\varepsilon_{-1}^i = \varepsilon_{-2}^i$, then only the first term of (10) constitutes the interface force. Thus, introduction of reinforcing fiber or shell involves strain and traction discontinuities on S_r, cf. Dems and Mróz [6].

2.3. Softening interface S_d

Assume now that at the interface S_d the traction vector is continuous but the displacement vector may suffer discontinuity, so that

$$[\![\underline{T}]\!] = 0 \quad , \quad [\![\underline{u}]\!] = \underline{v} = \underline{B}\,\underline{T} \quad \text{or} \quad [\![u_i]\!] = v_i = B_{ij}T_j \qquad (11)$$

Here the discontinuity vector $\underline{v}$ is assumed to be explicitly related to the traction vector $\underline{T}$ by the constitutive relation with a symmetric compliance matrix $\underline{B} = \underline{B}^T$. The displacement discontinuity does not involve any new terms in the interface force vector so that (7) and (8) still apply. In particular, when $[\![\underline{C}]\!] = 0$ and $[\![\underline{\varepsilon}^i]\!] = 0$, then $[\![\underline{a}]\!] = 0$ and the displacement gradient discontinuity vanishes on S_d. Here, the gradient discontinuity is calculated on both sides of S_d excluding the interface field. The interface S_d can now be conceived as a thin surface layer undergoing localized shear and normal straining induced by the displacement discontinuity. It may represent a soft surface layer introduced at the inclusion boundary in order to reduce local stress concentrations, or a delaminated area in the composite material.

3. VARYING INTERFACE: RATE EQUATIONS AND SENSITIVITY ANALYSIS

The variation of interface shape will now be considered as an evolution process specified by the transformation velocity field $\dot{\varphi}(\underline{x},t)$, such that each material element undergoes the transformation

$$\underline{x} = \underline{x}_o + \dot{\underline{\varphi}}\,dt \qquad (12)$$

When the inclusion interface S_i moves, the first equation of (1) provides

$$[\![\dot{u}_i]\!] = [\![\frac{\partial u_i}{\partial t}]\!] + u_{i,j}\dot{\varphi}_j = [\![\frac{\partial u_i}{\partial t}]\!] + a_i\dot{\varphi}_n = 0 \qquad (13)$$

and then

$$[\![\, \dot{\bar{u}}_i \,]\!] = [\![\, \frac{\partial u_i}{\partial t} \,]\!] = - \, a_i \dot{\varphi}_n \tag{14}$$

where $\dot{\varphi}_n = \dot{\varphi}_i n_i$ denotes the normal transformation velocity component, $\dot{u}_i$ denotes the total time derivative on the transformed element and $[\![\, \dot{\bar{u}}_i \,]\!]$ is the local time derivative. The second equation of (1) now provides

$$[\![\, \dot{\bar{T}}_i \,]\!] = [\![\, \frac{\partial \sigma_{ij}}{\partial t}]\!] n_j + [\![\, \sigma_{ij}]\!] \dot{n}_j + [\![\, \frac{\partial \sigma_{ij}}{\partial x_k}]\!] n_j \dot{\varphi}_k = 0 \tag{15}$$

The time derivative of the unit normal vector is, cf. [5]

$$\dot{n}_j = (n_j n_l - \delta_{jl}) n_k \dot{\varphi}_k{}'_l \quad \text{or} \quad \dot{\underline{n}} = (\underline{n} \cdot \underline{L} \, \underline{n}) \underline{n} - \underline{L}^T \underline{n} \tag{16}$$

where $L_{ij} = \dot{\varphi}_i{}'_j$. In view of (15) and (16), we obtain

$$[\![\, \dot{\underline{T}} \,]\!] = [\![\, \dot{\bar{\sigma}}_{ij}]\!] n_j = [\![\, \frac{\partial \sigma_{ij}}{\partial t}]\!] n_j = - [\![\, \sigma_{ij}]\!] (n_j n_l - \delta_{jl}) n_k \dot{\varphi}_k{}'_l \, -$$

$$[\![\, \frac{\partial \sigma_{ij}}{\partial x_k}]\!] n_j \dot{\varphi}_k = [\![\, \sigma_{il}]\!] n_k \dot{\varphi}_k{}'_l - [\![\, \sigma_{ij}{}'_k]\!] n_j \dot{\varphi}_k \tag{17}$$

Consider the local coordinate system (n,τ), $\tau = 1,2$, at the interface and assume that for a closed inclusion it is sufficient to consider $\dot{\varphi}_k = \dot{\varphi}_n$, $\dot{\varphi}_\tau = 0$. Equation (17) now provides

$$[\![\, \dot{\bar{\sigma}}_{nn}]\!] = [\![\, \frac{\partial \sigma_{nn}}{\partial t}]\!] = - [\![\, \frac{\partial \sigma_{nn}}{\partial n}]\!] \dot{\varphi}_n$$

$$[\![\, \dot{\bar{\sigma}}_{\tau n}]\!] = [\![\, \frac{\partial \sigma_{\tau n}}{\partial t}]\!] = [\![\, \sigma_{\tau \alpha}]\!] \dot{\varphi}_n{}'_\alpha - [\![\, \frac{\partial \sigma_{\tau n}}{\partial n}]\!] \dot{\varphi}_n \tag{18}$$

Equations (18) can also be expressed in the matrix form

$$\begin{bmatrix} [\![\, \dot{\bar{\sigma}}_{nn}]\!] \\[2mm] [\![\, \dot{\bar{\sigma}}_{\tau n}]\!] \end{bmatrix} = \begin{bmatrix} - [\![\, \sigma_{nn}{}'_n]\!] & 0 \\[2mm] - [\![\, \sigma_{\tau n}{}'_n]\!] & [\![\, \sigma_{\tau \alpha}]\!] \end{bmatrix} \begin{bmatrix} \dot{\varphi}_n \\[2mm] \dot{\varphi}_n{}'_\alpha \end{bmatrix} \tag{19}$$

where $\alpha = 1,2$. When the transformation rule is known and the equilibrium solution at instant t is specified, then the local stress rate discontinuities are specified by (17) or (19). On the other hand, the local displacement rate discontinuity is specified by (14). Thus (14) and (17) provide the boundary conditions for the rate transformation problem.

Denote by $\bar{\sigma}_1$, $\bar{\varepsilon}_1$, $\bar{u}_1$ and $\bar{\sigma}_2$, $\bar{\varepsilon}_2$, $\bar{u}_2$ the states within two body portions. Assume that the initial strain fields and the elasticity matrices do not vary. However, the interface motion

specified by the transformation rate $\dot{\varphi}_n(\underline{x},t)$ is assumed to occur. The rate fields therefore satisfy the field equations

$$\dot{\bar{\sigma}}_{1ij,j} = 0 \quad , \quad \dot{\bar{\sigma}}_1 = \underline{C}_1 \dot{\bar{\varepsilon}}_1 \quad , \quad \dot{\bar{\varepsilon}}_{1ij} = \frac{1}{2}(\dot{\bar{u}}_{1i,j} + \dot{\bar{u}}_{1j,i})$$

$$\dot{\bar{\sigma}}_{1ij}n_j = 0 \quad \text{on } S_T \quad , \quad \dot{\bar{u}}_i = 0 \quad \text{on } S_u \tag{20}$$

and similar equations in the domain V_2. Moreover, the discontinuity conditions (14) and (17) are satisfied on S_i. The virtual work equation can now be written as follows

$$\int \dot{\bar{\sigma}}_1 \cdot \dot{\bar{\varepsilon}}_1 dV_1 + \int \dot{\bar{\sigma}}_2 \cdot \dot{\bar{\varepsilon}}_2 dV_2 = \int (\dot{\bar{T}}_2 \cdot \dot{\bar{u}}_2 - \dot{\bar{T}}_1 \cdot \dot{\bar{u}}_1) dS_i = \int (\dot{\bar{T}}_2 \cdot [\![\dot{\bar{u}}]\!] +$$

$$[\![\dot{\bar{T}}]\!] \cdot \dot{\bar{u}}_1) dS_i = \int (\dot{\bar{T}}_1 \cdot [\![\dot{\bar{u}}]\!] - [\![\dot{\bar{T}}]\!] \cdot \dot{\bar{u}}_2) dS_i \tag{21}$$

We have thus a non-typical boundary-value problem when discontinuities in both displacement and traction rates are specified on the interface. To have a clear insight into this problem, we can consider it as a superposition of two problems. First, assume that there is a traction rate discontinuity on S_i and denote the respective solution by $\dot{\underline{\sigma}}'$, $\dot{\underline{\varepsilon}}'$, $\dot{\underline{u}}'$. The field $\underline{u}'$ is continuous on S_i but the stress rate field $\dot{\underline{\sigma}}'$ satisfies the condition $[\![\dot{\underline{\sigma}}']\!]\underline{n} = [\![\dot{\bar{T}}]\!]$ on S_i. We can conceive a distributed traction on surface S_i inducing the equilibrium states within V_1 and V_2. The rate potential and complementary energies are now of the form

$$\Pi^u(\underline{u}') = \int U(\dot{\underline{\varepsilon}}') dV - \int [\![\dot{\bar{T}}]\!] \cdot \dot{\underline{u}}' dS_i$$

$$\Pi^\sigma(\dot{\underline{\sigma}}') = \int W(\dot{\underline{\sigma}}') dV \tag{22}$$

where $U(\dot{\underline{\varepsilon}})$ and $W(\dot{\underline{\sigma}})$ are the specific strain and stress rate energies. The stationarity conditions provide weak formulations of the boundary value problem, namely

$$\delta\Pi^u = \int \dot{\underline{\sigma}}' \cdot \delta\dot{\underline{\varepsilon}}' \, dV - \int [\![\dot{\bar{T}}]\!] \cdot \delta\dot{\underline{u}}' dS_i = 0$$

$$\delta\Pi^\sigma = \int \dot{\underline{\varepsilon}}' \cdot \delta\dot{\underline{\sigma}}' \, dV = 0 \tag{23}$$

Consider now the second problem, when the displacement rate discontinuity is induced on S_i. The corresponding state fields are denoted by $\dot{\underline{\sigma}}''$, $\dot{\underline{\varepsilon}}''$, $\dot{\underline{u}}''$. Now the stress rate is continuous on S_i but the displacement rate satisfies the condition $[\![\dot{\underline{u}}'']\!] =$

$[\![\, \dot{\underline{u}} \,]\!]$ on S_i. We can conceive a thin layer on S_i along which both tangential and normal components of $\dot{\underline{u}}''$ undergo discontinuities (slip and dilatancy layer). The potential and complementary energies now are

$$\Pi^u(\dot{\underline{u}}'') = \int U(\dot{\underline{\epsilon}}'')dV$$

$$\Pi^\sigma(\dot{\underline{\sigma}}'') = \int W(\dot{\underline{\sigma}}'')dV - \int(\dot{\underline{\sigma}}''\underline{n})\cdot[\![\, \dot{\underline{u}} \,]\!] \, dS_i \tag{24}$$

and the stationarity conditions provide the relations

$$\delta\Pi^u = \int \dot{\underline{\sigma}}''\cdot\delta\dot{\underline{\epsilon}}'' \, dV = 0$$

$$\delta\Pi^\sigma = \int \dot{\underline{\epsilon}}''\cdot\delta\dot{\underline{\sigma}}'' \, dV - \int(\delta\dot{\underline{\sigma}}''\underline{n})\cdot[\![\, \dot{\underline{u}} \,]\!] \, dS_i = 0 \tag{25}$$

The solution of the rate problem associated with moving interface is now obtained by superposing two states of traction and displacement rate discontinuity problems, thus

$$\dot{\bar{\underline{\sigma}}} = \dot{\underline{\sigma}}' + \dot{\underline{\sigma}}'' \quad , \quad \dot{\bar{\underline{\epsilon}}} = \dot{\underline{\epsilon}}' + \dot{\underline{\epsilon}}'' \quad , \quad \dot{\bar{\underline{u}}} = \dot{\underline{u}}' + \dot{\underline{u}}'' \tag{26}$$

The potential and complementary energies of the states $\dot{\bar{\underline{u}}}$, $\dot{\bar{\underline{\epsilon}}}$, $\dot{\bar{\underline{\sigma}}}$ now are

$$\Pi^u(\dot{\bar{\underline{u}}}) = \int U(\dot{\bar{\underline{\epsilon}}})dV - \int[\![\, \dot{\bar{\underline{T}}} \,]\!]\cdot\dot{\bar{\underline{u}}}_1 dS_i$$

$$\Pi^\sigma(\dot{\bar{\underline{\sigma}}}) = \int W(\dot{\bar{\underline{\sigma}}})dV - \int(\dot{\bar{\underline{\sigma}}}_1\underline{n})\cdot[\![\, \dot{\underline{u}} \,]\!] \, dS_i \tag{27}$$

The present formulation provides a direct approach to sensitivity analysis by solving a rate or incremental problem associated with the moving interface. In many cases, however, we are interested in assessing the variation of an integral functional representing a global state property. As the potential energy represents the global stiffness and the complementary energy is a measure of global compliance, their variations are of fundamental interest.

The rate of variation of the potential energy can be expressed as follows

$$\dot{\Pi}^u(\underline{u},S_i) = \int\frac{\partial U}{\partial\underline{\epsilon}}\cdot\dot{\underline{\epsilon}} \, dV + \int[\![\, U \,]\!]\dot{\varphi}_n dS_i \tag{28}$$

However, in view of the virtual work principle and (14), there is

$$\int\underline{\sigma}\cdot\dot{\bar{\underline{\epsilon}}} \, dV = \int\underline{T}\cdot[\![\, \dot{\underline{u}} \,]\!]dS_i = -\int\underline{T}\cdot\underline{a} \, \dot{\varphi}_n dS_i \tag{29}$$

and (28) can be rewritten in the form

$$\dot{\Pi}^u = \int H \; \dot{\varphi}_n dS_i \tag{30}$$

where $H = [\![\; U \;]\!] - \underline{T} \cdot \underline{a}$ is the generalized force associated with the interface motion. This force can also be expressed interms of the Eshelby energy momentum tensor, namely, cf. [11]

$$\Sigma_{jk} = U\delta_{jk} - \sigma_{ij}u_i,_k \tag{31}$$

so that

$$\dot{\Pi}^u = \int [\![\Sigma_{jk}]\!] n_j n_k \dot{\varphi}_n dS_i = \int H \; \dot{\varphi}_n dS_i \tag{32}$$

and $H = \underline{n} \cdot [\![\; \underline{\Sigma} \;]\!] \underline{n}$.

Let us now pass to a discussion of the reinforcing interface S_r. The surface tractions are now discontinuous on S_r and are related to interface stresses by equilibrium conditions, so we have

$$[\![\; \underline{\sigma} \;]\!] = \underline{L}(\underline{N},\underline{q}) \neq 0 \quad , \quad [\![\; \underline{\varepsilon} \;]\!] = 0 \quad , \quad [\![\; \underline{u} \;]\!] = 0 \tag{33}$$

The plane case of such an interface was treated by Dems and Mróz [6] who discussed the optimal interaction of beam stiffeners within disks and plates. Consider, for example, a curvilinear plane stiffener introduced into a disk, Fig. 2a. Denote by
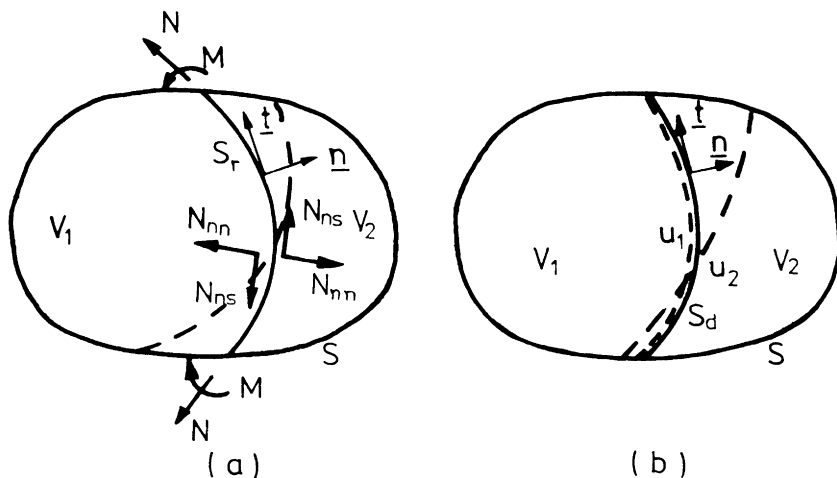
Figure 2. (a) Curvilinear stiffener in a disk;
(b) Displacement discontinuity line in a disk

$\underline{v}(v_s, v_n)$, $\underline{e}(\epsilon, \varkappa)$ and $\underline{Q}(N,M)$ the displacement vector, strain and generalized stress within the stiffener, where ϵ, $\varkappa$ are the axial elongation and curvature of the stiffener, N and M denote the cross sectional axial force and the bending moment. We have

$$\epsilon = v_s{,}_s - Kv_n \quad , \quad \varkappa = -\theta{,}_s = -(v_n{,}_s + Kv_s){,}_s \tag{34}$$

where K denotes the stiffener curvature, $\theta = v_n{,}_s + Kv_s$ is the angle of rotation of the stiffener cross section and s denote the stiffener parameter. The equilibrium equations of the stiffener are

$$N{,}_s - M{,}_s K - [\![N_{ns}]\!] = 0 \quad , \quad NK + M{,}_{ss} - [\![N_n]\!] = 0 \tag{35}$$

The potential energy now has the form

$$\Pi^u(\underline{u}, S_r) = \int U(\underline{\epsilon})\ dV - \int \underline{T}^o{\cdot}\underline{u}\ dS_T + \int \tilde{U}(\tilde{\underline{\epsilon}})\ dS_r \tag{36}$$

where the last term corresponds to stiffener elastic energy. The variation of Π^u due to stiffener variation is now expressed in the form, cf. [6]

$$\dot{\Pi}^u = \int \left\{ \tilde{U}K + [\![U]\!] - [\![N_{ns}\epsilon_{ns}]\!] - [\![N_n\epsilon_n]\!] - N\theta{,}_s + \right.$$

$$\left. (M{,}_s\epsilon){,}_s \right\} \dot{\varphi}_n dS_r - \int [u_s(\dot{T}_{ns} - T_{ns}{,}_s\dot{\varphi}_s) + u_n(\dot{T}_n - T_n{,}_s\dot{\varphi}_s)] dS_T \tag{37}$$

where the second term corresponds to the interaction of stiffener with the loaded boundary. For a closed stiffener, only the integral along interface S_r represents the potential energy variation.

Assume now that the displacement vector $\underline{u}$ undergoes the discontinuity along the softening interface S_d (which will be called the discontinuity line). We have

$$\underline{v} = \underline{u}_2(\underline{x}) - \underline{u}_1(\underline{x}) = [\![\underline{u}(\underline{x})]\!] \tag{38}$$

It is further assumed that the discontinuity vector is related to continuous internal tractions on S_d through the relations

$$\underline{N} = \frac{\partial U^d(\underline{v})}{\partial \underline{v}} = \underline{L}\ \underline{v} \quad , \quad \underline{v} = \underline{L}^{-1}\underline{N} = \underline{B}\ \underline{N} \tag{39}$$

where $\underline{L}$ and $\underline{B}$ are the interface stiffness and compliance matrices. The potential energy of the body now is

$$\Pi^u(\underline{u}, S_d) = \int U(\underline{\epsilon})\ dV - \int \underline{T}^o{\cdot}\underline{u}\ dS_T + \int U^d(\underline{v})\ dS_d \tag{40}$$

The variation of Π^u due to interface motion equals, cf. [7]

$$\dot{\Pi}^u = \int [-[\![U]\!] - U^d K + N_{n\alpha}v_{\alpha},_s - e_{3\alpha\beta}(N_{n\alpha}v_{\beta}),_s]\dot{\varphi}_n dS_d -$$

$$\int u_\alpha(\dot{T}_{n\alpha} - T_{n\alpha},_s\dot{\varphi}_s)dS_T + \int T_{n\alpha}(\dot{u}_\alpha - u_\alpha,_s\dot{\varphi}_s)dS_u \tag{41}$$

where $e_{3\alpha\beta}$ denotes the permutation symbol.

Consider now a more general functional which could represent global or local stress or displacement constraints, namely

$$G = \int \Psi(\underline{\sigma},\underline{u}) \, dV + \int h(\underline{u},\underline{T}) \, dS \tag{42}$$

and introduce an adjoint structure of the same shape and interface but subjected to initial strains, body forces and boundary conditions

$$\underline{\varepsilon}^{ai} = \frac{\partial \Psi}{\delta \underline{\sigma}} \quad , \quad \underline{f}^a = \frac{\partial \Psi}{\partial \underline{u}} \qquad \text{within V}$$

$$\underline{T}^{ao} = \underline{\sigma}^a \underline{n} = \frac{\partial h}{\partial \underline{u}} \qquad \text{on } S_T \quad , \quad \underline{u}^{ao} = -\frac{\partial h}{\partial \underline{T}} \qquad \text{on } S_u \tag{43}$$

Following the previous derivation, the variation of G can be expressed in terms of primary and adjoint fields and their discontinuities. For a closed interface S_i, we obtain

$$\dot{G} = \int \{ [\![\Psi]\!] - [\![\underline{\sigma}\cdot\underline{\varepsilon}^a]\!] + \underline{T}\cdot\underline{a}^a + \underline{T}^a\cdot\underline{a}\}\dot{\varphi}_n dS_i = \int \tilde{H}(\underline{u},\underline{u}^a)\dot{\varphi}_n dS_i \tag{44}$$

where $\underline{a}^a$ is the interface discontinuity vector of the adjoint displacement field, $[\![\underline{u}^a]\!] = \underline{a}^a \otimes \underline{n}$. The respective generalized *mutual energy momentum tensor* can be specified as follows

$$\tilde{\Sigma}_{jk} = (\Psi - \underline{\sigma}\cdot\underline{\varepsilon}^a)\delta_{jk} + \sigma_{ij}u^a_j,_k + \sigma^a_{ij}u_j,_k \tag{45}$$

so that (44) takes the form

$$\dot{G} = \int [\![\tilde{\Sigma}_{jk}]\!]n_j n_k\dot{\varphi}_n dS_i = \int \tilde{H}(\underline{u},\underline{u}^a)\dot{\varphi}_n dS_i \tag{46}$$

For the case of a closed beam stiffener within a disk structure, the functional G is now of the form

$$G = \int \Psi(\underline{\sigma},\underline{u}) \, dV + \int h(\underline{u},\underline{T}) \, dS + \int \Phi(\underline{Q},\underline{\tilde{\varepsilon}})dS_r \tag{47}$$

and its first variation with respect to shape of moving stiffening interface is expressed as

$$\dot{G} = \int \{-[\![N_s]\!]\varepsilon^a_s + [\![N_{ns}\varepsilon^a_{ns}]\!] + [\![N^a_n\varepsilon_n]\!] + N\theta^a,_s + N^a\theta,_s -$$

$$(M,_s\varepsilon^a),_s - (M^a,_s\varepsilon),_s - (N^a\varepsilon + M^a\chi)K + [\![\Psi]\!] - \Phi K\}\dot{\varphi}_n dS_r \tag{48}$$

Similarly, for a closed softening interface, we obtain

$$\dot{G} = \int \{ \ [\![\Psi]\!] \ - \Phi K - [\![\underline{\sigma} \cdot \underline{\varepsilon}^a_{\_}]\!] + T_{n\alpha} v^a_\alpha K - T_{n\alpha} v^a_\alpha{}_{,n} - T^a_{n\alpha} v_\alpha{}_{,n} +$$
$$\varepsilon_{3\alpha\beta} (T_{n\alpha} v^a_\beta + T^a_{n\alpha} v_\beta)_{,s} \} \dot{\varphi}_n dS_d \qquad (49)$$

where now $\Phi = \Phi(T_{n\alpha}, v_\alpha)$, $\alpha = \tau, n$, occurring in (45) depends on traction and displacement discontinuity on S_d. More general expressions are derived in [6] and [7] where the interaction with boundary surfaces was account for.

4. OPTIMAL REINFORCEMENT CONDITIONS

The sensitivity analysis associated with moving interfaces provides now a useful tool in generating the optimality criteria and also in determining proper reinforcement evolution rules which could be applied in numerical procedures.

Consider first a single reinforcing inclusion within the loaded body. A typical optimization problem could be formulated by requiring an extremum of a behaviour functional with constraint set on the inclusion volume. The design parameters would then specify position, orientation, size and shape of the inclusion. Let us note that translation or rotation of the inclusion does not affect its volume and there is no need for additional constraint.

Let us discuss the relevant optimality criteria for most typical cases of inclusion variations. When a rigid-body translation of inclusion specified by the vector $\dot{\varphi} = \underline{b}$ occurs, the potential energy variation follows from (30) and (31), namely

$$\dot{\Pi}^u = \int H \ \dot{b}_k n_k dS_i = \dot{b}_k \left[\int H^+ dS^+_k - \int H^- dS^-_k \right] = B_k \dot{b}_k \qquad (50)$$

where $H^+ = [\![U]\!]^+ - [\![\ \underline{T} \cdot \underline{a} \ ]\!]^+$, $H^- = [\![U]\!]^- - [\![\ \underline{T} \cdot \underline{a} \ ]\!]^-$, $dS_k = dS \cdot n_k$, and "+" , "−" denote values at respective interface portions with the translation vector directed outside or inside the inclusion, Fig. 3a.

When an arbitrary state functional G is considered, its variation follows from (44), that is

$$\dot{G} = \dot{b}_k \left[\int \tilde{H}^+ dS^+_k - \int \tilde{H}^- dS^-_k \right] = \tilde{B}_k \dot{b}_k \qquad (51)$$

where $\tilde{H}^+ = ([\![\Psi]\!] - [\![\ \underline{\sigma} \cdot \underline{\varepsilon}^a]\!] + \underline{T} \cdot \underline{a}^a - \underline{T}^a \cdot \underline{a})^+$ and $\tilde{H}^- = ([\![\Psi]\!] - [\![\ \underline{\sigma} \cdot \underline{\varepsilon}^a]\!] + \underline{T} \cdot \underline{a}^a - \underline{T}^a \cdot \underline{a})^-$.

The optimal position of the inclusion corresponding to an extremum of the potential energy is now specified by the condition $\dot{\Pi}^u_k = 0$, thus

$$B_k = 0 \quad \text{or} \quad \int H^+ dS_k = \int H^- dS_k \quad \text{on } S_i \ , \quad k=1,2,3 \qquad (52)$$

and when the stationary value of G is required, $\dot{G}_k = 0$, then

$$\tilde{B}_k = 0 \quad \text{or} \quad \int \tilde{H}^+ dS_k = \int \tilde{H}^- dS_k \quad \text{on } S_i \ , \quad k=1,2,3 \qquad (53)$$

These optimality conditions are expressed in terms of interface integrals. Alternative but similar conditions can be derived by using the concept of *path-independent integrals* discussed previously by Dems and Mróz [10]. Instead of inclusion translation with respect to a body , one can consider the body translation specified by the vector $-b_k$ with respect to inclusion, Fig. 3b.

$$(a) \qquad\qquad\qquad (b)$$
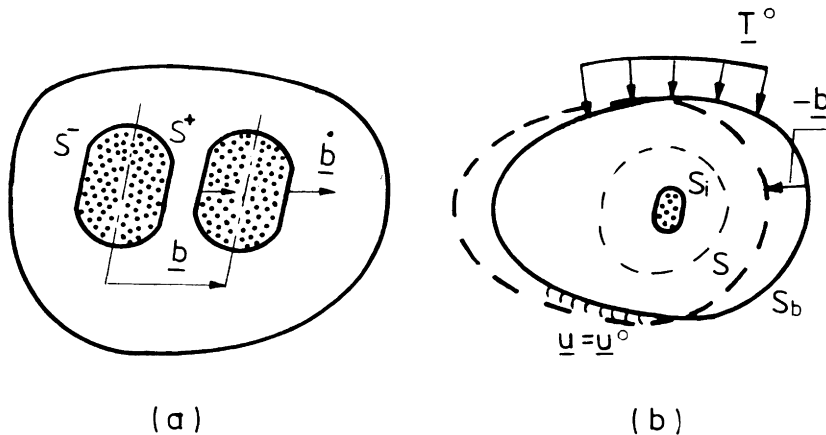
Figure 3. (a) Inclusion translation with respect to structure;
(b) Structure translation with respect to inclusion

Consider any closed surface S enclosing the inclusion. The variation of Π^u and G can now be expressed as follows

$$\dot{\Pi}^u = \dot{b}_k \left[\int (U\delta_{kj} - \sigma_{ij} u_i,_k) n_j dS \right] =$$

$$\dot{b}_k \left[\int U dS_k - \int T_i u_i,_k dS \right] = B_k^t \dot{b}_k \qquad (54)$$

and

$$\dot{G} = \dot{b}_k \left\{ \int [(\Psi - \underline{\sigma} \cdot \underline{\varepsilon}^a) \delta_{kj} + \sigma_{ij} u_i^a,_k + \sigma_{ij}^a u_i,_k] n_j dS \right\} =$$

$$\dot{b}_k \left\{ \int (\Psi U - \underline{\sigma} \cdot \underline{\varepsilon}^a) dS_k + \int (T_i u_i^a,_k + T_i^a u_i,_k) dS \right\} = \tilde{B}_k^t \dot{b}_k \qquad (55)$$

For a homogeneous body the surface integrals (54) and (55) vanish. However, when the surface encloses the inclusion, then (54) and (55) provide sensitivities of Π^u and G with respect to inclusion translation. In particular, the boundary surface can be used and the sensitivity can explicitly be expressed in terms of surface tractions and displacements. The relevant optimality conditions now follow from (54) and (55) by requiring $B_k^t = 0$ or $\tilde{B}_k^t = 0$.

Consider now the case of inclusion rotation, that is

$$x_k^* = x_k + \dot{\varphi}_k dt \quad , \quad \dot{\varphi}_k = e_{kpl} x_l \dot{\omega}_p \tag{56}$$

when $\dot{\omega}_p$ denotes the rotation rate vector and e_{kpl} is the permutation symbol. Following [10], the sensitivities of Π^u and G can be expressed as follows in terms of surface integrals on an enclosed arbitrary surface S

$$\dot{\Pi}^u = \dot{\omega}_p e_{kpl} \left[\int U x_l dS_k - \int (T_l u_k + T_i u_i{}_{,k} x_l) dS \right] = B_p^r \dot{\omega}_p \tag{57}$$

and

$$\dot{G} = \dot{\omega}_p e_{kpl} \left\{ \int (\Psi - \underline{\sigma} \cdot \underline{\varepsilon}^a) x_l dS_k + \int (T_l u_k^a + T_l^a u_k) dS + \int (T_i u_i{}^a{}_{,k} + T_i^a u_i{}_{,k}) x_l dS \right\} = \tilde{B}_p^r \dot{\omega}_p \tag{58}$$

The integrals can be calculated for any surface enclosing the inclusion, in particular, the boundary surface S_b or the interface S_i. When (57) and (58) are expressed as integrals over the interface, we obtain

$$\dot{\Pi}^u = \dot{\omega}_p e_{kpl} \left[\int ([\![U]\!] - \underline{T} \cdot \underline{a}) x_l dS_k^i \right] = B_p^r \dot{\omega}_p \tag{59}$$

and

$$\dot{G} = \dot{\omega}_p e_{kpl} \left[\int ([\![\Psi]\!] - [\![\underline{\sigma} \cdot \underline{\varepsilon}^a]\!] + \underline{T} \cdot \underline{a}^a + \underline{T}^a \cdot \underline{a}) x_l dS_k^i \right] = \tilde{B}_p^r \dot{\omega}_p \tag{60}$$

The optimality conditions corresponding to stationarity values of Π^u or G are now directly deduced from (57), (58) or (59), (60), namely $B_p^r = 0$ or $\tilde{B}_p^r = 0$, p =1,2,3.

Considering the expansion of inclusion, that is the transformation

$$x_k^* = x_k + \dot{\eta} x_k dt \tag{61}$$

the sensitivity of Π^u and G can be expressed as follows

$$\dot{\Pi}^u = \dot{\eta}\left[\int\int(\llbracket U \rrbracket - \underline{T}\cdot\underline{a})x_k dS_k^i = \dot{\eta}\left[\int\int(Ux_k n_k - T_i u_i,_k x_k - \frac{1}{2}T_i u_i)dS\right] = B^e\dot{\eta}\right. \tag{62}$$

and

$$\dot{G} = \dot{\eta}\left[\int\int(\llbracket \Psi \rrbracket - \llbracket \underline{\sigma}\cdot\underline{\epsilon}^a \rrbracket + \underline{T}\cdot\underline{a}^a + \underline{T}^a\cdot\underline{a})x_k dS_k^i = \tilde{B}^e\dot{\eta}\right. \tag{63}$$

When the integrand of (42) are $\Psi = \Psi(\underline{\sigma})$, $h = 0$ and Ψ_1 is a homogeneous function of stress of order p, then (63) can be expressed in terms of the surface integral on the arbitrary surface S enclosing the inclusion, namely

$$\dot{G} = \dot{\eta}\left\{\int[(\Psi_1 - \underline{\sigma}\cdot\underline{\epsilon}^a)x_k n_k + (T_i^a u_i,_k + T_i u_i^a,_k)x_k + \frac{2p-3}{p}T_i u_i^a + \frac{2p-3}{p}T_i^a u_i]dS\right\} \tag{64}$$

Finally, considering the parameter dependent shape variation, that is

$$\underline{\varphi} = \underline{\varphi}(\underline{x},d_l) \;,\; \dot{\underline{\varphi}} = \frac{\partial\underline{\varphi}}{\partial d_l}\dot{d}_l \;,\; \dot{\varphi}_n = (\frac{\partial\varphi_k}{\partial d_l}n_k)\dot{d}_l \;,\; l=1,2..m \tag{65}$$

the sensitivities of Π^u and G are expressed by

$$\dot{\Pi}^u = \dot{d}_l\left[\int\int(\llbracket U \rrbracket - \underline{T}\cdot\underline{a})\frac{\partial\varphi_k}{\partial d_l}n_k dS_i\right] = B_l^s\dot{d}l$$

$$\dot{G} = \dot{d}\left[\int\int(\llbracket \Psi \rrbracket - \llbracket \underline{\sigma}\cdot\underline{\epsilon}^a \rrbracket + \underline{T}\cdot\underline{u}^a + \underline{T}^a\cdot\underline{u})\frac{\partial\varphi_k}{\partial d_l}n_k dS_i\right] = \tilde{B}_l^s\dot{d}_l \tag{66}$$

Similar sensitivity expressions and optimality conditions can be derived for reinforcing and softening interfaces S_r and S_d.

Note that the path independent integrals (55),(60) and (64) can be applied for the case of translation, rotation and expansion of any interface, without using interface data.

5. REPRESENTATIVE ELEMENT OPTIMIZATION

The analysis of the previous Section can now be applied to a case of a representative material element subjected to homoge-

neous stress and strain. Consider the surface tractions $T_i^b = \sigma_{ij}^u n_j$ or displacements $u_i^b = \nu_{ij}^u x_j$ applied to the representative element, where σ_{ij}^u denotes the uniform stress tensor and ν_{ij}^u is a constant displacement gradient. The mean stress and strain tensors can now be expressed as follows, cf. Hill [12]

$$V^r \bar{\sigma}_{ij} = \frac{1}{2} \int (T_i^b x_j + T_j^b x_i) dS$$

$$V^r \bar{\varepsilon}_{ij} = \frac{1}{2} \int (u_i^b x_j + u_j^b x_i) dS \tag{67}$$

and it can easily be shown that $\bar{\sigma}_{ij} = \sigma_{ij}^u$, $\bar{\varepsilon}_{ij} = \frac{1}{2}(\nu_{ij}^u + \nu_{ji}^u)$. For the representative element volume there is

$$V^r \underline{\bar{\sigma}} \cdot \underline{\bar{\varepsilon}} = \int \underline{\sigma} \cdot \underline{\varepsilon} \, dV^r \tag{68}$$

Introduce the elastic stress and strain concentration matrices $\underline{A}(\underline{x})$, $\underline{B}(\underline{x})$, so that

$$\underline{\sigma}(\underline{x}) = \underline{A}(\underline{x})\underline{\bar{\sigma}} \quad , \quad \underline{\varepsilon}(\underline{x}) = \underline{B}(\underline{x})\underline{\bar{\varepsilon}} \tag{69}$$

Denoting by $\underline{C}$ and $\underline{D}$ the local stiffness and compliance matrices, we have

$$V^r \underline{\bar{\sigma}} = \int \underline{C} \, \underline{\varepsilon} dV^r = \int \underline{C} \, \underline{B} \, \underline{\bar{\varepsilon}} \, dV^r = \underline{\bar{C}} \, \underline{\bar{\varepsilon}} \quad , \quad \underline{\bar{C}} = \frac{1}{V^r} \int \underline{C} \, \underline{B} \, dV^r$$

$$V^r \underline{\bar{\varepsilon}} = \int \underline{D} \, \underline{\sigma} dV^r = \int \underline{D} \, \underline{A} \, \underline{\bar{\sigma}} \, dV^r = \underline{\bar{D}} \, \underline{\bar{\sigma}} \quad , \quad \underline{\bar{D}} = \frac{1}{V^r} \int \underline{D} \, \underline{A} \, dV^r \tag{70}$$

The effective moduli $\underline{\bar{C}}$ and $\underline{\bar{D}}$ now depend on the internal structure of the element, thus $\underline{A} = \underline{A}(\underline{s})$, $\underline{B} = \underline{B}(\underline{s})$, where $\underline{s}$ denotes collectively design parameters. Similarly to the previous analysis, the sensitivity of representative element behaviour with respect to variation of $\underline{s}$ can be studied.

Consider in this Section the case of rotation of an anisotropic element microstructure with respect to axes of mean stress or strain. Equations (57) and (58) when applied to homogeneous stress and strain fields at the boundary provide the optimality conditions

$$e_{kpl} \int T_l u_k dS = 0 \tag{71}$$

and

$$e_{kpl} \int (T_l u_k^a + T_l^a u_k) dS = 0 \tag{72}$$

Condition (71) requires coaxiality of surface traction and displacement. Similarly, (71) requires coaxiality of primary and adjoint tractions and displacements.

Considering the representative element, the optimality conditions can be derived by considering rotation of mean stress and strain tensors with respect to anisotropic microstructure. Let $\underline{Q}$ denotes the rotation matrix, so that $\underline{\sigma}^* = \underline{Q}\underline{\sigma}\,\underline{Q}^T$ and $\underline{\varepsilon}^* = \underline{Q}\underline{\varepsilon}\underline{Q}^T$ and the stress or strain components in the rotating frame do not vary. The corotational derivatives of stress or strain vanish, thus

$$\overset{\circ}{\underline{\sigma}} = \underline{Q}\,\overline{(\underline{Q}^T\underline{\dot{\overline{\sigma}}}\,\underline{Q})}\,\underline{Q}^T = \underline{\dot{\overline{\sigma}}} - \underline{\omega}\,\overline{\sigma} + \overline{\sigma}\,\underline{\omega} = 0 \quad , \quad \underline{\dot{\overline{\sigma}}} = \underline{\omega}\,\overline{\sigma} - \overline{\sigma}\,\underline{\omega}$$

$$\overset{\circ}{\underline{\varepsilon}} = \underline{Q}\,\overline{(\underline{Q}^T\underline{\dot{\overline{\varepsilon}}}\,\underline{Q})}\,\underline{Q}^T = \underline{\dot{\overline{\varepsilon}}} - \underline{\omega}\,\overline{\varepsilon} + \overline{\varepsilon}\,\underline{\omega} = 0 \quad , \quad \underline{\dot{\overline{\varepsilon}}} = \underline{\omega}\,\overline{\varepsilon} - \overline{\varepsilon}\,\underline{\omega} \quad (73)$$

where $\underline{\omega} = \underline{\dot{Q}}\,\underline{Q}^T$ denotes the spin of principal axes.

Consider now the variation of complementary energy under mean stress control

$$V^r\dot{W}(\overline{\sigma}) = V^r\,\frac{\partial W}{\partial\overline{\sigma}}\cdot\underline{\dot{\overline{\sigma}}} = V^r\,\overline{\varepsilon}\cdot\underline{\dot{\overline{\sigma}}} = V^r\overline{\varepsilon}\cdot(\underline{\omega}\,\overline{\sigma} - \overline{\sigma}\,\underline{\omega}) =$$

$$V^r(\overline{\varepsilon}\,\overline{\sigma} - \overline{\sigma}\,\overline{\varepsilon})\cdot\underline{\omega} \quad (74)$$

The variation of potential energy for mean strain control is

$$V^r\dot{U}(\varepsilon) = V^r\,\frac{\partial U}{\partial\overline{\varepsilon}}\cdot\underline{\dot{\overline{\varepsilon}}} = V^r\,\overline{\sigma}\cdot\underline{\dot{\overline{\varepsilon}}} = V^r\overline{\sigma}\cdot(\underline{\omega}\,\overline{\varepsilon} - \overline{\varepsilon}\,\underline{\omega}) =$$

$$V^r(\overline{\sigma}\,\overline{\varepsilon} - \overline{\varepsilon}\,\overline{\sigma})\cdot\underline{\omega} \quad (75)$$

The stationarity condition now requires *coaxiality of mean stress and strain tensors*, thus $\overline{\varepsilon}\,\overline{\sigma} = \overline{\sigma}\,\overline{\varepsilon}$.

Consider now the stress functional $G(\overline{\sigma}) = V^r\Psi(\overline{\sigma})$ representing the element response. To derive sensitivity of G, introduce an adjoint element subjected to the mean strain

$$\overline{\varepsilon}^a = \frac{\partial\Psi}{\partial\overline{\sigma}} \quad (76)$$

The sensitivity of G now equals

$$V^r\dot{G} = V^r\,\frac{\partial\Psi}{\partial\overline{\sigma}}\cdot\underline{\dot{\overline{\sigma}}} = V^r\,\overline{\varepsilon}^a\cdot\underline{\dot{\overline{\sigma}}} = V^r(\overline{\varepsilon}^a\,\overline{\sigma} - \overline{\sigma}\,\overline{\varepsilon}^a)\cdot\underline{\omega} \quad (77)$$

and the stationarity condition requires *coaxiality of mean stress and adjoint mean strain*, $\overline{\varepsilon}^a\overline{\sigma} = \overline{\sigma}\,\overline{\varepsilon}^a$. Note that coaxiality property does not depend on particular type of anisotropy. Such coaxiality condition was studied in detail for orthotropic

composites by Pedersen [8] and for orthotropic plastic texture anisotropy by Hill [9].

6. ILLUSTRATIVE EXAMPLES

In this Section three simple examples will be presented in which three types of interfaces discussed in previous Sections will be introduced and their optimal location will be considered.

Example I   Let be given a circular sandwich plate with constant sheet thickness, simply supported at the outer edge and uniformly loaded by a lateral pressure *p*. The plate sheets are made of two linear elastic materials with Young's moduli E_1 and E_2, so that $E_2 > E_1$, Fig. 4.
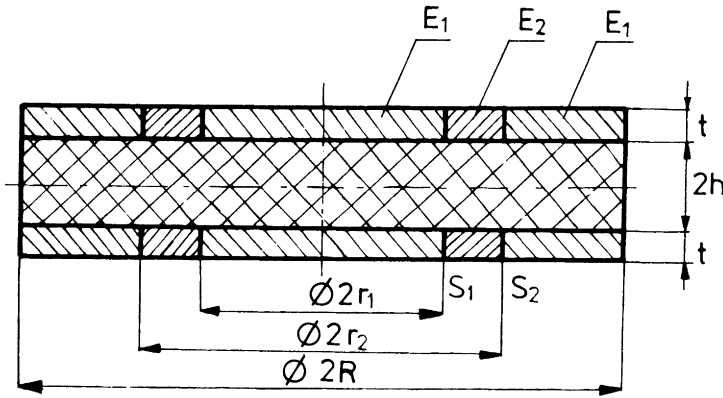
Figure 4. Circular sandwich plate with annular inclusion

The domain of higher Young's modulus, bounded by interfaces S_1 and S_2 of radii r_1 and r_2, respectively, can be treated as inclusion in matrix material of modulus E_1.

Assuming the complementary energy of the plate as the measure of mean plate compliance, the optimization problem is reduced to determining the radii r_1 and r_2 within the class of plate with constant inclusion volume. The complementary energy of plate equals

$$G = \Pi^\sigma = \frac{\pi}{th^2} \sum_{k=1}^{3} \frac{1}{E_k} \int_{r_{k-1}}^{r_k} (M_r^2 - 2\nu M_r M_t + M_t^2) r dr \qquad (78)$$

where M_r, M_t are the radial and circumferential bending moments and 2h is the core thickness. The constraint on the inclusion volume is expressed in the form

$$c = \left(\frac{r_2}{R}\right)^2 - \left(\frac{r_1}{R}\right)^2 = c_o < 1 = \text{const.} \tag{79}$$

Introducing the Lagrange functional $G' = G - \lambda(c - c_o)$, the op-timality conditions follows from stationarity of G', namely

$$\dot{G} = \lambda \dot{c} \quad , \quad \dot{\lambda}(c - c_o) = 0 \tag{80}$$

where $\dot{G}$ is defined by (44) and variation of constraint (79) equals

$$\dot{c} = 2\left(\frac{r_2}{R}\frac{\dot{r}_2}{R} - \frac{r_1}{R}\frac{\dot{r}_1}{R}\right) \tag{81}$$

The solution of optimality conditions (80) for the case $\nu = 0$ and $c_o = 0.1$ is illustrated in Fig.5 which shows the dependence of the optimal values of r_1/R and r_2/R on the ratio of elastic
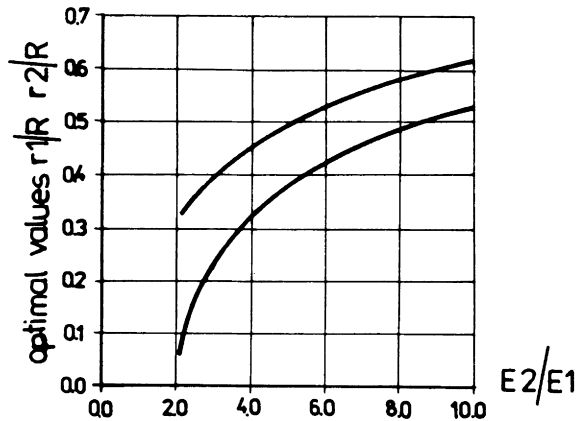
Figure 5. Optimal location of inclusion versus the ratio of elastic moduli

moduli E_2/E_1 for the inclusion and matrix materials. Figure 6 shows the variation of the plate compliance as the function of radius r_1 for $c_o = 0.1$ and $E_2/E_1 = 4$. It is easy to see that the values of r_1 and r_2 satisfying the optimality conditions (80) correspond to a global minimum of the mean plate compli-ance.

Example II   Consider a rotating circular disk of radius R with a central hole of radius r_o. The disk is stiffened with circular fibers of radii r_i and cross-sectional longitudinal rigidity D_i constituting the reinforcing interphases S_r, Fig. 7. The disk is made of linear elastic material with elastic constant E and ν. Assume the radii r_i and fiber longitudinal rigidity D_i as the design parameters and consider the complementary energy of a disk given in the form

$$G = \Pi^\sigma = \sum_{i=1}^{n+1} \frac{1}{Eh} \int_{r_{i-1}}^{r_i} (N_{r_i}^2 - 2\nu N_{r_i} N_{t_i} + N_{t_i}^2) r dr + \sum_{i=1}^{n} \frac{r_i N_i^2}{D_i} \qquad (82)$$
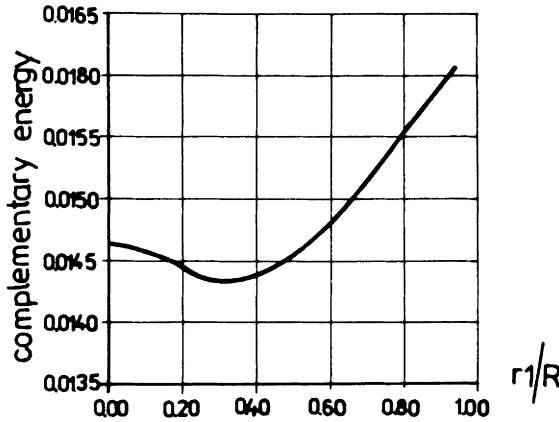
Figure 6. Plate compliance versus position of inclusion

where n denotes the number of reinforcing fibers.
   The optimization problem can now be stated as follows

$$\text{min. } G = \Pi^\sigma \quad \text{for} \quad c = \sum_{i=1}^{n} r_i \frac{D_i}{Eh} = c_o = \text{const.} \qquad (83)$$

The optimality conditions follow from the stationarity requirement of Lagrange functional and have the form

$$\dot{\Pi}^\sigma = \lambda \dot{c} \quad , \quad \dot{\lambda}(c - c_o) = 0 \qquad (84)$$

where now $\dot{\Pi}^\sigma$ follows from (46). The results of calculations are shown in Table 1, where the initial and optimal values of fiber radii and their longitudinal rigidities are given for prescri-

bed values of $\nu = 0.35$, $\rho\omega^2 = 1$, $c_o = 5$, $r_o = 0.1$ and $R = 1.1$. As the result of optimization procedure the value of complemen-
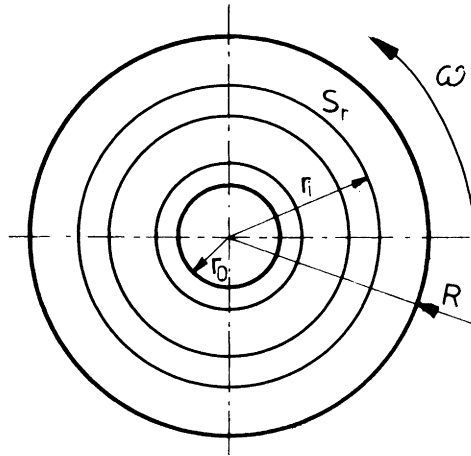
Figure 7. Rotating circular disk with reinforcing fibers

tary energy for optimal design is reduced about 19.25% in comparison to initial design.

Table 1
Fiber location and rigidities

Fiber No.	Initial		Optimal	
	r_i	D_i/Eh	r_i	D_i/Eh
1	0.26667	3.75000	0.46785	1.29476
2	0.43333	2.30769	0.69719	1.26836
3	0.60000	1.66667	0.84901	1.24543
4	0.76667	1.30435	0.96098	1.22480
5	0.93333	1.07143	1.04867	1.20614

Example III   As the last example consider a circular plate of external radius *a* with the softening interface S_d in the form of hinge line of radius R, Fig. 8. The plate is made of linear elastic material and its bending rigidity is denoted by D, while the hinge line has a constant stiffness *c*. The outer edge
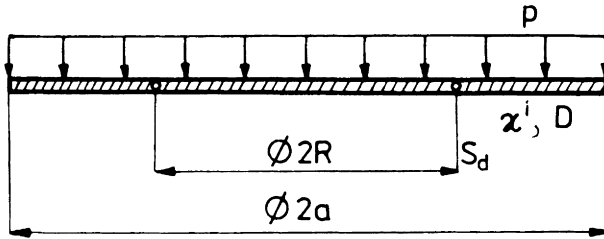
Figure 8. Circular plate with softening interface

of plate is rigidly supported and the uniform lateral pressure p as well as an imposed field of constant initial distortion $\underline{x}^i$ is applied to the plate. These initial distortion can be caused, for instance, by a difference in temperature between lower and upper plate surfaces.

We can now formulate the following optimization problem: for various combinations of lateral pressure and initial curvature find the optimal radius of softening interface, which minimizes the maximum effective moment within plate domain

$$\min_{0<R<a} \tilde{G} = G^{1/n} = \left\{ \int_0^a M_e^n \, rdr \right\}^{1/n} = \left\{ \int_0^a (M_r^2 + M_s^2 - M_r M_s)^{n/2} rdr \right\}^{1/n} \quad (85)$$
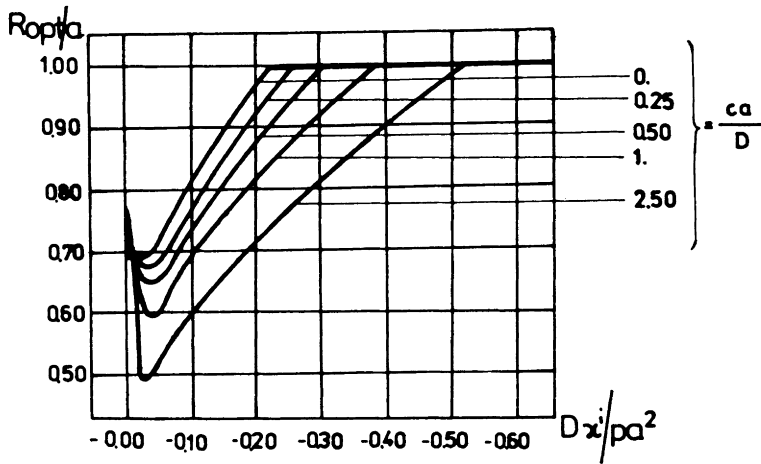
Figure 9. Optimal location of hinge line

where n is even and tending to infinity. The optimality condi-

tion of the problem (85) follows from stationarity requirements and takes the form

$$\overset{\approx}{G} = \frac{1}{n} G^{(1-n)/n} \dot{G} = 0 \tag{86}$$

where $\dot{G}$ follows from general expression (47). The results of the numerical solution of optimality condition (86) are shown in Fig. 9, where the plot of the optimal radius of the hinge line versus the ratio of initial curvature to lateral pressure is given for different values of hinge stiffness. It follows also from the calculations that on introducing he optimal hinge line within plate domain, them maximal effective moment is reduced about 35% in comparison with the plate without any softening interface.

REFERENCES

1 Garstecki, A. and Mróz, Z., Optimal design of elastic structures subjected to loads and initial distortions, J. Struct. Mech., 15, 47-68, 1987.
2 Lee,B.J. and Mear, M.E., Effect of inclusion shape on the stiffness of nonlinear two phase composites, J. mech. Phys. Sol.,39, 627-649, 1991.
3 Duva, J.M., A self-consistent analysis of the stiffening effect of rigid inclusions on a power law material, J. Eng. Mat. Techn., 106, 317-322,1984.
4 Home, C.L. and McMeeking, R.M., Plastic flow in ductile materials containing a cubic array of rigid spheres, Int. J. Plast., 7, 255-274, 1991.
5 Dems, K. and Mróz, Z., Variational approach by means of adjoint systems to structural optimization and sensitivity analysis, Int. J. Solids Struct., 20, 527-552, 1984.
6 Dems, K. and Mróz, Z., Optimal design of rib-stiffeners in disks and plates, Int. J. Solids Struct., 25, 9, 973-998,1989.
7 Dems, K. and Mróz, Z., Shape sensitivity analysis and optimal design of disks and plates with strong discontinuities of kinematic fields, Int. J. Solids Struct., 29, 4, 437-463, 1992.
8 Pedersen, P., Bounds on elastic energy in solids of orthotropic materials, Struct. Optimization, 2, 55-63, 1990.
9 Hill, R., Constitutive modeling of orthotropic plasticity in sheet metals, J. Mech. Phys. Sol., 38, 405-417, 1990.
10 Dems, K. and Mróz, Z., On a class of conservation rules associated with sensitivity analysis in linear elasticity, Int. J. Sol. Struct., 22, 737-758, 1986.
11 Eshelby, J.D., The continuum theory of lattice defects, Solid State Physics (Ed. F. Seitz *et al.*), vol. 3, 79, Academic press,1956.
12 Hill, R., The essential structure of constitutive laws for metal composites and polycrystales, J. Mech. Phys. Sol., 15, 79-95, 1967.

Optimization of composite topology for doubly-curved laminated shells under buckling constraints

A. Muc

Institute of Mechanics and Machine Design, Cracow University of Technology, ul. Warszawska 24, 31-155 Kraków, Poland.

Abstract
   The aim of the present paper is to present various types of the optimality conditions encountered in the analysis of laminated shell structures and their dependance on the kinematical and physical assumptions. Theoretical considerations are illustrated by various numerical examples dealing with buckling behaviour of doubly-curved composite shells.

1. INTRODUCTION

   Optimization of laminated structures is a complex task, the one which requires the integration of various factors related to composite mechanics, structural analysis, numerical programming and manufacturing. In general, most of the investigations in this area have been directed at two aspects: 1) design of a composite topology (layout), 2) optimization of a geometry (size and (or) shape of structures). In the optimization process the above two aspects may be considered separately or commonly. In the second case the optimization of a structural layout gives a full information for the design of structures. The proper design of laminated composite plated or shell structures subjected to various constraints has been one of a major topic of research in recent years. For thinwalled composite structures the examples of various formulations and solutions are discussed in Refs [1-7].
   In general, optimization of the structural layout under buckling constraints can be divided into two groups:
A Buckling loads of laminated structures are studied by means of analytical methods and simple mathematical representations.
B Numerical methods are applied to discretised models of practical design problems.
The fundamental difference in the both mentioned above approaches depends on the possibility (or not) of solving of geometrically nonlinear problems.
   In the first case (A) buckling loads are derived in the closed analytical form with the use of geometrically linear buckling theories (the Rayleigh-Ritz method, the Bubnov-Gallerkin method etc.). Thus, the optimality conditions under buckling constraints may be sought analytically. However,the solutions in the closed form have been found for axially compressed plates only (see Refs [8,9]). Therefore, in the case (A) the structural design is usually represented by a number of uknown parameters subjected to various constraints and the goal is to find their optimal values numerically. It is known that the stiffness characteristics of laminated thinwalled composites based upon the classical lamination

theory are governed by 12 lamination parameters and 4 independent stiffness invariants.In the orthotropic laminates, eliminating the coupling effects, the number of independent lamination parameters is reduced to four. The design method for tailoring the mechanical properties of the laminated thinwalled composite structures has been developed by Miki [10] and often used by many authors for solving of the optimization problems for plates [11] or cylindrical shells [12,13].

As the geometrically nonlinear theory is employed in the considerations (the case (B)) the problem of the laminate design for maximum buckling loads is much more difficult. We do not know in advance the continuous relations between buckling loads,composite topology and shell geometry, so that they have to be sought in a numerical way for each laminate configurations separately.

In both approaches,i.e. geometrically linear (A) and nonlinear (B), various optimization numerical procedures may be used, including integer, discrete or probabilistic search techniques, but we shall not dwell on it here. Some of them are presented and discussed in the references cited above.

The objective of the present paper is to discuss general results dealing with the optimization of laminated composite structures under buckling constraints and then to present numerical examples of the research in this area. Furthermore, in the interest of focusing the discussion, most of the presentation is limited to the design of laminated doubly-curved shells under buckling and first-ply failure constraints.

2. GOVERNING EQUATIONS

In our considerations we employ the global approach to the description of laminated composite shell deformations. The fundamental geometrical relations are formulated with the use of geometrically nonlinear Sander's equations [14] (large deflections,moderate rotations and small strains),extended for the case of first-order shear deformations theory - three displacements v_i,w and two angles of rotation of the normal to the shell midsurface γ_i. They take the following form:

$$\varepsilon_{ij} = e_{ij} + \tfrac{1}{2}\vartheta_i\vartheta_j + \tfrac{1}{2}g_{ij}\Psi^2, \Psi = \tfrac{1}{2}\epsilon_{ij}v_{j,i}, \quad \kappa_{ij} = \tfrac{1}{2}(\gamma_{i,j} + \gamma_{j,i}) + \tfrac{1}{2}(\epsilon_{ik}c_{kj} + \epsilon_{jk}c_{ki})\Psi,$$

$$\varepsilon_{i3} = \gamma_i + \vartheta_i, e_{ij} = \tfrac{1}{2}(v_{i,j} + v_{j,i}) - c_{ij}w, \quad \vartheta_i = w_{,i} + c_{ik}v_k, \quad i,j,k = 1,2 \qquad (1)$$

where g_{ij} and ϵ_{ij} mean metric and antymetric tensors, respectively. Derivatives with respect to surface coordinates are denoted by comma after subscripts.

Three-parametrical shell theory (the displacements v_i, w only) based on the Love-Kirchhoff hypothesis can be easily obtained by the following simplification:

$$\gamma_i = -\vartheta_i \qquad \Longleftrightarrow \qquad \varepsilon_{i3} = 0 \qquad (2)$$

The assumed form of the displacement field affects directly the number of terms in the stiffness matrix, i.e. the form of physical relations for composite thinwalled structures. It is obvious that the inclusion of transverse shear stresses σ_{i3} or transverse normal stresses σ_{33} expands the stiffness matrix in the comparison with the case as the Kirchhoff shell theory is applied in the analysis.On the other hand according to the laminated structures theory the number of nonzero terms in the stiffness matrix depends also on the laminate

configuration. As far as the author is concerned the most general form of the stiffness matrix is introduced in Ref. [15].

In the considered case of five-parametrical shell theory stress resultants and stress couples, N_{ij}, Q_{i3} and M_{ij} (rsp.) are related to direct ε_{ij}, ε_{i3} and bending κ_{ij} strains in the following fashion (see, for instance, Ref.[15]):

$$\left[\begin{array}{c} N_{ij} \\ Q_{i3} \\ M_{ij} \end{array} \right] = \left[\begin{array}{ccc} A & 0 & B \\ 0 & k'A^{S-D} & 0 \\ B & 0 & D \end{array} \right] \left[\begin{array}{c} \varepsilon_{ij} \\ \varepsilon_{i3} \\ \kappa_{ij} \end{array} \right] \tag{3}$$

With the help of the shear correction factor k' one can express easily three types of various formulations analysed herein:

-1° k' = 0 corresponds to the Kirchhoff shell theory (the constraint of type (2))

-2° k' = $\frac{5}{6}$ - transverse shear deformation theory of the first order

-3° k' variable and depends on the laminate configuration; it is determined by evaluations of average shear stresses with the use of the method suggested in Ref. [16].

It is worth to mention that k' is constant as G_{13} is equal to G_{23} and both ply thicknesses and orthotropic material properties are identical for each individual layers in the laminate. In that case the terms A^{S-D} in eqn (3) are uncoupled and independent on fibres orientations in plies. If G_{13} is not equal to G_{23} the shear coefficients are unequal even for symmetric laminates.

The numerical analysis bases on the functional formulation utilizing the functional of total potential energy J in the Lagrange form:

$$J = J_1 + J_2 + J_3 \tag{4}$$

where

$$J_1 = \frac{1}{2} \int_\Omega [P]^T [\ni] d\Omega, \quad J_2 = -\frac{p}{2} \int_\Omega [(2 + e_{ii})w - \vartheta_i v_i] d\Omega, \quad J_3 = \lambda_\alpha^I r_\alpha + \lambda_\alpha^{II} r_\alpha. \tag{5}$$

J_1 expresses the total strain energy, J_2 describes the work of the external uniform pressure p and has the form entirely consistent with the assumed kinematical relations (1) (see the results of the analysis in Ref. [17]). The last term in eqn (4) J_3 takes into account the possible types of kinematical boundary conditions with the help of the uknown Lagrange multipliers λ_α, at each shell boundaries I and II. In eqn (5) [P] represents the matrix of the stress resultants and stress couples, whereas [$\ni$] the matrix of the direct, transverse shear and bending strains, rsp.

In the prebuckling analysis, substitution of the kinematical variables by the interpolation functions in eqn (4), and then application of the principle of the virtual works to all nodal variables and Lagrange's multipliers lead finally to the basic system of nonlinear equations for which a solution is sought. Solution of the nonlinear equations is achieved by the modified Newton-Raphson method with a variable arc-length procedure.

If buckling analysis is carried out, for axisymmetric loading, each of the kinematical variables and in this way stress resultants components is expanded in a Fourier series in

the circumferential coordinate. Buckling equations are derived by employing perturbation technique to the functional (4). Then, by retaining linear and quadratic terms of the perturberation in the functional finally,one can obtain the following system of equations:

$$[K_1(p_o) + \eta K_2(\triangle p)][q^b] = 0 \qquad (6)$$

where the first term in eqn (6) is the stiffness matrix including the effects at the fixed load p_o,and the second is the load-geometric matrix and is proportional to the stress resultants increments due to known load increment $\triangle p$. $[q^b]$ means the vector of nodal displacements components at each nodal point on the shell meridian. The critical load can be calculated by means of a sequence of the eigenvalue problems (6).

3. DESIGN VARIABLES AND OPTIMALITY CONDITIONS

Thinwalled structures are commonly treated as two dimensional approximations of three dimensional bodies. Thus,the form of kinematical hypothesis and then of kinematical relations (large or small deflections, rotations etc. are taken into account or not) are the fundamental points in the whole analysis. The variety of used models and approaches (global or local) in the modelling of thinwalled structures is especially visible for composite or generally anisotropic plates and shells. Therefore the number of independent parameters describing composite material (by the physical relations) depends only on the kinematical assumptions. Generally, the applied shell theory should fulfill the basic requirement: the consistency of theoretical results with experimental ones. Thus, it is obvious that in geometrically nonlinear analysis the optimal design of laminated structures under buckling constraints as well as the proper choice of optimization algorithms are also strongly dependent on the assumed form of kinematical relations.

Let s_q (q=1,2,...) denote design variables for composite structures. Their number is directly connected with the applied kinematical hypothesis in integer (continuous) optimization only, and s_q are commonly equivalent to lamination parameters ξ_l.

With the regard to buckling problems it is wellknown that the first order shear deformation theory has to be used in the analysis due to the low Kirchhoff's modulus - to - Young's modulus (G_{13}/E_1) ratio. However, in this case the number of lamination parameters ξ_l increases from l=12 (Kirchhoff's shell theory) to 15 (as the transverse shear coefficient k'is constant - 2° or variable - 3°). The number of independent terms in the stiffness matrix may even be higher as more refined shell theories are taken into account.

For more general constraints that involve more complex combination of terms in the stiffness matrix the use of normalized integrals as design variables s_q is less atractive. Still, the integrals can be calculated for the purpose of characterizing the laminate and the illustration of the results. However, for the practical design each individual ply should be analyzed separately. Thus, the most logical design variables are ply-identity variables that define entirely mechanical and geometrical characteristics of each individual ply. In this way the number and the definition of design variables are not separated from kinematical relations and, as it will be shown below, the optimum conditions depend entirely on the form of an assumed kinematical hypothesis.

In our considerations we use the first variant of transverse shear deformation theory (2°) with the constant shear correction factor k'. In addition, we assume that Kirch-

hoff's modulus G_{13} is equal to G_{23}. As it was mentioned previously it causes that the terms A^{S-D} in the stiffness matrix (3) are uncoupled and independent on laminate configurations. Thus,even for five-parametrical shell theories the number of independent lamination parameters ξ_l can be equal to 12. This number can be reduced by additional assumptions. First of all let us notice that the coupling terms A_{i6}, B_{i6}, D_{i6} (i=1,2) in the stiffness matrix (3) have to be identically equal to zero (e.g. orthotropic materials and other models of laminate configurations). The above-mentioned terms couple sine and cosine coefficients of the Fourier expansion in the circumferential direction and we are not able to solve buckling problem without any additional expansions in Fourier series. Furthermore, from the point of view of the optimal design, it was proved by Onoda [13] (see also Refs [18,19]) that the nonzero terms A_{i6}, B_{i6}, D_{i6} reduce values of buckling loads. It can be easily verified by the analysis of the Rayleigh quotient that buckling loads usually decrease when the values A_{i6}, B_{i6}, D_{i6} become nonnegligible. Now, since only $\cos 2\alpha_q$ and $\cos 4\alpha_q$ appear in the stiffness expressions the orientational dependence is determined entirely by the interval $0^o \leq \alpha_q \leq 90^o$. Under the above assumptions one can find simply the global conditions of optimal configurations under buckling constraints. For the fixed wavenumber in buckling m the dimensionless buckling load $\Phi_m(p)$ can be written as the uknown in advance function F of the geometrical parameters g_j and of the coefficients $C_{\rho\beta}$ of the stiffness matrix:

$$\Phi_m(p) = F_m(g_j, C_{\rho\beta}) \tag{7}$$

In geometrically linear approach to buckling problems the relation (7) is equivalent to the Rayleigh quotient, whereas for nonlinear problems is the other form of eqn (6).

The differentials of eqn (7) with respect to the design variables s_q leads to the following relation:

$$\frac{\partial \Phi_m(p)}{\partial s_q} = \frac{\partial F_m}{\partial C_{\rho\beta}} \frac{\partial C_{\rho\beta}}{\partial s_q} = 0, \quad \rho, \beta = 1, 6 \tag{8}$$

The derivative $\frac{\partial C_{\rho\beta}}{\partial s_q}$ can be always expressed in the explicit form and for instance if the fibre orientations α_q are treated as the design variables s_q, it takes the following form:

$$\frac{\partial C_{\rho\beta}}{\partial \alpha_q} = -(2a_{\rho\beta} + 8b_{\rho\beta}\cos 2\alpha_q)\sin 2\alpha_q \tag{9}$$

It gives immediately one of the optimality conditions, i.e.:

$$\alpha_q = 0^o \quad or \quad 90^o \tag{10}$$

Let us notice also that if in the laminate $E_1 = E_2$ (e.g. woven roving materials) $a_{\rho\beta}$ is identically equal to zero and the condition (9) can be reduced to the following form:

$$sin(4\alpha_q) = 0 \iff \alpha_q = 0^o \quad or \quad 45^o \tag{11}$$

$a_{\rho\beta}$, $b_{\rho\beta}$ are known functions of the coefficients in the stiffness matrix (3). The above global optimality conditions explain completely the reason of the use for designing laminated thinwalled composite structures with the predetermined ply orientation angles in sublaminates, i.e. $0^o, \pm 45^o$ or 90° (see e.g. Refs [11,12]). In this approach the optimization process is reduced to the determination of stacking sequences and optimal thicknesses of sublaminates having prescribed fibre orientations.

It is worth to emphasize that the conditions (10) and (11) are general and derived without a reference to a special shell models as k' is constant and $G_{13} = G_{23}$. If $G_{13} \neq G_{23}$ and k' = $k'(\alpha_q)$ then one cannot obtain the stationarity conditions analogous to (10) or (11) because:

$$\frac{\partial C_{\rho\beta}}{\partial \alpha_q} = \frac{\partial k'}{\partial \alpha_q} c_{\rho\beta}(\alpha_q) + k' d_{\rho\beta}(\alpha_q) - (2a_{\rho\beta} + 8b_{\rho\beta}cos2\alpha_q)sin2\alpha_q \qquad (12)$$

This example is a very good illustration of problems encountered in the optimization of composite structures and highlights the role of modelling.

Thus, it is obvious that the relation (8) may give one global optimum condition in the form written symbolically by eqn (8) or after simplified assumptions two, one given by eqs (10) (or (11)) and the second in the following form:

$$\frac{\partial F_m}{\partial C_{\rho\beta}}(a_{\rho\beta} + 4b_{\rho\beta}cos2\alpha_q) = 0 \qquad (13)$$

Under the above-mentioned assumptions (dealing with the form of k', G_{13}, G_{23}) our optimization problem can be reduced to the analysis of eqn (13) only. However, in the futher analysis eqn (13) will be slightly modified for the generality of considerations and numerical purposes.

The conditions (10) and (13) are subjected to one additional constraint, the wavenumber in buckling m is fixed and constant during the analysis. On the other hand it is obvious that the fixed value of m corresponding to the minimum of buckling loads p (with respect to m) is not always the best with the regard to the optimization problem. This is illustrated in Fig.1 where the fibre orientation α_q is chosen as the design (control) parameter s_q. Among all plotted possible cases one can notice the situation (Fig. 1c) where for optimally oriented structures the global minimum corresponds neither to m nor to m+1. The maximum buckling load is reached at B which is the point of the intersection of curves for m and m+1. The value of s_q corresponding to the point B can be determined from the equation:

$$\Phi_m(p) = \Phi_{m+1}(p) \qquad (14)$$

Such a problem is often encountered for optimization of laminated structures under buckling constraints and in this case eqn (14) defines the location of so-called local minima.

Now, let us come back to the definition of lamination parameters. We consider the generalized symmetric balanced laminate of $[(\pm \alpha_1)/(\pm \alpha_2)/.../(\pm \alpha_N)]_S$. In this laminate,
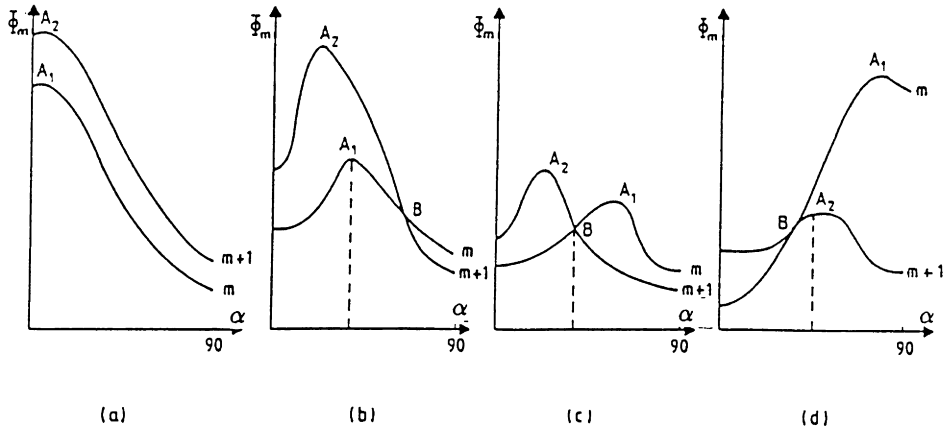
Figure 1: Possible variations of buckling loads with fibre orientations

eliminating coupling effects, the number of independent lamination parameters ξ_l is reduced to 4. They may be defined in the following fashion:

$$\xi_1 = \frac{1}{t} \int_{-t/2}^{t/2} cos2\alpha(z)dz, \quad \xi_2 = \frac{1}{t} \int_{-t/2}^{t/2} cos^2 2\alpha(z)dz,$$
$$\xi_9 = \frac{12}{t^3} \int_{-t/2}^{t/2} cos2\alpha(z)z^2 dz, \quad \xi_{10} = \frac{12}{t^3} \int_{-t/2}^{t/2} cos2\alpha(z)z^2 dz \tag{15}$$

where

$$\alpha(z) = \pm\alpha_i \ for \ t_i \leq z \leq t_{i+1} \tag{16}$$

The feasible regions of in-plane and out-of-plane lamination parameters are, respectively, expressed as follows:

$$-1 \leq \xi_1 \leq 1, \quad \xi_1^2 \leq \xi_2 \leq 1,$$
$$-1 \leq \xi_9 \leq 1, \quad \xi_9^2 \leq \xi_{10} \leq 1 \tag{17}$$

and for the in-plane lamination parameters (ξ_1, ξ_2) they form parabolas, whereas for out-of-plane parameters (ξ_9, ξ_{10}) are restricted by the values of ξ_1, ξ_2. A point on the parabola $\xi_2 = \xi_1^2$ corresponds to an angle-ply laminate $\pm\alpha$. For example the point $(0,0)$ corresponds to $\pm45^o$ laminate and $(0,\frac{1}{2})$ to a quasi-isotropic laminate.

The stiffness components $A_{ij}, A_{66}, D_{ij}, D_{66}$ (i,j = 1,2) of laminated composites are expressed as a linear function with respect to lamination parameters, whereas in our approach the coefficients $k'A^{S-D}$ are constant. However, to the author's knowledge, there is no information about the influence of B_{ij} terms on the optimization design, especially in geometrically nonlinear analysis. The results obtained with the aid of linear buckling theory for plates [9] or axially compressed cylinders [13] show evidently that the symmetric balanced laminate is the optimal configuration for composite structures.

Although we introduce herein lamination parameters, the optimization problems have been solved with the use of discrete (not continuous) design variables describing the properties of each individual ply. With the aid of eqn (16) the parameters ξ_l will be the illustrations of solutions though for symmetric 8-layered laminates four variables defined by eqs (15),(16) determine completely e.g. ply orientations α_i in the laminate.

4. OPTIMAL PROBLEM FORMULATION

We consider the buckling optimization problem of axisymmetric orthotropic doubly-curved shells under uniform external pressure p. One kind of laminate is analyzed herein, i.e. symmetric balanced laminate.

The optimization problem is stated as follows:

Objective function :
$$R1 = \max_{s_q}(\min_m p_{cr})$$
(18)

Design variables :
$$s_q = \{\alpha_i, t_i\}$$
(19)

The search of the local minima described by eqn (14) is carried out independently on the optimization procedures.

In our case the determinant (6) is the relation that gives the values of buckling pressures p_{cr}. In terms of the functional analysis it represents the second functional derivative (in the Frechet sense) of the functional of total potential energy (4). It is wellknown that in the pre-buckling state the above-mentioned derivative (and the determinant (6)) is positevely definite, whereas in the post-buckling range it changes its sign. It is worth to note also that the second term in eqn (6) is a linear function of the coefficients $C_{\rho\beta}$, so that its derivatives with respect to the design variables s_q - eqn (19) can be calculated analytically. In addition, for shells that fail in the axisymmetric mode (m=0) buckling pressures are always lower than those corresponding to bifurcation buckling mode (m$\neq$0). Since the appearance of the axisymmetric mode of bifurcation is detected by the lack of the convergence, the directions of searching for the optimum corresponding to such a case can be easily eliminated;it significantly simplifies and accelerates calculations.

5. NUMERICAL RESULTS AND DISCUSSIONS

As numerical examples two composite are considered (glass/ and boron/epoxy) where the elastic properties are shown in Table 1. The problems solved are for shells having the
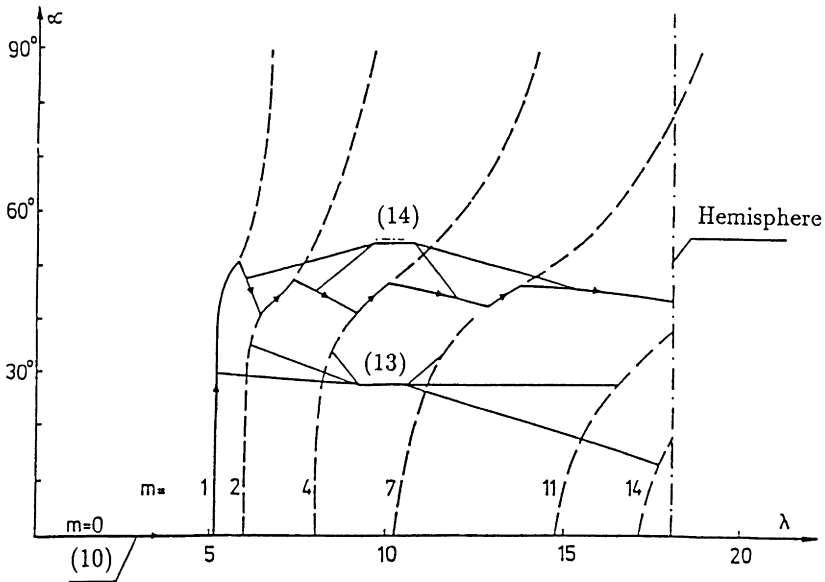
Figure 2: Optimal fibre orientations for angle-ply spherical shells made of GFRP

thickness-to-radius ratio t/R equal to 0.01.

Table 1
Material mechanical properties

Material	E_1	E_2	G_{12}	ν_{12}	X_t	X_c	Y_t	Y_c	S
	[GPa]				[MPa]				
Unidirectional GFRP	38.6	8.27	4.14	0.26	1062	610	31	118	72
Unidirectional BFRP	207.	20.7	7	0.3					
Steel	207.	207.		0.3					

The values of critical pressures p_{cr} are are presented in the dimensionless form, i.e. they are related to the following parameter:

$$\bar{\lambda} = \frac{2\sqrt{E_1 E_2}}{\sqrt{3(1 - \nu_{12}\nu_{21})}}\left(\frac{t}{R}\right)^2 \qquad (20)$$

5.1. Angle-ply spherical shells

As it is presented in Ref. [21] for spherical shells buckling pressures and modes are a function not only of fibre orientations $\pm\alpha$ but also of the shallowness parameter λ. Figure 2 is a plot of the optimal fibre orientations $\pm\alpha$ versus the shallowness parameter λ. The value $\lambda = 18.54$ corresponds to hemispherical shells. The calculations have been carried out for shells made of GFRP with the use of the transverse shear deformation

416

theory 2°. As it may be seen the optimal value $\alpha = 0^o$ (parallely to a shell meridian) can be reached only for shallow spheres ($\lambda < 5$) where the axisymmetric collapse (m=0) is a governing buckling mode - the optimality condition (10). As spherical shells fail in the antysymmetric mode (m $\neq$ 0) the optimal orientation rapidly changes - the condition (13) is now active. However, the skew direction of fibres with respect to an arbitrary shell meridian is very sensitive to the mode parameter m. In this case, one can obtain numerically the optimal orientations corresponding to the local minima (see eqn (14) and Fig.1c). The dashed parts of the plotted curves show the optimal orientations of spherical shells as the optimality condition (14) is not taken into account. Hence, it is obvious that the constraint condition (14) can change significantly the picture of the optimal fibres orientations and the values of the maximal buckling pressures in the comparison with the case as it is inactive. The influence of the local minima is particularly visible for angle-ply structures. The drawn distributions in Fig.2 resemble entirely those for angle-ply plates - Muc[9]. The obtained results show evidently that for shallow shells the optimal direction is equal to 0°, whereas for deeper shells corresponds to the isotropic state, i.e. $\alpha_{opt} = 45^o$.

5.2 Multilayered hemispherical shells

As the next example let us consider a hemispherical shell composed of N - identical layers made of GFRP, having the equal thicknesses t/N but arbitrarily oriented in the balanced symmetric laminate of $[(\pm\alpha_1)/(\pm\alpha_2)/.../(\pm\alpha_N)]_S$. Figure 3 shows the variations of the optimal (maximal) buckling pressures with the number of layers N. N=2 corresponds to
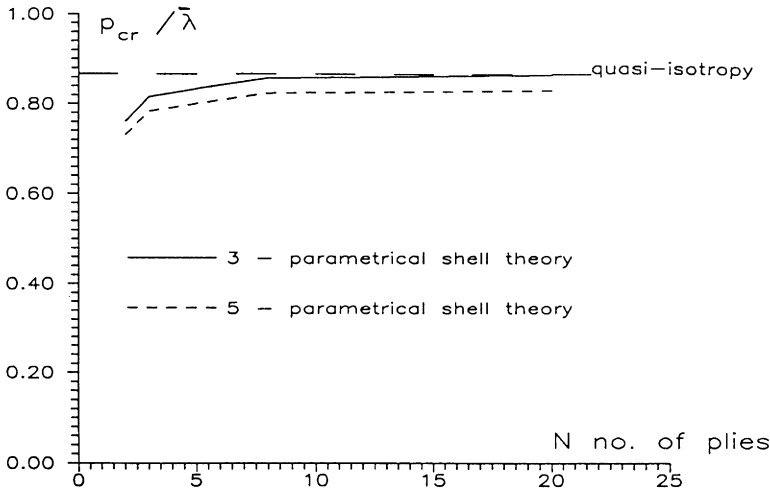
Figure 3: Maximal buckling pressures for optimally oriented GFRP shells (t/R = 0.01)

angle-ply hemispherical shells where the optimal fibre orientation is $\pm45^o$ (isotropy). In general, buckling loads increase with the increasing number value of N. However, there is a small amount of improvement in the buckling resistance, up to 17.2%, between the best and the worst cases. This is associated with the fact that the highest buckling load in Fig.

3 is obtained for the fibre orientation resembling quasi-isotropy, whereas the lowest value of p_{cr} corresponds to the isotropic state also (N=2, $\alpha = \pm45°$). The comparison of the optimal (maximal) buckling loads may lead to such results. However, for the determined number of layers N the improvement in the load carrying capability is a very significant and reaches even 90% between the worst and the best (with the regard to values of buckling loads) fibres orientations.

Figure 3 gives also the qualitative picture of the transverse shear effects on the values of buckling loads as well as on the optimal fibre orientation. As it may be seen the use of the transverse shear deformation theory (2°) results in the reduction of buckling loads in the comparison with the classical three-parametrical Kirchhoff shell theory (1°), and rather do not affect optimal fibre orientations. However, this effect is rather small here due to the low values of t/R (0.01) and of G_{13}/E_1 (0.055) ratios.

The plot of the buckling pressure contours on the lamination (ξ_1, ξ_2) plane (Fig.4) is treated as the illustration of the results and as the comparison of the buckling pressures
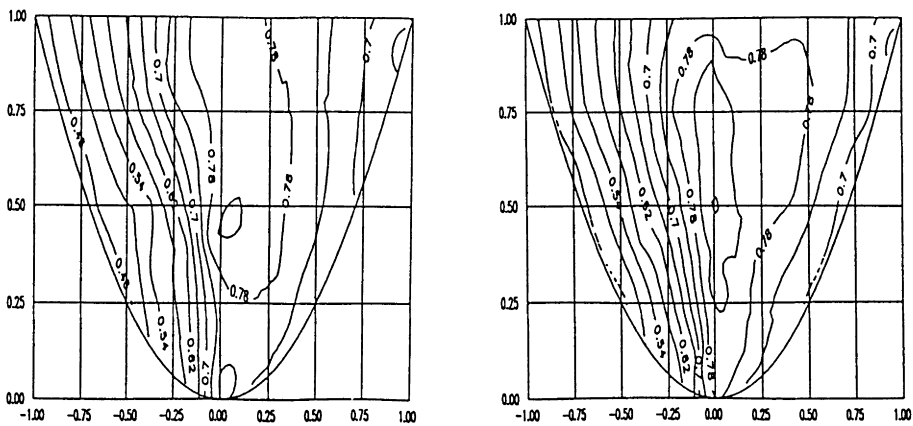
Figure 4: Contours of buckling pressures on the lamination in-plane parameter plane:a)N=3, b)N=8

for various fibre orientations. It is worth to resemble again that in the numerical analysis we use discrete not continuous optimization procedures. It is interesting to note that in the both cases plotted in Fig.4 the maximal buckling loads are always located in the surrounding of the point $(0,\frac{1}{2})$ - the quasi-isotropic state. However, this can be achieved for various fibre orientations dependly on the number of layers N in the laminate only. The angle-ply oriented hemispheres (N=2) have the other location of the optimum at the point (0,0) and in this case the mechanical properties of the shell are worse than those for the quasi-isotropic state.

The simplicity of finding fibre configurations in axisymmetric and antisymmetric buckling mode is the other very important feature of the contour presentation of the results on the lamination plane. The composite hemispheres made of GFRP that fail in the axisymmetric mode of buckling have the configurations of the laminate located on the left side of the ξ_2 axis (excluding the axis).

It is possible to express the engineering stiffnesses with the use of the in-plane lamination parameters:

$$E_1 = \frac{A_{11}A_{22} - A_{12}^2}{tA_{22}}, \quad E_2 = \frac{A_{11}A_{22} - A_{12}^2}{tA_{11}}, \quad G_{12} = \frac{A_{66}}{t} \quad and \quad \nu_{12} = \frac{A_{12}}{A_{22}} \tag{21}$$

For the quasi-isotropic state all material properties in eqn (21) should be constant. From the mathematical point of view a laminated shell becomes quasi-isotropic as the number of layers N tends to the infinity, whereas ply thicknesses to zero. For composite shells having finite number of layers N one can achieve easily quasi-isotropic state for the in-plane lamination parameters (ξ_1, ξ_2). However, the out-of-plane lamination parameters (ξ_9, ξ_{10}) - eqn (15) do not correspond to the quasi-isotropy. This fact indicates that as the number of layers N increases the mathematical conditions of the quasi-isotropy may be satisfied in a more rigorous way and it involves automatically that the maximal buckling loads increase - see Figs. 3 and 4. Such a result may be interpreted in one way only. The full symmetry of the shell geometrical properties, boundary conditions and external loadings imposes the requirement of the symmetry in the overall mechanical properties.

5.3 Optimization of hybrid torispheres

The aim of the present example is to see how fibre orientations can affect the values of
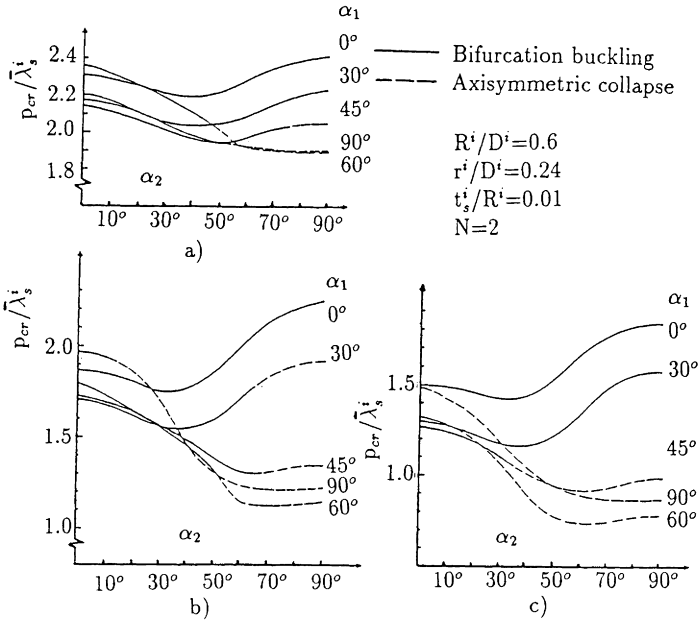
Figure 5: Influence of the thickness ratio on the variation of buckling pressures with fibre orientation:a)$t_c^a/t_s^a = \frac{1}{3}$,b)$t_c^a/t_s^a = 1$, c)$t_c^a/t_s^a = 3$

the critical pressures and the buckling modes of hybrid elastic torispheres made of a steel

layer and several composite layers (the number and thicknesses of the latter vary).The optimization has been carried out under the constraint that the total thickness of the members, i.e. steel and composite is always constant:

$$t_c + t_s = t = const. \tag{22}$$

The results of numerical calculations are presented in Figures 5 and 6. Figure 5 is a plot of buckling pressures for varying thicknesses of composite layers. However, for all cases
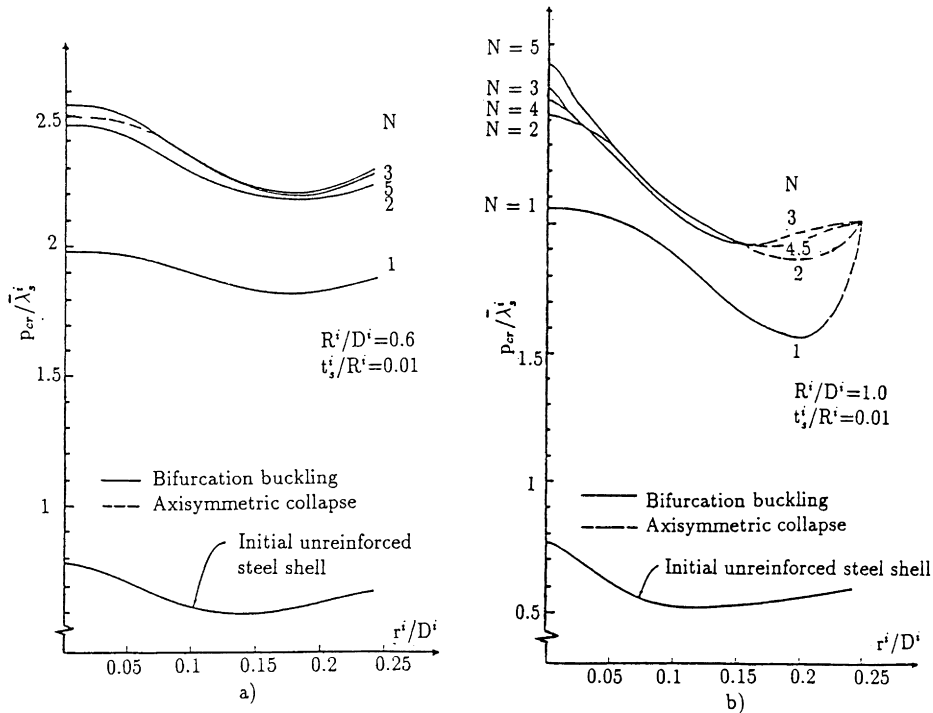
Figure 6: Optimal buckling pressures:a)R/D=0.6,b)R/D=1.0

considered the optimal fibre orientation satisfying the condition (22) corresponds to the cross/ply laminate ,i.e. $0°/90°$. Thus, the optimality condition is given by eqn (10). The optimal fibre orientaions for the torispheres considered herein are the combination of fibres oriented at $0°$ (the innermost surface) and $90°$ (near the shell mid-surface) independently on the shell geometry and number of the composite layers - see Fig.6. More detailed information about this problem can be found in Ref. [20]. In summary, it is worth to notice that the optimality conditions are always given by the relation (10). This is mainly caused by the fact that the chosen material properties of the steel and composite layers

are almost identical - see Table 1.

5.4 Buckling vs. first-ply failure

It is wellknown that buckling is one of various possible failure modes that occur for laminated structures. Among others one can list here e.g.:a) buckling of individual fibres in the matrix, b)ply failure (in the sense of the first or the last ply failure, c)delamination (including delamination buckling) - so called unilateral boundary conditions and others. Of course, in order to describe the mentioned above phenomena various failure criteria exist but we do not intend to dwell on them. On the other hand it is obvious that the optimization of the composite topology can be carried out in order to maximize loading carrying capability of composite structures. In the present analysis we focuse our attention on the one of possible failure modes of thinwalled structures made of FRP, i.e. the first-ply failure. Then, the obtained values of failure pressures will be compared with the optimal values of buckling pressures, in the sense of the optimization problem given by the conditions (18) and (19). The numerical analysis of the optimization problem with respect to the possible first-ply failure is carried out separately on the problem desribed by the set of eqs (18),(19).

In the present case the optimization problem is stated as follows:

Objective function :
$$R2 = \max_{s_q} p_f \qquad (23)$$

Design variables :
$$s_q = \{\alpha_i\} \qquad (24)$$

Constraint condition : $\quad F_1\bar{\sigma}_{11} + F_2\bar{\sigma}_{22} + F_{11}\bar{\sigma}_{11}^2 + F_{22}\bar{\sigma}_{22}^2 + 2F_{12}\bar{\sigma}_{11}\bar{\sigma}_{22} + F_{66}\bar{\sigma}_{12}^2 \leq 1 \quad (25)$

The constraint condition is the classical Tsai-Wu strength criterion. The bar over the symbols denotes the values of stresses determined in the local coordinate system associated with fibre directions in the each individual ply. The fullfilment of the constraint condition is checked independently on the top or bottom surfaces of plies in the laminate.

In the case analyzed herein it is convenient to introduce the definition of the failure envelope as the minimal value of pressures being the solution of the optimization problems R1 and R2,i.e.:
$$p_e = min(p_{cr}, p_f) \qquad (26)$$

Figure 7 presents the distributions of the failure envelopes (i.e. failure p_f or and buckling p_{cr} pressures) versus fibre orientations α for angle-ply spherical shells made of the unidirectional GFRP (see Table 1). As it may be seen the character of the curves is independent on the value of the shallowness parameter λ and the maximum is always obtained for α equal to 45° - the isotropic state. In the sense of the Tsai-Wu criterion the first-ply failure occurs at the shell apex and is directly associated with the shell deformations - see the results presented in Ref. [21]. The identical results to those shown in Fig.7 have been obtained for others values of material properties describing unidirectional FRP (for instance BFRP - Table 1). It is worth to mention that the failure criterion is active for
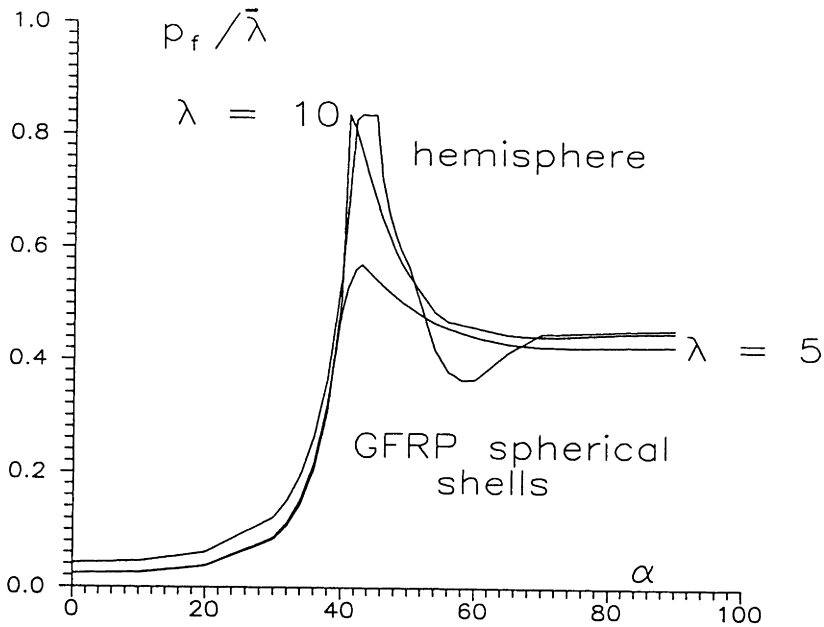
Figure 7: Variations of p_f with fibre orientations for angle-ply shells (t/R = 0.01)

$\alpha < 45°$. It turns out that the maxima on the failure envelopes ($\alpha = 45°$) corresponds to the bifurcation buckling, and for $\alpha > 45°$ the axisymmetric collapse is a failure mode.

With the regard to multilayered spherical shells one may observe almost the identical tendency as for angle-ply structures. The results of the calculations of failure envelopes conducted for shells made of 20 layers are plotted in Fig.8. The optimal fibre configurations for the optimization problems considered herein corresponds to the quasi-isotropic state, i.e. to the point $(0,\frac{1}{2})$ on the plane of the laminate parameters ξ_1, ξ_2. In addition, the dominating optimal failure mode (in the sense of the criterion (26)) corresponds to the bifurcation buckling. However, the optimal values of p_e do not always coincide with the values p_{cr} calculated with the aid of eqn (18). For shallow shells ($\lambda < 5$) the optimal laminate configuration with the respect to buckling loads (the problem R1) corresponds to $\alpha = 0°$, whereas with the respect to the FPF (the problem R2) the fibre orientations along meridians leads to the minimal values of p_f. However, for deeper shells ($\lambda > 5$) p_{cr} is equal to p_e.

6. CONCLUDING REMARKS

The present paper has shown an approach to stiffness (layout) optimization of orthotropic laminated doubly-curved shells using the discrete optimization methods. How-
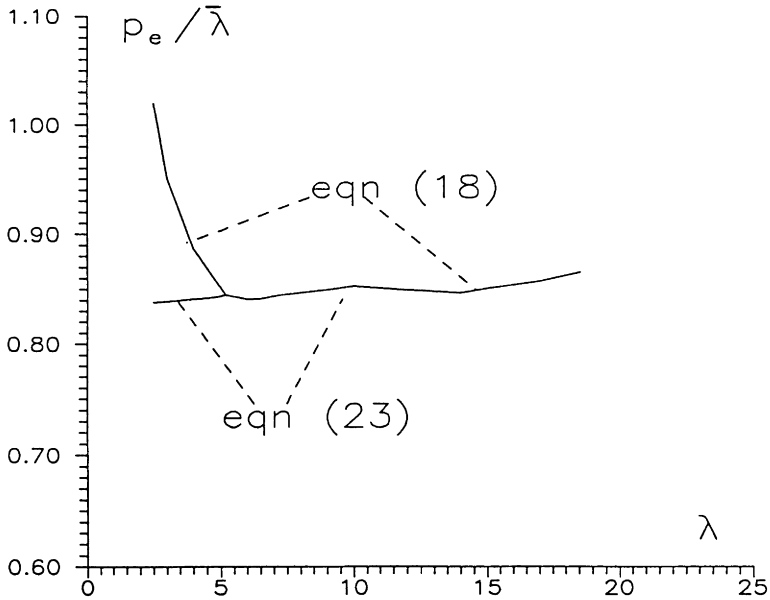
Figure 8: Failure pressures for 20-ply spherical shells made of GFRP (t/R = 0.01)

ever, the feasible regions of lamination have been also presented in order to demonstrate easily the results of optimization procedures.

The optimality conditions (global and local) have been formulated in a closed analytical form and then applied to numerical procedures solving buckling and first-ply failure problems for hemispherical and torispherical shells. The results have been demonstrated for two kinds of shell kinematical relations, i.e. three- and five-parametrical shell theories.

It is found that for hemispheres under buckling and first-ply failure constraints buckling is always the controlling failure mode. In addition, for shallow and deep laminated hemispheres the optimal laminate configurations correspond to the quasi-isotropic state on the in-plane lamination parameter plane with the one exception of two-layered (angle-ply N=2) shells.

7. REFERENCES

1. R.T. Haftka,Z.Gurdal and M.P.Kamat, Elements of structural optimization, Kluwer AcademicPubl.,Kluwer,1990.
2. P.Pedersen,Optimal orientation of anisotropic materials ...,"Optimization of large structural systems" (edt. G. Rozvany),1991,168.
3. G.A.Teters,R.B.Rikards and B.L. Narusberg, Optimization of laminated shells, Zinatne,Riga,1978 (in Russian).
4. B.L.Narusberg and G.A. Teters, Stability and optimization of composite shells, Zi-

natne,Riga,1988 (in Russian).

5. I.F.Obrastsov,V.V.Vasiliev and V.A. Burlakov, Optimal configurations of composite shells of revolution, Maszinostroenije, Moscow,1977 (in Russian).

6. D.Bushnell,Panda 2 - Program for minimum weight design of stiffened,composite, locally buckled panels,Comp.Str.,25 (1987) 469.

7. P.Hajela and C.J.Shih,Optimal design of laminated composites using a modified mixed integer and discrete programming algorithm,Comp.Str.,32 (1989) 213.

8. P.Pedersen,On sensitivity analysis and optimal design of specially orthotropic materials,Eng.Opt.,11 (1987) 305.

9. A.Muc,Optimal fibre orientation for simply-supported,angle-ply plates under biaxial compression,Composite Structures,9 (1988) 161.

10. M.Miki,Optimum design of fibrous laminated plates subjected to axial compression, Proc. 3-rd Japan-US Composite Materials Conf.,Tokyo,1986,673.

11. Z.Gurdal and R.T.Haftka,Optimization of composite laminates,"Optimization of large structural systems" (edt. G. Rozvany),1991,201.

12. H.Fukunaga and G.N.Vanderplaats,Stiffness optimization of orthotropic laminated composites using lamination parameters,AIAA J.,29 (1991) 641.

13. J.Onoda,Optimal laminate configurations of cylindrical shells for axial buckling,AIAA J.,23 (1985) 1093.

14. J.L.Sanders,Nonlinear theories for thin shells,Quart.Appl.Math.,21 (1963) 21.

15. J.R.Vinson and R.L.Sierakowski,The behaviour of structures composed of composite materials,Martinus Nijhoff Publ.,Dordrecht ,1987.

16. J.M.Whitney,Shear correction factor for orthotropic laminates under static loads,J. Appl. Mech.,40 (1973) 302.

17. W.T.Koiter,General equations of elastic stability for thin shells,Proc.Symp. "On the theory of shells",Houston,Texas,1967.

18. M.Uemura and T.Kasuya,Coupling effect on axial compressive buckling of laminated composite cylindrical shells,Proc.ICCM-IV,1982, 583.

19. J.W.Sawyer,Flutter and buckling of general laminated plates,J.Aircraft,14 (1977) 386.

20. G.D.Galletly and A.Muc,Buckling of fibre-reinforced plastic-steel torispherical shells under external pressure,Proc.Instn.Mech.Engrs,202 (1988) 409.

21. A.Muc,Buckling and post-buckling behaviour of laminated shallow spherical shells subjected to external pressure,I.J.Nonl.Mech.,27 (1992) 465.

8. ACKNOWLEDGEMENTS

425

DIRECT RELAXATION OF OPTIMAL LAYOUT PROBLEMS FOR PLATES[1]

K. A. Lurie[2]

Department of Mathematical Sciences, Worcester Polytechnic Institute, Worcester,
MA 01609-2280

[2]Professor, Department of Mathematical Sciences, Worcester Polytechnic Institute,
Worcester, Massachusetts.

Abstract.
   The paper suggests an application of a direct procedure initiated in Ref. 1 to
problems of optimal layout for plates. Optimal microstructures are explicitly indicated
for a number of special cases, particularly, for the case when the original and conjugate
strain tensors are coaxial.

Key Words. Direct relaxation, optimal microstructures, necessary conditions.

INTRODUCTION

   In this paper we consider nonselfadjoint optimization problems for thin anisotropic
plates subjected to transverse load. The state of equilibrium of such a plate is
described by the equation

$$\nabla \cdot \nabla \cdot \mathscr{D} \cdot \cdot \nabla\nabla w = q, \quad (x,y)\epsilon\Sigma \tag{1}$$

where w denotes the normal displacement, $\mathscr{D}$— the tensor of stiffness, and q the
transverse load density. The boundary $\partial\Sigma$ of a plate will be assumed clamped, this
property expressed by the boundary conditions

$$w\Big|_{\partial\Sigma} = \partial w/\partial n\Big|_{\partial\Sigma} = 0. \tag{2}$$

It will be assumed that $\mathscr{D} = \mathscr{D}(x,y)$ plays the role of control and may take one of two admissible values $\mathscr{D}_1$ or $\mathscr{D}_2$ at each point of the plate. The materials 1 and 2 with tensors $\mathscr{D}_1$ and $\mathscr{D}_2$ of stiffness will both be assumed isotropic, i.e.

$$\mathscr{D}_i = k_i a_1 a_1 + \mu_i (a_2 a_2 + a_3 a_3), \quad i = 1,2. \tag{3}$$

Here and below, a_1, a_2, a_3 represent an orthonormal basis in the space of 2nd rank symmetric tensors in the plane, i.e.

$$a_1 = (1/\sqrt{2})(ii+jj), \quad a_2 = (1/\sqrt{2})(ii-jj), \quad a_3 = (1/\sqrt{2})(ij+ij). \tag{4}$$

Introduce the characteristic function $\chi_1(x,y)$ of domain occupied by material 1 with tensor $\mathscr{D}_1$ of stiffness, and a similar function $\chi_2(x,y)$ for material 2; obviously, $\chi_1 + \chi_2 = 1$. It is required to find the distribution

$$\mathscr{D}(x,y) = \chi_1(x,y)\, \mathscr{D}_1 + \chi_2(x,y)\, \mathscr{D}_2 \tag{5}$$

of the stiffness tensor throughout Σ which maximizes some weakly continuous functional $I(w)$ of solution to the boundary value problem (1), (2). Weak continuity is supposed to be with respect to $W_2^2(\Sigma)$, this space naturally associated with (1), (2). Specifically, as a typical example, we will consider the functional

$$I(w) = - \int_\Sigma [w(x,y) - w_0(x,y)]^2 dxdy$$

where $w_0(x,y) \,\epsilon\, L_2(\Sigma)$.

This and similar optimization problems are known to be ill–posed and therefore requiring relaxation, i.e., the construction of an appropriate minimal extension of the initial set $U = \{\mathscr{D}_1,\, \mathscr{D}_2\}$ of admissible controls. Such an extension is currently offered on the basis of a precise knowledge of the G–closure of U, i.e. the set GU of invariants of the effective stiffness tensors $\mathscr{D}_0$ of all composites assembled from the elements of U (Ref. 2). However, the G–closures are known only for a few particular examples (Ref. 3), and the plate problem is not among them. Yet for these selected examples, the construction of GU represents difficulties, and for the plate problem these difficulties are still not overcome.

At the same time, for many applications we do not need to know the GU–set in full. Instead, it is often enough to specify some linear combination of components of $\mathscr{D}_0$; for our problem, this is the combination $\mathscr{D}_0 \cdot \cdot \nabla\nabla w$ which only matters in view of the Hooke's law. To determine this combination, we apply a *direct approach*, free from any reference to the G–closure.

This approach has originally been suggested for the 2nd order equation $\nabla \cdot \mathscr{D} \cdot \nabla w = f$ in Ref. 1 and received a further development in Refs. 9, 10. Here, we apply it to the 4th order equation (1) arising in the plate theory.

2. REDUCTION TO A SUP INF PROBLEM

We first reduce the problem to a convenient sup inf form. Introduce the Lagrange multiplier λ and consider the augmented functional

$$J = J(w,\lambda) = I(w) + \int_\Sigma \lambda(\nabla\cdot\nabla\cdot\mathscr{D}\cdot\cdot\nabla\nabla w - q)dxdy, \tag{6}$$

the second member at the right–hand side taking into account the equation (1).

Equating to zero the first variation of (6) with respect to w and bearing (2) in mind, we arrive at the conjugate equation

$$\nabla\cdot\nabla\cdot\mathscr{D}\cdot\cdot\nabla\nabla\lambda = 2(w - w_0) \tag{7}$$

and boundary conditions

$$\lambda\Big|_{\partial\Sigma} = \partial\lambda/\partial n\Big|_{\partial\Sigma} = 0. \tag{8}$$

After integration by parts with the boundary conditions (8), the functional (6) takes on the form

$$J = I + \int_\Sigma (\nabla\nabla\lambda\cdot\cdot\mathscr{D}\cdot\cdot\nabla\nabla w - \lambda q)dxdy \tag{9}$$

convenient for a subsequent use.

The problem

$$\sup_{\mathscr{D},w} I$$

subjected to (1), (2) is equivalent to

$$\sup_{\mathscr{D},w}\inf_{\lambda} J \tag{10}$$

subjected to (2), (8). This is since by (6),

$$\inf_{\lambda} J = I + \inf_{\lambda}\int_\Sigma \lambda(\nabla\cdot\nabla\cdot\mathscr{D}\cdot\cdot\nabla\nabla w - q)dxdy =$$

$$I + \begin{cases} 0 & \text{if } \nabla\cdot\nabla\cdot\mathscr{D}\cdot\cdot\nabla\nabla w = q, \\ -\infty & \text{otherwise.} \end{cases}$$

We observe that Eq. (1) appears as a necessary condition for a minimum in λ. Bearing (8) in mind, we may assume that J in (10) has the form (9). We have

finally for (10)

$$\sup_{\mathscr{D},w} \inf_{\lambda} \{I + \int_{\Sigma} (\nabla\nabla\lambda \cdot \cdot \mathscr{D} \cdot \cdot \nabla\nabla w - \lambda q)dxdy\} \tag{11}$$

where $\mathscr{D} \in U = \{\mathscr{D}_1, \mathscr{D}_2\}$, and w and λ satisfy, respectively, equations (2) and (8).

In the sequel, we will establish the upper and lower bounds for the functional (11). An upper bound will be constructed analytically through an appropriate mathematical construction, and the lower bound will be generated by a specially chosen composite assembled from the original constituents. Both bounds will be shown to coincide, and desired relaxation will thus be achieved.

3. UPPER BOUND FOR $\sup_{\mathscr{D},w} \inf_{\lambda} J$

This functional possesses the following upper bound:

$$\sup_{\mathscr{D},w} \inf_{\lambda} J = \sup_{w} \sup_{\mathscr{D}} \inf_{\lambda} J \leq \sup_{w} \inf_{\lambda} \sup_{\mathscr{D}} J =$$

$$= \sup_{w} \inf_{\lambda} [-\int_{\Sigma} (w - w_0)^2 dxdy - \int_{\Sigma} \lambda q dxdy + \int_{\Sigma} G(\nabla\nabla w, \nabla\nabla\lambda)dxdy] \tag{12}$$

where

$$G(\xi,\eta) = \begin{cases} \xi \cdot \cdot \mathscr{D}_1 \cdot \cdot \eta \ , \ \xi \cdot \cdot \mathscr{D}_1 \cdot \cdot \eta \geq \xi \cdot \cdot \mathscr{D}_2 \cdot \cdot \eta, \\[2mm] \xi \cdot \cdot \mathscr{D}_2 \cdot \cdot \eta \ , \ \xi \cdot \cdot \mathscr{D}_1 \cdot \cdot \eta \leq \xi \cdot \cdot \mathscr{D}_2 \cdot \cdot \eta. \end{cases} \tag{13}$$

The notation $\xi = \nabla\nabla w$, $\eta = \nabla\nabla\lambda$ will be used below. The function $G(\xi,\eta)$ is convex with respect to any of its arguments but non—convex with respect to their union. The problem

$$\sup_{w} \inf_{\lambda} [-\int_{\Sigma} (w - w_0)^2 dxdy - \int_{\Sigma} \lambda q dxdy + \int_{\Sigma} G(\nabla\nabla w, \nabla\nabla\lambda)dxdy] \tag{14}$$

is still ill—posed. It would be well—posed if the integrand $G(\xi,\eta)$ were a saddle function, i.e. concave in ξ for fixed η and convex in η for fixed ξ. The solution would then exist and operations sup and inf commute. For our problem it is obviously not the case. However, the requirement that the function $G(\xi,\eta)$ be saddle is too restrictive now that ξ and η are gradients; to ensure the existence of sup inf for this case, it is enough to require that this function be only quasisaddle (Ref. 1). The quasisaddle envelope $G^{**}(\xi,\eta)$ of $G(\xi,\eta)$ will be constructed applying the so called polysaddlification transform introduced in Ref. 1. This transform plays the same role for sup inf problems as the polyconvexification transform (Refs. 4–6) plays for the minimum problems. For the fourth order problem considered, the

polysaddlification transform is given by the formula

$$G^{**}(\xi,\eta) = \sup_{\omega,d} \sup_{b} \inf_{a} \{a \cdot \cdot \xi + b \cdot \cdot \eta + \omega \cdot \cdot (\xi \times \eta) + d\xi \cdot \cdot T \cdot \cdot \eta$$

$$- \inf_{\xi} \sup_{\eta} [a \cdot \cdot \xi + b \cdot \cdot \eta + \omega \cdot \cdot (\xi \times \eta) + d\xi \cdot \cdot T \cdot \cdot \eta - G(\xi,\eta)]\} \tag{15}$$

Here we introduced the notation T for a tensor

$$T = a_1 a_1 - a_2 a_2 - a_3 a_3; \tag{16}$$

the terms $\omega \cdot \cdot \xi \times \eta$ and $d\xi \cdot \cdot T \cdot \cdot \eta$ represent the null–Lagrangians $\xi \times \eta$ and $\xi \cdot \cdot T \cdot \cdot \eta$ (Refs. 3–6) taken into account with the aid of Lagrange multipliers ω and d.

The transform $G^{**}(\xi,\eta)$ defined by (15) satisfies the inequality

$$G^{**}(\xi,\eta) \geq G(\xi,\eta) \tag{17}$$

for any $G(\xi,\eta)$ convex in η and arbitrary in ξ (Ref. 1).

Applying $G^{**}(\xi,\eta)$ instead of $G(\xi,\eta)$ we arrive at the upper bound

$$\sup_{w} \inf_{\lambda} [-\int_{\Sigma} (w-w_0)^2 dxdy - \int_{\Sigma} \lambda q dxdy + \int_{\Sigma} G^{**}(\xi,\eta) dxdy] \tag{18}$$

for (14), and, consequently, for the original functional (10).

4. COMPUTATION OF $G^{**}(\xi,\eta)$

We first compute $\hbar(\xi,b) = \sup_{\eta}[b \cdot \cdot \eta - H(\xi,\eta)]$ with $H(\xi,\eta) = -\omega \cdot \cdot (\xi \times \eta) - d\xi \cdot \cdot T \cdot \cdot \eta + G(\xi,\eta)$:

$$b \cdot \cdot \eta - H(\xi,\eta) = \begin{cases} c^1 \cdot \cdot \eta & \text{if } \eta \in \xi \cdot \cdot (\mathscr{D}_1 - \mathscr{D}_2) \cdot \cdot \eta \geq 0, \\ c^2 \cdot \cdot \eta & \text{if } \eta \in \xi \cdot \cdot (\mathscr{D}_1 - \mathscr{D}_2) \cdot \cdot \eta \leq 0. \end{cases}$$

The tensors c^1, c^2 are defined as $(\text{dev}\xi = \xi_2 a_2 + \xi_3 a_3)$

$$c^1 = b + (d - k_1)\xi_1 a_1 - (d + \mu_1)\text{dev}\xi + \omega \times \xi,$$

$$c^2 = b + (d - k_2)\xi_1 a_1 - (d + \mu_2)\text{dev}\xi + \omega \times \xi. \tag{19}$$

By argument similar to that described in Ref. 1 we arrive at the formula

$$\bar{h}(\xi,b) = \sup_{\eta}[b\cdots\eta - H(\xi,\eta)] = \begin{cases} 0 & \text{if } b = \langle S \rangle \cdots \xi, \\ +\infty & \text{otherwise}. \end{cases} \tag{20}$$

In (20), the matrix $\langle S \rangle$ is defined as the convex hull

$$\langle S \rangle = t_1 S_1 + t_2 S_2, \quad t_1, t_2 \geq 0, \quad t_1 + t_2 = 1 \tag{21}$$

of matrices

$$S_i = \Delta_i + \omega \cdots \epsilon, \quad \Delta_i = \mathscr{D}_i - dT, \quad i = 1,2, \tag{22}$$

where the matrix

$$\epsilon = -E \times E \tag{23}$$

defines the Levi–Civita tensor of the 6th rank acting in the linear space of 2×2 symmetric tensors. The unit tensor E in this space can be defined as

$$E = a_1 a_1 + a_2 a_2 + a_3 a_3 \tag{24}$$

in the basis (4), and by a similar formula in any other orthonormal basis.
We make note of the formulas (Ref. 7)

$$\epsilon = -E \times E = -a_s a_s \times a_k a_k = -a_s a_t a_k \, \epsilon^{skt} = a_s a_t a_k \epsilon^{stk} \tag{25}$$

where

$$\epsilon^{skt} = a_s \cdots (a_k \times a_t) \tag{26}$$

are Levi–Civita symbols $(\epsilon^{123} = \epsilon^{231} = \epsilon^{312} = 1, \; \epsilon^{132} = \epsilon^{213} = \epsilon^{321} = -1, \; \epsilon^{stk} =$ otherwise); also

$$\omega \cdots \epsilon = -\omega \cdots E \times E = -\omega \times E = -E \times \omega = \epsilon \cdots \omega. \tag{27}$$

Geometrically, the function $\bar{h}(\xi,b)$ of ξ for fixed b is equal to positive infinity everywhere except for points of the set

$$b = \langle S \rangle \cdots \xi, \quad t_1, t_2 \in (21). \tag{28}$$

Equation (28) can be inverted to express ξ in terms of b. To this end we introduce symmetric tensors of the 4th rank (see (22))

$$\Delta_1 = \mathscr{D}_1 - dT, \quad \Delta_2 = \mathscr{D}_2 - dT, \quad \langle\Delta\rangle = t_1\Delta_1 + t_2\Delta_2 \tag{29}$$

and compute the inverse matrix $\langle S\rangle^{-1} = [\langle\Delta\rangle + \omega\cdot\cdot\,\epsilon]^{-1} = [\langle\Delta\rangle - \omega \times E]^{-1}$. We obtain by direct calculation

$$\langle S\rangle^{-1} = [1/(\det\langle\Delta\rangle + \omega\cdot\cdot\langle\Delta\rangle\cdot\cdot\omega)]\{(\det\langle\Delta\rangle)\langle\Delta\rangle^{-1} + \omega\omega + (\omega\cdot\cdot\langle\Delta\rangle)\times E\} = \delta + \Omega\times E \tag{30}$$

where

$$\delta = [1/(\det\langle\Delta\rangle + \omega\cdot\cdot\langle\Delta\rangle\cdot\cdot\omega)]\{(\det\langle\Delta\rangle)\langle\Delta\rangle^{-1} + \omega\omega\} \tag{31}$$

denotes the symmetric part of $\langle S\rangle^{-1}$ and

$$\Omega = [1/(\det\langle\Delta\rangle + \omega\cdot\cdot\langle\Delta\rangle\cdot\cdot\omega)](\omega\cdot\cdot\langle\Delta\rangle) \tag{32}$$

denotes the 2×2 tensor associated with its skew–symmetric part.

The set (28) is a segment of the curve in ξ–space traced as t_1 varies between 0 and 1. This segment connects points $\xi^{(1)}$ and $\xi^{(2)}$ corresponding, respectively, to $t_1 = 1$ and $t_1 = 0$:

$$\xi^{(1)} = S_1^{-1}\cdot\cdot b, \quad \xi^{(2)} = S_2^{-1}\cdot\cdot b. \tag{33}$$

We now compute the result of the operation

$$\inf_a\{a\cdot\cdot\xi - \inf_\xi[a\cdot\cdot\xi - (-\overline{h}(\xi,b))]\} \tag{34}$$

which comes second in the sequence (15). This one is known to put into correspondence with any given function $-\overline{h}(\xi,b)$ its concave ξ–envelope, i.e. the least concave function of ξ greater than or equal to $-\overline{h}(\xi,b)$. Particularly, if $-\overline{h}(\xi,b)$ is itself concave in ξ, then the operation (34) leaves this function intact.

In our special circumstances, this is obviously not the case. The concave envelope of $-\overline{h}(\xi,b)$ appears to be the function defined as negative infinity everywhere except for points of the convex hull Ξ of the curvilinear segment (28) where this envelope is equal to zero:

$$\inf_a\{a\cdot\cdot\xi - \inf_\xi[a\cdot\cdot\xi - (-\overline{h}(\xi,b))]\} = \begin{cases} 0 & , \ \xi \in \Xi \\ -\infty & , \ \xi \notin \Xi. \end{cases} \tag{35}$$

The hull Ξ is a convex body in the ξ–space. We will assume that the curvilinear segment (28) and a line segment

$$(\xi_1 - \xi_1^{(2)})/(\xi_1^{(1)} - \xi_1^{(2)}) = (\xi_2 - \xi_2^{(2)})/(\xi_2^{(1)} - \xi_2^{(2)}) = (\xi_3 - \xi_3^{(2)})/(\xi_3^{(1)} - \xi_3^{(2)}) \qquad (36)$$

connecting the endpoints $\xi^{(1)}$ and $\xi^{(2)}$ (see (33)) both belong to the boundary $\partial\Xi$ of Ξ.

For our future purposes we need to know the left–hand side of (35) as the function of b for fixed ξ. This function can be defined as equal to negative infinity everywhere in the b–space except for the body $\mathscr{B}$ which appears as the "b–image" of Ξ, specifically, the boundary $\partial\mathscr{B}$ of $\mathscr{B}$ is described by the same equation as that of $\partial\Xi$, this time, however, ξ should be kept fixed whereas b should be considered variable. Obviously, the set (28) which is perceived as a *curvilinear* segment in the ξ–space appears as a *line* segment in the b–space, and in this capacity belongs to $\partial\mathscr{B}$ Also, the set (36) which represents a *line* segment in the ξ–space appears as a *curvilinear* segment in the b–space, and this segment also belongs to $\partial\mathscr{B}$ Summarizing these results, we arrive at the following: the transform (15) reduces to a single operation

$$\sup_{\omega, d, b} [b \cdot\cdot \eta + \omega \cdot\cdot (\xi \times \eta) + d\xi \cdot\cdot T \cdot\cdot \eta] \qquad (37)$$

subjected to the constraint $b \in \mathscr{B}$ Note that the set $\mathscr{B}$ itself depends on ω and d.

The curvilinear segment (36) in the b–space obviously represents a rib on $\partial\mathscr{B}$ The calculation (37) of the supremum with respect to b will include among others the possibility that the supremum is attained at points belonging to this segment. In the sequel, we investigate this possibility in major detail. Equation (36) can be represented in the equivalent form (see (33))

$$\xi = (m_1 S_1^{-1} + m_2 S_2^{-1}) \cdot\cdot b = \langle S^{-1} \rangle \cdot\cdot b. \qquad (38)$$

Here, $m_1, m_2 \geq 0, m_1 + m_2 = 1$.

This relationship will be taken into account with the aid of the Lagrange multiplier Λ in the course of the maximization operation (37). We will examine stationary points of the function

$$\phi = b \cdot\cdot \eta + \omega \cdot\cdot (\xi \times \eta) + d\xi \cdot\cdot T \cdot\cdot \eta + \Lambda \cdot\cdot (\xi - \langle S^{-1} \rangle \cdot\cdot b) \qquad (39)$$

viewed as the function of b, ω, d and m_1.

A routine calculation shows that

$$\phi_b = \eta - \Lambda \cdot\cdot \langle S^{-1} \rangle = 0$$

which means that

$$\Lambda = \eta \cdot\cdot \langle S^{-1} \rangle^{-1}. \qquad (40)$$

With equations (38) and (40) in mind, the function ϕ becomes

$$\phi = \eta \cdot \cdot \langle S^{-1} \rangle^{-1} \cdot \cdot \xi + \omega \cdot \cdot (\xi \times \eta) + d \xi \cdot \cdot T \cdot \cdot \eta. \tag{41}$$

It can be shown (c.f. Ref. 7) that

$$\phi_\omega = -(\Lambda \cdot \cdot \langle S^{-1} \rangle \cdot \cdot b)_\omega + \xi \times \eta = m_1 (\Lambda \cdot \cdot S_1^{-1}) \times (S_1^{-1} \cdot \cdot b)$$

$$+ m_2 (\Lambda \cdot \cdot S_2^{-1}) \times (S_2^{-1} \cdot \cdot b) + \xi \times \eta.$$

This expression can be rewritten in either of two forms:

$$\phi_\omega = m_1 (\Lambda \cdot \cdot S_1^{-1}) \times (S_1^{-1} \cdot \cdot b) + m_2 (\Lambda \cdot \cdot S_2^{-1}) \times (S_2^{-1} \cdot \cdot b)$$

$$+ ((m_1 S_1^{-1} + m_2 S_2^{-1}) \cdot \cdot b) \times (\Lambda \cdot \cdot (m_1 S_1^{-1} + m_2 S_2^{-1})) = \tag{42}$$

$$= -m_1 m_2 (\Delta S^{-1} \cdot \cdot b) \times (\Lambda \cdot \cdot \Delta S^{-1}); \quad \Delta S^{-1} = S_2^{-1} - S_1^{-1},$$

or

$$\phi_\omega = \eta \cdot \cdot \langle S^{-1} \rangle^{-1} \cdot \cdot [m_1 S_1^{-1} \times S_1^{-1} + m_2 S_2^{-1} \times S_2^{-1}] \cdot \cdot \langle S^{-1} \rangle^{-1} \cdot \cdot \xi + \xi \times \eta. \tag{43}$$

The stationarity condition $\phi_\omega = 0$ can now be written as

$$\Delta S^{-1} \cdot \cdot b = (\Delta S^{-1}) \cdot \cdot \langle S^{-1} \rangle^{-1} \cdot \cdot \xi = \kappa \Lambda \cdot \cdot \Delta S^{-1} = \tag{44}$$

$$= \kappa \eta \cdot \cdot \langle S^{-1} \rangle^{-1} \cdot \cdot (\Delta S^{-1})$$

where κ is a scalar multiplier. An equivalent representation is associated with equation (43):

$$\eta \cdot \cdot \langle S^{-1} \rangle^{-1} \cdot \cdot [m_1 S_1^{-1} \times S_1^{-1} + m_2 S_2^{-1} \times S_2^{-1}] \cdot \cdot \langle S^{-1} \rangle^{-1} \cdot \cdot \xi + \xi \times \eta = 0 \tag{45}$$

Condition $\phi_d = 0$ reduces to

$$\phi_d = -m_1 m_2 (\Delta S^{-1} \cdot \cdot b) \cdot \cdot T \cdot \cdot (\Lambda \cdot \cdot \Delta S^{-1})$$

$$= -m_1 m_2 \kappa^{-1} (\Delta S^{-1} \cdot \cdot b) \cdot \cdot T \cdot \cdot (\Delta S^{-1} \cdot \cdot b) = 0. \tag{46}$$

or, equivalently,

$$\phi_d = -\eta \cdot \cdot \langle S^{-1} \rangle^{-1} \cdot \cdot [m_1 S_1^{-1} \cdot \cdot T \cdot \cdot S_1^{-1}$$
$$+ m_2 S_2^{-1} \cdot \cdot T \cdot \cdot S_2^{-1}] \cdot \cdot \langle S^{-1} \rangle^{-1} \cdot \cdot \xi + \xi \cdot \cdot T \cdot \cdot \eta = 0. \tag{47}$$

Note that the stationarity condition (46) applies as the necessary condition for a maximum if the corresponding root d is such that the function ϕ defined by (41) is concave in d for all ω. To guarantee this, we must require that det $S_i \geq 0 (i = 1,2)$, i.e. that

$$\det \Delta_i + \omega \cdot \cdot \Delta_i \cdot \cdot \omega \geq 0, \quad i = 1,2. \tag{48}$$

These inequalities should be considered as additional constraints influencing the d–maximization.

Computing the expression (41) for ϕ at the stationary values of ω and d we have to maximize it with regard to m_1. Before we do so we investigate this expression in terms of its attainability with the aid of special microstructures. This is a right time for such investigation since the aforementioned construction explicitly depends on m_1, this dependence being very special for a number of popular microstructures.

After maximization in m_1, the expression (41) should produce a final construction (37) for $G^{**}(\xi,\eta)$. This program is elaborate in its entirety, and we will begin with the analysis of several special cases.

5. CASE WHEN TENSORS ξ AND η ARE PROPORTIONAL

In this case, the assumption $\omega = \Omega = 0$ obviously satisfies equation (45) since the matrices S_1, S_2, $\langle S \rangle$ and $\langle S^{-1} \rangle$ are then symmetric. Equation (46) is reduced to

$$(\Delta \delta \cdot \cdot \langle \delta \rangle^{-1} \cdot \cdot \xi) \cdot \cdot T \cdot \cdot (\Delta \delta \cdot \cdot \langle \delta \rangle^{-1} \cdot \cdot \xi) = 0 \tag{49}$$

where (c.f. Eq. (31))

$$\Delta \delta = \delta_2 - \delta_1 = \Delta_2^{-1} - \Delta_1^{-1}, \quad \langle \delta \rangle^{-1} = (m_1 \Delta_1^{-1} + m_2 \Delta_2^{-1})^{-1}.$$

The tensors $\Delta_i (i = 1,2)$ are defined by Eqs. (29), (3) and (16) as

$$\Delta_i = K_i a_1 a_1 + M_i (a_2 a_2 + a_3 a_3), \quad K_i = k_i - d, \quad M_i = \mu_i + d. \tag{50}$$

We therefore obtain

$$\Delta \delta \cdot \cdot \langle \delta \rangle^{-1} \cdot \cdot \xi =$$

$$[\Delta K^{-1}a_1a_1 + \Delta M^{-1}(a_2a_2+a_3a_3)] \cdot \cdot [\langle K^{-1}\rangle^{-1}a_1a_1 + \langle M^{-1}\rangle^{-1}(a_2a_2+a_3a_3)] \cdot \cdot \xi$$

$$= (\Delta K^{-1})\langle K^{-1}\rangle^{-1}\xi_1 a_1 + (\Delta M^{-1})\langle M^{-1}\rangle^{-1}(\xi_2 a_2 + \xi_3 a_3) \tag{51}$$

where

$$\Delta K^{-1} = K_2^{-1} - K_1^{-1}, \quad \Delta M^{-1} = M_2^{-1} - M_1^{-1},$$

$$\langle K^{-1}\rangle^{-1} = (m_1 K_1^{-1} + m_2 K_2^{-1})^{-1}, \quad \langle M^{-1}\rangle^{-1} = (m_1 M_1^{-1} + m_2 M_2^{-1})^{-1}. \tag{52}$$

Equation (49) shows that the second invariant of (51) equals zero, i.e.

$$(\Delta K^{-1})^2 \langle K^{-1}\rangle^{-2}\xi_1^2 = (\Delta M^{-1})^2 \langle M^{-1}\rangle^{-2}(\xi_2^2 + \xi_3^2).$$

Introducing the ratio

$$\zeta = |\text{dev}\,\xi|/\xi_1 = \sqrt{(\xi_2^2 + \xi_3^2)}/\xi_1 \tag{53}$$

of deviatoric and spherical parts of tensor ξ, we arrive at the equation

$$\zeta^2 = \left[\frac{(k_2-k_1)(d+m_1\mu_2+m_2\mu_1)}{(\mu_2-\mu_1)(d-m_1k_2-m_2k_1)}\right]^2$$

defining the Lagrange multiplier d

$$d = (\zeta\tilde{k}\Delta\mu - \tilde{\mu}\Delta k)/(\zeta\Delta\mu + \Delta k), \tag{54}$$

$$\tilde{k} = m_1 k_2 + m_2 k_1, \quad \tilde{\mu} = m_1\mu_2 + m_2\mu_1,$$

$$\Delta k = k_2 - k_1, \quad \Delta\mu = \mu_2 - \mu_1. \tag{55}$$

Equation (54) has been obtained earlier by Gibianskii and Cherkaev in Ref. 8. We use (54) to eliminate d from the expression (39), the resulting construction is attainable by a laminar composite of the lst rank (Ref. 8).

6. CASE WHEN TENSORS ξ AND η ARE COAXIAL

This case generalizes the previous one but is related to a new situation when we *cannot* apply the G–closure technique (Ref. 3) to construct the required relaxation; on the contrary, the case of Section 5 is self–adjoint and therefore can be handled with the aid of such technique. In the new circumstances, no G–closure is known, and the

direct method demonstrates here its genuine power.

Because the tensors ξ and η are coaxial, we can choose the basis a_1, a_2, a_3 (see (4)) so that

$$\xi = \xi_1 a_1 + \xi_2 a_2, \tag{56}$$

$$\eta = \eta_1 a_1 + \eta_2 a_2; \tag{57}$$

the tensor ω will be assumed having only a_3–component, namely

$$\omega = \omega_3 a_3. \tag{58}$$

Direct calculation of the matrix $\langle S^{-1} \rangle^{-1}$ shows that

$$\langle S^{-1} \rangle^{-1} = Z^{-1}(PQ + \omega_3^2 R^2)^{-1}(QZa_1 a_1 + PZa_2 a_2 + PQa_3 a_3 + \omega_3^2 R^2 a_3 a_3 - \omega_3 RZa_3 \times E) \tag{59}$$

where

$$P = \left\langle M/(KM + \omega_3^2) \right\rangle, \quad Q = \left\langle K/(KM + \omega_3^2) \right\rangle, \quad R = \left\langle 1/(KM + \omega_3^2) \right\rangle, \quad Z = \langle 1/M \rangle, \tag{60}$$

and symbol $\langle \cdot \rangle$ denotes averaging, i.e., for example,

$$\langle 1/M \rangle = m_1/M_1 + m_2/M_2 = m_1/(\mu_1 + d) + m_2/(\mu_2 + d), \tag{61}$$

etc.

The tensor b computed as $b = \langle S^{-1} \rangle^{-1} \cdot \cdot \, \xi$ (c.f. (38)) turns out to be coaxial with ξ because of (56) and (59):

$$b = \langle S^{-1} \rangle^{-1} \cdot \cdot \, \xi = [1/(PQ + \omega_3^2 R^2)]\left[(Q\xi_1 + \omega_3 R\xi_2)a_1 + (P\xi_2 - \omega_3 R\xi_1)a_2\right]. \tag{62}$$

The matrix ΔS^{-1} can easily be computed, too; this one equals

$$\Delta S^{-1} = pa_1 a_1 + qa_2 a_2 + za_3 a_3 + \omega_3 ra_3 \times E \tag{63}$$

where

$$p = \Delta(M/(KM + \omega_3^2)), \quad q = \Delta(K/(KM + \omega_3^2)), \quad r = \Delta(1/(KM + \omega_3^2)), \quad z = \Delta(1/M), \tag{64}$$

and symbol $\Delta(\cdot)$ denotes the difference, i.e. for example,

$$\Delta(1/M) = 1/M_2 - 1/M_1, \tag{65}$$

etc.

The tensor $\Delta S^{-1} \cdot \cdot b = \Delta S^{-1} \cdot \cdot \langle S^{-1} \rangle^{-1} \cdot \cdot \xi$ is now computed as

$$\Delta S^{-1} \cdot \cdot b = [1/(PQ + \omega_3^2 R^2)]\{[(pQ + \omega_3^2 rR)\xi_1 + \omega_3(pR - rP)\xi_2]a_1 +$$

$$[(qP + \omega_3^2 rR)\xi_2 - \omega_3(qR - rQ)\xi_1]a_2\}.$$

A similar formula for $\Lambda \cdot \cdot \Delta S^{-1} = \eta \cdot \cdot \langle S^{-1} \rangle^{-1} \cdot \cdot \Delta S^{-1}$ is given by

$$\Lambda \cdot \cdot \Delta S^{-1} = [1/(PQ + \omega_3^2 R^2)]\{[(pQ + \omega_3^2 rR)\eta_1 - \omega_3(pR - rP)\eta_2]a_1$$

$$+ [(qP + \omega_3^2 rR)\eta_2 + \omega_3(qR - rQ)\eta_1]a_2\}.$$

Direct calculation shows that $(B_i = K_i M_i^2 + \omega_3^2, i = 1,2)$

$$-(\Delta S^{-1} \cdot \cdot b)(PQ + \omega_3^2 R^2)B_1 B_2 = (\tilde{M}\Delta k \xi_1 - \omega_3 \Delta \mu \xi_2)a_1 + (\tilde{K}\Delta \mu \xi_2 + \omega_3 \Delta k \xi_1)a_2, \quad (66)$$

$$-(\Lambda \cdot \cdot \Delta S^{-1})(PQ + \omega_3^2 R^2)B_1 B_2 = (\tilde{M}\Delta k \eta_1 + \omega_3 \Delta \mu \eta_2)a_1 + (\tilde{K}\Delta \mu \eta_2 - \omega_3 \Delta k \eta_1)a_2, \quad (67)$$

$$\tilde{K} = m_1 K_2 + m_2 K_1, \quad \tilde{M} = m_1 M_2 + m_2 M_1. \tag{68}$$

We are now ready to apply the necessary conditions (44) and (46). The first of them is reduced to

$$(\omega_3^2 - \overline{MK})(\xi_1 \eta_2 - \xi_2 \eta_1) + 2\omega_3(\overline{K}\xi_2 \eta_2 + \overline{M}\xi_1 \eta_1) = 0, \tag{69}$$

$$\overline{K} = \tilde{K}\,\Delta \mu / \Delta k, \quad \overline{M} = \tilde{M}\,\Delta k / \Delta \mu, \quad \overline{KM} = \tilde{K}\tilde{M}.$$

In view of (44), Eq. (46) can be rewritten as

$$(\Delta S^{-1} \cdot \cdot b) \cdot \cdot T \cdot \cdot (\Delta S^{-1} \cdot \cdot b) = 0. \tag{70}$$

Combining this with (66) we get

$$\xi_2 / \xi_1 = [(\tilde{M} \mp \omega_3)/(\omega_3 \pm \tilde{K})](\Delta k / \Delta \mu). \tag{71}$$

Equations (69) and (71) comprise a system that can be solved to determine ω_3 and d; we obtain $(\zeta = \xi_2 / \xi_1, \; \sigma = \eta_2 / \eta_1)$

$$\omega_3 = ((\tilde{k}+\tilde{\mu})/2)\Delta k \Delta \mu (\sigma-\zeta)/[(\sigma\Delta\mu\pm\Delta k)(\zeta\Delta\mu\pm\Delta k)] \tag{72}$$

and

$$d=[1/2(\sigma\Delta\mu\pm\Delta k)(\zeta\Delta\mu\pm\Delta k)]$$
$$[2\sigma\zeta\tilde{k}(\Delta\mu)^2\pm\Delta\mu\Delta k(\sigma+\zeta)(\tilde{k}-\tilde{\mu})-2\tilde{\mu}(\Delta k)^2]. \tag{73}$$

Equations (72), (73) provide a basis for the subsequent final calculations. We compute the bilinear form (41) making use of (72), (73). Direct calculation shows that

$$\phi = \phi_{1\pm} = \eta\cdot\cdot\langle\mathscr{D}\rangle\cdot\cdot\xi - [m_1 m_2/(\tilde{k}+\tilde{\mu})](\xi_1\Delta k\pm\xi_2\Delta\mu)(\eta_1\Delta k\pm\eta_2\Delta\mu) \tag{74}$$

where

$$\langle\mathscr{D}\rangle = m_1\mathscr{D}_1 + m_2\mathscr{D}_2.$$

The values (74) of $\phi_{1\pm}$ is attained by the rank 1 laminate with layers parallel to the main axes of tensor a_2, i.e. the main axes of ξ and η.

This regime will be valid within the range of parameters $\zeta = \xi_2/\xi_1$, $\sigma = \eta_2/\eta_1$ defined by Ineqs. (48) together with (72), (73). Without the range, rank 2 laminates will be applied to saturate the corresponding bounds.

To show this, consider for example, the case $\det\Delta_2 + \omega\cdot\cdot\Delta_2\cdot\cdot\omega = 0$ or, in view of (58),

$$B_2 = K_2 M_2 + \omega_3^2 = 0. \tag{75}$$

This is a manifold in the space (ω_3, d), and the variations $\delta\omega = a_3\delta\omega_3$, δd are therefore linked by the relationship (see (50))

$$2d\delta d - (k_2 - \mu_2)\delta d - 2\omega_3\delta\omega_3 = 0$$

as we move along this manifold. The latter relation can be rewritten as (see (50))

$$\delta d = 2\omega_3\delta\omega_3/(M_2-K_2), \tag{76}$$

and instead of two necessary conditions $\phi_\omega = \phi_d = 0$ (see (44) and (46)), we arrive at only one condition

$$(\Delta S^{-1}\cdot\cdot b)\times(\Lambda\cdot\cdot\Delta S^{-1})\cdot\cdot a_3\delta\omega_3 + (\Delta S^{-1}\cdot\cdot b)\cdot\cdot T\cdot\cdot(\Lambda\cdot\cdot\Delta S^{-1}) \, 2\omega_3\delta\omega_3/(M_2-K_2) = 0$$

or, equivalently,

$$(\Delta S^{-1} \cdot \cdot \mathbf{b}) \times (\Lambda \cdot \cdot \Delta S^{-1}) \cdot \cdot \mathbf{a}_3 + [2\omega_3/(M_2 - K_2)](\Delta S^{-1} \cdot \cdot \mathbf{b}) \cdot \cdot \mathbf{T} \cdot \cdot (\Lambda \cdot \cdot \Delta S^{-1}) = 0. \quad (77)$$

This condition should hold along with (75).

Equation (77) can be transformed with the aid of equations (66), (67) defining matrices $\Delta S^{-1} \cdot \cdot \mathbf{b}$ and $\Lambda \cdot \cdot \Delta S^{-1}$. We arrive at the relationship

$$\left[\tilde{M}\tilde{K} - \omega_3^2 + 2\omega_3^2(\tilde{M} - \tilde{K})/(M_2 - K_2) \right](\sigma - \zeta) + 2\omega_3\{[(\tilde{M}^2 - K_2 M_2)/(M_2 - K_2) - \tilde{M}](\Delta k/\Delta \mu)$$

$$- [(\tilde{K}^2 - K_2 M_2)/(M_2 - K_2) + \tilde{K}](\Delta \mu/\Delta k)\sigma\zeta\} = 0. \quad (78)$$

Expressions in the square brackets can be transformed as we use (75) to eliminate ω_3^2. After some algebra we arrive at the relationships

$$\tilde{M}\tilde{K} - \omega_3^2 + 2\omega_3^2(\tilde{M} - \tilde{K})/(M_2 - K_2) = [m_2/(M_2 - K_2)](\beta d + \gamma),$$

$$[(\tilde{M}^2 - K_2 M_2)/(M_2 - K_2) - \tilde{M}](\Delta k/\Delta \mu) - [(\tilde{K}^2 - K_2 M_2)/(M_2 - K_2) + \tilde{K}](\Delta \mu/\Delta k)\sigma\zeta =$$

$$- m_2 c/(M_2 - K_2). \quad (79)$$

Here, symbols β, γ and c are defined as

$$\begin{aligned} \beta &= -(u + v), \\ \gamma &= k_2 v - \mu_2 u, \\ c &= u - v\sigma\zeta, \end{aligned} \quad (80)$$

where

$$u = (k_2 + \tilde{\mu})\Delta k, \quad v = (\tilde{k} + \mu_2)\Delta \mu. \quad (81)$$

Eq. (78) now shows that

$$\omega_3 = (1/2c)(\beta d + \gamma)(\sigma - \zeta). \quad (82)$$

We now use this relation to eliminate ω_3 from (75). The result will be quadratic equation for d:

$$d^2[\beta^2(\sigma - \zeta)^2 - 4c^2] + 2[\beta\gamma(\sigma - \zeta)^2 + 2c^2(k_2 - \mu_2)]d$$

$$+ \gamma^2(\sigma - \zeta)^2 + 4c^2 k_2 \mu_2 = 0. \quad (83)$$

The discriminant of this equation is equal to

$$4c^2\{(\sigma-\zeta)^2(\gamma+\beta k_2)(\gamma-\beta\mu_2) + c^2(k_2 + \mu_2)^2\}.$$

From Eqs. (80), (82) it follows that

$$(\gamma + \beta k_2)(\gamma - \beta\mu_2) = -uv(k_2 + \mu_2)^2$$

and the discriminant turns out to be

$$4c^2(k_2+\mu_2)^2[-(\sigma^2 - 2\sigma\zeta + \zeta^2)uv + u^2 - 2uv\sigma\zeta + v^2\sigma^2\zeta^2]$$

$$= 4v^2c^2(k_2 + \mu_2)^2(\sigma^2 - u/v)(\zeta^2 - u/v) .$$

Eq. (83) now shows that

$$d = -\{1/[\beta^2(\sigma-\zeta)^2 - 4c^2]\}[\beta\gamma(\sigma-\zeta)^2 + 2c^2(k_2-\mu_2)$$

$$\mp 2vc(k_2 + \mu_2)\sqrt{(\sigma^2- u/v)(\zeta^2- u/v)]}. \tag{84}$$

The corresponding values of ω_3 will be

$$\omega_3 = \{(\sigma-\zeta)/[\beta^2(\sigma-\zeta)^2-4c^2]\}\{-\beta c(k_2-\mu_2) - 2\gamma c \pm \beta v(k_2+\mu_2)\sqrt{(\sigma^2-u/v)(\zeta^2-u/v)}\}$$

or, in view of (80),

$$\omega_3 = -\{(k_2 + \mu_2)(\sigma - \zeta)/[\beta^2(\sigma - \zeta)^2 - 4c^2]\}$$

$$\{c(v - u) \pm v(u + v)\sqrt{(\sigma^2-u/v)(\zeta^2-u/v)}\}. \tag{85}$$

Now it is easy to compute the bilinear form (41). After some algebra we obtain

$$\phi/\xi_1\eta_1 = [(K_2M_2 - K_1M_1)/(K_2\Delta\mu + \bar{M}\Delta k)][K_2 + M_2\sigma\zeta - \omega_3(\sigma - \zeta)] +$$

$$+ \omega_3(\sigma - \zeta) + d(1 - \sigma\zeta).$$

Making use of (50) and (68), we reduce this to the form

$$\phi/\xi_1\eta_1 = k_2 + \mu_2\sigma\zeta + \{m_1\Delta k\Delta\mu/[k_2\Delta\mu + \bar{\mu}\Delta k + d(\Delta k - \Delta\mu)]\}$$

$$[-k_2 + d + \omega_3(\sigma - \zeta) - (d + \mu_2)\sigma\zeta]. \tag{86}$$

With the aid of (84) and (85) one can show that

$$-k_2 + d + \omega_3(\sigma - \zeta) - (d + \mu_2)\sigma\zeta = \{(k_2 + \mu_2)/[(u + v)^2(\sigma - \zeta)^2 - 4c^2]\}\mathscr{L}$$

$$k_2\Delta\mu + \tilde{\mu}\Delta k + d(\Delta k - \Delta\mu) = \{1/[(u+v)^2(\sigma-\zeta)^2 - 4c^2]\}\mathscr{M},$$

where

$$\mathscr{L} = 2(1+\sigma\zeta)[c^2 - uv(\sigma-\zeta)^2] \pm v[2c(1-\sigma\zeta) - (u+v)(\sigma-\zeta)^2]\sqrt{(\sigma^2 - u/v)(\zeta^2 - u/v)},$$

$$\mathscr{M} = 2uv(u+v)(\sigma-\zeta)^2 - 2c\left[2cu - (u-v)\left[c \pm v\sqrt{(\sigma^2 - u/v)(\zeta^2 - u/v)}\right]\right].$$

Now it is easy to check by direct inspection that

$$\mathscr{L}/\mathscr{M} = -[(k_2+\mu_2)/u]\left[u/v + \sigma\zeta \pm \sqrt{(\sigma^2 - u/v)(\zeta^2 - u/v)}\right],$$

and from (86) we obtain

$$\phi/\xi_1\eta_1 = \phi_{2\pm}/\xi_1\eta_1 = k_2 + \mu_2\sigma\zeta - [m_1\Delta k\Delta\mu(k_2 + \mu_2)/2]$$

$$\left[1/v + (\sigma\zeta/u) \pm (1/u)\sqrt{(\sigma^2 - u/v)(\zeta^2 - u/v)}\right]. \tag{87}$$

The values (87) of $\phi_{2\pm}$ are attained by the rank 2 lamination with material $\mathscr{D}_1$ being the core and layers being parallel to the main axes of ξ and η. To show this, consider the formula

$$\mathscr{D}_0 = \mathscr{D}_2 + m_1[(\mathscr{D}_1 - \mathscr{D}_2)^{-1} + [2m_2/(k_2+\mu_2)](\alpha_1 nnnn + \alpha_2 tttt)]^{-1} = \mathscr{D}_2 + m_1 A^{-1} \tag{88}$$

for the effective tensor $\mathscr{D}_0$ of such a composite assembled from materials $\mathscr{D}_1$ and $\mathscr{D}_2$ taken with volume fractions m_1 and m_2, respectively. Parameters α_1, $\alpha_2 \geq 0$ ($\alpha_1 + \alpha_2 = 1$) are linked with the geometric parameters f, ρ of microstructure (see Figure) by the formulas
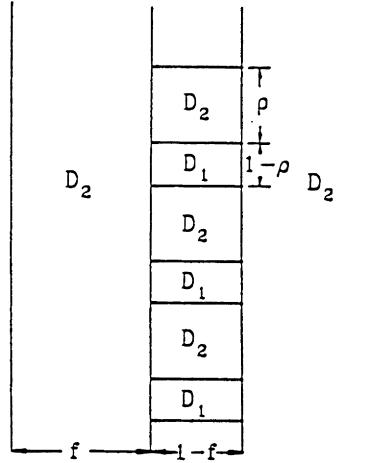
Rank 2 laminate

$$\alpha_1 = f(1-\rho)/m_2, \quad \alpha_2 = \rho/m_2.$$

The matrix A in (88) can be represented in the form

$$A = \pi\, a_1 a_1 + \theta(a_1 a_2 + a_2 a_1) + \theta a_2 a_2 + \tau a_3 a_3$$

where

$$\pi = -(\tilde{k}+\mu_2)/[(k_2+\mu_2)\Delta k] = -v/[(k_2+\mu_2)\Delta k\Delta\mu],$$

$$\theta = m_2(2\alpha_1-1)/(k_2+\mu_2), \qquad\qquad\qquad (89)$$

$$\rho = -(k_2+\tilde{\mu})/[(k_2+\mu_2)\Delta\mu] = -u/[(k_2+\mu_2)\Delta k\Delta\mu],$$

$$\tau = -1/\Delta\mu,$$

and the basis a_1, a_2, a_3 is chosen as suggested in (4) and (56), (57) with the unit vectors i, j oriented along the main axes of ξ and η.

The inverse matrix A^{-1} is computed as

$$A^{-1} = (\rho/\chi)a_1 a_1 - (\theta/\chi)(a_1 a_2 + a_2 a_1) + (\pi/\chi)a_2 a_2 + (1/\tau)a_3 a_3$$

where χ is defined by the formula

$$\chi = \pi\rho - \theta^2.$$

The bilinear form $\xi \,..\, \mathscr{D}_0 \,..\, \eta$ obviously depends on α_1; the extremal values of this parameter can be found from the relationship

$$(\xi..A^{-1}..\eta)_{\alpha_1} = \xi..(A^{-1})_{\alpha_1}..\eta = 0$$

or, equivalently, from

$$\xi..A^{-1}..A_{\alpha_1}..A^{-1}..\eta = 0.$$

This one is easily reduced to

$$(\theta^2 + \pi\rho)(\xi_1\eta_2 + \xi_2\eta_1) - 2\theta(\rho\xi_1\eta_1 + \pi\xi_2\eta_2) = 0,$$

and we obtain the extremal values of θ

$$\theta = [\pi/(\sigma + \zeta)]\left[(\rho/\pi) + \sigma\zeta \pm \sqrt{(\sigma^2 - \rho/\pi)(\zeta^2 - \rho/\pi)}\right] \tag{90}$$

(recall that $\xi = \xi_2/\xi_1$ and $\sigma = \eta_2/\eta_1$).

With these values for θ it is easy to arrive at the following expression for the bilinear form

$$\xi \cdot\cdot \mathscr{D}_0 \cdot\cdot \eta/\xi_1\eta_1 = k_2 + \mu_2\sigma\zeta + (m_1/2)\left[(1/\pi) + \sigma\zeta/\rho \right.$$
$$\left. \pm (1/\rho)\sqrt{(\sigma^2 - \rho/\pi)(\zeta^2 - \zeta/\pi)}\right]$$

or, in view of (89)

$$\xi \cdot\cdot \mathscr{D}_0 \cdot\cdot \eta/\xi_1\eta_1 = k_2 + \mu_2\sigma\zeta - [m_1\Delta k\Delta\mu(k_2+\mu_2)/2]\left[(1/v) + \sigma\zeta/u \right.$$
$$\left. \pm (1/u)\sqrt{\sigma^2 - u/v)(\zeta^2 - u/v)}\right].$$

This expression is the same as (87), and the attainability of the latter bound is thereby proved. A result similar to (87) can be established if the condition

$$B_1 = K_1M_1 + \omega_3^2 = 0 \tag{91}$$

holds instead of (75). We then arrive at the formula

$$\phi/\xi_1\eta_1 = \phi_{3\pm}/\xi_1\eta_1 = k_1 + \mu_1\sigma\zeta + [m_2\Delta k\Delta\mu(k_1+\mu_1)/2]$$

$$\left[(1/\overline{v}) + \sigma\zeta/\overline{u} \pm (1/\overline{u})\sqrt{(\sigma^2 - \overline{u}/\overline{v})(\zeta^2 - \overline{u}/\overline{v}\ )}\right] \qquad (92)$$

with $\overline{u}$, $\overline{v}$ defined as (cf. (81)).

$$\overline{u} = (k_1 + \tilde{\mu})\Delta k, \quad \overline{v} = (\tilde{k} + \mu_1)\Delta\mu. \qquad (93)$$

The values (92) are attained for the 2nd rank lamination with material $\mathscr{D}_2$ being the core and layers parallel to the main axes of ξ and η. Now it is easy to specify the ranges of parameters $\xi_1, \eta_1, \sigma, \zeta$ that maximize the function ϕ with respect to ω_3 and d (see (37) and (39)). Once this is done, the final operation of maximizing ϕ with respect to m_1 can be applied to construct the desired material pattern.

We arrive at the final expression for $\displaystyle\sup_{\mathscr{D},w}\inf_{\lambda} J$:

$$\sup_{\mathscr{D},w}\inf_{\lambda} J = \sup_{w}\inf_{\lambda}[I(w) - \int_\Sigma \lambda q\,dxdy + \sup_{m_1}\int_\Sigma \max(\phi_{1\pm},\phi_{2\pm},\phi_{3\pm})dxdy.]$$

The operation

$$\max(\phi_{1\pm},\phi_{2\pm},\phi_{3\pm})$$

is carried out explicitly at every point of the layout and thus provides with the required classification of ranges. In the context of a numerical implementation, this operation comes instead of the "inner loop" homogenization technique addressed by many authors (see, for example, Ref. 11) and generally providing suboptimal, rather than strictly optimal layouts.

REFERENCES

1. K.A. Lurie, The Extension of Optimization Problems Containing Controls in the Coefficients, Proceeding of the Royal Society of Edinburg, Vol. 114A, pp. 81–97, 1990.
2. K.A. Lurie., A.V. Fedorov and A.V. Cherkaev, Regularization of Optimal Design Problems for Bars and Plates, Parts 1 and 2, Journal of Optimization Theory and Applications, Vol. 37, pp. 499–521, 1982 and Vol. 37, pp. 523–543, 1982.
3. K.A. Lurie and A.V. Cherkaev, The Effective Characteristics of Composite Materials and Optimal Design of Constructions (in Russian), Advances in Mechanics (Poland), Vol. 9, No. 2, pp. 3–81, 1986.

4. J.M. Ball, Convexity Conditions and Existence Theorems in Nonlinear Elasticity, Archive for Rational Mechanics and Analysis, Vol. 63, pp. 337–403, 1977.

5. G. Strang, The Polyconvexification of $F(\nabla u)$, Research Report CMA–R09–83, Australian National University, 1983.

6. R.V. Kohn and G. Strang, Optimal Design and Relaxation of Variational Problems, Parts 1,2,3, Communications on Pure and Applied Mathematics, Vol. 39, pp. 113–137, 1986; Vol. 39, pp. 139–182, 1986; and Vol. 39, pp. 353–377, 1986.

7. A.I. Lurie, Nonlinear Theory of Elasticity, North Holland, Amsterdam, New York, Oxford, Tokyo, 1990.

8. L.V. Gibianskii and A.V. Cherkaev, Design of Composite Plates of Extremal Stiffness (in Russian), A.F. Ioffe Institute Report 914, Leningrad, 1984.

9. K.A. Lurie and R. Lipton, Direct Solution of an Optimal Layout Problem for Isotropic Heat Conductors in Three Dimensions, Theoretical Aspects of Industrial Design, Edited by David A. Field and Vadim Komkov, SIAM, Philadelphia, pp. 1–11, 1992.

10. K.A. Lurie, Direct Solution of an Optimal Layout Problem for Isotropic and Anisotropic Heat Conductors on a Plane, Journal of Optimization Theory and Applications, Vol. 72, pp. 553–575, 1992.

11. M.P. Bendsøe and N. Kikuchi, Generating Optimal Topologies in Structural Design Using a Homogenization Method, Computational Methods in Applied Mechanics and Engineering, vol. 71, pp. 197–224.

Necessary Weierstrass conditions
in problems of an optimal structural design

L.V. Petukhov

Department of Applied Mathematics, St. Petersburg Technical University, Russia

1   Introduction

In this paper problems of an optimal structural design are considered, control being inclusions of hard elastcic material into the soft one. Volumes of this materials are given. It is necessary to find such situations of the inclusions that a continious functional of stress tensor or strein tensor is minimized.

A central result of this paper is derivation of the necessary Weierstrass conditions for an inclusion of hard elastic material into the soft one and vise versa. The inequality of the necessary Weierstrass conditions includes a displacement vector with a solution of the problem of infinite two- or three-dimensional space with inclusions. Ellipse and ellipsoid inclusions are considered for two- and three-dimensional cases. For the problem of maximum stiffness the necessary Weierstrass conditions are obtained in a form of an algebraical expressions.

The Weierstrass conditions allow to analyse the functional sensitivity and can be used for optimal design with advanced composite materials.

2   The common optimization problem

Let $\mathbb{R}^N$ be the N-dimensional Euclidean space of vectors $\vec{x} = x_i \vec{e}_i$, where $\vec{e}_i$ are unit vectors of the Cartesian reference system (hereinafter indexes i, j, k, l take values from 1 to N, summation in products is assumed from 1 to N too).

Let $\Omega \subset \mathbb{R}^N$ denote a regular domain with a bound Γ [2] and a vector-function $\vec{f}(\vec{x}) = f_i(\vec{x})\vec{e}_i$ is defined in Ω, where $f_i(\vec{x}) \in \mathcal{L}^2(\Omega)$ and a vector-function $\vec{F}(\vec{y}) = F_i(\vec{y})\vec{e}_i$ is defined on $\Gamma_F \subset \Gamma$, where $F_i(\vec{y}) \in \mathcal{L}^2(\Gamma_F)$ (here $\mathcal{L}^2(\Omega)$ and $\mathcal{L}^2(\Gamma_F)$ are the Gilbert spaces). The domain Ω is occupied by two elastic materials with the shear moduluses μ_1, μ_2 ($\mu_2 \geq \mu_1$) and the Poisonn's ratios ν_1, ν_2. Besides soft and hard materials occupy domains $\Omega_1 \subset \Omega$, $\Omega_2 \subset \Omega$.

Volumes of soft and hard materials are assigned

$$\text{mes}\,\Omega_1 = \lambda_1, \ \text{mes}\,\Omega_2 = \lambda_2 = \text{mes}\,\Omega - \lambda_1. \tag{1}$$

Displacements $u_i(\vec{x})\vec{e}_i \in \mathcal{V}(\Omega)$ are determined by the integral identity

$$\int_{\Omega_1} A_1(\vec{u}, \vec{v})\, dx + \int_{\Omega_2} A_2(\vec{u}, \vec{v})\, dx - \int_{\Omega} \vec{f} \cdot \vec{v}\, dx - \int_{\Gamma_F} \vec{F} \cdot \vec{v}\, d\Gamma = 0, \tag{2}$$

$$\forall \vec{v} \in \mathcal{V}(\Omega) = \{\vec{v} = v_i(\vec{x})\vec{e}_i \mid v_i(\vec{x}) \in \mathcal{H}^1(\Omega),\ v_i(\vec{y}) = 0,\ \vec{y} \in \Gamma_u \subset \Gamma\},$$

where $\mathcal{H}^1(\Omega)$ is the Sobolev's space, $A_n(\vec{u}, \vec{v}) = a_{ijkl}^{(n)}\varepsilon_{ij}(\vec{u})\varepsilon_{kl}(\vec{v})$, $n = 1, 2$, $\varepsilon_{kl}(\vec{v}) = \frac{\frac{\partial v_k}{\partial x_l} + \frac{\partial v_l}{\partial x_k}}{2}$, components of the fourth rank tensor a_{ijkl} are calculated by μ_n, ν_n and the point denotes the inner product of vectors.

We are seeking the domains Ω_1^*, Ω_2^* of soft and hard material locations satisfied 1 such that a functional

$$J(\vec{u}) = \int_{\Omega} \varphi(\vec{u})\, dx + \int_{\Gamma_F} \psi(\vec{u})\, d\Gamma \tag{3}$$

is minimized. In the functional 3 the function $\varphi(\vec{u})$ depends on the displacement-vector components u_i and stress-tensor components $\sigma_{ij}(\vec{u})$, the function $\psi(\vec{u})$ depends on the displacement-vector components u_i.

The locations of soft and hard materials may have a very complicated structure. The aim of this paper is a consideration of functional sensitivity with reference to the inclusions.

3 Necessray optimal conditions

Let Ω_1^*, Ω_2^* are the optimal solutions (Ω_1^* is occupied by soft material, Ω_2^* is occupied by hard one) and Ω_1^*, Ω_2^* have the common boundary Γ_{12}^*. Adding the left-hand side of the integral identity 1 to the functional 3, we can obtain its first variation:

$$\begin{aligned}
\delta J &= \int_{\Omega} \left[\frac{\partial \varphi(\vec{u}^*)}{\partial \underline{\underline{\sigma}}} \cdot\cdot \underline{\underline{\sigma}}(\delta \vec{u}) + \frac{\partial \varphi(\vec{u}^*)}{\partial \vec{u}} \cdot \delta \vec{u} \right] dx + \tag{4} \\[2mm]
&+ \int_{\Gamma_F} \frac{\partial \psi(\vec{u}^*)}{\partial \vec{u}} \cdot \delta \vec{u}\, d\Gamma + \int_{\Omega_1^*} A_1(\delta \vec{u}, \vec{v})\, dx + \int_{\Omega_2^*} A_2(\delta \vec{u}, \vec{v})\, dx + \\[2mm]
&+ \int_{\Gamma_{12}^*} [A_1(\vec{u}^*, \vec{v}) + \varphi_1(\vec{u}^*) - A_2(\vec{u}^*, \vec{v}) - \varphi_2(\vec{u}^*)]\, \delta r\, d\Gamma + \\[2mm]
&+ \int_{\Gamma \cap \Gamma_2^*} [A_1(\vec{u}^*, \vec{v}) + \varphi_1(\vec{u}^*) - A_2(\vec{u}^*, \vec{v}) - \varphi_2(\vec{u}^*)]\, \delta r\, d\Gamma - \\[2mm]
&- \int_{\Gamma \cap \Gamma_1^*} [A_1(\vec{u}^*, \vec{v}) + \varphi_1(\vec{u}^*) - A_2(\vec{u}^*, \vec{v}) - \varphi_2(\vec{u}^*)]\, \delta r\, d\Gamma,
\end{aligned}$$

where two points denote the double inner product of tensors, $\vec{u}^*$ is the optimal solution of the optimal problem, $\delta\vec{u}$ is the firts variation of $\vec{u}$, δr is the first variation of the optimal boundaries Γ_{12}^*, $\Gamma\cap\Gamma_1^*$, $\Gamma\cap\Gamma_2^*$ satisfied condition [3]:

$$\int_{\Gamma_{12}^*}\delta r\,d\Gamma + \int_{\Gamma\cap\Gamma_1^*}\delta r\,d\Gamma + \int_{\Gamma\cap\Gamma_2^*}\delta r\,d\Gamma = 0. \tag{5}$$

We put $\vec{v}$ equal to $\vec{v}^*$ in 4, where $\vec{v}^*$ satisfies the integral identity

$$\int_{\Omega_1^*} A_1(\vec{v}^*,\vec{v})\,dx + \int_{\Omega_2^*} A_2(\vec{v}^*,\vec{v})\,dx + \tag{6}$$

$$+ \int_{\Omega}\left[\frac{\partial\varphi(\vec{u}^*)}{\partial\underline{\underline{\sigma}}}\cdot\cdot\underline{\underline{\sigma}}(\delta\vec{v}) + \frac{\partial\varphi(\vec{u}^*)}{\partial\vec{u}}\cdot\vec{v}\right]dx - \int_{\Gamma_F}\frac{\partial\psi(\vec{u}^*)}{\partial\vec{u}}\cdot\vec{v}\,d\Gamma = 0$$
$$\forall\vec{v}\in\mathcal{V}(\Omega).$$

Since $\delta\vec{u}\in\mathcal{V}(\Omega)$, we get from 4 an inequality

$$\delta J = \int_{\Gamma_{12}^*}[A_2(\vec{u}^*,\vec{v}^*) - \varphi_2(\vec{u}^*) - A_1(\vec{u}^*,\vec{v}^*) + \varphi_1(\vec{u}^*)]\,\delta r\,d\Gamma + \tag{7}$$

$$+ \int_{\Gamma\cap\Gamma_2^*}[A_2(\vec{u}^*,\vec{v}^*) - \varphi_2(\vec{u}^*) - A_1(\vec{u}^*,\vec{v}^*) + \varphi_1(\vec{u}^*)]\,\delta r\,d\Gamma -$$

$$- \int_{\Gamma\cap\Gamma_1^*}[A_2(\vec{u}^*,\vec{v}^*) - \varphi_2(\vec{u}^*) - A_1(\vec{u}^*,\vec{v}^*) + \varphi_1(\vec{u}^*)]\,\delta r\,d\Gamma \geq 0,$$

which must satisfy the constraint 5.

The inequality 7 for such δr is always satisfied if

$$A_2(\vec{u}^*,\vec{v}^*) - \varphi_2(\vec{u}^*) - A_1(\vec{u}^*,\vec{v}^*) + \varphi_1(\vec{u}^*) \;=\; \zeta,\ \vec{x}\in\Gamma_{12}^*, \tag{8}$$
$$A_2(\vec{u}^*,\vec{v}^*) - \varphi_2(\vec{u}^*) - A_1(\vec{u}^*,\vec{v}^*) + \varphi_1(\vec{u}^*) \;\leq\; \zeta,\ \vec{x}\in\Gamma\cap\Gamma_2^*, \tag{9}$$
$$A_2(\vec{u}^*,\vec{v}^*) - \varphi_2(\vec{u}^*) - A_1(\vec{u}^*,\vec{v}^*) + \varphi_1(\vec{u}^*) \;\geq\; \zeta,\ \vec{x}\in\Gamma\cap\Gamma_1^*, \tag{10}$$

where ζ is a constant.

4 Necessary Weierstrass conditions

We shall analyse the functional sensitivity when there is a soft inclusion into hard material or a hard inclusion into soft one. Let $\vec{x}_0\in\Omega_1^*$ ($\vec{x}_0\in\Omega_2^*$) and $\Omega_0(\eta)$ is a convex domain with a Lipschitz boundary $\Gamma_0(\eta)$. Points of $\Gamma_0(\eta)$ are determined by vectors $\vec{x}_0 + \eta\vec{y}$. For $\eta = 1$ we have a domain $\Omega_0 = \Omega_0(1)$, for $\eta\to 0$ the domain $\Omega_0(\eta)$ contracts to the point $\vec{x}_0$ and

$$\mathrm{mes}\,\Omega_0(\eta) = \eta^N\,\mathrm{mes}\,\Omega_0. \tag{11}$$

Let us suppose also that $\overline{\Omega}_0 \subset \Omega_1^*$ $(\overline{\Omega}_0 \subset \Omega_2^*)$ and hard (soft) material occupies the domain $\Omega_0(\eta)$. In order that the condition 1 is satisfied it is necessary to change the boundary Γ_{12}^* by a quantity $r(\vec{y}, \eta)$, $\vec{y} \in \Gamma_{12}^*$ [2], $r(\vec{y}, \eta) > 0$ $(r(\vec{y}, \eta) < 0)$ for a hard (soft) inclusion into soft (hard) material. In this case functional $J(\vec{u})$ will have a form

$$
\begin{aligned}
J(u) \;=\; & \int_{\Omega_1} [A_1(\vec{u}, \vec{v}) + \varphi_1(\vec{u})]\, dx + \int_{\Omega_2} [A_2(\vec{u}, \vec{v}) + \varphi_2(\vec{u})]\, dx + \quad (12) \\
& + \int_{\Gamma_F} \left[\psi(\vec{u}) - \vec{F} \cdot \vec{v} \right] d\Gamma - \int_{\Gamma} \vec{f} \cdot \vec{v}\, dx \pm \\
& \pm \int_{\Omega_0(\eta)} [A_1(\vec{u}, \vec{v}) + \varphi_1(\vec{u}) - A_2(\vec{u}, \vec{v}) - \varphi_2(\vec{u})]\, dx,
\end{aligned}
$$

where the sign $+(-)$ in the last integral corresponds to the soft (hard) material inclusion into the soft (hard) one.

Since the condition 11 must be satisfied, the function $r(\vec{y}, \eta)$ must be proportional to η^n and hence $\delta r = \ldots = \delta^{N-1} r = 0$. Since loadings in the integral identity are proportional to $\delta r, \ldots, \delta r^{N-1}$, variations $\delta \vec{u} = \ldots = \delta^{N-1}\vec{u} = 0$ correspondingly [2].

Putting $\vec{v} = -\vec{v}^*$ in 12 and using the integral idenity 6 for $\vec{v} = \delta^N \vec{u}$, we obtain

$$
\begin{aligned}
\delta^N J \;=\; & \int_{\Gamma_{12}^*} [A_2(\vec{u}^*, \vec{v}^*) - \varphi_2(\vec{u}^*) - A_1(\vec{u}^*, \vec{v}^*) + \varphi_1(\vec{u}^*)]\, \delta^N r\, d\Gamma \pm \quad (13) \\
& \pm \frac{d^N}{d\eta^N} \left\{ \int_{\Omega_0(\eta)} [A_2(\vec{u}, \vec{v}^*) - \varphi_2(\vec{u}) - A_1(\vec{u}, \vec{v}^*) + \varphi_1(\vec{u})]\, dx \right\}_{\eta=0}.
\end{aligned}
$$

Using the necessary conditions $\delta^N J \geq 0$, 8, the equality 11 and the signs of variations $\delta^N r$, we obtain from 13:

$$
\begin{aligned}
& \pm \frac{d^n}{d\eta^n} \left\{ \int_{\Omega_0(\eta)} [A_2(\vec{u}, \vec{v}^*) - \varphi_2(\vec{u}) - A_1(\vec{u}, \vec{v}^*) + \varphi_1(\vec{u})]\, dx \right\}_{\eta=0} \geq \quad (14) \\
& \geq \pm N! \zeta \operatorname{mes} \Omega_0.
\end{aligned}
$$

Here the sign $+(-)$ is taken for points $\vec{x}_0 \in \Omega_2^* (\vec{x}_0 \in \Omega_1^*)$.

The displacement-vector $\vec{u}$ in the left-hand side of 14 may be replaaced with a solution for the infinity space $\mathbb{R}^N$ with the inclusion Ω_0, when the main stresses $\sigma_k(\vec{u}^*(\vec{x}_0))$ of the stress-tensor $\underline{\sigma}(\vec{u}^*(\vec{x}_0))$ act in the infinity [3]. We shall denote this solution by $\vec{u}^0(\vec{x})$. The stress-tensors $\underline{\sigma}^{(1)}(\vec{u}^0(\vec{x}))$ and $\underline{\sigma}^{(2)}(\vec{u}^0(\vec{x}))$ do not depend on $\vec{x}$, the strain-tensor $\underline{\varepsilon}(\vec{v}^*(\vec{x}))$ is a continious function, therefore the inequality 14 takes the final form:

$$
\begin{aligned}
A_2(\vec{u}^0, \vec{v}^*) - \varphi_2(\vec{u}^0) - A_1(\vec{u}^0, \vec{v}^*) + \varphi_1(\vec{u}^0) &\geq \zeta, \; \forall \vec{x}_0 \in \Omega_2^*, \quad (15) \\
A_2(\vec{u}^0, \vec{v}^*) - \varphi_2(\vec{u}^0) - A_1(\vec{u}^0, \vec{v}^*) + \varphi_1(\vec{u}^0) &\leq \zeta, \; \forall \vec{x}_0 \in \Omega_1^*,
\end{aligned}
$$

where $\vec{u}^0 = \vec{u}^0(\vec{x}_0)$, $\vec{v}^* = \vec{v}^*(\vec{x}_0)$.

We shall call the inequalities 15 the necessary Weierstrass conditions. They must be satisfied for all points $\vec{x}_0 \in \Omega_1^*$ and $\vec{x}_0 \in \Omega_2^*$.

5 Elliptic and ellipsoidal inclusions

The displacement-vector $\vec{u}^0$ can not be determined for the arbitrary forms of inclusions. However, it is known for the elliptic, hypotrochoidal inclusions in two-dimensional case and for the ellipsoidal inclusions in three-dimensional case [1].

We shall consider in $\mathbb{R}^2$ the elliptic inclusion Ω_0 of soft material in hard one. Let $\eta(1+\xi)$ and $\eta(1-\xi)$ be semi-major and semi-minor axes of the ellipse. Let's put an origin of coordinates in point $\vec{x}_0$ and the let the unit vectors $\vec{e}_1$ and $\vec{e}_2$ be combined with the semi-major and semi-minor axes. Denoting the angle between the unit vector $\vec{e}_1$ and the first main direction of the stress-tensor $\underline{\sigma}(\vec{u}^*(\vec{x}_0))$ by β, we have the tensor components $\underline{\varepsilon}^0 = \underline{\varepsilon}(\vec{u}^0)$ and $\underline{\sigma}^0 = \underline{\sigma}(\vec{u}^0)$ in points of the elliptic inclusion [1]. They are independent on points $\vec{x} \in \Omega_0$ and are equal to constants:

$$
\varepsilon_{11}^0 = \frac{(\kappa_2 + 1)\left[(\kappa_1 - 1)C_1 - 2C_2\right]}{8},
$$

$$
\varepsilon_{22}^0 = \frac{(\kappa_2 + 1)\left[(\kappa_1 - 1)C_1 + 2C_2\right]}{8}, \qquad (16)
$$

$$
\varepsilon_{12}^0 = \frac{(\kappa_2 + 1)C_3}{4},
$$

$$
\sigma_{11}^0 = \frac{\mu_1(\kappa_2 + 1)(C_1 - C_2)}{2},
$$

$$
\sigma_{22}^0 = \frac{\mu_1(\kappa_2 + 1)(C_1 - C_2)}{2}, \qquad (17)
$$

$$
\sigma_{12}^0 = \frac{\mu_1(\kappa_2 + 1)C_3}{2},
$$

where $\kappa_k = 3 - 4\nu_k$ for the plane strained state, $\kappa_k = \frac{3-4\nu_k}{1+\nu_k}$ for the plane stressed state and

$$
C_1 = \frac{[(1+\xi^2)\mu_2 + (\kappa_2 - \xi^2)\mu_1](\sigma_1 + \sigma_2) - 2\xi(\mu_2 - \mu_1)(\sigma_1 - \sigma_2)\cos 2\beta}{(\mu_2 + \kappa_2\mu_1)[(\kappa_1 - 1)\mu_2 + 2\mu_1] - \xi^2(\mu_2 - \mu_1)[(\kappa_1 - 1)\mu_2 - 2\kappa_2\mu_1]},
$$

$$
C_2 = \frac{\xi[(\kappa_1 - 1)\mu_2 - (\kappa_2 - 1)\mu_1](\sigma_1 + \sigma_2)}{(\mu_2 + \kappa_2\mu_1)[(\kappa_1 - 1)\mu_2 + 2\mu_1] - \xi^2(\mu_2 - \mu_1)[(\kappa_1 - 1)\mu_2 - 2\kappa_2\mu_1]} -
$$

$$
- \frac{[(\kappa_1 - 1)\mu_2 + 2\mu_1](\sigma_1 - \sigma_2)\cos 2\beta}{(\mu_2 + \kappa_2\mu_1)[(\kappa_1 - 1)\mu_2 + 2\mu_1] - \xi^2(\mu_2 - \mu_1)[(\kappa_1 - 1)\mu_2 - 2\kappa_2\mu_1]},
$$

$$
C_3 = \frac{(\sigma_1 - \sigma_2)\sin 2\beta}{(1 - \xi^2)\mu_2 + (\kappa_2 + \xi^2)\mu_1}. \qquad (18)
$$

Here σ_1 and σ_2 are $\sigma_1(\vec{u}^*(\vec{x}_0))$ and $\sigma_2(\vec{u}^*(\vec{x}_0))$ respectively. The tensor components $\varepsilon_{ij}^0 = \varepsilon_{ij}^0(\vec{u}^0)$ and $\sigma_{ij}^0 = \sigma_{ij}^0(\vec{u}^0)$ for the case of inclusion Ω_0 of hard material into soft one are obtained from the formulas 16–18 if replace μ_1, μ_2 and κ_1, κ_2 by each other.

We shall consider now in $\mathbb{R}^3$ the ellipsoidal inclusion Ω_0 of soft material into hard one. Let $\eta a_1 \geq \eta a_2 \geq \eta a_3$ be semi axes of the ellipsoid. The origin of the coordinates is placed in the point $\vec{x}_0$ and the unit vectors $\vec{e}_1$, $\vec{e}_2$ and $\vec{e}_3$ are combined with major, middle and minor semi-axes of the ellipsoid. Stress-vectors $\vec{e}_k \cdot \underline{\underline{\sigma}}(\vec{u}^*(\vec{x}_0))$ act in the infinity at the ortogonal with respect to $\vec{e}_k$ planes.

Components of the stress-tensor $\underline{\underline{\sigma}}^0 = \underline{\underline{\sigma}}(\vec{u}^0(\vec{x}))$ are independent from $\vec{x}$ in the points of Ω_0 and are equal to [4]

$$\sigma_{ij}^0 = 2\mu_1 B_{ij}\sigma_{ij}, \quad i \neq j, \tag{19}$$

$$B_{12} = \frac{1-\nu_2}{\rho\Delta(\mu_1-\mu_2)[(1-2\nu_2)(\omega_1+\omega_2)-\left(\frac{2\rho^2}{e^2}-1\right)(\omega_1-\omega_2)]+2\mu_2(1-\nu_2)},$$

$$B_{23} = \frac{1-\nu_2}{\rho\Delta(\mu_1-\mu_2)[(1-2\nu_2)(\omega_2+\omega_3)-\left(\frac{2\rho^2}{1-e^2}-1\right)(\omega_2-\omega_3)]+2\mu_2(1-\nu_2)},$$

$$B_{31} = \frac{1-\nu_2}{\rho\Delta(\mu_1-\mu_2)[(1-2\nu_2)(\omega_1+\omega_2)-(2\rho^2-e^2)(\omega_1-\omega_2)]+2\mu_2(1-\nu_2)},$$

(components σ_{ii}^0 are governed by the linear algebraic equations.)

$$\left(E - \frac{\mu_2}{\mu_1}P \cdot Q^{-1} \cdot \Lambda_1\right) \cdot \sigma^0 = (E - Q^{-1} \cdot \Lambda_2) \cdot \sigma, \tag{20}$$

where $\sigma_{ij} = \sigma_{ij}(\vec{u}^*(\vec{x}_0))$, E - the unit matrix,

$$\sigma^0 = \begin{pmatrix} \sigma_{11}^0 \\ \sigma_{22}^0 \\ \sigma_{33}^0 \end{pmatrix}, \quad \sigma = \begin{pmatrix} \sigma_{11} \\ \sigma_{22} \\ \sigma_{33} \end{pmatrix}, \quad \Lambda_n = \frac{1}{1+\nu_n}\begin{pmatrix} 1 & -\nu_n, & -\nu_n \\ -\nu_n & 1 & -\nu_n \\ -\nu_n & -\nu_n & 1 \end{pmatrix}, \quad n = 1, 2,$$

matrix components P and Q are determined by relations

$$p_{m1} = (1-2\nu_2)[\omega_m - (\rho\Delta)^{-1}],$$

$$p_{m2} = (1-2\nu_2)(\rho^2-\xi_m)^{-1}\omega_m + \frac{\nu_2\omega_k}{\rho^2-\omega_k} -$$

$$- \frac{1}{2\rho\Delta}\left(\frac{1-2\nu_2}{\rho^2-\xi_m} - \sum_{k=1}^{3}\frac{1}{\rho^2-\xi_k}\right),$$

$$p_{m3} = (1-2\nu_2 2)\frac{(c_1-c_2)(\rho^2-\xi_m)}{(c_1-\xi_m)(c_2-\xi_m)}\omega_m + \nu_2\frac{(c_1-c_2)(\rho^2-\xi_k)}{(c_1-\xi_k)(c_2-\xi_k)}\omega_k -$$

$$- \frac{(1-\nu_2)(c_1-c_2)(\rho^2-\xi_m)}{(c_1-\xi_m)(c_2-\xi_m)\rho\Delta} - \frac{(\rho^2-c_1)^2}{c_1-\xi_m}\omega_4 + \frac{(\rho^2-c_2)^2}{c_2-\xi_m}\omega_5,$$

$$q_{m1} = (1 - 2\nu_2)\omega_m,$$

$$q_{m2} = (1 - 2\nu_2)\omega_m + (2\rho\Delta)^{-1},$$

$$q_{m3} = (1-2\nu_2)\frac{(c_1-c_2)(\rho^2-\xi_m)}{(c_1-\xi_m)(c_2-\xi_m)}\omega_m - \frac{(\rho^2-c_1)^2}{c_1-\xi_m}\omega_4 + \frac{(\rho^2-c_2)^2}{c_2-\xi_m}\omega_5,$$

$$m = 1, 2, 3,$$

where $\xi_1 = 0$, $\xi_2 = e^2$, $\xi_3 = 1$, $\Delta = \Delta(p) = \sqrt{(\rho^2 - e^2)(\rho^2 - 1)}$, $c_{1,2} = \frac{1+e^2\pm\sqrt{1+e^2+e^4}}{3}$, $a_k = \sqrt{\rho^2-\xi_k}$, $\omega_k = \int_\rho^\infty \frac{d\lambda}{(\lambda^2-\xi_k)\Delta(\lambda)}$, $\omega_{3+m} = \int_\rho^\infty \frac{d\lambda}{(\lambda^2-c_m)\Delta(\lambda)}$, $m = 1, 2$.

Sometimes it is necessary to have the strain-tensor components $\varepsilon_{ij}^0 = \varepsilon_{ij}(\vec{u}^0)$. To determine them, we'll make use of relations 19, 20 and obtain

$$\varepsilon_{ij}^0 = \frac{\sigma_{ij}^0}{2\mu_1}, \; i \neq j, \tag{21}$$

$$(2\mu_1 E - 2\mu_2\Lambda_1 \cdot P \cdot Q^{-1}) \cdot \varepsilon^0 = \Lambda_1 \cdot (E \cdot P \cdot Q^{-1} \cdot \Lambda_2) \cdot \sigma, \tag{22}$$

where

$$\varepsilon_{ij}^0 = \varepsilon_{ij}(\vec{u}^0), \; \varepsilon^0 = \begin{pmatrix} \varepsilon_{11}^0 \\ \varepsilon_{22}^0 \\ \varepsilon_{33}^0 \end{pmatrix}, \; \Lambda_1^{-1} = \frac{1}{1 - 2\nu_1} \begin{pmatrix} 1 - \nu_1 & \nu_1 & \nu_1 \\ \nu_1 & 1 - \nu_1 & \nu_1 \\ \nu_1 & \nu_1 & 1 - \nu_1 \end{pmatrix}.$$

6 Maximum stiffness construction

For this problem $\varphi(\vec{u}) = \vec{f} \cdot \vec{u}$, $\psi(\vec{u}) = \vec{F} \cdot \vec{u}$. From 6, 8 and 15 it follows that $\vec{v}^*(\vec{x}) = \vec{u}^*(\vec{x})$.

$$A_2(\vec{u}^*, \vec{u}^*) - A_1(\vec{u}^*, \vec{u}^*) = \zeta, \; \vec{x} \in \Gamma_{12}^*,$$

$$A_2(\vec{u}^*, \vec{u}^*) - A_1(\vec{u}^*, \vec{u}^*) \geq \zeta, \; \vec{x} \in \Gamma \cap \Gamma_2^*,$$

$$A_2(\vec{u}^*, \vec{u}^*) - A_1(\vec{u}^*, \vec{u}^*) \leq \zeta, \; \vec{x} \in \Gamma \cap \Gamma_1^*,$$

$$A_2(\vec{u}^*, \vec{u}^0) - A_1(\vec{u}^*, \vec{u}^0) \geq \zeta, \; \vec{x}_0 \in \Omega_2^*, \tag{23}$$

$$A_2(\vec{u}^*, \vec{u}^0) - A_1(\vec{u}^*, \vec{u}^0) \leq \zeta, \; \vec{x}_0 \in \Omega_1^*, \tag{24}$$

Inserting $\underline{\underline{\varepsilon}}^0$ from 16 into the left-hand side of the inequality 23, we get for $N = 2$

$$A_2(\vec{u}^*, \vec{u}^0) - A_1(\vec{u}^*, \vec{u}^0) = \chi(\sigma_1, \sigma_2, \mu_1, \mu_2, \kappa_1, \kappa_2, \beta, \xi)$$

where $\sigma_k = \sigma_k(\vec{u}^*(\vec{x}^0))$,

$$\chi = (\kappa_2 + 1)\frac{\mu_2(\kappa_1 - 1) - \mu_1(\kappa_2 - 1)}{8\mu_1(\kappa_1 - 1)}(\sigma_1 + \sigma_2)C_1 -$$

$$- \frac{(\kappa_2 + 1)(\mu_2 - \mu_1)}{4\mu_1}(\sigma_1 - \sigma_2)(C_2 \cos\beta - C_3 \sin\beta).$$

The function χ depends on $\beta \in [0, \pi]$ and $\xi \in [0, 1]$, therefore the inequality 23 will be satisfied if

$$\chi_2(\sigma_1, \sigma_2, \mu_1, \mu_2, \kappa_1, \kappa_2) \geq \zeta, \tag{25}$$

where

$$\chi_2 = \min \chi(\sigma_1, \sigma_2, \mu_1, \mu_2, \kappa_1, \kappa_2, \beta, \xi), \ \ \beta \in [0, \pi], \ \xi \in [0, 1]. \tag{26}$$

The left-hand side of the inequality 24 will be equal to

$$A_2(\vec{u}^*, \vec{u}^0) - A_1(\vec{u}^*, \vec{u}^0) = \chi(\sigma_1, \sigma_2, \mu_2, \mu_1, \kappa_2, \kappa_1, \beta, \xi).$$

The necessary Weierstrass condition will be satisfied if

$$\chi_1(\sigma_1, \sigma_2, \mu_2, \mu_1, \kappa_2, \kappa_1) \leq \zeta, \tag{27}$$

where

$$\chi_1 = \max \chi(\sigma_1, \sigma_2, \mu_2, \mu_1, \kappa_2, \kappa_1, \beta, \xi), \ \ \beta \in [0, \pi], \ \xi \in [0, 1]. \tag{28}$$

In general case the problem 26, 27 may not be exactly solvable, but, for instance, for $\mu_1 = 0$, $\mu_2 = \mu$, $\kappa_2 = \kappa$ the problem 26 have the solution which is got for $\beta = 0$ and

$$\xi = \begin{cases} (\sigma_1 + \sigma_2)(\sigma_1 - \sigma_2)^{-1}, & -1 \leq \sigma_1 \sigma_2^{-1} \leq 0, \\ (\sigma_1 - \sigma_2)(\sigma_1 + \sigma_2)^{-1}, & 0 \leq \sigma_2 \sigma_1^{-1} \leq 1. \end{cases}$$

Here $\sigma_1^2 \geq \sigma_2^2$. Thus, the Weierstrass condition 25 takes the form

$$\begin{aligned} A(\vec{u}^*, \vec{u}^*) - 4\kappa\sigma_1\sigma_2 &\geq \zeta, \ -1 \leq \sigma_1\sigma_2^{-1} \leq 0, \\ A(\vec{u}^*, \vec{u}^*) + 4\sigma_1\sigma_2 &\geq \zeta, \ 0 \leq \sigma_2\sigma_1^{-1} \leq 1. \end{aligned} \tag{29}$$

Inserting $\underline{\varepsilon}^0$ from 21, 22 into the left-hand side of the inequality 23, we get for $N = 3$

$$A_2(\vec{u}^0, \vec{u}^*) \ - \ A_1(\vec{u}^0, \vec{u}^*) = \sigma^T \cdot \left(E - \frac{\mu_1}{\mu_2}\Lambda_1 \cdot \Lambda_2^{-1} \right) \cdot \tag{30}$$

$$\cdot \ (2\mu_1 E - 2\mu_2\Lambda_1 \cdot P \cdot Q^{-1}) \cdot \Lambda_1 \cdot (E - P \cdot Q^{-1} \cdot \Lambda_2) \cdot \sigma \ +$$

$$+ \ 2\left(1 - \frac{\mu_1}{\mu_2}\right)(B_{12}\sigma_{12}^2 + B_{23}\sigma_{23}^2 + B_{31}\sigma_{31}^2) \geq \zeta.$$

This inequality must be satisfied for any disposition of the ellipsoid about the main axes of the stress-tensor $\underline{\sigma}(\vec{u}^*(\vec{x}_0))$. Denoting the matrix of cosines between $\vec{e}_k$ and the main axes of the stress-tensor $\underline{\sigma}(\vec{u}^*(\vec{x}_0))$ by $\underline{\gamma}$ (γ_{ij} is the cosine of angle between $\vec{e}_i$ and the direction $\sigma_j(\vec{u}^*(\vec{x}_0))$), we obtain

$$\sigma_{ij} = \gamma_{ik}\gamma_{jk}\sigma_k.$$

Let's introduce the Euler's angles (the precession, nutation and pure rotation angles) and express γ_{ij} by these angles:

$$
\begin{aligned}
\gamma_{11} &= \cos\beta_1\cos\beta_3 - \sin\beta_1\cos\beta_2\sin\beta_3, \\
\gamma_{12} &= -\cos\beta_1\sin\beta_3 - \sin\beta_1\cos\beta_2\cos\beta_3, \\
\gamma_{13} &= \sin\beta_1\sin\beta_2, \\
\gamma_{21} &= \sin\beta_1\cos\beta_3 + \cos\beta_1\cos\beta_2\sin\beta_3, \\
\gamma_{22} &= -\sin\beta_1\sin\beta_3 + \cos\beta_1\cos\beta_2\cos\beta_3, \\
\gamma_{23} &= -\cos\beta_1\sin\beta_2, \\
\gamma_{31} &= \sin\beta_2\sin\beta_3, \\
\gamma_{32} &= \sin\beta_2\cos\beta_3, \\
\gamma_{33} &= \cos\beta_2,
\end{aligned}
$$

then the left-hand side of 30 may be denoted by

$$
\chi(\sigma_1,\sigma_2,\sigma_3,\mu_1,\mu_2,\nu_1,\nu_2,\rho,e,\beta_1,\beta_2,\beta_3).
$$

This function χ depends on $\beta_k \in [0,\pi]$, $e \in [0,1]$ and $\rho \in [1,\infty)$, therefore the inequality 23 will be satisfied if

$$
\chi_2(\sigma_1,\sigma_2,\sigma_3,\mu_1,\mu_2,\nu_1,\nu_2) \geq \zeta, \tag{31}
$$

where

$$
\begin{aligned}
\chi_2 &= \min \chi(\sigma_1,\sigma_2,\sigma_3,\mu_1,\mu_2,\nu_1,\nu_2,\rho,e,\beta_1,\beta_2,\beta_3), \\
&\beta_k \in [0,\pi],\ e \in [0,1],\ \rho \in [1,\infty).
\end{aligned} \tag{32}
$$

The left-hand side of the inequality 24 will be equal to

$$
\chi(\sigma_1,\sigma_2,\sigma_3,\mu_2,\mu_1,\nu_2,\nu_1,\rho,e,\beta_1,\beta_2,\beta_3).
$$

The necessary Weierstrass condition will be satisfied if

$$
\chi_1(\sigma_1,\sigma_2,\sigma_3,\mu_2,\mu_1,\nu_2,\nu_1) \leq \zeta, \tag{33}
$$

where

$$
\begin{aligned}
\chi_1 &= \max \chi(\sigma_1,\sigma_2,\sigma_3,\mu_2,\mu_1,\nu_2,\nu_1,\rho,e,\beta_1,\beta_2,\beta_3), \\
&\beta_k \in [0,\pi],\ e \in [0,1],\ \rho \in [1,\infty).
\end{aligned} \tag{34}
$$

The problems 32, 34 may not be exactly solvable for any values of μ_1, μ_2, ν_1, ν_2, but for $\mu_1 = 0$, $\mu_2 = \mu$, $\nu_2 = \nu$ the inequality takes the form

$$
A(\vec{u}^*,\vec{u}^*) + \psi \geq \zeta,
$$

where the function $\frac{\psi}{\sigma_1^2}$ is shown at Figure 1 (it is supposed that $\sigma_1^2 \geq \sigma_2^2 \geq \sigma_3^2$), where $\alpha_1 = \frac{\sigma_2}{\sigma_1}$, $\alpha_2 = \frac{\sigma_3}{\sigma_1}$, $\mu = 2\cdot 10^6 \text{kg/cm}^2$, $\nu = 0.3$.

456
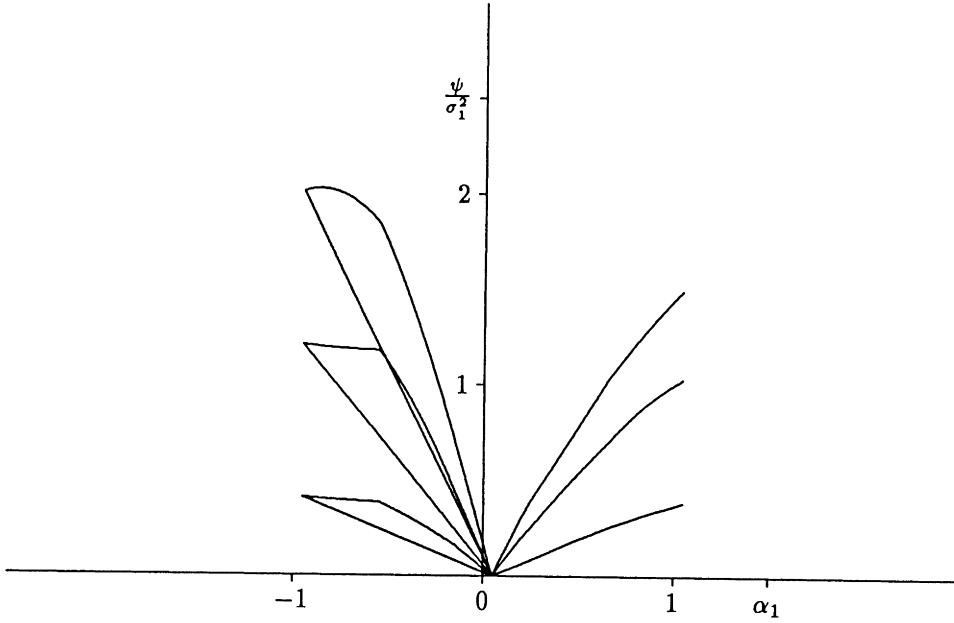
Figure 1

References

[1] A. I. Lurie. *The elasticity theory*. Nauka, 1970. In Russian.

[2] L. V. Petukhov. On optimal problems of the elacticity theory with unknown boundaries. *Applied Mathematics and Mechanics*, 2:231–236, 1986.

[3] L. V. Petukhov. Optimal elastic domains of maximal stiffness. *Applied Mathematics and Mechanics*, 1:88–95, 1989.

[4] J. N. Podylchuc. *Boundary problems of statics of elastic bodies*. Naukova Dumka, 1984. In Russian.

457

On Implementation of Partial Relaxation for Optimal Structural Compliance Problems.

Robert Lipton

Department of Mathematical Sciences, Worcester Polytechnic Institute, 100 Institute Road, Worcester, MA 01609

Abstract

The partial relaxation for optimal compliance design is independent of whether the underlying elastic problem is formulated in terms of displacements or strains. For the purposes of numerical experimentation and computation it may be advantageous to formulate optimal design problems in terms of displacements as is done in [8]. The relaxed problem delivered by the displacement based formulation is of min–min–max type. Because of this, efficient numerical implementation is hampered by the order of the last two min–max operations. We show here that the last two min–max operations may be exchanged facilitating an efficient numerical algorithm. We remark that the rigorous results given here corroborate the numerical methods and experiments given in [8].

1. INTRODUCTION

It is now well known that optimal design of structures made from two dissimilar elastic materials may involve zones of composite formed from the two constituent materials, see [4,9,13,15]. This observation motivates extension of the design space to incorporate the effective elastic properties of composites (see [13,15]). For many problems the design space need only be extended to include elastic composites with certain preferred extremal stiffness properties. This selective extension of the design space is commonly known as partial relaxation, (c.f. [11]).

In this paper we shall consider partial relaxation for problems of compliance optimization for 3 dimensional structures made from two isotropic materials with elasticities specified by shear and bulk moduli μ_i, κ_i $i = 1,2$ given by

$$C_i = 2\mu_i P_s + 3\kappa_i P_h \tag{1.1}$$

such that $\mu_2 \geq M_1$, $\kappa_2 \geq \kappa_1$. Here, P_s and P_h are the projections onto deviatoric and hydrostatic strains respectively. The results here apply equally well to the two dimensional design problems.

We suppose that the relatively stiff material characterized by C_2 is more costly.

Therefore, our goal is to minimize the compliance over all material layouts subject to a constraint on the amount of expensive material. The underlying elastic problem can be formulated variationally either in terms of stresses or elastic displacements.

It is easily seen (see section 2) that the partial relaxation for this problem is given by the well known extremal class of effective elastic tensors corresponding to finite rank laminar microstructures see, [2], [10], [11], and [14]. The relaxation is independent of the formulation of the underlying elastic problem.

For purposes of numerical experimentation and computation it may be advantageous to formulate the optimization problem in terms of displacements. The relaxed variational problem delivered by the displacement based approach is of min–min–max type, see (2.15). Because of this, an efficient numerical scheme is hampered by the order of the last two min–max operations. In this paper we provide a saddle point theorem justifying the exchange, see Theorem 3.2. The saddle point theorem is established with the aid of a convexity property enjoyed by the effective tensors of finite rank laminates (see Theorem 3.1) and the use of a tensor valued family of Young measures, see [16].

Once the exchange is made the compliance problem is of min–max–min type and the right most minimization reduces to the minimization of a local energy density at each point in the structural domain. This feature is computationally attractive, since the minimization of the local energy density can be done analytically, see Theorem 2.1. This saddle point theorem and max–min exchange has been incorporated in the recently developed numerical methods given in [8].

We illustrate the relationship between the relaxed Lagrangian for the displacement problem and its counter part for the stress based problem. The relaxed integrands appearing in both Lagrangians are nonlinear functions of their arguments, nevertheless there exists a duality relaxation between the two Lagrangians, see Section 4. We remark that the min–max interchange theorem easily generalizes to multi–load problems. The associated saddle theorem and relations between partially relaxed Lagrangians are given in Section 5.

2. MATHEMATICAL FORMULATION OF THE PROBLEM

The compliance or work done in the structural domain against body forces and boundary tractions by the resulting elastic displacement "u" is given by

$$\ell(u) = \int_{\Omega} f \cdot u dx + \int_{\partial\Omega} g \cdot u dS, \tag{2.1}$$

where f is the distributed force density in $H^{-1}(\Omega)^3$ and g is the prescribed boundary traction in $H^{-1/2}(\partial\Omega)$. The displacement u is an element of $H^1(\Omega)^3$ and satisfies the equilibrium equations

$$-\operatorname{div}\underline{\sigma} = f \quad \text{in } \Omega, \tag{2.2}$$

$$\underline{\sigma} \cdot n = g \quad \text{on } \partial\Omega, \tag{2.3}$$

$$\underline{\sigma} = C(x)\underline{e}(u), \tag{2.4}$$

where $\underline{e}(u)$ is the strain tensor given by

$$\underline{e}(u) = \frac{1}{2}(u_{i,j} + u_{j,i}). \tag{2.5}$$

Here the structural layout is prescribed by piecewise constant elasticity tensor $C(x)$ given by

$$C(x) = \chi_1 C_1 + \chi_2 C_2, \tag{2.6}$$

where χ_1 is the indicator function of material–1 and $\chi_2 = 1 - \chi_1$.

The choices of body force and boundary tractions are consistent with the solvability requirement

$$\int_\Omega f \cdot v dx - \int_{\partial\Omega} g \cdot v ds = 0 \tag{2.7}$$

for all $v \in C$, where

$$C = \{v : \underline{e}(v) = 0\}. \tag{2.8}$$

We consider the problem of minimizing the compliance over all layouts of materials–1 and 2 subject to a volume constraint on the stiffer and more expensive material 2. We note that a particular layout is specified by $C(x)$ and the volume constraint on material–2 is given by

$$v_2 = \int_\Omega \chi_2 dx. \tag{2.9}$$

The minimum compliance problem takes the form

$$\left.\begin{array}{l} \min_{C(x)} \ell(u) \\[4pt] \text{subject to: } u \text{ satisfying the equilibrium} \\[4pt] \text{conditions (2.2)–(2.5), and volume constraint,} \\[4pt] v_2 = \int_\Omega \chi_2 dx. \end{array}\right\} \tag{2.10}$$

Here we may view the above problem as one of distributed parameter optimal control, where the control is $C(x)$. Problem (2.10) can be written variationally over the space $H^1(\Omega)^3$ of admissible displacement fields as

$$\min_{C(x)} \ \max_{u \in H^1(\Omega)^3} \left\{ 2\ell(u) - \int_\Omega C(x)\underline{e}(u){:}\underline{e}(u)dx + \lambda v_2 \right\}. \tag{2.11}$$

Here λ denotes the lagrange multiplier associated with the volume fraction constraint. Alternatively problem (2.10) may be written variationally over the space "K" of admissible stress fields $\underline{\tau}$ as

$$\min_{C(x)} \quad \min_{\tau \underline{\epsilon} K} \left\{ \int_\Omega C^{-1}(x)\underline{\tau} : \underline{\tau} \; dx + \lambda \; v_2 \right\}. \tag{2.12}$$

Here K is given by

$$K = \begin{cases} \underline{\tau} \; \text{in} \; L^2(\Omega, S_3) \; \text{such that} \; -\text{div} \; \underline{\tau} = f \; \text{in} \; \Omega \\ \text{and} \; \underline{\tau} \cdot n = g \; \text{on} \; \partial\Omega. \end{cases}$$

It is well known from the work of (see, [4,13,15]), that problems of the type given by (2.10)–(2.12) are ill posed and require relaxation. This relaxation is accomplished through the extremal class of composites known as finite rank stiff laminates. The set of associated effective tensors is denoted by $\overline{GL}_{\theta_2}$ and the partially relaxed problem becomes

$$R = \min_{\theta_2 \epsilon L^\infty(\Omega,[0,1])} \quad \min_{\underline{\tau} \epsilon K} \int_\Omega [H(\tau.x) + \lambda\theta_2(x)]dx. \tag{2.13}$$

where

$$H(\tau,x) = \min_{C\epsilon\overline{GL}_{\theta_2}(x)} \{C^{-1}\underline{\tau} : \underline{\tau}\}. \tag{2.14}$$

Applying duality in (2.13) one may also argue that finite rank stiff laminates provide the partial relaxation for the compliance optimization problem given in displacement formulation. We find for this case that the partially relaxed problem is given by

$$\min_{\theta_2 \epsilon L^\infty(\Omega,[0,1])} \min_{C\epsilon\overline{GL}_{\theta_2}(x)} \max_{u\epsilon H^1(\Omega)^3} \left\{ 2\ell(u) + \int_\Omega [\lambda\theta_2(x) - C(x)\underline{e}(u):\underline{e}(u)]dx \right\}. \tag{2.15}$$

For the purposes of numerical implementation it is advantageous to switch the orders of minimization and maximization. Indeed if the last two operations are interchanged the subsequent minimization may be done analytically, see [8]. In what follows we see that it is possible to exchange the two right most operations of min–max, see Theorem 3.2. In this way we arrive (see Section 3) at the result.
Theorem 2.1. The partial relaxation for the displacement based optimal compliance design problem (2.11) is given by

$$\min_{\theta_2 \epsilon L^\infty(\Omega,[0,1])} \max_{u\epsilon H^1(\Omega)^3} \{2\ell(u) + \int_\Omega [\lambda\theta_2(x) + F(\underline{e}(u),x)]dx\}, \tag{2.16}$$

where for any constant strain ζ we have

$$F(\zeta,x) = - \max_{C\epsilon\overline{GL}_{\theta_2}(x)} C\zeta : \zeta . \tag{2.17}$$

We observe that $F(\zeta,x)$ is a nonlinear function of the strain variable ζ. Here $F(\zeta,x)$ can be computed analytically or numerically using formula (3.1). We remark that $F(\zeta,x)$ has been calculated explicitly for the two dimensional case in [8]. Similar strain energy functions have been computed earlier in the context of three dimensional incompressible elasticity and two dimensional elasticity, see [1], [7], and [10].

3. CONVEXITY PROPERTIES OF FINITE RANK LAMINATES AND A SADDLE POINT THEOREM.

The necessary new tool for deducing the saddle point theorem is a convexity property enjoyed by the effective elastic tensors for finite rank laminar microstructures. Before stating the convexity property we introduce the formulas for the effective tensors of finite rank laminar composites. They are given by

$$\overline{C} = C_2 - (1-\theta_2)[(C_2-C_1)^{-1} - \theta^2 \overset{*}{T}_2]^{-1} \tag{3.1}$$

and

$$\underline{C} = C_1 + \theta_2\left[(\mathbb{C}_2-\mathbb{C}_1)^{-1} + (1-\theta_2)\overset{*}{T}_1\right]^{-1} \tag{3.2}$$

for stiff and compliant composites respectively. Here the tensors $\overset{*}{T}_i$, $i = 1,2$ are of the form

$$\overset{*}{T}_i = \sum_{r=1}^{j} \rho_r \hat{\Gamma}_i(n_r), \ 1 \leq j < \infty, \tag{3.3}$$

where

$$\rho_r \geq 0 \ \text{and} \ \sum_{r=1}^{j} \rho_r = 1 \tag{3.4}$$

and $\hat{\Gamma}_i(v)$ are tensor valued functions of vectors "v" defined on the unit sphere S^2 given by

$$\hat{\Gamma}_i(v)_{mnop} = \frac{1}{4\mu_i}(v_m v_o \delta_{qs} + v_m v_p \delta_{mn} + v_n v_o \delta_{mp} + v_n v_p \delta_{mo})$$

$$+ (\frac{3}{3\kappa_i + 2\mu_i} - \frac{1}{\mu_i})v_m v_n v_o v_p, \quad i = 1,2. \tag{3.5}$$

These formulas were derived in [6] and have been rewritten in notation convenient for this exposition.

We introduce the convex sets of tensors Δ_1, Δ_2 formed by considering all convex combinations $\overset{*}{T}_1$ and $\overset{*}{T}_2$ delivered by formula (3.3). To understand the geometry of the sets Δ_1 and Δ_2 we regard $\hat{\Gamma}_1(v)$ and $\hat{\Gamma}_2(v)$ given by (3.5) as tensor valued maps mapping the surface of the unit sphere to surfaces in the space F of fourth order tensors. It is now evident from (3.3) that Δ_1 and Δ_2 correspond to the closed, bounded convex hulls of these surfaces.

We indicate the dependence of the effective tensors $\overline{C}$ and $\underline{C}$ on $\overset{*}{T}_1$, $\overset{*}{T}_2$ and θ_2 by writing

$$\overline{C} = \overline{C}(\overset{*}{T}_2, \theta_2) \tag{3.6}$$

$$\underline{C} = \underline{C}(\overset{*}{T}_1, \theta_2) \tag{3.7}$$

For any finite set of 3×3 symmetric matrices $\zeta^1, \zeta^2, ..., \zeta^\ell, \ell < \infty$ we form

$$\overline{f}(\overset{*}{T}_2) = \sum_{j=1}^{\ell} (\overline{C}(\overset{*}{T}_2, \theta_2)\zeta^j : \zeta^j) \tag{3.8}$$

and

$$\underline{f}(\overset{*}{T}_1) = \sum_{j=1}^{\ell} \underline{C}(\overset{*}{T}_1, \theta_1)\zeta^j : \zeta^j. \tag{3.9}$$

We now state the following convexity property for laminates.

Theorem 3.1. Convexity Property

For fixed θ_2 and for $\overset{*}{T}_1 \epsilon \Delta_1$ and $\overset{*}{T}_2 \epsilon \Delta_2$ the sum of energies $\overline{f}(\overset{*}{T}_2)$ is concave in $\overset{*}{T}_2$ and the sum $\underline{f}(\overset{*}{T}_1)$ is convex in $\overset{*}{T}_1$, i.e. for $\overset{*}{T}_2$ and $\overset{*}{T}_2'$ in Δ_2 and t in

[0,1] we have

$$\overline{f}(tT_2^* + ((1-t)T_2^{*\prime}) \geq t\overline{f}(T_2^*) + (1-t)\overline{f}(T_2^{*\prime}) \tag{3.10}$$

and for T_1^* and $T_1^{*\prime}$ in Δ_1 and t in [0,1] we have

$$\underline{f}(tT_1^* + (1-t)T_1^{*\prime}) \leq t\underline{f}(T_1^*) + (1-t)\underline{f}(T_1^{*\prime}). \tag{3.11}$$

Applying the convexity property and arguing as in [16] we obtain the following saddle point theorem.

Theorem 3.2

For fixed local volume fraction θ_2 in $L^\infty(\Omega,[0,1])$ and the Lagrangian $L(C,u)$ defined by

$$L(C,u) \equiv 2\ell(u) + \int_\Omega [\lambda\theta_2(x) - C(x)\underline{e}(u) : \underline{e}(u)]dx \tag{3.12}$$

we have

$$\min_{C\epsilon\overline{GL}_{\theta_2(x)}} \quad \max_{u \, \epsilon \, H^1(\Omega)^3} \quad L(C,u) = \max_{u\epsilon H^1(\Omega)^3} \quad \min_{C\epsilon\overline{GL}_{\theta_2(x)}} \quad L(C,u). \tag{3.13}$$

We remark that Theorem 2.1 follows immediately from Theorem 3.2. Indeed we may write

$$\min_{C\epsilon\overline{GL}_{\theta_2(x)}} \quad L(C,u) = 2\ell(u) + \int_\Omega [\lambda\theta_2(x) - \max_{C\epsilon\overline{GL}_{\theta_2(x)}} \{C(x)e(u):e(u)\}]dx$$

and Theorem 2.1 follows.

4. RELAXED LAGRANGIANS AND DUALITY

The saddle point Theorem 3.2 is used to provide a duality relation between partially relaxed Lagrangians appearing in the stress and displacement based optimal compliance design problems (2.13) and (2.16).
Indeed we have

Theorem 4.1

For prescribed volume fraction $\theta_2(x)$ in $L^\infty(\Omega,[0,1])$

$$\min_{\underline{\tau}\epsilon\kappa} \int_\Omega H(\underline{\tau},x)dx = \max_{u\epsilon H^1(\Omega)^3} \{2\ell(u) + \int_\Omega + \int_\Omega F(e(\underline{u}),x)dx\} \qquad (4.1)$$

where $H(\underline{\tau},x)$ and $F(\zeta,x)$ are nonlinear functions of $\underline{\tau}$ and ζ and are given by formulas (2.14) and (2.17) respectively.

Explicit formulas for $H(\underline{\tau},x)$ and $F(\zeta,x)$ have been worked out for the two dimensional design problem, and are given in [1], [7], and [8].

Proof. The proof of Proposition 4.1 follows from the following string of equalities

$$\min_{\underline{\tau}\epsilon K} \int_\Omega H(\underline{\tau},x)dx = \min_{\underline{\tau}\epsilon K} \min_{C\epsilon\overline{GL}^-_{\theta_2}(x)} \int_\Omega C^{-1}\underline{\tau}:\underline{\tau}\,dx$$

$$= \min_{C\epsilon\overline{GL}^-_{\theta_2}} \min_{\underline{\tau}\epsilon k} \int_\Omega C^{-1}\underline{\tau}:\underline{\tau}\,dx$$

$$= \min_{C\epsilon\overline{GL}^-_{\theta_2}(x)} \max_{u\epsilon H^1(\Omega)^3} \{2\ell(u) - \int_\Omega Ce(u):e(u)dx\}$$

$$= \max_{u\epsilon H^1(\Omega)^3} \min_{C\epsilon\overline{GL}^-_{\theta_2}(x)} \{2\ell(u) - \int_\Omega Ce(u):e(u)dx\}$$

$$= \max_{u\epsilon H^1(\Omega)^3} \{2\ell(u) + \int_\Omega F(\underline{e}(\underline{u}),x)dx\}. \qquad (4.2)$$

The second to last equality in (4.2) is an application of Theorem 3.2.

We note that the integrands $H(\tau,x)$ and $F(\zeta,x)$ have been portrayed in the literature as nonlinear constitutive laws for *smart* elastic materials, (see [8,11]). These materials are *smart* in the sense that they provide the optimal local elastic response for prescribed stress or displacement fields. We point out that Proposition 4.1 provides dual variational principles for such materials.

5. MULTI–LOAD PROBLEMS

Theorem 2.1 and Theorem 4.1 can be easily extended to multi–load optimal compliance design problems. Since the extension is straight forward and uses the techniques developed in earlier sections we shall only state the results.

We consider N load cases prescribed by the body force densities f^i and boundary tractions g^i, $i = 1,2,...,N$. Associated with each load case (f^i,g^i) is a displacement

field u^i satisfying equilibrium equations of the kind given by (2.2)–(2.6).
We consider minimizing a weighted sum of the compliances

$$\dot{\ell}(u^i) = \int_\Omega \dot{f}^i \cdot u^i dx + \int_{\partial\Omega} g^i \cdot u^i dS \tag{5.1}$$

given by

$$L = \sum_{i=1}^{N} w_i \dot{\ell}(u^i) \tag{5.2}$$

where $w_i \geq 0$ $i = 1,...,N$ and $\sum_{i=1}^{N} w_i = 1$. The goal here is to minimize L subject to
a volume constraint on the stiff elastic material characterized by elasticity tensor C_2.
Defining $U^N = \otimes^N H^1(\Omega)^3$ the constrained optimization problem written in terms of
displacements has the variational formulation

$$\min_{C(x)} \max_{(u^1,u^2,...,u^N)\epsilon U^N} [\sum_{i=1}^{N} w_i\{2\dot{\ell}(u^i) - \int_\Omega C(x)\underline{e}(u^i) : \underline{e}(u^i)dx\} + \lambda v_2]; \tag{5.3}$$

where v_2 is the volume of stiff material in the design and λ is the Lagrange
multiplier associated with the volume constraint. For N independently chosen
constant strains ζ^i $i = 1,...,N$ we define the function $J(\zeta^i,\zeta^2,...,\zeta^N,x)$ by

$$J(\zeta^i,\zeta^2,...,\zeta^N,x) = -\max_{C\epsilon\overline{GL}_{\theta_2(x)}} \sum_{i=1}^{N} w_i C\zeta : \zeta^i . \tag{5.4}$$

Then the partial relaxation is given by

Theorem 5.1.
The partial relaxation for the multi–load constrained compliance optimization
problem (6.3) is

$$\min_{\theta_2(x)\epsilon L^\infty(\Omega,[0,1])} \quad \max_{(u^1,u^2,\ldots,u^N)\epsilon U^N} \left[\sum_{i=1}^{N} 2w_i \dot{\ell}(u^i) + \right.$$

$$\left. + \int_\Omega [J(\underline{e}(u^1), \underline{e}(u^2),\ldots,e(u^N),x) + \lambda\theta_2(x)]dx \right] \qquad (5.5)$$

Theorem 5.1 is the extension of Theorem 2.1 to the multi–load case. Defining $K^N = \circledast^N K$ the constrained optimization problem written in terms of stresses has the variational formulation

$$\min_{C(x)} \quad \min_{(\underline{\tau}^1,\underline{\tau}^2,\ldots,\underline{\tau}^N)\epsilon K^N} \left\{\sum_{i=1}^{N} w_i \int_\Omega C^{-1}(x)\tau^i : \tau^i dx + \lambda V_2\right\}. \qquad (5.6)$$

Arguing as in [11] or as in Section 2 the partial relaxation of the compliance problem given in the stress based variational formulation is

$$\min_{\theta_2(x)\epsilon L^\infty(\Omega,[0,1])} \quad \min_{(\underline{\tau}^1,\underline{\tau}^2,\ldots,\underline{\tau}^N)\epsilon K^N} \left[\int_\Omega R(\tau^1,\tau^2,\ldots,\tau^N,x) + \lambda\theta_2(x)dx \qquad (5.7)\right.$$

where for any set of constant strains $\underline{\tau}^1,\ldots,\underline{\tau}^N$

$$R(\tau^1,\tau^2,\ldots,\tau^N,x) = \min_{C\epsilon\overline{GL}_{\theta_2(x)}} \sum_{i=1}^{N} w_i C^{-1}\tau^i : \tau^i. \qquad (5.8)$$

One also has a duality relation between the relaxed Lagrangians for both formulations.

Theorem 5.2.

For prescribed volume fraction $\theta_2(x)$ in $L^\infty(\Omega,[0,1])$

$$\min_{(\underline{\tau}^1,\underline{\tau}^2,\ldots,\underline{\tau}^N)\epsilon K^N} \left[\int_\Omega R(\tau^1,\tau^2,\ldots,\tau^N,x)dx = \right.$$

$$\max_{(u^1,u^2,\ldots,u^N)\epsilon U^N} \left\{\sum_{i=1}^{N} 2w_i \dot{\ell}(u^i) + \int_\Omega J(\underline{e}(u^1), \underline{e}(u^2),\ldots,e(u^N),x)dx\right\}. \qquad (5.9)$$

6. CONCLUSION

We remark that in general it is not possible to exchange minimization over volume fraction $\theta_2(x)$ and maximization over displacement fields in (2.16) or (5.5). This is due to the fact that the function resulting integrand is not quasiconcave for all values of the Lagrange multiplier "λ". This observation is seen in the numerical work of Jog, Haber, and Bendsoe [8].

6. REFERENCES

1. Allare, G. and Kohn, R.V., "Explicit optimal bounds on the elastic energy of a two–phase composite in two space dimensions," to appear in Q. Appl. Math., 1993.

2. Avellaneda, M., "Optimal bounds and microgeometries for elastic two–phase composites," SIAM J. Appl. Math. <u>47</u>, 1987, pp. 1216–1228.

3. Ball, J.M., "A version of the fundamental theorem for Young measures, in *Partial Differential Equations and Continuum Models of Phase Transitions* (ed. M. Rascle, D. Serre, and M. Slemrod), pp. 207–215. Springer Verlag, 1989.

4. Cheng, K.T., and Olhoff, N., "An investigation concerning optimal design of solid elastic plates," Int. J. Solids Structures, 1981, <u>17</u>, pp. 305–323.

5. Ekeland, I., and Teman, R. *Convex Analysis and Variational Problems*, North–Holland, Amsterdam, 1976.

6. Francfort, G.A., and Murat, F. "Homogenization and optimal bounds in linear elasticity," Arch. Rational Mech. Anal. <u>94</u>, 1986, pp. 307–334.

7. Gibianskii, L., and Cherkaev, A., "Design of composite plates of extremal rigidity; Ioffe Physicotechnical Institute, Preprint, 1984, (in Russian).

8. Jog. C.S., Haber, R.B., and Bendsoe, M.P., "A displacement–based topology design method with self–adaptive materials," in *Topology Design of Structures* (ed. M.P. Bendsoe), Kluwer, (to appear in 1992).

9. Klosowicz, B., and Lurie, K.A., "On the optimal non–homogeneity of a torsional elastic bar," Achieves of Mechanics, <u>24</u>, No. 2, 1971, pp. 239–249.

10. Kohn, R.V., and Lipton, R., "Optimal bounds for the effective energy of a mixture of isotropic, incompressible, elastic materials," Arch. Rational Mech. Anal. <u>102</u>, 1988, pp. 331–350.

11. Kohn, R., Recent progress in the mathematical modeling of composite materials," in *Composite Material Response: Constituitive Relations and Damage Mechanisms*, G. Sih et al, eds, Elsevier, 1988, pp. 155–177.

12. Lurie, K.A., Cherkaev, A.V., and Fedorov, A.V., "Regularization of optimal design problems for bars and plates," J. Opt. Theory Appl. <u>37</u>, 1982, pp. 499–523.

13. Lurie, K.A., and Cherkaev, A.V., "Optimal structural design and relaxed controls," Opt. Cont. Appl. and Methods <u>4</u>, 1983, p. 387.

14. Milton, G.W., and Kohn, R.V., "Variational bounds on the effective moduli of anisotropic composites," J. Mech. Phys. Solids Vol. 36, No. 6, 1988, pp. 597–629.

15. Murat, F., and Tartar, L., "Calcul des variations et homogénéisation," in *Les Methodes de l'Homogénéisation: Théorie et Applications en Physique,* Coll. de la Dir. des Etudes et Recherches de Electr. de France, Eyrolles, Paris, 1985, pp. 319–370.

16. Lipton, R., "On partial relaxation for problems of structural design," submitted to J.O.T.A.

Effects in the Optimization Using Brittle and Ductile Materials

H.A. Eschenauer and T. Vietor

Research Center for Multidisziplinary Analyses and Applied Structural Optimization (FOMAAS), Institute of Mechanics and Control Engineering, University of Siegen, D-W 5900 Siegen, Germany

Abstract

The use of advanced materials will increasingly gain importance in future developments of constructions in different disciplines. For this reason, the material behaviour in particular has to be considered when finding optimal layouts for components. Here, the different failure mechanisms of the applied materials must be taken into consideration. This paper presents a comparison between conventional, ductile materials and brittle ceramics as an example of an advanced material. In order to find a failure criterion which is characteristic for the material, stochastic models of the defects determining the failure of ceramic materials have been included. Two different approaches are compared. Because of the stochastic nature of the material parameters the classical deterministic optimization model is not sufficient. For this reason an augmented optimization procedure is introduced and tested for an example.

1. INTRODUCTION

The optimal layout of structures using advanced materials (e.g. ceramics, fibre-reinforced materials) calls for the augmentation of existing optimization procedures as well as for an multidisciplinary cooperation of mechanics, material sciences and design. Apart from considering the sometimes substantially diverging material characteristics, it becomes necessary to precisely describe the failure mechanisms of the different materials. An increased range of application is characteristic of one advanced material, namely ceramics which belong to the group of brittle materials. So far, results have been obtained in the field of structural optimization predominantly for the use of ductile materials. This paper presents first the optimal layout of a cantilever disc using the example of a specific ceramic (Al_2O_3). A comparison is made between the results for this brittle material and ductile materials (steel, aluminium). The goal is to find some basic effects of brittle materials on the optimal shape and compare these to the effects of ductile materials. In the following part the definition of the stochastic optimization problem is given and one possible method for solving this is introduced.

Shape optimization of structures is a well known problem which LAGRANGE (1736-1813) and CLAUSEN (1801-1885) already applied to bending beams using variational principles. But only the introduction of efficient and flexible analysis procedures like the Finite-Element (FE) Analysis allowed the application of the shape optimization to a wide range of problems.

FREUDENTHAL first dealt in his paper [10] with a probabilistic procedure for deriving a failure criterion for brittle materials. Here, the term *failure probability* is introduced,

and basic physical phenomenona of brittle materials are described mathematically. A large number of papers based upon this paper, i.g. EVANS [9] and BATDORF, CROSE [1], describe ways of calculating failure criteria for ceramic materials. KOSKI, SILVEN-NOINEN [12] show the result of a shape optimization using brittle materials.

2. FAILURE OF BRITTLE MATERIALS

2.1. Comparison of Ductile and Brittle Materials

In order to classify ductile and brittle materials, the value of the *critical stress intensity factor* K_{IC} which is a real material parameter proved useful. For a Griffith-crack in the one-dimensional stress state and the so-called crack opening mode I the stress intensity factor is given by the equation

$$K_{IC} = \sigma_c \sqrt{\pi x} \tag{1}$$

with σ_c as the critical stress value and x as the half length of the Griffith-crack. For brittle materials a range of $K_{IC} \leq 10MN/m^{3/2}$ and for ductile materials a range of $K_{IC} \geq 25MN/m^{3/2}$ is assumed. Correspondingly, the material behaviour lies between brittle and ductile for $10MN/m^{3/2} \leq K_{IC} \leq 25MN/m^{3/2}$.

Conventional Failure Criteria

For the conventional layout of components failure criteria are established by means of strength hypotheses which transform a multi-axial stress state into an equivalent one-axial stress state. With the obtained equivalent stress a statement concerning failure can be made by comparison with characteristic values generally determined under a one-axial stress. The type of hypothesis to be used depends on the failure mechanism which ultimately depends on the material.

a) Ductile materials

In the case of yielding before failure of a component the maximum strain energy theory according to LEVY, HUBER, VON MISES leads to the following expression for the equivalent stress:

$$\sigma_e = \frac{1}{\sqrt{2}} \sqrt{\left[(\sigma_{xx} - \sigma_{yy})^2 + (\sigma_{yy} - \sigma_{zz})^2 + (\sigma_{zz} - \sigma_{xx})^2 + 6(\tau_{xy}^2 + \tau_{yz}^2 + \tau_{zx}^2) \right]}. \tag{2}$$

b) Brittle materials

In the case of material failure caused by rupture perpendicular to the direction of the principal stress (e.g. cast materials), the normal stress hypothesis according to Rancine and Lame is valid. Here, the highest principal normal stress determines the failure:

$$\sigma_e = \sigma_1, \ \ \sigma_1 = \max_i \sigma_i. \tag{3}$$

This hypothesis can be applied only in parts to ceramics as it does not consider the stochastic distribution of defects which determine the failure.

2.2. Failure Criteria for Brittle Materials

As mentioned above, there is only a limited applicability of the stress hypotheses to ceramic materials. In the following the stochastic failure criterion used here shall be briefly introduced and derived.

Simple Approach

The derivation is based upon the following assumptions:

Assumption 1

The material behaviour is isotropic and all flaws are oriented perpendicular to the external load so it is the so-called crack opening mode I. Each component under consideration contains defects of different size. There is no mutual influence between the stress fields of the single defects. This means that the component can be subdivided in such a way that each volume element contains only one defect. Each defect therefore determines the strength of its surrounding volume element.

Assumption 2

The yield stress of a volume element is determined by means of the Griffith-theory (1921) according to (1):

$$\sigma_c x^{1/2} = const. \tag{4}$$

Assumption 3

The strenght of the whole component is determined by the weakest volume element. This corresponds to the Weakest-Link-Theory [10].

With the given distribution of the stochastic half crack length x given, the distribution of the failure stresses σ_c can be calculated from equation (4). As only the maximum defects determine the failure, the initial distribution is not drawn upon for the distribution of the crack length, but an extreme value distribution is used instead. Because of its favourable correspondence to reality the extreme value distribution of the polynomial type is used:

$$D(x) = \exp\left[-\left(\frac{x}{\mu}\right)^{-\alpha}\right], \tag{5}$$

where μ is the expected value of the crack length and α the form parameter of the distribution. By means of the stated assumptions and using the calculation of probability for the one-dimensional stress-state, the following expression for the reliability $P_r = 1 - P_f$ of a volume element i can be derived [3]

$$P_{ri} = \exp\left[-\left(\frac{\sigma}{\sigma_0}\right)^m\right], \tag{6}$$

where m is the so-called WEIBULL-modulus. The survival probability of the component can then be calculated as the product of the element reliabilities

$$P_r = \prod_i P_{ri} = \exp\left[-\sum_{\Delta V_i}\left(\frac{\sigma_i}{\sigma_0}\right)^m\right]. \tag{7}$$

For $\Delta V_i \rightarrow 0$ follows

$$P_r = \exp\left[-\frac{1}{V_0}\int_V \left(\frac{\sigma}{\sigma_0}\right)^m dV\right]. \tag{8}$$

Generalizing to the three-dimensional stress state yields after reformulation

$$P_f = 1 - \exp(-X) \tag{9}$$

with

$$X = \left(\frac{1}{m}!\right)^m \left(\frac{1}{\sigma_c}\right)^m \frac{1}{V_c} \int_V (\sigma_1^m + \sigma_2^m + \sigma_3^m) dV \tag{10}$$

and the material parameters σ_c and V_c. This failure model does not consider the mutual influence of the principal stresses on the failure probability. Thus, for higher accuracy in practical applications, an extension of the theory presented here is necessary.

Extended Approach

For improving the foregoing derivation additional assumptions are necessary:

Assumption 4

The material contains flaws with different orientations.

Assumption 5

The influence of the shape and size of the flaws to the failure is described with stress intensity factors. So it is possible to use different failure models.

For the description of the failure probability first one volume element containing only one flaw is considered. The flaw is critical if the stress value σ_{Ieq} is greater than a critical value σ_{Ic}. The value of σ_{Ieq} is calculated from the stress vector $\boldsymbol{\sigma}$ out of a failure criteria. A flaw is critical if its orientation lies between the solid angle Ω. The probability for the flaw lying in this angle is given with the equation

$$P_f(\Delta V_i) = \frac{\Omega(\boldsymbol{\sigma}, \sigma_{Ic})}{2\pi}. \tag{11}$$

For a volume element with a number of flaws greater than one the number of critical flaws is given with the equation

$$N_c = M\Delta V \frac{\Omega(\boldsymbol{\sigma}, \sigma_{Ic})}{2\pi}, \tag{12}$$

with M as the flaw density describing the mean number of flaws in the unit volume. For generalizing to the case of different sizes of the flaws the introduction of the function $N(\sigma_{Ic})$ is necessary giving the mean number of flaws with a strength lower than σ_{Ic} respectively the number of flaws greater the critical size a in the unit volume. With the density function $d(a)$ the following defintion is valid

$$N_c(\sigma_{Ic}) = M \int_a^\infty d(a)da = M(1 - D(a)). \tag{13}$$

The correlation between σ_{Ic} and a is described with K_{Ic} as the stress intensity factor. So it follows for the number of critical flaws in the range of $\sigma_{Ic} \leq \sigma \leq \sigma_{Ic} + d\sigma_{Ic}$

$$N_c(\sigma_{Ic} \leq \sigma \leq \sigma_{Ic} + d\sigma_{Ic}) = \Delta V_i \frac{dN(\sigma_{Ic})}{d\sigma_{Ic}} \frac{\Omega(\boldsymbol{\sigma}, \sigma_{Ic})}{2\pi} d\sigma_{Ic} \tag{14}$$

and for the total number of critical flaws in ΔV_i

$$N_i(\Delta V_i) = \Delta V_i \int_0^\infty \frac{dN(\sigma_{Ic})}{d\sigma_{Ic}} \frac{\Omega(\boldsymbol{\sigma}, \sigma_{Ic})}{2\pi} d\sigma_{Ic}. \tag{15}$$

With the assumption of a POISSON-distribution of the number k of flaws in the volume ΔV_i

$$P_k = \frac{N_i^k \exp(-N_i)}{k!} \tag{16}$$

for the reliability the equation

$$P_r(\Delta V_i) = P_{k=0} = \exp(-N_i) \tag{17}$$

is valid. For the complete volume the following expression follows:

$$P_r = \prod_i P_r(\Delta V_i) = \prod_i \exp(-N_i) = \exp\left(-\sum_i N_i\right). \tag{18}$$

After using equation (15), integration

$$P_r = \exp\left[-\int\limits_V \int\limits_0^\infty \frac{dN(\sigma_{Ic})}{d\sigma_{Ic}} \frac{\Omega(\sigma, \sigma_{Ic})}{2\pi} d\sigma_{Ic}\right] \tag{19}$$

and some further steps according to [1]

$$P_r(V) = \exp\left[-\int\limits_V \int\limits_0^{2\pi} \int\limits_0^{\frac{\pi}{2}} N(\sigma_{Ieq} = \sigma_{Ic})\sin\varphi\, d\varphi\, d\psi\, dV\right]. \tag{20}$$

For the function $N(\sigma_{Ieq} = \sigma_{Ic})$ there are different approaches. In many cases the assumption of a WEIBULL-distribution of the critical flaws is valid and leads to

$$N(\sigma_{Ic}) = \left(\frac{\sigma_{Ic}}{\sigma_{I0}}\right)^m. \tag{21}$$

In the following only the simple approach is used because the aim of this paper is to show only some basic effects of ceramics in comparison to ductile materials.

3. DEFINITION AND SOLUTION OF OPTIMIZATION PROBLEMS

3.1. General Stochastic Optimization Problem

Because of the stochastic nature of the material parameters and the design variables it is necessary to define the task as a stochastic optimization problem

$$\operatorname*{Min}_{\boldsymbol{x} \in D} \{\boldsymbol{f}_A(\boldsymbol{z})\}, \quad \boldsymbol{z}^T = (\boldsymbol{x}, \boldsymbol{p}), \tag{22}$$

$$f_{Ai} = k_1 E(f_i) + k_2 V(f_i), \tag{23}$$

$$D = \{\boldsymbol{x} \in R^n, P_{fi} = P[g_i(\boldsymbol{z}) < 0] < P_{imax} \ \forall i = 1, m_{st}; x_{il} \le x_i \le x_{iu} \ \forall i = 1, n\}, \tag{24}$$

with

f_{Ai}	:	augmented objective,
$\boldsymbol{z}$	:	vector of stochastic variables,
$\boldsymbol{x}$	:	vector of stochastic design variables,
$\boldsymbol{p}$	:	vector of stochastic parameters,
$E(f)$	:	expected value of the stochastic objective,
$V(f)$	:	variance of the stochastic objective,
k_1, k_2	:	weighting factors,
D	:	feasible domain,
P_{fi}	:	failure probability of the ith constraint,

P_{imax} : maximum feasible value for the failure probability,
m_{st} : number of stochastic constraints,
x_{il}, x_{iu} : lower and upper bounds for the design variables.

The failure probability is defined as

$$P_{fi} = P[g_i(z) < 0], \tag{25}$$

$$P_{fi} = \int_{D_i} d(z)dz, \quad D_i = \{z|g_i(z) < 0\}. \tag{26}$$

For solving the stochastic optimization problem different methods are possible. A survey to these is presented in [7]. Here the stochastic nature of the objectives is neglected. So the stochastic optimization problem is reduced to a problem with probabilistic constraints. These are calculated using an AFOSM-method which is shortly described in one of the following chapters.

For the calculation of the failure probabilities according to equations (25,26) an Advanced First Order Second Moment Method (AFOSM) is used. The necessary fundamentals, the used semi-anylytical sensitivity analysis and the augmentation using a special kind of transformation are described in [6]. For calculation of failure probabilities with high accuracy the transformation described by Wu [14] to standard-normally distributed variables is used in this paper. For low values of the standard deviation of the stochastic variables the simpler and easier to handle Normal-Tail-Transformation is sufficient. For the special example of a ceramic mirror this is shown in the following. In the AFOSM-procedure the actual failure surface is approximated by means of a linearization and only the first two moments of the failure conditions are used for the calculation. Here, the works by Hasofer and Lind [11] shall be mentioned as an example for a number of papers in this field. In this paper only the basic idea of this method is presented.

The transformation of the stochastic variables to independent, standard normally distributed variables $y = T(z)$ yields

$$P_{fi} = \int_{D_i} d(z)dz = \int_{\Delta_i} \prod_j \varphi(y_j)dy_j, \tag{27}$$

$$\Delta_i = \{y|h(y) < 0\}, \tag{28}$$

where $D_i \to \Delta_i$ is the transformation of the failure range and φ the density function of the standard normal distribution. The linear approximation of the boundary state function $h(y)$ in the point of maximum likelihood $y^\star$ yields

$$P_{fi} \approx \int_{\Delta_{il}} \prod_j \varphi(y_j)dy_j \approx \left\{ \begin{array}{c c} \Phi(-\beta) & | \quad h(\mathbf{o}) \geq 0 \\ \Phi(\beta) & | \quad h(\mathbf{o}) < 0 \end{array} \right. , \tag{29}$$

$$\Delta_{il} = \{y|l(y) < 0\}, \quad \beta : \underset{y}{\text{Min}} \left\{ \beta(y) = (y^T y)^{1/2} |h(y) = 0 \right\} \tag{30}$$

with the linearized boundary state function $l(y)$ in the point $y^\star$ and the standard normal distribution Φ. The optimization problem can be solved with the transformed variables y as well as with the original variables z. The latter case is characterized by the simpler description of the failure domain. The used transformation to independent, standard normal distributed variables determines the numerical effort for solving the optimization

problem and the accuracy of the failure probability.

3.2. Shape Optimization Problem

The shape optimization problem with muliple criteria can be formulated as follows [8]:

$$F^*[R^k(\xi^\alpha)] = \underset{R^k}{\text{Min}}\Big\{F[R^k(\xi^\alpha)] \,\Big|\, R^k(\xi^\alpha) \in G_R\Big\} \quad \forall k = 1, n_R, \tag{31}$$

$$\begin{aligned}
G_R = \Big\{R^k(\xi^\alpha) \in R^3 \,\Big|\, & H_i[R^k(\xi^\alpha)] = 0 \quad \forall i = 1, n_H, \\
& G_j[R^k(\xi^\alpha)] \geq 0 \quad \forall j = 1, n_G, \\
& R^{kl} \leq R^k \leq R^{ku} \quad \forall k = 1, n_R\Big\},
\end{aligned}$$

with

F	:	objective functional vector,
H_i, G_j	:	vector of equality and inequality constraint functional,
R^k	:	shape functions,
ξ^α	:	GAUSSians surface parameters,
R^{kl}, R^{ku}	:	lower and upper bounds of the shape functions,
G_R	:	set of feasible shape functions

and the assumption

$$R^k(\xi^\alpha) \approx \hat{R}^k(\xi^\alpha, x^k).$$

The optimal shape function is to be found so that the objective functional becomes minimal, considering the constraint functionals. This problem can be solved by means of direct and indirect solution procedures. The indirect procedures derive conditions for the optimal shape functions with the help of variational principles. The resulting differential equations have to be solved then. In the direct solution procedures the optimization problem is first of all transformed into a multicriteria optimization problem and then into a scalar optimization problem using preference strategies. The so-called SOP is solved by mathematical programming algorithms. The transformation is carried out by approach functions which describe a potentially large variety of shapes using free parameters. Obviously, the choice of shape functions limits the variety of solutions so that only an approach towards the optimal shape can be achieved. Especially various types of spline functions and the highly flexible Bezier functions have gained great importance as approach funtions.

4. AUGMENATIONS OF AN EXISTING OPTIMIZATION LOOP

Here two different augmentations of the optimization procedure SAPOP [2] are introduced. Firstly the procedure for stochastic optimization with the calculation of the reliability indices β_i and secondly the procedure for shape optimization.

4.1. Optimization procedure for stochastic optimization

The program system SAPOP is based upon the so-called "Three-Columns-Concept" consisting of structural model, optimization model and optimization algorithms. Fig. 1 shows the flow chart of the optimization procedure augmented by an AFOSM-method.

The figure presents that the integration of the AFOSM-method into an optimization procedure entails the interlocking of two optimization loops. The outer loop contains the actual optimization whereas the inner loop covers the calculation of the reliability indices and their sensitivities. The inner optimization problem is solved by using a modified, generalized reduced gradient algorithm which in this case works particularly effectively. By that, the only existing constraint, an equality constraint, is eliminated. In the optimal point the reliability index β and the Lagrange-multiplier μ occur as solution. The Lagrange-multiplier can be used for calculating the sensitivity.
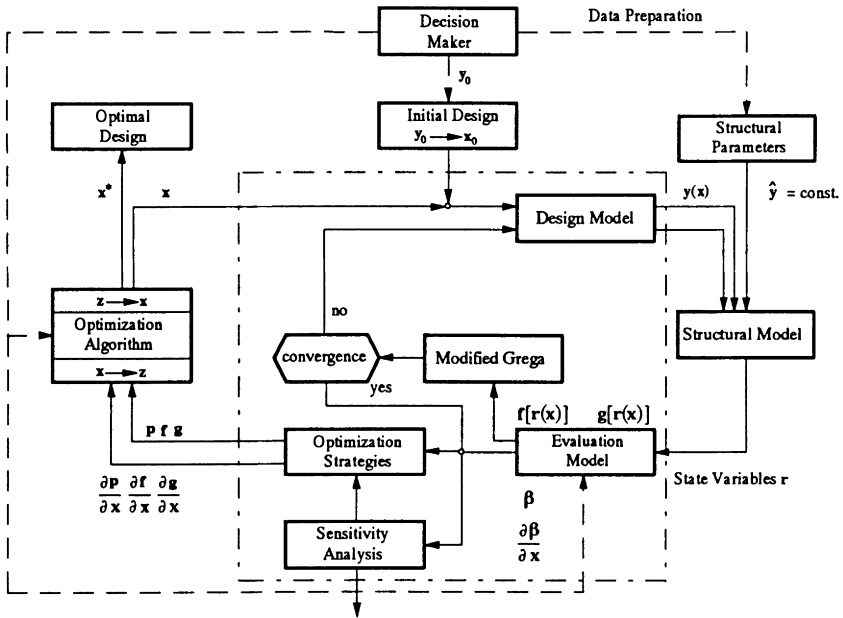
Figure 1: Diagram of the optimization procedure SAPOP for stochastic optimization.

4.2. Optimization procedure for shape optimization

In Fig. 2 the optimization loop including shape optimization and the calculation of the failure probabilities for ceramic material is presented. Here different kinds of approach functions are implemented. The Finite-Element program ANSYS [13] is used for structural analysis.

5. NUMERICAL RESULTS

5.1. Calculation of failure probabilities for a ceramic mirror plate

The following results refer to the ceramic mirror plate presented in [6]. The mirror plate with the design variables is shown in Fig. 3. The following stochastic model is assumed:
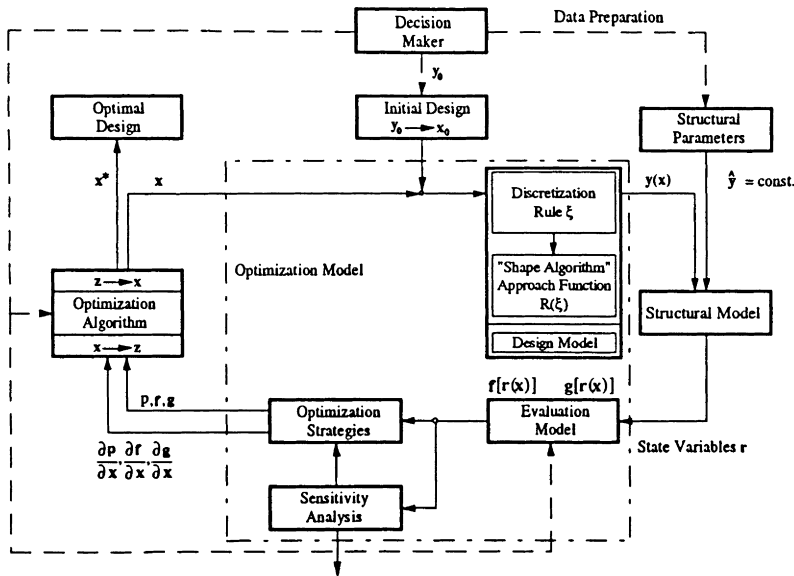
Figure 2: Diagram of the optimization procedure SAPOP for shape optimization.

design variables $x_1, \cdots x_6$ normal distributed,

Young's modulus E WEIBULL distributed,

pressure load p extrem value distributed.

Fig. 4 shows a comparison between the reliability indices β or β_E, respectively, calculated by the simple AFOSM-procedure with the transformation according to Rosenblatt and the procedure using the more complex Wu-Wirshing transformation. The index β correctly presents the tendency of the results, the reliability index, however, is always overestimated and the failure probability thereby underestimated. However, in the range of the standard deviation up to 10%, the deviations in the calculated indices are minimal. Since the augmented procedure is characterized by a high numerical effort, and since a semi-analytical sensitivity analysis is not possible, in the optimization presented in the following the simpler Rosenblatt-transformation is used, and, additionally, the variance range of 10% is not exceeded in the optimization. In the optimal design the failure probability which is more precise in each case has to be calculated and tested with regard to the augmented procedure.
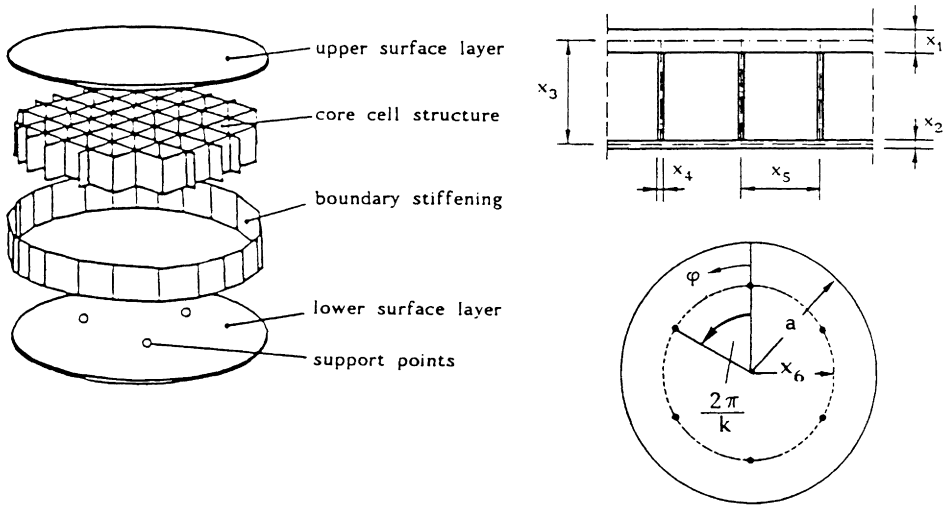
Figure 3: Model of the ceramic mirror.
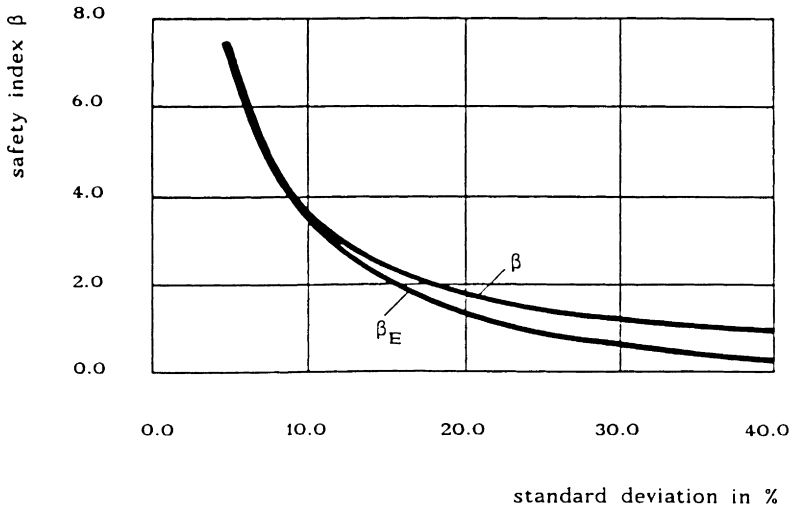
Figure 4: Comparison of the calculated reliability indices β, β_E.

5.2. Comparison of deterministic and stochastic optimization

Fig. 5 shows the results of the optimization of the ceramic mirror for the deterministic and the stochastic optimization problem. The results are presented in the form of functional-efficient boundaries. Each point on the functional-efficient boundary corresponds to an optimal design. By maintaining the reliability constraint the functional-efficient boundary of the stochastic optimization problem has been calculated as 99.86% which means a safety index of $\beta = 3$. A comparison between both boundaries shows that the deterministic optimization would lead to an obvious under-dimensioning of the structure.
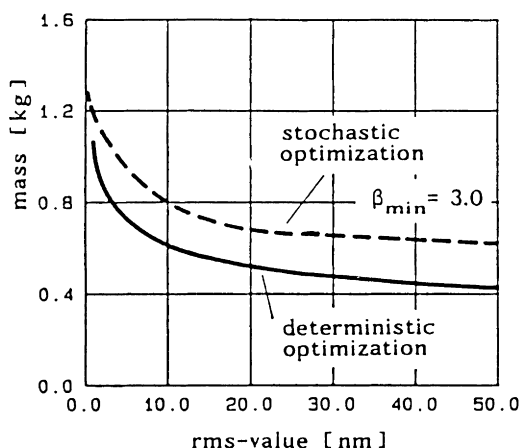
Figure 5: Functional-efficient boundaries for the point-supported mirror.

5.3. Shape optimization of a cantilever disc

Fig. 6 shows the initial design for a cantilever disc. The constant thickness of the disc is t = 10 mm. The initial design is a rectangular disc. The lower contours are described by cubic splines and the coordinates of the control points are chosen as the design variables of the optimization model. The optimization model is used in accordance with the Three-Columns-Concept due to [4].

a) **Column 1: Structural Model**
   The FE-program system ANSYS is used for structural analysis. The 8-nodes isoparametric shell element is used.

b) **Column 2: Optimization Model**
   Fig. 6 shows the definition of the design variables as control points of the spline function. The following items are used as objective functions: mass of the disc, failure probability (in the case of brittle material) or the maximum equivalent stress σ_e (in the case of ductile material).
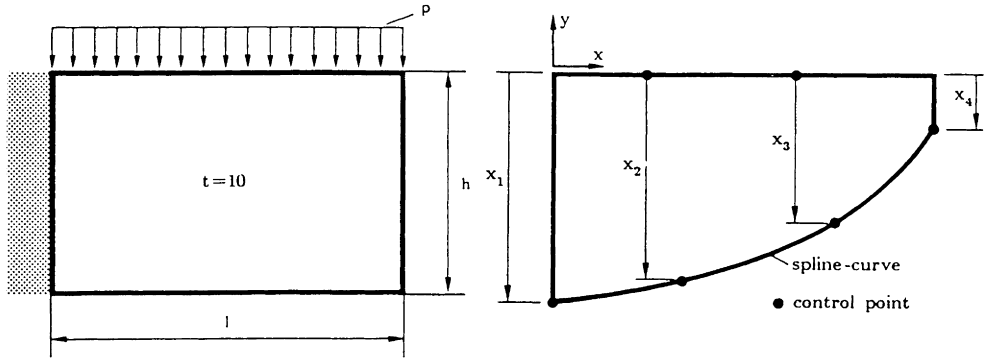
Figure 6: Initial design, control points and design variables of the cantilever disc.

c) Column 3: Optimization Algorithms

Two different optimization algorithms are used. First a Generalized Reduced Gradient Algorithm with an efficient strategy for finding feasible design points and second a Sequential Linearization Strategy.

The formulation of the objective functions reads as follows:

$$f_1(\boldsymbol{x}) \stackrel{\triangle}{=} \rho t \sum_i A_i(\boldsymbol{x}) \tag{32}$$

for the weight of the disc with ρ as the density of the material and t the thickness of the disc.

$$f_2(\boldsymbol{x}) \stackrel{\triangle}{=} \begin{cases} P_f & | \quad \text{brittle material} \\ \sigma_e & | \quad \text{ductile material} \end{cases} \tag{33}$$

as the failure criteria for the specified material according to eq. (2) or (9). Both objective functions create a multicriteria optimization problem which in the present case is transformed into a scalar optimization problem by applying a constrained oriented transformation. For that purpose, one objective function is transformed into a constraint by determining a demand level. So it is necessary to define maximum feasible values $P_{ffeas}, \sigma_{efeas}$. Figs. 7 and 8 show the optimization calculations in the form of functional-efficient boundaries and the optimal design of one point. Each point on the boundary corresponds to a best compromise design. For the feasible failure probabilities in Fig. 8 a logarithmic scale is used. For the brittle material the optimal boundary shape of the disc is concave in contrast to the optimal shape using the ductile material. This results from the volume effect with ceramics following equations (9,10). According to this effect the failure probability increases with constant stress and growing volume. It pre-dominates the stress reducing effect boundary for the ductile material. In Fig. 8 the influence of different WEIBULL-moduls m according to equation (10) is shown.
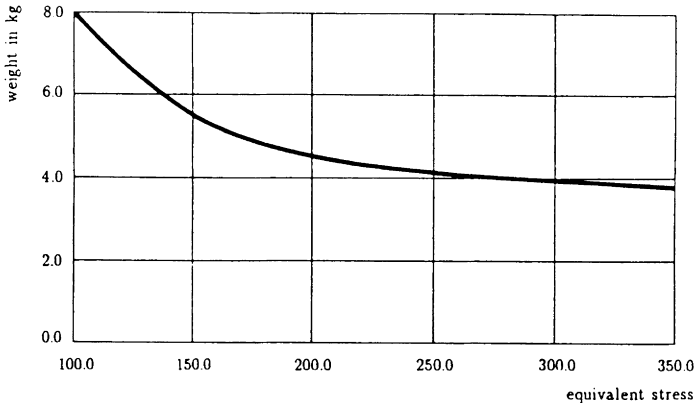
Figure 7: Functional-efficient boundary of the steel disc and one optimal design.
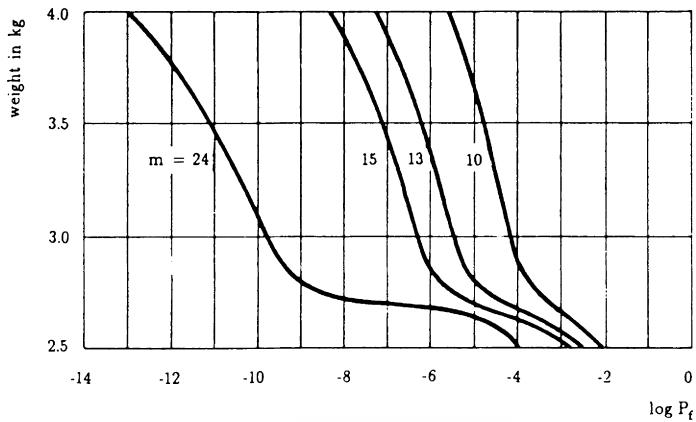
Figure 8: Functional-efficient boundaries of the ceramic disc and one optimal design.

6. CONCLUSION

The use of optimization procedures for the optimal layout of structures increasingly gains importance. The use of advanced materials call for a precise description and mathematical modeling of the failure criteria characterizing the material. Ceramics as an example of such advanced materials differ from the conventional, mostly ductile materials expecially by their property of brittleness and large scattering of the material parameters.

This paper presents the augmentation of an existing optimization procedure for stochastic optimization for including the scattering of the material parameters and the use of special failure criteria within the shape optimization. The results show on the one hand the fundamental difference in the shape of an optimal design made out of ductile and brittle materials. On the other hand the necessity of the stochastic optimization is shown.

In further studies the here presented two different methods will be used together for examples. For practical results the use of the extended failure criterion here also presented is necessary.

References

[1] BATDORF, S.B.; CROSE, J.G.: A Statistical Theory for the Fracture of Brittle Structures Subjected to Nonuniform Polyaxial Stresses. J. of Applied Mechanics, June 1974, 459-464.

[2] BREMICKER, M.; ESCHENAUER, H.A.; POST, P.: Optimization Procedure SAPOP - A General Tool for Multicriteria Structural Designs. In [4], 35-69.

[3] CREYKE, W.E.C.; SAINSBURY, I.E.J.; MORRELL, R.: Design with Non-Ductile Materials. Applied Science Publishers, London, New York, 1982.

[4] ESCHENAUER, H.A.; KOSKI, J.; OSYCZKA, A. (eds.): Multicriteria Design Optimization. Procedures and Applications. Springer-Verlag, Berlin, Heidelberg, New York, 1990.

[5] ESCHENAUER, H.A.; VIETOR, T.: Some Aspects on Structural Optimization of Ceramic Structures. In Eschenauer, H.A.; Mattheck, C.; Olhoff, N. (eds.): Engineering Optimization in Design Processes. Proceedings of the International Conference Karlsruhe Nuclear Research Center, Germany, September 3-4, 1990. Lecture Notes in Engineering. Springer-Verlag, Berlin, Heidelberg, New York, 1991, 145-154.

[6] ESCHENAUER, H.A.; VIETOR, T.: An Augmented Optimization Procedure for Stochastic Optimization and its Application to Design with Advanced Materials. Lecture Notes in Control and Information Sciences. Springer-Verlag, Berlin, Heidelberg, New York, 1992, 943-952.

[7] ESCHENAUER, H.A.; VIETOR, T.: The Efficiency of Several Methods in the Stochastic Structural Optimization. ZAMM 72, 1992, T570-T573.

[8] ESCHENAUER, H.A.; WEINERT, M.: Structural Optimization Techniques as a Mathematical Tool for Finding Optimal Shapes of Complex Shell Structures. To

appear 1992 in the Proceedings Volume of the Conference on Nonsmooth Optimization, Erice, Italy, 1991.

[9] EVANS, A.G.: A General Approach for the Statistical Analysis of Multiaxial Fracture. Journal of the American Ceramic Society, August 1978, 61(7-8), 302-308.

[10] FREUDENTHAL, A.M.: Statistical Approach to Brittle Fracture. In Liebowitz, H. (ed.): Fracture. An Advanced Treatise. Academic Press, New York, London, 1968, 592-618.

[11] HASOFER, A.M.; LIND, N.C.: Exact and Invariant Second-Moment Code Format. ASCE, Journal of the Engineering Mechanics Division, 100 (1974), 111-121.

[12] KOSKI, J.; SILVENNOINEN, R.: Multicriteria Design of Ceramic Components. In [4], 447-463.

[13] N.N.: ANSYS User's Manual. Vol I,II. Swanson Analysis Systems Inc. Houston, Pennsylvania.

[14] WU, Y.T.: Demonstration of a New, Fast Probability Integration Method for Reliability Analysis. Advances in Aerospace Structural Analysis. Papers of the Winter Annual Meeting, Miami Beach, FL, Nov. 17-22, 1985, O.M. Burnside (ed.), ASME, 63-73.

Acknowledgement

Optimal distribution of fibers in reinforced ceramics

F. Hild[a] and F.A. Leckie[b]

[a]Laboratoire de Mécanique et Technologie, E.N.S. Cachan/C.N.R.S./Université Paris 6,
61, avenue du Président Wilson, F-94235 Cachan Cedex, France

[b]Department of Mechanical and Environmental Engineering
University of California, Santa Barbara, CA 93106, U.S.A.

Abstract

Fiber pull-out is one of the fracture features of fiber reinforced brittle matrix composites. The onset of this mechanism is predicted by using Continuum Damage Mechanics, and corresponds to a localization of the deformations. After deriving a damage model from a uniaxial approach, different configurations are analyzed through analytical and numerical (F.E. calculations) methods. An extension to fibers in two perpendicular directions is proposed and a structure is analyzed. An optimal fiber distribution is discussed.

1. INTRODUCTION

The aim of this paper is to study the failure by fracture of fiber reinforced brittle matrix composites and to analyze an optimal fiber distribution. One of the features of the behavior of these composites is fiber pull-out due to fiber breakage. The occurrence of this mechanism is assumed to be described by the appearance of a macro-crack and will be described by a localization of the deformations. The initiation of macro-cracks in a structure during service often constitutes the early stage of the final failure of the structure. Starting from a material that is assumed free from any macro initial defect, the initiation of macro-cracks can be predicted using Continuum Damage Mechanics. The initiation stage is considered as the onset of a surface across which the velocity gradient is discontinuous. Under small deformations assumption, this phenomenon is mainly driven by the damage mechanism that causes strain-softening. For ceramic matrix composites, the damage mechanism is related to the percentage of broken fibers.

Although localization can be studied at the scale of fibers bonded to a matrix through an interface [1], i.e. at a micro-level, localization can also be analyzed at a meso-level, where the material behavior is homogenized. Continuum Damage Mechanics, which represents a local approach to fracture, constitutes an efficient tool for this purpose. The progressive deterioration of the material is modeled by an internal variable defined at the meso-level. This variable is called *damage*. The damage state and the evolution of this variable is obtained through a uniaxial study based on fiber breakage [2]. A 2-D plane stress analysis is

performed based on an extended model. The loss of uniqueness and the localization are studied for shear free states. A criterion referring to a critical value of the damage can describe the localization, which constitutes an objective criterion, from a design point of view. An extension to the case of fibers in two directions is proposed, based on a law of mixture in terms of the specific Helmholtz free energy.

This approach is also used to study a spinning disc made of a fiber reinforced ceramic matrix composite. The same criterion is implemented and studied through Finite Element computations. An extension to fibers in two perpendicular directions is proposed and an optimal fiber distribution is discussed in the case of the spinning structure.

2. LOCALIZATION AND LOSS OF UNIQUENESS

The failure at a meso-level, i.e. initiation of a macro-crack, is defined as the bifurcation of the rate problem in certain modes, viz. the appearance of a surface across which the velocity gradient is discontinuous. This phenomenon is referred to as *localization*, and corresponds to the failure of the ellipticity condition [1]. The condition of localization also can be compared to the loss of uniqueness of the rate problem.

Under small strain assumption and in elasticity coupled with damage, the behavior of a material is assumed to be described by the following piece-wise linear rate constitutive law

$$\dot{\sigma} = \begin{cases} \mathbb{E} : \dot{\varepsilon} & \text{if } \dot{D} = 0 \\ \\ \mathbb{H} : \dot{\varepsilon} & \text{if } \dot{D} \neq 0 \end{cases} \tag{1}$$

where $\dot{\sigma}$ and $\dot{\varepsilon}$ respectively denote the stress and strain rates, $\mathbb{E}$ and $\mathbb{H}$ are fourth rank tensors, $\mathbb{E}$ is assumed to be positive definite, and D is either a single damage variable or a set of damage variables. Localization occurs inside the body, *if and only if* [1,3]

Det $(\mathbf{n}.\mathbb{H}.\mathbf{n}) = 0$ for any vector $\mathbf{n} \neq 0$ and at any point *inside* a structure Ω (2)

This criterion corresponds to the failure of the ellipticity condition of the rate equilibrium equation; it also can be used as an indicator of the local failure of the material, i.e. at a meso-scale [4-5]. Any loss of uniqueness, considered as bifurcation of the rate boundary value problem, is excluded as long as the operator

$$\mathbb{H}_s = \frac{1}{2} (\mathbb{H} + \mathbb{H}^T) \tag{3}$$

is strictly positive definite everywhere within the structure. This condition is equivalent to the condition of hardening

$$\dot{\sigma} : \dot{\varepsilon} > 0 \tag{4}$$

In this study, the quantity that defines loss of uniqueness and localization is the linear tangent modulus $\mathbb{H}$. In the following, we analyze loss of uniqueness and loss of ellipticity (i.e. localization) for states when

$$\begin{cases} \varepsilon_{11} = \alpha \, \varepsilon_{22} \text{ with } \alpha \in \mathbb{R} \\ \varepsilon_{12} = 0 \end{cases} \tag{5.1}$$

These particular states only are considered, since we will deal with axisymmetric calculations, which are shear free. Consequently, only H_{1111}, H_{1122}, H_{2211}, H_{2222} and H_{1212} are different from zero. These states lead to a tangent modulus that takes the form

$$\mathbb{H} = \begin{bmatrix} H_{1111} & H_{1122} & 0 \\ H_{2211} & H_{2222} & 0 \\ 0 & 0 & H_{1212} \end{bmatrix} \tag{5.2}$$

For problems under hypothesis (5.1), the non-vanishing components of the vector $\mathbf{n}$ are n_1 and n_2, and the matrix $\mathbb{A} = \mathbf{n}.\mathbb{H}.\mathbf{n}$ reduces to [6]

$$\mathbb{A} = \begin{bmatrix} n_1^2 H_{1111} + n_2^2 H_{1212} & n_1 n_2 (H_{1212} + H_{1122}) \\ \\ n_1 n_2 (H_{1212} + H_{2211}) & n_1^2 H_{1212} + n_2^2 H_{2222} \end{bmatrix} \tag{5.3}$$
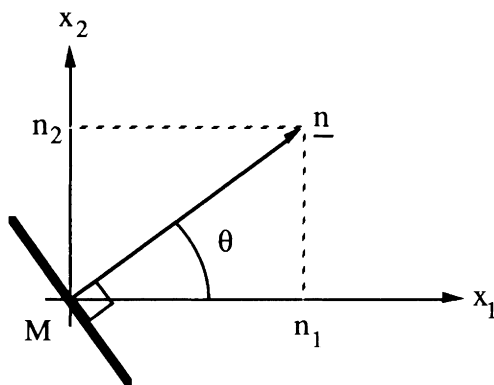
Figure 1. Localization mode.

If we rewrite $(n_1, n_2) = (\cos\theta, \sin\theta)$, $X = \tan^2\theta$, then the localization condition is to find real positive roots of the following equation

$$a\,X^2 + b\,X + c = 0 \tag{5.4}$$

with

$$a = H_{1212}H_{2222} \tag{5.5}$$
$$b = H_{1111}H_{2222} - H_{1122}H_{2211} - H_{1122}H_{1212} - H_{2211}H_{1212} \tag{5.6}$$
$$c = H_{1212}H_{1111} \tag{5.7}$$

If real positive roots are found, then the localization direction is perpendicular to the vector $(n_1, n_2, 0) = (\cos\theta, \sin\theta, 0)$, characterized by the angle θ (Fig. 1).

3. UNIAXIAL STUDY

This section is concerned with the development of a single damage variable model for tensile behavior of unidirectional fiber reinforced ceramic matrix composites. A schematic stress-strain diagram is shown in Fig. 2 for such a specimen. The micro-structural phenomena responsible for the features of curve 0ABC are now discussed. On initial loading from point 0 to A of Fig. 2 the composite behaves as a virgin, i.e. undamaged, elastic material with modulus E. Further loading from point A to B causes cracking of the matrix. The cracks traverse the entire load bearing section within the homogeneously stressed region. Further loading along BC involves further development of matrix cracks, which involves two processes. First the process of fiber debond, both at the front of the crack and in its wake, which is necessary to cause the stresses to redistribute. The second process is fiber failure, which precedes the process of fiber pull-out.
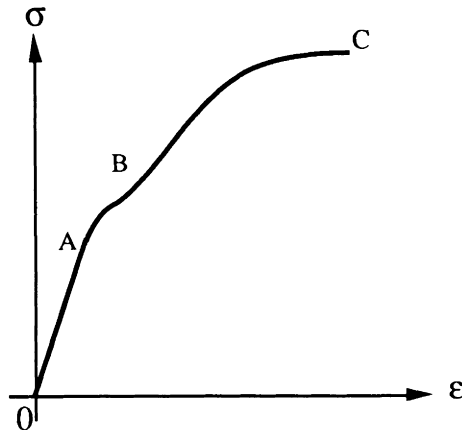
Figure 2. Schematic uniaxial stress-strain curve of a fiber reinforced brittle matrix composite.

The characteristics of fiber failure are determined by a statistical distribution of fiber strength [2]. This single mechanism is the *only* one considered in this study. Future development can be carried out by modeling the matrix cracking process and the fiber pull-out mechanism.

The model is based upon the assumption that the nominal stress applied to a bundle of fibers in parallel can be expressed in terms of a damage variable, denoted by $D = r/n$, where r is the number of failed fibers and n is the total number contained within the load bearing cross-section. This type of approach has been applied to perfectly brittle fiber systems [7-8]. It is shown that the nominal applied stress σ is related to the uniaxial strain ε by

$$\sigma = E\,(1-D)\,\varepsilon = \tilde{E}\,\varepsilon \tag{6}$$

where E is the Young's modulus of each unbroken fiber and $\tilde{E}$, the Young's modulus of the damaged bundle. If the nominal stress is the total current load divided by the total initial fiber area, then the average stress in the unbroken fibers is

$$\tilde{\sigma} = \frac{\sigma}{1-D} \tag{7}$$

This later expression refers to the concept of effective stress [9-10]. Although the nominal stress does not always increase with the applied strain ε, the stress in the unbroken fibers, $\tilde{\sigma}$, does increase whatever the applied strain, ε. Two regimes can be exhibited depending on the fiber length [11], and we are going to study both of them. We assume that the fiber failure probability, $P_F(\tilde{\sigma})$, at a stress $\tilde{\sigma}$ is given by a Weibull distribution [12]

$$P_F(\tilde{\sigma}) = 1 - \exp\left[-\frac{L}{L_0}\left(\frac{\tilde{\sigma}}{\sigma_0}\right)^m\right] \tag{8.1}$$

where σ_0 is the scale parameter of the in-situ fibers, m is the shape parameter, L is the fiber length, and L_0 is a gauge length for which m and σ_0 were identified. This first expression corresponds to the behavior of a fiber bundle, and will be referred to as model #0. On the other hand, due to interfacial sliding characterized by a shear stress τ, the fiber failure probability can be written as

$$P_F(\tilde{\sigma}) = 1 - \exp\left[-\left(\frac{\tilde{\sigma}}{\sigma_1}\right)^{m+1}\right] \tag{8.2}$$

where σ_1 is the characteristic strength multiplied by the fiber volume fraction [13]. This second expression takes consideration of the interfacial properties between fibers and matrix, and will be referred to as model #1.The ratio r/n characterized by damage variable D is

$$r/n = D = P_F(\tilde{\sigma}) \tag{9}$$

This definition is consistent with the bounded values of D for which D=0 for no failed fiber and D=1 for complete failure of all fibers. The damage is thus related to the nominal stress by

$$D = 1 - \exp\left[-\frac{L}{L_0} \left\{ \frac{\sigma}{(1-D)\sigma_0} \right\}^m \right] \quad \text{if } \varepsilon > 0 \text{ and } \dot{\varepsilon} > 0 \qquad \text{(model \#0)} \qquad (10.1)$$

$$D = 1 - \exp\left[-\left\{ \frac{\sigma}{(1-D)\sigma_1} \right\}^{m+1} \right] \quad \text{if } \varepsilon > 0 \text{ and } \dot{\varepsilon} > 0 \qquad \text{(model \#1)} \qquad (10.2)$$

The peak in the stress-strain plane (σ,ε) coincides with a critical value of damage

$$D = D_c = 1 - \exp(-1/m) \qquad \text{(model \#0)} \qquad (11.1)$$
$$D = D_c = 1 - \exp(-1/(m+1)) \qquad \text{(model \#1)} \qquad (11.2)$$

It can be noticed that the critical value of the damage is always *independent of* the fiber length, L. Conversely, the maximal nominal stress σ_{0M} may *depend upon* the length L for small volumes

$$\sigma_{0M} = \sigma_0 \left(\frac{L_0}{meL} \right)^{1/m} \qquad \text{(model \#0)} \qquad (12.1)$$

$$\sigma_{0M} = \sigma_1 \left[\frac{1}{e(m+1)} \right]^{1/(m+1)} \qquad \text{(model \#1)} \qquad (12.2)$$

The critical value of damage, D_c, is *only* related to the shape parameter m by Equ. (11) and is therefore a material dependent parameter. Conversely, σ_{0M} may depend upon the length of the fibers, so that it is not a material parameter.

Finally, as it has been underlined above, this model does not consider fiber pull-out. Thus this model constitutes a *lower* bound estimate up to the maximal nominal stress is reached, for a strain-controlled test. If the test is stress-controlled, then the point for which $\sigma = \sigma_{0M}$ constitutes the ultimate stable point.

4. 2-D STUDY WITH FIBERS IN ONE DIRECTION

This section deals with the study of a 2-D model extending the ideas of the previous section. The fibers are assumed to be parallel to the 2-direction. An analytical and numerical approach is studied.

4.1. Analytical study
In elasticity, under the plane stress hypothesis, with the small strain assumption, the relationship between stresses and strains is given by

$$\begin{bmatrix} \varepsilon_{11} \\ \varepsilon_{22} \\ \varepsilon_{12} \end{bmatrix} = \begin{bmatrix} 1/E_1 & -\nu_{12}/E_1 & 0 \\ -\nu_{21}/E_2 & 1/E_2 & 0 \\ 0 & 0 & 1/2G_{12} \end{bmatrix} \begin{bmatrix} \sigma_{11} \\ \sigma_{22} \\ \sigma_{12} \end{bmatrix} \qquad (13)$$

When fiber breaking in the 2-direction is considered, the damage state is described by damaged elastic constants $\tilde{E}_1$, $\tilde{E}_2$, $\tilde{\nu}_{12}$, $\tilde{\nu}_{21}$, $\tilde{G}_{12}$ instead of E_1, E_2, ν_{12}, ν_{21}, G_{12} respectively. The Young's modulus E_2 is no longer constant but depends upon the degradation of the fibers characterized by D_2 to become $\tilde{E}_2 = E_2(1-D_2)$: it is a straightforward extension of Equ. (6). Since pulling in the 1-direction has no effect on the strains in the 2-direction, $\tilde{\nu}_{12}$ is constant and equals ν_{12}. Finally we assume that $\tilde{E}_1 = E_1$ (no effect of the damage D_2 in the 1-direction) and that $\tilde{G}_{12} = G_{12}$ (the shear properties are slightly altered by fiber failure). We suppose also that the material is hyperelastic so that

$$\frac{\tilde{\nu}_{21}}{\tilde{E}_2} = \frac{\tilde{\nu}_{12}}{\tilde{E}_1} \qquad (14)$$

It can therefore be noticed that $\tilde{\nu}_{21} = \nu_{21}(1-D_2)$, and if $D_2 = 0$ then the behavior is purely elastic and is described by Equ. (13). if there is a damage evolution then the relationships between strains and stresses are given by

$$\sigma_{11} = \frac{E_2}{k[1-\nu_{12}^2(1-D_2)k]} [\varepsilon_{11} + \nu_{12}(1-D_2)k\varepsilon_{22}] \qquad (15.1)$$

$$\sigma_{22} = \frac{E_2(1-D_2)}{1-\nu_{12}^2(1-D_2)k} (\nu_{12}\varepsilon_{11} + \varepsilon_{22}) \qquad (15.2)$$

$$\sigma_{12} = 2G_{12}\varepsilon_{12} \qquad (15.3)$$

where $k = E_2/E_1$ is referred to as the Young's moduli ratio. As mentioned in section 2, the damage state of fibers in the 2-direction, D_2, can be related to the stress state through an implicit relationship

$$D_2 = 1 - \exp\left[-\frac{L}{L_0} \left\{ \frac{\sigma_{22}}{(1-D_2)\sigma_0} \right\}^m \right] \quad \text{if } \varepsilon_{22} > 0 \text{ and } \dot{\varepsilon}_{22} > 0 \quad \text{(model \#0)} \qquad (15.4.1)$$

$$D_2 = 1 - \exp\left[-\left\{ \frac{\sigma_{22}}{(1-D_2)\sigma_1} \right\}^{m+1} \right] \quad \text{if } \varepsilon_{22} > 0 \text{ and } \dot{\varepsilon}_{22} > 0 \quad \text{(model \#1)} \qquad (15.4.2)$$

It can be noticed that if $D_2 = D_c$ then H_{1122}, H_{2211} and H_{2222} vanish simultaneously and H_{1111}, H_{1212} are strictly positive. Therefore, this point corresponds to the loss of uniqueness *and* to a localization with $\theta = \pi/2$ (i.e. perpendicular to the fiber direction). It can be proven that $D_2 = D_c$ (viz. $H_{2222} = 0$ and $H_{1122} = H_{2211} = 0$) constitutes a *necessary and sufficient* condition for loss of uniqueness *and* localization. An initiation criterion can therefore be given by

$$D_2 = D_c \tag{16.1}$$

Since Equ. (16.1) implies that σ_{22} (see relations (15.4)) is constant and equals σ_{0M}, another criterion may be

$$\sigma_{22} = \sigma_{0M} \tag{16.2}$$

It also can be shown that criterion (16.2) can be expressed in terms of the strain energy release rate density Y [10], reaching a critical value Y_c

$$Y = Y_c = \frac{1}{2} \frac{\sigma_{0M}^2}{E_2(1-D_c)^2} \tag{16.3}$$

where $Y = \rho \frac{\partial \varphi_2}{\partial D_2}$, $\rho\varphi_2(\sigma,D_2)$ is the specific strain energy, which is a function of the Cauchy stress tensor σ, and the damage variable D_2, ρ denotes the material density, here assumed to be constant. Moreover, criterion (16.2) can be rewritten in terms of the strain ε_{22} by using Equ. (15.2) and yields

$$\varepsilon_{22}(1+\alpha\nu_{12}) = \varepsilon_0 \tag{16.4}$$

where ε_0 corresponds to the localization strain when the load ratio α is equal to zero. The localization angle, as expected, is equal to $\pi/2$ (viz. a localization mode perpendicular to the fiber direction) whatever the strain ratio α.

It is worth noting that if the failure of the matrix is considered, then localization cannot always occur: it exists another limit given by, for instance, the criterion $\sigma_{11} = \sigma_M$, where σ_M is the strength of the matrix in the transverse direction.

Knowing the analytical results, it is interesting to study the numerical sensitivity of the detection of the localization point (and therefore the loss of uniqueness as well). To get an accurate information in terms of the damage at localization, direction of localization and stress at localization, it is necessary to be as close as possible to the actual localization state [14]. This trend has also been observed when using a F.E. code to compute some more complicated situations.

In summary, this model leads to some very simple results. First, loss of uniqueness and localization occur simultaneously. Second, some very simple criteria (16) can be derived from criteria (2) and (3), and show that the relevant parameters are Weibull parameter m and Poisson's ratio ν_{12}. Third, the results are independent of the Young's modulus ratio $k = E_2/E_1$. Fourth, whatever the strain ratio α, the direction of localization is constant and perpendicular to the fiber direction. This model gives the same results as those found in a uniaxial approach and constitutes a straightforward generalization to 2-D cases. From a numerical standpoint, it is important to be as close as possible to the localization point to get accurate informations.

4.2. F.E.M. analysis: spinning disc

A problem that is given special attention is the case of a circular disc made of a fiber composite material. The analysis of this problem is performed not only due to its significant practical importance in, for example, turbines, but also due to the presence of a non-homogeneous stress state, a feature that distinguishes this problem from the 2-D study performed above.
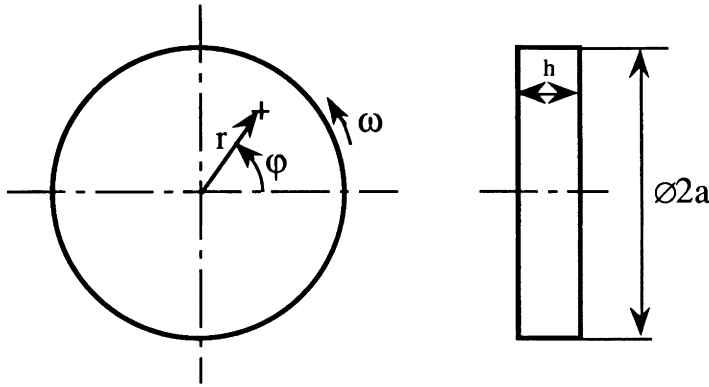
Figure 3. The geometry of the circular disc (a = .3 m, h = .01 m).

The geometry of the problem is shown in Fig. 3. Here ω represents the angular rotation speed, with dimension rad/s. The outer boundary of the disc, r = a, is assumed to be free from kinematic constraints and accordingly here the loading can be considered as stress controlled. In the present setting, the stress state is axisymmetric, at least up to the point where localization occurs, and hence a cylindrical coordinate system is introduced in Fig. 3. It is assumed that the fibers are oriented in the circumferential direction and coordinates x_1 and x_2 in the previous section are replaced with r and φ, respectively. The stress-strain relationship becomes

$$\sigma_r = \frac{E_\varphi}{k[1-v_{r\varphi}^2(1-D_\varphi)k]} [\varepsilon_r + v_{r\varphi}(1-D_\varphi)k\varepsilon_\varphi] \tag{17.1}$$

$$\sigma_\varphi = \frac{E_\varphi(1-D_\varphi)}{1-v_{r\varphi}^2(1-D_\varphi)k} (v_{r\varphi}\varepsilon_r + \varepsilon_\varphi) \tag{17.2}$$

in obvious notations. It should be remembered that no shear stress $\sigma_{r\varphi}$ is present due to axisymmetry. The expression for the damage parameter, D_φ, is in this problem either r-dependent (model #0)

$$D_{\varphi 0} = 1 - \exp\left[-\frac{r}{r_0}\left\{\frac{\sigma_\varphi}{(1-D_\varphi)\sigma_0}\right\}^m\right] \quad \text{if } \varepsilon_{\varphi\varphi} > 0 \text{ and } \dot{\varepsilon}_{\varphi\varphi} > 0 \tag{18.1}$$

or r-independent (model #1)

$$D_{\varphi 1} = 1 - \exp\left[-\left\{\frac{\sigma_\varphi}{(1-D_\varphi)\sigma_1}\right\}^{m+1}\right] \quad \text{if } \varepsilon_{\varphi\varphi} > 0 \text{ and } \dot{\varepsilon}_{\varphi\varphi} > 0 \qquad (18.2)$$

In relation (18.1), r_0 is a material constant representing the length dependence of the problem, while all the other parameters are defined earlier.

To describe completely the axisymmetric boundary value problem, small strains kinematics and equilibrium equations have also to be introduced. At this stage, it proved impossible to derive a closed-form solution for the stress state and for the damage variable. Instead the problem was solved using the finite element method. Constitutive relations (17) and (18) were implemented into a standard finite element code ABAQUS [15], and a solution was sought for by discretizing the problem using 2-node axisymmetric shell elements. Since the linear tangent modulus $\mathbb{H}$ also had to be implemented into the finite element code, the load, or angular rotation speed, required for loss of uniqueness and localization could be conveniently calculated using ABAQUS through a UMAT routine.

It should be noted that due to the non-explicit expression for the damage parameter given in (18) an iterative procedure had to be outlined to determine the damage state characterized by D_φ at every time the calculated strain field did change at a certain Gauss point [14]. Before focusing the attention on explicit results, one should first mention that the non-homogeneity of the stress field in this axisymmetric problem did not in any way change the important features of the mechanical (damage) behavior. All the conclusions drawn in the 2-D study are essentially confirmed. Therefore, it seems appropriate merely to comment on some numerical results derived from the finite element computations.

The material analyzed herein is a ceramic matrix composite with $E_r = 20$ GPa, $E_\varphi = 140$ GPa, $G_{r\varphi} = 13$ GPa, $\nu_{r\varphi} = .0214$, $m = 4$, $\sigma_0 = 1450$ MPa, $m = 3$, $\sigma_1 = 1293$ MPa, $r_0 = .002$ m, and the geometry of the disc is chosen with practical applications in mind, namely $a = .3$ m and $h = .01$ m.

In Fig. 4, the stress field is plotted as a function of the radial coordinate r at $\rho\omega^2 = .55 \; 10^{10}$ kg/m^3/s^2, that is just before localization. A comparison is made with an elastic solution where the effect of damage is ignored. As could be expected, the introduction of damage reduces the maximum stress acting within the disc and causes a redistribution of the whole stress field.

Localization and loss of uniqueness occur at the same value of ω and where r has the approximate value .248 m for model #0, and .234 m for model #1. Other critical values on important parameters are

$$\rho\omega_0^2 = .58598 \; 10^{10} \text{ kg/m}^3/\text{s}^2 \qquad (19.1)$$

$$\rho\omega_1^2 = 1.7076 \; 10^{10} \text{ kg/m}^3/\text{s}^2 \qquad (19.2)$$

$$D_{\varphi 0} = D_{\varphi 1} = .221199 \qquad (19.3)$$

where especially the two values of D_φ give further confidence in the numerical procedure since the critical value on the damage was previously proven (see Equ. (11) and (16.1) when m =4, or m+1=4) to be $1-\exp(-1/4) = .2211992...$
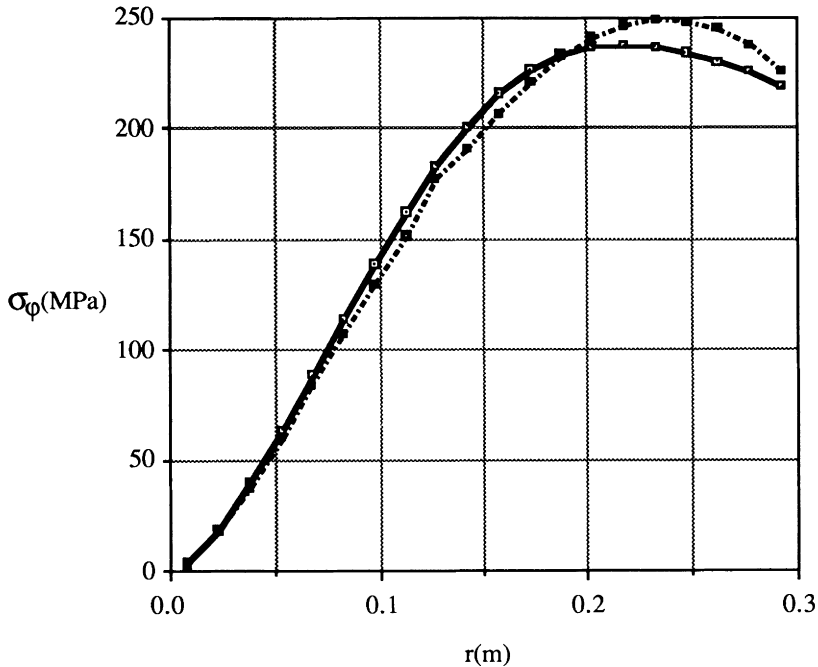
Figure 4. Hoop stress, σ_φ, as a function of the radial coordinate r, $\rho\omega^2 = .55 \ 10^{10} \ kg/m^3/s^2$, (——□——) damage model #0, and (·—··—■—··—) linear elastic model when $D_\varphi = 0$.

The direction of localization coincides with the direction perpendicular to the fiber direction, as already shown analytically. To find the actual value of the localization direction, the point at localization has to be determined with high accuracy [14].

5. 2-D STUDY WITH FIBERS IN TWO PERPENDICULAR DIRECTIONS

In this section the composite is constituted by a brittle matrix reinforced by fibers in two perpendicular directions. A local and a global analysis are performed to determine criteria to design such structures. Some optimization conclusions can be drawn from this section.

5.1. Local study

If the fibers are only in the 2-direction, the constitutive equations are given by relations (15.1-3). These relations can be derived from the specific Helmholtz free energy ψ_2, which is a scalar function of the state variables ε_{11}, ε_{22}, ε_{12}, and D_2

$$\rho\psi_2 = \rho\psi(\varepsilon_{11},\varepsilon_{22},\varepsilon_{12},D_2) \tag{20.1}$$

with

$$\rho\psi(x,y,z,d) = \frac{E_F}{2}\left[\frac{x^2+2\nu_{MF}(1-d)xy+k(1-d)y^2}{k\left\{1-\nu_{MF}^2(1-d)\right\}}\right] + z^2 G_{MF} \tag{20.2}$$

and

$$\sigma_{11} = \rho\frac{\partial\psi_2}{\partial\varepsilon_{11}} \quad , \quad \sigma_{22} = \rho\frac{\partial\psi_2}{\partial\varepsilon_{22}} \quad , \quad \sigma_{12} = \rho\frac{\partial\psi_2}{\partial\varepsilon_{12}} \tag{20.3}$$

It is worth noting that if the fibers are only in the 1-direction (perpendicular to the 2-direction), the breakage mechanism is defined by a damage variable denoted by D_1 and the corresponding specific Helmholtz free energy ψ_1 is given by

$$\rho\psi_1 = \rho\psi(\varepsilon_{22},\varepsilon_{12},\varepsilon_{12},D_1) \tag{21}$$

If the fibers are in both 1- and 2-directions, then we assume a state coupling [16] given by a law of mixture in terms of the total specific Helmholtz free energy $\rho\psi_{12}$

$$\rho\psi_{12} = (1-f)\rho\psi_1 + f\rho\psi_2 \tag{22}$$

where f is the percentage of fibers in the 2-direction. It is worth noting that equation (22) corresponds to a Lin-Taylor hypothesis. The elastic law is then given by

$$\sigma_{11} = \rho\frac{\partial\psi_{12}}{\partial\varepsilon_{11}} = (1-f)\rho\frac{\partial\psi_1}{\partial\varepsilon_{11}} + f\rho\frac{\partial\psi_2}{\partial\varepsilon_{11}} \tag{23.1}$$

$$\sigma_{22} = \rho\frac{\partial\psi_{12}}{\partial\varepsilon_{22}} = (1-f)\rho\frac{\partial\psi_1}{\partial\varepsilon_{22}} + f\rho\frac{\partial\psi_2}{\partial\varepsilon_{22}} \tag{23.2}$$

$$\sigma_{12} = \rho\frac{\partial\psi_{12}}{\partial\varepsilon_{12}} = (1-f)\rho\frac{\partial\psi_1}{\partial\varepsilon_{12}} + f\rho\frac{\partial\psi_2}{\partial\varepsilon_{12}} \tag{23.3}$$

The evolution of the damage variables D_1 and D_2 is assumed to be driven by the normal stresses in the corresponding direction, viz. σ_{11} and σ_{22}, respectively. It can be noticed that when the volume fraction ratio is either equal to zero or to one, the results of section 4.1 apply. In particular the localization direction is always perpendicular to the fiber direction. On the other hand, when the volume fraction ratio is not equal to zero or to one, a numerical method has to be used. The computations show that a loss of uniqueness *and* a localization criteria can both accurately be described by the two following criteria

$$\sigma_{11} = \sigma_{0M} \tag{25.1.1}$$

$$\sigma_{22} = \sigma_{0M} \tag{25.1.2}$$

$$Max(D_1, D_2) = D_c \tag{25.2}$$

The approximation is less than $\pm 1\%$. Criteria (25.1) are thus the actual criteria as far as the computations could spot any difference. Criteria (25) show that the maximum damage at localization or the maximum stress at localization *cannot* constitute parameters for an optimization process since they are insensitive to any change of the volume fraction ratio f and of the strain ratio α. On the other hand, the localization angle varies with the volume fraction ratio f and with the strain ratio α.

This first part of the study shows that from a local point of view, an optimization process is not interesting. The process has therefore to be addressed from a structural point of view at which the external load leads to a redistribution of the stress field when the volume fraction ratio f and the strain ratio α are altered. Thus different volume fractions, f, and different strain ratios, α, may lead to different maximum loads at localization.

5.2. F.E.M. Analysis: Spinning Disc

The same structure and material as in section 4.2 are analyzed ($E_M = 20$ GPa, $E_F = 140$. GPa, $G_{MF} = 13$ GPa, $\nu_{MF} = .0214$, m = 4, $\sigma_0 = 1450$ MPa, m = 3, $\sigma_1 = 1293$ MPa, $r_0 = .002$ m, a = .3 m, and h = .01 m). In the present setting, the stress state is axisymmetric, at least up to the point where localization occurs, and hence a cylindrical coordinate system is introduced. It is assumed that the fibers are oriented in the radial and circumferential directions, and coordinates x_1 and x_2 in the previous section are replaced with r and φ respectively. It should be remembered that no shear stress $\sigma_{r\varphi}$ is present due to axisymmetry. In this first analysis, we assume that there is an r-dependence in the hoop direction, which corresponds to the length of the fiber. The expression for the damage variables D_r and D_φ are given by (model #0)

$$D_{r0} = 1 - \exp\left[-\left\{\frac{\sigma_r}{(1-D_r)\sigma_0}\right\}^m\right] \quad \text{if } \varepsilon_{rr} > 0 \text{ and } \dot{\varepsilon}_{rr} > 0 \tag{26.1}$$

$$D_{\varphi 0} = 1 - \exp\left[-\frac{r}{r_0}\left\{\frac{\sigma_\varphi}{(1-D_\varphi)\sigma_0}\right\}^m\right] \quad \text{if } \varepsilon_{\varphi\varphi} > 0 \text{ and } \dot{\varepsilon}_{\varphi\varphi} > 0 \tag{26.2}$$

To describe completely the axisymmetric boundary value problem, small strains kinematics and equilibrium equations have also to be introduced. Again, it proved impossible to derive a closed-form solution for the stress state and for the damage variable. Instead the problem was solved using the finite element code ABAQUS [15]. The results of the computations are given in table 1. It can be noticed that the calculations can be performed only above f = .5. If the volume fraction ratio is less than .5 then a stress singularity arises at the center of the disc.

Table 1
Computations for the circular disc with different volume fraction ratios (model #0)

Volume fraction ratio f	1.	.9	.8	.7	.6	.55
$\rho\omega_0^2$ at localization (10^{10} kg/m^3/s^2)	.586	.672	.747	.817	.883	.914
Localization angle (°)	89.0	86.4	85.6	85.3	85.1	85.0
f $\rho\omega_0^2$ a^2/ σ_{0M}(r$_{loc}$)	2.2	2.2	2.2	2.0	1.8	1.7

When analyzing table 1 results, several conclusions can be drawn. First, at localization, an optimization process can be undertaken when the optimization parameter is the product of the density by the square of the angular velocity. The higher the volume fraction ratio, the lower the product. Second, the localization angle, as expected varies with the volume fraction ratio f. Third, a dimensionless parameter, f $\rho\omega_0^2$ a^2/ σ_{0M}(r$_{loc}$), where σ_{0M}(r$_{loc}$) denotes the stress level at the localization radius, r$_{loc}$, is constant over a large range of volume fraction.

In this part, we assume an r-independence in the hoop direction. The damage evolution is given by (model #1)

$$D_{r1} = 1 - \exp\left[- \left\{ \frac{\sigma_r}{(1-D_r)\sigma_1} \right\}^m \right] \quad \text{if } \varepsilon_{rr} > 0 \text{ and } \dot{\varepsilon}_{rr} > 0 \tag{27.1}$$

$$D_{\varphi 1} = 1 - \exp\left[- \left\{ \frac{\sigma_\varphi}{(1-D_\varphi)\sigma_1} \right\}^m \right] \quad \text{if } \varepsilon_{\varphi\varphi} > 0 \text{ and } \dot{\varepsilon}_{\varphi\varphi} > 0 \tag{27.2}$$

The results of the computations are given in table 2.

Table 2.
Computations for the circular disc with different volume fraction ratios (model #1)

Volume fraction ratio f	1.	.9	.8	.7	.6	.55
$\rho\omega_1^2$ at localization (10^{10} kg/m^3/s^2)	1.708	1.918	2.080	2.194	2.234	2.202
Localization angle (°)	89.0	86.4	85.6	85.3	85.1	85.1
f $\rho\omega_1^2$ a^2/ σ_{0M}(r$_{loc}$)	2.2	2.2	2.1	1.9	1.7	1.5

The same kind of conclusions as with model #0 can be drawn for model #1. It can also be noticed that an optimization process can be undertaken in terms of the angular velocity at localization.

6. CONCLUSIONS

Using a one-dimensional study of fiber breaking modeled by a single damage variable, a one-dimensional model is derived. This model is then generalized to a 2-D plane stress analysis with fibers in one direction. This generalized model gives rise to criteria identical to the one-dimensional model. Indeed, loss of uniqueness and localization can be described by some very simple criteria referring to Continuum Damage Mechanics. The conclusions drawn from the 2-D study are essentially confirmed by the finite element analysis of a spinning disc. This result is in itself interesting since it shows that the important features regarding loss of uniqueness and localization in fiber reinforced composites are independent of whether or not a homogeneous shear free stress field is present.

A model taking into account fibers in two perpendicular directions is studied. The same type of criteria as in the case of fibers in one direction can be derived. They refer to a maximal normal stress and to a maximal damage variable equal to a critical value. A finite element analysis confirms again these results in the case of more complicated stress fields.

Finally, since the criteria from a local stage are independent of the characteristics of the stress field, an optimization process can only be undertaken at a global stage.

7. ACKNOWLEDGMENTS

8. REFERENCES

1   Benallal, A., Billardon, R., and Geymonat, G., 3rd Conference on Constitutive Laws for Engineering Materials: Theory and Applications, Tucson, AZ, January 1991.
2   Coleman, B.D., J. Mech. Phys. Solids **7**, pp. 60-70 (1958).
3   Borré, G., and Maier, G., Meccanica **24**, pp. 36-41 (1989).
4   Billardon, R., and Doghri, I., C. R. Acad. Sci. Paris **308** [II], pp. 347-352 (1989).
5   Billardon, R., and Doghri, I., in *Strain Localization and Size Effect due to Cracking and Damage*. J. Mazars and Z.P. Bazant eds. Elsevier, pp. 295-307 (1989).
6   Ortiz, M., Leroy, Y., and Needelman, A., Comput. Meths Appl. Engrg. **61**, pp. 189-214 (1987).
7   Krajcinovic, D., and Silva, M.A.G., Int. J. Solids Structures **18** [7], pp. 551-562 (1982).
8   Hult, J., and Travnicek, L., Journal de Mécanique Théorique et Appliquée **2** [2], pp. 643-657 (1983).
9   Rabotnov, Y.N., in *Progress in Applied Mechanics*, Prager Anniversary Vol., McMillan, New-York, 307 (1963).
10 Lemaitre, J., and Chaboche, J.-L., in*Mechanics of Solid Materials*. Cambridge University Press. Cambridge (1990).

500

11 Hild, F., Domergue, J.-M., Evans, A.G., and Leckie, F.A., Int. J. Solids Structures, submitted (1992).
12 Weibull, W., Ing. Vetens. Akad., Handlingar Nr 151 (1939).
13 Curtin, W.A., J. Am. Ceram. Soc., **74** [11], pp. 2837-2845 (1991).
14 Hild, F., Larsson, P.-L., and Leckie, F.A., Int. J. Solids Structures, in press (1992).
15 Abaqus , Hibitt, H.D., Karlsson, B.I. and Sorenson, P., Inc., version 4.8 (1989).
16 Lemaitre, J., and Marquis, D., A.S.M.E., PVP-Vol 184, Visco-Plastic Behavior of New Materials, Edts. D. Hui and T.J. Kozik, Book No. H00567, pp. 53-57 (1989).

AUTHOR INDEX

R

S

T

V

W

Z

SUBJECT INDEX

508

List of

PARTICIPANTS

Professor Hiroyuki Abé
Dept. of Mechanical Engineering
Tohoku University
Aoba, Sendai 980
Japan

Professor Sarp Adali
Dept. of Mechanical Eng.
University of Natal
King George V Avenue
Durban 4001
Republic of South Africa

Professor N.V. Banichuk
Inst. for Problems in Mechanics
Academy of Science of Russia
Prospect Vernadscogo, 101
117526 Moscow
Russia

Docent Martin P. Bendsøe
Mathematical Institute
Technical University of Denmark
Building 303
DK–2800 Lyngby
Denmark

M.Sc. Torben Birker
FB 10, Universität Essen
Postfach 10 37 64
D–4300 Essen 1
Germany

Dr. J. Blachut
Dept. of Mechanical Engineering
The University of Liverpool
P.O. Box 147
Liverpool L69 3BX
U.K.

Professor Bernard Budiansky
313 Pierce Hall
Division of Appl. Sciences
Harvard University
29 Oxford Street
Cambridge, MA 02138
USA

Docent Esben Byskov
Dept. of Structural Engineering
Technical University of Denmark
Building 118
DK–2800 Lyngby
Denmark

Professor Gengdong Cheng
Research Inst. of Eng. Mechanics
Dalian Inst. of Technology
Dalian, 116024 Liaoning
Peoples Republic of China

Lektor Jes Christoffersen
Department of Solid Mechanics
Technical University of Denmark
Building 404
DK–2800 Lyngby
Denmark

Professor Krzysztof Dems
Lodz Technical University I – 26
ul. Zwirki 36
90–924 Lodz
Poland

Professor Alejandro Diaz
Dept. of Mechanical Engineering
Michigan State University
A231 Engineering Building
East Lansing, MI 48824–1226
USA

Jan Dvorak
Charles University
Mathematical Institute
Sokolovska 83
18000 Prague 8
Czechoslovakia

Dr. Piotr Fedelinski
Silesian Technical University
Mechanical Engineering Faculty
Dept. of Engineering Mechanics
ul. Konarskiego 18A
44–100 Gliwice
Poland

Per S. Frederiksen
Department of Solid Mechanics
Technical University of Denmark
Building 404
DK–2800 Lyngby
Denmark

Professor J.M. Guedes
CEMUL – Inst. Superior Técnico
Av. Rovisco Pais
P–1096 Lisboa Codex
Portugal

Dr.techn. Niels Hansen
Risø National Laboratory
Materials Department
DK–4000 Roskilde
Denmark

Professor John W. Hutchinson
Harvard University, Pierce Hall
Division of Applied Sciences
Cambridge, MA 02138
USA

Lektor Jarl Jensen
Department of Solid Mechanics
Technical University of Denmark
Building 404
DK–2800 Lyngby
Denmark

Professor Dr. H. Eschenauer
University of Siegen
FB 11, IMR
Paul–Bonatz–Str. 9–11
D–W 5900 Siegen 21
Germany

Professor Claude Fleury
Aerospace Laboratory
University of Liege
21 rue E. Solvay
B–4000 Liege
Belgium

Dr. Joachim Grenestedt
Lättkonstruktioner
KTH
S – 100 44 Stockholm
Sweden

Professor Robert B. Haber
Dept. of Theo. & Appl. Mech.
University of Illinois, Urabna–Champaign
104 S. Wright St., Urbana, Il. 61801
USA

Dr. Francois Hild
Laboratoire de Mécanique et Technologie
E.N.S. de Cachan
61, avenue du Président Wilson
F–94235 Cachan Cedex
France

Lektor Henrik Myhre Jensen
Department of Solid Mechanics
Technical University of Denmark
Building 404
DK–2800 Lyngby
Denmark

Professor B.L. Karihaloo
School of Civil and Mining Engn.
The University of Sydney
NSW 2006
Australia

Professor Noboru Kikuchi
Dept. of Mechanical Eng. and
Applied Mechanics
The University of Michigan
Ann Arbor, MI 48109–2215
USA

Professor Arne Kildegaard
Aalborg University
Pontoppidanstræde 101
9220 Aalborg Ø
Denmark

Professor F.A. Leckie
Dept. Mech. & Environmental Eng.
University of California
Santa Barbara
CA 93106–5070
USA

Dr. Tomasz Lekszycki
Inst. of Fundamental
Technological Research
Polish Academy of Sciences
ul. Swietokrzyska 21, 00 049 Warszawa
Poland

Prof. Robert Lipton
Dept. of Mathematical Sciences
Worchester Polytechnical Inst.
100 Institute Road
Worcester, MA 01609–2280
USA

Prof. Konstantin A. Lurie
Dept. of Mathematical Sciences
Worcester Polytechnic Inst.
100 Institute Road
Worcester, MA 01609–2280
USA

Civ.ing. Per Madsen
Danfoss
L7 S40
6430 Nordborg
Denmark

M.Sc. Mads Mammen
Grundfos A/S
DK–8850 Bjerringbro
Denmark

Arek Mezek
Silesian Technical University
Mechanical Engineering Faculty
Dept. of Engineering Mechanics
ul. Konarskiego 18A
44–100 Gliwice
Poland

Dr. S.K. Morton
Department of Engineering Math.
University of Bristol
Queen's Building
Bristol
England

Professor Zenon Mróz
Polish Academy of Sciences
Inst. Fundamental Tech. Research
Swietokrzyska 21
00–049 Warsaw
Poland

Dr. Aleksander Muc
Cracow University of Technology
Inst. Mechanics & Machine Design
Warszawska 42
31–155 Kraków
Poland

Professor Alan Needleman
Box D, Division of Engineering
Barus & Holley 7th Floor
Brown University
Providence, RI 02912
USA

Lektor Arne Gudmann Nielsen
Department of Solid Mechanics
Technical University of Denmark
Building 404
DK–2800 Lyngby
Denmark

514

Professor Frithiof Niordson
Department of Solid Mechanics
Technical University of Denmark
Building 404
DK–2800 Lyngby
Denmark

Professor Niels Olhoff
Inst. of Mechanical Engineering
Aalborg University
Pontoppidanstræde 101
DK–9220 Aalborg East
Denmark

Docent Pauli Pedersen
Department of Solid Mechanics
Technical University of Denmark
Building 404
DK–2800 Lyngby
Denmark

Prof. Preben Terndrup Pedersen
Department of Ocean Engineering
Technical University of Denmark
Building 101
DK–2800 Lyngby
Denmark

Prof. L.V. Petukhov
Dept. of Appl. Mathematics
St. Petersburg Tech. University
Lazazev emb. 20, 119
St. Petersburg 197042
Russia

Dr. Alija Picuga
Faculty of Mechanical Engineering
University "Dzemal Bijedic"
B. Parovica bb
88000 Mostar
Bosnia and Herzegovina

Professor Raymond H. Plaut
Department of Civil Engineering
Virginia Tech
Blacksburg, VA 24061–0105
USA

Assoc. Prof. Ryszard Pyrz
Inst. of Mechanical Engineering
University of Aalborg
Pontoppidanstræde 101
DK–9220 Aalborg East
Denmark

Dr. Stephane Quilici
Institut Méditerranéen de Tech./
Unité Modiles Numériques
Technopole de Chateau–Gombert
13451 Marseille Cedex 13
France

Professor F.G. Rammerstorfer
Inst Lightweight & Aerospace Eng.
Vienna University of Technology
Gusshausstrasse 27–29
A–1040 Vienna
Austria

Dr. John Rasmussen
Inst. of Mechanical Engineering
University of Aalborg
Pontoppidanstræde 101
DK–9220 Aalborg East
Denmark

Dipl.–Ing. Thomas J. Reiter
Inst Lightweight & Aerospace Eng
Vienna University of Technology
Gusshausstrasse 27–29
A–1040 Vienna
Austria

Professor Rolands Rikards
Riga Technical University
Kalku str. I
Riga, 226047
Latvia

Professor George Rozvany
FB 10, Universität Essen
Postfach 10 37 64
D–4300 Essen 1
Germany

M.Sc. Ole Sigmund
FB 10, Universität Essen
Postfach 10 37 64
D–4300 Essen 1
Germany

Professor John E. Taylor
Aerospace Engineering
University of Michigan
Ann Arbor, Mich. 48109
USA

Professor Dan Tortorelli
University of Illinois at
Urbana–Champaign
Dept. of Mechanical & Ind. Engn.
1206 W. Green Street
Urbana, IL 61801
USA

Dipl.–Ing. T. Vietor
University of Siegen
FB 11, IMR
Paul–Bonatz–Str. 9–11
D–W 5900 Siegen 21
Germany

Dr. Krzysztof Szuwalski
Cracow University of Technology
Inst. of Mech. and Machine Design
31–155 Krakow
ul. Warszawska 24
Poland

Dr. Vassili V. Toropov
Delft University of Technology
Dept. Mech. Eng. and Marine Tech.
Lab. for Engineering Mechanics
P.O. Box 5033
2600 GA Delft
Holland

Professor Viggo Tvergaard
Department of Solid Mechanics
Technical University of Denmark
Building 404
DK–2800 Lyngby
Denmark

Dipl.–Ing. H.–W. Wodtke
University of Siegen
FOMAAS
Paul–Bonatz–Str. 9–11
D–W 5900 Siegen 21
Germany